THE JOURNAL
OF
CHEMICAL PHYSICS

VOLUME 32, NUMBER 4 APRIL, 1960

Nuclear Magnetic Resonance in B_2O_3—H_2O Glasses and Boric Acids

A. H. SILVER

Scientific Laboratory, Ford Motor Company, Dearborn, Michigan

(Received October 13, 1959)

The class of materials B_2O_3—H_2O has been investigated over the range B_2O_3 to $B_2O_3 \cdot 3H_2O$. This includes "dry" glassy B_2O_3, "wet" glassy boron oxide of approximate composition $B_2O_3 \cdot \frac{1}{2}H_2O$, monoclinic and orthorhombic forms of metaboric acid, $B_2O_3 \cdot H_2O$, and triclinic orthoboric acid, $B_2O_3 \cdot 3H_2O$. The nuclear quadrupole interaction of the B^{11} isotope was measured and comparisons of the structures are made on the basis of this interaction. It is shown that all substances contain similar planar BO_3 triangular units. The presence of O—H—O hydrogen bonds, as in $B_2O_3 \cdot 3H_2O$, has a minor effect on the boron nuclear quadrupole interaction. It is concluded that BO_4 tetrahedral units exist in several of the wet glass samples as well as in monoclinic metaboric acid.

INTRODUCTION

THIS investigation was undertaken in order to determine what structural effect included water has on inorganic glasses. The boron oxide system was chosen because of the previous success in nuclear magnetic resonance (NMR) study of B_2O_3 glass[1] and because it was found that such glasses could easily be produced[2] containing about 35 mole % H_2O. Furthermore, the crystalline boric acids are available as reference materials in which the basic structural units are known.[3–5] Other research is being carried on in this laboratory by Milberg and co-workers on the boron oxide system using x-ray, infrared, and other techniques.

The B^{11} nuclear quadrupole interaction is a sensitive internal probe of the electron environment of the boron nucleus. It has been shown that the value of the quadrupole coupling constant, (eqQ) can be used to distinguish between certain local environments and bonding electron configurations.[1]

Previous study of boron oxide glasses by NMR methods has confirmed the existence of BO_3 triangles.[1] Addition of oxygen donating materials such as Na_2O and Li_2O results in conversion of some BO_3 groups to BO_4 tetrahedra. For the BO_3 triangles with predominantly covalent B—O bonds the quadrupole coupling constant was reported as 2.76 Mcps. If the BO_4 were perfect tetrahedra, (eqQ) would be zero. An upper limit of 0.57 Mcps was reported in the previous work.

EXPERIMENTAL

All samples were prepared starting from granular or powdered $B_2O_3 \cdot 3H_2O$. The $B_2O_3 \cdot 3H_2O$ sample was a pellet formed in a hydraulic press. This was necessary in order to provide a sufficient filling factor to observe the resonance. The monoclinic and orthorhombic metaboric acids were prepared by heating boric acid in an open container for about 24 hr at about 200°C and 100°C, respectively. The products were granular samples which were checked by infrared analysis. Wet glasses were produced by heating boric acid for 24 hr in a stoppered weighing bottle. The samples were formed in pyrex test tubes which fractured when the boron oxide glass solidified. Temperatures approximately 195°C, 230°C, and 260°C were used with resulting approximate composition for the products of $B_2O_3 \cdot 0.6H_2O$, $B_2O_3 \cdot 0.5H_2O$, and $B_2O_3 \cdot 0.4H_2O$, respectively. The water content was determined by chemical analysis on one of the samples made at each temperature. Slight variations in composition do occur but this will not affect the conclusions to be drawn in this paper. The dry B_2O_3 glass was prepared by heating at 1000°C in an open platinum crucible until all bubbling ceased. The melt was then poured into a carbon form. All samples were maintained in a dessicator. A low dielectric loss compound (Q dope) was applied to the glass samples before spectra were run. The metaboric acids were enclosed in quartz tubes. (Both Pyrex

[1] A. H. Silver and P. J. Bray, J. Chem. Phys. **29**, 984 (1958).
[2] M. E. Milberg and F. Meller, J. Chem. Phys. **31**, 126 (1959).
[3] H. Tazaki, J. Sci. Hiroshima Univ. **A10**, 55 (1940).
[4] W. H. Zachariasen, Acta Cryst. **5**, 68 (1952).
[5] W. H. Zachariasen, Acta Cryst. **7**, 305 (1954).

Copyright © 1960 by the American Institute of Physics

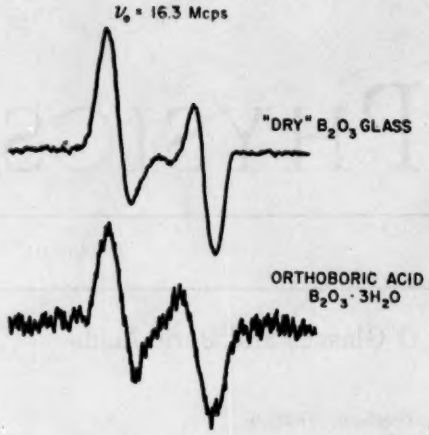

FIG. 1. B^{11} nuclear magnetic resonance in dry B_2O_3 glass and in polycrystalline $B_2O_3 \cdot 3H_2O$ at $\nu_0 = 16.3$ Mcps.

and commercial soft glass gave strong background B^{11} resonances and are not suitable sample holders for boron studies.)

The NMR spectra were obtained at room temperature using a Pound-Knight-Watkins type recording spectrometer and a Varian 12-in. electromagnet. Frequency calibration of the charts was obtained by using an electronic counter and digital printer. A cam on the recorder chart drive closes a microswitch at ½-in. intervals. This activates the counter for a fixed period of one second and the frequency is automatically printed. Closing the microswitch simultaneously shorts one input terminal of the recorder to ground through a 1.8 K resistor for ½ sec. The result is a sharp marker on the chart indicating the frequency calibration. This system eliminates the undesirable effects of beating a set of reference markers in the oscillating detector.

RESULTS

The previous experiments[1] on B_2O_3 glasses were performed at a B^{11} Larmor frequency of 7.177 Mcps. Attempts to observe the boron resonance in granular boric acid, $B_2O_3 \cdot 3H_2O$, had proved unsuccessful. The structure of boric acid[5] consists of planar BO_3 groups jointed by hydrogen bonding between oxygen atoms. The deviations from threefold symmetry are extremely small. It is an exceedingly good approximation to assume that the asymmetry parameter η is equal to zero. Previous failure to observe the resonance suggested that the presence of second-nearest neighbor hydrogen bonds was increasing the quadrupole coupling energy.

The present experiments were performed at 11.9 kilogauss, corresponding to a Larmor frequency for B^{11} of 16.3 Mcps. Using a cold-pressed powder slug the resonance has now been observed. Figure 1 illustrates the experimental derivative curves for the B^{11} resonance in "dry" B_2O_3 glass and in polycrystalline boric acid, $B_2O_3 \cdot 3H_2O$, at 16.3 Mcps. The relative signal-to-noise ratios suggest that the previous difficulty was a poor filling factor.

There are noticeable differences in the line shape, particularly in the central portion of the resonance. This difference can be assigned to a difference in the single component line width, i.e., the line width for a given orientation of the BO_3 plane relative to the external field. The theoretical dipolar second moment[6] for B^{11} has been calculated for a powdered sample. In boric acid, eight nearest hydrogen and three boron atoms were included; in the B_2O_3 glass, three boron neighbors were assumed at 2.76A. The result is 21.5 $(\text{kcps})^2$ for boric acid and 1.76 $(\text{kcps})^2$ for B_2O_3 glass. Assuming a Gaussian line shape, the rms deviation is

$$\sigma(B_2O_3 \cdot 3H_2O) = 4.6 \text{ kcps},$$
$$\sigma(B_2O_3) = 1.3 \text{ kcps}. \quad (1)$$

The peak-to-peak frequency separation, $(\Delta\nu)_{p-p}$, of the derivative extrema are measured as

$$(\Delta\nu)_{p-p}(B_2O_3 \cdot 3H_2O) = (0.0568 \pm 0.0005) \text{ Mcps},$$
$$(\Delta\nu)_{p-p}(B_2O_3) = (0.0623 \pm 0.0005) \text{ Mcps}. \quad (2)$$

Numerical calculations of the derivative line shape with dipolar broadening for $\sigma/(\Delta\nu)_0$ equal to 0.18 and 0.018 have been performed and are shown in Fig. 2. The quantity $(\Delta\nu)_0$ is the value of $(\Delta\nu)_{p-p}$ without dipolar broadening and is given by[1]

$$(\Delta\nu)_0 = 25(eqQ)^2/192\nu_0. \quad (3)$$

It appears that at least for $\sigma/\Delta\nu)_0 \leq 0.2$ the approximation

$$(\Delta\nu)_{p-p} = (\Delta\nu)_0 + \sigma \quad (4)$$

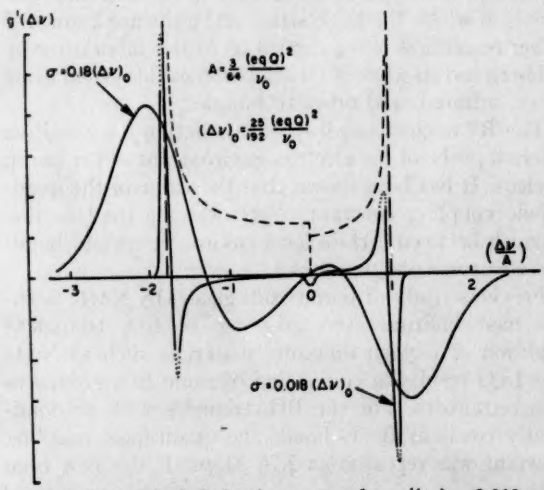

FIG. 2. Theoretical derivative curves for $\sigma/(\Delta\nu)_0 = 0.018$ and 0.18 for the central transition. The dashed curve is the frequency distribution neglecting dipolar broadening. σ is the rms deviation of a Gaussian function.

[6] J. H. Van Vleck, Phys. Rev. 74, 1168 (1948).

will be valid. On the other hand, it is clear that an upper limit exists on $\sigma/(\Delta\nu)_0$ for which (4) is valid, e.g., when $(\Delta\nu)_0/\sigma=0$, $(\Delta\nu)_{p-p}=2\sigma$. For the experiment discussed in reference 1, the correction to $(\Delta\nu)_{p-p}$ would amount to 1% corresponding to a ½% reduction in the quadrupole interaction. Considering the present data, one has

$$(\Delta\nu)_0(B_2O_3\cdot 3H_2O)=(0.0522\pm 0.0005)\ \text{Mcps},$$
$$(\Delta\nu)_0(B_2O_3)=(0.0610\pm 0.0005)\ \text{Mcps}. \quad (5)$$

From Eq. (3), the quadrupole coupling is

$$(eqQ)(B_2O_3\cdot 3H_2O)=(2.56\pm 0.02)\ \text{Mcps},$$
$$(eqQ)(B_2O_3)=(2.76\pm 0.02)\ \text{Mcps}. \quad (6)$$

The agreement with the previous value[1] for B_2O_3 glass is excellent. The difference of 0.2 Mcps between the boric acid and the glass is definitely outside the experimental error. This does not, however, indicate a basic structural difference in the BO_3 group. Quadrupole coupling constants of this magnitude have been attributed to the effects of a charged lattice in the borofluorides and borohydrides.[7] This small change might also be attributed to the influence of the hydrogen bonding of all oxygen atoms in the acid. For the present discussion, it is of note that the presence of hydrogen bonds has only a minor effect on the quadrupole interaction. The agreement between the values of (eqQ) for B_2O_3 glass and boric acid strengthens the concept of planar BO_3 triangles as the network former in the glass.

The width of the signal peaks for B_2O_3 glass can be attributed to the randomness of the structure. In the case of orthoboric acid the width is due to effects of the single component line width.

Figure 3 displays the B^{11} resonance in the orthorhombic and monoclinic forms of $B_2O_3\cdot H_2O$. Again, the

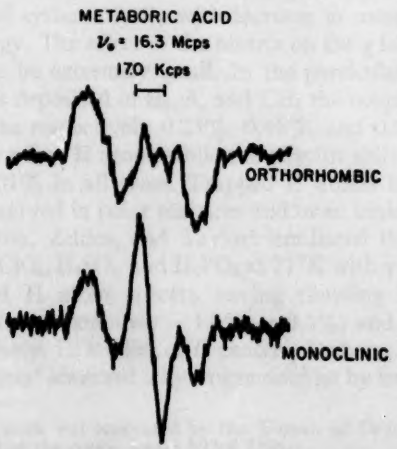

FIG. 3. B^{11} nuclear magnetic resonance in polycrystalline orthorhombic and monoclinic metaboric acids.

[7] A. H. Silver and P. J. Bray, J. Chem. Phys. (to be published).

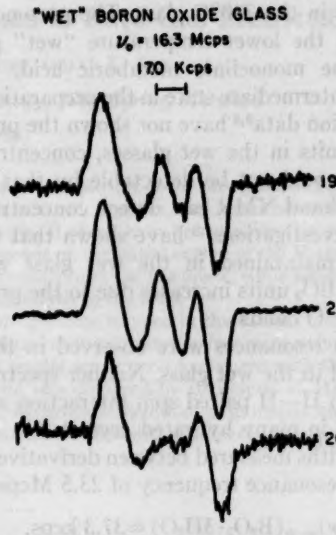

FIG. 4. B^{11} nuclear magnetic resonance in "wet" boron oxide glasses. The temperatures at which the samples were prepared are given.

broad outermost peaks correspond to the same resonance as observed in "dry" glass and in the orthoboric acid. Within the experimental accuracy the quadrupole interaction is again the same as in the boric acid, $B_2O_3\cdot 3H_2O$. From the x-ray structural investigations it is known that the boron has coordination 3 in the orthorhombic[4] and both 3 and 4 in the monoclinic[3] acids. Hence, this broad line is associated with the threefold boron atoms. Again, the atoms to which the oxygen neighbors are bonded apparently has little effect on the quadrupole interaction of the B^{11}. The two sharp peaks in the spectrum of the orthorhombic acid come from B^{11} nuclei with a small coupling constant. The peculiar shape is apparently due to the effects of modulation broadening. Since the infrared analysis of the sample showed a few percent of an unidentified impurity material, it is believed this narrow resonance results from the impurity. One can speculate that this impurity may be the cubic form of metaboric acid. In the case of the monoclinic acid, the large narrow resonance is assigned to the fourfold boron atoms. The width is presumably due to quadrupole broadening from the irregular BO_4 tetrahedra.

Figure 4 shows the boron resonances for the wet glasses produced at 195°, 230°, 260°C. All samples have the broad spectrum resulting from the triangularly coordinated boron atoms. The quadrupole interaction is the same as in the dry glass. No narrow resonance corresponding to BO_4 tetrahedra is observed in the 260°C glass whereas the narrow line does appear in the 195°C and 230°C glasses. In this respect the 260°C glass is similar to the "dry" B_2O_3 glass. The relative intensity of the narrow line in the 230°C glass is approximately 5%, as measured by direct integration. This means about 5% of the boron atoms have tetrahedral

environments in the 230°C glass. The presence of BO_4 tetrahedra in the lower temperature "wet" glasses is similar to the monoclinic metaboric acid, which is probably an intermediate state in the preparation. While x-ray diffraction data[2,8] have not shown the presence of tetrahedral units in the wet glasses, concentrations of 10% or less would not be detectable by that method. On the other hand NMR can detect concentrations of 1%. X-ray investigations[2,8] have shown that the basic BO_3 unit is maintained in the wet glass while the separation of BO_3 units increases due to the presence of longer O—H—O bonds.

The proton resonances were observed in the orthoboric acid and in the wet glass. Neither spectrum gave evidence of an H—H paired spin interaction similar to that observed in many hydrated crystals.[9]

The line widths measured between derivative maxima for a proton resonance frequency of 23.5 Mcps are

$$(\Delta\nu)_{p-p}(B_2O_3\cdot 3H_2O)=37.3 \text{ kcps},$$
$$(\Delta\nu)_{p-p}(B_2O_3\cdot 0.5H_2O)=25.7 \text{ kcps} \quad (7)$$

and the shapes are approximately Gaussian. The equivalent half-width of the resonance in gauss and hence, the local microscopic field is

$$(\Delta H)(B_2O_3\cdot 3H_2O)=4.4 \text{ gauss},$$
$$(\Delta H)(B_2O_3\cdot 0.5H_2O)=3.0 \text{ gauss}. \quad (8)$$

Calculation of the dipolar second moment for $B_2O_3\cdot 3H_2O$ considering three nearest boron and five nearest hydrogen atoms in the plane yields

$$(\langle\Delta H^2\rangle)^{\frac{1}{2}}(B_2O_3\cdot 3H_2O)=3.3 \text{ gauss}. \quad (9)$$

Assuming a local configuration for the wet glass similar to the orthorhomic metaboric acids[8] and considering three boron and two hydrogen neighbors one has

$$(\langle\Delta H^2\rangle)^{\frac{1}{2}}(B_2O_3\cdot 0.5H_2O)=3.0 \text{ gauss}. \quad (10)$$

The general agreement between these values and the lack of any strong H—H interaction indicates that water molecules do not exist in the glass. This agrees with the conclusions drawn from infrared[10] and x-ray studies.[8]

CONCLUSIONS

Comparison of the B^{11} nuclear resonance in the various boric acids and boron oxide glasses further conconfirms the planar BO_3 triangular unit as the basis of boron oxide glass. Presence of hydrogen bonding between BO_3 units does not appreciably affect the electron distribution near the boron atom. This is amply demonstrated by the consistency of the large quadrupole interaction in all the materials studied. The presence of H_2O in B_2O_3 glass does produce a small percentage of BO_4 units at the lower temperatures. At 260°C the BO_4 have apparently been transformed to the planar BO_3 units.

The absence of water molecules in the "wet" glass is supported by a study of the proton resonance.

ACKNOWLEDGMENTS

The author wishes to thank M. E. Milberg for his results prior to publication and to acknowledge helpful discussions. Infrared comparisons were performed by J. L. Parsons and chemical analyses were by R. K. Belitz. Thanks are due C. M. Savage for aid in the construction of the spectrometer and in the design of the frequency measuring system.

[8] F. Meller and M. E. Milberg (to be published).
[9] G. Pake, *Solid State Physics* (Academic Press, Inc., New York, 1956), Vol. 2.
[10] J. L. Parsons and M. E. Milberg, J. Am. Ceram. Soc. (to be published).

THE JOURNAL OF CHEMICAL PHYSICS VOLUME 32, NUMBER 4 APRIL, 1960

Multiple Trapping Sites for Hydrogen Atoms in Rare Gas Matrices*

S. N. Foner, E. L. Cochran, V. A. Bowers, and C. K. Jen

Applied Physics Laboratory, The Johns Hopkins University, Silver Spring, Maryland

(Received September 8, 1959)

Hydrogen atoms have been stabilized in nonequivalent lattice sites in matrices of the rare gases at liquid helium temperature. Electron spin resonance spectra of H atoms in argon, krypton, and xenon show that at least two trapping sites are involved in each case. In a neon matrix, H atoms have been stabilized in only one site. Attainability of the various trapping sites apparently depends on the initial energy of the H atom, a simple doublet spectrum being obtained when the atoms are deposited from the gas phase, while multiple trapping spectra are obtained when the atoms are produced by photolysis in the solid.

The hyperfine coupling contants and the electronic g factors for H atoms trapped in the various matrix sites have been determined. The deviation of the hyperfine coupling constant from the free-state value is positive in some cases and negative in others. The experimental results are in good agreement with theoretical predictions. A complex multicomponent H atom spectrum was obtained by photolysis of HI in xenon. The subsplitting in the spectrum is attributed to magnetic hyperfine interactions with matrix nuclei (Xe^{129} and Xe^{131}). The nature of the trapping sites in rare gas matrices is discussed. Evidence for trapping in substitutional sites and octahedral sites is presented.

I. INTRODUCTION

WHEN an atom or free radical is trapped in a solid, it is perturbed by the matrix fields and its energy levels are shifted. In electron spin resonance (ESR) experiments, the perturbations produced by the matrix are displayed as displacements of the resonance lines from their free-state positions. The spectral shifts correspond to deviations of the hyperfine coupling constant and the electronic g factor from the values for a radical in the free state. In addition, the widths and shapes of the spectral lines are influenced in a complex manner by the trapping medium, particularly through spin-lattice relaxation and matrix anisotropy.

The effect of the matrix field on the resonance spectra of various radicals has been studied by depositing the radicals in nonpolar matrices having different binding energies.[1] The deviation of the hyperfine coupling constant from the free-state value was generally small and increased systematically with increase in matrix binding energy. The effect of the matrix on the g factor was found to be extremely small. In the particular case of H atoms deposited in H_2, A, and CH_4 the coupling constant was respectively 0.23%, 0.46%, and 0.66% less than for a free H atom, while the g factor shift was less than 0.01% in all cases. Trapped H atoms have also been observed in polar matrices and in an ionic crystal. Livingston, Zeldes, and Taylor[2] irradiated the frozen acids $HClO_4$, H_2SO_4, and H_3PO_4 at 77°K with γ rays and observed H atom spectra having coupling constant shifts of approximately -1.0%, -0.4%, and $+0.2\%$, respectively. In studies of U centers, Delbecq, Smaller, and Yuster[3] observed a hydrogen doublet by irradiating a KCl—KH single crystal at 80°K with ultraviolet light. The doublet had a splitting of 500 ± 10 oe and the lines were quite broad (half-width $=68\pm5$ oe).

Since the spectrum of a trapped radical depends on its interaction with its environment, it is expected that the spectra of radicals trapped in nonequivalent lattice sites will be different. To be readily resolved, the spectra for the different sites should be displaced with respect to each other by at least the line width. The trapping of hydrogen atoms in different lattice sites in solid argon was recently reported by Cochran, Bowers, Foner, and Jen.[4] An ESR spectrum of three doublets was obtained by photolysis of HI in argon at 4.2°K. The resolution of the six lines as three independent H atom doublets was demonstrated by a warmup experiment which showed that the doublets disappeared at different temperatures. The doublet with highest thermal stability was identical with that obtained by deposition of H atoms in argon. The spectra were interpreted as the ESR spectra of H atoms in different lattice sites, the occupation of the additional sites in the photolytic experiment being made possible by the high initial energy of the photolytically released H atoms.

In this paper, we are concerned with the ESR spectra of H atoms trapped in the rare gas solids, with particular emphasis on the trapping of H atoms in nonequivalent lattice sites. The experimental results, together with the known crystallographic data on the rare gases, are combined with theoretical predictions to give a consistent picture of the nature of the trapping sites.

II. EXPERIMENTAL

The essential features of the apparatus have been described.[1] Two types of sample preparation are involved: (1) deposition of H atoms (from an electrical discharge in H_2) in various matrices; (2) photolytic

* This work was supported by the Bureau of Ordnance, Department of the Navy, under NOrd 7386.

[1] Jen, Foner, Cochran, and Bowers, Phys. Rev. **112**, 1169 (1958).

[2] Livingston, Zeldes, and Taylor, Discussions Faraday Soc. **19**, 166 (1955).

[3] Delbecq, Smaller, and Yuster, Phys. Rev. **104**, 599 (1956).

[4] Cochran, Bowers, Foner, and Jen, Phys. Rev. Letters **2**, 43 (1959).

generation of H atoms in solid media. A cross section of the sample deposition system is shown in Fig. 1. In the H atom deposition experiments, the sample was prepared by simultaneous deposition on the liquid helium-cooled sapphire rod of a molecular beam containing H atoms from the glass slit and molecular beams of rare gas atoms from the matrix slits. For photolytic experiments, the glass slit was replaced by an optical window of quartz or sapphire. A mixture of the photosensitive compound and the matrix gas was deposited on the sapphire rod via the matrix slits. The ratio of matrix gas to photosensitive compound was typically 100:1. After deposition, the sample was irradiated with ultraviolet light for periods of from 1 to 24 hours. For photolysis requiring a sapphire window the uv source was an rf discharge in hydrogen gas in the quartz tube shown in Fig. 1. For most of the experiments a quartz window was used and the uv source was a Hanovia SC 2537 Hg resonance lamp placed in front of the window. The samples used in these experiments were about 0.5 mm thick. After sample preparation, the sapphire rod was lowered into the microwave cavity for resonance observations.

The effect of temperature on the resonance spectra could be studied by removing the liquid helium from the cryostat. The heat leak into the cryostat resulted in a temperature rise of about 0.25°C per min. Samples containing H_2 could not be warmed up more than a few degrees because vaporization of H_2 degraded the vacuum in almost explosive fashion and caused the sample temperature to rise rapidly to that of the radiation shield (77°K).

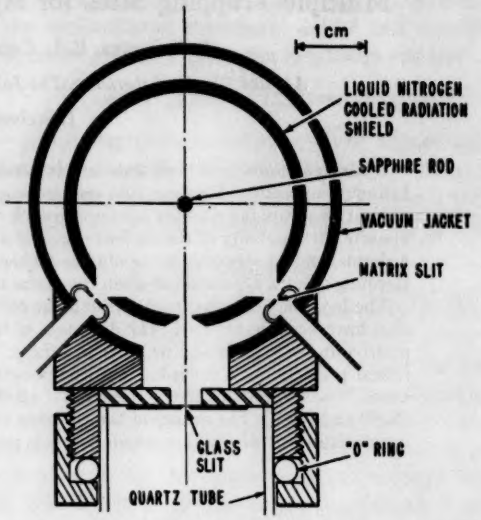

FIG. 1. Sample deposition system. For photolytic experiments, the glass slit is replaced by a suitable uv transmitting optical window.

III. ESR SPECTRA OF HYDROGEN ATOMS

A. Hyperfine Spectra of Hydrogen Atoms

In discussing the spectral perturbations experienced by a trapped H atom, we start by considering the spectrum of a free H atom. The magnetic energy levels for an atom in a $^2S_{\frac{1}{2}}$ state are given by the Breit-Rabi formula,[5,6]

$$W_{I\pm\frac{1}{2}}=-[\Delta W/2(2I+1)]+g_I\mu_0HM \pm(\Delta W/2)\{1+[4Mx/(2I+1)]+x^2\}^{\frac{1}{2}}, \quad (1)$$

where ΔW=hyperfine energy separation, I=nuclear spin, M is the magnetic quantum number of $\mathbf{F}=\mathbf{I}+\mathbf{S}$, $x=(g_J-g_I)\mu_0H/\Delta W$, g_J=electronic g factor, g_I=nuclear g factor, defined by $g_I=-\mu_I/\mu_0I$, μ_0=Bohr magneton and H=magnetic field. In an ESR experiment with H atoms ($I=\frac{1}{2}$) there are two allowed transitions: $(0,0\rightarrow1,1)$ and $(1,-1\rightarrow1,0)$ where each state is designated by its F, M value. If the microwave frequency is constant, as is the case for ESR experiments, the magnetic fields for the transitions are given by:

$$\nu=A\{\tfrac{1}{2}(1+x_1)+\tfrac{1}{2}(1+x_1^2)^{\frac{1}{2}}+g_I(\mu_0H_1/hA)\}, \quad (2)$$

$$\nu=A\{\tfrac{1}{2}(-1+x_2)+\tfrac{1}{2}(1+x_2^2)^{\frac{1}{2}}+g_I(\mu_0H_2/hA)\}, \quad (3)$$

where ν=microwave frequency, $A=\Delta W/h$=hyperfine coupling constant in frequency units, $x_1=(g_J-g_I)\mu_0H_1/hA$, $x_2=(g_J-g_I)\mu_0H_2/hA$, and H_1, and H_2 are respectively the magnetic fields for the low-field and high-field resonances.

The experimentally determined resonance fields (H_1 and H_2) for a trapped H atom and the microwave frequency (ν) are inserted in Eqs. (2) and (3) which are solved by iteration for A and g_J. The deviations of A and g_J from the free-state values are a phenomenological description of the interaction of the trapped H atom with its environment. In general, atoms trapped in nonequivalent sites will have different values for A and g_J, and thus give rise to multiple line spectra. If magnetic nuclei are present in the matrix, additional splitting of the lines by hyperfine interactions is possible.

A theory for the hfs and g factor shifts produced by the trapping matrix is given by Adrian[7] in the following paper. The perturbation produced by the matrix is treated as the sum of two effects: van der Waals interactions and Pauli exclusion effects. The van der Waals attraction leads to a reduction in the hyperfine coupling constant. The Pauli exclusion principle, which requires that the H wave functions be orthogonal to the wave functions of the matrix atoms, leads to an increase in the coupling constant. The net effect can be either a negative or a positive shift, depending on whether the attractive forces or exchange forces predominate. The

[5] G. Breit and I. I. Rabi, Phys. Rev. **38**, 2082 (1931).
[6] J. E. Nafe and E. B. Nelson, Phys. Rev. **73**, 718 (1948).
[7] F. J. Adrian, J. Chem. Phys. **32**, 972 (1960).

balance between these two effects is sensitive to the distance of the H atom from its nearest neighbor matrix atoms. The g factor shifts result from the Pauli exclusion forces and, therefore, relatively large g shifts are associated with positive shifts in the hyperfine coupling constants.

B. Hydrogen Atoms in Neon

Photolysis of a 1% mixture of HI in neon at 4.2°K produced a simple doublet H atom spectrum with the lines separated by 512.2 oe. The field separation is significantly greater than for free H atoms. The hfs constant, $A=1426.56$ mc/sec, is 0.43% greater than the free atom. The g factor shift, Δg_J, is -0.00019.

Several unsuccessful attempts were made to deposit H atoms in a neon matrix. On the supposition that the difficulty was due to inefficient condensation of H atoms on a neon surface at 4.2°K, an attempt was made to deposit the more easily condensed deuterium atoms. This experiment failed to show resonances. Lowering the temperature of the sapphire rod to about 2°K, by pumping on the liquid helium, was ineffective in stabilizing deposited H or D atoms.

C. Hydrogen Atoms in Argon

The stabilization of H atoms in argon has been reported.[1,4] Deposition of H atoms in argon at 4.2°K consistently results in a doublet spectrum with -0.46% shift in the hfs constant. Photolysis of HI in argon produces two additional doublets, one of which has a positive shift in the hfs constant. A part of the warmup recording of the low-field components of the ESR spectrum is shown in Fig. 2. The spectrum is being scanned every two minutes as the sample temperature rises. It is seen that the component labeled C disappears (at a temperature of about 12°K) in the third trace, starting from the top, while the intensities of the other lines are unaffected. Similar curves show that component B disappears at about 23°K and component A vanishes at about 39°K. The decay of the doublets at widely different temperatures is strong evidence that H atoms were stabilized in three different environments. It should be noted that the component labeled B is observed only occasionally in photolysis of HI in argon.

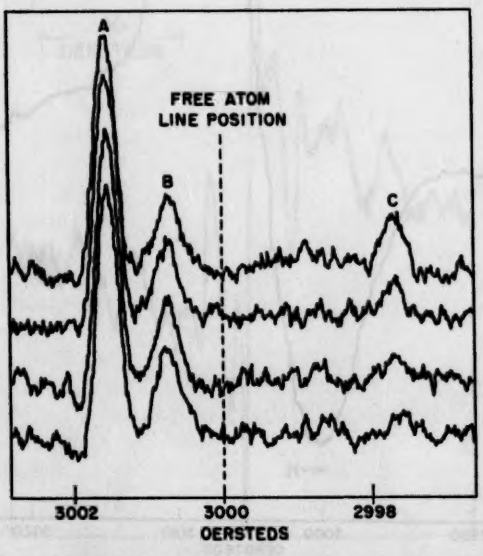

FIG. 2. ESR spectrum produced by photolysis of HI in argon. Recordings are being taken, in sequence, from top to bottom, as the sample is allowed to warm up.

FIG. 3. Low-field components of ESR spectrum of H atoms produced by photolysis of H_2O in argon at 4.2°K.

Multiple trapping of H atoms in argon has also been studied by photolysis of compounds other than HI. One reason for doing these experiments is to eliminate the possibility that the I atoms, which are generated simultaneously with the H atoms in the photolysis of HI, are responsible for the additional lines or affect the observed splittings. An I atom in the $^2P_{\frac{3}{2}}$ ground state, with nuclear spin $I=\frac{5}{2}$ and a moderately large nuclear electric quadrupole moment, would in the free state give a magnetic spectrum of 18 lines centered around the field corresponding to $g_J=\frac{4}{3}$, which is far removed from the observed doublets. In a polycrystalline sample the resonance lines are smeared out by matrix anisotropy so that they are not observed. The possibility of an indirect effect on the H atom resonances is, however, not excluded by this argument.

When a sample of 1% H_2O in argon was irradiated by uv from a discharge in hydrogen using a sapphire window, two hydrogen doublets were found. Fig. 3 shows a trace of the low-field components. The lines have the same field positions as the A and C lines in Fig. 2 obtained by photolyzing HI in argon. The photo-

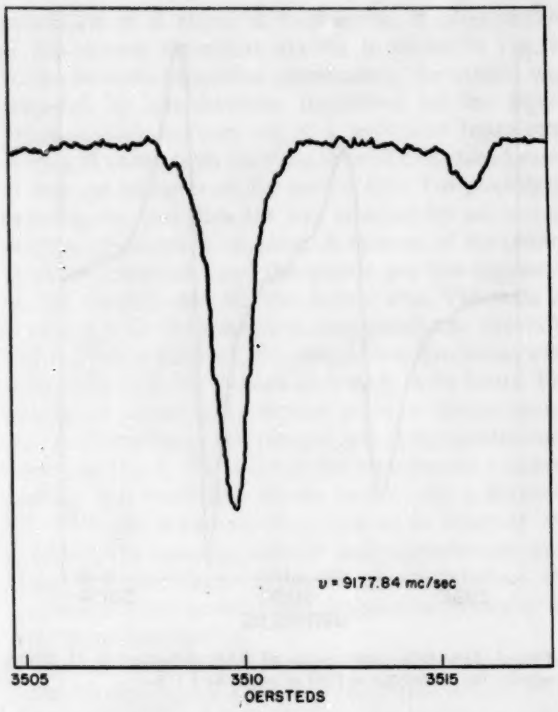

FIG. 4. High-field components of ESR spectrum of H atoms produced by photolysis of HI in krypton at 4.2°K.

lysis of NH_3 in argon also produced these two H atom doublets.

These experiments prove rather conclusively that there are at least two different trapping sites in an argon lattice where H atoms can be stabilized. The spectra for these two sites are independent of the photosensitive compound used (HI, H_2O, or NH_3), and thus exclude an indirect effect on the spectra by the other radical produced in the photolysis. The case for a third trapping site to explain doublet *B* in the photolysis of HI in argon is somewhat weakened by the absence of this doublet in photolyses of other compounds and by the infrequent occurrence of this doublet in the photolysis of HI in argon. Furthermore, the close proximity of the lines of this doublet with those of H atoms in H_2 is disturbing. On the other hand, the thermal stability of this doublet (23°K limit) is much higher than can be ascribed to H atoms in H_2 since the lines are observed even above the normal boiling point of H_2. A possible explanation is that under certain experimental conditions some of the argon crystallizes in a different structure which would give rise to the observed third doublet.

D. Hydrogen Atoms in Krypton

The hyperfine spectrum of H atoms deposited in krypton is a doublet with field separation of 506.9 oe. The hfs constant shift is −0.59%, and the *g* factor shift Δg_J is −0.00047.

Photolysis of HI in krypton produced an interesting and rather unexpected ESR spectrum. A trace of the high-field region is shown in Fig. 4. An additional line is observed 6.0 oe above the position of the normal (deposition) high-field line. A careful search of the low-field region disclosed only the low-field H atom deposition line. Since the H resonance lines must occur in pairs, failure to observe an additional low-field component requires an explanation. The simplest explanation is that the low-field component of the photolytically produced doublet is hidden under the low-field line. Because the missing line is only about $\frac{1}{10}$ as large as the observed low-field line, it is estimated that it could escape observation in roughly a ±1.0 oe range. On the assumption that the two low-field components fall on top of each other, the additional photolytically produced H atom doublet has a hfs shift of +0.47% and a *g* factor shift, ($\Delta g_J = -0.00259$). There is considerable uncertainty in these values. Although the calculated *g* factor shift is the largest observed in experiments on the rare gases, theoretical calculations, to be discussed later, indicate that the magnitude of the shift is reasonable.

E. Hydrogen Atoms in Xenon

The deposition of H atoms in xenon gives a doublet spectrum with field separation of 504.4 oe. The hfs

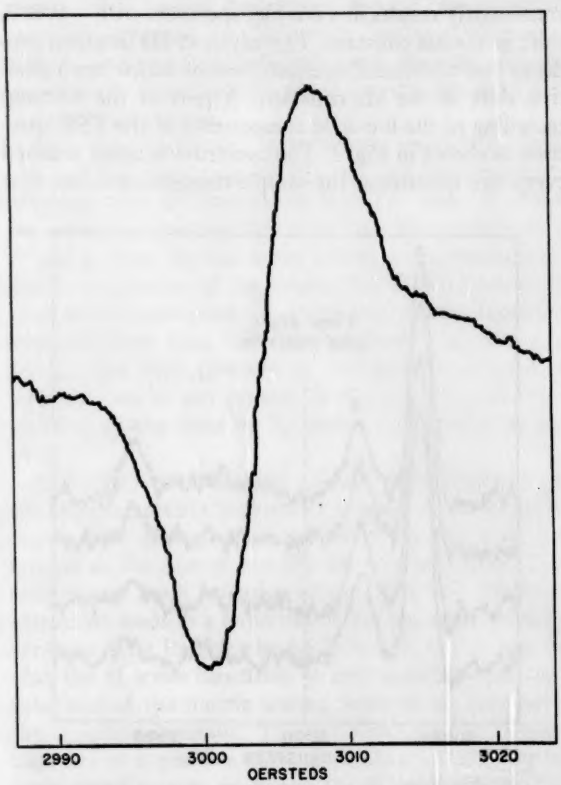

FIG. 5. Low-field component of ESR spectrum of deposited H atoms in xenon at 4.2°K.

constant shift is -1.09%, the largest negative shift observed for H atoms in these experiments. The g factor deviation $\Delta g_J = -0.00056$, is slightly larger than for krypton, although the difference is within the assigned limits of error. Figure 5 shows a trace of the low-field line. The resonance lines in xenon have an average half-width of 7.6 oe and thus are several fold wider than the resonance lines in the other rare gases.

Photolysis of HI in xenon produced a very complicated atomic hydrogen spectrum. To bring out the weaker components, a 1% HI in Xe sample was irradiated at 4.2°K with mercury resonance radiation for 23 hours. Figure 6 is a slow sweep recording of the low-field components of the spectrum. The number of lines and the over-all spread of the spectrum is not easy to establish. The spectrum has an apparent over-all spread of 98.2 oe (assuming that there are no additional lines further out, hidden in the noise background) and contains at least 13 components. The high-field spectrum is almost a mirror image of the low-field components and has the same apparent over-all spread. The spectrum was examined by taking expanded traces of the various regions of the spectrum. Line positions for the individual components were determined from these records. Figure 7 shows the field positions of the low-field spectral components. The indicated intensities are rough estimates based simply on the peak heights of the lines. The widths of the lines vary (for example, compare one of the end components in Fig. 6 with the sharp center component) and there are cases where the lines are not well resolved. Because of these factors, the intensities are subject to considerable uncertainty.

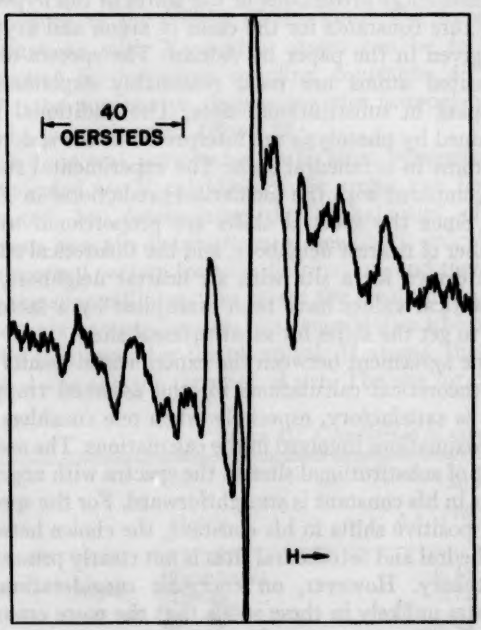

FIG. 6. Low-field components of ESR spectrum of H atoms produced by photolysis of HI in xenon at 4.2°K.

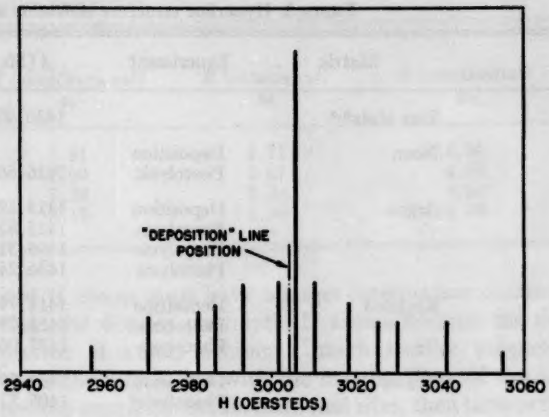

FIG. 7. Field positions of the low-field components of ESR spectrum of H atoms produced by photolysis of HI in xenon. Microwave frequency = 9177.84 Mc/sec.

The position of the "deposition" line is indicated. Contributions from the "deposition" line have been estimated and have been subtracted in obtaining the intensity pattern.

The center components of the low-field and high-field spectra are separated by 504.9 oe and can be characterized as a hydrogen doublet with hfs constant shift of -1.04% and a g factor shift, $\Delta g_J = -0.00169$. The symmetrical spacing of the other lines in the spectra about the center components suggests that they result from additional hyperfine interactions. Under these conditions the center components would give the correct values for the hydrogenic hyperfine structure constants, while the subsplitting in the spectral groups would determine the other hfs constants. The interpretation of the multiple line spectrum is considered in a following section where we discuss the nature of the trapping sites.

F. Summary of the Data for H Atoms in Rare Gas Matrices

The hyperfine coupling constants and g factors for H atoms trapped in rare gas matrices are given in Table I.

III. NATURE OF THE TRAPPING SITES

A. Trapping Sites in the Rare Gas Solids

The crystalline structure of the rare gas solids is face centered cubic. In a face centered cubic lattice there are three possible trapping sites: (1) substitutional site, (2) octahedral site, and (3) tetrahedral site. These are indicated in Fig. 8. Only one of the tetrahedral sites is shown. The number of nearest neighbor matrix atoms for the substitutional, octahedral, and tetrahedral sites are 12, 6, and 4, respectively. In addition to the regular crystalline trapping sites, there is the possibility of trapping at surface sites and at crystalline defects. The experimentally observed ESR lines are rather narrow, indicating that the H atoms are being subjected

TABLE I. Hyperfine structure constants and g factors for H atoms in rare gas matrices.[a]

Matrix	Experiment	A (Mc/sec)	$\Delta A/A$ (%)	g_J	$-\Delta g_J$
Free state[b,c]		1420.40573(5)		2.002256(24)	
Neon	Deposition		No resonances observed		
	Photolysis	1426.56(20)	+0.43	2.00207(8)	0.00019
Argon	Deposition	1413.82(40)	−0.46	2.00220(8)	0.00006
	Photolysis	1413.82(40)	−0.46	2.00220(8)	0.00006
	Photolysis	1416.31(80)	−0.29	2.00224(12)	0.00002
	Photolysis	1436.24(40)	+1.15	2.00161(8)	0.00065
Krypton	Deposition	1411.79(30)	−0.59	2.00179(8)	0.00047
	Photolysis	1411.79(30)	−0.59	2.00179(8)	0.00047
	Photolysis	1427.06(280)	+0.47	1.99967(31)	0.00259
Xenon	Deposition	1404.99(28)	−1.09	2.00170(8)	0.00056
	Photolysis[d]	1405.57(34)	−1.04	2.00057(8)	0.00169

[a] The numbers in parentheses indicate experimental and/or conversion errors in the last figures of the associated values.
[b] P. Kusch, Phys. Rev. **100**, 1188 (1955).
[c] R. Beringer and M. A. Heald, Phys. Rev. **95**, 1474 (1954).
[d] Coupling constant and g factor calculated for the center spectral components. The "deposition" doublet also appears in the photolysis experiment but cannot be accurately located because it is partially obscured by other lines.

to highly reproducible isotropic matrix fields. This suggests that trapping at surface sites or crystalline defects, where the fields are unsymmetrical, is probably not important in the present study.

A parameter which enters explicitly in the theory of the matrix effects on hyperfine spectra is the distance R (internuclear separation) of the trapped atom from its nearest neighbor matrix particles. When an H atom is trapped in the matrix, the lattice will experience some distortion: the substitutional sites are usually too large so that the matrix atoms tend to be drawn in toward the trapped atom; the interstitial sites are generally too small, in which case the matrix atoms are pushed away from the trapped atom. The calculations of the lattice distortions produced by trapped atoms are rather complicated and have not been carried out. In the comparison with theory that follows we shall use, as a first approximation, the crystal parameters of the undistorted lattice.

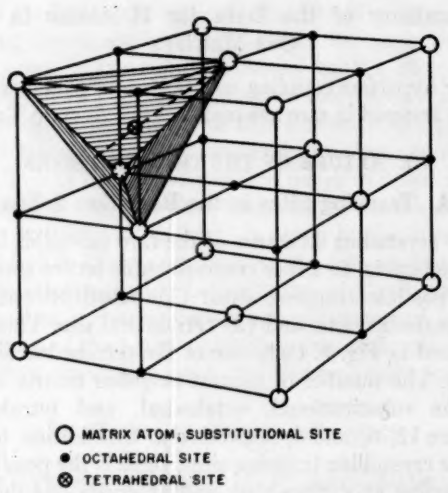

FIG. 8. Trapping sites in a face centered cubic lattice. All of the substitutional and octahedral sites are shown. Only one of the tetrahedral sites is indicated.

Table II gives the internuclear distances for the various sites in the rare gas solids. The lattice constants are taken from the compilation of Dobbs and Jones.[8] The distances are expressed in units of Bohr radii (a_0=0.5292 A).

B. Comparison with Theory for H Atoms in Argon and Krypton

Theoretical predictions of the shifts in the hyperfine structure constants for the cases of argon and krypton are given in the paper by Adrian. The spectra of the deposited atoms are most reasonably explained by trapping in substitutional sites. The additional lines obtained by photolysis are interpreted as the spectra of H atoms in octahedral sites. The experimental results are compared with the theoretical predictions[7] in Table III. Since the spectral shifts are proportional to the number of nearest neighbors, and the theoretical curves were drawn for a site with six nearest neighbors, the theoretical values have been multiplied by a factor of two to get the shifts for substitutional sites.

The agreement between the experimental results and the theoretical calculations for the assumed trapping sites is satisfactory, especially when one considers the approximations involved in the calculations. The assignment of substitutional sites to the spectra with negative shifts in hfs constant is straightforward. For the spectra with positive shifts in hfs constant, the choice between octahedral and tetrahedral sites is not clearly prescribed by theory. However, on energetic considerations it appears unlikely in these solids that the more cramped

[8] E. R. Dobbs and G. O. Jones, *Reports on Progress in Physics*, (The Physical Society, London, 1957), Vol. XX, p. 560.

TABLE II. Rare gas lattice parameters.

Crystal	Cubic cell dimension A	a_0	R (substitutional) a_0	R (octahedral) a_0	R (tetrahedral) a_0
Neon	4.35±0.15	8.22	5.81	4.11	3.56
Argon	5.31±0.01	10.03	7.09	5.01	4.34
Krypton	5.68±0.03	10.73	7.59	5.36	4.65
Xenon	6.1 ±0.1	11.52	8.15	5.76	4.99

tetrahedral site would be occupied in preference to the octahedral site. Furthermore, in the case of xenon, to be discussed later, there is independent evidence for occupation of octahedral sites rather than tetrahedral sites.

C. Complex Spectrum for H Atoms in Xenon

The large number of lines in the low-field and high-field spectra, together with regularities in the line spacings, suggest that the splittings are caused by magnetic Xe matrix atoms. Such an interaction, of course, could not occur in the nonmagnetic matrices, neon and argon. In the case of krypton, there is a magnetic isotope Kr^{83} ($I=\frac{9}{2}$, $\mu=-0.969\ \mu_N$) having a natural abundance of 11.48%. The low abundance of this isotope, together with its small nuclear g factor ($g_I=-0.215$) does not favor the observation of such an effect in krypton. In the case of xenon, however, about half of the matrix atoms are magnetic: 26.44% Xe^{129} ($I=\frac{1}{2}$, $\mu=-0.776786\ \mu_N$), and 21.18% Xe^{131} ($I=\frac{3}{2}$, $\mu=0.690635\ \mu_N$).

In a polycrystalline sample, such as we manufacture by condensation from the gas phase, the observed line splittings are due to isotropic hyperfine interactions. Anisotropic hyperfine interactions, if present, would contribute to the widths of the lines. The hyperfine interactions with Xe matrix atoms can be formally described by hyperfine coupling constants A^{129} and A^{131} (the superscript designating the isotope) which are in the ratio $A^{129}/A^{131}=3.38$.

The spectral pattern for an H atom symmetrically surrounded by N neighboring Xe atoms can be constructed by determining the probabilities of the various isotopic distributions of neighbors, calculating the spectral pattern for each distribution, and then adding the spectral intensities to get the resultant pattern. There are two regular sites in a xenon lattice which need to be considered for the photolytic H atoms: the octahedral site and the tetrahedral site. The site for deposited H atoms must have a larger internuclear distance than the site for photolytic H atoms because the deposited H atoms exhibit a much smaller magnetic hyperfine interaction with the matrix. Thus, if the deposited atoms are in substitutional sites, then both octahedral and tetrahedral sites are possibilities for the photolytic H atoms, whereas if the deposited H atoms are assigned to octahedral sites, only the tetrahedral site could be considered for the photolytic H atoms.

The calculated spectral patterns for octahedral and tetrahedral sites are shown in Fig. 9. Comparison of these patterns with the experimental distribution shows that the pattern for the octahedral site is, on the whole, in rather good agreement with experiment. The experimental line positions are, with some minor exceptions, rather accurately predicted. The variations in width of the experimental lines are also qualitatively predicted by this model. The experimentally observed "lines" generally are composed of several unresolved lines. The sharp center component is an exception in that it stands out very clearly. Considering the approximate nature of the intensity measurements of the experimental lines, the agreement between the experimental intensity distribution and the distribution for an octahedral site is satisfactory. The intensity pattern for a tetrahedral site, on the other hand, drops off too rapidly with displacement from the center, and in particular, predicts much too low intensities at displacements $\pm 3(A^{129}/2)$ and $\pm 4(A^{129}/2)$ to fit the observed spectrum. The octahedral site is, therefore, favored as the trapping site for photolytic H atoms. It is, of course, possible that trapping occurs in both sites with the spectrum of H atoms in tetrahedral sites, perhaps being responsible for the deviations between the experimental pattern and the theoretical pattern for an octahedral site. In this case, the observed symmetry of the low-field and high-field spectra would require that

TABLE III. Comparison of experiment with theory for assumed trapping sites.

Matrix		Substitutional site $\Delta A/A$(%)	Substitutional site Δg	Octahedral site $\Delta A/A$(%)	Octahedral site Δg
Argon	Experiment	−0.46	−0.00006	+1.15	−0.00065
	Theory	−0.72	−0.00003	+0.74	−0.00046
Krypton	Experiment	−0.59	−0.00047	+0.47	−0.0026
	Theory	−0.80	−0.00011	+0.36	−0.0021

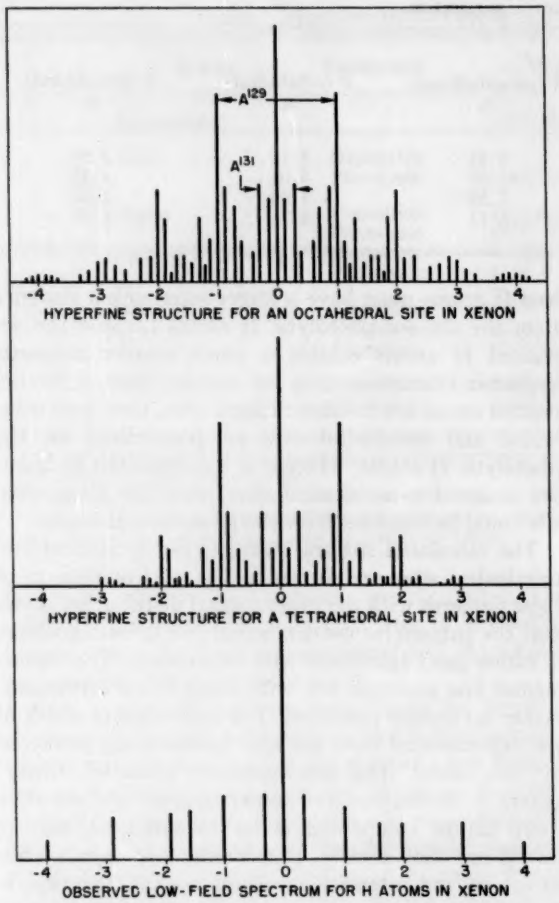
A129
A131
-4 -3 -2 -1 0 1 2 3 4
HYPERFINE STRUCTURE FOR AN OCTAHEDRAL SITE IN XENON
-4 -3 -2 -1 0 1 2 3 4
HYPERFINE STRUCTURE FOR A TETRAHEDRAL SITE IN XENON
-4 -3 -2 -1 0 1 2 3 4
OBSERVED LOW-FIELD SPECTRUM FOR H ATOMS IN XENON

FIG. 9. Spectral patterns for hyperfine splitting due to interactions with magnetic Xe nuclei in the matrix. Calculations for the octahedral and tetrahedral sites were made for natural abundances of the Xe isotopes. The hyperfine coupling constants for Xe^{129} and Xe^{131}, are designated by A^{129} and A^{131}. The experimental distribution is obtained from the data in Fig. 7 by setting $A^{129}=24.55$ oe.

the g factors for H atoms in the two sites be very nearly the same.

The hyperfine coupling constants that fit the octahedral site interpretation of the spectrum are $A^{129}=68.4$ Mc/sec and $A^{131}=20.2$ Mc/sec.

The doublet spectrum for deposited H atoms in xenon is attributed to H atoms trapped in substitutional sites. The lines are broadened by hyperfine interaction with magnetic Xe nuclei, but because the internuclear distance is considerably greater than for an octahedral trapping site the hyperfine splitting is much smaller.

D. H Atoms in Neon

The trapping situation in the case of neon is confused. Only a single doublet was observed, and only in the photolytic experiment. Thus, there is a single stable trapping site in neon, but the choice of site is not obvious. If neon followed the pattern set by the other rare gases, the substitutional site would be the most stable site and therefore would be the one occupied. The positive 0.46% shift in the hfs constant for an H atom in neon suggests that the H atom is in a cramped site. In a substitutional site in neon, however, an H atom has more space available than in any interstitial site in argon, krypton, or xenon. If the atoms in the matrix are represented by hard spheres, the sizes (radii) of the various trapping sites are: neon (subst.) $=2.91\ a_0$, neon (oct.) $=1.21\ a_0$, argon (oct.) $=1.47\ a_0$, krypton (oct.) $=1.57a_0$ and xenon (oct.) $=1.7\ a_0$. From this it would appear that the substitutional site might be too large to explain the hfs shift while the octahedral site would be too small. The assignment of the trapping site cannot be made solely on the experimental evidence.

The calculation of Adrian[7] on hfs shifts in neon furnishes additional information on the choice of trapping site. For the undistorted neon lattice the calculated hfs shift for the substitutional site is -0.09%, which is not in particularly good agreement with the experimental value $+0.43\%$. However, the alternative choice, the octahedral site would give a much too large positive shift. Since neon is more compressible than argon, krypton or xenon, the distortion of the lattice might be a more important factor than in the other cases. For a substitutional site, agreement between theory and experiment is obtained if the neon matrix atoms are drawn toward the H atom with the lattice parameter R changing from $5.81\ a_0$ to $5.33\ a_0$, a contraction of 8%. On the other hand, to fit the theory with an H atom in an octahedral site would require a lattice expansion with R (oct.) changing from $4.11\ a_0$ to $5.10\ a_0$, a 24% lattice distortion. The theoretical calculations, therefore, favor the substitional site as the trapping site for H atoms in neon.

The failure to observe resonances for deposited H atoms in neon is puzzling. There is no apparent reason for requiring that an H atom have excess energy to attain a substitutional site in a neon lattice. The difficulty has not been resolved. It may well be that under the conditions of our experiment condensation of H atoms on a neon surface is extremely inefficient.

IV. DISCUSSION

The spectrum for deposited H atoms was always included in the spectrum obtained by photolysis of HI in the solid. This is expected, since the photolytically generated H atoms are energetically capable of attaining any lattice site that would be accessible to deposited H atoms, which start essentially with room temperature thermal energy ($\sim$0.03 ev). In the case of neon, only a single doublet was observed in the photolysis experiment. This suggests that there is only one stable trapping site in neon, and furthermore, that if by some technique H atoms could be successfully deposited in neon, the spectrum would be identical with that obtained by photolysis.

Trapping of H atoms in a multiplicity of sites has been demonstrated for solid argon, krypton, and xenon.

Although the sites cannot be identified with certainty, the supposition that the deposited H atoms are stabilized in substitutional sites and the additional sites occupied by photolytic H atoms are octahedral (also, possibly, tetrahedral in the case of xenon) leads to good agreement between the experimental results and theoretical predictions. In the particular case of xenon, the splitting of the spectral lines is most readily interpreted as due to hyperfine interactions in a site with six nearest neighbors, i.e., an octahedral site.

The spectrum of H atoms in xenon is unusually interesting because both of the trapping sites have almost equal negative shifts in the hfs constant, in contrast to the cases of argon and krypton where one of the sites has a positive shift while the other has a negative shift. The $\Delta A/A$ *vs* R curve has essentially the shape of a Morse potential curve so that a given negative value of $\Delta A/A$ is satisfied by two values of the internuclear distance R. Thus, the observation of spectra with almost equal negative hfs shifts is not surprising, but the assigment of the trapping sites would, in general, be difficult. In the case of xenon, the matrix itself via magnetic hyperfine interactions serves to identify the sites. The differentiation between tetrahedral and octahedral sites is directly obtained from the spectral distribution in xenon without assistance from theoretical calculations on hfs matrix shifts.

The hyperfine interaction, which produces the splitting of the spectrum of H atoms in xenon, presumably arises from the overlap of the 1*s* H orbital with the 5*s* Xe orbitals, with the resultant admixture of a small amount of the Xe 5*s* orbital into the wave function of the unpaired electron. While the observed hyperfine splittings can be explained by this mechanism, there is the problem of explaining the apparent absence of an anisotropic hyperfine interaction due to expected admixture of the Xe 5*p* orbital which could have produced considerable line broadening. This is a problem which requires further study.

Trapping in a multiplicity of sites is clearly not restricted to H atoms. The phenonemon is probably quite general and may account for some of the discrepancies in the reported ESR spectra of free radicals. In the case of N atoms trapped in N_2, a triplet spectrum was observed,[9,10] as expected for an atom with nuclear spin $I=1$. In addition to the triplet, four satellite lines have been observed under various conditions,[1,9,11,12] although the triplet for N^{14} atoms can frequently be observed without any trace of the satellites.[10] The presence of the satellite lines has been explained[11] in terms of zero-field splitting of the $^4S_{\frac{3}{2}}$ state of nitrogen by an axially symmetric crystal field. The fact that the N atom spectrum sometimes has and at other times does not have satellites, indicates that the N atoms are in different crystalline environments. For more complicated radicals, the possibility of trapping in a multiplicity of sites is a potential source of error in the identifications of the radicals.

ACKNOWLEDGMENT

It is a pleasure to thank Dr. F. J. Adrian for undertaking a theoretical study of this problem and for many stimulating discussions during the course of this investigation.

[9] Cole, Harding, Pellam, and Yost, J. Chem. Phys. **27**, 593 (1957).
[10] Foner, Jen, Cochran, and Bowers, J. Chem. Phys. **28**, 51 (1958).
[11] T. Cole and H. M. McConnell, J. Chem. Phys. **29**, 451 (1958).
[12] Wall, Brown, and Florin, J. Chem. Phys. **30**, 602 (1959).

Matrix Effects on the Electron Spin Resonance Spectra of Trapped Hydrogen Atoms*

F. J. ADRIAN

Applied Physics Laboratory, The Johns Hopkins University, Silver Spring, Maryland

(Received September 8, 1959)

A study is made of the matrix effects on the electron spin resonance (ESR) spectra of hydrogen atoms stabilized in nonpolar matrices. It is assumed that the perturbing effect of the matrix consists of van der Waals interactions and the overlap or Pauli exclusion forces. These two effects are treated separately and the results added to get the net result. The van der Waals effect, which is treated by perturbation theory, leads to a reduction in the hfs splitting. The overlap effect, which is treated by requiring that the hydrogen atom wave function be orthogonal to the wave functions of the matrix particles, leads to an increase in the hfs splitting. In addition, the exclusion effect tends to introduce a small amount of the unpaired electron charge density onto the matrix particles. This can lead to a change in the electronic g factor, and also to hyperfine interactions with the nuclei of the matrix particles. The theory gives a good qualitative picture of the various matrix effects and their dependence on various properties of the matrix atoms and molecules.

I. INTRODUCTION

ELECTRON spin resonance (ESR) studies of atoms and free radicals trapped at low temperatures in various inert matrices show that the matrix fields perturb the trapped species.[1,2] In most cases studied to date the matrix perturbations have been quite small (weak matrix field), although easily discernable by the high resolution ESR experiments. In such cases, the trapped atom or radical is almost but not quite free, and the main features of the ESR spectrum pertain to the isolated radical, while the finer details are due to the interaction between the trapped radical and its environment.

Larger matrix effects are quite possible in matrices composed of polar molecules such as H_2O (strong matrix field), or in those cases where the ground state of the trapped paramagnetic species is degenerate, e.g., Cl and NO. Unfortunately, the experiments aimed at studying cases of this type have been rather unsuccessful,[1] most likely because the large matrix perturbations are sufficiently anisotropic to produce severe line broadening in a polycrystalline sample. It is quite likely that such experiments will have to be conducted in single crystal samples, a rather formidable complication. The strong matrix field case is probably best treated by some modification of crystal field theory. An example of this method is the work of Herzfeld[3] on the optical spectra of N atoms trapped in molecular nitrogen. However, because of the scarcity of ESR data on radicals trapped in polar matrices, we shall limit the present study to matrices such as molecular hydrogen and the monatomic gases where one can expect weak matrix fields.

The presence of an interaction between the trapped paramagnetic species and the matrix is quite expected. The matrix perturbation can, however, affect the ESR spectrum in a surprisingly large number of ways, and these various effects can combine to produce rather puzzling spectra. The following is a partial list of phenomena which can be caused by matrix effects[4]:

1. Shifts in the hyperfine structure (we abbreviate this term as hfs) splitting constants. These arise because the matrix perturbs slightly the unpaired electron density at the nuclei of the paramagnetic species. For H atoms trapped in H_2, and in various monatomic gases these shifts are roughly 0.5 to 1.0% of the free atom value. Both positive and negative shifts have been observed.[2]

2. Shift in the spectroscopic splitting factor or g factor g_J. This effect is due to the spin-orbit interaction of the unpaired electron in the field of the matrix particles.[2]

3. Multiple lines can arise if there are different trapping sites within a matrix which produce different shifts in the hfs constants, and/or in g_J.[2]

4. Hyperfine interactions with magnetic nuclei belonging to the matrix particles. Such interactions produce additional lines in the ESR spectrum.[2a]

In this paper we shall present a semiquantitative discussion of the above phenomena for the case of H atoms trapped in molecular hydrogen and in various monatomic gas matrices. Similar considerations will apply to more complicated radicals trapped in such matrices, although numerical estimates will be more difficult to obtain. This limitation is of secondary importance, since the present model is rather crude, even for the simplest case of trapped H atoms, and must be regarded as a qualitative rather than a quantitative theory. The goal of the present study is to show that interactions between the trapped H atom and the

* This work supported by the Bureau of Ordnance, Department of the Navy, under NOrd 7386.

[1] Jen, Foner, Cochran, and Bowers, Phys. Rev. **112**, 1169 (1958).

[2] (a) Foner, Cochran, Bowers, and Jen, J. Chem. Phys. **32**, 963 (1960); (b) Cochran, Bowers, Foner, and Jen, Phys. Rev. Letters **2**, 43 (1959).

[3] C. M. Herzfeld, Phys. Rev. **107**, 1239 (1957).

[4] An additional effect is the presence of satelite lines which occur when the electron spin transition is accompanied by a nuclear spin flip. This effect was first observed by Zeldes and Livingston, Phys. Rev. **96**, 1702 (1954), and the theory was developed by Trammell, Zeldes, and Livingston, *ibid.* **110**, 630 (1958).

matrix particles can account qualitatively for the observed matrix effects, and to relate the matrix effect to various properties of the matrix atoms or molecules.

The matrices studied here are composed of uncharged, spherically symmetric molecules and atoms. Thus, the only interactions which need be considered are the van der Waals interaction and the Pauli exclusion forces. The latter arise when the electron cloud of the H atom penetrates the closed shell of a matrix atom or molecule. The effect of these two different interactions will be treated separately and the results added to get the net effect. It will be shown that the van der Waals interaction tends to reduce the hfs splitting of the trapped H atom. The Pauli exclusion forces, on the other hand, will tend to increase the hfs splitting. Thus, there is a competition between these two effects, the former predominating in sites where the H atom is relatively far from the nearest neighbor matrix particles, and the latter predominating in relatively cramped sites. It will also be shown that the Pauli exclusion effect tends to introduce a small amount of the charge density of the unpaired electron onto the matrix particles. This results in a spin-orbit interaction of the unpaired electron in the field of the matrix particles which produces a slight shift in the g factor g_l. This effect can also lead to a hyperfine interaction with the nuclei of the matrix particles.

II. GENERAL THEORY

A. Nature of the Trapping Sites

The present background of experimental and theoretical work on trapped H atoms gives us a fairly good qualitative picture of the trapping sites. It appears that the hydrogen atoms can be trapped at both substitutional and interstitial sites in the rare gas matrices. In the preceding paper,[2a] it is shown that a comparison of the experimental results with the theoretical estimates presented here substantiates this view, and that it is usually possible to distinguish between substitutionally and interstially trapped atoms. It is very unlikely that any of the observed H atom ESR lines come from atoms trapped at surface sites, because of the relative scarcity of such sites, and also because the unsymmetrical matrix fields experienced by such atoms would broaden their ESR lines considerably.

On the other hand, there is likely to be a considerable amount of lattice distortion in the vicinity of a trapped atom, since it is generally true for the matrices considered here that the H atom is too small to fill the available volume in a substitutional site, and too large to fit exactly into an interstitial site. A theoretical investigation of the lattice distortion problem would require the solution of a rather complicated problem in lattice dynamics. Unfortunately, it is not possible to estimate the lattice distortion by comparison of the experimental results with the theoretical predictions, since the present theory is not accurate enough for this exacting task.

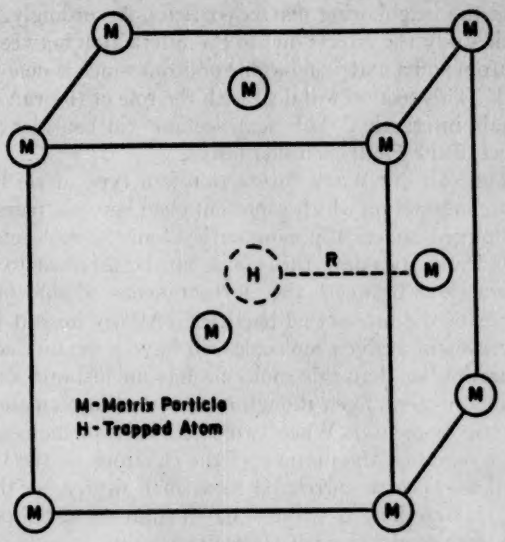

FIG. 1. A H atom trapped interstially at a body center point in a face centered cubic lattice of matrix particles. M denotes a matrix particle, and H denotes the trapped atom.

The present study is based on a rather general model for a trapping site in which the trapped H atom is surrounded more or less symmetrically by N nearest neighbor matrix particles. Since the matrix interactions dealt with here are of relatively short range it can be assumed that the nearest neighbor particles provide the chief contributions to the various matrix effects. It can also be assumed that all the nearest neighbor matrix particles are at the same distance from the trapped atom, (this distance we call R). One possible trapping site is illustrated in Fig. 1.

Since the nearest neighbor matrix particles will be arranged symetrically around the trapped atom there will be no anisotropic matrix effects (i.e., effects depending on magnetic field orientation). Moreover, for the weak interactions dealt with here it can be assumed that the trapped H atom interacts independently with each of the neighboring matrix particles. Thus, one adds the separate contributions of the nearest neighbors to obtain the net perturbation (i.e., the magnitude of a given matrix effect is proportional to N), which quantity may vary from roughly 4 to 12.

It will be seen that the calculated matrix effects are quite sensitive to the distance R between the trapped atom and its nearest neighbor matrix particles. Thus, it will be possible to estimate R from the observed matrix effects, and then to ask whether the values of R are reasonable from energy considerations.

B. van der Waals Interaction

As discussed in the previous section, one can find the net matrix perturbation of the trapped atom by calculating the effect due to the interaction between the H atom and a given matrix particle, and then summing

over the neighboring matrix particles. Accordingly, we shall study the effects due to the interaction between a H atom and a matrix molecule or atom which is denoted as M. This section will deal with the role of the van der Waals interaction. The next section will consider the effect of the Pauli exclusion forces.

The van der Waals interaction is a type of electrostatic interaction which is present even between pairs of uncharged spherically symmetric atoms or molecules.[5] Classically speaking, this effect can be ascribed to an interaction between the instantaneous dipole moments of the interacting particles. (At any instant the electrons in a given molecule will have a definite configuration so that this molecule has an instantaneous dipole moment, even though it possesses no permanent electric moments). When two such atoms or molecules come together, the motions of the electrons on the two particles become correlated to a small degree, so that the interaction between the instantaneous dipole moments produces a net attractive energy.

Of course the van der Waals interaction also perturbs the wave functions of the interacting species. The present calculations indicate that the Van der Waals interaction causes a slight expansion in the electronic charge clouds of the interacting atoms or molecules, i.e., the mean atomic or molecular radius is increased slightly. Such an expansion of the electronic charge cloud of the H atom will tend to reduce the charge density at the proton, thereby decreasing the hyperfine interaction between the electron and the nucleus. This result is physically reasonable since the expansion of the electronic charge cloud around an atom or molecule increases the magnitude of its instantaneous dipole moment, which in turn increases the van der Waals interaction energy. The expansion of the electron charge distribution by the van der Waals interaction is naturally very small, because it is opposed by the much stronger binding between the electrons and the nuclei of the parent molecule.

In the formal development of the theory the important changes in the electronic charge distribution of the H atom will correspond to second order terms in the van der Waals perturbed wave function. (First order changes in the wave function are also present, but they do not change the hyperfine interaction energy). That is, the change in the hyperfine interaction energy will appear in third order energy terms due to the perturbation,

$$\mathcal{H}=\mathcal{H}_V+\mathcal{H}_{hfs}, \tag{1}$$

where $\mathcal{H}_V$ describes the electrostatic interaction between the H atom and the matrix molecule or atom, and $\mathcal{H}_{hfs}$ describes the hyperfine interaction between the unpaired electron and the proton. The zero order problem is, naturally, described by the Hamiltonian

$$\mathcal{H}_0=\mathcal{H}_H+\mathcal{H}_M, \tag{2}$$

where $\mathcal{H}_H$ is the Hamiltonian for an isolated H atom and $\mathcal{H}_M$ is the corresponding quantity for the isolated matrix particle M. The solutions of the zero order problem are of the form

$$\psi_{ij}=h_i m_j, \tag{3}$$

where h_i denotes the ith state of H, and m_j denotes the jth state of M.

As discussed previously, the trapped atom is surrounded in a symmetrical fashion by the matrix particles, and, consequently, anisotropic matrix effects do not appear. Thus, we need consider only the isotropic hfs interaction[6]

$$\mathcal{H}_{hfs}=(8\pi/3)g_J\beta(\mu_H/I_H)\delta(\mathbf{r}_H)\mathbf{I}_H\cdot\mathbf{S}. \tag{4}$$

Here, μ_H and I_H are, respectively, the magnetic moment and spin of the proton, $\mathbf{r}_H$ is the position vector of the electron of the H atom measured with the proton as the origin, and β is the Bohr magneton. The H atom hfs splitting is thus determined by the unpaired electron density at the proton, which quantity we denote as $|h(H)|^2$. For simplicity, a number of subsequent formulas and results will be given in terms of this quantity.

So long as the charge clouds of the interacting particles do not overlap, the interaction energy consists of interactions between various instantaneous multipole moments. That is, $\mathcal{H}_V$ has the familiar form,[7]

$$\mathcal{H}_V=(e^2/R^3)\sum_\mu(2z_H z_\mu-x_H x_\mu-y_H y_\mu)$$
$$+\text{terms in } (1/R^4),\ (1/R^5),\ \text{etc.}, \tag{5}$$

where the first term is the dipole-dipole interaction, the next term is the dipole-quadrupole interaction, etc. Here, R is the separation between the interacting particles, z_H, x_H, and y_H are the coordinates of the hydrogenic electron measured from the proton, and z_μ, x_μ, and y_μ are the coordinates of the μth electron of M measured from the centroid of the charge distribution of M.

Since the interaction between the particles involves only nonzero order multipole moments, one has the following selection rule governing the matrix elements of $\mathcal{H}_V$

$$(h_0 m_0\,|\,\mathcal{H}_V\,|\,h_i m_j)=0 \quad \text{if } h_i \text{ is an } s \text{ state}. \tag{6}$$

An equivalent statement of the above rule is that there are no spherical harmonics of zero order in the expansion of $\mathcal{H}_V$ which can connect the ground s state of the $\mathcal{H}$ atom to an excited s state. The above selection rule,

[5] For a discussion of these interactions see Hirschfelder, Curtiss, and Bird, *Molecular Theory of Gases and Liquids* (John Wiley & Sons, Inc., New York, 1954), p. 955.

[6] A. Abragam and M. H. L. Pryce, Proc. Roy. Soc. (London) **A205**, 135 (1951).

[7] See reference 5, p. 923.

coupled with the selection rule,

$$(h_0m_0 \mid 3\mathcal{C}_{hfs} \mid h_im_0)=0 \quad \text{if } h_i \text{ is not an } s \text{ state}, \qquad (7)$$

simplifies considerably the application of the perturbation theory.

We wish to find those terms in the energy due to the perturbation $3\mathcal{C}$ which are linear in $3\mathcal{C}_{hfs}$. The first order term is just the hfs splitting of the isolated H atom. It can be shown by using the selection rules (6) and (7) that there is no second order energy term which is linear in $3\mathcal{C}_{hfs}$. The third order term in the perturbation energy is,[8]

$$W_3=\sum_{i,j}{}' \sum_{k,l}{}' \frac{(00 \mid 3\mathcal{C} \mid ij)(ij \mid 3\mathcal{C} \mid kl)(kl \mid 3\mathcal{C} \mid 00)}{(E_{00}-E_{ij})(E_{00}-E_{kl})}$$

$$-(00 \mid 3\mathcal{C} \mid 00)\sum_{kl}{}' \frac{(00 \mid 3\mathcal{C} \mid kl)(kl \mid 3\mathcal{C} \mid 00)}{(E_{00}-E_{kl})^2}. \qquad (8)$$

Here, the symbol $(ij \mid 3\mathcal{C} \mid kl)$, is an abbreviation for the quantity $(h_im_j \mid 3\mathcal{C} \mid h_km_l)$. The prime on the summation signs indicates that the ground state h_0m_0 is omitted from the summation. If we select out of W_3, those terms which are linear in $3\mathcal{C}_{hfs}$, and use the selection rules (6) and (7), we get the following expression for the change produced by the van der Waals interaction in the hfs energy:

ΔE_{hfs}

$$=2\sum_{i}{}' \sum_{kl}{}' \frac{(00 \mid 3\mathcal{C}_{hfs} \mid i0)(i0 \mid 3\mathcal{C}_V \mid kl)(kl \mid 3\mathcal{C}_V \mid 00)}{(E_{00}-E_{i0})(E_{00}-E_{kl})}$$

$$-(00 \mid 3\mathcal{C}_{hfs} \mid 00)\sum_{kl}{}' \frac{(00 \mid 3\mathcal{C}_V \mid kl)(kl \mid 3\mathcal{C}_V \mid 00)}{(E_{00}-E_{kl})^2}. \qquad (9)$$

The foregoing expression for ΔE_{hfs} can be greatly simplified by replacing the energy differences between the ground state and the various excited states by appropriate average excitation energies. We shall denote the average energy for the excited states of the H atom by E_H, and the corresponding quantity for the matrix molecule or atom by E_M. We shall determine the average excitation energies by taking the average of the energy of the first excited state and of the ionization energy. This approximation allows us to use matrix multiplication methods to eliminate the sums over the various excited states. These procedures, which are described in detail in the Appendix, give the following result for the change in the unpaired electron density at the proton:

$$\Delta \mid h(H)\mid^2=-\mid h_0(H)\mid^2\{(2/E_H)+[1/(E_H+E_M)]\}E_V. \qquad (10)$$

Here, $\mid h_0(H)\mid^2$ is the unpaired electron density at the proton in the isolated hydrogen atom, and E_V is the van der Waals interaction energy. It is to be noted that E_V will be negative (since the van der Waals forces are attractive), and E_H and E_M are negative quantities, so that [(10)] predicts that the van der Waals interaction will reduce the hfs splitting.

The van der Waals interaction energy can be estimated using the polarizabilities of the interacting particles. This well-known expression for E_V is[9]

$$E_V=-c_1/R^6-c_2/R^8-\cdots \qquad (11)$$

where

$$c_1=\tfrac{3}{2}[E_HE_M/(E_H+E_M)]\alpha_H\alpha_M; \qquad (12)$$

$$c_2=\tfrac{45}{8}\frac{E_HE_M\alpha_H\alpha_M}{e^2}\left[\frac{\alpha_HE_H}{2E_H+E_M}+\frac{\alpha_ME_M}{E_H+2E_M}\right]. \qquad (13)$$

The quantities α_H and α_M are the polarizabilities of the H atom and matrix particle, respectively.

At the distances which will be encountered in the present study, the second term in (11) cannot be neglected. The inclusion of this term can be troublesome, however, for at sufficiently small values of R it becomes larger than the first term and produces an unrealistic behavior in the variation of $\mid h(H) \mid^2$ with separation. (Presumably the third term in (11) would produce similar difficulties at even smaller values of R.) For example, in the results for H atoms in argon, cf. Fig. 4, there is an incipient decrease in slope at the smallest values of R which is due to this effect. This anamolous behavior is due to the fact that the above equation for E_V becomes incorrect as the charge clouds of the interacting particles begin to overlap. (It will be remembered that Eq. (5) for $3\mathcal{C}_V$, from which Eq. (11) was derived, is correct only when there is no overlapping of the charge clouds.) Brooks[10] has analyzed this problem for the van der Waals interaction between two He atoms, and has shown that the quantities c_1, c_2, etc., are actually functions of R which decrease to zero as the interacting charge clouds begin to overlap. Moreover, the higher coefficients fall off more rapidly with decreasing R. Accordingly, at small values of R it will be necessary to take this effect into account. This was not required for the present calculation, where the lowest values of R considered appeared to be just short of the point where this difficulty became acute.

C. Pauli Exclusion Forces

The Pauli exclusion or exchange forces arise when the separation between the trapped H atom and the nearest neighbor matrix particles becomes sufficiently short so that the electron charge cloud of the H atom overlaps the electron charge clouds of the matrix particles. The penetration of the closed shell matrix atoms and molecules by the unpaired electron of the H atom violates the exclusion principle, and the consequence is a repulsive interaction energy between the particles involved. This interaction can change both the H atom wave function, and the wave functions of

[8] K. F. Niessen, Phys. Rev. 34, 253 (1929).

[9] Reference 5, p. 964.

[10] F. C. Brooks, Phys. Rev. 86, 92 (1952).

FIG. 2. A H atom and a He atom with interpenetrating charge clouds. The exclusion principle is violated in the region of overlap.

the matrix particles, with a number of corresponding changes in the ESR spectrum of the system.

We shall illustrate the general features of the problem by considering the interaction between a H atom and a He atom, as depicted in Fig. 2. To the extent that the charge clouds of the two atoms overlap, there is a violation of the exclusion principle which requires alteration of the orbitals of the electrons involved. It is likely that this alteration can be qualitatively described as a shrinking of both the H orbital and the He orbital having the same spin as the H electron, since this will reduce the forbidden overlap between the two orbitals. It will be seen presently that this prediction is upheld by the actual calculation. This shrinkage of the orbitals has the following effects:

1. The contraction of the H orbital will increase the unpaired electron charge density at the proton, thus increasing the observed hfs splitting.

2. Only that He orbital having the same spin as the hydrogenic electron is contracted by the exclusion effect. Thus, the magnetic interaction of the two helium electrons with the helium nucleus no longer completely cancels. In this way the exclusion forces can lead to isotropic magnetic hyperfine interactions with the nuclei of neighboring matrix particles.

3. For more complex matrix atoms and molecules, such as the monatomic gases neon, argon, etc., which have outer shell p electrons, the considerations just described can also lead to an unbalancing of the spins of these electrons. This can lead to several effects, one of which is a magnetic hyperfine interaction between the unbalanced p electrons and the nuclei of the matrix particle. This magnetic hyperfine interaction will be anisotropic, i.e., it will depend on the angle between the p orbitals involved and the external magnetic field. In polycrystalline media such an effect will lead to line broadening.

4. The spin-orbit interaction involving the unbalanced p electrons can lead to a shift in the g factor g_J. As shown for the case of the F center[11] this spin-orbit interaction is quenched in first order, so that the shifts in g_J are relatively small second order effects.

This problem has already been studied for the case of color centers in alkali halides, particularly the F center. It was found that the effect of the exchange or exclusion forces on the unpaired electron charge density could be fairly well accounted for by requiring that the total electronic wave function of the system be a properly antisymmetrized (i.e., determinantal) product of one-electron wave functions of all the electrons in the system.[12] It was further shown that this many-electron formalism was equivalent to using a one-electron orbital for the unpaired electron, which had been orthogonalized by the Schmidt process to all the other one-electron orbitals of the system. These arguments, although derived for the case of the F center, are quite general, and can be applied to the present problem. The method does, however, entail certain approximations, which will be discussed presently in some detail, and whose validity must be considered separately for different systems. For the case of a hydrogen atom stabilized in an inert matrix, the properly orthogonalized wave function is

$$h=[h_0-\sum_i(h_0\,|\,\psi_i)\psi_i]/[1-\sum_i(h_0\,|\,\psi_i)^2]^{\frac{1}{2}}, \qquad (14)$$

where the sum is taken over all the one-electron orbitals ψ_i of the neighboring matrix particles.

We shall illustrate this method by using it to calculate the unpaired electron density at the proton for the case of a H atom interacting with a He atom. The approximations involved can also be clearly described, although not avoided, for this relatively simple system. This is a three-electron system, and the exclusion principle is satisfied by using the antisymmetrized wave function

$$\Psi=[1-(h_0\,|\,he)^2]^{-\frac{1}{2}}(3!)^{-\frac{1}{2}}\det|\,h_0\uparrow(1)he\uparrow(2)he\downarrow(3)|. \qquad (15)$$

Here, he is a helium $1s$ electron, the arrows denote the electron spin orientation, and $(h_0\,|\,he)$ is the overlap integral between the H and He orbitals. The unpaired electron density at the proton is given by the expression,

$$|\,h(\mathrm{H})\,|^2 = (1/S_z)\langle\Psi\,|\,\delta(\mathbf{r}_1)S_{z1}+\delta(\mathbf{r}_2)S_{z2}+\delta(\mathbf{r}_3)S_{z3}\,|\,\Psi\rangle, \qquad (16)$$

where $\mathbf{r}_1$, $\mathbf{r}_2$ and $\mathbf{r}_3$, are the position vectors (measured from the proton as the origin) of the three electrons, S_{z1}, S_{z2}, and S_{z3} are the spin projection operators for the three electrons, and S_z is the net spin projection operator. It is easily shown that the above formalism leads to the following result for $|\,h(\mathrm{H})\,|^2$,

$$|\,h(\mathrm{H})|^2=\frac{|\,h_0(\mathrm{H})-(h_0\,|\,he)he(\mathrm{H})\,|^2}{1-(h_0\,|\,he)^2}. \qquad (17)$$

Clearly the same result would be obtained by using an orthogonalized wave function for the unpaired electron.

On the other hand, the above method of estimating the effect of the Pauli exclusion forces is incomplete. It recognizes the exclusion principle by using a properly antisymmetrized wave function, but it does not allow for the fact that the exclusion forces may cause the one-electron orbitals to differ somewhat from the free

[11] F. J. Adrian, Phys. Rev. **107**, 488 (1957).

[12] B. S. Gourary and F. J. Adrian, Phys. Rev. **105**, 1180 (1956).

atom orbitals. To take proper account of this aspect of the problem it would be necessary to take suitable trial functions for the orbitals h_0 and he, which orbitals would be determined by minimizing the energy of the system. It should also be recognized that the He electron with the same spin as the H electron has a somewhat different interaction with the H electron from that of the other He electron. Consequently, the spatial part of two functions $he\uparrow$ and $he\downarrow$ may be slightly different. This last point is the phenomenon of exchange polarization, which has been discussed by several authors in connection with somewhat different problems.[13] Unfortunately, the energy calculations required to treat this aspect of the problem are quite difficult, and they would greatly reduce the simplicity and generality of the method. It appears from the results obtained for the F center and the results of the present study that one can neglect these effects and still obtain a good semi-quantitative picture of the various effects due to interactions between a paramagnetic species and its environment. On the other hand, effects which cannot be explained by the present simplified theory may be clarified by making the indicated improvements in the theory. It appears that a few points of gross disagreement between theory and experiment already exist, and their number will likely increase as additional experiments are made.

Numerical calculation of the exclusion effect using (17) indicates that at the separations of importance in this problem ($4<R<8a_0$) the normalization factor of the orthogonalized wave function accounts for the major part of the change in the unpaired electron density at the proton. This result is also true for more complicated matrix particles, so that the orthogonalized H atom wave function (14) leads to the following simplified formula for the effect of the exclusion forces on the unpaired electron density at the proton

$$|h(\mathrm{H})|^2 \cong |h_0(\mathrm{H})|^2(1+S^2). \tag{18}$$

Here S^2 is the sum of the squares of the overlap integrals of the H orbital with the one-electron orbitals of the matrix particles

$$S^2=\sum_i (h_0 \mid \psi_i)^2. \tag{19}$$

Clearly the exclusion forces act to increase the charge density at the proton.

The effect of exchange interactions in producing small shifts in the g factor g_J has been investigated for the case of the F center,[11] using the requirement that the wave function for the unpaired electron be orthogonal to the electron orbitals of the surrounding particles. The arguments used for the F center can be applied directly to the present problem. The basic point is that the orthogonality requirement admixes small components of the p orbitals of the matrix particles into the wave function of the unpaired electron. To the extent that the unpaired electron moves in these p orbitals, it experiences a strong spin-orbit interaction and a consequent shift in its electronic g factor.

The actual calculation of Δg is carried out by treating the spin-orbit interaction due to each matrix atom or molecule separately, expanding about the particle in question. It is essential that one start with a Hamiltonian which is gauge invariant, since otherwise the transformation of the origin from the proton to the matrix particle will introduce spurious terms. This requirement is met by starting with a Hamiltonian which is derived by a suitable reduction of the Dirac equation.[11] After the expansion has been performed, the perturbing Hamiltonian associated with particle α has the form

$$\mathcal{H}_\alpha' = -(e\hbar/2mc)\mathbf{H}\cdot\mathbf{L}+(e\hbar^2/2m^2c^2)r^{-1}(dU_\alpha/dr)\mathbf{L}\cdot\mathbf{S}. \tag{20}$$

The second term in the preceding expression is the spin-orbit interaction due to matrix particle α, U_α being the potential energy of the unpaired electron in the field of this particle.

The unsymmetrical fields due to the interaction between the trapped species and the matrix particle quenches the orbital angular momentum $\mathbf{L}$, i.e., $\mathcal{H}_\alpha'$ vanishes in first order. The contribution of particle α to the g factor shift, denoted by Δg_α, is given by that part of the second order energy which is linear in H and M_S. In order to sum the resulting expression for Δg_α over the various excited states of the trapped H atom, the average excitation energy E_H is introduced. This leads to the following expression for Δg_α

$$\Delta g_\alpha = (e\hbar^2/m^2c^2E_\mathrm{H})(h \mid r^{-1}(dU_\alpha/dr)L_z^2 \mid h). \tag{21}$$

Here the z axis is in the direction of the applied magnetic field, and h is the orthogonalized wave function (14). The major contributions to Δg_α will come from the p orbitals of α which are admixed into the hydrogen atom wave function by the orthogonalization process. Thus, we can rewrite (21) in the following convenient form,

$$\Delta g_\alpha = (4/3E_\mathrm{H})(h \mid \psi_{\alpha p\sigma})^2\lambda_{\alpha p\sigma}(\psi_{\alpha p\sigma} \mid L_z^2 \mid \psi_{\alpha p\sigma}). \tag{22}$$

Here, $\psi_{\alpha p\sigma}$ is the outermost $p\sigma$ orbital of matrix particle α, the notation $p\sigma$ denoting that p orbital, which is directed along the line joining the matrix particle and the H atom. The quantity $\lambda_{\alpha p\sigma}$, is the spin-orbit splitting constant for this p orbital.[14] It can be deter-

[13] Abragam, Horowitz and Pryce, Proc. Roy. Soc. (London) **A230**, 169 (1955); J. H. Wood and G. W. Pratt, Jr., Phys. Rev. **107**, 995 (1957); and V. Heine, *ibid.* **107**, 1002 (1957).

[14] In deriving the above formula we have used the equation,

$$\lambda_{\alpha p\sigma} = 3(\beta^2/e)\langle\psi_{\alpha p\sigma} \mid r^{-1}(dU_\alpha/dr) \mid \psi_{\alpha p\sigma}\rangle,$$

cf R. G. Barnes and W. V. Smith, Phys. Rev. **93**, 96 (1954). The sign has been changed in this relation, because we shall use experimental data for atoms which have a missing p electron or hole in an otherwise closed shell, whereas the original formula was given for a single p electron outside a closed shell.

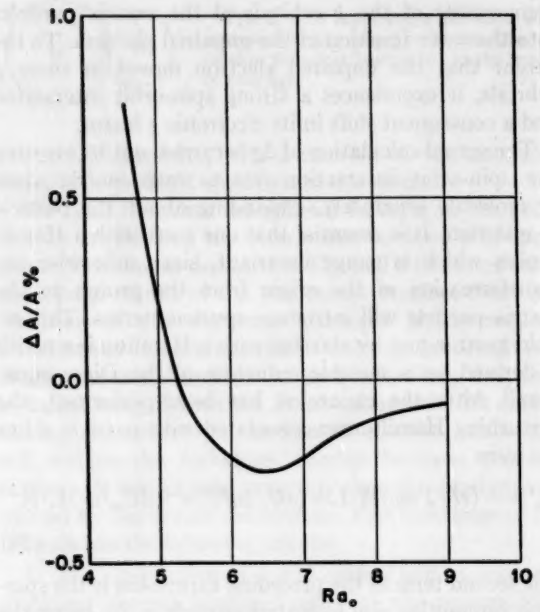

FIG. 3. The effect of a molecular H matrix on the hfs splitting of a trapped H atom. Results were calculated for six neighboring matrix particles a distance R from the trapped atom.

mined from experimental results on highly similar atoms or ions (e.g., for argon the data on Cl are used and Br provides the necessary results for Kr).

For a trapped H atom isotropically surrounded by matrix particles, the g-factor shift will also be isotropic. In this case the sum over the N nearest neighbor matrix particles is readily performed and yields the result

$$\Delta g = (8N/9E_{\mathrm{H}})\,(h\,|\,\psi_{p\sigma})^2\lambda_{p\sigma}. \qquad (23)$$

As defined, E_{H} is negative, and the spin-orbit splitting constant $\lambda_{p\sigma}$ is positive so that the net g factor shift will be negative.

RESULTS AND DISCUSSION

For the sake of clarity and conciseness, the results presented here have been calculated for the specific case of a H atom interacting with six nearest neighbor matrix particles, which particles are arranged with cubic symmetry about the trapped atom. As illustrated in Fig. 1, this model might correspond to a H atom trapped interstially at the body-center point of a face-centered cubic lattice of matrix particles. The choice of a specific model, however, will in no way affect the general features of the results. Moreover, all the results presented here are proportional to the number of nearest neighbor matrix particles, so that these results may be readily extended to other types of sites with different numbers of neighboring particles. In the preceding paper a more direct comparison is made between the experimental results and the theoretical predictions.[2a] It is shown that one can usually distinguish between substitutionally and interstially trapped atoms on the basis of their ESR spectra.

A. Molecular Hydrogen Matrix

The effect of the van der Waals interaction on the hfs splitting of the H atom was calculated from (11). The effective excitation energy of the H molecule was taken to be the sum of the excitation energy of the H atom and the binding energy of the molecule. The polarizability of the H molecule was determined by taking the average of the two experimental polarizabilities corresponding to an electric field parallel to and perpendicular to the bond axis.[15]

The effect of the Pauli exclusion forces on the H atom hfs splitting was estimated from Eq. (18). The one-electron orbitals for the H molecule were approximated by the molecular orbital $(\psi_a+\psi_b)/(2+2S_{ab})^{\frac{1}{2}}$, where ψ_a and ψ_b are atomic orbitals for the two bonded H atoms. These atomic orbitals are hydrogenlike $1s$ orbitals, but, following the work of Wang[16] on valence-bond wave functions employing orbitals of this type,

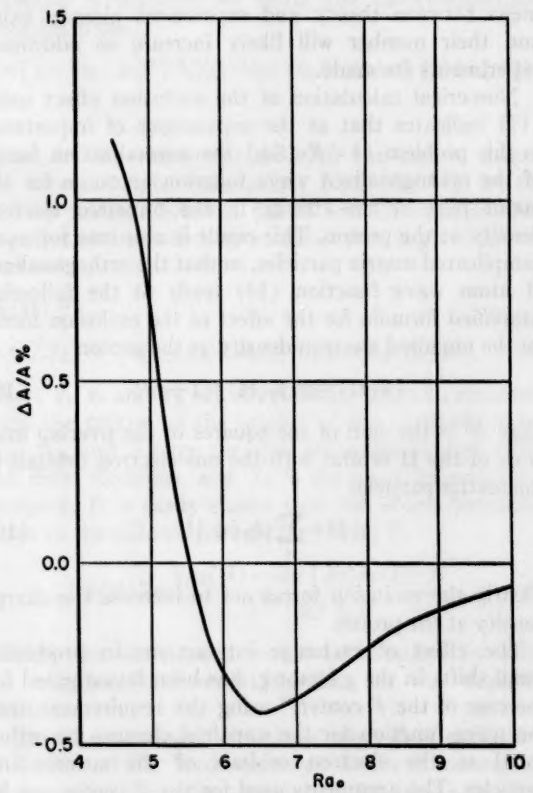

FIG. 4. The effect of an argon matrix on the hfs splitting of a trapped H atom. Results were calculated for six neighboring matrix particles a distance R from the trapped atom.

[15] Reference 5, p. 950.
[16] S. Wang, Phys. Rev. **31**, 579 (1928).

their effective charge is taken to be 1.188 instead of the free atom value of unity.

The percentage change in the hfs splitting of the H atom, which is denoted as $\Delta A/A$, is plotted *vs* nearest neighbor distance R in Fig. 3. The experimental value[1] of (-0.23%) for the change in the hfs splitting corresponds to a value of R between 6.0 and 7.0 a_0. This value of R is in agreement with an estimate based on the expected line broadening caused by hyperfine interactions with the nuclei of the surrounding H molecules. If R were appreciably less than 5.5 a_0, these hyperfine interactions would yield broader lines than are actually observed.

Since there is no appreciable spin-orbit coupling for an electron associated with either a H atom or a H molecule, we do not expect any shift in the electronic g factor due to the molecular H matrix. The experimental result[1] $[g_J=2.00230(8)]$ confirms this prediction.

B. Argon Matrix

The nature of the H atom ESR spectrum in noble gas matrices depends on whether the trapped atoms were produced by an electrical discharge in H gas and then codeposited with the matrix gas (deposition experiment),[1] or produced by photolysis of hydrogen iodide which had been codeposited with the matrix gas (photolysis experiment).[2] So far the multiple trapping sites have been observed only in the photolysis experiment. The results of the various experiments are listed in Table I of the preceding article.[2a]

The experimental results show that H atoms can be stabilized in three different sites in an argon matrix with correspondingly different hfs splittings and electronic g factors. Moreover, as the temperature of the matrix is raised from 4°K, the lines corresponding to the different sites vanish at different temperatures,[2] indicating different degrees of stability for the various sites.

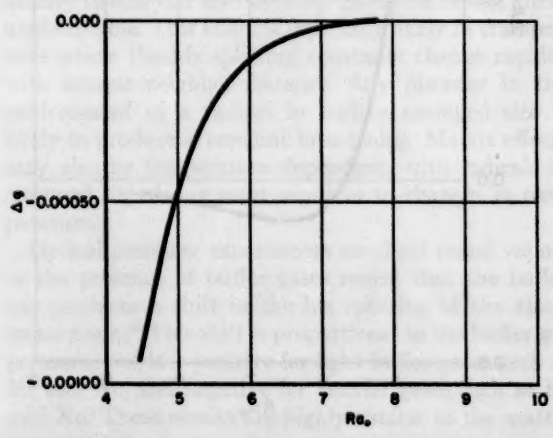

FIG. 5. The effect of an argon matrix on the g factor of a trapped H atom. Results were calculated for six neighboring matrix particles a distance R from the trapped atom.

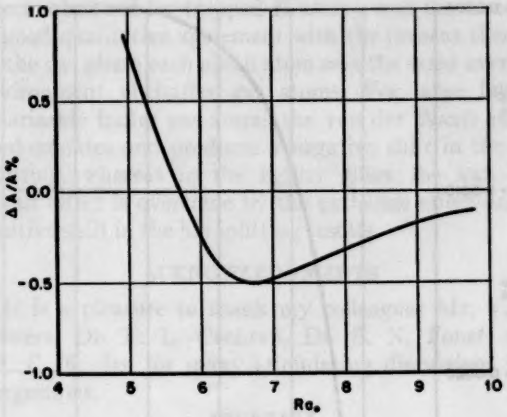

FIG. 6. The effect of a Kr matrix on the hfs splitting of a trapped H atom. Results were calculated for six neighboring matrix particles a distance R from the trapped atom.

The theoretical results are given in Fig. 4.[17] The observed sites, correspond to reasonable values of R. It is also noteworthy that the positive shift, which corresponds to the smallest value of R, is associated with the site of lowest thermal stability. This is quite reasonable since the sites having relatively small separations between the trapped atom and the nearest neighbor matrix atoms are likely to be under considerable strain.

The theoretical results for the g-factor shift Δg are plotted against nearest neighbor distance in Fig. 5. The results are in qualitative agreement with experiment. Since the exclusion effect, which is solely responsible for Δg, also produces the positive shift in the hfs splitting, one would expect only that site having the positive shift in the hfs splitting to have an appreciable g-factor shift. This is actually the case since Δg is negligible except at the smaller values of R where the shift in the hfs splitting is positive. For $\Delta A/A=1.15\%$, $R=4.5a_0$ and this gives $\Delta g=-0.00089$ as compared with the experimental value of -0.00065. The predicted g-factor shift for the other sites is much smaller, in agreement with experiment.

C. Krypton Matrix

The experimental results[2a] indicate that there are two possible lattice sites in the krypton matrix. The theoretical results for the hfs splitting and g-factor shift are given in Figs. 6 and 7, respectively.[18] The normal site, which is the site observed in both photolysis and deposition experiments, has an experimental hfs shift of -0.59%, which corresponds to a separation of 6.5 to 7.0 a_0. The theoretical g-factor shift is small (~-0.00047) for these separations, in agreement with the experimental result. The other line has an experi-

[17] The SCF argon orbitals of D. R. Hartree and W. Hartree, Proc. Roy. Soc. (London) **166**, 450 (1938) were used in this calculation.

[18] The SCF krypton orbitals of B. H. Worsley, Proc. Roy. Soc. (London) **247**, 390 (1958) were used in this calculation.

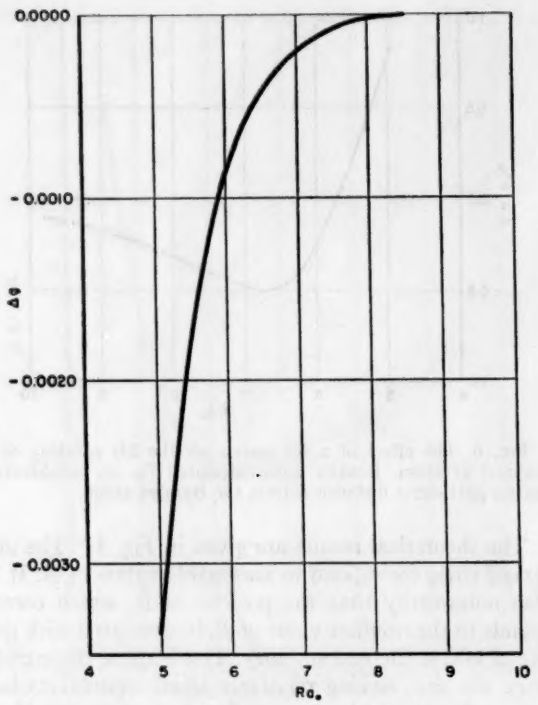

FIG. 7. The effect of a Kr matrix on the g factor of a trapped H atom. Results were calculated for six neighboring matrix particles a distance R from the trapped atom.

mental hfs shift of 0.47%, which corresponds to $R=5.25\ a_0$. This gives a theoretical value of -0.0024 for Δg, which is comparable with the experimental result of -0.0026.

D. Neon Matrix

Only a single site has been observed for H atoms trapped in neon, and that for the photolysis experiment only.[2a] Attempts to deposit H atoms from a discharge into a neon matrix have been unsuccessful. The observed shift in the hfs splitting is 0.43%. The theoretical results for the shift in the hfs splitting are given in Fig. 8.[19] As shown in the preceding article,[2a] a comparison of the experimental results and the theoretical predictions indicates that the H atoms are trapped substitutionally. In most cases substitutional trapping leads to negative shifts in the hfs splitting. The polarizability of neon is so low, however, that the van der Waals effect is overcome by the exchange effect at relatively large separations in this matrix.

E. Xenon Matrix

The spectrum of H atoms produced by photolysis of HI in xenon is very complicated, and has not been completely analyzed.[2a] There are definitely two and possibly three sites for the trapped atoms. At least one site has a multiple line spectrum due to hyperfine interactions between the unpaired electron and the Xe nuclei. The order of magnitude of the observed Xe hyperfine splittings is in agreement with theoretical estimates based on the orthogonalized wave function (14). There is, however, the following serious difficulty. The orthogonality requirement admixes into the unpaired electron wave function small amounts of the Xe5s orbital with the same spin, which orbital can yield the observed isotropic hyperfine interaction. But the orthogonality requirement also admixes slightly larger amounts of the Xe5p orbital into the unpaired electron wave function. The presence of this 5p orbital will yield an anisotropic hyperfine interaction with the Xe nuclei, which, in the polycrystalline samples studied, should have broadened the Xe hyperfine lines considerably more than was observed. It may be, as discussed in Sec. IIC, that the exchange interaction between the unpaired electron and the Xe5p orbitals are not adequately treated by the simple orthogonalization procedure. This problem will require further theoretical study and a more detailed analysis of the observed spectrum.

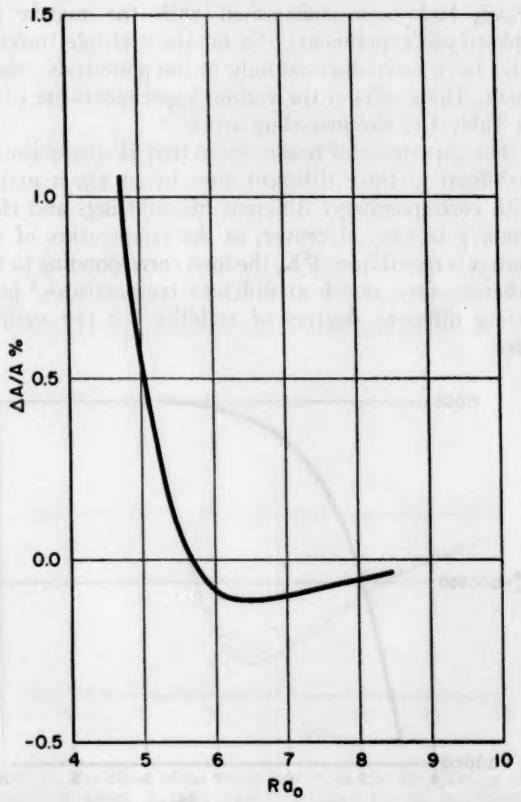

FIG. 8. The effect of a neon matrix on the hfs splitting of a trapped H atom. Results were calculated for six neighboring matrix particles a distance R from the trapped atom.

[19] The analytic approximations of W. E. Bleick and J. E. Mayer, J. Chem. Phys. **2**, 252 (1934), to the SCF neon orbitals calculated by F. W. Brown, Phys. Rev. **44**, 214 (1933), were used in this calculation.

The results obtained by deposition of H atoms in xenon are quite reasonable. The shift in the hfs splitting is negative and large ($\Delta A/A=-1.09\%$). This is the largest negative hfs shift yet observed, and it is to be expected since the van der Waals effect is greatest for large highly polarizable atoms such as Xe. The lines are considerably broader than usual, due, most likely to unresolved hyperfine interactions with the Xe nuclei. The observed g-factor shift is large (-0.00056) for a site exhibiting a negative shift in the hfs splitting. This result is most likely due to the large spin-orbit interaction to be expected for a Xe5p electron.

CONCLUSIONS

It appears that the present model, although rather crude, gives a satisfactory qualitative description of the interactions experienced by a H atom trapped in a nonpolar matrix. The theory is also able to give the dependence of the matrix effects on various characteristics of the matrix, such as polarizability and spin-orbit interaction constants. This allows us to predict the trend in the matrix effect for a series of identical matrix substances, of which the noble gases are an ideal example.

On the other hand, the quantitative agreement between theory and experiment, although rather good for the cases discussed here, is not to be taken too seriously. For example, the net shift in the hfs splitting is the difference between two competing effects which themselves can only be roughly estimated. For this reason, the quantitative details are often rather sensitive to the approximations used. Fortunately, however, the qualitative features of the results are not.

An understanding of matrix effects on the ESR spectra of trapped radicals is quite important, because these effects may complicate what would otherwise be simple, readily interpretable spectra. An example of this occurs for H atoms in krypton where an accidental coincidence gives the appearance of a missing line. Matrix effects can also broaden lines and render them unobservable. This effect is especially likely in cramped sites where the hfs splitting constants change rapidly with nearest neighbor distance. Any disorder in the environment of a radical in such a cramped site is likely to produce severe line broadening. Matrix effects may also be temperature dependent, with radicals in cramped sites being most sensitive to changes in temperature.

Optical pumping experiments on alkali metal vapors in the presence of buffer gases reveal that the buffer gas produces a shift in the hfs splitting of the alkali metal atom.[20] This shift is proportional to the buffer gas pressure, and it is positive for light buffer gases such as He and Ne, and negative for heavier gases such as Kr and Xe. These results are highly similar to the matrix effects observed for trapped H atoms, and the trend is in good qualitative agreement with the present theory. In the gas phase each alkali atom sees the same average environment of buffer gas atoms. For large highly polarizable buffer gas atoms the van der Waals effect predominates and produces a negative shift in the hfs splitting, whereas in the lighter gases the van der Waals effect is overcome by the exchange effect and a positive shift in the hfs splitting results.

[20] M. Arditi and T. R. Carver, Phys. Rev. **112**, 449 (1958); Beaty, Bender and Chi, *ibid.* **112**, 450 (1958); and Bender, Beaty and Chi, Phys. Rev. Letters **1**, 311 (1958).

ACKNOWLEDGMENTS

It is a pleasure to thank my colleagues Mr. V. A. Bowers, Dr. E. L. Cochran, Dr. S. N. Foner, and Dr. C. K. Jen for many stimulating discussions and suggestions.

APPENDIX

The problem is to simplify the formula

$$\Delta E_{\rm hfs}=2\sum_i{}'\sum_{kl}{}'\frac{(00\,|\,3\mathcal{C}_{\rm hfs}\,|\,i0)\,(i0\,|\,3\mathcal{C}_V\,|\,kl)\,(kl\,|\,3\mathcal{C}_V\,|\,00)}{(E_{00}-E_{i0})\,(E_{00}-E_{kl})}$$
$$-(00\,|\,3\mathcal{C}_{\rm hfs}\,|\,00)\sum_{kl}{}'\frac{(00\,|\,3\mathcal{C}_V\,|\,kl)\,(kl\,|\,3\mathcal{C}_V\,|\,00)}{(E_{00}-E_{kl})^2},$$

by matrix multiplication techniques after replacing the various excitation energies by average excitation energies, that is, $E_{00}-E_{i0}=E_{\rm H}$, and $E_{00}-E_{kl}=E_{\rm H}+E_M$. It should be noted that the ground state is omitted from all the sums in the above equation. Thus, in order to use matrix multiplication techniques the sums must first be completed by adding and subtracting the ground state terms wherever necessary.

The quantity $(00\,|\,3\mathcal{C}_V\,|\,00)=0$, so that the sum over kl gives the result

$$\Delta E_{\rm hfs}=\frac{2}{E_{\rm H}(E_{\rm H}+E_M)}\sum_i{}'(00\,|\,3\mathcal{C}_{\rm hfs}\,|\,i0)\,(i0\,|\,3\mathcal{C}_V{}^2\,|\,00)$$
$$-\frac{(00\,|\,H_{\rm hfs}\,|\,00)\,(00\,|\,3\mathcal{C}_V{}^2\,|\,00)}{(E_{\rm H}+E_M)^2}.$$

The quantity $(00\,|\,3\mathcal{C}_{\rm hfs}3\mathcal{C}_V{}^2\,|\,00)$, which results from summing over all states i including the ground state, vanishes because the terms in $3\mathcal{C}_V{}^2$ vanish at the H nucleus, while $3\mathcal{C}_{\rm hfs}$ vanishes everywhere else. Thus, the sum over i gives the result

$$\Delta E_{\rm hfs}=-(00\,|\,3\mathcal{C}_{\rm hfs}\,|\,00)$$
$$\times\left(\frac{2}{E_{\rm H}}+\frac{1}{E_{\rm H}+E_M}\right)\frac{(00\,|\,3\mathcal{C}_V{}^2\,|\,00)}{E_{\rm H}+E_M}.$$

It is readily shown using the same procedures that the quantity, $(00\,|\,3\mathcal{C}_V{}^2\,|\,00)/(E_{\rm H}+E_M)$, is an approximate expression for the van der Waals energy E_V. Thus, the change in the hfs splitting of the H atom, or, equivalently, the change in the unpaired electron density at the proton, is given by the expression

$$\Delta\,|\,h(\mathrm{H})|^2=-|\,h_0(\mathrm{H})|^2\{(2/E_{\rm H})+[1/(E_{\rm H}+E_M)]\}E_V.$$

Infrared Absorption of Zinc Oxide and of Adsorbed CO_2. I

SANJURO MATSUSHITA AND TOSHIKO NAKATA

Faculty of Science, Hokkaido University, Sapporo, Japan

(Received August 13, 1959)

For measuring the absorption spectra of a powdered solid in contact with a gas and adsorbed gas molecules, a new disk technique has been developed by which the powder can be formed into optical samples having sufficiently high transmissivity and a well-defined thickness. By the use of this technique the spectrum of zinc oxide under varying heat treatments and gaseous conditions was studied at 20° and 300°C mainly in the region 2000~1200 cm^{-1}. With samples made from zinc nitrate and evacuated at 300°C a distinct symmetrical band was observed at 1550 cm^{-1} which was investigated in detail. From its intensity, behavior, and correlation with absorption by free electrons, the band was attributed to an electronic absorption associated with zinc vacancies in the crystal lattice. Samples made from zinc carbonate showed strong absorption by free electrons on being evacuated, affording a useful basis for observing its variation.

INTRODUCTION

RECENTLY Eischens *et al.* have observed infrared absorption spectra of gas molecules adsorbed on the surface of metals or oxides.[1,2] This was achieved by measuring the transmission of a powder sample placed in an evacuable cell with and without adsorbed gas. Catalytic chemists are interested not only in the state of adsorbed molecules but in the nature of the solid which adsorbs gas and the correlation between them. On the other hand, observations of the spectral changes of a solid under the conditions that properties of the solid vary sensitively with varied atmospheres will provide useful information in the field of solid state physics. Therefore, infrared spectroscopy as applied to a gas-powder system should have wider application as a means of investigation in these fields, if one can observe correctly the spectrum of the solid as well as that of the adsorbed gas.

Employing a method analogous to Eischens' but improved especially in sample preparation, we have studied zinc oxide and its adsorption of gas by means of infrared spectroscopy. The present paper reports on a new technique involved in the method and the spectra of zinc oxide taken under various conditions. The properties which have been investigated with particular interest in these spectra are the behavior of a certain new absorption band and the absorption due to free electrons in the solid, the latter bearing a relation to the study of gas adsorption which will be reported in a subsequent paper.

EXPERIMENTAL

Preparation of Sample

Three kinds of zinc oxide samples were used in this work. Two of them, with which most of the data were obtained, consisted of zinc oxide dispersed in Aerosil silica[3,4] after Eischens. Dispersion was attained by drying and calcining a homogeneous paste made from a solution of zinc salt and the silica powder. In order to obtain adequate optical samples for the transmission measurement we developed a disk technique by which the powder was pressed into a very thin disk. The powder was ground in an agate mortar, weighed and pressed in a die which was analogous to that for the KBr disk but had particularly well-polished surfaces. About 40 kg/cm^2 of pressure was applied. Advantages of the disk sample over a sample of unpressed powder are that the scattering loss of radiation is markedly reduced so that the sample becomes suitably transparent for absorption measurement, and that a sample of desired and uniform thickness can be prepared which permits precise quantitative treatment. The method has been proved useful also in application to other samples containing metal or not containing silica. The disk of dispersed zinc oxide used in this work had a white or faintly yellowish white color and flat and fine surfaces as if polished. Visual observation of the disk placed above an electric lamp showed that its transparency was quite homogeneous. The apparent density of pressed samples (dispersed ZnO) used was 0.50 to 0.54 g/cm^3, and calculation indicated that about 80% of the total volume was vacant space. The BET area (N_2) was not materially changed by pressing. The thickness of the disk was chosen in many cases with a special care such that the transmission amounted to around 37%, where percentage transmission changes most sensitively in response to a change in absorptivity of the sample.

The powder samples used in this work were of four kinds, as given in the following, of which the fourth was a sample for blank tests containing no zinc oxide. Every one of them was pressed into disks when used for optical measurement.

[1] Eischens, Pliskin, and Francis, J. Chem. Phys. **22**, 1786 (1954).

[2] Eischens, Francis, and Pliskin, J. Phys. Chem. **60**, 194 (1954). R. P. Eischens, Z. Elektrochem. **60**, 782 (1956). R. P. Eischens and W. A. Pliskin, Advances in Catalysis **10**, 1 (1958).

[3] Supplied by Degussa, Frankfurt/Main, Germany. For physical and chemical properties of the material, see references 1, 4, and 8 in addition to the report of the maker.

[4] Zettlemoyer, Chessick, and Mollabaugh, J. Phys. Chem. **62**, 489 (1958).

Sample I: The paste was made with aqueous solution of zinc nitrate, dried at room temperature and heated at 300°C in air for 24 hr. Weight percentage of zinc oxide was 20 or 30. The BET area (per gram of the powder) was approximately 80 m^2.

Sample II: The paste was made with ammoniac solution of zinc carbonate and calcined at 500°C after drying. The sample contained 30% of zinc oxide and had BET area of 110 m^2/g.

Sample III: Zinc oxide alone, made by calcination of zinc carbonate at 500°C; BET area 6.2 m^2/g. Zinc carbonate was prepared by precipitation from a solution of zinc nitrate and ammonium carbonate.

Sample IV: Aerosil silica alone. Paste was made with pure water; the subsequent treatment was the same as in Sample I; BET area 160 m^2/g.

Electron Microscopic Study of Samples[5]

The state of dispersion of zinc oxide in silica was studied with an electron microscope. The carbon replica method[6] was applied to a portion of the dispersed-zinc oxide sample (not yet pressed) which had been prepared for the spectroscopic study. This procedure consists in first covering the particles of the sample with carbon by an evaporation method and then removing zinc oxide by dissolution with hydrochloric acid so that the spaces which have been occupied by zinc oxide become cavities. An electron micrograph of Sample I containing 30% of zinc oxide is shown in Fig. 1. The white area forming something like a contour line around a spherical Aerosil particle shows the vacancy produced by dissolution of zinc oxide, indicating that zinc oxide had covered surfaces of some of Aerosil particles. Judging from the photograph, the thickness of zinc oxide layer was estimated to be roughly 100 A. The distribution of zinc oxide in silica was found homogeneous insofar as infrared wavelength is concerned. Analogous electron micrographs were obtained with Sample II. Formation of zinc silicate seems most improbable in view of the method of sample preparation and, in fact, was not recognized by x-ray study.

Measurement of Spectra

The absorption cell was essentially the same as that used by Eischens *et al.*[2] or by Yang and Garland.[7] It was connected with a vacuum system set by the side of a spectrometer through a freezing trap for intercepting undesired vapor. The procedures such as evacuation, introduction of gas, and heating of sample could be performed without removing the cell from the optical path. Since a double-beam instrument was used, a reference

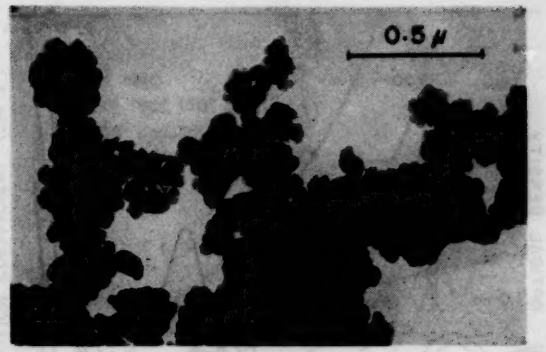

FIG. 1. Electron micrograph of ZnO dispersed in silica (by carbon replica method). Locations of ZnO in the powder are shown by white narrow areas surrounding silica particles.

cell which was optically equivalent to the sample cell, but contained no sample, was placed in the path of reference beam. It was connected with the sample cell by a vacuum line so that the conditions of gaseous phase in both cells were kept identical at any stage of the experiment. The spectrometer used, a Hilger model H800, was modified through rearrangement of some optical units, in such a way that each beam was made to pass through each cell vertically with the sample placed horizontally at a focal point of the sample beam. Further, after the optical, electrical, and recording systems of the instrument were examined thoroughly, several alterations were made in order to make the instrument suitable for the present purpose, especially to improve the accuracy and reproducibility in transmission measurement. A CaF_2 prism was used, and the resolution was less than 5 cm^{-1} near 1500 cm^{-1} under the operating conditions employed. The standard signal-to-noise ratio adopted was usually 500 (for "100% signal") but 800 for samples with poor transparency. Recording of the spectrum was made with the transmission scale magnified by placing an appropriate net in the path of reference beam to reduce the intensity.

Absorption spectra were usually measured at sample temperature of 20°C (regulated room temperature), but in some cases at 300°C, where the following procedure was adopted. With the sample kept at 300°C the "absorption spectrum" was recorded in the usual way, and subsequently the same scanning was repeated under the condition that the sample beam was blocked with an added shutter before the cell. The second record gives the emission spectrum of the sample for which the intensity distribution is relative to that of the reference beam. The first record corrected by the second gives, therefore, the true absorption spectrum of the sample at 300°C. (Under the conditions of the present experiment the induced emission was estimated to be a small fraction.)

In the present work, a change in transmission of a sample is assumed to be wholly due to the change in absorption. This is because the scattering power of

[5] This part of the work was done by Dr. T. Matsui of Hokkaido University.

[6] T. Matsui, J. Research Inst. Catalysis, Hokkaido Univ. 4, 112 (1956).

[7] A. C. Yang and C. W. Garland, J. Phys. Chem. 61, 1504 (1954).

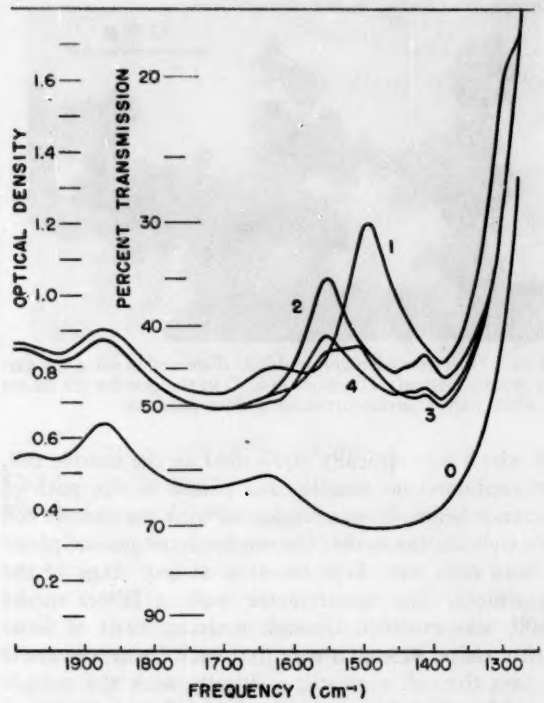

FIG. 2. Spectra of ZnO (1.2 mg/cm² in thickness) dispersed in silica, measured after various treatments given in succession. 1, after evacuation at 20°C. 2, after evacuation at 300°C. 3, after heating with oxygen. 4, after a second evacuation at 300°C. 0, spectrum of silica alone, showing the background.

the sample was not expected to change substantially in the process in question, although the scattering loss itself was by no means negligible even in the sample prepared by the disk technique.

SPECTRA OF SOLID

There were no essential differences between the spectra obtained with samples made from different original materials. But, the proportions in which certain features of the solid were exhibited in the spectrum varied considerably with the kind of the sample, so that in observing a feature in detail use was made of the sample that exhibited the feature in the most pronounced way.

1. Bell-Shaped Band at 1550 cm^{-1}

This section summarizes the experimental results of an investigation using Sample I. It is to be noted that the band at 1550 cm^{-1}, which is the main topic in this section, appears also in the spectra of Samples II and III, as will be seen in figures shown subsequently.

The spectra of Sample I of 4 mg/cm² in thickness containing 30% of zinc oxide which was treated under various conditions are shown in Fig. 2. An exception is the curve denoted by 0, which is the spectrum of silica alone (Sample IV, 2.8 mg/cm²) taken under the same condition as in Spectrum 2, forming the background of the absorption of zinc oxide in the other spectra. The limit of transmission of the silica was at 1200 cm^{-1}. The disk of Sample I prepared in air was first evacuated in the cell at 20°C to the order of 10^{-5} mm Hg and then subjected to spectroscopic examination, which yielded Spectrum 1. A distinct symmetrical band is seen at 1490 cm^{-1}, while weak absorptions at 1630 and 1320 cm^{-1} are attributed, respectively, to water and nitrogen dioxide which were not sufficiently desorbed.[8] The sample which gave Spectrum 1 was further evacuated to 10^{-5} mm Hg at 300°C for two hours and cooled down to 20°C. This gave Spectrum 2, where the band at 1490 cm^{-1} is missing, whereas a band of the same type appears at 1550 cm^{-1}. The transition from Spectrum 1 to 2 has been studied in more detail in another experiment. The experiment was such that the evacuation of the sample lasting 10 min was repeated several times at gradually increasing temperatures and between every two evacuation processes the spectrum was observed at 20°C. It is seen in Fig. 3 that the peak at 1490 cm^{-1} shifts to 1550 cm^{-1}. In the intermediate state the absorption seems not to be a single band.

When the sample which gave Spectrum 2 was heated at 300°C with oxygen of 30 cm Hg pressure admitted, the peak at 1550 cm^{-1} was gradually lowered as the heating time lengthened, and at the same time a shoulder appeared which grew on the longer wavelength side, so that the band acquired a shape of two peaks. The change was so slow that ten hours heating was required before the two peaks attained about the same height, and after twenty hours, when Spectrum 3 was obtained, no further change could be detected by more prolonged heating. Even in another experiment using the oxygen pressure of about one atmosphere, the behavior of the spectrum was substantially the same. By evacuating

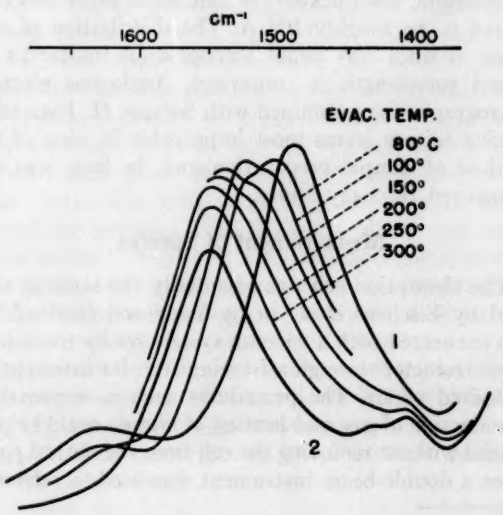

FIG. 3. The observation of transition from Spectrum 1 to 2 in Fig. 2. Ten minutes evacuation was repeated at gradually elevated temperatures.

[8] R. S. McDonald, J. Am. Chem. Soc. 79, 850 (1957).

again at 300°C for two hours, the sample giving Spectrum 3 was easily restored to the state which gave the single symmetrical band centering at 1550 cm^{-1}, as seen in Spectrum 4. It seems natural for zinc oxide, with the employed oxygen pressure taken into account, that the oxidation proceeded far more slowly than the reduction. The integrated intensities of the band in Spectra 3 and 4 are approximately equal to each other. That the band at 1550 cm^{-1} in Spectrum 4 did not recover the height of the band in Spectrum 2 can be interpreted by assuming that the concentration of the absorber, which will be discussed subsequently, decreased owing to the prolonged heating. In fact, when a newly prepared sample in the state of Spectrum 2 was heated in a vacuum at 300°C for more than 15 hr, the peak was lowered to the extent of that in Spectrum 4. The sample which attained the state of Spectrum 4 was proved to be stable on heating for more several hours; accordingly, such samples were used in the experiment in which the spectrum of adsorbed molecules was determined (to be reported in a subsequent paper).

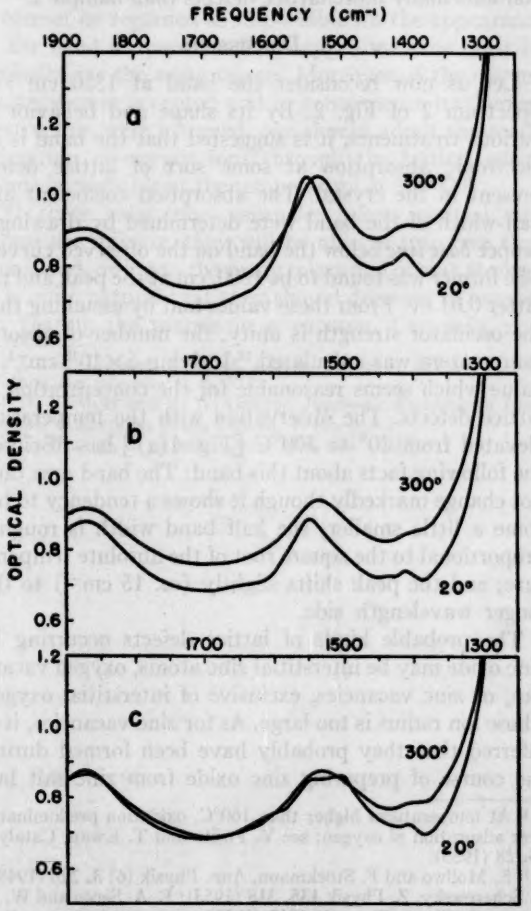

FIG. 4. Spectra measured at 300°C compared with those at 20°C. (a) Evacuated sample exhibiting a strong absorption at 1550 cm^{-1}. (b) Evacuated sample with the band weakened. (c) Sample heated with oxygen. The 20°C spectra are the same as Spectra 2, 4, and 3 in Fig. 2, respectively.

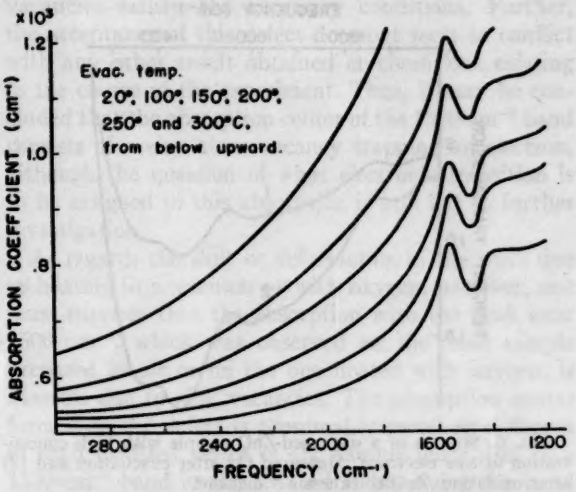

FIG. 5. Spectra of ZnO (unmixed sample) measured at 20°C after evacuations at several temperatures. The increasing absorption is attributed to production of free electrons. (The absorption coefficient shown may include that due to scattering, which can be assumed not to vary by evacuation.)

All the spectra described so far are those measured with the sample kept at 20°C; the sample in course of heating at a higher temperature was likewise cooled to 20°C each time it was subjected to a measurement. Spectra measured with the sample kept at 300°C are shown in Fig. 4 in comparison with those which were measured with the same sample at 20°C. Figures 4(a), (b), and (c) correspond to Spectra 2, 4, and 3 in Fig. 2, respectively. It is seen in Fig. 4(a) that by elevating the temperature the absorption becomes stronger over almost the whole range, and that the increment is larger the longer the wavelength, except in the region near 1550 cm^{-1} where a deformation of the band occurs simultaneously. Such an increase in absorption due to temperature elevation occurs in a greater degree in the case of (b),* and can scarcely be seen in the case of oxidized sample (c).

2. Absorption by Free Electrons

Zinc oxide is a semiconductor of the reduction type. It is known that the electrical conductivity increases after heating in a vacuum and decreases on standing in air.[9,10]† In Fig. 5, the spectra of Sample III (ZnO alone, 25 mg/cm^2) which were measured at 20°C after evacuation at various temperatures are shown. It is seen that in the range of longer wavelength the absorption increases rapidly with elevation of the evacuation temperature. These increases in absorption are to be considered as being due to free electrons in the solid.

* This result was confirmed by using a thicker sample. The ratio of the increase in the case of (b) to that of (a) was of the order of 1.3 at 1700 cm^{-1}.

[9] E. Mollwo, *Photoconductivity Conference* (John Wiley & Sons, Inc., New York, 1956), p. 521.

[10] Barnard, Winter, and Briscoe, J. Chem. Soc. **1954**, 1518.

† Y. Fuïta of Hokkaido University also confirmed this result, using the same sample as that used in the observation of Fig. 5.

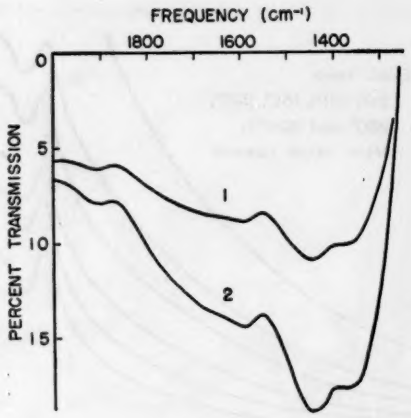

FIG. 6. Spectra of a dispersed-ZnO sample with high concentration of free electrons. Measured (1) after evacuation and (2) after oxidation. ZnO thickness 1.8 mg/cm².

For the absorption by free electrons, it is expected theoretically that the absorption coefficient should be approximately proportional to the square of the wavelength in the region here investigated,[11] and the present observed results are in good accord with this requirement.

The increase in absorption of Sample I on being heated at 300°C, which was illustrated in Fig. 4, may also be attributed to an increase in absorption of free electrons. According to reported data,[9] the static conductivity of zinc oxide increases on raising the temperature from 20° to 300°C by a factor of the order of ten. Drude's equation for free electrons, when the relaxation time and the effective number of electrons are taken as 10^{-14} sec and 10^{18} cm^{-3}, respectively, gives the absorption coefficient 100/cm at frequency 1700 cm^{-1},‡ while the difference in absorption at 20° and 300°C in Fig. 4(a) corresponds to the absorption coefficient 250/cm at the same frequency. (The observed absorption coefficient can be determined directly, since the reduced thickness of zinc oxide alone in the sample is clearly known.) The above values of relaxation time and number of electrons give a mean free path of 15 A, considerably smaller than the particle size, and the values of conductivity and mobility in harmony with the data hitherto reported.[12] The fact that the spectra of this sample observed at 20°C do not appear to show the distinct variation in free electron absorption that should accompany a change of state of the sample may be accounted for by proposing that the absolute number of free electrons was too small to be observed under the optical conditions employed.

The result obtained with a disk of Sample II (30% ZnO, 6 mg/cm²) is shown in Fig. 6. Spectrum 1 was measured at 20°C after the evacuation of the sample at 300°C for two hours, the condition being the same as in the case of Spectrum 2 in Fig. 2. The poor transmission of the sample seems, at least in part, attributable to high concentration of free electrons. In fact, in the case of this sample, heating in oxygen (10 cm Hg) at 300°C for two hours markedly reduced the absorption over a wide range of wavelength, as is shown in Spectrum 2.[13] Such a change in absorption can be most reasonably interpreted as being caused by a change in the number of free electrons. The absorption coefficient corresponding to this difference is about 1400/cm at 1700 cm^{-1}. By evacuating again at 300°C for 2 hr, the sample which gave Spectrum 2 resumed the state giving Spectrum 1. The richness of free electrons implies that there exist a large number of lattice defects. Despite the dilution of zinc oxide to 30%, the color of the disk was faintly yellowish white in contrast with the pure white disk of Sample I, which indicates that Sample II contains many more lattice defects than Sample I.[14]

3. Discussion

Let us now reconsider the band at 1550 cm^{-1} in Spectrum 2 of Fig. 2. By its shape and behavior in various treatments, it is suggested that the band is an electronic absorption at some sort of lattice defect present in the crystal. The absorption coefficient and half-width of the band were determined by drawing a proper *base line* below the band on the observed curve.[15] The former was found to be 1800/cm at the peak and the latter 0.01 ev. From these values and by assuming that the oscillator strength is unity, the number of absorption centers was calculated,[16]‡ giving 5×10^{17} cm^{-3}, a value which seems reasonable for the concentration of lattice defects. The observation with the temperature elevated from 20° to 300°C [Fig. 4(a)] has disclosed the following facts about this band: The band area does not change markedly though it shows a tendency to become a little smaller; the half band width is roughly proportional to the square root of the absolute temperature; and the peak shifts slightly (*ca.* 15 cm^{-1}) to the longer wavelength side.

The probable kinds of lattice defects occurring in zinc oxide may be interstitial zinc atoms, oxygen vacancies, or zinc vacancies, exclusive of interstitial oxygen whose ion radius is too large. As for zinc vacancies, it is inferred that they probably have been formed during the course of preparing zinc oxide from zinc salt but

[11] F. Seitz, *The Modern Theory of Solids* (McGraw-Hill Book Company, New York, 1940), p. 639.

‡ It is assumed that the effective mass of an electron is the same as the electronic mass and that the refractive index is unity.

[12] P. H. Miller, Jr., Phys. Rev. **60**, 890 (1941); E. E. Hahn, J. Appl. Phys. **22**, 855 (1951); S. E. Harrison, Phys. Rev. **93**, 53 (1954); A. R. Hutson, *ibid.* **108**, 222 (1957).

[13] At temperatures higher than 160°C, oxidation predominates over adsorption of oxygen; see Y. Fujita and T. Kwan, Catalyst **15**, 28 (1958).

[14] E. Mollwo and F. Stöckmann, Ann. Physik (6) **3**, 226 (1948); E. Scharowsky, Z. Physik **135**, 318 (1953); E. A. Secco and W. J. Moore, J. Chem. Phys. **26**, 942 (1957).

[15] N. Wright, Anal. Chem. **13**, 1 (1941); Heigl, Bell, and White, *ibid.* **19**, 293 (1947). The method was modified by taking the background into account.

[16] A. Smakula, Z. Physik **59**, 603 (1930).

their number cannot increase in any subsequent reduction process. Now we shall inquire whether any of these three kinds of defects can fit in with the experimental facts observed on the band at 1550 cm^{-1}. Those facts, among others, which serve as particularly useful criteria are (1) that the band is weakened by heating the sample for a long time, and (2) that the absorption due to free electrons increases as the band is weakened. The former indicates that the lattice defect responsible for this band can be extinguished thermally at 300°C, and the latter means that the defect acts as a trap for electrons.

In zinc oxide evacuated at a high temperature, there exist almost certainly interstitial zinc atoms acting as donors. Although, in view of the fact that the ionization energy of a donor in zinc oxide is about 0.05 ev,[12] the absorption by neutral interstitial zinc atoms does not come into question, the electronic transition $Zn^+(4s) \rightarrow Zn^+(4p)$ may occur in the singly ionized interstitial zinc,[17] and the energy of the transition might be reduced in the medium to 1550 cm^{-1}.[18] Evidently, however, a defect of this kind cannot be a trap for electrons; hence it cannot be regarded as responsible for the appearance of the band in question. The oxygen vacancy must be excluded for the same reason. Moreover, if the oxygen vacancy were accepted and in consequence its thermal destruction were assumed, one should admit the ready migration of oxygen ions through the lattice, which seems improbable at the temperature of 300°C.[19]

If there exist zinc vacancies where neutral zinc atoms are missing, they will be able to trap free electrons, and, owing to the ready migration of zinc atoms,[17] it is quite natural that they should decrease in number on heating the sample in a vacuum. Certainly, zinc vacancies satisfy the necessary conditions. Further, the acceptance of this defect does not seem to conflict with any other result obtained or conditions existing in the course of the experiment. Thus, it may be concluded that the absorption center of the 1550-cm^{-1} band consists of a zinc atom vacancy trapping an electron, although the question of what electronic transition is to be assigned to this absorption is still left to further investigation.

As regards the shift or deformation of the band due to heating in a vacuum or with oxygen, however, one must suppose that the absorption with the peak near 1500 cm^{-1}, which was observed on the fresh sample prepared in air or on the one heated with oxygen, is likewise due to zinc vacancies. The absorption center formed on the defect is presumably somehow different in such oxidized states of the sample from that of a 1550-cm^{-1} band in the reduced state, giving the band that is shifted about 50 cm^{-1}. That is, it is supposed that the growth of 1550-cm^{-1} band coupled with the disappearance of the 1500-cm^{-1} peak, which was observed invariably after the evacuation of oxidized samples, should be accounted for by a change in absorption centers but not by new formation of zinc vacancies. If otherwise, it is hard to explain the fact that the same procedure of heating a sample in a vacuum at 300°C initially gives rise to a new band at 1550 cm^{-1} and then lowers it.

As to the weak band appearing near 1400 cm^{-1}, it is not clear at present whether it has any relation to the 1550-cm^{-1} band or not.

ACKNOWLEDGMENTS

We wish to express our sincere thanks to Dr. T. Matsui for his collaboration in a part of this work. Thanks are also due to Professor J. Horiuti, Professor T. Hori, Professor A. Kobayashi, and Professor T. Kwan for their support and valuable discussions.

[17] D. G. Thomas, J. Phys. Chem. Solids **3**, 235 (1957); E. Mollwo, see reference 9, p. 513.

[18] H. F. Mott and R. W. Gurney, *Electronic Processes in Ionic Crystals* (Clarendon Press, Oxford, 1940), p. 83.

[19] C. Wagner, Z. physik. Chem. **22B**, 181 (1933).

Electronic Structure of LiH. V. A Radially Correlated Wave Function*

J. M. ROBINSON, *Department of Physics, Texas College of Arts and Industries, Kingsville, Texas*

AND

J. D. STUART AND F. A. MATSEN, *Departments of Chemistry and Physics, University of Texas, Austin, Texas*

(Received July 20, 1959)

The electronic energy and dipole moment of LiH have been calculated with valence-bond wave functions into which some radial correlation has been introduced by assigning different orbitals to different electrons. The energy as calculated from the radially correlated functions is 0.76 ev lower than from the corresponding uncorrelated functions. The calculated dipole moment agrees well with that obtained in previous calculations. Moffitt's concept of "atoms in molecules" is applied to the correlated and uncorrelated functions.

INTRODUCTION

An important source of error in calculations of the electronic energy of atoms and molecules is that there is a very incomplete allowance for electron correlation in the wave function employed. For atoms, correlation error is defined as the difference between the experimental and the Hartree-Fock energies after suitable corrections have been made for relativistic effects. While exact Hartree-Fock calculations have not been made for molecules so that the correlation error has not been precisely defined for molecules, the concept itself is useful.

The correlation error in atomic calculations can be decreased by configuration interaction or by assigning different orbitals to different electrons. Such a wave function has been called an "open configuration wave function." In particular, if s orbitals are employed, the assignment of different orbitals to different electrons introduces some radial correlation and the wave function has been called a "radially correlated wave function." This terminology has lead to some confusion in the past and it is here proposed that the symbol DODE, different orbitals for different electrons, be used to describe such calculations. The term SODE, same orbitals for different electrons (within the restriction of the Pauli principle), is used for the conventional calculation.

DODE energy calculations on atoms are consistently better than both SODE and Hartree-Fock calculations.[1–4] While the extension of DODE calculations to molecules is fairly obvious, it is only recently that such calculations have been made.[5,6]

In this paper the electronic energy and dipole moment of lithium hydride have been calculated by using DODE wave functions representing the "structures" ($1s$, $1s'$, $2s$; h), ($1s$, $1s'$, $2p_\sigma$; h), and ($1s''$, $1s'''$; h'', h''') (see Table II). These have been shown to be the three most important structures.[7,8] The point of comparison is a calculation made with the corresponding SODE wave function representing the structures ($1s^2$, $2s$; h), ($1s^2$, $2p_\sigma$; h), and ($1s^2$, h^2).

One might expect the DODE calculations to be superior to the SODE calculation for two reasons: (1) the energy of each of the three structures should be lowered because of the introduction of radial correlation into the $1s$ shell on lithium, and (2) the energy of the ionic structure Li^+H^- should have a greater relative lowering than the two covalent structures because of the introduction of additional radial correlation in H^- so that its participation in the ground state should be greater (see Table I). A further incentive for performing a DODE calculation is to test still further the dependence of the calculated dipole moment for lithium hydride on the type of function used. This quantity has shown a surprising invariance to function type.[8–12]

Finally, the calculation provides an opportunity to test the "atoms-in-molecules" concept of Moffitt by improving the atomic and ionic wave function used in the calculation.[13]

CALCULATIONS

The wave function used was

$$\Psi=[1/(4!)^{\frac{1}{2}}]\sum_{i=1}^{3}C_i\Phi_i, \qquad (1)$$

where the Φ_i's are listed in Table II and the parameter sets in Table III. The C_i's and the electronic energy

* Supported by the Robert A. Welch Foundation of Houston, Texas, and the Office of Ordnance Research, U. S. Army. Paper presented at the American Physical Society meeting April, 1959, Austin, Texas.

[1] H. Shull and P.-O. Löwdin, J. Chem. Phys. **25**, 1035 (1956).
[2] G. H. Brigman and F. A. Matsen, J. Chem. Phys. **27**, 829 (1957).
[3] Brigman, Hurst, Gray, and Matsen, J. Chem. Phys. **29**, 251 (1958).
[4] Hurst, Gray, Brigman, and Matsen, Mol. Phys. **1**, 189 (1958).
[5] LiH, J. M. Robinson, Ph.D. dissertation, University of Texas, 1957. The present paper is based in part on this dissertation.
[6] He_2^+, P. Csavenszky, J. Chem. Phys. **31**, 178 (1959).
[7] Miller, Friedman, Hurst, and Matsen, J. Chem. Phys. **27**, 1385 (1957).
[8] Hurst, Miller, and Matsen, J. Chem. Phys. **26**, 1092 (1957).
[9] A. M. Karo and A. R. Olson, J. Chem. Phys. **30**, 1232 (1959).
[10] F. T. Ormand and F. A. Matsen, J. Chem. Phys. **29**, 100 (1958).
[11] O. Platas and F. A. Matsen, J. Chem. Phys. **29**, 965 (1958).
[12] Bernard J. Ransil, "Electronic properties of selected first row diatomic molecules in LCAO-MO-SCF approximation," University of Chicago (unpublished).
[13] W. Moffitt, Proc. Roy. Soc. (London) **210**, 245 (1951).

were determined in the usual way from

$$\sum_{i=1}^{3}(H_{ij}-S_{ij}E)C_i=0, \qquad j=1,2,3. \tag{2}$$

The matrix elements H_{ij} and S_{ij} are listed in Table IV. The C_i's and energy and dipole moment results are given in Table V.

The orbital exponents for the SODE wave function Ψ_{I} were chosen by Slater's rules for atoms.[14] The orbital exponents for the DODE wavefunction Ψ_{II} are essentially those which minimize the energy of Li$(1s, 1s', 2s)$, $Li^+(1s, 1s')$, and $H^-(1s, 1s')$[4]. The Slater value is used for the $2p_\sigma$ orbital.

Calculations with the DODE wave functions Ψ_{III}, Ψ_{IV}, and Ψ_{V} were made to investigate the effect of radial correlation in the ionic structure, Φ_3 of Table II. Φ_1 and Φ_2 of these three wave functions are identical with Φ_1 and Φ_2 of Ψ_{II}. Φ_3 of Ψ_{III} is a SODE function with $\delta_{1s''}=\delta_{1s'''}=2.70$ and $\delta_{h'}=\delta_{h''}=1.00$. Ψ_{IV} permits some radial correlation in Li^+, and Ψ_{V} permits some radial correlation in both Li^+ and H^-. Ψ_{V} differs from Ψ_{II} in that 1.00 rather than 0.6875 is used as the "scale factor"[1] in the selection of the orbital exponents for H^-.

The experimental internuclear distance $R_e=3.01$ au[15] was used in all calculations.

The exchange integrals were computed by using a program developed for the IBM 650 by Dr. J. M. Miller.[16] The remaining integral and analysis programs were developed by the authors initially for the IBM CPC and later for the IBM 650.†

DISCUSSION

The DODE calculation did satisfy expectation (1) that the energies of the three structures are lowered so that the energy of the molecule is lowered. There is obtained an energy 0.76 ev lower than the SODE calculation and an energy 0.35 ev below the best previously reported energy.[9] Contrary to expectation (2), introduction of radial correlation into H^- does not improve the energy significantly. Indeed, the use of the optimum hydride ion orbitals has an adverse effect upon the calculated energy, compare Ψ_{II} and Ψ_{IV}.

TABLE I. SODE–DODE energies (infinite separation).[a]

$\{\mathrm{Li}(1s^2, 2s)+H(1s)\}-\{\mathrm{Li}(1s1s'2s)+H(1s)\}=0.699$ ev.
$\{Li^+(1s^2)+H^-(1s^2)\}-\{Li^+(1s1s')+H^-(1s'1s'')\}=1.811$ ev.

[a] See Table II for explanation of symbols.

TABLE II. Wave functions.

$\Phi_1=(1s, 1s', 2s; h)$[a,b]
$\Phi_2=(1s, 1s', 2p_\sigma; h)$
$\Phi_3=(1s'', 1s'''; h'h'')$
$1s(i)\cdot\equiv\cdot 1s$ on Li$=(\delta_{1s}^3/\pi)^{\frac{1}{2}}\exp(-\delta_{1s}r_i)$
$2s(i)\cdot\equiv\cdot 2s$ on Li$=(\delta_{2s}^5/3\pi)^{\frac{1}{2}}r_i\exp(-\delta_{2s}r_i)$
$2p_\sigma(i)\cdot\equiv\cdot 2p_\sigma$ on Li$=(\delta_{2p}^5/\pi)^{\frac{1}{2}}r_i\exp(-\delta_{2p}r_i)\cos\theta_i$
$h(i)\cdot\equiv\cdot 1s$ on H$=(\delta_h^3/\pi)^{\frac{1}{2}}\exp(-\delta_h r_i)$

[a] Primes are used to indicate different orbital exponents.

[b] $(abcd)=[abcd]+[bacd]+[abdc]+[badc]$. In the foregoing expression

$$[abcd]=\begin{vmatrix}(a\alpha)_1 & (b\beta)_1 & (c\alpha)_1 & (d\beta)_1\\ (a\alpha)_2 & (b\beta)_2 & (c\alpha)_2 & (d\beta)_2\\ (a\alpha)_3 & (b\beta)_3 & (c\alpha)_3 & (d\beta)_3\\ (a\alpha)_4 & (b\beta)_4 & (c\alpha)_4 & (d\beta)_4\end{vmatrix}.$$

The reason for this becomes apparent when the problem is considered from the standpoint of perturbation theory. We may write

$$\Psi=\lambda\psi_C+\mu\psi_{\mathrm{I}}, \tag{3}$$

where

$$\psi_C=\alpha\Phi_1+\beta\Phi_2 \tag{4}$$

$$\psi_{\mathrm{I}}=\Phi_3. \tag{5}$$

Then from perturbation theory, the energy E is given by

$$E=E^0+E^1, \tag{6}$$

where

$$E^0=\mathcal{H}_{CC}, \tag{7}$$

$$E^1=-[(\mathcal{H}_{C\mathrm{I}}-\mathcal{H}_{CC}\mathcal{S}_{C\mathrm{I}})^2]/(\mathcal{H}_{\mathrm{II}}-\mathcal{H}_{CC}), \tag{8}$$

$$\mathcal{H}_{AB}=[1/(S_{AA}S_{BB})^{\frac{1}{2}}]\int\psi_A H\psi_B d\tau, \tag{9}$$

$$\mathcal{S}_{AB}=[1/(S_{AA}S_{BB})^{\frac{1}{2}}]\int\psi_A\psi_B d\tau, \tag{10}$$

$$S_{AA}=\int\psi_A\psi_A d\tau, \qquad S_{BB}=\int\psi_B\psi_B d\tau. \tag{11}$$

The perturbation term couples the ionic structure Φ_3 with the covalent structures, Φ_1 and Φ_2. Relative to function Ψ_{IV}, Ψ_{II} decreases the denominator but simultaneously decreases the numerator, principally by raising $S_{C\mathrm{I}}$ (see Table VI), so that Ψ_{II} has an almost negligible effect on this term. An interpretation of the increase in $S_{C\mathrm{I}}$ is that Ψ_{II} has made the ionic function more covalent and has thereby not improved it as a proper variation term. This result underscores the difficulty of making a clear cut distinction between nonorthogonal valence-bond structures. For apparently the same reason, similar results for H_2 have been obtained by Robinson and Weigang.[17]

[14] Eyring, Walter, and Kimball, *Quantum Chemistry* (John Wiley & Sons, Inc., New York, 1944), p. 163.

[15] G. Herzberg, *Spectra of Diatomic Molecules* (D. Van Nostrand Company, Inc., Princeton, New Jersey, 1950), p. 546.

[16] See also Miller, Gerhauser, and Matsen, *Quantum Chemistry Integrals and Tables* (University of Texas Press, Austin, Texas, 1959).

† The authors are grateful to Texas Instruments, Inc., of Dallas, Texas and the Humble Oil and Refining Company of Baytown, Texas for the donation of computer time.

[17] J. M. Robinson and O. Weigang, University of Texas (unpublished).

TABLE III. Orbital exponents.[a]

	δ_{1s}	$\delta_{1s'}$	δ_{2s}	δ_{2p}	δ_h	$\delta_{1s''}$	$\delta_{1s'''}$	$\delta_{h'}$	$\delta_{h''}$
Ψ_I	2.700	2.700	0.650	0.650	1.000	2.700	2.700	1.000	1.000
Ψ_{II}	3.300	2.065	0.650	0.650	1.000	3.300	2.065	1.000	0.325
Ψ_{III}	3.300	2.065	0.650	0.650	1.000	2.700	2.700	1.000	1.000
Ψ_{IV}	3.300	2.065	0.650	0.650	1.000	3.300	2.065	1.000	1.000
Ψ_V	3.300	2.065	0.650	0.650	1.000	3.300	2.065	1.380	0.620

[a] R_e=3.01 au (see reference 15).

TABLE IV. Matrix elements.

	Ψ_I	Ψ_{II}	Ψ_{III}	Ψ_{IV}	Ψ_V
H_{11}	−18.672	−68.326	−68.326	−68.326	−68.326
S_{11}	2.3506	8.5741	8.5741	8.5741	8.5741
H_{22}	−20.537	−76.062	−76.062	−76.062	−76.062
S_{22}	2.5971	9.5855	9.5855	9.5855	9.5855
H_{33}	−7.7482	−79.933	−7.7482	−28.590	−92.894
S_{33}	0.98230	10.039	0.98230	3.6129	11.714
H_{12}	−4.1638	−15.285	−15.285	−15.285	−15.285
S_{12}	0.51011	1.8665	1.8665	1.8665	1.8665
H_{13}	−7.3222	−63.142	−13.997	−26.799	−55.038
S_{13}	0.91180	7.9056	1.7376	3.3265	6.8412
H_{23}	−8.7918	−43.649	−16.896	−32.536	−57.692
S_{23}	1.0991	5.4486	2.1051	4.0539	7.1776

$H_{ij} \cdot\equiv\cdot \int \Phi_i H \Phi_j d\tau$ $\quad S_{ij} \cdot\equiv\cdot \int \Phi_i \Phi_j d\tau$

TABLE V. Energy, dipole moment, and coefficients.

	Ψ_I	Ψ_{II}	Ψ_{III}	Ψ_{IV}	Ψ_V
C_1	0.6123	0.7899	0.6323	0.6091	0.5627
C_2	0.3719	0.5185	0.4002	0.3797	0.3757
C_3	0.2606	−0.03249	0.2200	0.2581	0.2903
E(ev)[a]	−216.96	−217.40	−217.62	−217.67	−217.72
μ(D)	−5.98	−5.40	−5.94	−6.02	−6.18

Experimental energy −219.71 ev

C's normalized to $\int \psi\psi d\tau = 1$ and $\int \phi_i \phi_i d\tau = 1$

[a] 1 au=27.19 ev.

TABLE VI. Perturbation calculation.

	Ψ_I	Ψ_{II}	Ψ_{III}	Ψ_{IV}	Ψ_V
$\mathcal{H}_{CC}$	−7.9692	−7.9954	−7.9954	−7.9954	−7.9954
$\mathcal{S}_{CC}$	1.0000	1.0000	1.0000	1.0000	1.0000
$\mathcal{H}_{II}$	−7.8879	−7.9620	−7.8879	−7.9131	−7.9304
$\mathcal{S}_{II}$	1.0000	1.0000	1.0000	1.0000	1.0000
$\mathcal{H}_{CI}$	−6.4550	−7.4549	−6.4748	−6.4801	−6.9548
$\mathcal{S}_{CI}$	0.80515	0.93253	0.80507	0.80568	0.86479
α[a]	0.76993	0.76426	0.76426	0.76426	0.76426
β[a]	0.49867	0.50648	0.50648	0.50648	0.50648
$(\mathcal{H}_{CI}-\mathcal{H}_{CC}\mathcal{S}_{CI})^2$	0.0014882	0.0000009	0.0014399	0.0014733	0.0016401
$(\mathcal{H}_{II}-\mathcal{H}_{CC})$	0.081313	0.033372	0.10750	0.082262	0.064949
E^0(au)	−7.9692	−7.9954	−7.9954	−7.9954	−7.9954
E^1(au)	−0.018302	−0.000029	−0.013394	−0.017910	−0.025252

[a] Normalized to $\int \psi\psi d\tau = 1$, $\int \Phi_A \Phi_A d\tau = 1$.

TABLE VII.

Wave function[a]	Directly calculated energy (ev)	Directly calculated atomic energy (ev) Li(^2S)+H	Li$^+$+H$^-$	Moffitt energy (ev)	Sum of experiments atomic energy (ev) Li(^2S)+H	Li$^+$+H$^-$
Ψ_{I}	−216.96	−215.28	−206.58	−220.66	−217.03	−212.38
Ψ_{IV}	−217.67	−215.98	−207.28	−220.65	−217.03	−212.38
Ψ_{II}	−217.40	−215.98	−211.00	−218.50	−217.03	−212.38

[a] See Tables II and III.

In the DODE calculation there is a considerable improvement in the energies of the separate atoms; thus, the DODE calculations move in the direction envisaged by Moffitt in his "atoms-in-molecules" theory.[13] In the Moffitt theory the calculated energy is "improved" by replacing the inexact atomic energies calculated from the inexact wave functions by the experimental atomic energies without changing the inexact interaction terms. In Table VII are listed for three cases the Moffitt energies calculated from

$$\sum_{i=1}^{3}(\tilde{H}_{ij}-S_{ij}E)\Gamma_i=0, \qquad j=1,2,3, \tag{12}$$

where

$$\tilde{H}_{ij}=H_{ij}+\tfrac{1}{2}[S_{ij}(W_i-\bar{W}_i)+(W_j-\bar{W}_j)S_{ij}] \tag{13}$$

$$H_{ij}=\int\Phi_i H\Phi_j d\tau \tag{14}$$

$$S_{ij}=\int\Phi_i\Phi_j d\tau \tag{15}$$

$$\bar{W}_i=\int\Phi_i H_0\Phi_i d\tau, \qquad H_0=H \text{ (infinite separation)} \tag{16}$$

W_i and W_j = exact atomic energies (infinite separation).

The directly computed energies for the three cases are listed in Table VII for comparison. Several features should be noted: (1) ψ_{II}, which used "best" atomic and ionic functions, yields the highest Moffitt energy. (2) ψ_{I} and ψ_{IV} with poorer atomic functions yield a Moffitt energy$\sim$1 ev below experiment. (3) While ψ_{IV} yields a directly calculated energy$\sim$0.7 ev. below that from ψ_{I}, the Moffitt energies of ψ_{I} and ψ_{IV} are equal. Similar effects have been observed by Hurley[18] and Pauncz[19] for the hydrogen molecule. The results, together with the rather drastic change in orbital exponents between separated atoms and ions in the corresponding terms in the molecule, emphasize that there are, in reality, no atoms (or ions) in molecules.

The dipole moment associated with the lowest energy is 6.18D (hydrogen negative). This is larger than has heretofore been calculated with valence-bond wave functions. It is believed that this result is too high since the treatment does not include polarization on the hydrogen atom, the inclusion of which in an earlier calculation[11] lowered the dipole moment by 0.4D. It is apparent that an exact prediction of the dipole moment cannot be made for some time, but it is encouraging that all the recent calculations put the moment in a rather narrow range, 5.5 to 6.5D.

[18] A. C. Hurley, Proc. Phys. Soc. (London) A68, 1949 (1955).
[19] R. Pauncz, Acta Phys. Acad. Sci. Hung. 4, 237 (1954).

On the Mechanism of the Lewis-Rayleigh Nitrogen Afterglow

K. D. BAYES AND G. B. KISTIAKOWSKY

Gibbs Chemical Laboratory, Harvard University, Cambridge, Massachusetts

(Received August 19, 1959)

The relative intensities in the nitrogen afterglow, from 5000 to 11 000 A, have been measured in pure nitrogen and after addition of several foreign gases. Most of the bands in the recently discovered $Y-B\,^3\Pi_g$ system are overlapped by $B\,^3\Pi_g-A\,^3\Sigma_u^+$ bands but intensity assignments have been made. Changes in relative intensities accompanying changes in external conditions show that the bands can be classified into five groups of different kinetic origins. The vibrational levels of the $B\,^3\Pi_g$ and Y states just below D_e, the energy of two separated ground state nitrogen atoms, are not populated. At low temperature the highest populated levels of the $B\,^3\Pi_g$ and Y states tend to a limit about 850 cm^{-1} below D_e. It is suggested that this is approximately equal to the dissociation energy of the $^5\Sigma_g^+$ state of the nitrogen molecule. Some of the emission from the low vibrational levels of the $B\,^3\Pi_g$ state is associated with the radiation cascade $Y\rightarrow B\,^3\Pi_g\rightarrow A\,^3\Sigma_u^+$, but the rest has a different kinetic origin. The emission from $B\,^3\Pi_g$ ($v=7$, 6, 5) is probably the second step in the cascade $^3\Delta_u\rightarrow B\,^3\Pi_g\rightarrow A\,^3\Sigma_u^+$.

Foreign gases modify the vibrational population distribution of the upper levels of the $B\,^3\Pi_g$ state, each in its characteristic fashion. Some gases quench the emission from the lowest vibrational levels of $B\,^3\Pi_g$ more effectively than the rest of the spectrum. The quenching of the emission from the higher levels depends on the pressure of nitrogen. A mechanism accounting for most of the afterglow emission is discussed.

INTRODUCTION

THE extensive literature on the Lewis-Rayleigh nitrogen afterglow has been previously summarized.[1–3] It is well established that the recombination of ground state (^4S) nitrogen atoms is mainly responsible for the afterglow. Berkowitz, Chupka, and Kistiakowsky (BCK)[4] proposed that weakly bound $^5\Sigma_g^+$ nitrogen molecules, essentially in equilibrium with the atoms, could undergo collision-induced transitions into the $B\,^3\Pi_g$ state. This mechanism satisfactorily explains the strong emission from the 12th, 11th, and 10th vibrational levels of $B\,^3\Pi_g$ but does not account for the emission from its lower levels. Recent work has demonstrated the existence of another band system in the afterglow[5–7] for which $B\,^3\Pi_g$ is the lower state. The present study of the relative intensities in the afterglow spectrum from the visible to 11 000 A was undertaken in an effort to elucidate additional features of the afterglow mechanism. Some of these findings have been reported previously.[6,8]

EXPERIMENTAL

Most of the runs were made with a flow system. The flows of nitrogen and other gases were metered by measuring the pressure drop across capillaries of known cross sections. Active nitrogen was formed in an electrodeless discharge created by a 2450-Mc, 125-w Raytheon Microtherm machine. A Wood's light trap prevented light of the bright discharge from entering the observation cell. The latter was a horizontal Pyrex tube 30 mm in diameter and 27 cm long. A 8-cm section at the front of the cell was isolated by two sealed-in windows and the space between them evacuated to prevent fogging of the front window when the rest of the cell was cold. The inlet and outlet tubes entered from the top so that the whole cell could be immersed in dry ice or liquid nitrogen. A polyethylene bag surrounded by a Styrofoam box contained the coolant.

Below about 10 mm Hg the afterglow would disappear upon coming in contact with the glass walls at 77°K. This was attributed to efficient wall recombination of the atoms since no emission was observed downstream from the cold cell. Adding 30 mm of argon to the nitrogen slowed the diffusion to the walls so that spectra at 77°K could be recorded. At the lower pressures it was possible to record spectra by only partially covering the cell with liquid nitrogen but then the emitting gas was not at a well-defined temperature.

The discharge was 60 cm upstream from the observation cell, which corresponded to 50 msec transit time for the largest flow rate used. The rare gases and nitrogen were introduced above the discharge but the other gases were introduced 30 cm upstream from the cell. A small McLeod gauge recorded the pressure at the outlet of the cell.

For experiments with N_2^{15} a closed circulating system was used. A mercury diffusion pump circulated the gas. A 35-mm diameter cold trap stuffed with glass wool kept mercury vapour from entering the discharge. Except for these changes the vacuum system was the same.

A small Pyrex lens concentrated the light from the cell onto the entrance slit of a $f/4.5$ spectrograph.[9] The collimator was an 8-degree off-axis parabolic mirror

[1] H. O. Kneser, Ergeb. exakt. Naturw. **8**, 229 (1929).
[2] S. K. Mitra, *Active Nitrogen—A New Theory*, Association for the Cultivation of Science, Calcutta, India, 1945.
[3] K. R. Jennings and J. W. Linnett, Quart. Revs. **12**, 116 (1958).
[4] Berkowitz, Chupka, and Kistiakowsky, J. Chem. Phys. **25**, 457 (1956).
[5] M. Brook, Science Report No. 2, Contract AF19(122)–453 of U. S. Air Force Geophysics Directorate with UCLA.
[6] G. B. Kistiakowsky and P. Warneck, J. Chem. Phys. **27**, 1417 (1957).
[7] LeBlanc, Tanaka, and Jursa, J. Chem. Phys. **28**, 979 (1958).
[8] K. D. Bayes and G. B. Kistiakowsky, J. Chem. Phys. **29**, 949 (1958).
[9] W. E. Brown, thesis, Harvard University, 1948.

5 in. in diameter. The blazed 5-in. grating had 15 000 lines per inch. Light from the grating returned to the parabolic mirror and was focused on an exit slit adjacent to the entrance slit. Because of the low intensity of the afterglow, both slits were 0.5 mm wide which gave a resolution of 30 A. This was sufficient to resolve much of the vibrational structure of the afterglow spectrum. The grating was rotated reproducibly by a motor-driven micrometer head pushing against a lever attached to the grating table. A pip marker correlated the position of the micrometer head with the chart of the recorder. Line spectra of several rare gases were used to calibrate the position of the micrometer head against the wavelength. This calibration was accurate to better than ±3 A. Twenty minutes were required to sweep the spectrum from 11 000 to 5000 A.

A RCA 7102 infrared-sensitive photomultiplier tube, operated at 1300 v and cooled with dry ice, was placed 10 cm from the exit slit. A chopper in front of the entrance slit modulated the light at 450 cps. A magnetic tachometer mounted on the shaft of the chopper provided a 450 cps reference signal. The photomultiplier and reference signals were amplified and compared in a Baird-Atomic phase-sensitive amplifier, the output going to a Brown recorder.

TABLE I. Intensities of N_2^{14} afterglow at 4 mm Hg. Intensities proportional to number of quanta.

$B\,^3\Pi_g - A\,^3\Sigma_u^+$	$Y - B\,^3\Pi_g$	300°K	200°K	100°K*
12–6, 11–5, 10–4		0.07	0.08	0.04
12–7, 11–6, 10–5		0.87	1.14	0.51
12–8, 11–7, 10–6		4.29	4.86	2.25
9–5, ... 5–1	7–0	0.77	0.65	0.39
12–9		0.37	0.71	0.60
11–8	8–1	1.54	1.60	0.73
10–7		0.57	0.43	0.18
9–6		0.21	0.15	0.06
8–5		0.30	0.20	0.09
7–4		0.39	0.47	0.28
6–3	6–0	1.18	1.45	0.54
5–2		0.65	0.77	0.45
4–1, 11–9	7–1	0.75	1.10	0.60
3–0		0.33	0.36	0.16
	8–2	0.22	0.67	0.59
7–5		0.15	0.18	0.15
6–4	5–0	0.82	0.91	0.38
5–3, 11–10		0.87	0.93	0.49
4–2	6–1	1.23	1.71	1.12
3–1	7–2	2.35	3.32	1.78
2–0		2.72	3.16	1.49
	8–3	0.90	2.33	2.29
6–5, 11–11		0.79	0.81	0.41
5–4		0.23	0.25	0.10
4–3	5–1	0.26	0.32	0.21
3–2	6–2	0.84	0.89	0.64
2–1	7–3	4.34	5.60	3.16
1–0	8–4	5.12	7.16	5.69
5–5		0.36	0.43	0.34
4–4	4–1	0.62	0.87	0.71
3–3	5–2	0.88	1.15	1.12
2–2	6–3	0.92	1.00	0.94
1–1	7–4	1.10	1.50	1.38
0–0	8–5	5.93	10.07	8.98

* This indicates a rather ill-defined temperature between 77° and 200°K.

TABLE II. Intensities of N_2^{15} afterglow at 5 mm Hg.

$B\,^3\Pi_g - A\,^3\Sigma_u^+$	$Y - B\,^3\Pi_g$	300°K	200°K
12–6, 11–5, 10–4		0.12	...
12–7, 11–6, 10–5		1.76	0.26
12–8, 11–7, 10–6		6.84	1.03
9–5, ... 5–1	7–0	0.99	0.22
12–9		1.21	0.25
11–8	8–1	1.30	0.17
10–7		0.31	0.07
9–6		0.37	0.05
8–5		0.37	0.04
7–4		1.03	0.17
6–3, 5–2	6–0	2.79	0.76
4–1		1.04	0.28
3–0	7–1	0.62	0.12
	8–2	0.69	1.19
7–5		0.34	0.17
6–4		0.75	0.15
5–3	5–0	1.04	0.23
4–2	6–1	1.72	0.56
3–1		3.13	0.64
2–0	7–2	3.29	0.63
	8–3	2.41	1.69
6–5	9–4	0.85	0.19
5–4		0.31	0.08
4–3	5–1	0.24	0.19
3–2	6–2	1.15	0.70
2–1		3.07	0.64
1–0	7–3	7.03	2.24
	8–4	2.03	2.29
5–5	9–5	0.57	0.30
4–4		0.64	0.30
3–3	5–2	1.05	0.56
2–2	6–3	0.79	0.25
1–1	7–4	0.96	0.25
0–0	8–5	6.61	2.37

Airco prepurified nitrogen (0.003% O_2) was used without further purification. The N_2^{15} was isotopically 99.7% pure.* Other gases used were the best grade available in tanks. There was spectroscopic evidence for slight mercury contamination when the circulating system was used. The CO probably contained traces of hydrocarbons.

To calibrate the spectral response of the system, the spectrum of an NBS calibrated tungsten filament bulb was repeatedly recorded and its output in quanta per wavelength interval was assumed to be that given by the Planck formula. The relative intensities of bands in the afterglow spectrum were determined by measuring the areas of the peaks on the recorder charts with a radial planimeter and dividing the area by the relative response per quantum at that wavelength, as determined in the calibration. Much difficulty was caused by progressive deterioration of the infrared response of the photomultipliers.

DATA

Band intensities are given in Tables I through IV in arbitrary units proportional to quanta. The first two columns give the vibrational quantum numbers, with the upper state first, of the $B\,^3\Pi_g - A\,^3\Sigma_u^+$ and $Y-$

* We are grateful to Professor T. I. Taylor for providing the N_2^{15}.

TABLE III. Intensities of N_2^{14}+argon afterglow.

	N_2:Ar Pressure, mm Hg Temperature	1:4.5 18 300°K	1:4.6 16 200°K	1:13 35 77°K
$B\,^3\Pi_g - A\,^3\Sigma_u^+$	$Y - B\,^3\Pi_g$			
12–6, 11–5, 10–4		0.04	0.05	...
12–7, 11–6, 10–5		0.94	0.87	0.13
12–8, 11–7, 10–6		4.93	4.29	0.79
9–5, ... 5–1	7–0	1.24	0.77	...
12–9		0.30	0.37	0.23
11–8	8–1	1.62	1.52	0.27
10–7		1.41	0.87	0.11
9–6		0.88	0.35	0.02
8–5		0.63	0.28	0.03
7–4		0.59	0.36	0.05
6–3	6–0	1.10	1.07	0.14
5–2		0.73	0.66	0.18
4–1, 11–9	7–1	0.89	1.33	0.34
3–0		0.31	0.20	0.03
	8–2	0.26	0.73	0.97
7–5		0.21	0.34	0.16
6–4		0.76	0.64	0.10
5–3, 11–10		1.00	0.99	0.24
4–2	6–1	1.60	1.39	0.33
3–1	7–2	2.49	4.02	1.23
2–0		3.60	2.89	0.22
	8–3	0.91	2.04	2.92
6–5, 11–11		0.80	0.69	0.05
5–4		0.50	0.36	...
4–3	5–1	0.77	0.48	0.13
3–2	6–2	1.62	1.69	0.37
2–1	7–3	6.09	8.26	2.15
1–0	8–4	5.46	6.84	4.04
5–5		0.51	0.47	0.14
4–4	4–1	0.85	0.65	0.27
3–3	5–2	1.47	1.47	0.30
2–2	6–3	2.24	2.00	0.27
1–1	7–4	1.85	3.15	1.15
0–0	8–5	12.69	12.85	4.79

$B\,^3\Pi_g$ transitions which are expected to contribute to the measured peak. The half-widths of the peaks were in the range 110 to 160 cm^{-1} and the transitions whose band heads, as reported by Pierce and Gaydon[10] for the First Positive system and by LeBlanc, Tanaka, and Jursa (LBTJ)[7] for the $Y - B\,^3\Pi_g$ system, fell within this interval were assigned to the observed peak. Transitions not listed in the tables are thought to be insignificant. The green ($\Delta v = 5$) and yellow ($\Delta v = 4$) sequences of the $B\,^3\Pi_g - A\,^3\Sigma_u^+$ system were not resolved sufficiently to record separate intensities. The maximum errors in the intensities are estimated to vary from 0.10 unit in the visible part of the spectrum to 0.5 unit of the $B(0) - A(0)$† band. The intensities in the N_2^{15} spectra are somewhat less accurate due to an uncertain calibration of phototube sensitivity. One or two bands were present between 10 500 and 11 000 A but the peaks were too small for intensity measurements.

The effect of foreign gases on relative intensities of the red ($\Delta v = 3$) sequence of the $B\,^3\Pi_g - A\,^3\Sigma_u^+$ system, which is comparatively free of overlaps, is shown in Table V. It should be stressed that these effects were determined by the mole fraction of the added gas, rather than by its partial pressure. In experiments with increasing mole fractions of foreign gases a composition was reached where further additions of foreign gas did not alter the relative band intensities. It is this "fully modified" spectrum which is recorded in Table V for CO, CO_2, Ar, and CH_4. For the other gases listed this limiting intensity distribution could not be observed because of the low afterglow intensity. However it was possible to plot the relative intensities against mole fraction of foreign gas and extrapolate to the fully modified spectrum. This was done for He, NH_3, N_2O, and H_2, the extrapolation for the latter two being quite large. The last column of Table V gives the relative effectiveness of the foreign gas, compared to nitrogen, in modifying the intensity distribution of the red sequence. This was estimated from the mole fractions of foreign gases which gave an intensity distribution halfway between that of pure nitrogen and the fully modified distribution. For gases which had a distribution very similar to nitrogen the relative effectivenesses were estimated by comparing the effects of nitrogen and of foreign gas on the spectrum of a 1:25 N_2:Ar mixture. Other sequences of the $B\,^3\Pi_g - A\,^3\Sigma_u^+$ system originating in high vibrational levels of the

TABLE IV. Intensities of 1:2 N_2^{14}: CO afterglow at 5 mm Hg.[a]

$B\,^3\Pi_g - A\,^3\Sigma_u^+$	$Y - B\,^3\Pi_g$	300°K	200°K
12–7, 11–6, 10–5		1.01	1.39
12–8, 11–7, 10–6		5.21	6.19
9–5, ... 5–1	7–0	0.43	0.47
12–9		0.63	1.09
11–8	8–1	1.45	1.56
10–7		0.76	0.91
9–6		0.40	0.37
8–5		0.30	0.37
7–4		0.38	0.53
6–3, 5–2	6–0	1.26	1.58
4–1, 11–9	7–1	0.46	0.77
3–0		0.15	0.38
	8–2	0.20	0.74
7–5		0.15	0.56
6–4, 5–3, 11–10	5–0	1.36	1.55
4–2	6–1	0.85	1.19
3–1	7–2	1.38	1.74
2–0		0.76	1.09
	8–3	1.01	2.15
6–5, 11–11		0.61	0.91
5–4		0.38	0.53
4–3	5–1	0.31	0.56
3–2	6–2	0.72	0.92
2–1	7–3	1.49	2.30
1–0	8–4	1.14	2.11
5–5		0.36	0.52
4–4	4–1	0.43	0.64
3–3	5–2	0.73	0.87
2–2	6–3	0.70	0.54
1–1	7–4	0.65	0.80
0–0	8–5	0.64	1.00

[a] A weak background of CN bands makes these intensities less accurate than the previous runs.

[10] R. W. B. Pearse and A. G. Gaydon, *The Identification of Molecular Structure* (Chapman and Hall, Ltd., London, 1950).

† This notation indicates the $B\,^3\Pi_g$ ($v = 0$) $- A\,^3\Sigma_u^+$ ($v = 0$) band.

TABLE V. Intensities of the $\Delta v=3$ sequence of the $B\,^3\Pi_g - A\,^3\Sigma_u^+$ system when foreign gases are added in excess at 300°K.

$B\,^3\Pi_g - A\,^3\Sigma_u^+$	Ar	He	H_2	CO_2	CH_4	NH_3	CO	N_2O
12–9	<0.05	<0.05	0.26	0.36	0.33	0.77	0.53	0.36
11–8	0.18	0.20	1.00	1.00	1.00	1.00	1.00	1.00
10–7	0.25	0.65	2.10	0.75	0.85	0.57	0.63	0.77
9–6	0.63	0.98	1.75	0.49	0.59	0.18	0.27	0.63
8–5	1.00	1.00	0.38	0.42	0.41	0.19	0.25	0.37
7–4	0.48	1.03	0.38	0.28	0.53	...	0.30	0.29
6–3	0.28	0.83	0.47	0.31	0.59	...	0.47	0.33
5–2	0.14	0.40	0.35	0.24	0.53	...	0.35	0.25

$B\,^3\Pi_g$ state were modified in the same manner as shown in Table V.

Additions of the foreign gases (except argon and helium) reduced the afterglow intensity more than could be expected on the basis of a simple dilution effect. It has been shown, except for carbon dioxide, that these gases do not react significantly with nitrogen atoms.[10a] Ammonia was most efficient in quenching the light emission and quantitative measurements of this effect on the visible emission are shown in Fig. 1.‡ The bands originating from the lowest vibrational levels of the $B\,^3\Pi_g$ state were quenched more efficiently and according to a different quenching law, as is shown in Fig. 2 for the case of ammonia quenching.

Incomplete resolution of the vibrational structure and extensive overlapping of rotational structure created a difficult problem in assigning intensities of individual bands. This problem was solved by using the careful intensity measurements by Turner and Nicholls[11] of the $B\,^3\Pi_g - A\,^3\Sigma_u^+$ system as excited in a discharge.

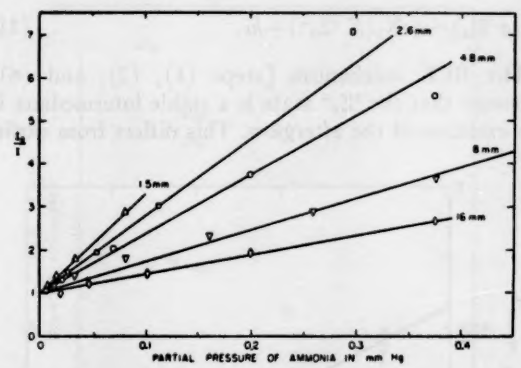

FIG. 1. Quenching of the emission from $B\,^3\Pi_g$ ($v=12$, 11, 10) by ammonia at 300°K and at several pressures of nitrogen indicated in the figure. The runs at 8 mm nitrogen pressure were carried out to $I_0/I=15$ and the solid line shown is drawn using all the points.

Combining the relative intensities of bands originating in a given upper vibrational level of $B\,^3\Pi_g$, as measured by them, with the intensity of a band in the afterglow spectrum which was comparatively free of overlap, it was possible to evaluate the sum of intensities of bands from a given level of $B\,^3\Pi_g$.

It was found that the $Y(8)-B(m)$ progression could be measured nearly free from overlap by $B(n)-A(m)$ bands under certain conditions. Table VI shows the data obtained from the spectrum of a 1:5:1, N_2:Ar:CO mixture at 77°K. By using these relative intensities in combination with the relative intensities of the $B\,^3\Pi_g - A\,^3\Sigma_u^+$ bands as calculated in the foregoing it was also possible to evaluate the intensities of bands originating from a given level of Y. The details of these calculations will be found elsewhere.[12]

We define the population B_n as the sum of the intensities, in units of quanta, of all the bands which originate from the nth vibrational level of $B\,^3\Pi_g$. Likewise Y_m is the sum of intensities of all bands which have $Y(m)$ as their upper state. I_n is defined as the sum of

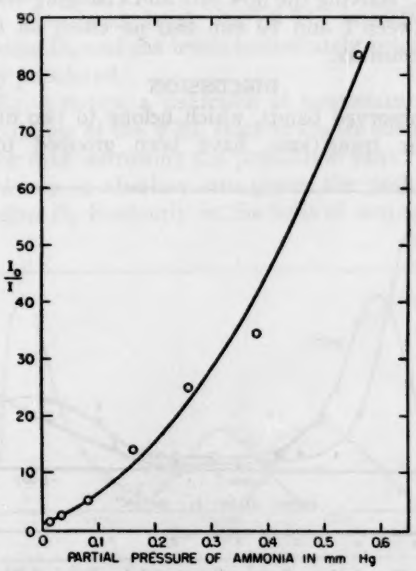

FIG. 2. Quenching of the $B\,^3\Pi_g(O) - A\,^3\Sigma_u^+(O)$ band by ammonia at 300°K. Nitrogen pressure 8 mm Hg.

[10a] G. B. Kistiakowsky and G. G. Volpi, J. Chem. Phys. **27**, 1141 (1957); **28**, 665 (1958); P. A. Gartaganis and C. A. Winkler, Can. J. Chem. **34**, 1457 (1956).

‡ A similar run reported by Kistiakowsky and Volpi[10a] quantitatively disagrees with the foregoing runs. This is probably because of their indirect measurement of ammonia concentration by ion current intensity.

[11] R. G. Turner and R. W. Nicholls, Can. J. Phys. **32**, 468 (1954).

[12] K. D. Bayes, thesis, Harvard University, 1959.

TABLE VI. Relative intensities of the bands originating from the 8th vibrational level of Y.

$Y(m)-B\,^3\Pi_g(n)$:	8–1	8–2	8–3	8–4	8–5
Intensity:	0.07	0.98	2.63	2.35	0.77

intensities of all the $Y-B\,^3\Pi_g$ bands which have the nth vibrational level of $B\,^3\Pi_g$ as their lower state.

It was previously discovered[6] that when B_n is plotted against the energy of the levels below the dissociation limit D_e a smooth curve can be fitted to the populations of both isotopes. This is shown in Fig. 3 for pure nitrogen at room temperature and liquid nitrogen temperature. It will be noted that the main population peak is narrower and its maximum is shifted to higher energy for the lower temperature. The shift of the energy of the peak maximum with temperature is shown in Fig. 4. The limits shown in the figure are maximum possible errors. The line extrapolates at 0°K to 850 cm^{-1} below D_e, the extremes being 1100 and 700 cm^{-1}.

The population curves for spectra which have been completely modified by a foreign gas are shown in Fig. 5. The curve for N_2O was identical with that shown for CO_2 and the CH_4 curve is similar except for a larger rise at low $B(n)$. The curve for He is of the same shape as the argon curve but its maximum is shifted to slightly lower energies. Figure 6 shows that there is a definite correlation between the effectiveness of a gas and the population which it produces.

The complete population analyses of three spectra are shown in Figs. 7 to 9. The B_n's are indicated by circles. The I_n's are shown as triangles and represent the contribution of $Y-B\,^3\Pi_g$ bands to the populations B_n. Halving the flow rate and changing the pressure between 1 and 10 mm had no effect on the relative intensities.

DISCUSSION

The observed bands, which belong to two different electronic transitions, have been grouped together according to their response to changing conditions. The Morse potential energy curves of the electronic states of nitrogen which are thought to be involved in the afterglow are shown in Fig. 10 and each group of bands is indicated by a single vertical arrow.

As a basis for the discussion we expand the mechanism proposed by BCK[4]:

$$N(^4S)+N(^4S)+M \underset{k_{-1}}{\overset{k_1}{\rightleftharpoons}} N_2(^5\Sigma_g^+)+M \quad (1)$$

$$N_2(^5\Sigma_g^+)+M \xrightarrow{k_2} N_2(B\,^3\Pi_g, v=12, 11, 10)+M \quad (2)$$

$$\longrightarrow N_2(Y\,^3\Sigma_u^-, v=8, 7, 6)+M \quad (3)$$

$$\longrightarrow N_2(^3\Delta_u)+M \quad (4)$$

$$\longrightarrow N_2(a\,^1\Pi_g)+M \quad (5)$$

$$N_2(B\,^3\Pi_g, v=12, 11, 10) \longrightarrow N_2(A\,^3\Sigma_u^+, v=8, 7, 6)+h\nu \text{ (group 1)} \quad (6)$$

$$N_2(Y\,^3\Sigma_u^-, v=8, 7, 6) \longrightarrow N_2(B\,^3\Pi_g, v=4, 3, 2)+h\nu \text{(group 2)} \quad (7)$$

$$N_2(B^3\Pi_g, v=4, 3, 2) \longrightarrow N_2(A\,^3\Sigma_u^+, v=2, 1, 0)+h\nu \text{ (group 3a)} \quad (8)$$

$$N_2(^3\Delta_u) \longrightarrow N_2(B\,^3\Pi_g, v=7, 6, 5)+h\nu \quad (9)$$

$$N_2(B\,^3\Pi_g, v=7, 6, 5) \longrightarrow N_2(A\,^3\Sigma_u^+, v=4, 3, 2)+h\nu \text{ (group 4)} \quad (10)$$

$$N_2(a\,^1\Pi_g) \longrightarrow N_2(X\,^1\Sigma_g^+)+h\nu. \quad (11)$$

The BCK mechanism [steps (1), (2), and (6)] proposes that the $^5\Sigma_g^+$ state is a stable intermediate in the emission of the afterglow. This differs from earlier

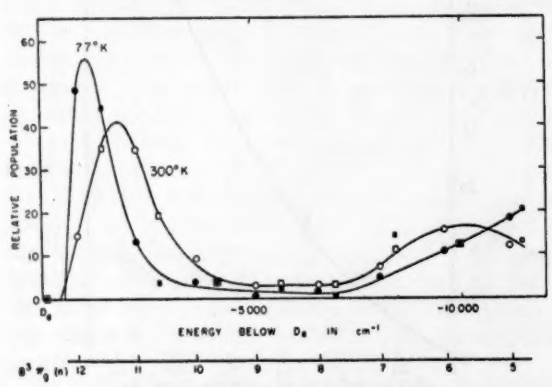

FIG. 3. Population of the vibrational levels of $B\,^3\Pi_g$ in the afterglow. For each isotope the sum B_5 to B_{12} is normalized to 100. N_2^{14} data are indicated by circles, N_2^{15} data by squares. The vibrational numbering on the abscissa is for N_2^{14}. Open symbols are for 4 mm Hg at 300°K. Solid symbols are for 2:1 Ar:N_2 mixtures at 12 mm Hg and 77°K.

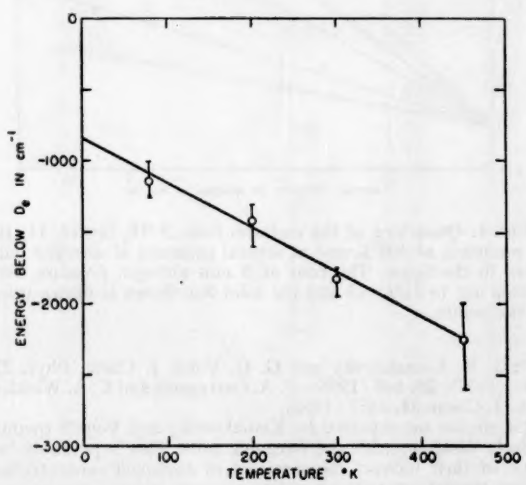

FIG. 4. The shift of the maximum of the $B\,^3\Pi_g$ (12, 11, 10) population curve with temperature.

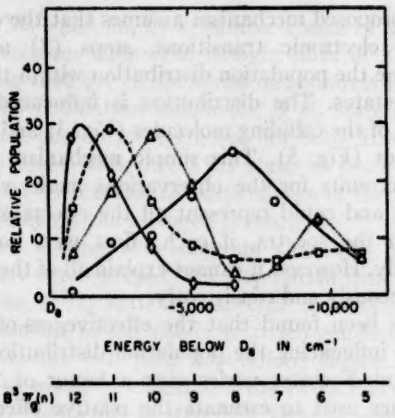

FIG. 5. The $B\,^3\Pi_g$ population curves in presence of excess of foreign gases; diamonds: ammonia; squares: carbon dioxide; triangles: hydrogen; circles: argon.

proposals[13] in that the $^5\Sigma_g^+$ molecule is supposed to undergo many collisions during its lifetime and a near equilibrium between ground state atoms N(^4S) and the $^5\Sigma_g^+$ molecules is established. A separate step, involving a collision-induced radiationless transition (2), forms $B\,^3\Pi_g$ molecules primarily in the $v=12$, 11 and 10 levels, which then emit the group 1 bands.

A collision-induced radiationless transition into the Y state, competitive with step (2), explains the emission of the group 2 bands. The process forming Y state molecules in the 8, 7, and 6 levels must be analogous to the process forming the $B\,^3\Pi_g$ state molecules in

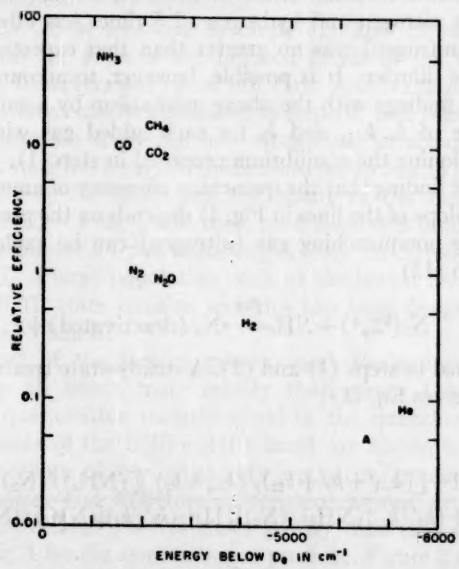

FIG. 6. The relative effectiveness of various gases in influencing the $B\,^3\Pi_g$ population curve plotted against the position of the maximum of the fully modified population curve.

[13] A. G. Gaydon, *Dissociation Energies* (Chapman and Hall, Ltd., London, 1947); G. Cario and L. H. Reinecke, Abhandl. braunschweig. wiss. Ges. 1, 8 (1949).

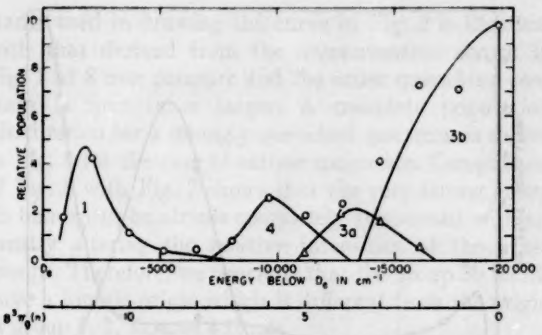

FIG. 7. Population of the vibrational levels of $B\,^3\Pi_g$ for N_2^{14} at 4 mm Hg and 300°K. Circles represent B_n, the total emission from $B\,^3\Pi_g$ ($v=n$); triangles are I_n, the sum of $Y-B\,^3\Pi_g$ bands which fall into $B\,^3\Pi_g$ (n). The lines are drawn to indicate different band groups.

the 12, 11 and 10 levels. A decrease in temperature narrows the population curve of the Y state and shifts it to higher energies as can be seen in Table VII. The analysis of the spectrum of a 24:1 argon to nitrogen mixture shows a broadening of the population curve of the Y state, comparable with that shown for the $B\,^3\Pi_g$ state in Fig. 5. Also the cutoff in the population of vibrational levels of Y and $B\,^3\Pi_g$ occurs at the same energy.

An important finding is that the vibrational levels of the $B\,^3\Pi_g$ and Y states which lie just below the dissociation energy of the nitrogen molecule ($D_e=79\,900$ cm^{-1}) are virtually unpopulated. This is true of N_2^{15} [B $^3\Pi_g$ ($v=13$)], 120 cm^{-1} below D_e, and N_2^{14} [$Y(v=9)$], 240 cm^{-1} below, while the population of N_2^{15}[$Y(v=9)$], 650 cm^{-1} below, is barely detectable, being at the most 0.05 of that of N_2^{15} [$Y(v=8)$], even at 77°K. The next highest vibrational level, N_2^{14}[$B\,^3\Pi_g$ ($v=12$)], 860 cm^{-1} below D_e, and the levels immediately below it are strongly populated.

As Fig. 4 shows, a reduction of temperature shifts the population of the $B\,^3\Pi_g$ state to higher energies (at the same time narrowing the population peak) and an extrapolation to absolute zero places the peak at 850 cm^{-1} below D_e. Evidently, in the limit of zero tempera-

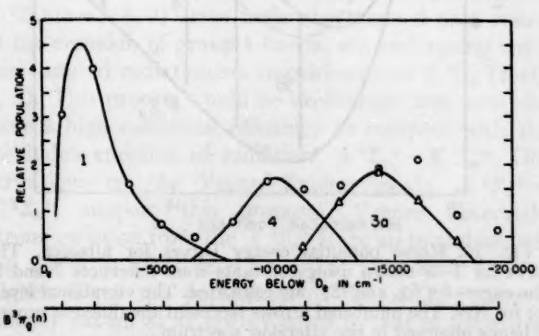

FIG. 8. Population of the vibrational levels of $B\,^3\Pi_g$ for N_2^{14}: CO=2:1 at 6 mm Hg and 300°K. Circles represent B_n, the total emission from $B\,^3\Pi_g(n)$; triangles: I_n, the sum of $Y-B\,^3\Pi_g$ bands which fall into $B\,^3\Pi_g$ (n).

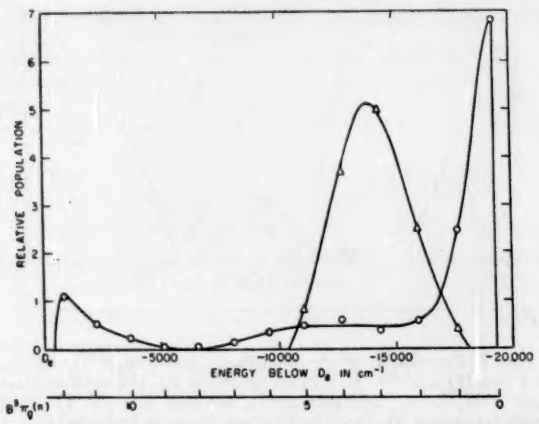

FIG. 9. Population of the vibrational levels of $B\,^3\Pi_g$ for N_2^{14}: Ar=1:3 at 35 mm Hg and 77°K. Circles represent B_n, the total emission from $B\,^3\Pi_g(n)$; triangles: I_n, the sum of $Y-B\,^3\Pi_g$ bands which fall into $B\,^3\Pi_g$ (n).

ture, and hence soft molecular collisions, the $B\,^3\Pi_g$ molecules would be uniformly formed with an energy of about 850 cm^{-1} less than the energy of two recombining atoms.

These findings suggest that the $^5\Sigma_g^+$ state has a dissociation energy of about 850 cm^{-1}. This is somewhat larger than the estimates made from predissociations, 350 cm^{-1} from $B\,^3\Pi_g$ and 100 cm^{-1} from $a\,^1\Pi_g$.[14] The direct spectroscopic evidence for the $^5\Sigma_g^+$ state[15] has been discredited.[16]

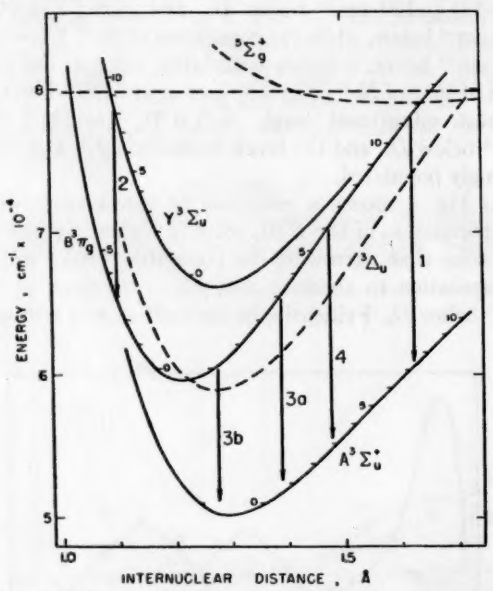

FIG. 10. Morse potential energy curves for nitrogen. The curve for Y is drawn using constants from references 7 and 8. The curves for $^3\Delta_u$ and $^5\Sigma_g^+$ are estimated. The vibrational levels are for N_2^{14}. The numbered arrows represent the different groups of bands observed in the afterglow spectrum.

[14] A. E. Douglas and G. Herzberg, Can. J. Phys. **29**, 294 (1951).
[15] C. M. Herzfeld and H. P. Broida, Phys. Rev. **101**, 606 (1956); A. M. Bass and H. P. Broida, *ibid.* **101**, 1740 (1956).
[16] M. Peyron and H. P. Broida, J. Chem. Phys. **30**, 139 (1959).

The proposed mechanism assumes that the collision-induced electronic transitions, steps (2) and (3), determine the population distribution within the $B\,^3\Pi_g$ and Y states. The distribution is influenced by the energies of the colliding molecules (Fig. 3) and by their properties (Fig. 5). This simple mechanism satisfactorily accounts for the observations made with pure nitrogen and could represent all the effects of foreign gases on the spectra, if each effect were considered separately. However it cannot explain all of the findings simultaneously and consistently.

It has been found that the effectiveness of various gases in influencing the population distribution in the $B\,^3\Pi_g$ and Y states varies over a factor of 10^3. The techniques used to estimate the relative effectiveness are not very accurate but the range of effectiveness is certainly not less than 10^2. However, the rate of light emission does not vary over a large range for gases of different effectiveness. Even though argon is 20 times less effective than nitrogen in influencing the population of the $B\,^3\Pi_g$ and Y states, BCK found no suggestion of a decrease of the ratio (afterglow intensity)/$(N)^2$ as the mole fraction of argon was increased.§ The

TABLE VII. Ratio of the total emission from the 8th and the 7th vibrational levels of Y.

Spectrum	N_2^{14} 300°K	N_2^{14} 200°K	N_2^{14} 100°K	N_2^{15} 300°K	N_2^{15} 200°K
Y_8/Y_7	1.04	1.35	1.60	1.87	>10

decrease in emission which we observed for mixtures of active nitrogen and hydrogen (2.5 times less effective than nitrogen) was no greater than that expected for simple dilution. It is possible, however, to account for these findings with the above mechanism by a suitable choice of k_1, k_{-1}, and k_2 for each added gas without abandoning the equilibrium proposed in step (1).

The finding that the quenching efficiency of ammonia (the slope of the lines in Fig. 1) depends on the pressure of the nonquenching gas (nitrogen) can be explained if step (12)

$$N_2(^5\Sigma_g^+)+NH_3 \xrightarrow{k_{12}} N_2 \text{ (deactivated)}+? \quad (12)$$

is added to steps (1) and (2). A steady-state treatment then gives Eq. (1);

$$I_0/I = \frac{\{1+[(k_{-1}'+k_2'+k_{12})/(k_{-1}+k_2)][(NH_3)/(N_2)]\}}{\{1+(k_2'/k_2)[(NH_3)/(N_2)]\}\{1+(k_1'/k_1)[(NH_3)/(N_2)]\}} \quad (1)$$

where I and I_0 are the light intensity with and without added ammonia, the rate constants are defined in the foregoing and the primes refer to the added gas, am-

§ The gradual increase in $I/(N)^2$ noted by BCK for decreasing afterglow intensity could be attributed to stray radiation.

monia. This equation, by a suitable choice of rate constants, describes either the straight lines of Fig. 1 or the finding that the effectiveness of ammonia in determining the population within the $B\,^3\Pi_g$ state is much higher than that of nitrogen, but not both. Having the ammonia react with the $B\,^3\Pi_g$ state in place of step (12) would not explain the dependence of the quenching efficiency on the nitrogen pressure.

Another finding also suggests that the proposed mechanism is too simple. The population distributions within the $B\,^3\Pi_g$ state for spectra of varying mole fractions of an added gas in nitrogen are not simply additive in the two pure populations shown in Figs. 3 and 5, as would be expected if the two kinds of molecules were competing in step (2). Thus in some argon-nitrogen mixtures the emission from the 10th and 9th levels of the $B\,^3\Pi_g$ state is a greater percentage of the total emission from $B\,^3\Pi_g$ ($v \geq 5$) than either in pure nitrogen or in argon with a vanishingly small mole fraction of nitrogen.

We conclude, therefore, that the event or events which determine the population distribution within the $B\,^3\Pi_g$ and Y states are not simply steps (2) and (3). It is possible to construct mechanisms similar to the one presented which do account for all the observed facts[11] but they will not be discussed here because of the lack of independent evidence for the necessary additional steps. It would appear that further progress in elucidating the initial steps of the afterglow mechanism requires experiments in which the atomic concentration and the intensities in the afterglow spectrum are simultaneously measured.

Step (3) is followed by steps (7) and (8) which account for some of the infrared bands of the afterglow. However, not all of the First Positive bands in the infrared can be attributed to step (8) and therefore the emission from the low vibrational levels of the $B\,^3\Pi_g$ state has been subdivided into group 3a and group 3b. Group 3a bands are the result of the cascade, $Y \rightarrow B\,^3\Pi_g \rightarrow A\,^3\Sigma_u^+$, and their contribution is indicated by the sums I_n. Upon deducting I_n from the corresponding B_n, a large population peak at the lowest levels of the $B\,^3\Pi_g$ state remains and this has been designated group 3b bands.

Most of the foreign gases quench the emission of group 3b bands more readily than group 1 bands. The quantitative measurements of the quenching by ammonia of the $B(0)-A(0)$ band are shown in Fig. 2. The slope of the line at very low partial pressures of ammonia, and therefore at constant atomic nitrogen concentration[10a], is five times greater than that shown in Fig. 1 for the same nitrogen pressure. Figure 2 shows an upward curvature, in contrast to the quenching of group 1 bands seen in Fig. 1, which can be fitted to an equation that is quadratic in ammonia pressure. Kinetically this could be interpreted as the reaction between ammonia and two consecutive precursors of the emission of radiation. One of the quenching constants used in drawing the curve in Fig. 2 is identical with that derived from the measurements shown in Fig. 1 at 8 mm pressure and the other quenching constant is four times larger. A complete population distribution for a strongly quenched spectrum is shown in Fig. 8 for the case of carbon monoxide. Comparison of Fig. 8 with Fig. 7 shows that the very strong group 3b bands can be almost completely suppressed without greatly altering the relative intensities of the other groups. Therefore, we conclude that the group 3b bands have a kinetic origin which is different from the origin of group 1, 2, 3a, and 4 bands.

The strong emission from the lowest vibrational levels of the $B\,^3\Pi_g$ state is not caused by the vibrational relaxation of molecules initially formed in higher vibrational levels of $B\,^3\Pi_g$. The relative intensities of the pure nitrogen afterglow are not altered, within the accuracy of these measurements, between the pressures of 1 and 10 mm Hg.

However, vibrational relaxation of molecules in the $B\,^3\Pi_g$ state can be observed under conditions of very high collisional frequency and is undoubtedly important in the spectrum of LBTJ[7] in which the $Y-B\,^3\Pi_g$ bands are virtually free from overlapping $B\,^3\Pi_g-A\,^3\Sigma_u^+$ bands. The analysis of a spectrum taken under conditions similar to those used by LBTJ is shown in Fig. 9. Vibrational relaxation has slightly skewed the group 1 peak and has shifted the 3a band emission to the lowest levels [the radiative lifetime of $B\,^3\Pi_g$ (low) is roughly five times greater than the lifetime of $B\,^3\Pi_g$ (12, 11, 10) because of the factor ν^3 in the Einstein radiation law]. Group 2, and hence 3a, bands are much stronger than group 1 bands in Fig. 9 because the low temperature and the added argon both favor population of the Y state over population of the $B\,^3\Pi_g$ state. For this spectrum the sum of low B_n's (12.8) is equal within experimental error to the sum of I_m's (14.3): the absence of 3b bands can probably be attributed to the quenching by the impurities present in the large excess of argon used.

A possible kinetic explanation of the group 3b bands, which is consistent with the quenching data, is that the $A\,^3\Sigma_u^+(v=7, 8, 9)$ state molecules, formed as a result of the emission of group 1 bands, are undergoing collision-induced radiationless transitions into $B\,^3\Pi_g$ ($v=0$, 1, 2). This process would be exothermic and need not have a high collisional efficiency to compete with the forbidden emission of radiation, $A\,^3\Sigma_u^+-X\,^1\Sigma_g^+$. Observations on the Vegard-Kaplan bands, $A\,^3\Sigma_u^+-X\,^1\Sigma_g^+$, support this proposal. Vegard observed[17] strong emission from the $A\,^3\Sigma_u^+$ state up to and including the sixth vibrational level, but none from $v=7$ or higher. Thus the population of the $A\,^3\Sigma_u^+$ state is sharply cut off at an energy equal to that of the lowest vibrational level of the $B\,^3\Pi_g$ state. Kaplan[18] found that

[17] L. Vegard, Z. Physik **75**, 30, 44 (1932).
[18] J. Kaplan, Phys. Rev. **54**, 176 (1938).

the emission from the $A\ ^3\Sigma_u^+$ state is suppressed by even trace impurities in nitrogen, indicating that the electronic energy of the $A\ ^3\Sigma_u^+$ state is readily quenched. Unfavorable for this proposed source of group 3b bands is the fact that the intensity of group 1 bands is insufficient, by at least a factor of three, to account for the total intensity of the 3b bands.

An additional source of group 3b bands could be molecules in $A\ ^3\Sigma_u^+(v=7$ and higher) which are formed directly from ground state nitrogen atoms in triple collisions and are then converted into the lowest levels of the $B\ ^3\Pi_g$ state either by the emission of low frequency radiation or by collisions. These conversion processes would be in competition with the step-wise vibrational relaxation of the $A\ ^3\Sigma_u^+$ state, which would be very efficient for the vibrational levels near the dissociation limit,[19] but would become slower as the spacing of the levels increases. Because of the Frank-Condon principle it is expected that the transitions into the low levels of $B\ ^3\Pi_g$ would become more probable as the $A\ ^3\Sigma_u^+$ molecules relax vibrationally. Thus the quenching of the electronic energy of the $A\ ^3\Sigma_u^+$ molecules could result in the curved plot seen in Fig. 2. It must be admitted, however, that this is only a speculation and that the kinetic origin of bands of group 3b remains uncertain.

A combination of Mulliken's considerations on the nature of his predicted $^3\Sigma_u^-$ and $^3\Delta_u$ states,[20] with the identification of the Y state as $^3\Sigma_u^-$,[21] leads us to place the potential energy curve of the $^3\Delta_u$ state as indicated in Fig. 10. It intersects the curve of the $^5\Sigma_g^+$ state and could be populated by collision-induced radiationless transitions, as indicated by step (4). There would follow the only optically allowed transition, $^3\Delta_u - B\ ^3\Pi_g$, and steps (4) and (9) may be responsible for the population peak centered on $v=6$ of the $B\ ^3\Pi_g$ state. The similar shape of this population peak and that of the population peak formed by the emission of $Y - B\ ^3\Pi_g$ bands (compare in Fig. 8 the I_n curve with the population peak centered on $v=6$) supports this suggestion. The bands comprising this $^3\Delta_u - B\ ^3\Pi_g$ transition would lie too far in the infrared to be detectable by the photomultiplier and hence further experiments are needed to test this hypothesis. Another possible source of the population peak centered on $v=6$, a direct collision-induced radiationless transition from the $^5\Sigma_u^+$ state, does not seem plausible, because for pure nitrogen at lower pressures and low temperature the population of $v=9$ and 8 of the $B\ ^3\Pi_g$ state is virtually zero and yet the $v=6$ population peak remains present.

Qualitatively it has been found that the total emission from the Y state is increased and the emission from the $^3\Delta_u$ state (i.e., the importance of the $B\ ^3\Pi_g$ ($v=7, 6, 5$) population peak) is decreased relative to the emission of the group 1 bands as the temperature is lowered.

Step (5) has been included in the mechanism to account for the weak $a\ ^1\Pi_g - X\ ^1\Sigma_g^+$ emission, step (11), which has been observed in the afterglow.[22]

Summing up, we have quantitatively determined the contribution of the various emissions in the afterglow spectra and have attempted to show that parallel and consecutive processes involving the $^5\Sigma_g^+$ state account for much of the observed spectrum. A source of the remaining afterglow emission has been proposed.

The authors acknowledge the financial assistance of the Mallinckrodt Chemical Company in the purchase of research supplies and thank Professor W. Klemperer and Professor O. Oldenberg for the loan of equipment. Thanks are also due to Dr. LeBlanc, Dr. Tanaka, Dr. Jursa, Dr. Broida, and Professor Wilkinson for preprints of their publications. One of us (KDB) thanks the Standard Oil Foundation and the Monsanto Chemical Company for financial support.

[19] R. N. Schwartz and K. F. Herzfeld, J. Chem. Phys. **22**, 767 (1954).

[20] M. Zelikoff, *Threshold of Space* (Pergamon Press, New York, 1957), p. 169.

[21] P. G. Wilkinson (to be published).

[22] Tanaka, Jursa, and LeBlanc in reference 20, p. 89.

Mechanics of Atomic Recombination Reactions*

DON L. BUNKER

Los Alamos Scientific Laboratory, University of California, Los Alamos, New Mexico

(Received August 3, 1959)

A treatment is developed by means of which it is possible to calculate an equilibrium constant for the formation of a collision complex from a pair of chemically interacting atoms. For iodine atoms, this leads to a value of the rate constant for $I+I+M \rightarrow I_2+M$, if the mechanism is $2I \rightleftharpoons I_2^*(^1\Sigma)$, $I_2^*+M \rightarrow I_2+M$. The rate constant so calculated agrees with that obtained by a statistical procedure [J. Keck, J. Chem. Phys. **29**, 410 (1958)].

The calculation also furnishes enough information about the mechanical details of collisions so that the contribution of molecular states other than $^1\Sigma$ to recombination may be deduced. As a result a fairly conclusive discussion may be given of the plausibility of the various detailed mechanisms thus far suggested. A most likely mechanism and a possible calculation based on it are proposed.

INTRODUCTION

IN the study of homogeneous gas-phase atomic recombination reactions,

$$X+X+M \rightarrow X_2+M, \tag{1}$$

the sequence of elementary steps

$$X+X \rightleftharpoons X_2^*, \tag{2a}$$

$$X_2^*+M \rightarrow X_2+M, \tag{2b}$$

immediately suggests itself as a probable mechanism. It is found, however, that simple calculations based on this model (e.g., taking the lifetime of X_2^* equal to the vibration period of X_2, and assuming the third body M to be a hard sphere) lead to results inconsistent with the measured rates of these reactions.

Recently Keck[1] has advanced a theoretical treatment with which it is possible to make a much more sophisticated study of this mechanism. His approach is of a statistical nature; the mechanics of formation of a three-body complex is assumed to be fairly unimportant, and attention is focused instead on the relative probabilities of decomposition of this complex into various possible sets of products. This perfectly general procedure may be specialized for any particular mechanism by specifying the interactions between X, X, and M.

The alternate mechanism

$$X+M \rightleftharpoons XM \tag{3a}$$

$$XM+X \rightarrow X_2+M \tag{3b}$$

also has been invoked,[2] with some success, in order to explain some of the observed features of recombination reactions. This paper presents the results of a treatment of mechanism (2), based on mechanics, of a precision comparable to that obtained in the theoretical treatment of mechanism (3). The objectives of this study were (a) to provide a nonstatistical test of Keck's theory as applied to mechanism (2); (b) to elucidate the mechanical details of this type of process; (c) to draw conclusions, if possible, about the relative merits of mechanisms (2) and (3).

The specific reaction which will be considered is the recombination of iodine atoms in the presence of, usually, argon.[3] This much-studied system has already been interpreted in terms of both the treatments cited above. In both our and Keck's treatments of mechanism (2) argon is regarded as a hard sphere.

DETAILS OF THE CALCULATION

For either mechanism the rate constant for the overall reaction (1) is given by

$$k=PZK, \tag{4}$$

where K is a pseudo-equilibrium constant for reaction (2a) or (3a), and P and Z are the probability factor and collision number for reaction (2b) or (3b). In the present case we want to calculate K for reaction (2a).[4]

A collision between two atoms is to be described in plane polar center-of-mass coordinates. If the interaction potential V is central and μ is the reduced mass,

$$\mu -\mu r\dot{\theta}^2+\mathrm{d}V/\mathrm{d}r=0. \tag{5}$$

To describe a collision we employ the impact parameter b and the incident kinetic energy E. The relations between these and the angular momentum L and the incident relative velocity v are: $L=\mu r^2\dot{\theta}$; $b=L/\mu v$; $E=\frac{1}{2}\mu v^2$. Substituting these in (5) and integrating once, we get

$$\tfrac{1}{2}\mu\dot{r}^2=E(1-b^2/r^2)-V \tag{6}$$

if the zero of V is chosen to correspond to dissociation. Equation (6) describes the behavior of the separation

* This work was sponsored by the U. S. Atomic Energy Commission.

[1] J. Keck, J. Chem. Phys. **29**, 410 (1958).

[2] D. L. Bunker and N. Davidson, J. Am. Chem. Soc. **80**, 5090 (1958).

[3] These data have been summarized by D. L. Bunker and N. Davidson, J. Am. Chem. Soc. **80**, 5085 (1958).

[4] A more complete description of the mathematical procedure is available in Report LA-2295 (unclassified), Los Alamos Scientific Laboratory, Los Alamos, New Mexico, July 2, 1959.

coordinate r during the collision specified by E and b; we can find the time required to cover the portion of the trajectory between any two values of r by means of

$$t=(\mu/2)^{\frac{1}{2}}\int_{r_1}^{r_2}[E(1-b^2/r^2)-V]^{-\frac{1}{2}}\mathrm{d}r.$$

We obtain K by integrating the product of the collision number and the complex lifetime, for reaction (2a), over all values of b and E:

$$K=\int_0^\infty\int_0^{b_{\max}}Z(E,b)\tau(E,b)\,\mathrm{d}b\mathrm{d}E. \tag{8}$$

Here $b_{\max}$ is a naturally arising upper limit to b and will be discussed shortly. Equation (8) can be rearranged to

$$K=\int_0^\infty Z(b_{\max})n(E)\tau(E)\,\mathrm{d}E. \tag{9}$$

In this expression $Z(b_{\max})$ is a collision number whose cross-section term is $b_{\max}^2$, $n(E)$ is a normalized Maxwell-Boltzmann distribution function $(E/k^2T^2)\exp-E/kT$, and $\tau(E)$ is the average lifetime of X_2^* when the incident energy is E;

$$\tau(E)=(2\mu)^{\frac{1}{2}}b_{\max}^{-2}\int_0^{b_{\max}}b\oint[E(1-b^2/r^2)-V]^{-\frac{1}{2}}\mathrm{d}r\mathrm{d}b. \tag{10}$$

In (10) the inner integral covers the portion of the trajectory beginning and ending at the value of r (called $r_{\max}$) at which we say the collision starts. This quantity, like $b_{\max}$, arises in a natural way.

To illustrate the origin of $b_{\max}$ and $r_{\max}$, let us take $V=-4\epsilon_0(\sigma/r)^6$, the attractive part of a Lennard-Jones potential. For each E in the inner integrand of (10) there will then be a value of b sufficiently large that the integrand becomes imaginary over a range of r, which therefore cannot be crossed. This is the way in which the "rotation barrier" appears in this formulation. We propose to let $b_{\max}$ be the maximum b for which the barrier is crossed ($b_{\max}$ is then about the size of a collision diameter); similarly, $r_{\max}$ is the location of the barrier. For this potential,

$$b_{\max}=3^{\frac{1}{2}}\sigma(\epsilon_0/E)^{1/6};\quad r_{\max}(\text{for } b=b_{\max})=(\tfrac{2}{3})^{\frac{1}{2}}b_{\max}. \tag{11}$$

Here $r_{\max}$ increases slowly with decreasing b and becomes infinite for $b=0$. Therefore, in carrying out the calculation for this potential, we adopt two conventions which later prove unnecessary. V is cut off at an arbitrary large value of $r(=\rho')$ to prevent interactions at absurdly great distances, and also at an arbitrary small value $(=\rho)$ because $V\to-\infty$ as $r\to0$. An evaluation of $\tau(E)$ was made[5] as a function of ρ and ρ'. It was found that the results for $(\rho/r_{\max})=0.85$, $(\rho'/r_{\max})=1.24$, with $r_{\max}$ defined as in Eq. (11), were half as large as for $\rho=0$, $\rho'=\infty$. Thus one might as well adopt the latter values, in which case

$$\tau(E)=1.50\sigma\mu^{\frac{1}{2}}\epsilon_0^{1/6}E^{-\frac{1}{2}}. \tag{12}$$

The integration over the Maxwell-Boltzmann distribution, Eq. (9), then yields

$$K=\tfrac{8}{3}(2\pi)^{\frac{1}{2}}\sigma^3(\epsilon_0/kT)^{\frac{1}{2}}. \tag{13}$$

It remains to be determined how good an approximation was this choice of V. The easiest way to do this is to repeat the calculation with a more accurate potential function, which need not appear simple except to the 704. The function used was

$$V=\alpha D_e\left\{\exp[-2\beta(r-r_e)]-2\frac{\exp[-\beta(r-r_e)]}{[1+(r-r_e)^2]^n}\right\}+4\epsilon_0'[(\sigma'/r)^m-(\sigma'/r)^6]. \tag{14}$$

In (14) the first term is a Morse function, multiplied by a constant (α), and with its attractive part divided by a quantity which makes it approach zero more rapidly. The second term grafts an inverse-sixth "tail" onto the potential. The terms ϵ_0', σ', and m are chosen by imposing the following three conditions: (1) and (2), that the first and second terms have coincident zeros and minima, and (3), that $\epsilon_0'\sigma'^6=\epsilon_0\sigma^6$. (For X=I, we take $\epsilon_0^{\mathrm{I}}=\epsilon_0^{\mathrm{X}_e}$ and $\sigma^{\mathrm{I}}=\sigma^{\mathrm{X}_e}$.) Next α is selected to give the correct dissociation energy. The remaining parameter n regulates the separation at which the transition from Morse to r^{-6} behavior occurs. A determination of n was made by calculating the energy E_{50} of the 50th vibrational level of I_2, using all available anharmonicity constants,[6] and requiring that

$$\oint[2\mu(E_{50}-V)]^{\frac{1}{2}}\,\mathrm{d}r=50.5h, \tag{15}$$

where h is Planck's constant and the integration is over one cycle of motion.[7] For the purposes of our calculation, the following parameters adequately describe I_2: $m=9$, $n=1$, $\alpha=0.784$, $\sigma'=2.29$ A, and $\epsilon_0'=0.573$ ev.

When K is recalculated using the V of Eq. (14), the results are about half as large as given by (13), and the temperature dependence is altered slightly. The reason for the comparatively small difference between these two results is that the rotation barrier most often occurs at an r such that the r^{-6} potential is a somewhat better approximation than the Morse function. The results of the more elaborate computation were adopted as final, and k for X=I, M=argon calculated according to (4) with $P=1$. In the Z of Eq.

[5] All numerical calculations reported were programmed for an IBM 704 computer.

[6] G. Herzberg, *Molecular Spectra and Molecular Structure. I. Spectra of Diatomic Molecules* (D. Van Nostrand Company, Inc., Princeton, New Jersey, 1950), pp. 540–541.

[7] This is a modification of the semiclassical method of Klein and Rydberg; cf. R. Rydberg, Z. Physik **73**, 376 (1932).

(4), the cross-section term was $\frac{1}{4}(\sigma_M+\bar{r}_{max})^2$, where $\bar{r}_{max}$ is the r_{max} for $E=kT$. This is commensurate with the assumptions made in the treatments of mechanism (3); it is possible that the cross-section estimates are somewhat small in both cases.

Thus far the false assumption has been made that *all collisions occur along the* $^1\Sigma$ *potential curve to which* (14) *applies*. If we wish to consider only the process $I(^2P_{\frac{1}{2}})+I(^2P_{\frac{1}{2}})\rightleftarrows I_2^*(^1\Sigma)$, we must now introduce into K an electronic degeneracy factor, $g=\frac{1}{16}$. More remains to be said about g (see discussion); however, for display purposes (Fig. 1), this factor has been included.

DISCUSSION

It is necessary to admit in advance that our lack of knowledge about the quantity P in Eq. (4) limits our ability to determine the exact course of events in a recombination reaction. P represents the probability per collision that reaction (2b) or (3b) occurs; it arises partly from geometry and partly from quantum-mechanical transition probabilities. So long as a calculated result can be made to match the observed rate constants, by assigning to P an appropriate variation with T and/or M, the mechanism on which the calculation is based cannot be eliminated. Only if a mechanism requires $P>1$ can it be discarded.

Let us first compare our results for X = I, M = Ar with those of Keck. Both are shown in Fig. 1 (with $g=\frac{1}{16}$), along with the experimental results. Within its precision, our result is an upper limit to Keck's, as is his to the observed rate constant. This is expected, since we take $P=1$, whereas Keck's treatment (which assumes transitions are sufficiently rapid that there is a uniform density of representative points in the region of phase space corresponding to the three-body complex) takes account of the geometrical part of P only. If one also expects that the quantum-mechanical part of P decreases with increasing T, the conclusion is that the appearance of Fig. 1 is exactly as it should be if Keck's

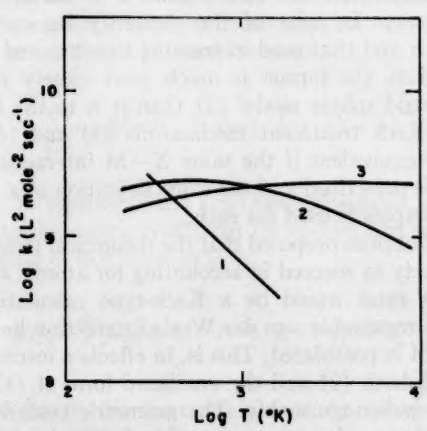

FIG. 1. Log$k$ (I+I+Ar→I_2+Ar) *vs* log$T$. Curve 1, experimental (reference 3); curve 2, Keck's results (reference 1); curve 3, calculation described in this paper.

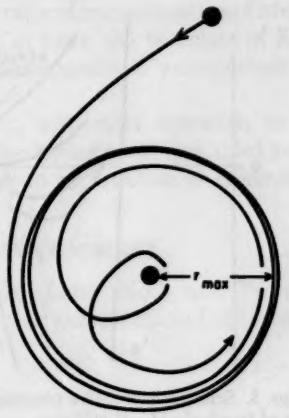

FIG. 2. Schematic trajectory for most important type of two-body (X—X) collision.

postulates about the relative unimportance of detailed mechanics are reasonable.

On the other hand, the closeness of all three curves at ordinary temperatures indicates P for argon is nearly unity. A property of mechanisms such as (2), in which M is a rigid sphere, is that all M are about equally efficient except for variations in P. Therefore, neither our nor Keck's treatment of this mechanism can explain the observed wide variation of third-body efficiency among different gases unless for argon $P\ll 1$. There are two ways of removing this serious contradiction. One is to make the collision diameter in (2b) larger, which helps only to a limited extent; the other is to allow $g>\frac{1}{16}$.

The alternate mechanism (3) has been treated[2] in two variations. In one (the "relaxed XM" hypothesis) only bound states of XM are counted as complexes. The rates calculated on this basis reproduce the experimental results remarkably well *provided* g *is not much less than* $\frac{1}{4}$. Again the situation can be somewhat improved by adjusting the cross section for reaction (3b). In the "unrelaxed XM" case, where all aggregates of X and M are counted whether bound or not, the striking agreement with the observed temperature dependence is lost, but the calculated rates are an order of magnitude larger and can be made to agree with experiment regardless of the value of g. In both variations of mechanism (3) the correct dependence of k on M is predicted.

The crucial point in determining which is the most plausible mechanism is therefore a decision about the value of the electronic degeneracy factor g. This factor g arises because each of the $^2P_{\frac{1}{2}}$ I atoms has its ground state split into 4 components by the approach of the other. There are thus 16 possible combinations, of which 1 gives rise to the $^1\Sigma$ molecular state, 4 or more others to other mildly attractive states, and the balance to repulsive states. If only the $^1\Sigma$ state leads to recombination, $g=\frac{1}{16}$; if all attractive states (i.e., $^3\Pi$ and $^1\Sigma$) produced recombination, we would have $g=\frac{5}{16}$; and if all states gave recombination (e.g., by transitions among molecular electronic states) g would be 1.

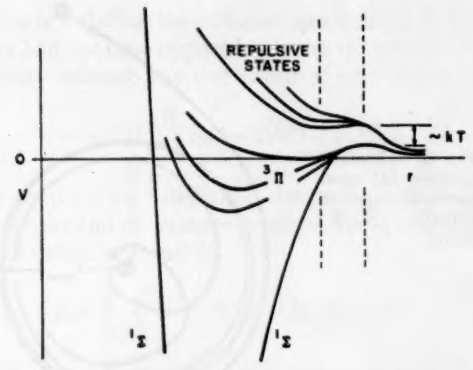

FIG. 3. Schematic effective potential curves for most important type of two-body (I—I) collision.

All three of these possibilities have been argued in the older literature.[8] However, we can bypass these arguments and adopt a new point of view which arises as a result of the calculations reported in this paper. Inspection of the tabulated results reveals that one type of collision is so important in determining K that all others may be neglected: *viz.*, the collision with b nearly equal to b_{max}. In other words, *collisions with the largest allowable angular momentum determine the behavior of the system, and the mental picture associated with "head-on" collisions should be avoided.* A typical trajectory is shown schematically in Fig. 2, in which one of the atoms is regarded as stationary. The incident particle spends substantially all its time orbiting in the vicinity of r_{max}. For the simple inverse-sixth potential used in our approximate calculation, it can be shown that when $b=b_{max}$ the interaction energy at r_{max} is $\frac{1}{2}E$. Thus the separation of the attractive and repulsive curves at r_{max} is only of the order of kT, and we should not be surprised if more or less free transitions occurred between the incipient electronic states of I_2.

The situation we have to examine in determining g for I_2 is illustrated in Fig. 3. The potential curves have been drawn to include the rotation barrier in the conventional way. We have 5 attractive curves which virtually coincide in the region of importance (between the dashed lines) and, about kT higher, 11 repulsive curves which also coincide. (Some of the curves are degenerate and coincide for all values of r.) The value of g depends on whether the interval between transitions among the various potential curves is large or small compared with the lifetime of I_2^*. Unfortunately we do not known which is the case, so we consider both possibilities.

If transitions between curves are infrequent, then we have the adiabatic collisions postulated by Keck. Only the $^1\Sigma$ state leads to recombination, and g is indeed $\frac{1}{16}$.

Conversely, if transitions occur rapidly, either spontaneously or because of perturbations arising from the proximity of a third body, the incoming particles become distributed Boltzmann fashion among the I_2 molecular levels, with the energies of these levels measured in the vicinity of r_{max}. If the separation of the attractive and repulsive states is about kT, the statistical weight of an attractive state is $1/(5+11/e)\cong 1/9$ instead of $\frac{1}{16}$. Whether or not attractive states other than $^1\Sigma$ contribute to recombination can be decided as follows. The binding energy for these states is no more than $3kT$ at room temperature. To this must be added, for the oblique collisions we are considering, the height of the rotation barrier. By a very simple argument it can be shown that when $b=b_{max}$ and $r=r_{max}$, the angular and radial kinetic energies are $\frac{2}{3}E$ and 0, respectively, (for the r^{-6} potential), and the height of the barrier for this most favorable case is E. Thus the most strongly bound state other than $^1\Sigma$ is never more than about 4 kT away from dissociation, and we expect that only $^1\Sigma$ will lead to recombination. The others are so weakly bound that they cannot be deactivated enough to avoid the range of r (dashed lines) in which rapid re-equilibration among states would occur. *Regardless of whether the collisions are adiabatic, as Keck suggests, the electronic degeneracy factor g is close to* $\frac{1}{16}$. It might possibly be as large as about $\frac{1}{8}$.

As has already been pointed out, both the "relaxed XM" hypothesis and the rigid sphere mechanism (2) run afoul of this conclusion to some extent. The former leads to results which are too small, for all M; the latter gives high rates for simple third bodies and (even if full use is made of the possible M-variation of P) low rates for complicated ones, so that the relative efficiencies of different M are not predicted correctly. In this situation it is natural to take a second look at the "unrelaxed XM" model. It has already been shown,[2] by a procedure involving calculation of the equilibrium constant for XM formation, that this model is capable of accounting for the observations if P varies in the proper way. In spite of the similarity between this approach and that used in treating the "relaxed XM" mechanism, the former is much more closely related to the rigid sphere model (2) than it is to the latter. In the Keck treatment mechanisms (2) and (3) are entirely equivalent if the same X—M interaction potential is prescribed and the same definition of a three-body complex is used for each.

It is therefore proposed that the theoretical treatment most likely to succeed in accounting for atomic recombination rates would be a Keck-type calculation in which a reasonable van der Waals interaction between X and M is postulated. This is, in effect, a mechanism in which both (2) and the unrelaxed form of (3) participate indistinguishably. The geometric contribution to P, taken as $\frac{1}{2}$ in the treatment of (3), should arise naturally in Keck's treatment. The calculation should be done for X=I with M=Ar, H_2 and D_2 (to see if an

[8] E. P. Wigner, J. Chem. Phys. **5**, 720 (1937); E. Rabinowitch, Trans. Faraday Soc. **33**, 283 (1937); E. P. Wigner, J. Chem. Phys. **7**, 646 (1939).

isotope effect is predicted; none is found[3]), and for various polyatomic third bodies.

SUMMARY

The principal conclusions of this study are

(1) collisions between atoms are not necessarily adiabatic;

(2) the visualization of head-on rather than oblique collisions, in the study of reaction rates, is likely to be a misleading procedure;

(3) neither the rigid-sphere third body nor the bound intermediate hypothesis can, by itself, account completely for the observed rates of recombination of atoms;

(4) for heavy atoms, at least, the postulate of Keck (that detailed collision mechanics is unimportant) is supported;

(5) Keck's treatment, with more attention to the interaction between recombining atom and third body, offers a promising route to explanation of recombination rates.

ACKNOWLEDGMENT

I am indebted to Dr. James Keck and Professor Norman Davidson for their comments and criticism.

THE JOURNAL OF CHEMICAL PHYSICS VOLUME 32, NUMBER 4 APRIL, 1960

Thermal Conductivity of Gas Mixtures in Chemical Equilibrium. II

RICHARD S. BROKAW

Lewis Research Center, National Aeronautics and Space Administration, Cleveland, Ohio

(Received November 2, 1959)

The expression for the thermal conductivity of gas mixtures in chemical equilibrium is presented in a simpler and less restrictive form. This new form is shown to be equivalent to the previous equations.

IN a previous paper[1] an explicit expression for the increase in thermal conductivity due to chemical reaction was developed for gas mixtures in which chemical equilibrium exists locally throughout the temperature gradient. This expression is applicable to mixtures involving any number of reactants, inert diluents, and chemical equilibria. It is the purpose of this brief paper to present the expression for thermal conductivity due to reaction in a simpler and less restrictive form, and to show that this form is equivalent to previous equations.

A system of ν independent chemical reactions involving μ chemical species (both reactants and diluents) may be written in balanced form as

$$\sum_{k=1}^{\mu} n_{ik} X^k = 0 \qquad i = 1, 2, \cdots j, \cdots \nu. \tag{1}$$

Here X^k represents the kth chemical species and n_{ik} is the stoichiometric coefficient for species k in reaction i. The heat of this reaction is

$$\Delta H_i = \sum_{k=1}^{\mu} n_{ik} H_k \qquad i = 1, 2, \cdots j, \cdots \nu, \tag{2}$$

where the H_k are the enthalpies of the species referred to a common base. For this system the thermal conductivity due to reaction is

$$\lambda_r = -\frac{1}{RT^2} \frac{\begin{vmatrix} A_{11} & \cdots & A_{1\nu} & \Delta H_1 \\ \vdots & & \vdots & \vdots \\ A_{1\nu} & \cdots & A_{\nu\nu} & \Delta H_\nu \\ \Delta H_1 & \cdots & \Delta H_\nu & 0 \end{vmatrix}}{\begin{vmatrix} A_{11} & \cdots & A_{1\nu} \\ \vdots & & \vdots \\ A_{1\nu} & \cdots & A_{\nu\nu} \end{vmatrix}} \tag{3}$$

where

$$A_{ij} = A_{ji} = \sum_{k=1}^{\mu-1} \sum_{l=k+1}^{\mu} (RT/D_{kl}P) x_k x_l [(n_{ik}/x_k) - (n_{il}/x_l)][(n_{jk}/x_k) - (n_{jl}/x_l)] \quad i, j = 1, 2, \cdots \nu. \tag{4}$$

Here R is the gas constant in pressure-volume units, T is the absolute temperature, P the pressure, and D_{kl} the binary diffusion coefficient between components k and l; x_k and x_l are the corresponding mole fractions. Any gas inert to reaction i or j must be included, but has a zero stoichiometric coefficient for the reaction in which it does not participate.

Equations (1)–(4) are most easily verified by assuming them correct and deriving the previous result (Eqs. (10)–(12) of reference 1). In the previous paper an independent component was identified in each reaction and given a stoichiometric coefficient of -1. This

[1] J. N. Butler and R. S. Brokaw, J. Chem. Phys. 26, 1636 (1957).

form can be achieved as follows: First Eq. (1) is rewritten

$$X^i = \sum_{k=1,k\neq i}^{\mu} n_{ik}' X^k \quad i=1, 2, \cdots j, \cdots \nu, \qquad (5)$$

where $n_{ik}' \equiv -n_{ik}/n_{ii}$. We can transform Eq. (3) by dividing each row and column by the $-n_{ii}$ or $-n_{jj}$ appropriate to that row or column in both numerator and denominator determinants. The form of Eq. (3) is maintained, but the quantities ΔH_i and A_{ij} are transformed, and indicated by primes:

$$\Delta H_i' \equiv -(\Delta H_i/n_{ii}) = \sum_{k=1,k\neq i}^{\mu} n_{ik}' H_k - H_i \qquad (6)$$

The A_{ij}' are given by Eq. (4) if the n_{ik}, n_{il}, n_{jk}, and n_{jl} are replaced by n_{ik}', n_{il}', n_{jk}', and n_{jl}'. Equations (5) and (6) are now of the form used in reference 1. It remains only to show that the A_{ij}' are equal to the A_{ik} and A_{kk} defined by Eqs. (10) and (11) of reference 1. To prove this we split the double sum of Eq. (4) into two series. The first series sums over the independent components from 1 to ν; summation in this series is indicated by the index p or q. The second series sums over all other species from $\nu+1$ to μ; summation in this instance is over indices r and s. Accordingly,

$$A_{ij}' = \tfrac{1}{2}\sum_{k=1}^{\mu}\sum_{l=1}^{\mu} = \tfrac{1}{2}\sum_{p=1}^{\nu}\sum_{q=1}^{\nu} + \sum_{p=1}^{\nu}\sum_{r=\nu+1}^{\mu} + \tfrac{1}{2}\sum_{r=\nu+1}^{\mu}\sum_{s=\nu+1}^{\mu}. \qquad (7)$$

Since by definition the independent species occur in only one reaction, we find

$$n_{ip}' = n_{iq}' = -1, \quad p, q = i; \qquad n_{jp}' = n_{jq}' = -1, \quad p, q = j$$
$$= 0, \quad p, q \neq i; \qquad = 0, \quad p, q \neq j.$$

If we define $\Delta_{kl} \equiv RT/D_{kl}P$, we find that the terms of Eq. (7) are

$$\tfrac{1}{2}\sum_{p=1}^{\nu}\sum_{q=1}^{\nu} = -\Delta_{ij}, \quad j\neq i$$

$$= \sum_{p=1,p\neq i}^{\nu} \Delta_{pi}(x_p/x_i), \quad j=i$$

$$\sum_{p=1}^{\nu}\sum_{r=\nu+1}^{\mu} = \sum_{r=\nu+1}^{\mu}\sum_{p=1}^{\nu} n_{ir}' n_{jr}' \Delta_{pr}(x_p/x_r)$$

$$+ \sum_{r=\nu+1}^{\mu} (n_{ir}'\Delta_{jr} + n_{jr}'\Delta_{ir}), \quad j\neq i$$

$$= \sum_{r=\nu+1}^{\mu}\sum_{p=1,p\neq i}^{\nu} n_{ir}'^2 \Delta_{pr}(x_p/x_r)$$

$$+ \sum_{r=\nu+1}^{\mu} \Delta_{ir}[(x_r + n_{ir}'x_i)^2/x_i x_r], \quad j=i$$

$$\tfrac{1}{2}\sum_{r=\nu+1}^{\mu}\sum_{s=\nu+1}^{\mu} = \sum_{r=\nu+1}^{\mu-1}\sum_{s=r+1}^{\mu} \Delta_{rs}\frac{(n_{ir}'x_s - n_{is}'x_r)(n_{jr}'x_s - n_{js}'x_r)}{x_r x_s}, \quad j\neq i$$

$$= \sum_{r=\nu+1}^{\mu-1}\sum_{s=r+1}^{\mu} \Delta_{rs}[(n_{ir}'x_s - n_{is}'x_r)^2/x_r x_s], \quad j=i$$

After summing the appropriate terms of Eq. (7), the elements A_{ij}' and A_{ii}' are found to be identical to the elements A_{ik} and A_{kk} of reference 1. (There are differences in the symbols, particularly in the letters chosen for the indices.) Hence, Eqs. (1) through (4) are entirely equivalent to the expression for the thermal conductivity of a reacting gas presented heretofore.

In conclusion, it is perhaps worthwhile to state specifically how the formulas presented here are superior to the previous expressions. First and foremost, it is not necessary to identify a specific independent component with each reaction; that is to say Eq. (1) is less restrictive than Eq. (5). As a consequence the contribution of each component to each reaction is handled entirely through the stoichiometric coefficients, and a single, and relatively simple, expression suffices for all the A_{ij} [Eq. (4)]. This is not only convenient for hand calculations; it should also simplify programing for computing machines.

NMR Chemical Shifts of Aluminum: Experimental Data and Variational Calculation

D. E. O'REILLY

Gulf Research and Development Company, Pittsburgh 30, Pennsylvania

(Received October 6, 1959)

Chemical shifts of Al^{27} for aluminum alkyl halides, halides, alkyls, alkoxides, AlH_4^-, and $Al(OH)_4^-$ are given. The magnitude of the resonance line width of aluminum compounds as liquids or in solution is indicative of the cubic or noncubic molecular symmetry around the Al^{27} nucleus. The chemical shift of Al^{27} in AlH_4^- is calculated by a variation procedure using both valence bond and molecular orbital type wave functions. Requirements on variational functions due to time reversal and inversion symmetry are given. Factors determining the shifts of other aluminum compounds are discussed.

INTRODUCTION

SINCE the initial observation[1] of the "chemical shift" of the resonance frequency of a nucleus in different chemical environments, the effect has been measured for many different nuclei and in some cases used to elucidate the electronic and chemical structure of molecules. The chemical shifts of the proton, in particular, have been measured with considerable precision in a large number of molecules. These shifts have been correlated with parameters such as bond ionic character. Ramsey[2] developed a theory of the magnetic shielding of nuclei using a perturbation theory approach which, for rigorous application to the calculation of shifts, requires the knowledge of matrix elements of the orbital angular momentum operator between the ground electronic state and all excited states of the molecule. Detailed knowledge of these excited states is, in general, not available. Approximations of the formulation involving an average excitation energy are equally unsatisfactory, since one does not generally know what value to choose for this energy. More recently, following a procedure suggested by the work of Tillieu and Guy[3] and Hornig and Hirschfelder,[4] both Das and Bersohn[5] and McGarvey[6] have developed a variational calculation of the shift and successfully applied it to the hydrogen molecule. McGarvey[6] has also calculated proton shifts for the hydrogen halides with considerable success. The great advantage in the variational formulation lies in the fact that the final expression for the shift involves only expectation values of appropriate operators for the ground electronic state of the molecule. With reasonably good expressions for the ground electronic state wave functions, the shift can be calculated to good approximation, as is illustrated by the calculations mentioned in the foregoing H_2 molecule. In the present paper variation calculations are given for the AlH_4^- molecule which are in reasonably good agreement with the experimental value.

Aluminum-27 (100% abundant, $I=5/2$) has a moderately large electric quadrupole moment ($Q=0.149\times10^{-24}$ cm^2). At Al molecular positions of noncubic symmetry, large electric field gradients are generally present and the Al^{27} nuclear spin is coupled with the molecular framework because of the interaction of the quadrupole moment with the molecular electric field gradient. This interaction thus results in a short spin-lattice relaxation time and correspondingly large line width[7] in liquids due to transitions of the magnetic dipole moment induced by the molecular tumbling.

This effect generally permits an assignment of cubic (octahedral or tetrahedral) or noncubic symmetry to the surroundings of the molecular site occupied by the aluminum nucleus on the basis of the magnitude of the line width. Similar observations for the N^{14} nucleus have been made by Ogg and Ray[8].

EXPERIMENTAL

Nuclear resonances of Al^{27} were observed and chemical shifts measured with a Varian Associates V–4200A NMR spectrometer, Varian 12-in. electromagnetic and V-2100 power supply. A BC-221-D Bendix Radio Corporation frequency meter was used in the calibration of the V-4200A helipot used for scanning the magnetic field. Shifts were measured at 7.20 Mcps and a magnetic field strength near 6490 gauss. The first derivative of resonance absorption was recorded using audio modulation (20 cps) of the static field and subsequent narrow-band audio amplification of the NMR signal. Dispersion mode first derivatives were recorded at high rf power and sweep modulation amplitude in the case that the resonance line width was greater than 1 gauss.

Aluminum compounds studied were initially more than 99% pure. Reagent grade solvents were used in preparing solutions. Aluminum alkyls and alkyl halides were obtained from the Process Division of Gulf Research & Development Company and the

[1] W. D. Knight, Phys. Rev. **76**, 1259 (1949).
[2] N. F. Ramsey, Phys. Rev. **77**, 567 (1950); **78**, 699 (1950); **86**, 243 (1952).
[3] J. Tillieu and G. Guy, J. Chem. Phys. **24**, 1117 (1956).
[4] J. F. Hornig and J. O. Hirschfelder, J. Chem. Phys. **23**, 474 (1955).
[5] T. P. Das and R. Bersohn, Phys. Rev. **104**, 849 (1956).
[6] B. R. McGarvey, J. Chem. Phys. **27**, 68 (1957).
[7] N. Bloembergen, *Nuclear Magnetic Relaxation* (Nijhoff, The Hague, The Netherlands, 1948); Y. Ayant, Compt. rend. **238**, 1876 (1954).
[8] R. A. Ogg and J. D. Ray, J. Chem. Phys. **25**, 1285 (1956).

TABLE I. NMR chemical shifts and widths of aluminum compounds at 25°C.

	δ, ppm	width, guass
1. $Al(H_2O)_6^{3+}$ (aq. acidic solution)	0	*n* (0.05)
2. $Al(OiBu)_3$ (*n*-heptane solution)	−7	*n* (0.09)
3. AlF^{2+} (KF added to 1)	−15	*b* (0.3)
4. Al_2I_6 (ethyl ether solution)	−39	*n* (0.08)
5. $Al(OH)_4^-$ (aq. basic solution)	−80	*n* (0.08)
6. $Al(iBu)Cl_2$ (pure)	−86	*b* (3.7)
7. $Al(OCH_3)Cl_2$ (pure)	−90	*b*
8. $AlCl_3$ (toluene solution)	−91	*b* (0.3)
9. $Al(CH_3)_2Cl \cdot Al(CH_3)Cl_2$ (pure)	−93	*b*
10. Al_2Br_6 (ethyl ether solution)	−96	*n* (0.09)
11. Al_2Br_6 (liquid Br_2 solution)	−101	*b* (0.3)
12. AlH_4^- ($LiAlH_4$ in ethyl ether)	−103	*n* (0.06)
13. Al_2Cl_6 (ethyl ether solution)	−105	*n* (0.10)
14. $Al(CH_3)_3$ (pure)	−156	*b* (0.4)
15. $HAl(iBu)_2$ (pure)	−162	*b* (8.9)
16. $Al(Et)_3$ (pure)	−171	*b* (1.5)
17. $Al(iBu)_3$ (pure)	−220	*b* (5.4)

B. F. Goodrich Research Laboratory, Brecksville, Ohio.

The error involved in shift measurements is estimated to be ±3 parts per million (ppm) for "narrow" resonances (less than 0.1 gauss in width) and ±10 ppm for "broad" resonances (greater than 0.1 gauss in width).

EXPERIMENTAL RESULTS

In Table I is listed the chemical shift δ for various molecules. We define δ as follows:

$$\delta = [(H_c - H_r)/H_r] \times 10^6. \quad (1)$$

Here H_r is the magnetic field for which resonance occurs for the reference compound and H_c is the resonance field for the compound for which δ is given. All δ values are referred to a solution of $AlCl_3 \cdot 6H_2O$ in water for which the chemical shift was independent of concentration. Also in Table I each Al resonance is denoted by *n* (narrow) if the width between points of maximum slope is less than 0.1 gauss and by *b* (broad) if the width is greater than 0.1 gauss.

We ascribe the narrow resonances to Al-containing molecules or complexes which have octahedral or tetrahedral symmetry around the Al, at least on the average for times longer than about the correlation time of molecular tumbling in the liquid. The broad resonances on the other hand correspond to molecules with noncubic point group symmetry around the Al.

These assignments are verified for several of the complexes for which the symmetry is known or presumed to be known. These are Al^{3+} (aq.), AlF^{2+},[9] $Al(OH)_4^-$,[10] and AlH_4^-.[11]

The addition of KF to an acidic, aqueous solution of $AlCl_3 \cdot 6H_2O$ results in the immediate development of a broad resonance and a decrease in intensity of the narrow resonance due to Al^{3+} (aq.); the resultant absorption derivative is shown in Fig. 1. From consideration of the equilibrium constants[9] for the complexes $AlF_x^{3+(-x)}$ $(0<x<6)$ and the concentration of the Al^{3+} and F^- ions in the solution, the broad resonance is primarily due to the AlF^{2+} complex ion.

A somewhat analogous effect occurs in a solution of anhydrous aluminum chloride in ethyl ether. A freshly prepared solution is light yellow in color and shows only a narrow, symmetrical resonance presumably due to the Al_2Cl_6 dimer. Upon standing the solution turns to a red-brown color and an additional, broad Al^{27} resonance appears which is ascribed to the formation of etherates such as $AlCl_3 \cdot Et_2O$.

The narrow Al^{27} resonances from freshly prepared ether solutions of the aluminum halides indicate that these solutions contain the dimer ions Al_2X_6, which, by electron diffraction studies[12] in the gaseous phase, are known to have nearly tetrahedral symmetry around each Al. Similarly, the narrow resonance from $Al(OiBu)_3$ solutions in *n*-heptane indicates this resonance is due to a polymer with approximately cubic symmetry about the Al, probably formed by an oxygen bridge between aluminum nuclei. This conclusion is in agreement with the results of cryoscopic and dipole moment measurements[13] on aluminum alkoxides in hydrocarbon solvents. Pure trimethyl aluminum shows a relatively narrow "broad" resonance indicating that dimers are present in the liquid, probably formed by bonding of the Al to methyl protons (rather than methyl carbon) as suggested by Pitzer and Gutowsky.[14] Aluminum triisobutyl gives a considerably broader resonance than aluminum trimethyl indicating the monomer form is predominant.

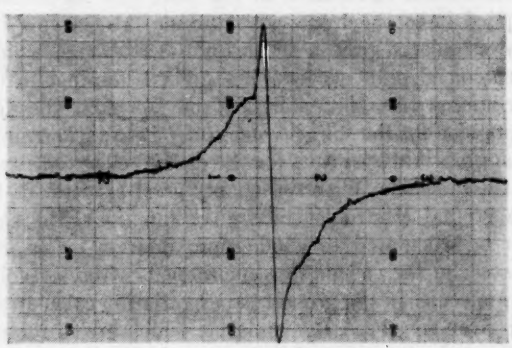

FIG. 1. Al^{27} NMR absorption derivative of solution of $AlCl_3 \cdot 6H_2O$ in water with KF added. Broad component corresponds to AlF^{2+}; the narrow component is due to Al^{3+}.

[9] Wendell M. Latimer, *Oxidation Potentials* (Prentice-Hall, Inc., Englewood Cliffs, New Jersey, 1952).
[10] Lippincott, Psellos, and Tobin, J. Chem. Phys. **20**, 536 (1952).
[11] D. A. Brown, J. Chem. Phys. **29**, 451 (1958).
[12] K. J. Palmer and N. Elliot, J. Am. Chem. Soc. **60**, 1852 (1938).
[13] H. Ulich and W. Nespital, Z. physik. Chem. **165**, 294 (1933).
[14] K. S. Pitzer and H. S. Gutowsky, J. Am. Chem. Soc. **67**, 2204 (1946).

The spectrum of lithium aluminum hydride in ethyl ether consists of five overlapping resonances in the approximate intensity ratio of 1:4:6:4:1 which are ascribed to spin-spin splitting of the Al^{27} resonance by four equivalent protons in a tetrahedral configuration about the aluminum. The spin-spin coupling constant is 110 cps. A recorder derivative of this resonance is shown in Fig. 2.

Only weak broad Aluminum-27 NMR signals were observed for the pure liquids $Al(CH_3)_2F$, $Al(i\text{Bu})_2Br$; $Al(i\text{Bu})_2I$, $Al(CH_3)_2I$ and $Al(i\text{Bu})Br_2$, presumably due to lifetime broadening by large molecular electric field gradients.

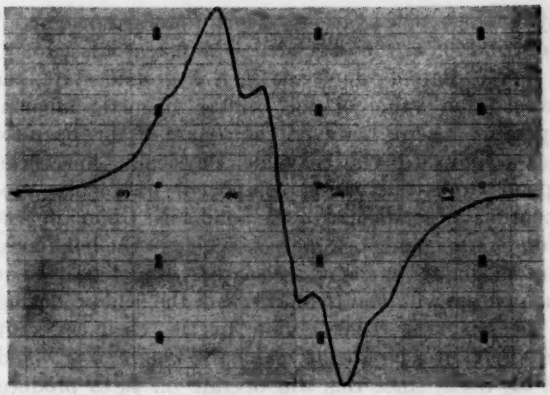

FIG. 2. First derivative of Al^{27} NMR absorption of $LiAlH_4$ dissolved in ethyl ether ($\nu = 7.20$ Mcps). Five partially resolved peaks are present due to spin-spin splitting of the Al^{27} resonance by four equivalent protons bonded to Al. ($J \approx 110$ cps.)

VARIATIONAL CALCULATIONS FOR AlH_4^-

The variational method hinges on choosing a wave function which will give a close approximation to the energy E when the energy is computed by minimization of Eq. (2) below:

$$E(\mu, H) = \int \psi^* \mathcal{H} \psi d\tau \Big/ \int \psi^* \psi d\tau. \tag{2}$$

In the above equation $\mathcal{H}$ is the Hamiltonian operator for the molecular electrons and nuclei in an external magnetic field H. If one considers the magnetic moment μ of only the Al^{27} nucleus and the z direction to be the direction of the external field, $\mathcal{H}$ can be written as[2]

$$\mathcal{H} = \mathcal{H}_0 + \boldsymbol{\mu} \cdot \mathcal{H}_1 + \mathbf{H} \cdot \mathcal{H}_2 + \mu H \mathcal{H}_3. \tag{3}$$

$\mathcal{H}_0$ is the energy operator in the absence of the field H and nuclear magnetic dipole moment μ,

$$\mathcal{H}_1 = (e/mc) \sum_k (\mathbf{l}_k / r_k^3)$$

is the electron orbital magnetic flux density operator, $\mathcal{H}_2 = (e/2mc)\mathbf{L}$ is the total orbital magnetic moment operator, $\mathbf{L}$ being the total orbital angular momentum of the electrons. The expression

$$\mathcal{H}_3 = (e^2/2mc^2) \sum_k [(x_k^2 + y_k^2)/r_k^3]$$

is proportional to the energy of the diamagnetic circulation of electronic charge in the externally applied field and the field due to the nuclear moment. The coordinate system is centered at Al^{27}.

Analogous to the case of an atom in an electric field, the trial wave function is chosen as follows:

$$\psi = \psi_0 + \mathbf{H} \cdot \mathbf{g} \psi_0, \tag{4}$$

where $\mathbf{g}$ is a vector operator and ψ_0 is the wave function of the electrons in the absence of μ and H. The electronic ground state of the molecule is considered to be nondegenerate.

There is a basic condition $\mathbf{g}$ must satisfy. This condition may be derived by consideration of the behavior of (3) and (4) under time reversal.[15] The time-dependent Schroedinger equation is

$$\mathcal{H} \psi = i\hbar (\partial \psi / \partial t), \tag{5}$$

and the complex conjugate of (5) is

$$\mathcal{H}^* \psi^* = -i\hbar (\partial \psi^* / \partial t). \tag{5a}$$

The Wigner[15] time-reversal operator K which reverses time is now employed. Under K, $\mathcal{H}_0 \rightarrow \mathcal{H}_0$, $\mathcal{H}_1 \rightarrow \mathcal{H}_1$, $\mathcal{H}_2 \rightarrow \mathcal{H}_2$, $\mathcal{H}_3 \rightarrow \mathcal{H}_3$, $\boldsymbol{\mu} \rightarrow -\boldsymbol{\mu}$ and $\mathbf{H} \rightarrow -\mathbf{H}$. Hence

$$K\mathcal{H} = \mathcal{H}^* K$$

so that the time-reversed Schroedinger equation is

$$\mathcal{H}^* K\psi = -i\hbar (\partial K\psi / \partial t). \tag{6}$$

Thus the eigenfunctions of (6) are those of (5a) so that

$$K\psi = \psi^*. \tag{6a}$$

If $\mathbf{g}$ is a function of the quantum mechanical operators of coordinates, linear momenta, and (or) angular momenta, then (6a) requires that $\mathbf{g}$ be a purely imaginary operator, i.e.,

$$\mathbf{g}^* = -\mathbf{g}. \tag{7}$$

Furthermore, since $\mathcal{H}$ is invariant under the inversion operation I,

$$I\mathbf{g} = \mathbf{g}I. \tag{8}$$

As may be readily verified, the z component of $\mathcal{H}_2$ commutes with $\mathcal{H}_{1z}$ and $\mathcal{H}_3$. For a diatomic molecule ($C_{\infty v}$ or $D_{\infty h}$ symmetry) $\mathcal{H}_{2z}$ commutes with $\mathcal{H}_0$ when the z direction corresponds to the symmetry axis of the molecule. Thus with the magnetic field H directed along the molecular symmetry axis z', $\mathcal{H}_{2z'}$ is conserved and has an expectation value of zero if the molecule is in a Σ ground state. A similar result holds for $\mathcal{H}_{1z}$ from

[15] E. Wigner, Nach. Akad. Wiss. Göttingen, Math.-physik. Kl. 1932, 546.

symmetry considerations. Thus the "paramagnetic" contribution $\sigma_{||}^{p}$ to the chemical shift tensor is zero.

For a diatomic molecule in a Σ ground state, the expectation value of the orbital magnetic moment operator is zero; however, the square of this operator has a finite expectation value. Physically, this corresponds to a fluctuating component of angular momentum perpendicular to the bond axis. Upon application of a magnetic field perpendicular to the bond axis, the magnetic moment associated with the angular momentum will tend to line up with the field producing a paramagnetic contribution to the chemical shift tensor. Thus a physically reasonable choice of $\mathfrak{g}$ would be $\mathfrak{IC}_2$ itself, since this will operate on ψ_0 to produce a finite value for the expectation value of the angular momentum in the state ψ. Also $\mathfrak{IC}_2^{*}=-\mathfrak{IC}_2$ and $I\mathfrak{IC}_2=\mathfrak{IC}_2 I$ so that (7) and (8) are satisfied. This choice for $\mathfrak{g}$ is that of Hornig and Hirschfelder[4] and McGarvey.[6]

The result for the chemical shift σ is as follows[6]:

$$\sigma_\lambda=\langle\psi_0\,|\,\mathfrak{IC}_3\,|\,\psi_0\rangle_\lambda-\frac{2\langle\psi_0\,|\,\mathfrak{IC}_{1x}\mathfrak{IC}_{2x}\,|\,\psi_0\rangle_\lambda\langle\psi_0\mathfrak{IC}_{2x}{}^{2}\psi_0\rangle_\lambda}{\langle\psi_0\,|\,\mathfrak{IC}_{2x}[\mathfrak{IC}_0,\,\mathfrak{IC}_{2x}]\,|\,\psi_0\rangle_\lambda},\quad(9)$$

where λ refers to a particular orientation of the molecule relative to the external field. Equation (8) can be written more compactly[6] by defining ΔE as the difference between the diagonal matrix element of $\mathfrak{IC}_0$ corresponding to the states $\mathfrak{IC}_{2x}\psi_0$ and to ψ_0,

$$\sigma_\lambda=\langle\psi_0\,|\,\mathfrak{IC}_3\,|\,\psi_0\rangle_\lambda-\frac{2\langle\psi_0\,|\,\mathfrak{IC}_{1x}\mathfrak{IC}_{2x}\,|\,\psi_0\rangle_\lambda}{\Delta E}.\quad(10)$$

The expression (9) for the shift involves only expectation values of operators for the ground state of the molecule.

A relatively simple molecule containing aluminum is AlH_4^-. The following antisymmetrized, valence bond wave function $\psi_{c_{0v}}$ for an Al—H covalent bond will be used where

$$\psi_{c_{0v}}=(2+2S^2)^{-\frac{1}{2}}(\psi_1+\psi_2),$$

$$\psi_1=\frac{1}{\sqrt{2}}\sum_P(-1)^P P t_a\alpha(1)s_h\beta(2),$$

$$\psi_2=\frac{1}{\sqrt{2}}\sum_P(-1)^P P s_h\alpha(1)t_a\beta(2),$$

and

$$S=\int s_h t_a\,d\tau.\quad(11)$$

Here t_a is one orbital of the aluminum sp^3 hybrid directed toward a proton on which a $1s$ orbital s_h is centered; α and β are the electron spin wave functions corresponding to spin-up and spin-down, respectively, and P is the permutation operator. After using (11), the contribution $\sigma_{c_{0v}}{}^{d}$ of $\mathfrak{IC}_3$ to σ, averaged over all orientations of the symmetry axis of the Al—H bond relative to the external magnetic field, is as follows:

$$\sigma_{c_{0v}}{}^{d}=(e^2/3mc^2)[1/(1+S^2)]\Big((1/R)+2S\int(t_a s_h/r_a)\,d\tau+\tfrac{1}{4}\langle 1/r_a\rangle_{3s}+\tfrac{3}{4}\langle 1/r_a\rangle_{3p}\Big),\quad(12)$$

where r_a is the radial coordinate measured from the aluminum nucleus and $\langle 1/r_a\rangle_{3s}$ and $\langle 1/r_a\rangle_{3p}$ are the expectation values of $1/r$ for the $3s$ and $3p$ orbitals of aluminum, respectively. Here R is the Al—H bond distance. Additional terms which are much smaller than those given are omitted in (12). The procedure of McGarvey was followed in evaluation of the matrix elements of $\mathfrak{IC}_{1x}\mathfrak{IC}_{2x}$, $\mathfrak{IC}_{2x}{}^{2}$, and $\mathfrak{IC}_{2x}[\mathfrak{IC}_0,\,\mathfrak{IC}_{2x}]$. After some reduction one obtains

$$\Delta E=\frac{Z_h e^2\Big(\int(s_h y^2/r_h{}^4)\cdot(\partial s_h/\partial r)\,d\tau\Big)}{\tfrac{3}{4}\{[1+(4/\sqrt{3})S^2]/R^2\}-\int s_h(\partial^2 s_h/\partial y^2)\,d\tau}\quad(13)$$

and

$$\langle\psi_{c_{0v}}\,|\,\mathfrak{IC}_{1x}\mathfrak{IC}_{2x}\,|\,\psi_{c_{0v}}\rangle=\frac{e^2\hbar^2}{2m^2c^2}\frac{\sin^2\alpha}{1+S^2}\Big(\tfrac{3}{4}\int\frac{p_{x'a}{}^{2}}{r_a{}^{3}}d\tau+\sqrt{3}S\int\frac{s_h p_{xa}}{r_a{}^{3}}d\tau-R^2\int\Big(\frac{\partial s_h}{\partial y}\Big)^2\frac{d\tau}{r_a{}^{3}}\Big).\quad(14)$$

Here Z_h is the effective nuclear charge of the hydrogen atom and α is the angle between direction of the symmetry axis z' of the molecule and the external field direction z. After using hydrogenic wave functions for s_h and $p_{x'a}$, we find

$$\Delta E=\frac{\tfrac{2}{3}(Z_h{}^4e^2/a_0{}^3)}{\tfrac{3}{4}\{[1+(4/\sqrt{3})S^2]/R^2\}+[\tfrac{1}{3}(Z_h/a_0)^2]}\quad(15)$$

and

$$\langle\psi_{c_{0v}}\,|\,\mathfrak{IC}_{1x}\mathfrak{IC}_{2x}\,|\,\psi_{c_{0v}}\rangle=\frac{e^2\hbar^2}{2m^2c^2}\frac{\sin^2\alpha}{1+S^2}\Big[\frac{Z_a{}^{3}}{108a_0{}^{3}}+\sqrt{3}S\int\frac{s_h p_{x'a}}{r_a{}^{3}}d\tau-\frac{1}{3R}\int_0^R(R_h')^2r_h{}^2dr_h-\frac{R^2}{3}\int_R^\infty\frac{(R_h')^2}{r_h}dr_h\quad(16)$$

where Z_h and Z_a are the effective nuclear charges for $1s$ hydrogen and $3p$ aluminum electrons, respectively.

The second term in Eq. (9) averaged over all orientations of the Al—H bond relative to the external field is denoted by σ^{p}; the averaged contribution to this term by the covalent wave function being denoted by $\sigma_{c_{0v}}{}^{p}$.

For the ionic form of the Al—H bond we use the following wave function corresponding to Al^+—H^-:

$$\psi_{ion}=(1/\sqrt{2!})\sum_P(-1)^P Ps_h\alpha(1)s_h\beta(2). \quad (17)$$

The evaluation of matrix elements of Eq. (10) for this case was done following the procedure of McGarvey; one obtains the following result for σ_{ion}:

$$\sigma_{ion}=(2e^2/3mc^2)\int_R^\infty rR_{1s}^2dr. \quad (18)$$

Here R_{1s} is a radial 1s hydrogen wave function corresponding to s_h; σ_{ion} has been evaluated using a hydrogen radial wave function with $Z=11/16$. This value of Z is that obtained for H^- by a variational calculation of the energy using hydrogen 1s wave functions with Z as a parameter.

The ionic character is defined as follows:

$$i=a^2/(1+a^2), \quad (19)$$

where a is defined by the following equation:

$$\psi_0=\psi_{cov}+a\psi_{ion}. \quad (20)$$

In the usual definition of the ionic character, the overlap integral between ψ_{cov} and ψ_{ion} is neglected. Thus, matrix elements of the operators in (9) which involve both ψ_{ion} and ψ_{cov} are also omitted. The error involved in this approximation is small for AlH_4^- since i is small. There are several sources of values of the ionic character. The ionic character has generally been correlated with electronegativity differences. For the Al—H bond the electronegativity difference is 0.6 and the ionic character given by Dailey and Townes[16] is 0.17, that given by Pauling[17] is 0.10. Pauling's value has been used in the calculation since it gives slightly better agreement of the calculated shift with the experimental value. Thus the chemical shift σ for a single Al—H bond is as follows:

$$\sigma=(1-i)\sigma_{cov}+i\sigma_{ion}, \quad (21)$$

where σ_{cov} is the average shift for the covalent wave function.

TABLE II. Values of quantities used in chemical shift calculation.

R/a_0	3.08[a]
Z_h	1.00
S	0.730
$a_0\int(s_hl_a/r_a)d\tau$	0.259
$a_0^3\int(s_hp_{za}/r_a^3)d\tau$	0.052
Z_a	5.94[b]

[a] See reference 11.

[b] R. Sternheimer, Phys. Rev. **80**, 102 (1950); the value of $1/r^3$ corresponding to this value of Z_a is somewhat greater than that given by R. G. Barnes and W. V. Smith, Phys. Rev. **93**, 95 (1954).

[16] B. P. Dailey and C. H. Townes, J. Chem. Phys. **23**, 118 (1955).

[17] Linus Pauling, *The Nature of the Chemical Bond* (Cornell University Press, Ithaca, New York, 1948).

TABLE III. Results of chemical shift calculation.

	Valence bond	Molecular orbital $\lambda=1.00$
ΔE, ev	35.6	33.2
$\langle\psi_0\|\mathcal{H}_2\mathcal{H}_2\|\psi_0\rangle$, ev	6.30×10^{-4}	5.67×10^{-4}
σ_{cov}^p	-35.4×10^{-6}	-34.1×10^{-6}
σ_{cov}^d	15.8×10^{-6}	15.4×10^{-6}
σ_{ion}	0.53×10^{-6}	...
i	0.10[a]	...
$\sigma(AlH_4^-)$	-70×10^{-6}	-75×10^{-6}
$\delta(AlH_4^-)$	-103×10^{-6}	

[a] See reference 17.

Using the approximation of perfect pairing the wave function for the AlH_4^- molecule is written as a Slater determinant of four orbitals of the form in Eq. (20) with one orbital for each bond and two electrons in each orbital. Thus the chemical shift for the AlH_4^- molecule is four times that of Eq. (21) within this approximation. All overlap type integrals occurring in (12), (15), and (16) have been evaluated using Slater-type orbitals and the numerical tables of Mulliken *et al.*[18] and Rosen.[19] These and other quantities used in the calculation of the shift are given in Table II. The calculated shift compares fairly well with the experimental value as shown in Table III. It must be borne in mind that the shift is relative to Al^{3+} (aq.) which is considered to be a closed shell ion with no covalent bonding between the solvent water and the ion. In view of the simplicity of the wave functions used in the calculation, the agreement obtained is probably satisfactory.

In the preceding calculation we have implicitly assumed that the closed shell wave functions of the 1s, 2s, and 2p electrons are not affected by the bonds formed so that the diamagnetic shift due to these electrons is not changed. Hartree[20] has given the potential of the closed shell electrons at the nucleus in Al^{3+}; using this quantity, we obtain $+754\times10^{-6}$ for the shift due to the closed shell, with the aid of Lamb's[21] expression for the diamagnetic shift in atoms. Calculations of polarization effects of the valence electrons on the atomic core in Al(III)[22] and Al(I)[23] indicate that the core wave functions are not much affected by the valence electrons.

A calculation of the shift of AlH_4^- was also carried out using a molecular orbital wave function of the following form for an Al—H bond:

$$\psi_0=N\{t_a(1)+\lambda s_h(1)\}\{t_a(2)+\lambda s_h(2)\}\cdot\{\alpha(1)\beta(2)-\alpha(2)\beta(1)\}, \quad (22)$$

[18] Mulliken, Rieke, Orloff, and Orloff, J. Chem. Phys. **17**, 1248 (1949).

[19] N. Rosen, Phys. Rev. **38**, 255 (1931).

[20] D. R. Hartree, Proc. Roy. Soc. (London) **A151**, 96 (1935).

[21] W. E. Lamb, Jr., Phys. Rev. **60**, 817 (1941).

[22] K. Katterback, Z. Astrophys. **32**, 165 (1953).

[23] L. Biermann and K. Lübeck, Z. Astrophys. **25**, 325 (1948).

where l_a and s_h are as previously defined and N is given by the following equation:[24]

$$N^{-1}=(1+2\lambda S+\lambda^2). \tag{23}$$

The evaluation of σ^d and σ^p using the molecular orbital wave function (22) is quite straightforward. The results are as follows:

$$\sigma^d=\frac{2e^2N}{3mc^2}\left\{\tfrac{1}{4}\langle 1/r_a\rangle_{3s}+\tfrac{3}{4}\langle 1/r_a\rangle_{3p}+2\lambda\int\frac{l_a s_h}{r_a}d\tau+(\lambda^2/R)\right\},$$

$$\langle\psi_0\,|\,\mathcal{H}_{1z}\mathcal{H}_{2z}\,|\,\psi_0\rangle=(e^2\hbar^2/m^2c^2)N\sin^2\alpha\{\tfrac{3}{4}\langle 1/r_a^3\rangle_{3p}$$

$$+\sqrt{3}\lambda\int(s_h p_{z'a}/r_a^3)d\tau-\lambda^2R^2\int(\partial s_h/\partial y)^2(d\tau/r_a^3)\},$$

$$\Delta E=\frac{\frac{2}{3}\lambda^2e^2(Z_h^4/a_0^3)}{\{\frac{3}{4}[1+(4/\sqrt{3})S\lambda]/R^2\}+(\lambda^2/3)(Z_h/a_0)^2}. \tag{24}$$

The quantity λ may be evaluated by calculation of the electric dipole moment due to Eq. (22) and comparison with the experimental value. Unfortunately, an experimental value of the dipole moment of the Al—H bond is not available and there is no satisfactory way of estimating it. Since the electronegativity of Al (1.5) is nearly equal to that of H (2.1), one would expect λ to be equal to approximately unity. Hence, the quantities of Eqs. (24) have been evaluated with $\lambda=1.00$ and are given in Table III. The value of the chemical shift calculated in this way is somewhat smaller in magnitude than the experimental value. Choosing $\lambda=0.87$ yields agreement between the calculated and observed value of the shift. This value of λ corresponds to a MO wave function in which the electron density of the two electrons of an Al—H bond is greater in the aluminum orbital than the hydrogen orbital. In valence bond language this corresponds to invoking the polar structure Al^-H^+ into the valence bond wave function. This is in contrast to the slightly greater electronegativity of H compared to that of Al which indicates that the polar structure of Al^+H^- is the most important polar structure to be considered.

[24] C. A. Coulson, *Valence* (Oxford University Press, New York, 1953).

VARIATIONAL CALCULATION FOR OTHER MOLECULES

The approximate agreement obtained between the calculated and observed chemical shift for AlH_4^- in the preceding section suggests that at least a parametric correlation of the observed shifts with such quantities as ionic character and bond distance for more complex aluminum-containing molecules can be obtained through the variational approach. With this end in mind, the variational method has been applied to the aluminum halides; the calculation is similar to that of the preceding section, a valence bond wave function made up of aluminum and halide atomic functions being used.

With the use of hydrogenic wave functions for the aluminum and halide orbitals and the value of Z_a given in Table II, quantitative agreement of the calculated shifts with the observed shifts was not found. A value of 8.0 for Z_a was necessary to obtain fair agreement between observed and calculated shifts. This result is perhaps not unexpected in view of the simplicity of the valence bond wave function and orbitals used, since this function is not an exact solution of the molecular Hamiltonian $\mathcal{H}_0$ as was assumed in the derivation of Eq. (9). The paramagnetic contribution to the shift is found to depend inversely on the effective nuclear charge of the halide and directly on the covalent character of the aluminum-halide bond. In terms of Eq. (10), ΔE increases with the halide effective nuclear charge while $\langle\psi_0\,|\,\mathcal{H}_{1z}\mathcal{H}_{2z}\,|\,\psi_0\rangle$ is approximately constant. The decrease in the magnitude of the observed shift in the sequence Cl, Br, I is thus due to the increase of the effective nuclear charge of the halide which predominates over the increase in covalent character of the bonds in the order Cl, Br, I.

ACKNOWLEDGMENTS

Several informative discussions of alkyl aluminum compounds were received from Dr. H. Scott of B. F. Goodrich Research Laboratory. Dr. C. P. Poole, Jr., and Dr. R. H. Hughes made helpful comments on the manuscript.

THE JOURNAL OF CHEMICAL PHYSICS VOLUME 32, NUMBER 4 APRIL, 1960

Electrical Properties of Organic Solids. I. Kinetics and Mechanism of Conductivity of Metal-Free Phthalocyanine*

GORDON TOLLIN,† DAVID R. KEARNS,‡ AND MELVIN CALVIN

Lawrence Radiation Laboratory and Department of Chemistry, University of California, Berkeley, California

(Received July 30, 1959)

Techniques involving the use of high-intensity, short-duration light pulses have been applied to the study of the kinetics of photoconductivity in films of metal-free phthalocyanine. These experiments, in conjunction with measurements of steady-state photoconductivity, are consistent with the following scheme. The principal route for the formation of charge carriers is via the first excited singlet state, although the lowest triplet state can, to some extent, contribute to charge carrier production. The mobility of the carriers is low and is concentration-dependent, being lower at higher carrier concentration. The decay of the photocurrent is the result of a diffusion-limited bimolecular recombination, with a capture radius of approximately one molecular diameter. The experiments indicate that carriers produced thermally in the dark do not interact with light-produced carriers.

A. INTRODUCTION

PREVIOUS work from this laboratory[1] has suggested that the mechanism of quantum conversion in photosynthesis involves processes which are characteristic of ordered arrays of pigment molecules. For this reason, it has seemed important to investigate in detail the electronic properties of these systems. Furthermore, investigations of this nature are of great interest in their own right.

The general properties of organic semiconductors have recently been reviewed by Garrett.[2] It is apparent from this article that, in spite of the large volume of information that has been accumulated, little is known either theoretically or experimentally about the fundamental processes of charge carrier formation and migration in these systems. Almost all the work in this field has been concerned with steady-state conductivity properties and very little attention has been paid to kinetics, although Nelson[3] has conducted a series of experiments on the kinetics of photoconductivity in solid cationic dyes such as basic fuchsin, rhodamine *B*, and crystal violet. However, these ionic systems in many ways are different from the nonionic dyes.

For these reasons, we felt that an investigation of the kinetics of photoconductivity in nonionic dye molecules would be of interest. Metal-free phthalocyanine was chosen for the present study because: (a) its properties appear to be typical of this class of substances, (b) a great many electrical measurements have been performed on it,[4,5] and (c) its structure corresponds to the prophyrins, of which class chlorophyll is a member. With this in mind, techniques have been developed which permit the study of the kinetics of photoconductivity in solid organic dye materials.

B. MATERIALS AND METHODS

The material used in the experiments was prepared from crude metal-free phthalocyanine (DuPont) by vacuum sublimation in a muffle furnace. This yielded crystalline material in the form of needles 0.1–1 cm in length. The cell used for most of the conductivity measurements is diagramed in Fig. 1. Additional measurements were also carried out using a sandwich-type cell. The samples were applied to the electrodes by another vacuum sublimation of the crystalline material. A variety of ambient atmospheres (air, O_2, natural gas) were used in the sublimations, but the results appeared to be independent of the gas used. Subsequent to the sublimation of the sample, the entire cell was coated with a clear acrylic resin. This coating served merely a protective function and produced no changes in any of the measured properties of the phthalocyanine. For the conductivity measurements, the sample cell was mounted on one end of a copper rod, the temperature of which could be varied. For most of the measurements, field strengths of the order of 10^4 v/cm were used. X-ray diffraction indicated that the sublimed films of phthalocyanine were essentially amorphous. However, the films could be made microcrystalline by annealing the entire cell at 270°C for several days under reduced natural gas pressure. The crystals formed in this manner were about 1 μ in diameter and 10 μ long.

Figure 2 shows a block diagram of the apparatus used in these studies. For kinetic studies, the samples

* The work described in this paper was sponsored by the United States Atomic Energy Commission, and the Department of Chemistry, University of California, Berkeley, California.

† Present address: Department of Chemistry, University of Arizona, Tucson, Arizona.

‡ A substantial portion of this paper is the subject of David R. Kearns, Ph.D. dissertation, "Electric and magnetic properties of organic molecular crystals," University of California, Berkeley, California.

[1] Tollin, Sogo, and Calvin, Ann. N. Y. Acad. Sci. **74**, 310 (1958).

[2] C. G. B. Garrett, *Semiconductors*, N. B. Hannay, editor (Reinhold Publishing Corporation, New York, 1959), Chap. 15. This article should be referred to for a more complete bibliography.

[3] R. C. Nelson, J. Chem. Phys. **22**, 885, 890, 892 (1954).

[4] Eley, Parfitt, Perry, and Taysum, Trans. Faraday Soc. **49**, 79 (1953).

[5] D. D. Eley and G. D. Parfitt, Trans. Faraday Soc. **51**, 1529 (1955).

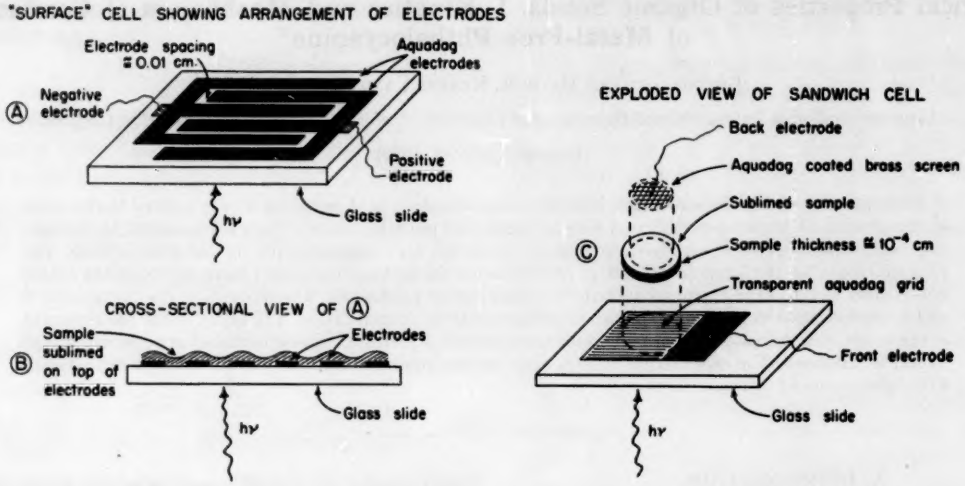

FIG. 1. Diagram of sample cells.

were illuminated by a General Electric FT-230 flashtube operated at 1500 v with a load capacitance of 2 microfarads. This produced a light pulse with a one μsec rise time and which decayed to about 10% of its peak intensity in about 5 μsec. A standard triggering system was used. The calculated output of this lamp is thus $\sim 10^{24}$ quanta per sec/cm^2 of which 10% may impinge on the sample.

Photocurrent generated in the sample by the light pulse was passed through a known resistance with values ranging from 1000 ohms to 1 megohm, depending upon the experiment. The voltage developed across this resistance was fed through a cathode follower and dc amplifier (gain=2000) into the various recording devices. In this manner, it was possible to measure the decay curve of the photocurrent from about 10 μsec after flashing to about 100 sec. The photosignal itself was used to trigger the oscilloscope sweep, and thus it was also possible to observe the rise time of the photocurrent.

For the measurement of action spectra and steady-state photoconductivity, a Hanovia 800-w xenon arc lamp or a 500-w tungsten filament projection lamp and a Bausch and Lomb 500-mm grating monochromator were used in place of the flashtube. The impinging visible intensity from these lamps is about 10^{17}–10^{19} quanta/sec/cm^2.

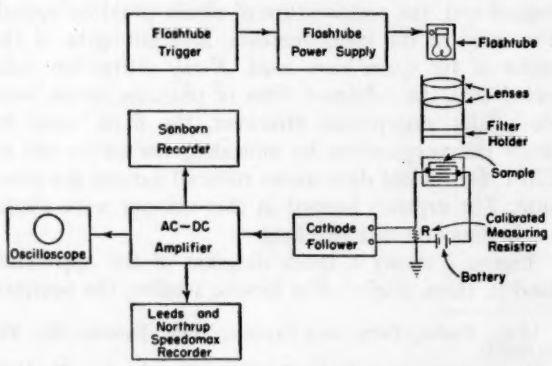

FIG. 2. Block diagram of conductivity apparatus.

C. RESULTS AND DISCUSSION

1. Kinetics of Photocurrent Decay

Typical photocurrent decay curve data are shown in Fig. 3. These were obtained with unannealed, metal-free phthalocyanine in the "surface" cell shown in Fig. 1. Unless otherwise stated, all of the following results apply to samples of this type. The rise time of the photocurrent in the flash experiments is never slower than ~ 1 μsec even if a neutral filter of 1% transmission is placed between flash light and sample. This indicates that the rise time of the photocurrent is limited by the rise time of the circuitry.

In Fig. 4, a plot of log photocurrent (i/e) *vs* log time (t) is shown for data obtained at 23°C and at −35°C. From these curves, it is apparent that the current decay from several hundred microseconds to several seconds obeys the relation,

$$I = i/e = ct^{y} \quad (e = \text{electronic charge}), \qquad (1)$$

where $y = -\frac{1}{2}$ at 23°C and −0.43 at −35°C. This was the general result for all of the samples studied under all conditions, with y varying between −0.6 and −0.4.

The curves in Fig. 4 also show a break at longer times (greater than one second at 23°C and greater than 15 sec at −35°C) with y approaching −1. If one replots the long-time data, it is possible to show that the curves follow a bimolecular law

$$1/I = Kt + \text{constant}. \qquad (2)$$

Such plots are shown in Fig. 5 for both 23°C and −35°C. Thus, at low carrier concentrations, the

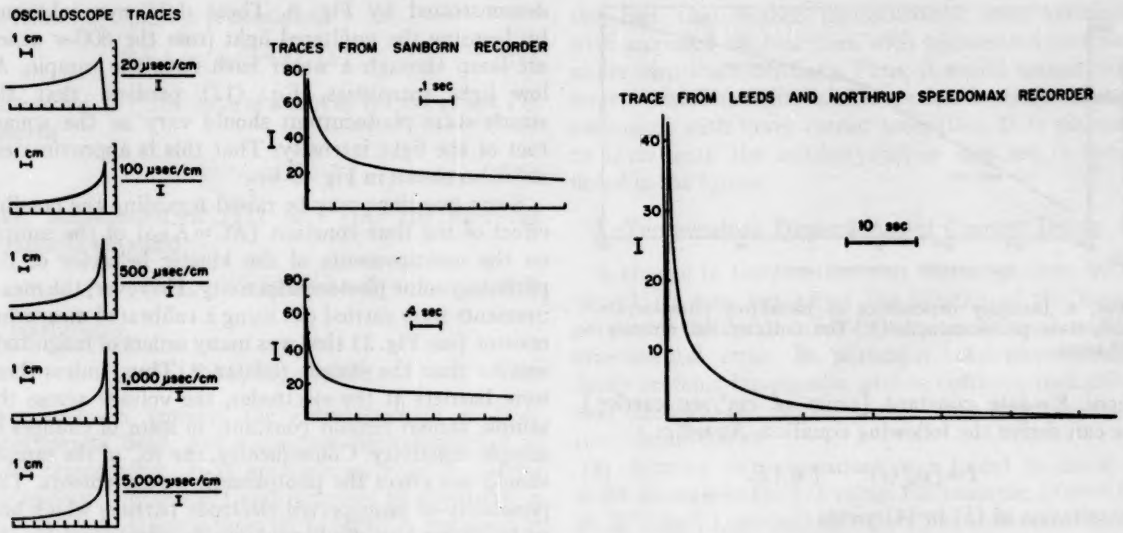

FIG. 3. Typical photoconductivity decay data for metal-free phthalocyanine at room temperature.

current decay is strictly bimolecular, and at higher carrier concentrations, the current decay is slower than bimolecular.

At the shortest times (10–100 μsec), the current decays even more slowly than at the longer times (>100 μsec).

The decay law at low current is precisely what one would expect for a process involving the recombination of oppositely charged carriers. The slower decay at the higher currents may be accounted for simply by assuming a concentration-dependent charge carrier mobility, analogous to what is observed for ion mobilities in solutions of high ionic strength.[6]

If one makes the above assumptions, it is possible to obtain an equation which adequately expresses the time dependence of the photocurrent at all except the very earliest times (less than 100 μsec). An empirical relation between current I and carrier concentration n, which will lead to a satisfactory description of the experimental results is

$$I=[\mu_0/(n+c)^{1-1/x}]\cdot nAE \qquad (3)$$

where n = total carrier concentration $=n_+ + n_-$, E = field strength, A = cross-sectional area of conducting material, $\bar{\mu}=\mu_0/[(n+c)^{1-1/x}]$ = apparent average carrier mobility at a particular value of n, and c and x are constants for a given sample and temperature, c representing a critical concentration of carriers, below which the mobility is concentration independent.

Assuming a bimolecular rate law,

$$dn/dt=-Kn^2, \qquad (4)$$

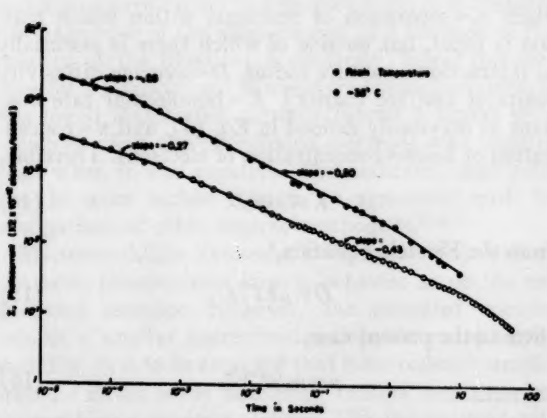

FIG. 4. Log photocurrent *vs* log time for a metal-free phthalocyanine sample at room temperature and −35°C.

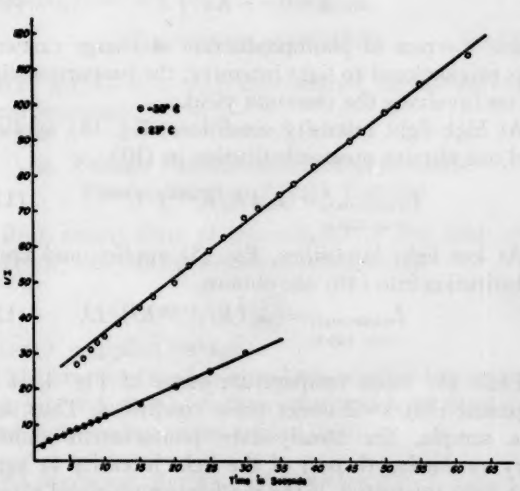

FIG. 5. $1/I$ *vs* t for metal-free phthalocyanine at room temperature and −35°C. The unit on the ordinate is 2×10^9 amps^{-1}.

[6] W. J. Moore, *Physical Chemistry* (Prentice-Hall, Inc., Englewood Cliffs, New Jersey, 1950), p. 451.

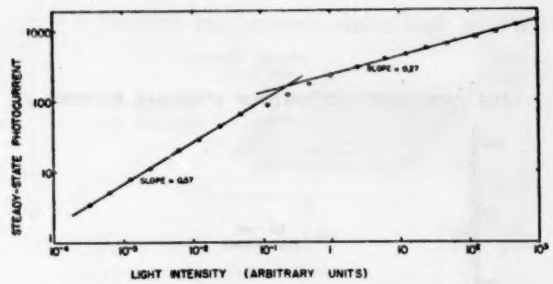

FIG. 6. Intensity dependence of metal-free phthalocyanine steady-state photoconductivity. The unit on the ordinate is 10^{-8} amps.

where K=rate constant [units of cm³/sec carrier], one can derive the following equation. At $n \ll c$:

$$I=[\mu_0/(c)^{1-1/x}]\cdot nAE. \tag{5}$$

Substitution of (5) in (4) yields

$$dI/dt=-(Kc^{1-1/x}/\mu_0 AE)\cdot I^2 \tag{6}$$

or, upon integration,

$$1/I=(Kc^{1-1/x}/\mu_0 AE)\cdot t+\text{const.} \tag{7}$$

For $n \gg c$:

$$I=\mu_0 n^{1/x} AE, \tag{8}$$

and upon substitution in (4) and integration, one obtains

$$I=(\mu_0 AE/K^{1/x})\cdot t^{-1/x}+\text{const.} \tag{9}$$

Thus, at low carrier concentrations, I should decay according to Eq. (7) and at high carrier concentrations according to Eq. (9), in agreement with experiment.

It is also possible to write equations for the steady-state photoconductivity. At the steady-state, Eq. (4) becomes

$$dn/dt=0=-Kn^2+L \tag{10}$$

where L=rate of photoproduction of charge carriers. L is proportional to light intensity, the proportionality factor involving the quantum yield.

At high light intensity conditions, Eq. (8) applies, and one obtains upon substitution in (10)

$$I_{\substack{\text{steady-state}\\(\text{high light})}}=(\mu_0 AE/K^{1/2x})\cdot L^{1/2x}. \tag{11}$$

At low light intensities, Eq. (5) applies, and upon substitution into (10) one obtains:

$$I_{\substack{\text{steady-state}\\(\text{low light})}}=(\mu_0 AE/c^{1-1/x}K^{\frac{1}{2}})\cdot L^{\frac{1}{2}}. \tag{12}$$

From the room temperature curve of Fig. 4, it is apparent that $x=2$ under these conditions. Thus, for this sample, the steady-state photocurrent should vary as the fourth root of the light intensity at very high light intensities, if the mechanism proposed above is correct. That this is approximately the case is demonstrated by Fig. 6. These data were obtained by focusing the unfiltered light from the 800-w xenon arc lamp through a water bath onto the sample. At low light intensities, Eq. (12) predicts that the steady-state photocurrent should vary as the square root of the light intensity. That this is approximately so is also shown in Fig. 6.

Some questions may be raised regarding the possible effect of the time constant ($RC=K\epsilon_0\rho$) of the sample on the measurements of the kinetic behavior of the phthalocyanine photoconductivity. However, the measurements were carried out using a calibrated measuring resistor (see Fig. 2) that was many orders of magnitude smaller than the sample resistance. Thus, unless there were barriers at the electrodes, the voltage across the sample should remain constant, in spite of changes in sample resistivity. Consequently, the RC of the sample should not effect the photokinetic measurements. The possibility of unsuspected electrode barriers which had to be charged or discharged can be eliminated by the observations that (1) the decay of flash photoconductivity is not exponential as would be expected for a process involving discharge of a condenser, and (2) the resistivity of the sample may be changed by a factor of 10^7 (see paper II) without effect on the kinetics of the initial decay of the flash photoconductivity. Such a change in resistance would produce a large change in the RC of the sample.

The fact that photocurrent may be observed for several minutes after flash illumination suggests a low mobility and that carrier recombination may be diffusion-limited. The mathematics of diffusion-limited reactions have been treated by Waite.[8] For a bimolecular diffusion-limited process, Waite derives the following expression for the rate law at low reactant concentrations.

$$dn/dt=4\pi r_0 Dn^2=-Kn^2, \tag{13}$$

where r_0=separation of reactants within which reaction is rapid, but outside of which there is essentially no interaction=capture radius, D=average diffusivity [units of cm²/sec carrier], K=bimolecular rate constant as previously defined in Eq. (4), and n=concentration of holes=concentration of electrons. Therefore,

$$K=4\pi r_0 D. \tag{14}$$

From the Einstein equation,[9]

$$D=\mu kT/e \tag{15}$$

where in the present case,

$$\mu=\mu_0/c^{1-1/x}, \tag{16}$$

[7a] L. E. Lyons, J. Chem. Phys. **23**, 220 (1955).
[7b] Compton, Schneider, and Waddington, J. Chem. Phys. **27**, 160 (1957).
[8] T. R. Waite, Phys. Rev. **107**, 463 (1957).
[9] N. F. Mott and R. W. Gurney, *Electronic Processes in Ionic Crystals* (Clarendon Press, Oxford, England, 1950), p. 63.

the following equation is obtained,

$$K=4\pi r_0(\mu_0/c^{1-1/x})\cdot(kT/e). \quad (17)$$

From Eq. (7), the slope of a plot of $1/I$ *vs* t at low I is equal to

$$Kc^{1-1/x}/\mu_0 AE=B. \quad (18)$$

Upon substitution of (17) into (18) the following equation is obtained:

$$(4\pi r_0/AE)\cdot(kT/e)=B \quad (19)$$

or, rearranging,

$$r_0=(BAE/4\pi)\cdot(e/kT). \quad (20)$$

This equation permits the calculation of r_0 from experimental data. For metal-free phthalocyanine at room temperature, r_0 is approximately 25 A (about one molecular diameter) and increases to about 200 A at −35°C. At temperatures up to 50°C, r_0 remained at about the room temperature value, within experimental error.

The fact that one can obtain reasonable values for r_0 suggests that the assumption that recombination is diffusion-limited is a moderately accurate one. The observed increase in r_0 at low temperatures may be due to a decrease in thermal scattering.

2. Results with Sandwich Cells and Annealed Samples

Room temperature photoconductivity decay curves were also measured for sandwich-type cells of metal-free phthalocyanine. These gave essentially the same kinetics as did the "surface" cells. In general, the sandwich cells were more difficult to prepare and had about a 100 times poorer signal to noise ratio than did the "surface" cells.

A common method used to indicate the sign of the majority charge carrier in a sandwich cell is to measure the magnitude of the photocurrent as a function of the polarity of the illuminated electrode. When this was done for a sandwich cell of metal-free phthalocyanine, it was found that higher currents (about 2 times) were obtained when the illuminated electrode was positive than when it was negative. This indicates that holes are the more mobile carriers, in agreement with investigations of other organic compounds.[7,10,11]

Microcrystalline (annealed) "surface" cells exhibit the same photocurrent kinetic behavior as do the unannealed samples. However, the annealed samples exhibit a smaller concentration dependence of carrier mobility. It is to be expected that more ordered samples would contain fewer scattering centers and therefore possess higher carrier mobilities. This is consistent with the fact that higher photocurrents were obtained with annealed samples than with unannealed samples, under identical conditions. Thus, it would appear that larger carrier mobility concentration dependences are associated with lower carrier mobilities. It is planned to investigate the microcrystalline samples in more detail in the future.

3. Temperature Dependence of Current Decay

A change in temperature over the range from 60°C to −35°C does not affect the kinetics of the major portion of the decay curve (20 μsec to 100 sec), within experimental error. In particular, the photocurrent decay remains bimolecular at low currents, indicating that there are no trapping centers with depths greater than about 0.05 ev.

A decrease in temperature was found to cause a slight decrease in the $1/x$ value. For example, $1/x=0.50$ at 23°C and $1/x=0.43$ at −35°C, as shown in Fig. 4. Inasmuch as one would expect a decrease in mobility at lower temperatures, these results again indicate that there is an inverse relationship between mobility and concentration dependence of mobility. This is further demonstrated by the fact that the concentration-dependent portion of the decay curve extends to longer times at the lower temperature (see Fig. 4).

4. Temperature Dependence of Steady-State Photocurrent and Dark Current

The steady-state photocurrent as a function of temperature obeyed the following equation[12]:

$$I_{\text{steady-state}}=c\exp(-\Delta E/kT), \quad (21)$$

where $\Delta E\cong 0.2$ ev, in agreement with other reported values.

The temperature dependence of the dark current was more difficult to measure, but was found to obey the following relation[13]:

$$I_{\text{dark}}=c\exp(-\Delta E/2kT), \quad (22)$$

where $\Delta E\cong 1$–2 ev., in approximate agreement with reported values.

5. Voltage Dependence of Steady-State Photocurrent and Dark Current

Both steady-state photoconductivity and dark conductivity obeyed the following relationship,

$$I\alpha V^1, \quad (23)$$

where V = applied voltage.

The kinetics (the functional relationship between the current and time) of flash photoconductivity decay were independent of the applied field.

[10] H. P. Kallman and M. Silver, *Symposium on Fluorescence and Semiconductors* (Garmisch-Partenkirchen, 1956).

[11] D. C. Northrup and O. Simpson, Proc. Roy. Soc. (London) **A244**, 377 (1958).

[12] Kommandeur, Korinek, and Schneider, Can. J. Chem. **35**, 998 (1957).

[13] N. F. Mott and R. W. Gurney, reference 12, pp. 156 ff.

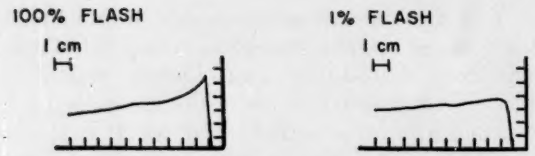

FIG. 7. Intensity dependence of initial photoconductivity decay for a typical metal-free phthalocyanine sample. The flash intensity was varied with neutral density filters; sweep times are 20 μsec per cm.

6. Flash Intensity Dependence of Photocurrent Decay

A study of the kinetics of photocurrent decay demonstrated that, for a given sample, the functional relationship between measured photocurrent, I, and carrier concentration, n, as given in Eq. (3), did not change with flash intensity, for times after flashing greater than about 200 μsec. For shorter times (<200 μsec), it was found that as the flash intensity decreased the photocurrent decayed more slowly. This effect is shown in Fig. 7.

7. Spectral Response of Steady-State Photoconductivity

The photoconductivity action spectra for both thick and thin samples are shown in Fig. 8, along with the absorption spectrum of a thin film of metal-free phthalocyanine. It is apparent that it is light absorbed by phthalocyanine which is effective in producing photoconductivity. Furthermore, from the fact that illumination of the back side of thick samples yields an action spectrum which is the inverse of the absorption spectrum, it can be concluded that light absorbed close to the electrodes is more effective in causing photoconductivity than is light which is absorbed on the back side of the sample.

8. Effect of Ambient Illumination on Photoconductivity

If a sample is illuminated with a steady light source and simultaneously subjected to flash illumination, the photocurrent due to the flash decays more rapidly than it would in the absence of the ambient light (see Fig. 9). This effect is greater the higher the intensity of the ambient light. At highest ambient light intensity, the flash photocurrent decay becomes approximately unimolecular after about 0.01 sec. This effect may be interpreted simply as a concentration effect in which the ambient light-produced carriers are present in concentrations greater than flash-produced carriers at the longer times. This causes the flash current to decay pseudo-unimolecularly. This hypothesis is supported by the spectral response curves of the long-time decay where the wavelength of the ambient light was varied. In these experiments, the sample was flashed from one side and illuminated with ambient light from the other side. It was found that the ambient light had its greatest effect on the decay curve at wavelengths which correspond to the inverse of the phthalocyanine absorption spectrum, indicating a direct interaction between flash-produced carriers and ambient light-produced carriers. Wavelengths in the infrared region of the spectrum had no effect on the decay, again indicating the absence of trapping.

In these samples, the room temperature dark current was approximately twice as great as the photocurrent produced by the highest intensity ambient light. In addition, as indicated in Sec. 3 above, neither an increase nor a decrease in this dark current over several orders of magnitude produced any change in the kinetics of decay of the flash photocurrent. This might suggest that the measured dark current was not an intrinsic property of the phthalocyanine, but rather an artifact of the sample cell. This possibility was eliminated by the observation that the photocurrent produced by a standard light was essentially proportional to the measured dark current for a series of seven different samples. These results and the ambient light experiments suggest that the dark current is somehow different from the photocurrent. At present we cannot offer an account of this difference.

D. CONCLUSIONS

The fact that the rise time of flash-induced photoconductivity is limited by the circuitry (ca. 1 μsec) indicates that the electronically excited state which gives rise to charge carriers has a lifetime of less than 1 μsec. This immediately suggests the first excited singlet state, inasmuch as one would expect the lowest

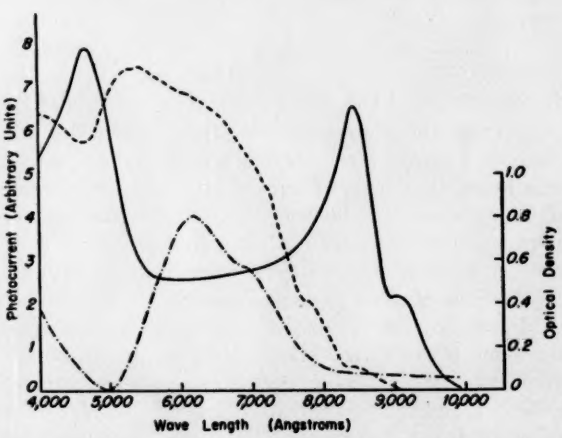

FIG. 8. Spectral response of steady-state photoconductivity and absorption spectrum of metal-free phthalocyanine films. (50 A bandwidth.) —— Photoconductivity: thick sample, back side illumination. – – – Photoconductivity: thick sample, front side illumination; thin sample, front and back side illumination. —.—. absorption spectrum of sublimed film of metal-free phthalocyanine.

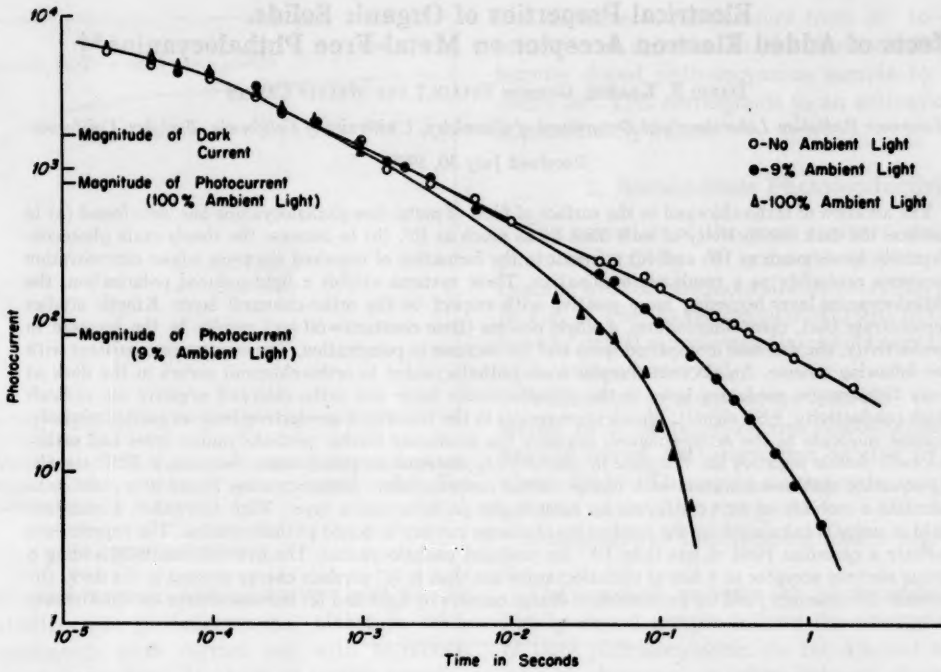

FIG. 9. Log photocurrent *vs* log time of a metal-free phthalocyanine sample with varying amounts of ambient light. The unit on the ordinate is 10^{-8} amp.

triplet state to have a much longer lifetime (of the order of 10^{-4} sec or greater).[14]

The first 10 μsec of the photocurrent decay are complicated by the decay of the light pulse itself and therefore no attempt will be made to discuss this region in any detail.

It was noted above that the photocurrent from 20 μsec to several hundred μsec after flashing decayed significantly more slowly than would be predicted by the proposed mechanism, and that this effect became even more pronounced and lasted for a longer period of time at lower flash intensities. This suggests that there exists a long-lived (of the order of 10^{-4} sec) high-energy intermediate which contributes to carrier production, but to a smaller extent than does the excited singlet state. One possibility for such an intermediate is the lowest triplet state. Such an hypothesis would be consistent with the low intensity flash behavior of the current decay, inasmuch as the triplet lifetime would be longer under low intensity illumination due to a decreased probability of self-quenching.

The next question which arises is the detailed mechanism for the conversion of nonconducting excited electronic states into charge carriers. It is possible to gain some insight into this problem by a consideration of the results reported in the following paper.

[14] G. Porter and M. R. Wright, Discussions Faraday Soc. (to be published).

Electrical Properties of Organic Solids. II. Effects of Added Electron Acceptor on Metal-Free Phthalocyanine*†

DAVID R. KEARNS, GORDON TOLLIN,‡ AND MELVIN CALVIN

Lawrence Radiation Laboratory and Department of Chemistry, University of California, Berkeley, California

(Received July 30, 1959)

The addition of ortho-chloranil to the surface of films of metal-free phthalocyanine has been found (a) to increase the dark conductivity of such films by as much as 10^7, (b) to increase the steady-state photoconductivity by as much as 10^6, and (c) to result in the formation of unpaired electrons whose concentration decreases reversibly as a result of illumination. These systems exhibit a light-induced polarization, the phthalocyanine layer becoming more positive with respect to the ortho-chloranil layer. Kinetic studies demonstrate that, upon illumination, a single process (time constant=60 sec) results in the increase in conductivity, the decrease in unpaired spins and the increase in polarization. The results are consistent with the following scheme. An electron transfer from phthalocyanine to ortho-chloranil occurs in the dark at room temperature producing holes in the phthalocyanine layer and ortho-chloranil negative ion radicals (high conductivity, ESR signal). Illumination results in the transfer of an electron from an excited phthalocyanine molecule to the ortho-chloranil negative ion producing further phthalocyanine holes and ortho-chloranil double negative ion (increase in conductivity, increase in polarization, decrease in ESR signal). By equating spin concentration with charge carrier concentration (phthalocyanine holes) it is possible to calculate a mobility of 10^{-4} cm²/v/sec for holes in the phthalocyanine layer. With this value, a quantum yield of unity is calculated for the production of charge carriers in doped phthalocyanine. The experiments indicate a quantum yield of less than 10^{-1} for undoped phthalocyanine. The over-all results of adding a strong electron acceptor to a film of phthalocyanine are thus to (a) produce charge carriers in the dark, (b) increase the quantum yield for production of charge carriers by light and (c) increase charge carrier lifetime.

INTRODUCTION

A NUMBER of studies have indicated that the conductivity of organic semiconductors may be significantly altered by the presence of impurity materials. For example, gases such as O_2, Cl_2, and NO_2 have been found to increase both the semiconductivity and photoconductivity of anthracene crystals by several orders of magnitude.[1,2] Similar effects have been observed with O_2 and the metal phthalocyanines.[3] These effects appear to be due to alteration of surface conductivity. Akamatu *et al.*[4,5] have studied complexes between halogens and polycyclic aromatic compounds and have found 10^7–10^9-fold increases in bulk conductivity over that of the pure hydrocarbon. All of the foregoing effects have been tentatively interpreted by the respective authors as due to an increase in the mobility of charge carriers[1–3,6,7] caused by interaction between the impurity and the host molecules.

The results quoted in the foregoing suggest that there may be a general effect of oxidizing agents (electron acceptors) upon the conductivity properties of certain organic substances (donors). Therefore, we felt it to be of interest to investigate the effects of organic oxidizing agents upon such properties. Further interest in this problem is generated by the fact that aggregates of porphyrin molecules (chlorophyll) and organic oxidizing agents (quinones, coenzyme *Q*,[8] etc.), as well as reducing agents (carotenoids)[9,10] occur together in photosynthetic materials, and their interaction may be of importance in the primary quantum conversion process.

High conductivities have been observed[11] in chloranil, iodanil, and bromanil complexes of dimethylaniline; electron spin resonance (ESR) has been observed[12] in molecular compounds of diamines and substituted benzoquinones. Previous work from this laboratory[13] has demonstrated that one can achieve large increases in dark conductivity of metal-free phthalocyanine upon the addition of small amounts of ortho-chloranil. In addition, a qualitative parallelism between the ESR signal and the conductivity of various phthalocyanine samples was observed.[14] The present studies represent an extension of this work.

* The work described in this paper was sponsored in part by the United States Atomic Energy Commission.

† A substantial portion of the work presented in this paper is the subject of: David R. Kearns, Ph.D. dissertation, "Electric and magnetic properties of organic molecular crystals," University of California, Berkeley, California.

‡ Present address: Department of Chemistry, University of Arizona, Tucson, Arizona.

[1] W. G. Schneider and T. C. Waddington, J. Chem. Phys. **25**, 358 (1956).

[2] D. M. J. Compton and T. C. Waddington, J. Chem. Phys. **25**, 1075 (1956).

[3] A. T. Vartanyan and I. A. Karpovich, Doklady Akad. Nauk S.S.S.R. **111**, 561 (1956).

[4] Akamatu, Inokuchi, and Matsunaga, Bull. Chem. Soc. Japan **29**, 213 (1956).

[5] H. Akamatu and H. Inokuchi, *Proceedings of the Third Conference on Carbon* (Pergamon Press, New York, 1959), p. 51.

[6] Akamatu, Inokuchi, and Matsunaga, Bull. Chem. Soc. Japan **29**, 213 (1956), see p. 218.

[7] Lyons, Bree, and Morris, reference 5, p. 87.

[8] F. L. Crane, Plant Physiol. **34**, 128 (1959).

[9] Blass, Anderson, and Calvin, Plant Physiol. (to be published).

[10] Sapozhnikov, Kayasovskaya, and Maevskaya, Doklady Akad. Nauk S.S.S.R. **113**, 74 (1957).

[11] D. D. Eley and H. Inokuchi, reference 5, p. 91.

[12] Bijl, Kainer, and Rose-Innes, J. Chem. Phys. **30**, 765 (1959).

[13] D. Kearns and M. Calvin, Bio-Organic Chemistry Quarterly Report, UCRL-8457, September, 1958, p. 25.

[14] D. R. Kearns and M. Calvin (unpublished results).

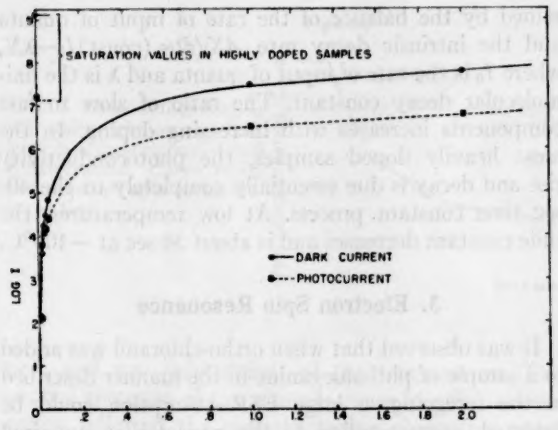

FIG. 1. Variation of dark conductivity and photoconductivity of phthalocyanine with amount of ortho-chloranil added. The unit on the ordinate is 10^{-11} amp.

EXPERIMENTAL

The principal organic semiconductor used in the present studies was phthalocyanine, although additional experiments were carried out with tetracene, coronene, and decacylene. Methods of sample preparation and conductivity measurements were as described previously.[15] The oxidizing agents were applied by spraying a benzene solution onto the exposed area of a surface cell[15] of the organic semiconductor. Occasional samples were prepared from solutions containing both donor and acceptor molecules, but results from such samples require further investigation.

Electron spin resonance measurements were carried out with a previously described spectrometer.[16]

RESULTS

In a series of preliminary experiments, it was found that the dark conductivity and photoconductivity of phthalocyanine, tetracene, decacyclene, and coronene were increased to varying degrees by the addition of small amounts of either ortho-chloranil, chloranil, or phenanthrenequinone. Inasmuch as the largest effects were obtained with ortho-chloranil-phthalocyanine mixtures, it was decided to limit the present investigation to this system.

1. Dark Conductivity

The variation of the room temperature dark conductivity of a phthalocyanine sample with the amount of added ortho-chloranil is shown in Fig. 1. It is apparent that the dark conductivity increases with increasing amounts of ortho-chloranil added (doping) to a maximum value of about 10^7 times that of the pure phthalocyanine.

A decrease in temperature from 25° to −100°C resulted in a decrease in the dark conductivity of a heavily doped phthalocyanine sample by a factor of about 10^3. This corresponds to an activation energy of approximately 0.2 ev.

2. Steady-State Photoconductivity

The variation of the room temperature steady-state photoconductivity of ortho-chloranil-doped phthalocyanine with ortho-chloranil concentration is also shown in Fig. 1. The maximum photocurrent obtained with a heavily doped sample was about 10^5 times that obtained with undoped material.

A decrease in temperature from 25° to −100°C resulted in a decrease in the photoconductivity of a heavily doped phthalocyanine sample by a factor of about 4×10^2. This again corresponds to approximately a 0.2-ev activation energy.[17]

A summary of the foregoing results is given in Table I.

The spectral response of photoconductivity in a lightly doped sample follows the absorption spectrum of pure phthalocyanine. As the amount of doping increases, however, a photoinduced *decrease* in conductivity can be observed at certain wavelengths. The magnitude of this effect increases with increasing doping, but is never more than a few percent of the photoinduced increase in conductivity produced by phthalocyanine absorption. The spectral response of this effect is shown in Fig. 2. The significance of this action spectrum is not unambiguous inasmuch as it represents the resultant of two opposing processes. Cooling the sample causes this effect to disappear, with the result that wavelengths which produced a decrease in conductivity at room temperature produce an increase in conductivity at the low temperatures. It is also possible to observe the replacement of the decrease at room temperature

TABLE I. Comparison of the maximum values of the conductivity of ortho-chloranil-doped metal-free phthalocyanine with the conductivity of pure metal-free phthalocyanine. The room temperature specific resistivity of pure metal-free phthalocyanine was approximately 10^9 ohm cm and that for the doped material was approximately 10^2 ohm cm, both measured at a field strength of 10^4 volts/cm. The units in the table are relative to the value for pure phthalocyanine photoconductivity at −100°C.

	Undoped		Doped	
Temperature °C	Dark cond.	Steady-state photoconductivity	Dark cond.	Steady-state photoconductivity
25	10^3	10^3	10^{10}	10^6
−100	10^{-7}	1	10^7	2.5×10^5

[15] Tollin, Kearns, and Calvin, J. Chem. Phys. **32**, 000 (1960).
[16] Sogo, Pon, and Calvin, Proc. Natl. Acad. Sci. U. S. **43**, 387 (1957).
[17] Due to the experimental difficulties involved in measuring the temperature dependence of dark conductivity in cells of the type used in these experiments (see reference 15), it is not certain that the slightly larger decrease in dark conductivity upon cooling is significant.

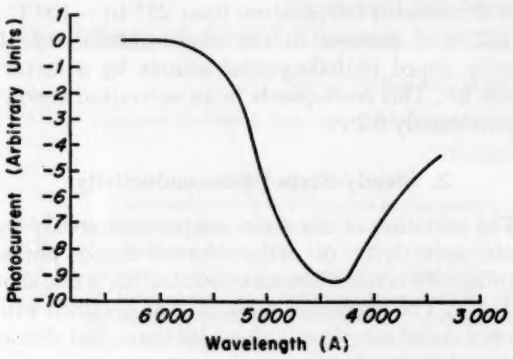

FIG. 2. Action spectrum of the reverse photoconductivity effect (100 A bandwidth). The spectrum was measured under the condition of constant energy at all wavelengths, and a scanning rate of approximately 100 A/3 sec.

by an increase in photoconductivity if the illumination at that wavelength is prolonged.

The rise and decay curves for photoconductivity in ortho-chloranil-doped phthalocyanine induced by light in the phthalocyanine absorption bands consist of two components. One of these is quite rapid and has time constants essentially the same as those of the undoped material. The other component is very much slower and is unimolecular for both rise and decay with a time constant of about 60 sec. This is shown for the photoconductivity decay in Fig. 3. The fact that rise time equals decay time required that the process be determined by the balance of the rate of input of quanta and the intrinsic decay rate, $dX/dt = (\text{const})I_0 - \lambda X$, where I_0 is the rate of input of quanta and λ is the unimolecular decay constant. The ratio of slow to fast components increases with increasing doping. In the most heavily doped samples, the photoconductivity rise and decay is due essentially completely to the 40-sec time constant process. At low temperatures, the time constant decreases and is about 36 sec at −100°C.

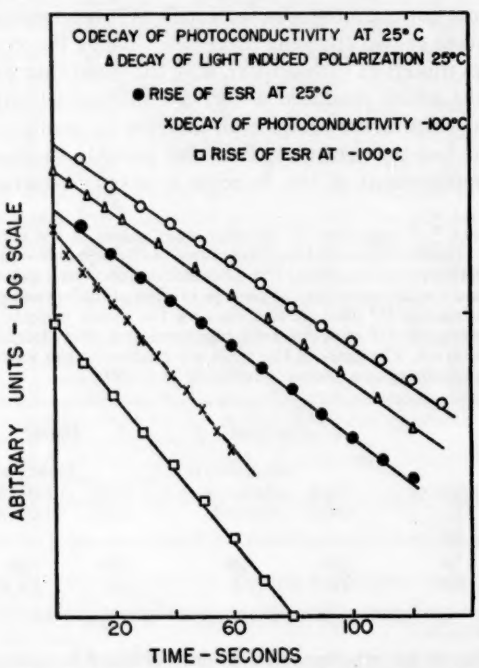
○ DECAY OF PHOTOCONDUCTIVITY AT 25° C
△ DECAY OF LIGHT INDUCED POLARIZATION 25°C
● RISE OF ESR AT 25°C
× DECAY OF PHOTOCONDUCTIVITY -100°C
□ RISE OF ESR AT -100°C
ABITRARY UNITS - LOG SCALE
20
60
100
TIME - SECONDS

FIG. 3. Semilog plots of time-dependence of photoconductivity, light-induced ESR and light-induced polarization in doped phthalocyanine. The relative positions of each of the curves in this figure are not comparable.

3. Electron Spin Resonance

It was observed that when ortho-chloranil was added to a sample of phthalocyanine in the manner described in the foregoing, a large ESR absorption could be detected, corresponding to the presence of unpaired electron spins in the sample (see Fig. 4). The greater the extent of doping, the greater the ESR signal. When the sample was cooled to about −100°C in the spectrometer cavity, no change in spin concentration or line shape could be observed.

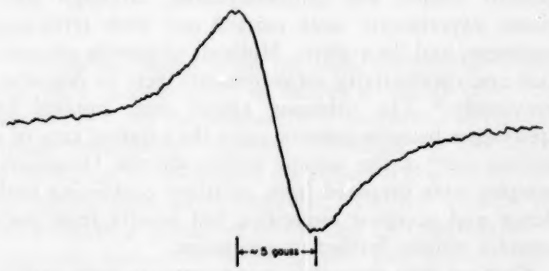

FIG. 4. Electron spin resonance spectrum of ortho-chloranil-doped phthalocyanine. The curve represents the first derivative of the absorption.

Inasmuch as it was not possible to achieve uniform mixing of phthalocyanine and ortho-chloranil, it was therefore not possible to measure the ratio of unpaired spins to the number of ortho-chloranil molecules in actual contact with phthalocyanine molecules. The number (by comparison with diphenylpicrylhydrazyl) of unpaired spins per total number of ortho-chloranil molecules added is 0.01. It is of interest to note that even in those cases for which stoichiometric compounds between electron donor (reductant) and electron acceptor (oxidant) have been measured, the number of unpaired electron spins is always much smaller than that expected for simple complete electron transfer complexes ($[D\cdot]^+[A\cdot]^-$).[18,19]

When a heavily doped sample was illuminated in the ESR spectrometer, a *decrease* in unpaired spins could be observed (see Fig. 5). The magnitude of this effect corresponded to approximately a 5–20% decrease in the spin concentration, depending upon the sample

[18] Y. Matsunaga, J. Chem. Phys. **30**, 855 (1959).
[19] Buck, Lupinski, and Oosterhoff, Mol. Phys. **1**, 196 (1958), and private communication.

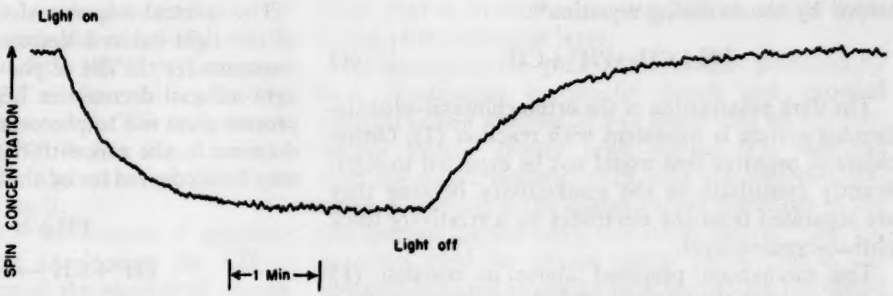

FIG. 5. Effect of illumination with white light on the ESR signal in ortho-chloranil-doped phthalocyanine. Curve represents unpaired spin concentration *vs* time.

used, and was independent of the temperature. The spectral response of the photodecrease in spin concentration followed the phthalocyanine absorption spectrum. The photoinduced decrease in ESR and the subsequent rise in spin concentration, when the light was turned off, followed unimolecular kinetics with a time constant of approximately 60 sec (see Fig. 3). At −100°C, the time constant decreased to about 36 sec (see Fig. 3).

4. Light-Induced Polarization

When an ortho-chloranil-doped phthalocyanine film was placed between the plates of a condenser, a charging of the condenser could be observed, using a vibrating-reed electrometer to measure the voltage developed (see Fig. 6). The sign of the induced charge on the condenser plates indicated that the phthalocyanine layer was positive with respect to the ortho-chloranil. When such a cell was illuminated, an increase in polarization was observed. The spectral response of the photoinduced charge produced on the plates corresponded to phthalocyanine absorption. The polarity of the effect demonstrated that the phthalocyanine layer became more positive with respect to the ortho-chloranil layer upon illumination.

The rise and decay of the light-induced charge on the condenser plates followed unimolecular kinetics with a room temperature time constant of about 60 sec (see Fig. 3). The experimental arrangement did not permit cooling of the sample.

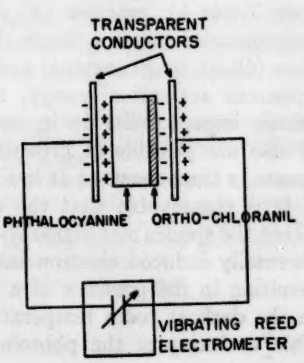

FIG. 6. Schematic diagram of polarization apparatus. The plates of the condenser were approximately 10^{-2} cm apart. The maximum voltage obtainable in this system upon illumination was about 100 mv.

5. Flash-Induced Photoconductivity

A moderately doped sample of phthalocyanine was examined by the flashing light method described previously.[15] The decay of the photoconductivity produced by light in the phthalocyanine absorption region is shown in Fig. 7, together with a decay curve for undoped material with and without ambient illumination.[15] This fast process represents only a fraction of the changes described in the three foregoing paragraphs.

DISCUSSION AND CONCLUSIONS

The concurrent increase in dark conductivity and ESR in phthalocyanine upon the addition of ortho-chloranil may be explained in the following manner. Ortho-chloranil is a strong oxidizing agent and therefore might be expected to remove electrons from the phthalocyanine if the two substances were placed in intimate contact. The relative ease of transfer of electrons from the phthalocyanine to the ortho-chloranil would depend upon the electron affinity of ortho-chloranil and the ionization potential of phthalocyanine. It is postulated, then, that such an electron transfer takes place in the dark in the doped samples. This gives rise to the observed ESR. Positive holes which can conduct are formed in the phthalocyanine layer as a result of the transfer and give rise to the large dark currents. This electron-transfer process may be repre-

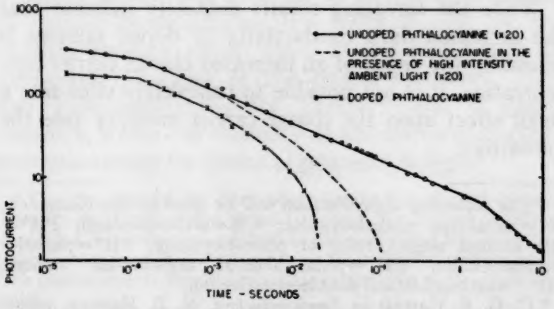
UNDOPED PHTHALOCYANINE (x20)
UNDOPED PHTHALOCYANINE IN THE PRESENCE OF HIGH INTENSITY AMBIENT LIGHT (x20)
DOPED PHTHALOCYANINE
PHOTOCURRENT
TIME - SECONDS

FIG. 7. Flash-induced photoconductivity in doped phthalocyanine as compared with that in undoped phthalocyanine with and without ambient illumination. The unit on the ordinate is 5×10^{-7} amp.

sented by the following equation[20]:

$$PH+CH \rightarrow PH^{+}+CH^{-}. \quad (1)$$

The dark polarization of the ortho-chloranil–phthalocyanine system is consistent with reaction (1). Ortho-chloranil negative ions would not be expected to significantly contribute to the conductivity because they are separated from the electrodes by a relatively thick phthalocyanine layer.

The mechanism proposed above in reaction (1) postulates that the increase in dark conductivity upon doping is due to the actual formation of charge carriers, as opposed to an increase in the mobility of charge carriers already present in the undoped material. This is supported by the following observations: (a) The dark conductivity of pure phthalocyanine has an activation energy of about 1 ev.[15] This has been ascribed primarily to the process of formation of charge carriers.[21] On the other hand, the photoconductivity of pure phthalocyanine has an activation energy of only 0.2 ev,[15] and this can be interpreted in terms of charge carrier mobility.[22] The fact that cooling a doped phthalocyanine sample to $-100°C$ does not decrease the ESR signal and produces a much smaller decrease in dark conductivity (see Table I) than is produced in an undoped sample demonstrates that the primary process which occurs in the dark upon doping is not appreciably reversed at the low temperature. Therefore, the decrease in dark conductivity in doped material at $-100°C$ can be attributed to the temperature dependence of mobility. Such an identification is supported by the fact that photoconductivity in both doped and undoped samples has this same temperature dependence. This, we feel, is strong evidence that the main result of doping is to produce charge carriers. (b) When moderately doped samples are subjected to flash illumination the decay curves for photoconductivity are essentially identical with the curves obtained with undoped samples in the presence of high intensity ambient illumination[15] (see Fig. 7). This indicates that charge carriers are indeed produced by doping and that these carriers behave in the same manner as do photoproduced carriers.

While the foregoing results definitely indicate that the increased dark conductivity in doped samples is primarily the result of an increased charge carrier concentration, it is not possible to completely eliminate a small effect upon the charge carrier mobility (see the following).

The spectral response of the photoconductivity and of the light-induced decrease in ESR, and the time constants for the rise of photoconductivity and for the light-induced decrease in ESR indicate that the same process gives rise to photoconductivity and results in a decrease in the concentration of unpaired spins. This may be accounted for by the following processes.

$$PH+h\nu \rightarrow PH^{*} \quad (2)$$

$$PH^{*}+CH^{-} \rightarrow PH^{+}+CH^{-\,-}. \quad (3)$$

This requires that the paramagnetic species observed in ESR be CH^{-} and that PH^{+}, although paramagnetic, is not detected, perhaps due to broadening of the resonance line. The decrease in ESR, then, is the result of the transformation of CH^{-} radicals into $CH^{-\,-}$ ions which, due to aromatization of the pi-electron system, would not be paramagnetic. The 60-sec time constant observed in these experiments demonstrates that charge carriers have a considerably longer lifetime in the doped material than in the undoped material. This would result in a large increase in steady-state photoconductivity upon doping, in agreement with experiments.

It is also possible to interpret the light-induced polarization phenomenon in terms of reaction (3). It is apparent from the method of doping and from Fig. 6 that most of the CH^{-} radicals will be in fixed positions near one surface of the phthalocyanine layer. Therefore, the postulated electron transfer from PH^{*} to CH^{-} should result in an increased polarization, in which the ortho-chloranil layer becomes more negative with respect to phthalocyanine. The rise time, spectral response, and measured polarity of the polarization effect are consistent with this hypothesis.

It was noted above that the decay of photoconductivity, the rise of ESR and the polarization decay, after illumination ceased, were all unimolecular processes having the same time constant. This can be interpreted in terms of the following reaction as the rate-limiting step in all of these processes:

$$PH^{+}+CH^{-\,-} \rightarrow PH+CH^{-}. \quad (4)$$

Inasmuch as the concentration of PH^{+} is high in the dark and is not appreciably changed by illumination (see Table 1), reaction (4) should result in pseudo-unimolecular kinetics. Since this reaction is relatively slow (60-sec time constant) and yet has only a negligible apparent activation energy, there must be some intrinsic improbability in it, as yet not understood. It is also not possible at present to account for the decrease in time constant at low temperatures.

It is conceivable that the energy relationships between the species mentioned above are such as to allow a thermally induced electron transfer from PH to CH^{-} resulting in the presence of a small amount of $CH^{-\,-}$ in the dark at room temperature. It is therefore possible to interpret the photoinduced decrease in con-

[20] The following abbreviations will be used in the discussion: PH = metal-free phthalocyanine; CH = ortho-chloranil; PH^{*} = first excited singlet state of phthalocyanine; PH^{+} = phthalocyanine holes; CH^{-} = ortho-chloranil negative-ion radical; $CH^{-\,-}$ = ortho-chloranil double-negative ion.

[21] C. G. B. Garrett in *Semiconductors*, N. B. Hannay, editor (Reinhold Publishing Corporation, New York, 1959), Chap. 15, p. 662 ff.

[22] Kommandeur, Korinek, and Schneider, Can. J. Chem. **35**, 998 (1957).

ductivity (see Fig. 2) as the result of an excitation of CH^{--} with the subsequent transfer of an electron to PH^+ forming PH and CH^-.§ At −100°C the amount of CH^{--} becomes vanishingly small, resulting in the disappearance of this photoreversal. The wavelength for maximum response at 4300 A (see Fig. 2) might very well correspond to the absorption of CH^{--} in the matrix in which it finds itself.

According to reaction (1), the number of unpaired spins produced by doping (neglecting the CH^{--} concentration) is a measure of the number of charge carriers produced in the phthalocyanine layer. Thus, by measuring the conductivity of a sample with a measured spin concentration, it is possible to calculate a charge carrier mobility by the following equation:

$$I=\mu NEA, \tag{5}$$

where I=current in electrons per second; μ=mobility in $cm^2/v/sec$; N=number of charge carriers/cm^3; E=field strength; and A=cross-sectional area of conductor.

Such a calculation results in a value of 10^{-4} $cm^2/v/sec$ for the mobility of holes in ortho-chloranil-doped phthalocyanine. By measuring the number of light quanta required to produce a given current,[23] it is possible to calculate a quantum yield for the production of holes in such a system, using the above value for the mobility. This was found to be approximately unity.

It is interesting to compare the mobility given in the foregoing with those obtained in inorganic semiconductors such as germanium and silicon. These latter normally range from 1 to 1000 $cm^2/v/sec$ at room temperature. Therefore, a value of 10^{-4} $cm^2/v/sec$ for an organic material is in keeping with the large differences between the crystal interactions in valence crystals and those in organic molecular crystals. For example, heats of sublimation are about 3–4 ev for valence crystals and about 10^{-2} ev for molecular crystals.

It is of interest to inquire into the relationship between charge carriers in doped and undoped phthalocyanine. It was noted above that the behavior of the flash-induced photoconductivity of doped phthalocyanine was essentially identical with that of pure phthalocyanine in the presence of high-intensity ambient light. This would argue that the dark carriers and the light-produced carriers in doped material are the same as those produced by light in undoped material, that is, in both cases current is carried by holes in the phthalocyanine layer.

By comparing the peak photocurrents produced by flash illumination in heavily doped and undoped phthalocyanine samples, it was found that an approximately 10-fold greater peak current was obtained with the doped material than with the undoped material. Therefore, if the charge carrier mobilities in the two systems are the same, this would require[24] that the quantum yield for charge carrier production in the undoped material be about 10% of that for the doped material (that is, approximately 0.1). However, due to the concentration dependence of mobility,[15] one would expect that carrier mobility in doped phthalocyanine would be smaller than in undoped material, as a result of the higher dark carrier concentration in the doped samples. Thus, the intrinsic quantum yield for undoped phthalocyanine is probably lower than 0.1.

It was noted that doping produces a 10^5-fold increase in steady-state photocurrents but only a 10-fold increase in flash-induced photoconductivity is observed. This may be attributed to the fact that the use of a short-duration light pulse to produce charge carriers tends to eliminate effects caused by differences in recombination times in the two systems, whereas steady-state experiments accentuate these differences.

The considerations presented in this section indicate that the over-all result of adding a strong electron acceptor to a phthalocyanine film is to increase the quantum yield for charge carrier production and to increase charge carrier lifetime. Thus, the ortho-chloranil negative ions act as efficient centers for the conversion of electromagnetic energy, which may be absorbed by phthalocyanine molecules situated many molecular diameters away, into charge carriers, and also act as effective electron traps. Similar, but apparently less effective, impurity centers existing in small amounts in undoped phthalocyanine could be responsible for its photoconductivity. Alternatively, the host molecules themselves could function as ionization centers.[25]

The present results indicate that the presence of electron-accepting impurities in organic semiconducting systems will increase the probability of utilization of charge carriers for chemical or biological processes by making recombination less probable and by increasing quantum yields. These factors would tend to counteract the effect of low carrier mobilities. This may have significance for photosynthesis in plant materials, where the efficiency of utilization of electromagnetic energy for chemical processes is high.

§ It is also possible that an excited CH^{--} could transfer an electron to PH, forming PH^- and CH^-. The PH^- could recombine with a PH^+ to give the same net result.

[23] The quantum yield was determined by measuring the ratio of the initial rate of rise of photoconductivity to the rate of input of quanta. The measurement was carried out over a time interval of one second. The fact that the time constant for photocurrent decay was 60 sec would minimize any errors due to carrier recombination during the course of the measurement.

[24] The rise time of the flash photocurrent (*ca.* 3 μsec) is considerably smaller than the decay time (see Fig. 7) and therefore errors due to carrier recombination are minimized by using the peak photocurrent in the comparison. Thus the ratio of the peak flash photocurrents should approximate the ratio of the quantum yields.

[25] L. E. Lyons, J. Chem. Soc. **1957**, 5001.

Dynamical Theory of Diffusion in Crystals. IV. Some Aspects of the Introduction of Irreversibility

STUART A. RICE*† AND HARRY L. FRISCH

Bell Telephone Laboratories, Incorporated, Murray Hill, New Jersey

(Received October 21, 1959)

The origin of irreversibility in the phenomenon of crystal diffusion is examined from a dynamical point of view. It is shown that straightforward considerations lead to the establishment of two time scales, one for jumps between lattice sites and one for vibrations about a given lattice point. The dissipation of energy is shown to occur almost entirely by relaxation of "recaptured" particles, little energy being lost in the transit across the barrier. The quasi-equilibrium and nonequilibrium formulations are compared and shown to be quite similar in structure and functional dependence.

1. INTRODUCTION

In several preceding papers[1–4] there has been developed a dynamical theory of self-diffusion in crystals. The basis of the theory lies in the observation that, in general, the path an atom must follow in making a diffusive jump does not lie along a normal coordinate. The motion along the diffusive trajectory is therefore determined by the superposition of all normal vibrations with nonvanishing projections on the given path. This motion is not purely harmonic, but has a character and mean period determined by the superposition of harmonic motions. When the contributing normal vibrations are in proper phase, the amplitude of the motion along the diffusive path can be large and the atom can move from its original lattice site into that of the vacancy.

The last sentence of the preceding paragraph represents three approximations in the theory. First, the motion of the atom is described in terms of the equilibrium distribution of normal vibrations without consideration of the perturbation to equilibrium caused by the transport process itself. In extensive investigations, Prigogine,[5] Curtiss,[6] Montroll,[7] and Bak[8] have shown that when the energy of activation is greater than 10–20 kT the error made in using the equilibrium distribution for rate calculations is negligible. This approximation is therefore very good for the case of diffusion where the heat of activation often exceeds 20 kT.

The second approximation is contained in the words "normal vibration." The implication of these words is that anharmonic forces are negligible. In fact, it has been shown that in the absence of anharmonicity, there would be no pressure dependence of the diffusion coefficient.[2] As we shall see in this paper, the anharmonic terms are fundamental to the coupling leading to irreversibility, but need not be considered when calculating the functional form of the jump frequency to first order.

The third approximation is of a more fundamental nature since it concerns the question of irreversibility. The diffusive motion has been described as irreversible by the use of the Einstein relation,

$$\mathfrak{D}=\Gamma[(\Delta x)^2/2], \tag{1}$$

with Γ the frequency of jumps, Δx the length of a jump and $\mathfrak{D}$ the diffusion coefficient. The difficulty lies not so much in the use of the Einstein relationship, as in the criterion for the irreversible jump. An atomic displacement along the diffusive path was taken as a diffusive jump only if it exceeded a critical distance, q_0. In this declaration of irreversibility by fiat, no account is taken of the loss of energy necessary to render the jump irreversible. In a classical mechanical picture such as discussed herein, the reflection of the particle from the vacancy site is certain unless there is some de-excitation process. It is the mechanism of de-excitation which is the subject of this paper.

The problem we have set for ourselves is clearly one of vibrational relaxation. The theory of vibrational relaxation of diatomic molecules coupled to a heat bath has been studied in detail by Montroll and co-workers.[7] In this theory, it is assumed that the approach to equilibrium is characterized by the stochastic process generated by the set of differential equations,

$$dx_n/dt=\sum_m(W_{nm}{}^*x_m-W_{mn}{}^*x_n) \tag{2}$$

where $x_n(t)$ is the fraction of molecules in the nth energy state at time t, and the $W_{mn}{}^*$ are the transition

* Alfred P. Sloan Fellow.

† Permanent address: Department of Chemistry and Institute for the Study of Metals, University of Chicago, Chicago 37, Illinois.

[1] S. A. Rice, Phys. Rev. **112**, 804 (1958).

[2] S. A. Rice and N. H. Nachtrieb, J. Chem. Phys. **31**, 135 (1959).

[3] Lawson, Rice, Corneliussen, and Nachtrieb, J. Chem. Phys. **32**, 447 (1960).

[4] O. P. Manley and S. A. Rice, Phys. Rev. **117**, 632 (1960).

[5] I. Prigogine, Physica **15**, 913 (1949); **16**, 51 (1950).

[6] C. F. Curtiss, "The equilibrium assumption in the theory of absolute reaction rates," University of Wisconsin, Dept. CM-476 (June, 1948).

[7] E. W. Montroll and K. E. Shuler, J. Chem. Phys. **26**, 454 (1957), Advances in Chem. Phys. **1**, 361 (1958), and references cited therein.

[8] T. Bak and I. Prigogine, J. Chem. Phys. **31**, 1368 (1959).

probabilities for the process $n \rightarrow m$. The coupling of the diatomic molecule to the heat bath results in transitions for which W_{mn}^* is taken to be given by the Landau-Teller relation[9]

$$P_{mn} = P_{10}[(m+1)\delta_{n-1,m} + m\delta_{n+1,m}]$$

$$W_{n+1,n}^* = Z^* N^* \exp(-h\nu/kT) P_{n,n+1}$$

$$W_{n,n+1}^* = Z^* N^* P_{n+1,n} \tag{3}$$

where P_{10} is the transition probability per collision for the transition $0 \rightarrow 1$ and P_{mn} is similarly defined. The total transition probability depends in the indicated manner on the collision number, Z^*, and the concentration of heat bath molecules, N^*. Now, a molecule initially in the nth state wanders at random amongst the energy levels until equilibrium is attained. Both increases and decreases in n are permitted, subject only to the values of W_{mn}^*. This model is the quantum mechanical analog of the Kramers formulation of the Brownian motion of a harmonic oscillator.[10]

The approach to equilibrium in a crystal could be based on a similar analysis to the one outlined above. Note that Eq. (2) is a first order differential equation with the inherent property of time irreversibility. Since our object is to examine the mechanical basis for diffusion, we shall use a different approach. What is required is the study of the de-excitation of specific normal modes of vibration. Since a normal mode in a crystal represents a collective motion of many atoms, the synthesis of the contributing normal modes into a wave packet becomes necessary to define the motion of an atom. Thus, the description of the approach of an atom to equilibrium with its surroundings in this analysis requires the discussion of the simultaneous relaxation of many normal modes and their interactions. We shall carry out these formal calculations in Sec. III. However, since such an approach tends to focus attention on the normal modes rather than on the diffusing atom and is, moreover, difficult to carry through, we have adopted an alternative procedure to introduce the relevant physical phenomena.

The method we shall use to introduce the discussion of de-excitation depends on two observations. First, the time scale on which diffusive motion occurs is bifurcated into a long time interval during which there is relaxation between lattice sites, and a short time interval during which relaxation of very short displacements about a given lattice site occur. A significant fraction of our efforts will be devoted to the demonstration that such a distribution of relaxation times indeed exists. Second, the fact that any given motion is the resultant of a very large number of superposed normal vibrations suggests that the atom executes a random walk about its lattice site. The relaxation of small amplitude displacements, being weakly coupled to the crystal, satsifies a diffusion relationship. The diffusion coefficient, or relaxation time, will be seen to be related to the distribution of normal modes. The random walk which defines the relaxation is a reflection of the spectrum of interactions being random in time and is caused by the essentially continuous direct and indirect interactions between an atom and its surroundings.

In the following, we shall proceed by first considering a one-dimensional model for which we shall make a detailed analysis of the anharmonic behavior of an atom during one period of the motion. With this background, we then turn to a study of the relaxation of an atom in three dimensions.

II. A ONE-DIMENSIONAL MODEL

Consider a system of N coupled point masses in a one-dimensional lattice, with coordinates $x_{-N/2}, \cdots, x_{N/2}$, and a vacant site at the center of the lattice. Let a be the lattice spacing and y the resultant deviation in distance between the masses associated with the lattice points ± 1. The problem to be considered is the migration of the mass points located at 1 or -1 into the vacancy located at lattice point 0 formed at time $t=0$ in this system. It will be assumed that the masses associated with lattice points j, where $|j|>1$, are bound harmonically to their near neighbors. The masses at -1 and 1 will be subjected to a nonlinear force due to the presence of the vacancy. When a diffusive jump occurs, the nonlinear potential is assumed to shift and always act only between the atoms bracketing a vacancy.

A qualitative analysis of the problem outlined above is pertinent at this point. We note that the lattice $j=\pm 2, \cdots \pm N/2$ will act as a heat bath coupled to the wandering particles at ± 1. A diffusive jump carries a point mass from ± 1 to 0 where it carries out a number of vibrations with lifetimes of order ν^{-1} where ν is a characteristic lattice frequency. After a longer time, Γ^{-1}, the particle may either jump back to its original lattice site or a neighbor may jump into the vacancy created by the first jump. We restrict consideration to the first jump.

Our qualitative analysis is aided by the reduction of the system to the simplest possible model. We take as a simple nonlinear potential acting between particle ± 1

$$\Phi(y) = \Phi_0 y^2 (y-a)^2. \tag{4}$$

Note that when y is small compared with a, the potential is harmonic being given by $\Phi = \Phi_0 a^2 y^2$. Letting $y_{\pm j}$, $2<j<N/2$, be the resultant deviation in distance between particles $\pm j$ and $\pm(j+1)$, the Hamiltonian

[9] L. Landau and E. Teller, Physik. Z. Sowjetunion **10**, 34 (1936).

[10] H. A. Kramers, Physica **7**, 284 (1940); S. Chandrasekhar, Revs. Modern Phys. **15**, 1 (1943).

of our system is

$$E=H(y,\dot{y},y_{\pm i},\dot{y}_{\pm i})$$
$$=(m/2)\dot{y}^2+\Phi(y)+H_{N-2}(y_{\pm i},\dot{y}_{\pm i}) \quad (5)$$

where

$$H_{N-2}(y_{\pm i},\dot{y}_{\pm i})=\sum_{j=2}^{N/2}[(m/2)\dot{y}_{\pm i}^2+(k/2)y_{\pm i}^2] \quad (6)$$

with k a harmonic spring constant.

Since the system is initially at equilibrium, the mean time interval required for an extension dy to be obtained is given for a very large heat bath by

$$\langle dT\rangle=\lim_{\tau\to\infty}(1/\tau)\int_0^\tau dt\lim_{N\to\infty}\int_{\Omega_{N-2}}d\Omega_{N-2}{}^0 \quad (7)$$
$$\cdot[dy/(dy/dt)]\exp[-H(\Omega_N{}^0)/kT]$$
$$=\lim_{\tau\to\infty}(1/\tau)\int_0^\tau dt\lim_{N\to\infty}\int_{\Omega_{N-2}}d\Omega_{N-2}{}^0$$
$$\cdot[dy/(dy/dt)]\exp[-H_{N-2}(\Omega_{N-2}{}^0)kT]/Z$$
$$\cdot\exp[-H-H_{N-2})/kT]=\langle[dy/(dy/dt)]$$
$$\cdot\exp[-(H-H_{N-2})/kT]\rangle, \quad (8)$$

where Z is the partition function for the system. Thus, the mean time required for a jump of distance a is given by

$$\langle T\rangle=\int_0^a\langle[dy/(dy/dt)]\exp[-(H-H_{N-2})/kT]\rangle. \quad (9)$$

The appearance of the exponential factor in the above relation arises naturally from the canonical weighting of a fluctuation leading to the occurrence of the diffusive jump.

The simplest way of evaluating the above expression, which introduces also the element of irreversibility in this description, is by assuming that the effect of the diffusive jump on the detailed dynamics of the remainder of the lattice heat bath can be ignored due to the large size of the heat bath. With this decoupling, it is consistent to consider the heat bath to have its equipartition energy of $(N-2)kT$. Thus, if

$$H-H_{N-2}=E-H_{N-2}\approx E-\langle H_{N-2}\rangle=\epsilon,$$

is the average energy possessed by the wandering mass, we find

$$\langle T(\epsilon)\rangle=\int_0^a\frac{dy}{\{(2/m)[\epsilon-\Phi(y)]\}^{\frac{1}{2}}}\exp(-\epsilon/kT)$$
$$\epsilon\geq\epsilon^+$$
$$=\infty \qquad \epsilon<\epsilon^+ \quad (10)$$

and $\epsilon^+=\Phi(a/2)=\Phi_0a^4/16$ is the minimum activation energy. A mass with insufficient energy $\epsilon<\epsilon^+$ can never make a displacement as large as $a/2$. It is convenient to rewrite the above elliptic integral in the standard form[11]

$$\langle T(\epsilon)\rangle/\exp(-\epsilon/kT)=\int_0^a\frac{dy}{(2\Phi_0/m[b^4-y^2(y-a)^2])^{\frac{1}{2}}}$$
$$=(m/2\Phi_0)\cdot(\sqrt{2}/b)[K(k)-F(\varphi,k)], \quad (11)$$

where

$$k^2=[(a^2/4)+b^2]/2b^2, \quad (12)$$

$$\varphi=\cos^{-1}\left\{\frac{a/2}{[(a^2/4)+b^2]^{\frac{1}{2}}}\right\}, \quad (13)$$

$$b^2=(\epsilon/\Phi_0)^{\frac{1}{2}}, \quad (14)$$

with $F(\varphi,k)$ Legendre's normal elliptic integral of the first kind and $K(k)=F(\pi/2,k)$ the corresponding complete elliptic integral.[11] The diffusion coeficient is obtained immediately from the combination of Eqs. (1) and (11).

The ratio of the frequencies of small and large displacements (at constant ϵ) is

$$\frac{\langle T_S\rangle}{\langle T_L\rangle}=\frac{b_L}{b_S}\frac{K(k_S)-F(\varphi_S,k_S)}{K(k_L)-F(\varphi_L,k_L)} \qquad \epsilon\geq\epsilon^+$$
$$\approx 0, \qquad \epsilon<\epsilon^+. \quad (15)$$

The small displacements are characterized by energies $\epsilon\approx kT\ll\epsilon^+$ so that in fact the ratio of the two mean time intervals is small. The preceding statement contains the implication that the rate-determining step in the atomic jump is the acquisition of the energy required to surmount the barrier. That this is true may be easily seen from the form of Eq. (15) and the interpretation of Eq. (7) in terms of energy fluctuations.

If we follow the analysis introduced by Kirkwood,[12] a description of the particle motion in time intervals, long compared to $\langle T_S\rangle$ but short relative to $\langle T_L\rangle$, will have the character of irreversibility. The specific implementation of such an analysis requires a more detailed investigation of the dynamics of our one-dimensional lattice and vacancy to exhibit explicitly the existence of two time scales arising naturally from the mechanical motions of our system.

Consider the motion of the masses located at 1 and -1. The equations of motion are

$$\ddot{x}_j+\tfrac{1}{2}\omega_0^2(x_j-x_{j-1})+\tfrac{1}{2}\omega_0^2(x_j-x_{j+1})=0;$$
$$j=\pm 2,\cdots,\pm\tfrac{1}{2}N$$
$$\ddot{x}_1-\tfrac{1}{2}\lambda\psi(x_1-x_{-1})+\tfrac{1}{2}\omega_0^2(x_1-x_{-1})+\tfrac{1}{2}\omega_0^2(x_1-x_2)=0$$
$$\ddot{x}_{-1}+\tfrac{1}{2}\lambda\psi(x_1-x_{-1})+\tfrac{1}{2}\omega_0^2(x_{-1}-x_1)+\tfrac{1}{2}\omega_0^2(x_{-1}-x_{-2})=0,$$
$$\omega_0^2=k/m, \quad (16)$$

with k the force constant of the harmonic potential, λ a coupling constant and where $(m\lambda/2)\psi(x_1-x_{-1})$ is the

[11] P. F. Byrd and M. D. Friedman, *Handbook of Elliptic Integrals* (Springer-Verlag, Berlin, 1954).
[12] J. G. Kirkwood, J. Chem. Phys. **14**, 180 (1946).

nonlinear force acting on the particles adjacent to the vacancy. We seek the amplitude, $y=x_1-x_{-1}$, on condition that the remainder of the lattice act as a heat bath and be little effected by the anharmonicity of the motions adjacent to the vacancy. The procedure followed is to reduce the N-body problem in the simplest possible manner to a nonlinear vibration of one degree of freedom under the influence of an external force. The reduction is effected by utilizing the linear equations of motion for the remainder of the lattice, and then regarding the heat bath as the source of the external driving force. The nonlinear excited vibration problem can then be solved to an accuracy of order λ^2 by the method of Krylov and Bogolubov.[13]

In the absence of the nonlinear force, the solution of Eq. (16) is

$$x_j^0(t)=\sum_{k=-N/2}^{N/2}[\alpha_{jk}\sin(\omega_k t+\delta_k)+\beta_{jk}\cos(\omega_k t+\delta_k)] \quad (17)$$

where ω_k is the kth eigenfrequency of the linear lattice, α_{jk} and β_{jk} are the contributions of the kth normal vibration to the motion of the jth atom, and δ_k are the phases of the normal vibrations.

To a sufficient approximation, all the $x_j(|j|>1)$ can be approximated in the equations of motion of x_1 and x_{-1} by Eq. (17). This ansatz leads to the two relations,

$$\ddot{x}_1-(\lambda/2)\psi(y)+\tfrac{1}{2}\omega_0^2 y+\tfrac{1}{2}\omega_0^2(x_1-x_2^0)=0,$$
$$\ddot{x}_{-1}+(\lambda/2)\psi(y)-\tfrac{1}{2}\omega_0^2 y+\tfrac{1}{2}\omega_0^2(x_{-1}-x_{-2}^0)=0. \quad (18)$$

By subtraction of the second of Eqs. (18) from the first

$$\ddot{y}-\lambda\psi(y)+\tfrac{3}{2}\omega_0^2 y=\tfrac{1}{2}\omega_0^2(x_{-2}^0-x_2^0)=F^0(t)/m, \quad (19)$$

and it is seen that y indeed executes a forced nonlinear oscillation under a rapidly varying external force, $F^0(t)$, whose explicit form in terms of initial positions, velocities, and time is given by Eq. (15). $F^0(t)$ corresponds to a kind of Brownian motion force in the sense that its mean frequency is relatively large as compared with the jump frequency. That is, $F^0(t)$ corresponds to the superposition of many sinusoidal functions with widely varying frequencies. The resultant of this superposition has, in general, local fluctuations superimposed on any periodic or quasi-periodic time dependence. It is these fluctuations which provide a rapid local variation to $F^0(t)$. From Eq. (17) we see that $F^0(t)$ is a trigonometric polynomial. In a certain sense, Eq. (17) may be regarded as the spectrum of the force $F^0(t)$.

To obtain a solution to Eq. (19) put

$$y=z+(x_1^0-x_{-1}^0)=z+Y(t). \quad (20)$$

With the substitution of (20) into (19) we find

$$\ddot{z}+(3\omega_0^2/2)z=\lambda\psi[z+Y(t)] \quad (21)$$

since, by virtue of Eq. (17),

$$\ddot{Y}+\tfrac{3}{2}\omega_0^2 Y=F^0(t)/m. \quad (22)$$

Consider the generating solutions,

$$z=A\sin(\omega t+\delta)$$
$$\dot{z}=A\omega\cos(\omega t+\delta)$$
$$\omega^2=\tfrac{3}{2}\omega_0^2 \quad (23)$$

obtained from Eq. (21) by setting $\lambda=0$. If we take ψ to be a polynomial and use Eq. (17), it follows that

$$\psi[z+Y(t)]=\psi_0(z)+\sum_n^M[\psi_{n,1}(z)\cos\gamma_n t+\psi_{n,2}(z)\sin\gamma_n t], \quad (24)$$

where the Fourier expansion of ψ contains only a finite number of terms because $F^0(t)$ is a finite sum of functions. Note that one term has been separated from the sum for later convenience. The index n indicates the finite set of frequencies γ_n which are linear combinations of the eigenfrequencies ω_k. To obtain the desired first-order approximation, take a trial solution of the form,

$$z(t)=A(t)\sin v(t)=A(t)\sin(\omega t+\delta(t)), \quad (25)$$

Eq. (24) then becoming

$$\psi_0(A\sin v)=\sum_{k\geq 0}^{N'}h_k(A)\sin kv,$$
$$\psi_{n\,i}(A\sin v)=\sum_{k\geq 0}^{N'}h_{n\,i,k}(A)\sin kv, \quad (26)$$

since we again deal with finite sums of functions in $\psi_{n,1}$ and $\psi_{n,2}$ and the expansion coefficients h_k, $h_{n\,i,k}$ are functions of the amplitude A.

Consider now that a time smoothing is introduced over an interval τ long compared with ω_k^{-1} but short compared with ν^{-1}.[12] The time smoothing of Eq. (21) leads to

$$\langle F^0(t)/m\rangle_{\mathrm{Av},t}=\langle\tfrac{1}{2}\omega_0^2(x_{-2}^0-x_2^0)\rangle_{\mathrm{Av},t}$$
$$=\tfrac{1}{2}\omega_0^2[x_{-2}^0(0)-x_2^0(0)]+R(t) \quad (27)$$

where $R(t)$ contains the contributions to the motion from the very low frequency lattice vibrations, $\omega_k<\nu$. The time averaged random force is seen to contain two components, one being a constant dependent upon the initial conditions, and one being slowly varying in time. To complete the necessary transformations, we now consider an ensemble of linear lattices and, following Kirkwood,[12] take the ensemble average of the time average of the random force. This gives

$$\langle\langle F^0(t)/m\rangle_{\mathrm{Av},t}\rangle=2a\omega_0^2, \quad (28)$$

since

$$\langle\langle x_{-2}^0(0)-x_2^0(0)\rangle_{\mathrm{Av},t}\rangle=4a$$
$$\langle\langle R(t)\rangle_{\mathrm{Av},t}\rangle\cong 0. \quad (29)$$

[13] See for example N. Minorsky, *Introduction to Nonlinear Mechanics* (Edwards Brothers, Inc., Ann Arbor, Michigan, 1946).

It may then be shown[13] that the use of Eqs. (25) and (26) to solve the ensemble averaged and time smoothed equation of motion leads to

$$dA/dt=0, \qquad dv/dt=\omega-(\lambda/2\omega A)h_1(A) \tag{30}$$

and

$$y=A\sin v$$

$$+\lambda\sum_{k=2}^{N'}\frac{h_k\sin kv}{(1-k^2)\omega^2}-(\lambda/2)\sum_n^M\sum_{k\geq 0}^{N'}\frac{h_{n2,k}\cos(kv+\gamma_n t)}{\omega^2-k(\omega+\gamma_n)^2}$$

$$+(\lambda/2)\sum_n\sum_k\left[\frac{h_{n2,k}\cos(kv+\gamma_n t)}{\omega^2-(k\omega+\gamma_n)^2}+\frac{h_{n2,k}\cos(kv-\gamma_n t)}{\omega^2-(k\omega-\gamma_n)^2}\right.$$

$$\left.+\frac{h_{n1,k}\sin(kv+\gamma_n t)}{\omega^2-(k\omega+\gamma_n)^2}-\frac{h_{n2,k}\sin(kv-\gamma_n t)}{\omega^2-(k\omega-\gamma_n)^2}\right]. \tag{31}$$

As in Eqs. (26), the expansion coefficients exhibited are functions of the amplitude A. Note that A is constant in time and is determined by the initial average velocity $\langle\dot{y}(0)\rangle$. Moreover, there are two time scales involved, one of the order of ω_k^{-1} and the other of the order of v^{-1}. The magnitude of the ratio of the two basic time intervals depends upon the amplitude of the vibration and the form and magnitude of the nonlinear term in the equation of motion. We reserve the discussion of these results for Sec. IV.

III. THREE DIMENSIONAL CRYSTALS

In the preceding section, we have shown how the inherent anharmonicity in the potential acting on an atom adjacent to a vacancy leads to two time scales of dynamical interest. For the present, we seek a different representation of this basic fact in terms of dissipative behavior.

The central theme of our argument is the contention that the motion of the atom is like that of a Brownian particle. For the purposes of the following, it is not necessary to use the anharmonic nature of the atomic potential in the same manner as before. For, having established that the motion may be discussed in terms of two time scales, what must be shown is that dissipation is rapid. Once again, the anharmonicity will play a dominant role, but the discussion will be couched in terms of normal modes and their interactions, and not explicitly in terms of the anharmonicity of the motion of a single atom.

Let the potential energy of the crystal be of the form,

$$V_T=\sum\alpha_{ij}q_iq_j+\sum\sum b_{ijkl}q_iq_jq_kq_l. \tag{32}$$

If the coefficients b_{ijkl} are small we may consider the problem to consist of the interaction between the normal modes defined by just the quadratic term of (32). In terms of these normal modes, the amplitude of motion of the diffusing particle is governed by the superposition

$$q_1=\sum_i\alpha_{1i}Q_i \tag{33}$$

with α_{1i}, the weight contributed by the ith normal mode Q_i to the motion along q_1. Each of the Q_i represents a harmonic oscillator of one degree of freedom. The equations of motion of such an oscillator are, of course,

$$\dot{Q}_i=P_i/m,$$
$$\dot{P}_i=m\omega_i^2Q_i+F_i, \tag{34}$$

where P_i is the momentum conjugate to Q_i and m is the mass of an atom. When the interaction force F_i vanishes, the oscillator describes a circle in the phase plane. It is therefore convenient to use the rotating coordinates

$$\xi_i=Q_i\cos\omega_i t-(P_i/m\omega_i)\sin\omega_i t,$$
$$\eta_i=m\omega_iQ_i\sin\omega_i t+P_i\cos\omega_i t, \tag{35}$$

whereupon the equations of motion become

$$\dot{\xi}_i=-(F_i/m_i)\sin\omega_i t,$$
$$\dot{\eta}_i=F_i\cos\omega_i t, \tag{36}$$

and ξ_i and η_i would be constants if F_i were to vanish.

Resulting from the interactions between the normal vibrations, the motion of the diffusing atom is coupled to all other motions in the lattice. The potential defined in Eq. (32) suggests the following simple form for the interaction between normal vibrations,

$$\lambda V=\sum\lambda_{ij}Q_iQ_j, \tag{37}$$

with λ_{ij} a coupling constant.

It is necessary at this point to analyze carefully the implications of Eq. (37). So far as the normal modes of the system are concerned, the product of normal coordinates can be transformed away by the use of a new set of system coordinates. Such a term cannot lead to dissipation if only modes within the system interact. Equation (37) is to be interpreted, therefore, as an interaction between the system and the reservoir. The interaction may be written in terms of all the normal modes of both system and reservoir, but only the interactions with the reservoir contribute to the dissipation. We now require a careful distinction between system and reservoir. Consider a large crystal. About some one vacancy imagine there to be excised a volume element with linear dimensions very large compared to atomic spacing, say of the order of a vacancy-vacancy separation. This volume will be considered to form the system and the remainder of the crystal will be considered to form the reservoir. Only the normal modes of the system will be assumed to contribute to motions along the diffusive path. By this criterion, very long wavelength (greater than a linear dimension of the volume) modes are prohibited from contributing to

diffusion. It might be argued that such a division of system and reservoir is untenable, because although the density of normal modes decreases as ν^2, the corresponding amplitudes increase as ν^{-2}, and thereby the contribution per mode is approximately constant. However, it should be noted that although the long wavelength modes may indeed contribute to motion, they do not contribute to diffusive motion. For, the long wavelength modes correspond to *in-phase* motions of large numbers of atoms, and thereby the relative separation of atom and vacancy is unchanged. Motions which do not change the relative separation of atom and vacancy cannot aid diffusion. Finally, note that the division of the crystal into system and reservoir implies that the number of degrees of freedom of the reservoir is very much greater than the number of degrees of freedom of the system.

The force acting on the ith normal mode caused by this interaction is easily seen to be

$$F_i=-\sum_{i\neq j}\lambda_{ij}Q_j$$
$$=-\sum_{i\neq j}\lambda_{ij}[\xi_j\cos\omega_j t+(\eta_j/m\omega_j)\sin\omega_j t]. \tag{38}$$

The interaction force acting on the diffusing atom becomes, with the aid of Eqs. (33) and (37)

$$F_1=\sum_i\alpha_{1i}F_i$$
$$=-\sum_i\sum_{i\neq j}\alpha_{1i}\lambda_{ij}[\xi_j\cos\omega_j t+(\eta_j/m_j)\sin\omega_j t]. \tag{39}$$

Equation (39) again expresses the principle of superposition. Resulting from the linearity of the atomic displacement in the normal modes, and that of the force acting on one normal mode in the amplitudes of all other normal modes, the motion of the atom is effectively coupled piecewise to the motions of the contributing vibrations.

If the coupling constants λ_{ij} are small, the rate of change of ξ_i and η_i with time is small and it is convenient to write[14]

$$\xi_i=\bar{\xi}_i+\xi_i'(\bar{\xi},\bar{\eta},t)$$
$$\eta_i=\bar{\eta}_i+\eta_i'(\bar{\xi},\bar{\eta},t), \tag{40}$$

with $\bar{\xi}_i$ and $\bar{\eta}_i$ the values when $F_i=0$ and ξ_i' and η_i' have the same time derivatives as ξ_i and η_i. Suppose that the interaction is turned on adiabatically in the past at a rate determined by e^{st} where the limit as $s\to 0$ will be taken later. Then, it may be shown that[14]

$$F_1(t)=-\sum_i\sum_{i\neq j}\alpha_{1i}\lambda_{ij}[\bar{\xi}_j\cos\omega_j t+(\bar{\eta}_j/m\omega_j)\sin\omega_j t]$$
$$+\tilde{F}_1(t) \tag{41}$$

with

$$\tilde{F}_1(t)=-\sum_i\alpha_{1i}\sum_{i\neq j}(\lambda_{ij}/m\omega_j)$$
$$\sum_{k\neq j}\lambda_{jk}[\bar{\xi}_k\{-(\pi/2)\delta(\omega_k-\omega_j)\sin\omega_j t+[\omega_j/(\omega_k^2-\omega_j^2)]$$
$$\cdot\cos\omega_k t\}+(\bar{\eta}_k/m\omega_k)\{(\pi/2)\delta(\omega_k-\omega_j)\cos\omega_j t$$
$$+[\omega_j/(\omega_k^2-\omega_j^2)]\sin\omega_k t\}],$$

and the force $\tilde{F}_1(t)$ fluctuates rapidly. Consider now an ensemble of replicas of the central atom and its surroundings. We introduce the ansatz that the surrounding medium is always at thermal equilibrium, (see Sec. II). Under these circumstances, Toda's analysis has shown that[14]

$$\langle\dot{P}_i\rangle+m\omega_i^2\langle Q_i\rangle=\Lambda_i\langle Q_i\rangle-\zeta_i(\langle P_i\rangle/m), \tag{43}$$

$$\Lambda_i=\sum(1/m)[\lambda_{ij}^2/(\omega_j^2-\omega_i^2)], \tag{44}$$

$$\zeta_i=(\pi/2m)\sum(\lambda_{ij}^2/m\omega_i^2)\delta(\omega_i-\omega_j), \tag{45}$$

where Λ_i is the frequency shift of the ith normal vibration due to the reaction field of the other normal vibrations and ζ_i is the friction constant for the motion of the ith mode. By the use of Eq. (33), the equation of motion of the diffusing atom becomes

$$0=m\sum\alpha_{1i}\langle\ddot{Q}_i\rangle+\sum\alpha_{1i}\zeta_i\langle\dot{Q}_i\rangle+\sum\alpha_{1i}(m\omega_i^2-\Lambda_i)\langle Q_i\rangle, \tag{46}$$

which clearly shows that the motion is irreversible. It should be noted that the friction constant depends upon the spectrum of vibrations and is proportional to the square of the coupling constant. The dissipated energy is thereby also proportional to λ^2. Within the approximation used of small coupling, the normal modes of the system constitute also a Markov process in that they are linear (mutually independent) superpositions of the Markoffiian normal modes of the individual atoms.

Because of the assumption that the coupling constants λ_{ij} are small, the friction constant obtained from Eq. (45) corresponds to the strongly underdamped motion of the ith oscillation. In this case, the time of relaxation τ_r is very much longer than the mean period of oscillation, $2\pi/\omega_i$. Nevertheless, since the interlattice point jump frequency is very much smaller than ω_i, it is pertinent to investigate the order of magnitude of the relaxation time. We proceed to use an approximate model for this calculation.

The preceding arguments indicate that the diffusing atom executes a random walk under the influence of the superposed (damped) harmonic vibrations. Under these conditions, the particle may be considered to diffuse between two points of the trajectory it follows. The solution of Eq. (46) is well known for the case of a

[14] We here follow the analysis given by M. Toda, J. Phys. Soc. Japan 14, 722 (1959).

single oscillator undergoing Brownian motion. In the underdamped case,[10]

$$\langle\dot{Q}\rangle = Q_0 \exp(-\zeta t/2m)\cos(\omega t+\delta)\cos^{-1}\delta - \omega Q_0 \exp(-\zeta t/2m)\sin\omega' t\cos^{-1}\delta, \quad (47)$$

$$\omega\langle Q\rangle = \dot{Q}_0 \exp(-\zeta t/2m)\sin\omega' t\cos^{-1}\delta + \omega Q_0 \exp(-\zeta t/2m)\cos(\omega' t-\delta)\cos^{-1}\delta, \quad (48)$$

$$\omega'^2 = \omega^2 - (\zeta^2/4), \quad (49)$$

$$\delta = \tan^{-1}(\zeta/2\omega' m). \quad (50)$$

The frictional coefficient may be estimated from the theory of diffusion given previously.[1] For the case when there are very small displacements, the activation energy tends to zero quadratically in the size of the displacement. We have then the approximate relation,

$$\mathfrak{D} \approx \nu[(\Delta q)^2/2],$$
$$\nu^2 = \sum\alpha_{1j}^2\nu_j^2/\sum\alpha_{1j}^2. \quad (51)$$

For a Debye crystal it may be shown[3] that

$$\sum\alpha_{1j}^2 = (1/m)(h/\pi k\Theta_D)^2 \quad (52)$$

with the Θ_D the Debye temperature of the lattice. Moreover, for very small displacements, the greatest contributions to ν arise from the highest frequency modes and we may estimate $\nu \approx k\Theta_D/h$. The approximate frictional coefficient is, thereby,

$$\zeta = kT/\mathfrak{D} \approx 2h^2T/\pi m^2 k\Theta_D^2(\Delta q)^2. \quad (53)$$

If we take $\Theta_D \approx 200°K$, $m=100$ amu, $\Delta q = 10^{-9}$ cm and $T=300°K$, then the value of ζ is 2×10^{-10} g sec^{-1}. The relaxation time, $\tau_r = 2m/\zeta$ is thereby 1.6×10^{-12} sec. This is larger than the inverse vibrational frequency, which in this calculation is 2.5×10^{-13} sec. The motion of the mode is underdamped. The superposition of nearly independent modes suggests that the relaxation time for the motion of the atom is of the same order of magnitude as the relaxation time of a single contributing mode. We observe that τ_r is very much shorter than the mean time between diffusive jumps between lattice positions, since these are commonly of the order of magnitude, 10^{-6} -10^{-10} sec. Thus, the "hot" atom which has just jumped into a lattice vacancy will very likely not be instantaneously reflected to its original site.

It is important to note where the energy is lost. For large displacements, say $(\Delta q)=10^{-8}$ cm, the relaxation time estimated from Eq. (53) is 1.6×10^{-10} sec, a factor of 100 longer than that for small displacements. Thus, the diffusing particle loses energy very slowly at the top of the barrier; the energy dissipation occurs rapidly only when the particle is "recaptured" in the vicinity of one of the potential wells.

IV. DISCUSSION

It is pertinent to start this discussion by noting that we have shown that there are at least two relaxation times of dynamical interest for the study of the motion of a diffusing atom. The time scales are separated not only in magnitude, but also in the rate of dissipation of energy. A particle which has just escaped from a lattice site loses energy to the lattice at a rate much smaller than the rate at which it loses energy when recaptured. Thus a particle, once it escapes, may make or, dependent upon the magnitude of the damping, may not make several oscillations between the two lattice positions before enough energy is lost to confine it to one or the other of the two wells. Once so confined, the rate of loss of energy is large and the particle rapidly comes to equilibrium with the lattice. The several oscillations amongst lattice sites constitute a randomization process by which the particle forgets from which of the lattice points it originated.

In each of the calculations presented, it has been seen that the anharmonicity of the vibrations plays a dominant role in the irreversibility of the basic dynamical event. The question which immediately arises then is the relevance of the extant theories of diffusion, all of which are based on quasi-equilibrium harmonic lattice models. Certain aspects of this question may be answered unequivocally. As mentioned in the introduction, numerous studies[5-8] have shown that the exponential dependence of rate constants on the activation energy is unaltered by either the disturbance to the equilibrium distribution, or the presence of anharmonic effects provided that U^+/kT is large. In effect, the results of detailed calculation support the naive physical picture which suggests that if the particle spends most of the time in the vicinity of the minimum of a potential well, all properties are determined to first order by the shape of the well in the vicinity of that minimum. When the well is deep, anharmonicity would in this simple picture be expected to play a minor role. On the other hand, the pre-exponential factor in the diffusion coefficient is a measure of the coupling between the diffusing particle and the remainder of the system. As can be seen from the simplest case, this coupling depends intimately upon the details of the shape of the potential, especially the anharmonic portion. The detailed one dimensional theory of Bak and Prigogine[8] gives for the frequency factor,

$$\nu = \kappa\gamma/\mu c^3 m^2 \quad (54)$$

with μ the mass per unit length of lattice, c the velocity of sound, m the mass of the migrating atom, γ the force constant for the displacement of the migrating atom from its original lattice site, and κ is a reduced coupling constant defined by

$$\kappa = \lambda^2 |V_f|^2/\omega_f^2 \quad (55)$$

with λ the coupling constant in the potential energy, and $|V_f|$ the Fourier coefficient of the potential energy corresponding to frequency ω_f. Equations (45) and (46) are valid for a Debye crystal. The structure of the

frequency factor is best studied if some elementary decompositions are made. Using the fact that Θ_D is proportional to c, and that γ is proportional to the square of a vibrational frequency, we obtain the functional dependence on frequency

$$\nu M(\lambda^2 \mid V_f \mid^2/\omega_f^2\Theta_D^3)\omega^2; \qquad \omega^2=\gamma/m. \tag{56}$$

Following Bak and Prigogine, $\lambda^2 \mid V_f \mid^2/\omega_f^2$ may be taken as a constant from which we deduce that, other things being equal, the jump frequency is weighted by the square of the vibrational frequency of the migrating atom. This is in complete agreement with the quasi-equilibrium analysis leading to the second of Eqs. (51). In the equilibrium analysis, it is a mean-square frequency which appears. The difference is just in the other factors of Eq. (54), which implicitly include the coupling leading to the change from the squared to the mean-squared frequency.

It is also pertinent to observe that the constancy $\lambda^2 \mid V_f \mid^2/\omega_f^2$ has an analog in the equilibrium theory. For, the role of this reduced coupling constant is played by the superposition of normal modes and the associated coefficients α_{1i}. The weighting coefficients are dependent upon the frequency of the vibration as

$$\alpha_{1i}^2=\cos^2\eta_{1i}/2\pi^2 mN\nu_i^2 \tag{57}$$

with $\cos\eta_{1i}$ the angle between q_1 and the direction of the ith vibrational mode. The sum $\sum\alpha_{1i}^2\nu_i^2$ is thus seen to be a constant independent of the frequency. Note that the structure of (57) is the same as the structure of (56) in the sense that both have an inverse square frequency, and that $\cos\eta_{1i}$ is the coupling constant between the ith mode and the selected motion along q_1.

The major difference between Eq. (54) and the equilibrium analysis lies in the prediction by Bak and Prigogine of an isotope effect proportional to the square of the mass ratio. This stands in contrast to the fractional power prediction of all equilibrium analyses. We believe this result to be a partial consequence of the assumption that inertial effects may be neglected and that the coupling constant λ is independent of the mass of the foreign atom. In the equilibrium analysis, the coupling of the diffusing particle to the lattice depends on its mass through the effective mass of the cooperatively vibrating system. It is just this effect which is lost when λ is taken to be independent of mass. It remains to be determined experimentally which of these two alternatives is closer to reality. We may conclude from the preceding arguments that the pre-exponential factors in the equilibrium and non-equilibrium theory have more in common than is apparent from superficial examination. The important difference is the presence of the anharmonic coupling constant. Anharmonicity is sufficient to provide irreversibility. Whether or not anharmonicity is necessary for all types of irreversibility, remains an unanswered question.

The most difficult problem faced in diffusion theory is the introduction of irreversibility. There has been employed in each of the sections of this paper the following hypotheses: (a) the lattice surrounding a diffusing atom is in thermal equilibrium, (b) the equation of motion of the diffusing atom is to be solved in a coarse-grained sense and to an order linear in the anharmonic coupling constant. It is the relationship between hypotheses (a) and (b) which we now study.

The general theory of irreversibility has been approached from several points of view of which only those of Kirkwood[12] and of Van-Hove,[15] and Prigogine[16] have been developed to any great extent. We exclude from consideration here the interesting theory of Bogolubov,[17] which rests on the ansatz that the higher order distribution functions become functionals of the singlet distribution function after some small time interval. Since no attempt is made to justify this assertion, the Bogolubov theory does not represent an attempt to understand the nature of the difference between mechanically reversible and macroscopically irreversible events. The analysis of Van-Hove, Prigogine, and Brout utilizes a Fourier decomposition of the N-body distribution function and the subsequent neglect of some of the Fourier coefficients. On the other hand, the analysis of Kirkwood is based upon analogies between the theory of Brownian motion and the motion of a molecule in a dense medium. The frictional force is obtained in terms of the autocorrelation function of the intermolecular force acting on a molecule and is assumed to be independent of time after a certain time interval τ. The time τ is to be chosen so as to render the basic dynamical event independent of both prior and future events. For example, in the case of a dilute gas, τ is chosen as long compared to the duration of a collision but short compared to the time between collisions. Thus, a Fourier expansion of the distribution function after coarse graining with respect to time would lack those Fourier components describing the details of the trajectory in time τ. During this interval, only an average trajectory would be described. It is thereby seen, as was shown in general by Rice,[18] that coarse graining is related to the neglect of certain Fourier coefficients. Because of this relationship, we shall use whichever language is appropriate.[19]

It may be readily shown that the solution of the Liouville equation for the case of N harmonic oscillators is, in angle (α) and action (J) variables,[16]

$$f^{(N)}=\sum_{\{n\}} f_{\{N\}}^{(N)}(J_1\cdots J_N)\exp\Big(i\sum_k n_k(\alpha_k-\omega_k t)\Big) \tag{58}$$

[15] L. Van-Hove, Physica **21**, 517 (1955).
[16] I. Prigogine, Physica **22**, 35 (1956); **23**, 555, 567 (1957); **24**, 214, 705 (1958); and others cited therein.
[17] Bogolubov, *Problems of a Dynamical Theory in Statistical Physics* (Moscow, 1947).
[18] S. A. Rice, J. Chem. Phys. **30**, 587 (1959).
[19] Another example of the relationship between the two approaches is provided by P. Mazur, Physica **25**, 149 (1959).

where $\{n\}$ is the set of numbers $n_1, \cdots, n_N$ and the summation is over all values of all numbers of this set. If the frequencies ω_k are commensurable, they can all be written as an integer multiplied by some frequency ω_p. The period of the Poincaré cycle is then $2\pi/\omega_p$. If the frequencies are incommensurable, the Poincaré cycle depends upon the accuracy of the specification of the state.[20] As $N \to \infty$, the approximation to ω_p must be better and better, and therefore the period of the Poincaré cycle tends to infinity. However, the system does not display irreversible behavior since there is no mechanism of interaction by which an arbitrary initial distribution of energy in the normal modes can relax to the equilibrium distribution ion.

The macroscopic theory of irreversibility is based on the fact that every system has a small number of macroscopic variables which change slowly in time. These may be thought of as approximate thermodynamic integrals of motion. The existence of these macroscopic variables depends upon the existence of local equilibrium, i.e., all microscopic quantities which affect the experiment vary so rapidly on the time scale of the experiment that they come into equilibrium with the instantaneous values of the macroscopic parameters. What we must seek then is not only a perturbation which permits the exchange of energy between otherwise isolated parts of the system but also a solution to the equations of motion which corresponds to a macroscopic experiment. By the latter is meant a solution which preserves the feature that the irreversible process is determined by a few averaged parameters. This solution will be of necessity a coarse description of the phenomenon since the macroscopic experiment deals only with averages.

In the one-dimensional model discussed in this paper, the above factors enter in two related ways. First, the environment of the diffusing atom is always taken to be at thermal equilibrium. This assumption removes coherences between the motion of an atom and its surroundings, and thereby permits only one direction of evolution. The specific manner in which the coherences in atomic motion are removed can be seen from the detailed calculations of Sec. II. For, when the equations of motion are averaged over an interval of time long compared with the vibrational period of an atom in the "heat bath" just those motions which are nondissipative are neglected. In a sufficiently short time interval, it is nearly always true that the mean-square displacement is proportional to the square of the product of the velocity and time. It is only when the time interval is long enough to include many interactions that the mean-square displacement becomes linear in the time. Thus, the effect of coarse graining in time is to add a statistical assumption which, strictly speaking, violates the Newtonian laws of motion. The coarse graining is also seen to be equivalent to the decoupling effected by assuming the remainder of the lattice to be always in thermal equilibrium. The other necessary feature, the coupling required to effect energy transfer is, of course, provided by the anharmonicity.

The same two features are found in the treatment of the three-dimensional crystal and need little further comment. It is pertinent to mention that Toda's analysis,[14] which we have used extensively, is based on a solution of the equations of motion neglecting terms quadratic in the coupling constant λ. The terms which arise from the thermostat are eliminated by the assumption of thermal equilibrium. Since the terms involved are of an oscillatory nature, they could have been removed equally well by a time smoothing.

ACKNOWLEDGMENT

We wish to thank Professor M. H. Cohen of the University of Chicago and Dr. M. Lax of the Bell Telephone Laboratories for several valuable discussions and incisive criticisms.

[20] H. L. Frisch, Phys. Rev. **104**, 1 (1956).

Variational Theory of Chemical Reaction Rates Applied to Three-Body Recombinations*

JAMES C. KECK

Avco-Everett Research Laboratory, Everett, Massachusetts

(Received October 8, 1959)

A "variational" theory, which gives a least upper bound to the rate of a chemical reaction, is presented. The reaction is represented by the motion of a point in phase space across a trial surface dividing the "initial" and "final" chemical states. The trial surface is well defined in regions of phase space where interactions causing reaction are negligible, but is subject to arbitrary variations otherwise. It is shown that a least upper bound to the reaction rate can be obtained by calculating the rate at which representative points cross the "trial" surface and then minimizing this rate with respect to allowed variations of the surface. Explicit calculations of the recombination rate of attracting atoms in the presence of repulsive third bodies are made for a simple trial surface having one adjustable parameter. At low temperatures, the experimental rate constants are quite close to the theoretical bounds; at high temperatures, the experimental data fall away from the bounds in a manner which can be understood in terms of various approximations contained in the theory. Promising methods of improving the agreement between theory and experiment are discussed.

I. INTRODUCTION

A BASIC assumption of kinetic theories of chemical reaction rates is that transitions between states are induced by collisions. This leads to the concept of a "collision complex" through which reacting systems pass from the initial to the final state.[1] The "collision complex" includes those particle configurations for which the interaction inducing the transition is in some sense appreciable, and except for the case of "square well" interactions, its boundaries can only be loosely defined. Thus, absolute calculations of reaction rates based on a knowledge of the interaction potentials are not possible using kinetic theories, and for this reason they have been severely criticized.

In the present paper, we shall present a method for calculating a rigorous upper bound to the rate of a chemical reaction which is free of this difficulty and provides an explicit connection between the reaction rate and the interaction potentials. The method is based on a variational principal and is similar to an approach outlined by Wigner[2] in 1937. The reaction is represented by the motion of a point in phase space across a trial surface which divides the initial and final states of the system. In regions of phase space where interactions causing reaction are unimportant, the trial surface is uniquely defined by the chemical reaction. In the remaining regions, it is ambiguous and will be assumed arbitrary, except that it must not have any "holes." The division of the phase space into "initial" and "final" states by the trial surface will, of course, not be exact. However, for cases where the volume per particle in a gas is large compared to the interaction volume, this will have a negligible effect on the calculation of the gas properties. Since passage through the trial surface is a necessary condition for reaction, a calculation of the rate at which systems cross it in one direction will yield an upper bound to the reaction rate. The least upper bound is obtained by varying the trial surface to find the minimum crossing rate. It will be shown that for appropriately chosen trial surfaces, it is possible to obtain bounds which lie very close to experimentally observed rates, and thus, the theory offers a promising approach to the problem of understanding reaction rates.

Although we shall apply the method specifically to the three-body recombination reaction, it should be noted that the general principle involved in defining a trial surface, which can be varied to yield a least upper bound to a reaction rate, is applicable to a wide class of both chemical and physical problems.

II. MATHEMATICAL DEVELOPMENT

We are interested in reactions of the type

$$A \rightarrow B \qquad (1)$$

in which a system of three or more atoms in the initial chemical state A goes over into the final chemical state B. We shall assume that electronic transitions do not occur during the reaction and that the motion of the nuclei may be treated classically. With these approximations, the state of the system can be specified by a point in the phase space of the nuclei. Let S be a surface in this phase space which divides the "initial" state A from the "final" state B. In regions where interactions causing reaction are negligible, S is defined by the requirement that it coincide with the surface used to calculate the equilibrium constant for the reaction. In the remaining regions, S is ambiguous and, for practical purposes, arbitrary. In these regions, S can be chosen to suit our convenience, and any particular choice of S can be regarded as a trial surface subject to arbitrary variations. As usual, such variations will be made by the adjustment of a set of arbitrary parameters α_j on which S depends.

* This work was sponsored by the U. S. Army Rocket and Guided Missile Agency, Army Ordnance Missile Command, United States Army, Huntsville, Alabama under Contract No. DA-19-020-ORD-4862.

[1] J. C. Keck, J. Chem. Phys. **29**, 410 (1958).

[2] E. P. Wigner, J. Chem. Phys. **5**, 720 (1937).

Since the crossing of S is a necessary condition for reaction, an upper bound to the rate of reaction (1) can be obtained by calculating the rate $R(\alpha_j)$ at which representative points in phase space flow across S in one direction. $R(\alpha_j)$ can be expressed as an integral over S of the product of the phase space density ρ and the normal component of the generalized velocity of representative points. Thus,

$$R(\alpha_j)=\int_{\mathbf{v}\cdot\mathbf{n}>0}^{S}\mathbf{v}\cdot\mathbf{n}\rho d\sigma, \tag{2}$$

where $d\sigma$ is an element of the surface S, $\mathbf{n}$ is the unit normal to $d\sigma$, and $\mathbf{v}$ is the generalized velocity of a representative point.

In general, one will not be able to specify the density exactly at points in phase space where three-body interactions are important. However, as a consequence of Liouville's theorem, we know that, for regions connected by trajectories satisfying the known conservation laws, the density where interactions are important cannot exceed the maximum density ρ_m where interactions are unimportant. Thus, we will still obtain an upper bound to the reaction rate if we substitute ρ_m for ρ in Eq. (2):

$$R_m(\alpha_j)=\int_{\mathbf{v}\cdot\mathbf{n}>0}^{S}\mathbf{v}\cdot\mathbf{n}\rho_m d\sigma, \tag{3}$$

Equation (3) may be transformed into an expression more convenient for calculation as follows: We define S by means of the equation,

$$\phi(p_i, q_i, \alpha_j)=0. \tag{4}$$

In terms of ϕ the unit normal to S may be written,

$$\mathbf{n}=\nabla\phi/|\nabla\phi|. \tag{5}$$

By substituting Eq. (5) into Eq. (3) and expanding the dot product gives

$$R_m(\alpha_j)=\sum_i\int\rho_m\left(\dot{p}_i\frac{\partial\phi}{\partial p_i}+\dot{q}_i\frac{\partial\phi}{\partial q_i}\right)\frac{d\sigma}{|\nabla\phi|}. \tag{6}$$

Substituting Hamilton's equation of motion into Eq. (6) gives

$$R_m(\alpha_j)=\sum_i\int\rho_m\left(-\frac{\partial H}{\partial q_i}\frac{\partial\phi}{\partial p_i}+\frac{\partial H}{\partial p_i}\frac{\partial\phi}{\partial q_i}\right)\frac{d\sigma}{|\nabla\phi|}. \tag{7}$$

The quantity in parenthesis is the Jacobian J_i of the transformation from $dHd\phi$ to dp_idq_i. Thus, Eq. (7) may be rewritten,

$$R_m(\alpha_j)=\sum_i s_i\int\rho_m\frac{dHd\phi d\sigma}{dp_idq_i|\nabla\phi|}, \tag{8}$$

where

$$s_i=\begin{cases}J_i/|J_i|, & J_i\neq 0\\ 0, & J_i=0.\end{cases} \tag{9}$$

Since $d\phi/|\nabla\phi|$ is the element of length perpendicular to $d\sigma$, the factor $d\sigma d\phi/|\nabla\phi|$ is just the volume element in phase space $\prod_i dp_idq_i$, and Eq. (8) may be rewritten,

$$R_m(\alpha_j)=\sum_i s_i\int\rho_m dH\prod_{k\neq i}dp_kdq_k. \tag{10}$$

The integration of Eq. (10) is to be performed subject to the constraints $\phi=0$ and $\mathbf{v}\cdot\mathbf{n}=\sum_i J_i\geq 0$.

Having obtained the value of $R_m(\alpha_j)$ from Eq. (10), we may find the values of α_j, for which it is a minimum by setting

$$\partial R_m(\alpha_j)/\partial\alpha_l=0. \tag{11}$$

Substitution of the values of the α_j obtained from Eq. (11) into Eq. (10) gives the least upper bound to the true reaction rate which can be obtained for the assumed "trial" surface and the given interaction potential.

We should like to reiterate the reasons $R_m(\alpha_j)$ is an overestimate of the reaction rate, because it is important to keep them in mind in comparing theory and experiment. First, we have included in our calculation all crossings of S in one direction, and some of these will be due to single trajectories which cross S more than once. Second, we have extended our integral over all of S and may have included regions which are inaccessible to trajectories originating outside the interaction zone. Finally, we have replaced the true density of points on S by the maximum value it can have consistent with the conservation laws.

In concluding this discussion, we should like to point out that for the special case of a gas in thermodynamic equilibrium

$$\rho_m=\rho_e=\rho_0\exp(-H/kT). \tag{12}$$

In Eq. (12) H is the total energy of a three-particle system which is, of course, conserved along a trajectory, and ρ_0 is a constant.

III. THREE-BODY RECOMBINATION

To illustrate the application of the foregoing principles, we shall calculate a least upper bound to the equilibrium recombination rate constant for the reaction

$$A_1+A_2+A_3\rightarrow A_1A_2+A_3. \tag{13}$$

For simplicity, we shall assume that A_3 is a repulsive catalyst so that no other reactions are possible. The trial surface S we shall use in this calculation is shown in Fig. 1. It is one of the simplest that can be constructed which includes the effect of the rotational barrier. It depends on a single arbitrary parameter a in terms of which it may be decomposed into two faces S^A and S^B.

The face S^A is defined by the relations,

$$r_3=a: \quad H_{12}\leq B: \quad r_{12}\leq z, \tag{14}$$

where

$$H_{12}=p_{12}^2/2\mu_{12}+l_{12}^2/2\mu_{12}r_{12}^2+V_{12} \tag{15}$$

is the internal energy of A_1A_2,

$$B=V_{12}(z)+\tfrac{1}{2}z\frac{dV_{12}}{dr_{12}}\bigg|_z \tag{16}$$

is the energy of the rotational maximum in the effective potential, $V_{12}+l_{12}^2/2\mu_{12}r_{12}^2$, and z is the position of the rotational maximum defined by the condition,

$$(\partial/\partial r_{12})[V_{12}+l_{12}^2/(2\mu_{12}r_{12}^2)]\,|_z=(dV/dr_{12})|_z - (l_{12}^2/\mu_{12}z^3)=0. \tag{17}$$

In the above equations, r_3 is the separation of A_3 and the center-of-mass of A_1 and A_2, r_{12} is the separation of A_1 and A_2, p_{12} is the radial momentum of A_1A_2, l_{12} is the angular momentum of A_1A_2, V_{12} is the potential energy of A_1A_2, which is assumed to depend only on r_{12}, and $\mu_{12}=m_1m_2/(m_1+m_2)$ is the reduced mass of A_1A_2. The rate at which representative points in phase space flow across S^A is simply the rate of binary collisions between molecules A_1A_2 and third bodies A_3 for a collision diameter a. In the present problem, we shall be interested in the rate of binary collisions in which the energy to dissociate A_1A_2 is available in the center-of-mass system of $A_1A_2+A_3$. This rate will be called the "available energy" collision rate.

The face S^B is defined by the relations,

$$H_{12}=B: \quad r_3\geq a: \quad r_{12}\leq z. \tag{18}$$

The rate at which representative points in phase space flow across S^B is the analog of the Wigner rate, including the effect of the rotational barrier, and will be called the barrier rate.

It should be clear from Fig. 1 and the definitions of S^A and S^B that S satisfies the requirements for an acceptable trial surface. The total rate of flow of representative points across S is just the sum of the available

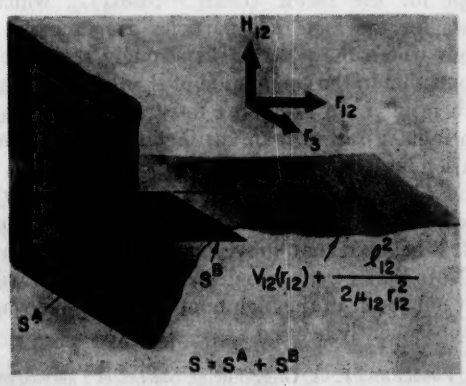

FIG. 1. Cross section of the trial surface used to calculate variational rate constant for three-body recombination.

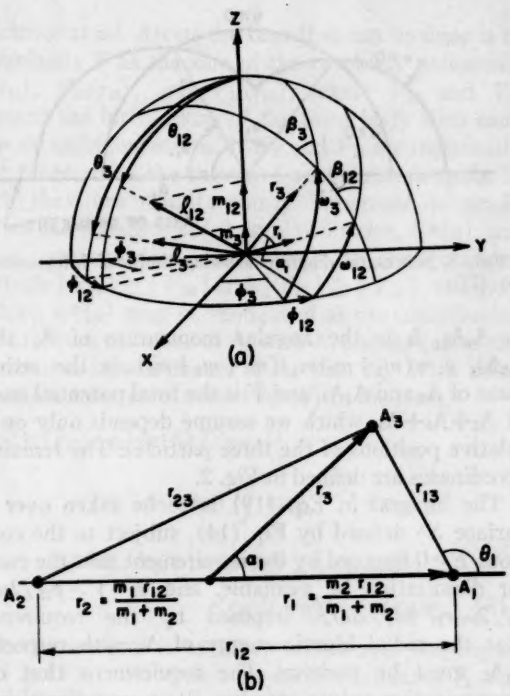

FIG. 2. Part (a) shows angular coordinates used in the present calculation. Part (b) shows coordinates giving the relative positions of the three atoms A_1, A_2, and A_3.

energy and barrier rates and is a function of the parameter a. The minimum value of this sum with respect to variations of a will be called the variational rate.

Available Energy Rate

The equilibrium rate constant

$$k^A(a)=R_m^A(a)/[A_1][A_2][A_3]$$

corresponding to the available energy rate can be obtained by combining Eqs. (10) and (12) and eliminating the center-of-mass coordinates. The result is

$$k^A(a)=(g_{12}/Z_f)\int \exp(-E/kT) \times dE dl_3 d\omega_3 dm_3 d\phi_3 dp_{12} dr_{12} dl_{12} d\omega_{12} dm_{12} d\phi_{12}, \tag{19}$$

where g_{12} is the electronic degeneracy associated with the potential V_{12},

$$Z_f=g_1g_2(2\pi\mu_{12}kT)^{\frac{3}{2}}(2\pi\mu_3kT)^{\frac{3}{2}} \tag{20}$$

is the partition function for $A_1+A_2+A_3$ in the center-of-mass system, g_1 and g_2 are the electronic degeneracies of A_1 and A_2, respectively,

$$E=(p_{12}^2/2\mu_{12})+(l_{12}^2/(2\mu_{12}r_{12}^2)+(p_3^2/2\mu_3) +(l_3^2/2\mu_3r_3^2)+V \tag{21}$$

is the total energy of $A_1+A_2+A_3$ in the center-of-mass system, p_3 is the radial momentum of A_3 with respect

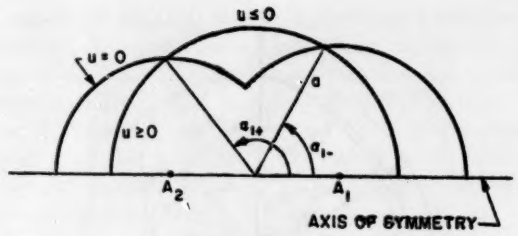

FIG. 3. Schematic diagram showing limits of integration for Eq. (22).

to A_1A_2, l_3 is the angular momentum of A_3 about A_1A_2, $\mu_3=(m_1+m_2)m_3/(m_1+m_2+m_3)$ is the reduced mass of A_3 and A_1A_2, and V is the total potential energy of $A_1+A_2+A_3$, which we assume depends only on the relative positions of the three particles. The remaining coordinates are defined in Fig. 2.

The integral in Eq. (19) is to be taken over the surface S^A defined by Eq. (14), subject to the conditions $E\geq 0$ imposed by the requirement that the energy for dissociation be available, and $E-V\geq p_{12}^2/2\mu_{12}+l_{12}^2/2\mu_{12}r_{12}^2+l_3^2/2\mu_3 r_3^2$, imposed by the requirement that the radial kinetic energy of A_3 with respect to A_1A_2 must be positive. The requirement that only representative points crossing S^A in one direction be included has been satisfied in Eq. (19) by taking the factor s defined by Eq. (9) equal to $+1$.

In order to evaluate Eq. (19), it is convenient to introduce the angles α_1 and β_3 shown in Fig. 2 in place of m_{12} and ϕ_{12}. This transformation, for which the Jacobian is simply $l_{12}\sin\alpha_1$, enables us to express the total potential energy V in terms of r_{12}, r_3, and α_1. The integration with respect to $dEdl_3dm_3d\phi_3d\omega_{12}d\beta_3$ may then be carried out in a straightforward manner and gives

$$k^A(a)=(g_{12}/g_1g_2)4\pi a^2(2kT/\mu_3)^{\frac{1}{2}}\int(I_1+I_2)r_{12}^2dr_{12}d\cos\alpha_1, \tag{22}$$

where

$$I_1=\int[1-e^{-(x^2+y+u)}]dxdy, \quad 0<x^2+y<-u, \tag{23a}$$

and

$$I_2=\int\exp[-(x^2+y+u)]dxdy, \quad -u<x^2+y<b-u_{12}. \tag{23b}$$

In the foregoing equations,

$$u=V/kT,$$
$$u_{12}=V_{12}/kT,$$
$$b=B/kT,$$
$$x=p_{12}/(2\mu_{12}kT)^{\frac{1}{2}},$$
$$y=l_{12}^2/2\mu_{12}kTr_{12}^2.$$

The integration of Eq. (23a) is elementary and gives

$$I_1=\begin{cases}2[\frac{4}{15}(-u)^{5/2}+\frac{2}{3}(-u)^{\frac{1}{2}}], & u<0\\ 0, & u>0.\end{cases} \tag{24}$$

The integration of Eq. (23b) involves transcendental functions and is quite complicated. Fortunately, it has been found numerically that in all practical cases the contribution to the final result arising from I_2 is smaller than that from I_1, and, therefore, to a first approximation we can neglect I_2.

We can now integrate Eq. (22) approximately with respect to $d\cos\alpha_1$. To do this, we divide the range of integration into two parts, in which $u\leq 0$ and $u\geq 0$ as shown schematically in Fig. 3. We then assume that the interaction with A_3 varies sufficiently rapidly as a function of α_1 so that it will be a reasonable approximation to set $u=u_{12}$ over the entire range where $u\leq 0$. As a result of this approximation, we obtain

$$k^A(a)=(g_{12}/g_1g_2)8\pi a^2(2kT/\mu_3)^{\frac{1}{2}}\int_{u_{12}<0}[\tfrac{4}{15}(-u_{12})^{5/2}+\tfrac{2}{3}(-u)_{12}^{\frac{1}{2}}](\cos\alpha_{1-}-\cos\alpha_{1+})r_{12}^2dr_{12}. \tag{25}$$

To perform the remaining integration over dr_{12}, we first observe that the integrand in Eq. (25) has a strong maximum in the vicinity of the radius r_e, where u_{12} has its minimum. Thus, as a first approximation we can expand the potential u_{12} about r_e in a Taylor series

$$u_{12}\approx -D_{12}[1-\beta_{12}^2(r_{12}-r_e)^2]/kT, \tag{26}$$

and evaluate the relatively slowly varying term $(\cos\alpha_{1-}-\cos\alpha_{1+})r_{12}^2$ at r_e. The remaining integration then gives

$$k^A(a)=(g_{12}/g_1g_2)4\pi^2a^2r_e^2\beta_{12}^{-1}(\cos\alpha_{1-}-\cos\alpha_{1+})_{r_e}\times(2D_{12}/\mu_3)^{\frac{1}{2}}\sum_{n=2}^{3}(1/n!)(D_{12}/kT)^{n-1}, \tag{27}$$

where the angles α_{1-} and α_{1+} are defined in Fig. 3. This is the final form of our result. It is identical with the ordinary expression for the available energy rate[3] except for the factor $(\cos\alpha_{1-}-\cos\alpha_{1+})_{r_e}$, which accounts for the fact that particles are excluded from regions where the potential is strongly repulsive, and the omission in the summation of the terms $n=0$ and 1, which result from extending integrations over p_{12} and l_{12} to infinity rather than cutting them off at the dissociation limit as we have done.

The approximations made in obtaining $k^A(a)$ are expected to be quite good from a physical standpoint, and it is believed that no serious errors result from their use. Note that a weak van der Waals attraction will not affect our result in the high temperature range where it will subsequently be used.

[3] R. Fowler and E. A. Guggenheim, *Statistical Thermodynamics* (Cambridge University Press, Cambridge, England, 1939), Chapter XII.

Barrier Rate

The equilibrium rate constant

$$k^B(a)=R_m{}^B(a)/[A_1][A_2][A_3]$$

corresponding to the barrier rate can be obtained by combining Eqs. (10) and (12) and eliminating the center-of-mass coordinates. The result may be expressed in the form,

$$k^B(a)=(g_{12}/Z_f)\int\exp(-E/kT)\,dE(s_p dl_{12}d\omega_{12}+s_l dp_{12}dr_{12})$$
$$\times dm_{12}d\phi_{12}dp_3dr_3dl_3d\omega_3dm_3d\phi_3, \quad (28)$$

where $s_p=\pm1$ and $s_l=(\partial V/\partial\omega_{12})/|\,\partial V/\partial\omega_{12}\,|$. The integrations are to be carried out over the surface S^B defined by Eq. (18) subject to the restriction,

$$s_p\,|\,\partial(V-V_{12})/\partial r_{12}\,|+s_l\,|\,\partial V/\partial\omega_{12}\,|\cdot|\,\partial p_{12}/\partial l_{12}\,|\geq 0 \quad (29)$$

imposed by the requirement that only representative points crossing S^B in one direction be counted.

Note that the first and second terms in Eq. (28) give, respectively, the contribution to $k^B(a)$ due to vibrational and rotational transitions.

To integrate Eq. (28) it is convenient to replace $dEd\omega_{12}dm_{12}d\phi_{12}$ in the vibrational term by $dr_{12}d\alpha_1d\beta_3d\beta_{12}$ and $dEdp_{12}dm_{12}d\phi_{12}$ in the rotational term by $dl_{12}d\alpha_1d\beta_3d\beta_{12}$. These transformations, for which the Jacobians are, respectively, $[\partial(V-V_{12})/\partial r_{12}]l_{12}\sin\alpha_1$ and $[\partial(V-V_{12})/\partial\alpha_1](\partial p_{12}/\partial l_{12})l_{12}\sin\alpha_1\cos\beta_{12}$, permit the integration over $d\beta_3d\beta_{12}dp_3dl_3d\omega_3dm_3d\phi_3$ to be carried out. The result is

$$k^B(a)=(g_{12}/g_1g_2)4\pi(8kT/\pi u_{12})^{\frac{1}{2}}\int\exp[-(b+u-u_{12})]$$
$$\times[\,|\,\partial(u-u_{12})/\partial r_{12}\,|\,r_{12}\eta_1+|\,\partial(u-u_{12})/\partial\alpha_1\,|\,\gamma\cos\eta_1]$$
$$\times r_3{}^2dr_3r_{12}dr_{12}dyd\cos\alpha_1, \quad (30)$$

where

$$\eta_1=\begin{cases}\pi/2, & \gamma^2\tan^2\theta_1\leq 1\\ \tan^{-1}(\gamma^2\tan^2\theta_1-1)^{-\frac{1}{2}}, & \gamma^2\tan^2\theta_1\geq 1,\end{cases}$$

and

$$\gamma=r_{12}\,|\,\partial p_{12}/\partial l_{12}\,|.$$

As before, $u=V/kT$, $u_{12}=V_{12}/kT$, $b=B/kT$, $y=l_{12}{}^2/2\mu_{12}kTr_{12}{}^2$. The angle θ_1 is shown in Fig. 2(b).

It is interesting to note that Eq. (30) shows that if the total potential V is spherically symmetric about the center-of-mass of A_1A_2 (i.e., independent of α_1), then the contribution to the reaction rate from rotational transitions is identically zero.

To proceed further, we must specify the potentials V_{12} and V. Two-body potentials have been determined for many molecules from spectroscopic measurements and scattering experiments and we can assume V_{12} is known. Three-body potentials are virtually nonexistent, however, and we cannot specify V with any degree of confidence at all. About the best that can be done is to approximate V as the sum of the two-body potentials, $V_{12}(r_{12})$, $V_{13}(r_{13})$, and $V_{23}(r_{23})$, where V_{13} and V_{23} represent the interactions of the third body with each of the recombining atoms. If V_{13} and V_{23} are sufficiently short range, then the region of configuration space in which they are simultaneously important is small, and we can separate $k^B(a)$ into two parts, $k_1{}^B(a)$ and $k_2{}^B(a)$, corresponding, respectively, to configurations in which $|\,V_{13}\,|\geq|\,V_{23}\,|$ and $|\,V_{23}\,|\geq|\,V_{13}\,|$. Roughly speaking $k_1{}^B(a)$ may be thought of as the contribution to $k^B(a)$ from collisions of A_3 with A_1 and $k_2{}^B(a)$ as the contribution from collision of A_3 with A_2. With these approximations, we can write $k_1{}^B(a)$ in the form,

$$k_1{}^B(a)=(g_{12}/g_1g_2)4\pi(8kT/\pi\mu_{12})^{\frac{1}{2}}$$
$$\cdot[m_2/(m_1+m_2)]\int\exp[-(b+u_{13})]$$
$$\times|\,du_{13}/dr_{13}\,|\,(\eta_1\cos\theta_1+\gamma\cos\eta_1\sin\theta_1)$$
$$\times r_{13}{}^2dr_{13}r_{12}{}^2dr_{12}dyd\cos\theta_1, \quad (31)$$

where the integral is to be extended over the region $|\,V_{13}\,|\geq|\,V_{23}\,|$. Note that we have eliminated r_3 and α_1 in favor of r_{13} and θ_1.

The corresponding expression for $k_2{}^B$ can be obtained from Eq. (31) by simply interchanging the subscripts 1 and 2.

The integration over $d\cos\theta_1$ may now be performed and gives

$$k_1{}^B(a)=(g_{12}/g_1g_2)\pi^2(8kT/\pi\mu_{12})^{\frac{1}{2}}$$
$$\times[m_2/(m_1+m_2)]\int\exp[-(b+u_{13})]\,|\,du_{13}/dr_{13}\,|$$
$$\times(f_p+\gamma^2f_l)(1+\gamma^2)^{-\frac{1}{2}}r_{13}{}^2dr_{13}r_{12}{}^2dr_{12}dy, \quad (32)$$

where

$$f_p=\begin{cases}1-\dfrac{\tan\theta_{1m}}{|\tan\theta_{1m}|}(2/\pi)\{\tan^{-1}[(1+\gamma^2)^{\frac{1}{2}}\tan\eta_{1m}]\\ \quad-(1+\gamma^2)^{\frac{1}{2}}\eta_{1m}\sin^2\theta_{1m}\}, & \gamma^2\tan^2\theta_{1m}\geq 1\\ 1-\dfrac{\tan\theta_{1m}}{|\tan\theta_{1m}|}[1-(1+\gamma^2)^{\frac{1}{2}}\sin^2\theta_{1m}], & \gamma^2\tan^2\theta_{1m}\leq 1\end{cases} \quad (33a)$$

and

$$f_l=\begin{cases}1-\dfrac{\tan\theta_{1m}}{|\tan\theta_{1m}|}(2/\pi)\left\{\tan^{-1}[(1+\gamma^2)^{\frac{1}{2}}\tan\eta_{1m}]\right.\\ \quad\left.+\dfrac{(1+\gamma^2)^{\frac{1}{2}}}{\gamma^2}\dfrac{\cos^2\theta_{1m}}{\tan\eta_{1m}}\right\}, & \gamma^2\tan^2\theta_{1m}\geq 1\\ 1-\dfrac{\tan\theta_{1m}}{|\tan\theta_{1m}|}, & \gamma^2\tan^2\theta_{1m}\leq 1.\end{cases} \quad (33b)$$

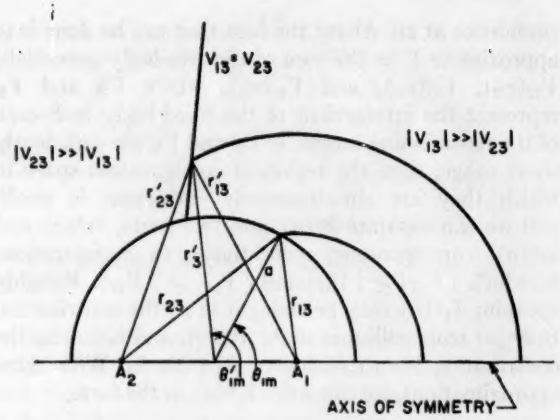

FIG. 4. Schematic diagram showing limits of integration for Eq. (31). The primed and unprimed quantities refer to the two cases given in Eq. (34).

The angle θ_{1m} is defined by the relations,

$$\theta_{1m}=\begin{cases}[(r_3^2-r_1^2-r_{13}^2)/2r_1r_{13}]_{V_{13}=V_{23}}, \\ \qquad (r_3)_{V_{13}=V_{23}}\geq a \\ [(a^2-r_1^2-r_{13}^2)/2r_1r_{13}]_{V_{13}=V_{23}}, \\ \qquad (r_3)_{V_{13}=V_{23}}\leq a.\end{cases} \tag{34}$$

and is shown in Fig. 4 for the two cases indicated.

The functions f_p and f_l are essentially the effective solid angles over which A_3 induces vibrational and rotational transitions. They are roughly of the form $(1-\cos\theta_{1m})$ and are shown in Fig. 5 as a function of θ_{1m} for several values of γ^2. As one might expect the derivative of f_p with respect to θ_{1m} has maxima in the neighborhood of 45° and 135°, indicating that vibrational transitions are most important at these angles,

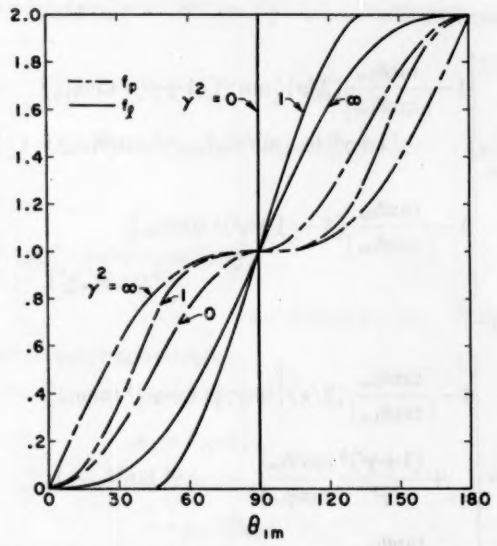

FIG. 5. Curves showing the function f_p and f_l defined by Eqs. (33a) and (33b).

while the derivative of f_l has a maximum at 90°, indicating that rotational transitions are most important at this angle. Also note that for all values of γ^2, except infinity, there are finite regions in which f_l has zero derivative, indicating that rotational transitions are forbidden.

We now assume that the potential V_{13} has the form shown in Fig. 6(a), i.e., it is strongly repulsive for small separations and has a weak van der Waals attraction at larger separations. The factor $|du_{13}/dr_{13}|\exp(-u_{13})$ will thus have the form shown in Fig. 6(b). Note that there are two strong maxima at separations α_{1+} and α_{1-} defined by the condition,

$$(d/dr_{13})[|du_{13}/dr_{13}|\exp(-u_{13})]_{\alpha_{1\pm}}=0 \tag{35}$$

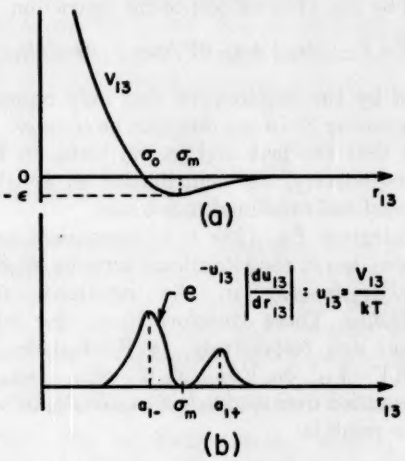

FIG. 6. Part (a) shows the form of the interaction potential V_{13}. Part (b) shows the maxima in the function $|du_{13}/dr_{13}|\exp(-u_{13})$.

and separated by a zero at σ_m where u_{13} has its minimum. The integration over r_{13} can thus be divided into two parts $0\leq r_{13}\leq\sigma_m$ and $\sigma_m\leq r_{13}\leq\infty$. Since the factor $(f_p+\gamma^2 f_l)r_{13}^2$ varies relatively slowly we may evaluate it a_{1-} in the part $0\leq r_{13}\leq\sigma_m$ and α_{1+} in the part $\sigma_m\leq r_{13}\leq\infty$ and factor the integrand. The remaining integration is elementary and gives

$$k_1^B(a)=(g_{12}/g_1g_2)\pi^2(8kT/\pi\mu_{12})^{\frac{1}{2}}[m_2/(m_1+m_2)]$$
$$\times\{a_{1-}^2I_{1-}\exp(\epsilon/kT)+a_{1+}^2I_{1+}[\exp(\epsilon/kT)-1]\}, \tag{36}$$

where

$$I_{1\pm}=\int e^{-b}(f_p+\gamma^2f_l)_{\alpha_{1\pm}}(1+\gamma^2)^{-\frac{1}{2}}r_{12}^2dr_{12}dy. \tag{37}$$

Note that in performing the r_{13} integration above we have assumed there is an equilibrium population of A_1A_3 bound by the van der Waals potential. This implies that the rate-limiting step in the chain

$$A_1+A_3+X\rightarrow A_1A_3+X$$
$$A_2+A_1A_3\rightarrow A_2A_1+A_3$$

is the latter reaction. This is almost certainly true when $\epsilon/kT \lesssim 1$.

At this point, we may check our results against those obtained by Wigner for the case where the surface separating free and bound states was taken as $H_{12}=0$. To do this, we simply set $b=0$ and neglect the van der Waals attraction, i.e., set $\epsilon=0$. The integration over dy may then be carried out and gives

$$k_1^{W}=(g_{12}/g_1g_2)[8\pi^2a_{1-}^2/(2\pi\mu_{12}kT)^{\frac{1}{2}}]$$
$$\times[m_2/(m_1+m_2)]\int_{V_{12}<0}|V_{12}|(1-\cos\theta_{1m})r_{12}^2dr_{12}. \quad (38)$$

By adding to this the corresponding expression for k_2^{W}, we obtain the Wigner result,

$$k^{W}=(g_{12}/g_1g_2)4\pi a_{1-}^2(2\pi\mu_{12}/kT)^{\frac{1}{2}}\int_{V_{12}<0}|V_{12}|$$
$$\times[(1/m_1)(1-\cos\theta_{1m})+(1/m_2)(1-\cos\theta_{2m})]r_{12}^2dr_{12}. \quad (39)$$

In the present calculation, we wish to include the effects of the rotational barrier explicitly. To do this, we carry out an approximate integration with respect to dy using a technique previously employed in the integration of Eq. (32). We first make a change of variables introducing the position of the rotational barrier, z, in place of y. Equation (37) can then be written

$$I_{1\pm}=\int_{z_m}^{\infty}e^{-b}|db/dz|[F_p^{1\pm}(z)+F_l^{1\pm}(z)](z-z_1)z^2dz, \quad (40)$$

where

$$F_p^{1\pm}(z)=(z-z_1)^{-1}\int_{z_1}^{z}(f_p)_{a_{1\pm}}(1+\gamma^2)^{-\frac{1}{2}}dr_{12} \quad (41a)$$

and

$$F_l^{1\pm}(z)=(z-z_1)^{-1}\int_{z_1}^{z}\gamma^2(f_l)_{a_{1\pm}}(1+\gamma^2)^{-\frac{1}{2}}dr_{12}. \quad (41b)$$

The range of integration for Eq. (40) is defined by the requirement that a rotational barrier exist. For many potentials, this is only true if the angular momentum l_{12} is less than some maximum value l_m. If z_m is the position of the rotational barrier corresponding to l_m, $l_{12}\leq l_m$ implies $z\geq z_m$. The range of integration for Eqs. (41a) and (41b) is defined by the requirement that the effective potential at r_{12} must be less than the barrier height, so that the radial momentum p_{12} will be real. Thus, z_1 is defined as a function of z by the equation

$$u_{12}(z_1)+(z^2/2z_1^2)(du_{12}/dr_{12})|_z=u_{12}(z)$$
$$+\tfrac{1}{2}z(du_{12}/dr_{12})|_z. \quad (42)$$

We now make the assumption that b increases strongly with decreasing z, so that the factor $|db/dz|\exp(-b)$ in the integrand has a sharp maximum at a radius z_2 defined by the condition,

$$(d/dz)[|db/dz|\exp(-b)]_{z_2}=0, \quad (43)$$

while the remainder of the integrand varies sufficiently slowly so that it may be approximated by its value at z_2. The integral may then be factored and integrated with respect to dz. The result is

$$I_{1\pm}=[F_p^{1\pm}(z_2)+F_l^{1\pm}(z_2)](z_2-z_1)z_2^2$$
$$\times[1-\exp(-B_m/kT)], \quad (44)$$

where B_m is the maximum value of B and corresponds to z_m. Our final result is obtained by inserting Eq. (44) into Eq. (36) and adding the corresponding expression for $k_2^{B}(a)$. Thus,

$$k^{B}(a)=(g_{12}/g_1g_2)2\pi(2\pi\mu_{12}kT)^{\frac{1}{2}}(z_2-z_1)z_2^2$$
$$\times[1-\exp(-B_m/kT)]$$
$$\times\{m_1^{-1}\{a_{1-}^2(F_p^{1-}(z_2)+F_l^{1-}(z_2))\exp(\epsilon/kT)$$
$$+a_{1+}^2(F_p^{1+}(z_2)+F_l^{1+}(z_2))[\exp(\epsilon/kT)-1]\}$$
$$+m_2^{-1}[a_{2-}^2(F_p^{2-}(z_2)+F_l^{2-}(z_2))\exp(\epsilon/kT)$$
$$+a_{2+}^2(F_p^{2+}(z_2)+F_l^{2+}(z_2))[\exp(\epsilon/kT)-1]\}\}. \quad (45)$$

This is a rather formidable expression, but considering the complexity of the problem we might have expected worse. Actually, the only real complication is that involved in integrating Eq. (41a) and (41b) to obtain the F's. This must be done either graphically or numerically. In cases where a rough estimate of the rate will suffice, the F's may be taken equal to unity.

The most important difference between the calculation made above and the one carried out by Wigner is that we have included explicitly, both the effect of the rotational barrier and the van der Waals force. This leads to a considerably more complicated temperature dependence than the simple $T^{-\frac{1}{2}}$ law found by Wigner, as well as a substantial reduction in the rate constant at low temperatures.

It is worth nothing that our expression for the barrier rate constant contains a good deal of the correct mechanics of the problem. What is missing is the consideration of trajectories which cross S^{B} more than once.

Variational Rate

To obtain the variational rate constant $k^{V}(a)$ we simply add the available energy rate constant $k^{A}(a)$ and the "barrier" rate constant $k^{B}(a)$, and minimize with respect to variations of the parameter a. While in principle this can be done analytically, in practice it has been found more convenient to simply calculate $k^{A}(a)+k^{B}(a)$ for several values of a and locate the minimum graphically.

The actual calculations of $k^{A}(a)$ and $k^{B}(a)$ were programmed for an IBM 650 computer for which this

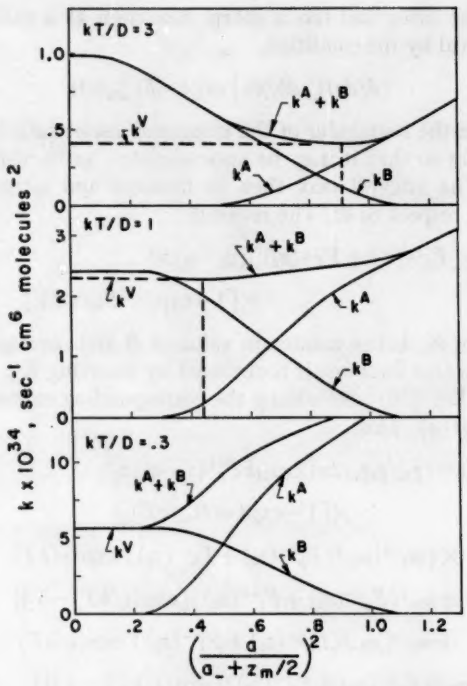

FIG. 7. Curves illustrating the method used to determine the variational rate constant k^V for the process $O+O+A=O_2(^3\Sigma_g^-)+A$ for several values of kT/D where D is the binding energy of $O_2(^3\Sigma_g^-)$. Note that, as kT/D increases, the position of the minimum corresponding to the "variational" rate constant moves from $a=0$ toward $a=a_-+z_m/2$, beyond which point the "barrier" rate constant $k^B(a)$ is essentially 0.

problem is trivial. Only the case of symmetrical molecules, i.e., $A_1=A_2$, was treated, and the interaction potential V_{12} was assumed to have the Morse form. A detailed discussion of this potential and a summary of the constants employed is given in part I of Appendix A. The potential V_{13} between the third body and a recombining atom was assumed to have the Lennard-Jones form at large separation and the Mason-Vanderslice[4] form at small separation. The two forms were smoothed graphically in the region of overlap. A detailed discussion of these potentials and a summary of the parameters used is given in parts II and III of Appendix A.

Some typical results, which serve to illustrate the procedure for locating the minimum rate constant are shown in Fig. 7 for the case

$$O+O+A\rightarrow O_2(^3\Sigma_g^-)+A.$$

In this figure, the rate constants $k^A(a)$, $k^B(a)$ and $k^A(a)+k^B(a)$ are plotted as functions of $a^2/(a_-+z_m/2)^2$ for several values of the dimensionless temperature kT/D. It can be seen that for $kT/D\ll 1$ the best value of $a/(a_-+z_m/2)$ is zero, in which case $k^V\approx k^B(0)$, while for $kT/D\gg 1$ the best value of $a/(a_-+z_m/2)$ is unity, in which case $k^V\approx k^A(a_-+z_m/2)$. As shown in Fig. 8, the transition region in which $k^A(a)$ and $k^B(a)$ are simultaneously important is relatively narrow, and in practice k^V can easily be interpolated so that it is unnecessary to carry out the detailed analysis illustrated in Fig. 7.

An analysis similar to that just described was also carried out for the case,

$$I+I+A\rightarrow I_2(^1\Sigma_g^+)+A,$$

and the results were essentially identical except that the crossing point for $k^B(0)$ and $k^A(a_-+z_m/2)$ occurred at $kT/D\approx 3$.

From a practical point of view, the temperature range of primary interest is that for which $kT/D<1$. Since the preceding analysis showed that in this range $k^V=k^B(0)$ for both iodine and oxygen, it seems fairly safe to conclude that this will be the case in general and, thus, the properties of the "barrier" rate constant are of special importance. In this connection, it is of interest to compare the relative contributions to $k^B(0)$ made by vibrational and rotational transitions. This is done in Fig. 9, where $k_p^B(0)$ and $k_l^B(0)$ are plotted along with $k^B(0)$ as functions of kT/D. It can be seen that at low temperatures the major contribution to $k^B(0)$ arises from $k_p^B(0)$, while at high temperatures the major contribution is from $k_l^B(0)$. The ratio of $k_l^B(0)/k_p^B(0)$ varies approximately as $T^{\frac{1}{2}}$, and it can be shown that this is a result of including the effect of the rotational barrier in the calculations. In the Wigner calculation, which neglects the rotational barrier, there is no difference in the temperature dependence of

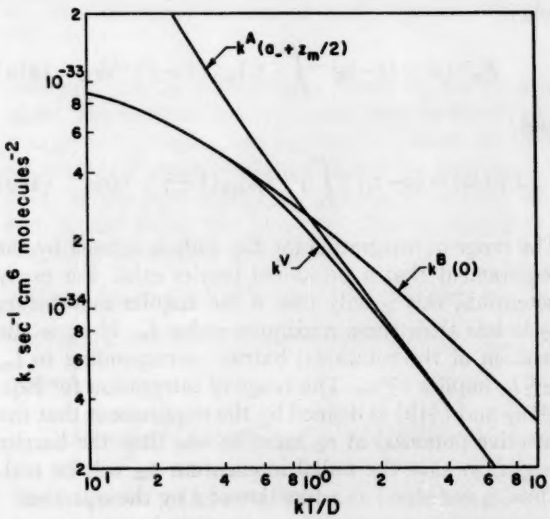

FIG. 8. The curve labeled k^V shows the variational rate constant for the process $O+O+A=O_2(^3\Sigma_g^-)+A$ as a function of kT/D, where D is the binding energy of $O_2(^3\Sigma_g^-)$. The curves labeled $k^B(0)$ and $k^A(a_-+z_m/2)$ are, respectively, the low and high temperature asymptotes for k^V. Note that k^V is quite well approximated by the smaller of $k^B(0)$ and $k^A(a_-+z_m/2)$ and can easily be interpolated in the transition region.

[4] E. A. Mason and J. T. Vanderslice, J. Chem. Phys. **28**, 432 (1958).

the vibrational and rotational contributions. The reason for pointing out this effect is that, as will be seen later, the experiments show a stronger negative temperature dependence than the theory, and it is tempting to speculate that at least part of the difference may be due to the fact that rotational transitions are less important than the theory predicts. This would be the case if the true three-body potential were more nearly spherically symmetric than the dumbbell shape assumed.

Figure 9 also shows that the barrier rate constant is a considerably better bound than the Wigner rate constant, especially at low temperatures. This is a simple result of the fact that the rotational barrier limits the number of trajectories which can reach the surface $H_{12}=0$ from the free state. An interesting project would be to calculate this correction. It would also be of interest to consider the general case where H_{12} is set equal to an arbitrary constant. This would give bounds on the frequency of vibrational and rotational transitions in molecules.

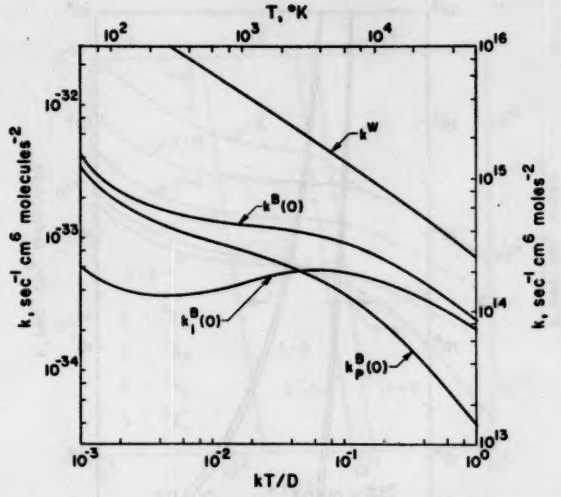

FIG. 9. Recombination rate constants for O+O+A→O_2 ($^3\Sigma_g^-$)+A. The curve labeled $k^B(0)$ shows the "barrier" rate constant evaluated for $a=0$. The curves labeled $k_p^B(0)$ and $k_i^B(0)$ show, respectively, the contributions to $k^B(0)$ due to vibrational and rotational transitions. Note that at low temperatures vibrational transitions are dominant, while at high temperatures rotational transitions are dominant. The curve labeled k^w shows the Wigner rate constant for comparison.

IV. ELECTRONIC TRANSITIONS

Before we can make a meaningful comparison of theory and experiment, we must first consider the effect of transitions between the various bound electronic states of a molecule, which are degenerate in the free state. This is necessary because what is usually measured in experiments is either the depopulation of the free state or the population of the ground state, and the existence of intermediate electronic states can provide alternative paths by which this can occur. Such a path is the chain reaction,

$$A+A+M \xrightarrow{k_{fi}} A_2^i+M \qquad (46a)$$

$$A_2^i+X \xrightarrow{k_{i0}} A_2+X, \qquad (46b)$$

where A_2^i denotes a molecule in an intermediate electronic state.

The general solution of these equations involves considerable complication and will not be undertaken here. Instead, we shall consider the two limiting cases in which either the reaction,

$$A_2^i+M \xrightarrow{k_{if}} A+A+M, \qquad (47a)$$

or the reaction

$$A_2^i+X \xrightarrow{k_{i0}} A_2+X \qquad (47b)$$

dominates in depopulating A_2^i. If reaction (47a) is dominant, then we may assume reaction (46a) is in equilibrium and the over-all reaction rate is

$$R_{f0}=k_{f0}[A]^2[M], \quad k_{f0}\ll k_{fi}, \qquad (48)$$

where

$$k_{f0}=(k_{i0}K_{fi}^{-1})([X]/[M]) \qquad (49)$$

is the effective three-body rate constant for the over-all reaction with M as the third body and K_{fi} is the equilibrium constant for reaction (47a). If the reaction (47b) is dominant, then we can assume A_2^i is in a steady state of near zero concentration, and the over-all reaction rate is

$$R_{f0}=k_{fi}[A]^2[M], \quad k_{fi}\ll k_{f0}. \qquad (50)$$

Thus, we see that the rate-limiting rate constant is the smaller of k_{fi} and k_{f0}.

For our subsequent discussion, it is convenient to express k_{f0} in terms of the cross section σ_e for electronic transitions, from the intermediate to ground state. A straightforward calculation involving essentially only the evaluation of K_{fi} leads to the result,

$$k_{f0}=\sigma_e(2D_i/\mu)^{\frac{1}{2}}(g_i/g_f)(8\pi r_i^2/\beta_i)\chi_i\{[X]/[M]\}, \qquad (51)$$

where

$$\chi_i=2(hc\omega_i/D_i)[\cosh(D_i/kT)-1][1-\exp(-hc\omega_i/kT)]^{-1} \qquad (52)$$

is a dimensionless factor shown as a function of temperature in Fig. 10, g_i/g_f is the ratio of the electronic degeneracy of the intermediate and free states, and μ is the reduced mass for a collision of A_2 and X. The constants D_i, ω_i, r_i, and β_i are, respectively, the binding energy, vibrational constant, equilibrium separation, and decay constant for A_2^i and are tabulated in Appendix A for a few molecules of interest.

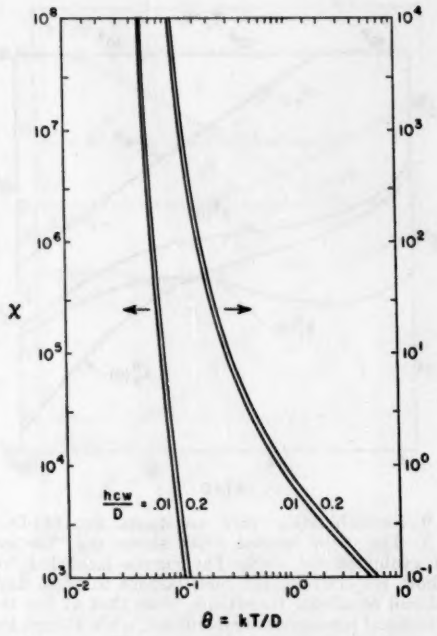

FIG. 10. Curves of the function χ, defined in Eq. (53), as a function of kT/D for two values of the parameter $hc\omega/D$. This function determines the temperature dependence of recombination via the chain mechanism (46) in cases where the electronic transition is the rate-limiting step. The left scale should be used for the two curves on the left and the right scale for the two curves on the right.

To obtain numerical values for $k_{f\to 0}$, we require a knowledge of the cross section σ_e for electronic transitions from the intermediate to ground state. These transitions usually involve spin flips and are expected to be very improbable except in cases where atom exchange occurs. Fortunately, due to the exceedingly steep temperature dependence of the factor χ_i, all we need for our present purposes is an estimate of the cross section good to one, or two orders of magnitude. We have, therefore, assumed that only atoms of the recombining species induce electronic transitions and that the cross section for the reaction is of the order of g_0/g_f times the kinetic cross section. The factor g_0/g_f is the ratio of the electronic degeneracy of the ground and free states, and is included on the loose argument that for a reaction to occur the reacting atoms must be appropriately oriented. The only other unknown factor in $k_{f\to 0}$ is the ratio [X]/[M] which, with our assumption that X=A, is time-dependent. Again, because of the extremely steep temperature dependence of the factor χ_i, this complication can be glossed over for the present and we have simply taken $[X]/[M]=10^{-2}$, which is typical of all the experiments we shall discuss.

V. COMPARISON OF THEORY AND EXPERIMENT

Temperature Dependence

The rate constants for recombination of iodine, bromine, oxygen, and nitrogen atoms in the presence of argon have been calculated as a function of the temperature for both the direct and chain mechanisms and are shown in Figs. 11–14 along with the available experimental data. The curves labeled $f\to 0$, $f\to 1$, etc., refer to direct recombination of atoms into the bound electronic states, 1, 2, etc., identified in the figures. The curves labeled $1\to 0$, $2\to 0$, etc., refer to recombination to the ground state via the chain mechanism under conditions where the rate-limiting step is assumed to be the transition between electronic states. In this connection, note that the curves are shown as solid lines where the corresponding process is the rate-limiting step and are dashed otherwise. Also, note that the crossing points are uncertain due to our ignorance of the cross sections for electronic transitions, although a change of one or two orders of magnitude is required to produce an appreciable effect. The curves labeled Σ represent the sum of all processes leading to the ground

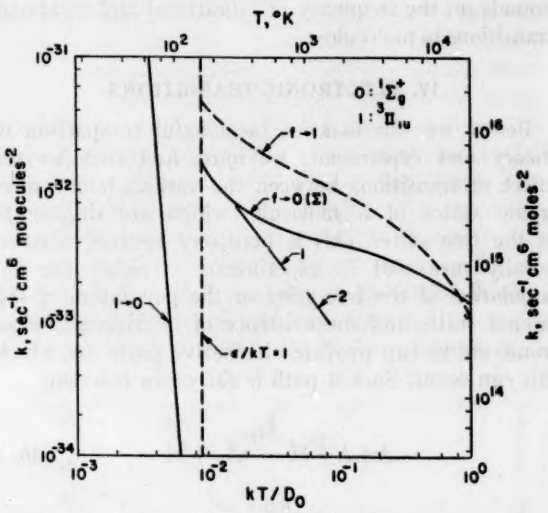

FIG. 11. Three-body recombination rate constants for I+I+A→I_2+A as a function of kT/D_0, where D_0 is the binding energy of $I_2(^1\Sigma_g^+)$. The curves labeled $f\to 0(\Sigma)$ and $f\to 1$ are the rate constants for direct recombination to the $^1\Sigma_g^+$ and $^3\Pi_{1u}$ states of I_2. These curves have been cut off at $\epsilon/kT=1$, where ϵ is the depth of the van der Waals potential, since the theory is no longer applicable below this point. The curve labeled $1\to 0$ is an estimate of the effective rate constant for transitions from the $^3\Pi_{1u}$ to the $^1\Sigma_g^+$ state. Note that in the range $\epsilon/kT\leq 1$ the transition $1\to 0$ is always the rate-limiting step for recombination to the 0 state via the chain mechanism Eq. (46). To indicate this, we have used a solid line for the curve $1\to 0$ and a dashed line for the curve $f\to 1$. Curve (1) shows the low temperature experimental data obtained in flash photolysis experiments.[5,6] Curve (2) shows the high temperature recombination rate constants deduced from dissociation rates measured in shock tubes.[7] The experimental data lie very close to the theoretical upper bound $f\to 1(\Sigma)$ at low temperatures but exhibit a steeper temperature dependence than the theory. Possible explanations for this are discussed in the text.

[5] D. L. Bunker and N. Davidson, J. Am. Chem. Soc. **80**, 5085 (1958).

[6] Strong, Chien, Graf, and Willard, J. Chem. Phys. **26**, 1287 (1957).

[7] Britton, Davidson, Gehman, and Schott, J. Chem. Phys. **25**, 804 (1956).

state, and it is these with which the experimental data should be compared.

In making the comparison of theory and experiment, it should be remembered that the theory gives a rigorous upper bound to the rate constant. Thus, we expect the observed rate constants to fall below the Σ curves. It is interesting to note that at low temperatures all the experimental data lie quite close to the theoretical bound. This is shown more clearly in Fig. 15 where we have plotted the ratio of the observed rate constants to the upper bound represented by the Σ curve as a function of kT/D_0, where D_0 is the binding energy of the ground state. Although points for oxygen and nitrogen and a portion of the bromine curve actually lie above the bound, this is not considered serious, since a rather large error is quoted for the oxygen result, the nitrogen result disagrees with another measurement, and the bromine data are uncorrected for the effect of Br_2 as catalyst and are expected to be "high."

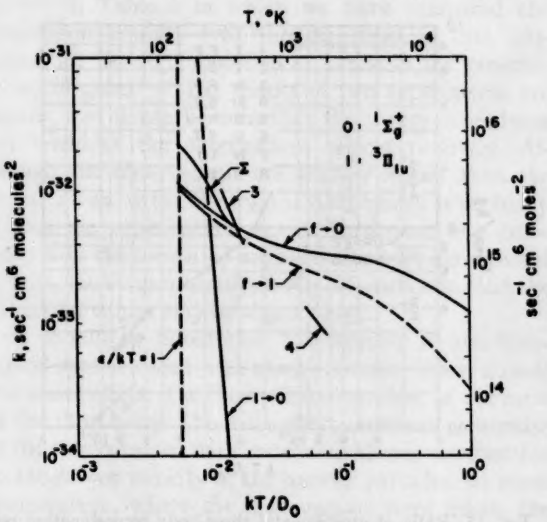

FIG. 12. Recombination rate constants for Br+Br+A→Br_2+A as a function of kT/D_0, where D_0 is the binding energy of Br_2 ($^1\Sigma_g^+$). The curves marked $f\to0$ and $f\to1$ are the rate constants for direct recombination to the $^1\Sigma_g^+$ and $^3\Pi_{1u}$ states of Br. These curves have been cut off at the point $\epsilon/kT=1$, where ϵ is the depth of the van der Waals potential, since the theory is no longer applicable below this point. The curve labeled 1→0 is an estimate of the effective rate constant for transitions from the $^3\Pi_{1u}$ to the $^1\Sigma_g^+$ state. The portions of the curves shown as solid lines indicate the regions in which the corresponding process is the rate-limiting step in recombination to the 0 state via the chain mechanism, Eq. (46). The curve labeled Σ shows the rate constant for recombination to the 0 state via both direct and chain mechanisms. Curve (3) shows the low temperature experimental data obtained in flash photolysis experiments.[8] Curve (4) shows the high temperature recombination rate constants deduced from dissociation rates measured in shock tubes.[8,9] Although the experimental rate constant exceeds the theoretical upper bound Σ at low temperatures, there is a strong possibility that the experimental results may be high, and this is not regarded as a serious disagreement. As in the case of iodine, the experimental data show a steeper temperature dependence than the theoretical bound. Reasons for this are discussed in the text.

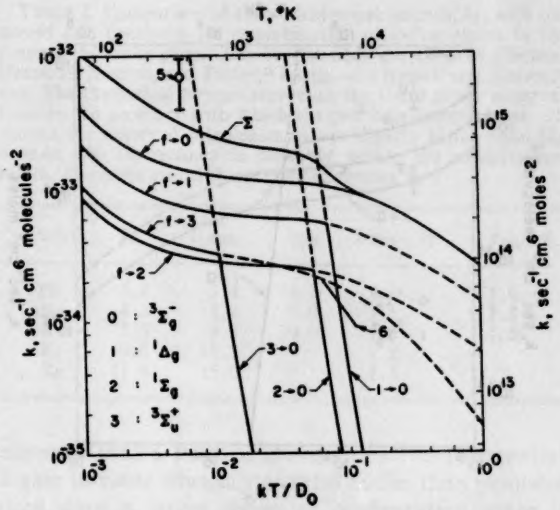

FIG. 13. Three-body recombination rate constants for O+O+A→O_2+A as a function of kT/D_0, where D_0 is the binding energy of $O_2(^3\Sigma_g^-)$. The curves labeled $f\to0$, $f\to1$, $f\to2$, and $f\to3$ are the rate constants for direct recombination to the $^3\Sigma_g^-$, $^1\Delta_g$, $^1\Sigma_g$, and $^3\Sigma_u^+$ states of O_2. The curves labeled 1→0, 2→0, and 3→0 are estimates of the effective rate constants for transitions from the $^1\Delta_g$, $^1\Sigma_g$, and $^3\Sigma_u^+$ to the $^3\Sigma_g^-$ state. The portions of the curves shown as solid lines indicate the regions in which the corresponding process in the rate-limiting step in recombination to the 0 state via the chain mechanism Eq. (46). The curve labeled Σ shows the rate constant for recombination to the 0 state via both direct and chain mechanisms. The point (5) shows the result of discharge experiments in which the atom concentration was determined from the photon yield of the reaction O+NO→NO_2+$h\nu$.[10] The curve (6) shows the recombination rate constant deduced from dissociation rates measured in shock tubes.[11,12] Although the experimental point at low temperatures is somewhat above the theoretical bound Σ, the error quoted is quite large and the discrepancy is not considered significant. As in the cases of iodine and bromine, the experimental data show a steeper temperature dependence than the theoretical bound. Reasons for this are discussed in the text.

Assuming our approximation to the three-body potential is at all reasonable, we can draw the tentative conclusion that recrossing of the "barrier" surface by single trajectories, (i.e., recombination and dissociation in a single collision) is a small effect at low temperatures. This would not be an unreasonable thing to expect, since at low temperatures, the phase volume associated with bound states tremendously outweighs that associated with free states and, thus, a trajectory which once crosses the barrier surface has a good chance of coming out in a bound state.

At high temperatures, the observations do fall somewhat below the theoretical bound. The interesting feature to note in this region is that the ratios of k_{exp}/k_Σ for all the species studied appear to lie more or less on a smooth curve when plotted as a function of kT/D_0.

[8] D. Britton and N. Davidson, J. Chem. Phys. **25**, 810 (1956).
[9] H. B. Palmer and D. F. Hornig, J. Chem. Phys. **26**, 98 (1957).
[10] C. B. Kretschmer, Aerojet Report 1611, Azusa, California, (1959).
[11] S. R. Byron, J. Chem. Phys. **30**, 1380 (1959).
[12] M. Camac, private communication.

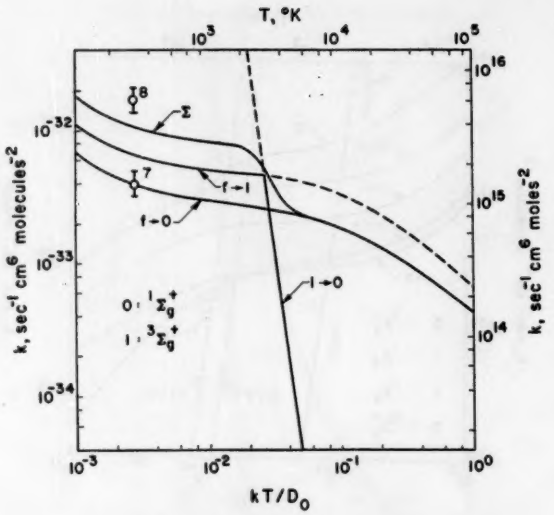

FIG. 14. Three-body recombination rate constants for N+N+A→N_2+A as a function of kT/D_0, where D_0 is the binding energy of $N_2(^1\Sigma_g^+)$. The curves labeled $f\to0$ and $f\to1$ are the rate constants for direct recombination to the $^1\Sigma_g^+$ and $^3\Sigma_g^+$ states of N_2. The curve labeled 1→0 is an estimate of the effective rate constants for transition from the $^3\Sigma_g^+$ to the $^1\Sigma_g^+$ state. The portions of the curves shown as solid lines indicate the regions in which the corresponding process is the rate-limiting step in recombination to the 0 state via the chain mechanism Eq. (46). The curve labeled Σ shows the rate constant for recombination to the 0 state via both direct and chain mechanisms. The points (7) and (8) show the results of flow experiments in which the atom concentration was determined by titrating with NO.[13,14] The two experiments give values which bracket the theoretical upper bound Σ.

This suggests that the mechanism responsible for depressing the observed rate constant below the theoretical bound depends in the first approximation only on the binding energy of the ground state. It is not surprising that the correlation should be with the ground state binding energy since for iodine, bromine, and oxygen the ground state plays the dominant role. At the present time, it does not seem unreasonable to suppose that other molecules will exhibit a similar departure from the theoretical upper bound, and thus, we may use the observed correlation as a basis for making fairly precise theoretical predictions of recombination rates. In this connection, it will be of considerable interest to see if the recombination rate of nitrogen atoms follows the same pattern at high temperatures. Note, however, that in nitrogen a correction may have to be made for the increased importance of recombination via the chain mechanism.

There are two possible explanations for the decrease in the ratio of k_{exp}/k_Σ with increasing temperature:

First, multiple crossings of the barrier surface can be expected to become more important as the temperature increases. Since this is an effect which is probably associated with the ratio of free to bound states, it is reasonable to expect a dependence on kT/D_0. The question of whether this effect is important is one which could be answered quite easily by Monte Carlo trajectory calculations, and it is proposed as a very important problem for those working in this area.

Second, our approximation to the three-body potential is certainly rather poor. As an example of how the three-body potential can affect the temperature dependence of the rate constant, we recall the previous discussion of the difference in the temperature dependence of rotational and vibrational transitions. In this discussion, it was noted that the major contribution to the rate constant at high temperatures came from rotational transitions and that these are dependent on the asymmetry of the three-body potential. A more nearly symmetric potential would result in a smaller contribution from rotational transitions and,

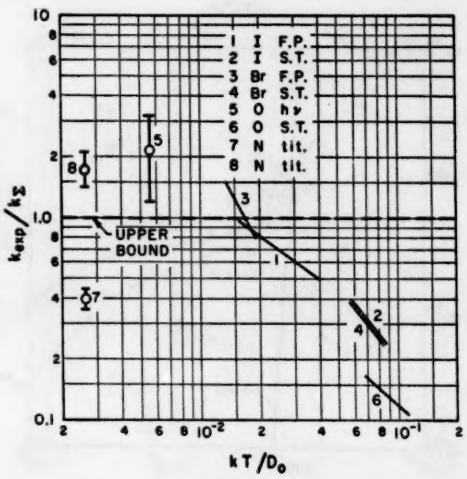

FIG. 15. Ratio of experimental three-body recombination rate constants k_{exp} to theoretical upper bounds k_Σ as a function of kT/D_0, where D_0 is the ground state binding energy. In all cases, the third body is argon. Curve (1) summarizes the results of flash photolysis experiments on recombination of iodine atoms.[5,6] Curve (2) summarizes the results of shock tube experiments on the dissociation of iodine.[7] Curve (3) summarizes the results of flash photolysis experiments on the recombination of bromine atoms.[8] Curve (4) summarizes the results of shock tube experiments on the dissociation of bromine.[8,9] Point (5) is the result of discharge experiments on the recombination of oxygen atoms in which the atom concentration was determined from the photon yield of the reaction NO+O→NO_2+$h\nu$.[10] Curve (6) summarizes the results of shock tube experiments on the dissociation of oxygen.[11,12] Points (7) and (8) are the results of flow experiments on the recombination of nitrogen atoms in which the atom concentration was determined by titrating with NO.[13,14] At low temperatures, the experimental results scatter about the theoretical upper bound. The fact that some of the data lie slightly above the bound is not considered serious at present due to the likelihood of experimental errors of this magnitude. At high temperatures, the experimental data fall away from the bound in a more-or-less smooth manner, which suggests that the mechanism responsible is nonspecific and may well be the same for all molecules. If this is the case, the theory can be empirically corrected to give recombination rate constants to about a factor of 2. Possible explanations of this effect and suggestions for improving the theory are given in the text.

[13] Herron, Franklin, Bradt, and Dibeler, J. Chem. Phys. **30**, 879 (1959).

[14] Hartech, Reeves, and Mannella, J. Chem. Phys. **29**, 608 (1958).

hence, a steeper temperature dependence of the rate constant.

The above discussion suggests that the study of reaction rates can be a means of investigating three-body potentials. A possible approach to the problem would be to represent the three-body interaction as an expansion in cylindrical harmonics with unknown coefficients to be determined by comparison with experiment. It is reasonable to suppose that such an expansion would converge rapidly so the number of undetermined coefficients might be quite small. It would be of considerable interest to observe the form of the various terms in the expansion. We already know, for example, that there would be no rotational contribution from the spherically symmetric part.

Atomic Number Dependence

A further comparison of theory and experiment is shown in Table I in which we have compared the theoretical bounds with the experimental rate constants for the recombination of iodine in the presence of noble gases.[15,16] The results of two experiments are shown, and it can be seen that the theory reproduces the trend of the observations almost perfectly. Although the observations are slightly higher than the bound given by the theory, the discrepancy is probably within the experimental error. Furthermore, a comparison of the tabulated argon results with more recent results, shown graphically in Fig. 11, indicates that the tabulated values may be slightly high.

It should be noted that the increase in the theoretical rate constant with atomic number is not a mass but a size effect. The theory is independent of the mass of the third body. The mass effect results in a decrease of the rate constant with increasing atomic number due to the slower velocity of the heavier particles. At room temperature, where the observations were made, the size effect is governed almost entirely by the van der Waals force, and since this was interpolated from measurements on noble gases there is room for improvement here.

At this point, it seems appropriate to inject a few remarks on the probable effect of other third bodies on the recombination reaction. It was already noted that the theoretical rate constants are independent of third body mass. They are also independent of the internal complexity of the third body as long as its internal state does not affect the external force field. We expect the present theory to share the success of the Bunker and Davidson theory[17] in explaining the relative efficiencies of complex catalysts at low temperatures since the van der Waals force enters in much the same way. It is also expected that attractive atoms will have a somewhat higher intrinsic efficiency as third bodies than repulsive ones since a larger region of configuration space is open to them. It should be noted, however, that in most cases the electronic degeneracy of attractive configurations is small compared to that of repulsive configurations so the over-all effect on the rate constant will be considerably diminished. The important effect in connection with attractive atoms is expected to be their ability to induce electronic transitions between the various bound states of a molecule by exchange collisions. Attractive third bodies with internal degrees of freedom have not been considered in any detail, but they should be very efficient due to the high probability of forming long-lived complexes.

TABLE I. Comparison of theoretical upper bounds, k_Σ, with observed rate constants for recombination of iodine atoms in the presence of noble gases. The observations are those of Christie, Harrison, Norrish, and Porter,[15] k_{CHNP}, and Russell and Simons,[16] k_{RS}. The theoretical bounds reproduce the trend of the observations to the accuracy with which the two experiments agree. Although the observed rate constants are slightly higher than the bounds, the discrepancy is probably within the experimental errors. The units are 10^{-33} sec^{-1} cm^6 molecules^{-2}.

Catalyst	k_Σ	k_{CHNP}	k_{RS}	k_{CHNP}/k_Σ	k_{RS}/k_Σ
He	3.0	3.4	4.7	1.1	1.6
Ne	4.3	4.6	5.0	1.1	1.2
A	7.5	9.2	10.0	1.2	1.4
Kr	9.1	11.3		1.2	
Xe	11.4	15.0		1.3	

VI. CONCLUDING REMARKS

Considering the simple "trial" surface used and the crude approximation to the three-body potential assumed, the comparison between theory and experiment is quite encouraging. At low temperatures, the observed recombination rate constants lie very near the predicted upper bounds, while at high temperatures they fall away from the bounds in a relatively smooth manner that can be qualitatively explained in terms of various approximations contained in the theory. Among the most important problems requiring investigation in connection with these approximations are: (1) the representation of the three-body potential, (2) the effect of multiple crossing of the "trial" surface by single trajectories, and (3) the treatment of electronic transitions between bound states. Improvement in the treatment of all these problems is certainly feasible, and some possible approaches have been mentioned. There is also the possibility of reducing the theoretical bound through the systematic investigation of other and perhaps more complicated trial surfaces. In view of the many opportunities available for refinement of the theory, it does not seem unreasonable to hope that a very satisfactory description of three-body recombination and dissociation can be obtained with the present approach.

[15] Christie, Harrison, Norrish, and Porter, Proc. Roy. Soc. (London) **A231**, 446 (1955).
[16] K. E. Russell and J. Simons, Proc. Roy. Soc. (London) **A217**, 271 (1953).
[17] D. L. Bunker and N. Davidson, J. Am. Chem. Soc. **80**, 5090 (1958).

TABLE II. Summary of parameters for the Morse potential.[a]

Molecule	μ	State	D_M/k °K	β_M A^{-1}	r_e A	$\beta_M r_e$	ω cm^{-1}
N_2	7	$^1\Sigma_g^+$	1.15[5]	2.69	1.09	2.94	2360
		$^3\Sigma_u^+$	4.25[4]	2.74	1.29	3.54	1460
O_2	8	$^3\Sigma_g^-$	6.01[4]	2.65	1.21	3.20	1580
		$^1\Delta_g$	4.86[4]	2.82	1.22	3.42	1509
		$^1\Sigma_g^+$	4.11[4]	2.93	1.23	3.59	1433
		$^3\Sigma_u^+$	8.16[3]	3.74	1.42	5.3	819
Br_2	40	$^1\Sigma_g^+$	2.31[4]	1.94	2.28	4.44	323
		$^3\Pi_{1u}$	3.24[3]	2.80	3.1	8.7	171
I_2	63.5	$^1\Sigma_g^+$	1.81[4]	1.86	2.67	4.96	215
		$^3\Pi_{1u}$	9.65[2]	1.66	5.9	9.8	44

[a] G. Herzberg, *Spectra of Diatomic Molecules* (D. Van Nostrand Company, Inc., Princeton, New Jersey, 1950).

In concluding, we should like to point out the relationship of the present variational theory of reaction rates to the "statistical" theory previously proposed by the author.[1] The two theories are in a sense complimentary, since the trial surfaces of the variational theory form appropriate boundaries for the collision complex of the statistical theory. In fact, it was the problem of defining the boundaries of the collision complex which led to the development of the variational theory. Coupling of the two theories provides a reasonable method for estimating the rate constants in cases where two or more trial surfaces are found which give comparable bounds to the reaction rate. For example, we have already employed the ideas of the statistical theory in a qualitative manner in arguing that multiple crossing of the barrier surface by single trajectories should be unimportant at low temperatures. However, because the statistical theory is non-

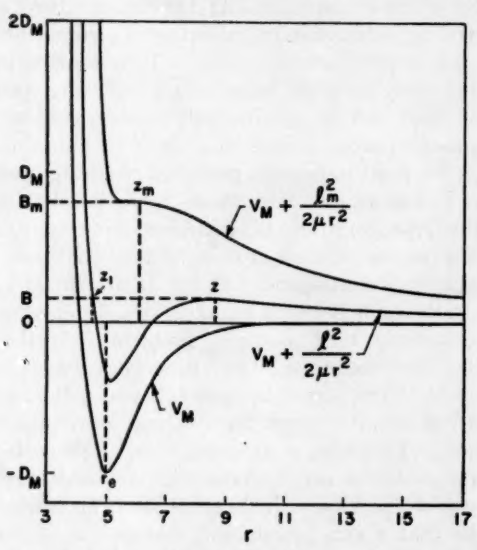

FIG. 16. Curves showing effective Morse potential for several values of angular momentum.

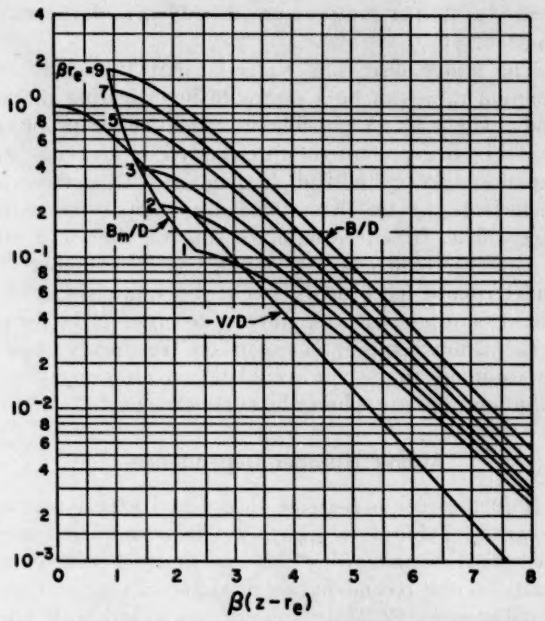

FIG. 17. Curves relate various parameters identified in Fig. 16. The curve labeled $(-V/D)$ was obtained from Eq. (A1). The curves labeled B/D were obtained by substituting Eq. (A1) into Eq. (16). The curve labeled B_m/D is the locus of the maxima of the B/D curves.

rigorous and leads to involved calculations, it is felt that quantitative treatment of the coupling problem should await the solution to the more important problems in connection with the variational theory.

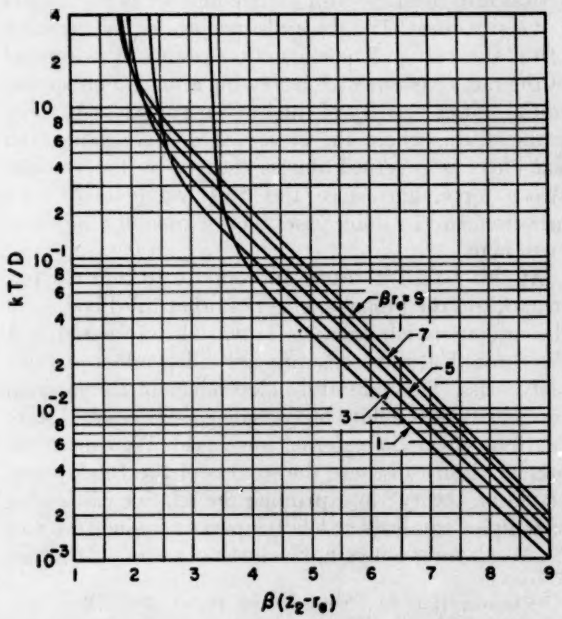

FIG. 18. Curves showing the relation between position z_2 of the maximum in the function $|dB/dz|\exp(-B/kT)$ and the temperature T. The curves were obtained by combining Eqs. (A1), (16), and (43).

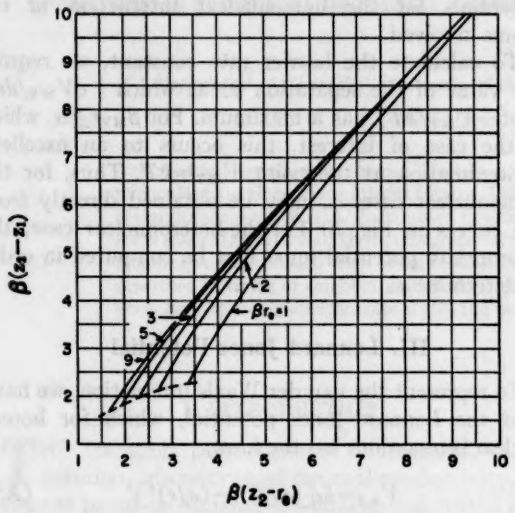

FIG. 19. Curves showing the relation between (z_2-z_1) and z_2. The curves were obtained by numerical solution of Eq. (42), with $u_{12}=V_M/kT$.

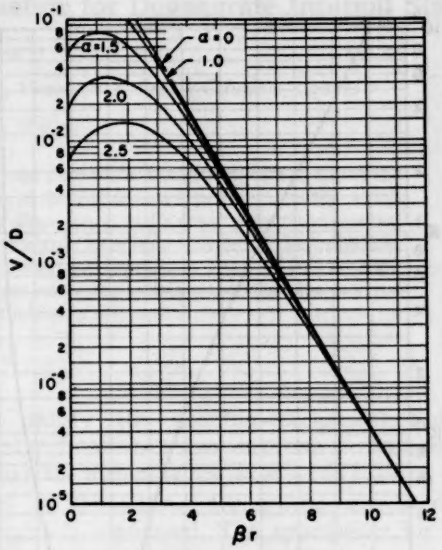

FIG. 20. Mason-Vanderslice potential for several values of the parameter α. The curves are plots of Eq. (A3) with $\beta'=\beta_{MV}$.

ACKNOWLEDGMENT

The author wishes to thank A. R. Kantrowitz for his enthusiastic support of this work, B. T. Feld and E. E. Salpeter for many stimulating discussions, some of which resulted directly in ideas discussed in the present paper, N. Davidson for pointing out the importance of including the van der Waals force, H. K. Brown for assistance with the more involved mathematics, W. K. Goldsmith for programming the calculations, and B. Kivel and H. Petschek for critical reading of the manuscript.

APPENDIX

I. Morse Potential

The Morse potential is described by the equation,

$$V_M(r)=D_M\{\{1-\exp[-\beta_M(r-r_e)]\}^2-1\}. \quad \text{(A1)}$$

The corresponding effective potential is

$$V_M'(r)=V_M(r)+l^2/2\mu r^2, \quad \text{(A2)}$$

where l is the angular momentum of the molecules and the constants D_M, β_M, r_e, and μ are tabulated for the molecular states of interest in the present work in Table II. The general form of the effective potential is shown in Fig. 16 for several values of l. Note there is a maximum value of angular momentum l_m for which the effective potential has a relative minimum.

Some useful curves relating various parameters appearing in the theory are shown in Figs. 17–19. These were obtained by inserting Eq. (A1) into the defining equations.

II. Mason-Vanderslice Potential

For homonuclear interactions, the Mason-Vanderslice potential[4] may be written in the form,

$$V_{MV}(r)=D_{MV}\exp[-\beta' r-2\alpha\exp(-\beta' r/\alpha)], \quad \text{(A3)}$$

where

$$\beta'=(1-V_{MV}/D_{MV})\beta_{MV}. \quad \text{(A4)}$$

D_{MV}, β_{MV}, and α are constants related to the atomic properties of the interacting atoms, and a summary

TABLE III. Summary of parameters for Mason-Vanderslice potential.

Atom	A	D_{MV}/k °K	β_{MV} A^{-1}	α
He	4	4.11[6]	4.83	1.50
Ne	20	1.58[7]	4.24	1.54
A	40	1.53[7]	3.10	2.18
Kr	84	2.38[7]	2.74	2.39
Xe	131	2.71[7]	2.38	2.24
N	14	4.96[6]	2.84	1.55
O	16	5.06[6]	2.67	1.24
Br	80	1.65[7]	2.31	2.18
I	127	2.03[7]	2.08	2.31

TABLE IV. Summary of parameters for Lennard-Jones potential. The values for the noble gases were taken from reference 19. The values for the remaining atoms were obtained by interpolation on Z.

Atom	A	Z	ϵ/k	σ
He	4	2	10	2.6
Ne	20	10	33	2.79
A	40	18	120	3.42
Kr	84	36	173	3.60
Xe	131	54	223	4.04
N	14	7	25	2.7
O	16	8	30	2.7
Br	80	35	170	3.6
I	127	53	220	4.0

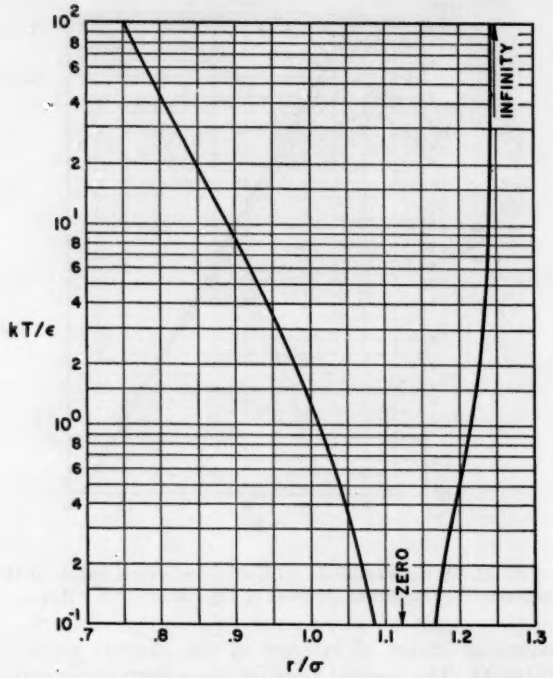

FIG. 21. Curve showing the relation between the position r of the maxima in the function $|dV_{LJ}/dr|\exp(-V_{LJ}/kT)$ and the temperature T. The curve was obtained by inserting Eq. (A5) into Eq. (35).

of values for the atoms of interest in the present work is given in Table III. Note that, since the definition of β' involves V_{MV}, Eq. (A3) gives only an implicit definition of V_{MV} and this produces some complication. Fortunately, in all cases of interest in the present work, $V_{MV}/D_{MV}\ll 1$ and we can, therefore, set $\beta'\approx\beta_{MV}$ Figure 20 shows curves of V_{MV}/D_{MV} for $\beta'=\beta_{MV}$ as a function of $\beta_{MV}r$ for several values of α. At low energies, the curves are all asymptotic to a simple exponential.

For heteronuclear interactions, Mason and Vanderslice suggest using the geometric mean of the two potentials for the homonuclear interaction of the atoms involved.

To calculate the barrier rate constant, we require the value of the separation a_- at which $|dV_{MV}/dr|\exp(-V_{MV}/kT)$ has a maximum. For $\beta_{MV}r\geq\alpha$, which is the case of interest, this occurs to an excellent approximation at the point $V_{MV}=kT$. Thus, for the homonuclear case, a_- may be obtained directly from the curves in Fig. 20. For the heteronuclear case, the appropriate potential must first be computed in order to determine a_-.

III. Lennard-Jones Potential

To represent the van der Waals interaction, we have used the Lennard-Jones potential, which for homonuclear interactions has the form,

$$V_{LJ}=4\epsilon[(\sigma/r)^{12}-(\sigma/r)^{6}]. \tag{A5}$$

The constants ϵ and σ for the atoms of interest in the present paper are given in Table IV.

For the heteronuclear interactions, the combination rules

$$\epsilon_{12}=(\epsilon_1\epsilon_2)^{\frac{1}{2}} \tag{A6}$$

and

$$\sigma_{12}=\tfrac{1}{2}(\sigma_1+\sigma_2) \tag{A7}$$

are recommended by Hirschfelder, Curtiss, and Bird.[18]

To calculate the barrier rate constant, we require the separations a_- and a_+ at which

$$|dV_{LJ}/dr|\exp(-V_{LJ}/kT)$$

has maxima. These may be obtained from the graph in Fig. 21 which represents the solution of Eq. (35).

It should be noted that the values of a_- obtained from the Lennard-Jones and Mason-Vanderslice potentials do not join smoothly. In the present calculations, smoothing was done graphically.

[18] Hirshfelder, Curtiss, and Bird, *Molecular Theory of Gases and Liquids* (John Wiley & Sons, Inc., New York, 1954).

Quantum-Mechanical Modified Boltzmann Equation for Degenerate Internal States

ROBERT F. SNIDER

Department of Chemistry, University of British Columbia, Vancouver 8, British Columbia, Canada

(Received October 22, 1959)

A modified quantum-mechanical Boltzmann equation has been derived for the general case in which the molecules have degenerate internal states. This is an equation of the Boltzmann type for a quantity which is simultaneously a Wigner distribution function in molecular phase space, and a density matrix in internal state space. In particular, the nondiagonal terms of this density matrix have been included in the formalism, resulting in the collision term being modified from the usual Boltzmann expression. Thus the collisions are described in terms of combinations of the Lippmann-Schwinger scattering matrix rather than the collision cross section. For nondegenerate states the usual collision term is obtained again.

I. INTRODUCTION

THE transport phenomena of dilute gases, such as diffusion, viscosity, and thermal conductivity, usually are based on Boltzmann's integro-differential equation.[1-2] This equation is assumed to hold under certain restrictive conditions, namely that the gas is sufficiently dilute and that the gas is not too far from being distributed uniformly in its vessel. The first derivation of this equation was given by Boltzmann,[3] who derived it from physical arguments. More recently, attempts have been made to derive this equation from the mechanical equations of motion of a gas.[4-17] These derivations have used both classical mechanics[4-9] and quantum mechanics[13-17] in their derivations, while in this paper only quantum mechanics will be considered.

Classically, the Boltzmann equation is an integro-differential equation for the phase-space distribution function. However, there is no complete analog in quantum mechanics to this function, since position and momentum cannot be specified simultaneously in quantum mechanics. The function which corresponds closest to the classical distribution function is the Wigner distribution function,[18] which is a certain Fourier transform of the quantum-mechanical density matrix. It is this function (for one particle) which must satisfy the quantum-mechanical Boltzmann equation. In all the above quantum derivatives except the last, the molecules are assumed to have no internal states. In the latter,[17] the special case of diatomic molecules is considered. The appropriate function to describe the gas in this case consists of a set of one-particle Wigner distribution functions, one for each of the terms in a matrix of internal states, i.e., a Wigner distribution function-density matrix which is a distribution function in position-momentum space and a density matrix in internal state space. This is required for degenerate states since, as indicated more explicitly in Sec. IV, Eq. (41), the internal state of a molecule may be any linear combination of the degenerate internal states. In sharp contrast to this is the case when the internal states are nondegenerate. Then the internal state wave function for a free particle contains only one possible state, and the corresponding density matrix will be diagonal in internal states. Thus, although it is sufficient to use a distribution function or population density when the internal states are nondegenerate, this does not give a sufficiently accurate description of the system when there are degenerate states. Correspondingly, a density in internal states must be used then. However, Dahler[17] considers only the diagonal elements of this Wigner distribution function-density matrix.

In this paper a Boltzmann-like equation is proposed for this Wigner distribution function-density matrix, which takes into account the nondiagonal terms of this function. Such an equation should form the basis for the discussion of gases with degenerate internal states. In particular, it should be possible to investigate the quantal analog of the recent classical mechanical work of Curtiss and Muckenfuss[19-21] on the transport of angular momentum in dilute gases.

The method of deriving this modified Boltzmann equation bears some resemblance to the recent deriva-

[1] S. Chapman and T. G. Cowling, *The Mathematical Theory of Non-Uniform Gases* (Cambridge University Press, New York, 1952), second edition.
[2] Hirschfelder, Curtiss, and Bird, *Molecular Theory of Gases and Liquids* (John Wiley & Sons, Inc., New York, 1954).
[3] L. Boltzmann, Wein. Ber. **66**, 275 (1972). (Collected Works 1,316).
[4] N. Bogolubov, J. Phys. (U.S.S.R.) **10**, 265 (1946).
[5] J. G. Kirkwood, J. Chem. Phys. **15**, 72 (1947).
[6] M. Born and H. S. Green, *A General Kinetic Theory of Liquids* (Cambridge University Press, New York, 1949).
[7] H. Grad, unpublished lecture notes.
[8] M. Schönberg, Nuovo Cimento **10**, 419 (1953).
[9] M. S. Green, J. Chem. Phys. **25**, 836 (1956).
[10] E. A. Uehling and G. E. Uhlenbeck, Phys. Rev. **43**, 552 (1933).
[11] H. Mori and S. Ono, Progr. Theoret. Phys. **8**, 327 (1952).
[12] S. Ono, Progr. Theoret. Phys. **12**, 113 (1954).
[13] H. S. Green, Proc. Phys. Soc. (London) **A66**, 325 (1953).
[14] J. Ross and J. G. Kirkwood, J. Chem. Phys. **22**, 1094 (1954).
[15] A. W. Saenz, Phys. Rev. **105**, 546 (1957).
[16] H. Mori and J. Ross, Phys. Rev. **109**, 1877 (1958).
[17] J. Dahler, J. Chem. Phys. **30**, 1447 (1959).
[18] E. Wigner, Phys. Rev. **40**, 479 (1932).
[19] C. F. Curtiss, J. Chem. Phys. **24**, 225 (1956).
[20] C. F. Curtiss and C. Muckenfuss, J. Chem. Phys. **26**, 1619 (1957).
[21] C. Muckenfuss and C. F. Curtiss, J. Chem. Phys. **29**, 1257 (1958).

tions by Saenz,[15] and by Mori and Ross,[16] in that it uses the formal scattering theory of Lippmann and Schwinger[22,23] to describe the collisions rather than the perturbation approach used by Dahler[17] and earlier workers.[10–14] Thus the resulting expressions normally would use the complete collision cross section rather than the Born approximation to the cross section. However, since the Boltzmann-like equation which is obtained is for a nondiagonal Wigner distribution function-density matrix, the collision cross section as such is not involved but rather, elements of the Lippmann Schwinger scattering matrix t. The combinations of this matrix which arise can be shown to reduce easily to the ordinary collision cross section if the distribution function is diagonal.

In contrast to the derivation by Mori and Ross,[16] a coarse graining in time is not used, nor is a time-smoothing operation carried out[5]—instead, physical requirements are made on the solution of the modified Boltzmann equation, namely that the Wigner distribution function-density matrix must be only macroscopically position-dependent and further that it is diagonal in the internal energy. These requirements suffice to accomplish the same effect as the coarse graining of time. Lastly, the technique used in this derivation for introducing the ordinary flux terms in the Boltzmann equation is new.* The method used here has some logical resemblance to Ono's[12] cell-function method but is formally very different.

II. GENERAL FORMULATION

A gas in a macroscopic state is represented quantum mechanically by a symmetric (Bose-Einstein) or antisymmetric (Fermi-Dirac) N-particle density matrix $\rho^{(N)}$ where N is the number of molecules in the gas. $\rho^{(N)}$ is taken here to be normalized to $N!$. As is well known,† this density matrix satisfies the operator equation

$$i\hbar(\partial\rho^{(N)}/\partial t)=H^{(N)}\rho^{(N)}-\rho^{(N)}H^{(N)}, \tag{1}$$

where $\hbar$ is Planck's constant divided by 2π, and t is the time. $H^{(N)}$ is the N-particle Hamiltonian assumed to be of the form

$$H^{(N)}=\sum_{i=1}^{N}H_i^{(1)}+\tfrac{1}{2}\sum_{i\neq j}V_{ij}, \tag{2}$$

where $H^{(1)}$ is a one-particle Hamiltonian, e.g., the kinetic energy, while V_{ij} is the short-range intermolecular potential between molecules i and j and is responsible for molecular collisions.

This equation, because of its great number of degrees of freedom, is impossible to solve except in a very formal manner. However, when dealing with a gas at a sufficient dilution, several approximations can be made to obtain approximate solutions of this equation. An assumption that is basic to the theory is that in a dilute gas the molecules are far apart most of the time and consequently independent of one another. The mathematical relation that expresses this is the Boltzmann property,[24–25]

$$\rho^{(N)}=\prod_{i=1}^{N}\rho_i^{(1)}, \tag{3}$$

i.e. that the N-particle density matrix is a product of one-particle density matrices.‡ This property will be assumed to hold almost everywhere in the gas, in fact, everywhere except where two or more molecules are interacting or colliding. For sufficiently dilute gases the number of molecules that are colliding at any one instant is very small so that the Boltzmann property then should hold almost everywhere. However, because of the intermolecular potential V, the molecules do collide and this has an effect on the singlet density matrix.

The equation of change of $\rho^{(1)}$ is obtained by taking the trace of Eq. (1) over all molecules but one, namely,

$$i\hbar(\partial\rho^{(1)}/\partial t)=H^{(1)}(1)\rho^{(1)}(1)-\rho^{(1)}(1)H^{(1)}(1)+\operatorname*{Tr}_{(2)}[V(1,2)\rho^{(2)}(1,2)-\rho(1,2)V(1,2)]. \tag{4}$$

In this equation, the quantities

$$\rho^{(2)}(1,2)=[1/(N-2)!]\operatorname*{Tr}_{(3\cdots N)}\rho^{(N)}(1,2,3,\cdots N) \tag{5}$$

and

$$\rho^{(1)}(1)=[1/(N-1)]\operatorname*{Tr}_{(2)}\rho^{(2)}(1,2) \tag{6}$$

have been used to denote the pair density matrix for molecules 1 and 2 and the singlet density matrix for molecule 1, respectively. The physical interpretation of Eq. (4) is that the time derivative of $i\hbar\rho^{(1)}$ is a sum of a flux term given by $H^{(1)}\rho^{(1)}-\rho^{(1)}H^{(1)}$, and a collision term expressed in terms of the intermolecular potential and the pair density matrix. This latter term will vanish except when molecule 1 is colliding with another molecule, molecule 2. To express the collision term in terms of $\rho^{(1)}$ requires a knowledge of $\rho^{(2)}$ when the molecules are colliding and this is just when the Boltzmann property does not hold. Since the Boltzmann property is assumed to hold when the molecules are not colliding, it is sufficient to express $\rho^{(2)}$ during the collision in terms of $\rho^{(2)}$ before the collision occurred, where

[22] B. A. Lippmann and J. Schwinger, Phys. Rev. **79**, 469 (1950).
[23] M. Gell-Menn and M. L. Goldberger, Phys. Rev. **91**, 398 (1953).
* It was pointed out by the referee that this is similar to a proof by E. C. McErvine and A. W. Overhauser in application to the theory of metals. E. C. McErvine, Bull. Am. Phys. Soc. Ser. II, **3**, 367 (1958) and Thesis, Cornell University (unpublished).
† See, for example reference 2, Chap. 2.
[24] M. Kac, Proc. Berkeley Symposium on Mathematical Statistics (1954).
[25] R. Brout, Physica **22**, 509 (1956).
‡ The symmetry of the molecules has been neglected completely in this paper.

now the Boltzmann property will hold and, consequently, $\rho^{(2)}$ and the collision term can be expressed in terms of $\rho^{(1)}$. This will yield then an equation which must be satisfied by $\rho^{(1)}$. The problem is thus to express $\rho^{(2)}$ during a collision in terms of $\rho^{(2)}$ before a collision; this can be done with the help of the equation of change for $\rho^{(2)}$, namely,

$$i\hbar[\partial\rho^{(2)}(1,2)/\partial t]=H^{(2)}(1,2)\rho^{(2)}(1,2)-\rho^{(2)}(1,2)H^{(2)}(1,2)+\operatorname{Tr}_{(3)}[(V_{13}+V_{23})\rho^{(3)}(1,2,3)-\rho^{(3)}(1,2,3)(V_{13}+V_{23})], \quad (7)$$

which is obtained from Eq. (1) in the same manner as was Eq. (4). In fact, Eq. (4) is obtained from Eq. (7) by taking the trace over molecule 2. The triplet density matrix $\rho^{(3)}$ is defined analogously to $\rho^{(1)}$ and $\rho^{(2)}$, while the pair Hamiltonian is

$$H^{(2)}(1,2)=H^{(1)}(1)+H^{(1)}(2)+V(1,2). \quad (8)$$

Equations (4) and (7) are exact. However, for the cases considered here, namely that of a dilute gas, the possibility of triple collisions is very small, so that, when using Eq. (7) for calculating the pair density matrix when molecules 1 and 2 are colliding, the terms involving a third molecule may be neglected and Eq. (7) simplifies to

$$i\hbar(\partial\rho^{(2)}/\partial t)=H^{(2)}\rho^{(2)}-\rho^{(2)}H^{(2)}. \quad (9)$$

It must be remembered that this equation is correct only during the collision between molecules 1 and 2. The procedure that is followed is to find a suitable formal solution to Eq. (9) which describes the collision and then to use this solution to express the collision term of Eq. (4) in terms of $\rho^{(1)}$. After some rearranging this reduces to a more recognizable form. Finally, in Sec. IV, the Wigner distribution function[18] is defined and a modified Boltzmann equation is obtained for it.

III. APPLICATION OF FORMAL SCATTERING THEORY

The appropriate solution of Eq. (9) will be obtained in terms of the formal scattering of Lippmann and Schwinger,[22,23] the relevant portions of this theory being reproduced here for completeness. Equation (9) is solved formally by the expression

$$\rho(t)=\exp[-iH(t-t_0)/\hbar]\rho(t_0)\exp[iH(t-t_0)/\hbar], \quad (10)$$

where the superscript (2) will be understood unless otherwise indicated. Here t and t_0 are times, $\rho(t)$ the pair density matrix at time t, and

$$\exp[-iH(t-t_0)/\hbar] \quad (11)$$

is the unitary operator transforming a wave function at time t_0 to a wave function at time t due to the action of the pair Hamiltonian H. This transformation operator describes both the motion due to the kinetic energy of the molecules and the collisional effect due to the potential. To separate these effects it is useful to introduce the kinetic and internal state energy operator

$$K=H^{(1)}(1)+H^{(1)}(2), \quad (12)$$

so that the total Hamiltonian for the pair of molecules may be written

$$H=K+V. \quad (13)$$

With the aid of this operator, a transformation to the "interaction representation" allows a separation of the kinetic and collisional effects, thus the density matrix in interaction representation,

$$\rho_I(t)=\exp(iKt/\hbar)\rho(t)\exp(-iKt/\hbar), \quad (14)$$

does not change due to the kinetic motion of the molecules but only due to the potential or collisional effects. The corresponding time dependence of ρ_I may be written as

$$\rho_I(t)=U(t,t_0)\rho_I(t_0)U^*(t,t_0), \quad (15)$$

where $U(t,t_0)$ is found from Eqs. (10), (14), and (15) to be

$$U(t,t_0)=\exp(iKt/\hbar)\exp[-iH(t-t_0)/\hbar]\cdot\exp(-iKt_0/\hbar); \quad (16)$$

$U^*(t,t_0)$ is the adjoint of $U(t,t_0)$. It is useful to rewrite this equation for $U(t,t_0)$ in the form

$$U(t,t_0)=\exp(iKt/\hbar)\exp[+iH(t_0-t)/\hbar]\cdot\exp[-iK(t_0-t)/\hbar]\exp(-iKt/\hbar)=\exp(iKt/\hbar)U(0,t_0-t)\exp(-iKt/\hbar). \quad (17)$$

Equation (15) will be used to evaluate the collision term in Eq. (4). An expression for $\rho(t)$ is needed. This may be written in terms of $\rho(t_0)$ with the help of Eqs. (14), (15), and (17) as

$$\rho(t)=U(0,t_0-t)\exp[-iK(t-t_0)/\hbar]\rho(t_0)\cdot\exp[iK(t-t_0)/\hbar]U^*(0,t_0-t). \quad (18)$$

The physical significance of the times t and t_0 is that, at time t the molecules are in the midst of a collision whereas time t_0 is an earlier time before the collision begins, and so the Boltzmann property will hold, i.e.,

$$\rho(t_0)=\rho^{(1)}(1;t_0)\rho^{(1)}(2;t_0). \quad (19)$$

The effect of the operator $U(0,t_0-t)$ is to transform a wave function in interaction representation at time t_0-t before a collision to time 0 in the midst of a collision. Now since $U(0,t_0-t)$ transforms wave functions in interaction representation and since such a wave function is unchanged by $U(0,t_0-t)$ as long as the molecules have not yet collided, it follows that $U(0,t_0-t)$ is insensitive to the value of the negative time t_0-t provided that this is before the collision occurs if they are in the midst of the collision at time 0. Thus t_0-t may be replaced by any previous time (in $U(0,t_0-t)$)

in fact even by the limit $-\infty$. The existence of this well-known limit recently has been clarified by Jauch.[26] The limit operator usually is denoted by

$$U(0,-\infty)=\lim_{\tau\to-\infty}\exp(iH\tau/\hbar)\exp(-iK\tau/\hbar)=\Omega^{(+)}. \tag{20}$$

Finally, for Eq. (18), one needs to know the effect of $\exp[-iK(t-t_0)/\hbar]$ on $\rho(t_0)$. This is, however, merely the transformation operator which takes a wave function at time t_0 to time t under the action of a pair Hamiltonian which contains no interaction. Thus, utilizing Eqs. (12) and (19) and obvious commutivity properties,

$$\exp[-iK(t-t_0)/\hbar]\rho(t_0)\exp[iK(t-t_0)/\hbar]=\rho^{(1)}(1_{t-t_0};t)\rho^{(1)}(2_{t-t_0};t), \tag{21}$$

where

$$\rho^{(1)}(1_{t-t_0};t)=\exp[-iH^{(1)}(1)(t-t_0)/\hbar]\rho(1;t_0)\cdot\exp[iH^{(1)}(1)(t-t_0)/\hbar] \tag{22}$$

is the singlet density matrix evaluated at time t for the coordinates 1_{t-t_0}. The meaning of the transformation in Eq. (22) is that it is a translation in position space (provided that $\rho^{(1)}$ is diagonal in the internal state energy, which is later assumed in this paper, Sec. IV.

The Boltzmann equation is known to be applicable only to dilute gases, when the density is not too nonuniform. In particular, there cannot be sizable variations in the distribution function over distances and times of the order of collision distances and times. Consequently, in the low density limit, $\rho^{(1)}(1_{t-t_0};t)$ will be replaced by $\rho^{(1)}(1;t)$. The correction term arising from this difference corresponds to part of the density correction terms found by Bogolubov[4] and Green[27] for the classical Boltzmann equation. These take into account the faster position dependence of the density of the gas than is usually accounted for in the ordinary Boltzmann equation and is responsible for certain density corrections to the transport coefficients.[28]

The above considerations allow Eq. (4) to be written

$$i\hbar[\partial\rho^{(1)}(1)/\partial t]=H^{(1)}(1)\rho^{(1)}(1)-\rho^{(1)}(1)H^{(1)}(1)+\operatorname*{Tr}_{(2)}[V(1,2)\Omega^{(+)}\rho^{(1)}(1)\rho^{(1)}(2)\Omega^{(+)*}(1,2)-\Omega^{(+)}(1,2)\rho^{(1)}(1)\rho^{(1)}(2)\Omega^{(+)*}(1,2)V(1,2)], \tag{23}$$

which is an equation for the singlet density matrix. Eq. (23) involves the quantum mechanical operators V and $\Omega^{(+)}$, neither of which usually is used to represent the results of a collision. To express the collisional results in a more usual form, one needs certain well-known formulas from the formal theory of scattering. The derivation of these formulas are indicated here for completeness of presentation.

By differentiating Eq. (16) with respect to t_0 and casting the results into an integral equation, an integral expression is obtained for $U(t,t_0)$, namely,

$$U(t,t_0)=1-(i/\hbar)\int_{t_0}^{t}\exp(iKt/\hbar)\exp[-iH(t-t')/\hbar]V\cdot\exp[-iKt'/\hbar]dt'. \tag{24}$$

Provided the limit exists,

$$\Omega^{(+)}=U(0,-\infty)=1-(i/\hbar)\int_{-\infty}^{0}\exp(iHt'/\hbar)V\cdot\exp(-iKt'/\hbar)dt', \tag{25}$$

where 1 is the identity operator. As mentioned in the discussion before Eq. (20), $\Omega^{(+)}$ is to be the limit of $U(0,\tau)$ as $\tau\to-\infty$, where $U(0,\tau)$ is insensitive to the value of τ. To make this limit operator exist, a convergence factor is introduced in the integral of Eq. (25). For the justification of this, see the original literature[22-23] and especially Jauch's article.[26] With this convergence factor

$$\Omega^{(+)}=1-(i/\hbar)\lim_{\epsilon\to0}\int_{-\infty}^{0}\exp(\epsilon t'/\hbar)\exp(iHt'/\hbar)V\exp(-iKt'/\hbar)dt', \tag{26}$$

where ϵ is an arbitrary small number of dimensions of energy.

The effect of this operator on an eigenfunction χ_a of K, i.e.,

$$K\chi_a=E_a\chi_a, \tag{27}$$

is that it transforms χ_a to a new wave function $\psi_a^{(+)}$, namely

$$\begin{aligned}\psi_a^{(+)}&=\Omega^{(+)}\chi_a\\&=\chi_a-(i/\hbar)\lim_{\epsilon\to0}\int_{-\infty}^{0}\exp(\epsilon t'/\hbar)\exp(iHt'/\hbar)\exp(-iE_at'/\hbar)dt'V\chi_a\\&=\chi_a+\lim_{\epsilon\to0}(E_a-H+i\epsilon)^{-1}V\chi_a.\end{aligned} \tag{28}$$

This may be rearranged to have the following form,

$$\psi_a^{(+)}=\chi_a+G_a^{(+)}V\psi_a^{(+)}, \tag{29}$$

where

$$G_a^{(+)}=\lim_{\epsilon\to0}(E_a-K+i\epsilon)^{-1}=[1/(E_a-K)]_P-\pi i\delta(E_a-K). \tag{30}$$

The last form for $G_a^{(+)}$ follows easily from the theory of complex functions, the definition of the principal value $(\ )_P$ of an operator, and the Dirac δ function. Equation (29) is known as the Lippmann-Schwinger equa-

[26] J. M. Jauch, Helv. Phys. Acta. **31**, 127 (1958).
[27] H. S. Green, *Molecular Theory of Fluids* (North Holland Publishing Company, Amsterdam, Holland, 1952).
[28] R. F. Snider and C. F. Curtiss, Phys. Fluids **1**, 122 (1958).

tion. This may be changed to an operator equation for $\Omega^{(+)}$, namely

$$\Omega^{(+)}=1+G^{(+)}V\Omega^{(+)}, \tag{31}$$

in which the energy eigenvalue E in $G^{(+)}$ must correspond to the eigenfunction χ upon which $\Omega^{(+)}$ operates.

The connection between $\Omega^{(+)}$ and the collision cross section may be expressed in terms of the $t^{(+)}$ matrix defined by

$$t^{(+)}=V\Omega^{(+)}. \tag{32}$$

The collision cross section for scattering *"in relative coordinates"* from state a to state b can be shown to be

$$\sigma_{a\to b}=(2\pi)^4\mu^2\hbar^2(k_b/k_a)\,|\,t_{ba}{}^{(+)}\,|^2, \tag{33}$$

where k_a and k_b are the magnitudes of the relative momentum wave numbers of states a and b, respectively, and μ is the reduced mass of the colliding molecules. Here a and b refer to relative momentum eigenfunctions which are normalized to Dirac δ functions in the position. Now $\Omega^{(+)}$ can be eliminated from Eq. (23) by the use of Eqs. (31) and (32), giving the result

$$\begin{aligned}i\hbar[\partial\rho^{(1)}(1)/\partial t]&=H^{(1)}(1)\rho^{(1)}(1)-\rho^{(1)}(1)H^{(1)}(1)\\&+\operatorname*{Tr}_{(2)}[t(1,2)\rho^{(1)}(1)\rho^{(1)}(2)-\rho^{(1)}(1)\rho^{(1)}(2)t^*(1,2)]\\&+\operatorname*{Tr}_{(2)}[t(1,2)\rho^{(1)}(1)\rho^{(1)}(2)t^*(1,2)G^{(+)*}(1,2)\\&\quad-G^{(+)}(1,2)t(1,2)\rho^{(1)}(1)\rho^{(1)}(2)t^*(1,2)],\end{aligned} \tag{34}$$

where the $(+)$ on t is to be understood. t will be written for $t^{(+)}$ in the rest of this paper for notational convenience.

In applications to the kinetic theory of gases, $\rho^{(1)}$ has the special property that it is almost diagonal in the energy; this property is discussed more fully in Sec. IV (Eq. (59) and sequence). By requiring this property of $\rho^{(1)}$ on both sides of Eq. (34), a simplification of this equation is obtained when it is written out in matrix notation. For this purpose, the basic set of functions for the expansion are chosen as the eigenfunctions χ of K, Eq. (27), which are normalized to Dirac δ functions in the position. Thus, Eq. (34) becomes

$$\begin{aligned}\partial\rho_{a_1b_1}/\partial t^{(1)}&=[(H_{a_1}{}^{(1)}\rho_{a_1b_1}{}^{(1)}-\rho_{a_1b_1}{}^{(1)}H_{b_1}{}^{(1)})/i\hbar]\\&+(2\pi/\hbar)\sum_{cc'a_2b_2}t_{ac}\rho_{c_1c_1'}{}^{(1)}\rho_{c_2c_2'}{}^{(1)}t_{c'b}{}^*\delta_{a_2b_2}\delta(E_b-E_{c'})\\&+(1/i\hbar)\sum_{ca_2b_2}[t_{ac}\rho_{c_1b_1}{}^{(1)}\rho_{c_2b_2}{}^{(1)}-\rho_{a_1c_1}{}^{(1)}\rho_{a_2c_2}{}^{(1)}t_{cb}{}^*]\delta_{a_2b_2},\end{aligned} \tag{35}$$

where $\delta_{a_2b_2}$ is the Kronecker δ function and summations have been written symbolically for sums over all states even though these are continuous. In this equation, a_1 is the eigenvalue of $H^{(1)}$ for molecule 1, a_2 that for molecule 2, and a is the comprehensive eigenvalue denoting a_1, a_2. This holds for b, c, and c' as well. The energy δ function in the second term arises from the remark made at the beginning of this paragraph, namely that $E_a\simeq E_b$ and $E_c\simeq E_{c'}$, together with the fact that

$$G^{(+)*}-G^{(+)}=2\pi i\delta(E-K), \tag{36}$$

which is easily seen from Eq. (30).

Finally, as a special case of Eq. (35) which shows the connection to the usual formula, if $\rho^{(1)}$ is diagonal, Eq. (35) becomes

$$\begin{aligned}\partial\rho_{a_1}{}^{(1)}/\partial t&=(1/\hbar^3)\sum_{ca_2}[\delta(E_a-E_c)/\mu_a{}^2]\\&\cdot[(k_c/k_a)\rho_{c_1}{}^{(1)}\rho_{c_2}{}^{(1)}\sigma_{c\to a}-(k_a/k_c)\rho_{a_1}{}^{(1)}\rho_{a_2}{}^{(1)}\sigma_{a\to c}],\end{aligned} \tag{37}$$

which is recognizable as an equation of the Boltzmann or Uehling-Uhlenbeck form for a spatially uniform dilute gas (quantum statistics have been neglected). To obtain this form, Eq. (33) for the cross section and the identity

$$t^*-t=t^*(G^{(+)*}-G^{(+)})t=2\pi i t^*\delta(E-K)t \tag{38}$$

have been used. With the help of Eq. (37), some physical interpretation of the terms in Eq. (35) may be made. Thus, by analogy, the time rate of change of $\rho_{a_1b_1}{}^{(1)}$ is given by the sum of, (1) a flux term [which vanishes in Eq. (37)]; (2) a term describing the number of molecular collisions which result in one of the molecules having a density matrix $\rho_{a_1b_1}{}^{(1)}$; (3) a term which describes the collisional removal of molecules having a density matrix $\rho_{a_1b_1}{}^{(1)}$.

IV. MODIFIED BOLTZMANN EQUATION FOR THE WIGNER DISTRIBUTION FUNCTION

Equation (35) bears some resemblance to the Boltzmann equation and the various terms have been given a physical interpretation at the end of the last section. However, the Boltzmann equation is given in terms of the distribution function in classical problems and in terms of the Wigner distribution function[18] in quantum-mechanical problems. It is the purpose of this section to change Eq. (35) for the singlet-density matrix into a modified Boltzmann equation for the corresponding Wigner distribution function. In order to do this, it first is necessary to make the form of $H^{(1)}$ and $\rho^{(1)}$, as used in the previous sections, more explicit.

The one-particle Hamiltonian $H^{(1)}$ is assumed to be a sum of a kinetic energy operator and an internal state energy operator H_{int}, thus in coordinate representation

$$H^{(1)}=-(\hbar^2/2m)\nabla^2+H_{\text{int}}, \tag{39}$$

where m is the mass of the molecule and ∇^2 is the Laplacian for the position (center of gravity) of the molecule. H_{int} is assumed to have orthonormal eigenfunctions such that

$$H_{\text{int}}S_{lm}(\sigma)=\epsilon_l S_{lm}(\sigma), \tag{40}$$

where σ denotes the internal coordinations of the molecule and l and m are the quantum numbers specifying the internal state of the molecule. Here the quantum numbers have been labeled as for rotational states, m is

the magnetic quantum number about some specified axis, and l is comprehensive index, denoting, for example, the total angular momentum quantum number. What is important is that l denotes the energy levels which are degenerate in m.

Since ϵ_l does not depend on m, the stationary internal states may be any linear combination of states with the same l; thus any function of the form

$$\psi(\sigma)=\sum_m c_m S_{lm}(\sigma), \tag{41}$$

provided only that normalization is preserved, i.e., that

$$\sum_m |c_m|^2=1. \tag{42}$$

This corresponds physically to the molecule rotating about some other axis than the specified one. The total wave function for a molecule is a product of one of the above internal wave functions with a position wave function, which will describe, for a molecule in a gas, the molecule moving with some average momentum $\mathbf{p}$. If $\varphi(\mathbf{r})$ is such a function, then the singlet density matrix has the form

$$\begin{aligned}\rho^{(1)}(\mathbf{r},\sigma;\mathbf{r}',\sigma')&=\sum_{\substack{\text{occupied}\\ \text{states}}}\varphi(\mathbf{r})\varphi(\mathbf{r}')^*\psi(\sigma)\psi(\sigma')^*\\ &=\sum_{\substack{\text{occupied}\\ \text{states}}}\varphi(\mathbf{r})\varphi(\mathbf{r}')^*\sum_{mm'}c_m c_{m'}{}^* S_{lm}(\sigma)\,S_{lm}{}^*(\sigma')\\ &=\sum_{lmm'}\rho\begin{pmatrix}lm & lm'\\ \mathbf{r} & \mathbf{r}'\end{pmatrix}S_{lm}(\sigma)\,S_{lm'}{}^*(\sigma')\end{aligned} \tag{43}$$

which, in terms of internal state quantum numbers, gives a density matrix which is diagonal in l but not diagonal in m.

Although in quantum mechanics the position and momentum of a molecule may not be given simultaneously, in discussing the behavior of a gas one speaks of the momentum distribution of the molecules at some position in space. In fact, in nonequilibrium systems, this is one of the quantities (or set of quantities) which vary from position to position. Thus, it is necessary to introduce the Wigner distribution function,[18]

$$\begin{aligned}&f_{lm;lm'}(\mathbf{r},\mathbf{p},t)\\ &=[1/(\pi\hbar)^3]\int\exp[(2i\mathbf{p}\cdot\mathbf{R})/\hbar]\rho\begin{pmatrix}lm' & lm'\\ \mathbf{r}+\mathbf{R} & \mathbf{r}-\mathbf{R}\end{pmatrix}d\mathbf{R}\S\end{aligned} \tag{44}$$

as the quantum-mechanical function most suited to describe the gas. The time dependence comes from the time dependence of ρ (not explicitly shown), and it is noted that the distribution function here defined is still a density matrix in the space of internal state quantum numbers, diagonal in l but not in general diagonal in m. From the normalization requirements of Sec. II, it follows that f is normalized so that

$$\sum_{lm}\int f_{lm;lm'}(\mathbf{r},\mathbf{p},t)d\mathbf{p}=n(\mathbf{r},t), \tag{45}$$

where $n(\mathbf{r},t)$ is the density of molecules in the gas at position $\mathbf{r}$ at time t.

When dealing with a dilute gas in nonequilibrium situations, one normally is interested in systems which are not too far removed from equilibrium. In this case, f will vary only slowly with position. To make this more explicit, it will be assumed that there is a distance a such that f is essentially constant over distances of this magnitude but may vary over distances of several a. With this in mind it is useful to introduce the "macroscopic position" vector

$$\mathbf{R}=\mathbf{n}a, \tag{46}$$

where $\mathbf{n}$ is the vector

$$\mathbf{n}=(n_x,n_y,n_z) \tag{47}$$

with n_x, n_y, n_z integers (both positive and negative). The only restriction on these integers is such that $\mathbf{R}$ must remain inside any box in which the gas might lie, e.g., if the gas is in a cubic box of volume L^3 then n_x, n_y, n_z are restricted so that

$$-(L/2a)<n_x,n_y,n_z<(L/2a). \tag{48}$$

Any position $\mathbf{r}$ then may be described as being the sum of a macroscopic position $\mathbf{R}$ and a "microscopic position" $\mathbf{r}_a$ such that

$$\mathbf{r}=\mathbf{R}+\mathbf{r}_a, \tag{49}$$

where

$$|r_{a_x}|,\quad |r_{a_y}|,\quad |r_{a_z}|<a/2. \tag{50}$$

Thus position space has been divided into cells of volume a^3 such that f is constant inside of each cell. Expressed differently, f depends on position only as a function of $\mathbf{R}$ and does not depend on $\mathbf{r}_a$.

In discussing collision problems, it is most suitable to use momentum representation. Thus the density matrix in the previous section, Eq. (35), was written in momentum representation. The relation of the density matrix in momentum representation to the Wigner distribution is the following

$$\begin{aligned}\rho\begin{pmatrix}lm & lm'\\ \mathbf{p} & \mathbf{p}'\end{pmatrix}&=\int\exp\{[i(\mathbf{p}-\mathbf{p}')\cdot\mathbf{r}]/\hbar\}f_{lm;lm'}[\mathbf{r},(\mathbf{p}+\mathbf{p}')/2,t]d\mathbf{r}\\ &=\int\exp\{[i(\mathbf{p}-\mathbf{p}')\cdot\mathbf{r}_a]\hbar\}d\mathbf{r}_a\sum_{\mathbf{R}}\exp\{[i(\mathbf{p}-\mathbf{p}')\cdot\mathbf{R}]/\hbar\}f_{lm;lm'}[\mathbf{R},(\mathbf{p}+\mathbf{p}')/2,t],\end{aligned} \tag{51}$$

§ This is the Wigner distribution function for a single molecule.

since $\mathbf{R}$ is a discrete variable. To evaluate the consequences of this expression, it is useful to introduce macroscopic and microscopic momenta, thus

$$\mathbf{p}=\mathbf{P}+[\mathbf{p}], \tag{52}$$

where

$$\mathbf{P}=\mathbf{l}(h/a) \tag{53}$$

and

$$[\mathbf{p}]=\mathbf{g}(h/L). \tag{54}$$

Here $\mathbf{l}$ and $\mathbf{g}$ are vectors whose x, y, and z components are positive or negative integers similar to $\mathbf{n}$ except that the range of $\mathbf{l}$ is from $-\infty$ to ∞ while that of $\mathbf{g}$ is restricted so that

$$|g_x|,\quad |g_y|,\quad |g_z|<L/2a. \tag{55}$$

This has the same effect in momentum space as the division of $\mathbf{r}$ had in position space, namely a dividing of momentum space into cells. Provided that L is finite, a continuum of momenta is not required; however, in practice $L\to\infty$ and $[\mathbf{p}]$ becomes a continuous variable ranging for each coordinate from $-h/a$ to h/a. As the notation suggests, each component of $[\mathbf{p}]$ is the corresponding component of $\mathbf{p}$ modulo h/a.

A simplification of Eq. (51) comes from the fact that

$$\mathbf{R}\cdot\mathbf{P}=2\pi\mathbf{n}\cdot\mathbf{l}\hbar \tag{56}$$

which follows from Eqs. (46) and (52). Now since $\mathbf{n}\cdot\mathbf{l}$ is an integer

$$\exp[(i\mathbf{P}\cdot\mathbf{R})/\hbar]=\exp(2\pi i\mathbf{n}\cdot\mathbf{l})=1, \tag{57}$$

and Eq. (51) becomes

$$\rho\begin{pmatrix} lm \\ \mathbf{p}\end{pmatrix}\begin{pmatrix} lm' \\ \mathbf{p}'\end{pmatrix}=\int \exp\{[i(\mathbf{p}-\mathbf{p}')\cdot\mathbf{r}_a]/\hbar\}d\mathbf{r}_a\sum_{\mathbf{R}}$$
$$\cdot\exp\{[i([\mathbf{p}]-[\mathbf{p}'])\cdot\mathbf{R}]/\hbar\}f_{lm;\,lm'}[\mathbf{R},\,(\mathbf{p}+\mathbf{p}')2,\,t]. \tag{58}$$

Finally, since $[\mathbf{p}]\ll\mathbf{P}$, the integrand in Eq. (58) may be approximated by replacing $\mathbf{p}$ by $\mathbf{P}$. This has the effect of uncoupling the macroscopic and microscopic motion and implies mathematically that

$$\rho\begin{pmatrix} lm \\ \mathbf{p}\end{pmatrix}\begin{pmatrix} lm' \\ \mathbf{p}'\end{pmatrix}=a^3\delta_{\mathbf{P},\mathbf{P}'}\sum_{\mathbf{R}}\exp\{\{i[\mathbf{p}]-[\mathbf{p}'])\cdot\mathbf{R}\}/\hbar\}$$
$$\cdot f_{lm;\,lm'}\{\mathbf{R},\,\mathbf{P}+\tfrac{1}{2}([\mathbf{p}]+[\mathbf{p}']),\,t\}, \tag{59}$$

where the δ function is the 3-dimensional Kronecker δ function. Eq. (59) shows that ρ, in momentum representation, is nearly diagonal in the linear momentum $\mathbf{p}$ and consequently also almost diagonal in the energy (diagonal in l and almost diagonal in kinetic energy), a fact which was used to derive Eq. (35) in the previous section.

Considering Eq. (35) to be in the $(lm\mathbf{p})$ representation, this equation for ρ may be transformed into an equation for the Wigner distribution f by using Eq. (51) and its Fourier inverse

$$f_{lm;\,lm'}(\mathbf{r},\mathbf{p},t)$$
$$=(1/h^3)\int\exp[(i\mathbf{q}\cdot\mathbf{r})/\hbar]\rho\begin{pmatrix} lm \\ \mathbf{p}+\frac{1}{2}\mathbf{q}\end{pmatrix}\begin{pmatrix} lm' \\ \mathbf{p}-\frac{1}{2}\mathbf{q}\end{pmatrix}d\mathbf{q}. \tag{60}$$

In this integral and subsequent integrals over the momenta, the momenta will be considered as continuous variables in spite of Eqs. (52–54); this corresponds to the limit $L\to\infty$. Thus Eq. (35) becomes

$$\frac{\partial f_{lm;\,lm'}(\mathbf{r},\mathbf{p},t)}{\partial t}+\frac{\mathbf{p}}{m_l}\cdot\frac{\partial f_{lm;\,lm'}(\mathbf{r},\mathbf{p},t)}{\partial\mathbf{r}}\equiv\frac{\partial_c f_{lm;\,lm'}(\mathbf{r},\mathbf{p},t)}{\partial t}$$

$$=\frac{2\pi}{h^3\hbar}\sum_{L\,L_1\,l_1m_1;\,nn'n_1n_1'}\int\cdots\int\exp[(i\mathbf{q}\cdot\mathbf{r})/\hbar]\exp\{[-i(\mathbf{p}'-\mathbf{n})\cdot\mathbf{r}']/\hbar\}\exp\{[-i(\mathbf{p}_1'-\mathbf{n}')\cdot\mathbf{r}_1]/\hbar\}$$
$$\cdot\left\langle\begin{matrix} lm & l_1m_1 \\ \mathbf{p}+\frac{1}{2}\mathbf{q} & \mathbf{p}_1\end{matrix}\middle|\,t\,\middle|\begin{matrix} Ln & L_1n_1 \\ \mathbf{p}' & \mathbf{p}_1'\end{matrix}\right\rangle f_{Ln;\,Ln'}[\mathbf{r}',\tfrac{1}{2}(\mathbf{p}'+\mathbf{n}),t]f_{L_1n_1;\,L_1n_1'}[\mathbf{r}_1,\tfrac{1}{2}(\mathbf{p}_1'+\mathbf{n}'),t]$$
$$\cdot\left\langle\begin{matrix} Ln' & L_1n_1' \\ \mathbf{n} & \mathbf{n}'\end{matrix}\middle|\,t^*\delta(E)\,\middle|\begin{matrix} lm' & l_1m_1 \\ \mathbf{p}-\frac{1}{2}\mathbf{q} & \mathbf{p}_1\end{matrix}\right\rangle d\mathbf{q}d\mathbf{p}'d\mathbf{p}_1d\mathbf{p}_1'd\mathbf{n}d\mathbf{n}'d\mathbf{r}'d\mathbf{r}_1 \tag{61}$$
$$+\frac{1}{h^3i\hbar}\sum_{l_1m_1n_1n}\int\cdots\int\exp[(i\mathbf{q}\cdot\mathbf{r})/\hbar]\Big[\exp\{[-i(\mathbf{p}'-\mathbf{p}+\tfrac{1}{2}\mathbf{q})\cdot\mathbf{r}']/\hbar\}\exp\{[-i(\mathbf{p}_1'-\mathbf{p}_1)\cdot\mathbf{r}_1]/\hbar\}$$
$$\cdot\left\langle\begin{matrix} lm & l_1m_1 \\ \mathbf{p}+\frac{1}{2}\mathbf{q} & \mathbf{p}_1\end{matrix}\middle|\,t\,\middle|\begin{matrix} ln & l_1n_1 \\ \mathbf{p}' & \mathbf{p}_1'\end{matrix}\right\rangle f_{ln;\,lm'}[\mathbf{r}',\tfrac{1}{2}(\mathbf{p}'+\mathbf{p}-\tfrac{1}{2}\mathbf{q}),t]f_{l_1n_1;\,l_1m_1}[\mathbf{r}_1,\tfrac{1}{2}(\mathbf{p}_1'+\mathbf{p}_1),t]$$
$$-\exp\{-i(\mathbf{p}-\mathbf{p}'+\tfrac{1}{2}\mathbf{q})\cdot\mathbf{r}']/\hbar\}\exp[-i(\mathbf{p}_1-\mathbf{p}_1')\cdot\mathbf{r}_1/\hbar]f_{lm;\,ln}[\mathbf{r}',\tfrac{1}{2}(\mathbf{p}+\mathbf{p}'+\tfrac{1}{2}\mathbf{q}),t]f_{l_1m_1;\,l_1n_1}[\mathbf{r},\tfrac{1}{2}(\mathbf{p}_1+\mathbf{p}_1'),t]$$
$$\cdot\left\langle\begin{matrix} ln & l_1n_1 \\ \mathbf{p}' & \mathbf{p}_1'\end{matrix}\middle|\,t^*\,\middle|\begin{matrix} lm' & l_1m_1 \\ \mathbf{p}-\frac{1}{2}\mathbf{q} & \mathbf{p}_1\end{matrix}\right\rangle\Big]d\mathbf{q}d\mathbf{p}'d\mathbf{p}_1d\mathbf{p}_1'd\mathbf{r}'d\mathbf{r}_1$$

where the $t^*\delta(E)$ matrix element is to be interpreted as the t^* matrix element times a δ function of the energy between the same states. This equation has been written as an equation for the collisional rate of change $(\partial_c/\partial t)$ of f which is the total time rate of change of f minus the flux change of f due to the motion of the molecules [m_l is the mass of a molecule in the lth state (possibly a different molecular species)]. Equation (61) bears some resemblance to the Boltzmann equation, but differs among other things in that the f's in the Boltzmann equation are evaluated at the same position variable $\mathbf{r}$. This fact arises also in this case from considerations similar to those resulting in Eq. (59), as will be shown now.

The t matrix describes the results of a collision process. However, the collision proper does not depend on the motion of the center of gravity of the colliding molecules and this results in the conservation of the total momentum of the molecules during the collision. A consequence is that the t matrix may be written in the special form

$$\left\langle \begin{matrix} lm & l_1m_1 \\ \mathbf{p} & \mathbf{p}_1 \end{matrix} \middle| t \middle| \begin{matrix} Ln & L_1n_1 \\ \mathbf{p}' & \mathbf{p}_1' \end{matrix} \right\rangle = \left\langle \begin{matrix} lm & l_1m_1 \\ (\mathbf{p},\mathbf{p}_1) & \end{matrix} \middle| t \middle| \begin{matrix} Ln & L_1n_1 \\ (\mathbf{p}',\mathbf{p}_1') & \end{matrix} \right\rangle \delta(\mathbf{p}'+\mathbf{p}_1'-\mathbf{p}-\mathbf{p}_1) \quad (62)$$

which indicates explicitly that the total momentum is conserved and that t depends only on the relative momenta of the molecules; thus,

$$(\mathbf{p},\mathbf{p}_1)=(m_l\mathbf{p}_1-m_{l_1}\mathbf{p})/(m_l+m_{l_1}) \quad (63)$$

is the relative momentum of a molecule of species l_1 with momentum $\mathbf{p}_1$ with respect to a molecule of species l with momentum $\mathbf{p}$.

The right-hand terms of Eq. (61) may now be simplified with the use of Eq. (62) and the fact that f depends only on $\mathbf{R}$ rather than $\mathbf{r}$. This latter fact allows the integration over $\mathbf{r}_a'$ and $\mathbf{r}_{1a}$ to be performed immediately. Thus the first term on the right side of Eq. (61) becomes

$$\frac{a^6}{\hbar^3}\frac{2\pi}{\hbar}\sum_{LL_1l_1m_1;nn'n_1n_1'}\sum_{\mathbf{R}_1\mathbf{R}'}\int\cdots\int \exp\{(i[\mathbf{q}]\cdot\mathbf{r})/\hbar\}\exp\{\{-i([\mathbf{p}']-[\mathbf{n}])\cdot\mathbf{R}'\}/\hbar\}\exp\{\{-i([\mathbf{q}]-[\mathbf{p}']+[\mathbf{n}])\cdot\mathbf{R}_1\}/\hbar\}$$

$$\cdot\left\langle \begin{matrix} l_m & l_1m_1 \\ (\mathbf{p}+\frac{1}{2}[\mathbf{q}], & \mathbf{p}_1) \end{matrix} \middle| t \middle| \begin{matrix} Ln & L_1n_1 \\ (\mathbf{p}', & \mathbf{p}+\mathbf{p}_1-\mathbf{p}'-\frac{1}{2}\mathbf{q}) \end{matrix} \right\rangle f_{Ln;\,Ln'}\{\mathbf{R}',\mathbf{p}'+\tfrac{1}{2}([\mathbf{n}]-[\mathbf{p}']),t\} \quad (64)$$

$$\cdot f_{L_1n_1;\,L_1n_1'}\{\mathbf{R}_1,\mathbf{p}+\mathbf{p}_1-\mathbf{p}'+\tfrac{1}{2}([\mathbf{p}']-[\mathbf{n}]),t\}\left\langle \begin{matrix} Ln' & L_1n_1' \\ (\mathbf{P}'+[\mathbf{n}], & \mathbf{p}+\mathbf{p}_1-\frac{1}{2}[\mathbf{q}]-\mathbf{P}'-[\mathbf{n}]) \end{matrix} \middle| t^*\delta(E) \middle| \begin{matrix} lm' & l_1m_1 \\ (\mathbf{p}-\frac{1}{2}[\mathbf{q}], & \mathbf{p}_1) \end{matrix} \right\rangle$$

$$d[\mathbf{q}]d\mathbf{p}'d[\mathbf{n}]d\mathbf{p}_1,$$

where, as in the derivation of Eq. (59), terms of the order $[\mathbf{p}]\cdot\mathbf{r}_a'$ have been neglected so that the integration over the microscopic positions $\mathbf{r}_a'$ and $\mathbf{r}_{1a}$ have yielded Kronecker δ functions of the form

$$\int \exp[i(\mathbf{P}-\mathbf{P}')\cdot\mathbf{r}_a/\hbar]d\mathbf{r}_a=a^3\delta_{\mathbf{P},\mathbf{P}'}. \quad (65)$$

Consequently the macroscopic part of $\mathbf{n}$ is equal to $\mathbf{P}'$, while the macroscopic part of $\mathbf{q}$ is zero.

Since $[\mathbf{q}]$ is a small momentum compared to $\mathbf{p}$, and if the t matrix elements are assumed to remain constant over ranges of the momenta of the order of $\hbar/a$ (a criterion associated with this is that the intermolecular potential has a range much smaller than a), then $[\mathbf{q}]$ may be neglected in the t matrix elements. Since $[\mathbf{q}]\cdot\mathbf{r}\simeq[\mathbf{q}]\cdot\mathbf{R}$, the term [Eq. (64)] is independent of $\mathbf{r}_a$ and the integration over $[\mathbf{q}]$ may be carried out, thus

$$\int \exp\{\{i[\mathbf{q}]\cdot(\mathbf{R}-\mathbf{R}_1)\}/\hbar\}d[\mathbf{q}]=(h/a)^3\delta_{\mathbf{R},\mathbf{R}_1}. \quad (66)$$

Lastly, a further simplification is obtained by a notational change, namely replacing $\mathbf{p}'$ by $\mathbf{p}'+\frac{1}{2}([\mathbf{n}']-[\mathbf{p}'])$. This change, together with the previously mentioned constancy of the t matrix elements, allows the integration over $[\mathbf{n}]$ to be performed yielding the final result for term [Eq. (64)],

$$h^3(2\pi/\hbar)\sum_{LL_1l_1m_1;nn'n_1n_1'}\iint\left\langle \begin{matrix} lm & l_1m_1 \\ (\mathbf{p}, & \mathbf{p}_1) \end{matrix} \middle| t \middle| \begin{matrix} Ln & L_1n_1 \\ (\mathbf{p}', & \mathbf{p}+\mathbf{p}_1-\mathbf{p}') \end{matrix} \right\rangle f_{Ln;\,Ln'}(\mathbf{r},\mathbf{p}',t)$$

$$\cdot f_{L_1n_1;\,L_1n_1'}(\mathbf{r},\mathbf{p}+\mathbf{p}_1-\mathbf{p}',t)\left\langle \begin{matrix} Ln'L_1n_1' \\ (\mathbf{p}', & \mathbf{p}+\mathbf{p}_1-\mathbf{p}') \end{matrix} \middle| t^*\delta(E) \middle| \begin{matrix} lm'l_1m_1 \\ (\mathbf{p}, & \mathbf{p}_1) \end{matrix} \right\rangle d\mathbf{p}_1d\mathbf{p}', \quad (67)$$

where $\mathbf{r}$ has been written for $\mathbf{R}$, a macroscopic position being implied.

By similar arguments, the second term on the right side of Eq. (61) may be simplified so that the modified Boltzmann equation for the Wigner distribution function is

$$\frac{\partial f_{lm;\,lm'}(\mathbf{r},\mathbf{p},t)}{\partial t}+\frac{\mathbf{p}}{m_l}\cdot\frac{\partial f_{lm;\,lm'}(\mathbf{r},\mathbf{p},t)}{\partial \mathbf{r}}$$

$$=(2\pi h^3/\hbar)\sum_{LL_1l_1m_1;nn'n_1n_1'}\iint\left\langle\begin{matrix}lm & l_1m_1\\(\mathbf{p},\mathbf{p}_1)\end{matrix}\right|t\left|\begin{matrix}Ln & L_1n_1\\(\mathbf{p}',\mathbf{p}+\mathbf{p}_1-\mathbf{p}')\end{matrix}\right\rangle f_{Ln;\,Ln'}(\mathbf{r},\mathbf{p}',t)$$

$$\cdot f_{L_1n_1;\,L_1n_1'}(\mathbf{r},\mathbf{p}+\mathbf{p}_1-\mathbf{p}',t)\left\langle\begin{matrix}Ln' & L_1n_1'\\(\mathbf{p}',\mathbf{p}+\mathbf{p}_1-\mathbf{p}')\end{matrix}\right|t^*\delta(E)\left|\begin{matrix}lm' & l_1m_1\\(\mathbf{p},\mathbf{p}_1)\end{matrix}\right\rangle d\mathbf{p}_1d\mathbf{p}'$$

$$+(h^3/i\hbar)\sum_{lm_1n_1n'}\int\left[\left\langle\begin{matrix}lm & l_1m_1\\(\mathbf{p},\mathbf{p}_1)\end{matrix}\right|t\left|\begin{matrix}ln & l_1n_1\\(\mathbf{p},\mathbf{p}_1)\end{matrix}\right\rangle f_{ln;\,lm'}(\mathbf{r},\mathbf{p},t)f_{l_1n_1;\,l_1m_1}(\mathbf{r},\mathbf{p}_1,t)\right.$$

$$\left.-f_{lm;\,ln}(\mathbf{r},\mathbf{p},t)f_{l_1m_1;\,l_1n_1}(\mathbf{r},\mathbf{p}_1,t)\left\langle\begin{matrix}ln & l_1n_1\\(\mathbf{p},\mathbf{p}_1)\end{matrix}\right|t^*\left|\begin{matrix}lm' & l_1m_1\\(\mathbf{p},\mathbf{p}_1)\end{matrix}\right\rangle\right]d\mathbf{p}_1, \tag{68}$$

where in the last term it is also necessary to assume that f is not sensitive to changes in momentum of the order of h/a.

The physical interpretation of the two terms on the right side of Eq. (68) is that the first is the number of molecules which, due to a collision, end in a state contributing to $f_{lm;\,lm'}(\mathbf{r},\mathbf{p},t)$; the second term is the number of molecules which are removed by collisions from states contributing to $f_{lm;\,lm'}(\mathbf{r},\mathbf{p},t)$. This is emphasized by analogy to the special case when f is diagonal in the internal states, i.e., there are no m indices. Then Eq. (68) reduces to the usual quantum-mechanical Boltzmann equation, namely

$$\frac{\partial f_l(\mathbf{r},\mathbf{p},t)}{\partial t}+\frac{\mathbf{p}}{m_l}\cdot\frac{\partial f_l(\mathbf{r},\mathbf{p},t)}{\partial \mathbf{r}}=\sum_{LL_1l_1}\iiint[f_L(\mathbf{r},\mathbf{p}',t)f_{L_1}(\mathbf{r},\mathbf{p}_1',t)-f_l(\mathbf{r},\mathbf{p},t)f_{l_1}(\mathbf{r},\mathbf{p}_1,t)]$$

$$\cdot(k_{LL_1}/\mu_{ll_1}k_{ll_1})\sigma(LL_1(\mathbf{p}',\mathbf{p}_1')\rightarrow ll_1(\mathbf{p},\mathbf{p}_1))\delta(E_{ll_1}-E_{LL_1})\delta(\mathbf{p}'+\mathbf{p}_1'-\mathbf{p}-\mathbf{p}_1)d\mathbf{p}'d\mathbf{p}_1d\mathbf{p}_1', \tag{69}$$

where Eq. (33) has been used for the cross section, and the energy E_{LL_1} denotes the total energy of the pair of molecules, one in state L with momentum $\mathbf{p}'$, the other in state L_1 with momentum $\mathbf{p}_1'$ and similarly for E_{ll_1}. Moreover, the fact that

$$k_{ll_1}{}^2\sigma(ll_1(\mathbf{p},\mathbf{p}_1)\rightarrow LL_1(\mathbf{p}',\mathbf{p}_1'))$$

$$=k_{LL_1}{}^2\sigma(LL_1(\mathbf{p}',\mathbf{p}_1')\rightarrow ll_1(\mathbf{p},\mathbf{p}_1)) \tag{70}$$

has been used to group the right-hand terms in this manner. Eq. (70) follows from symmetry arguments of nondegenerate states.[29] Lastly, it should be remarked that f is a Wigner distribution function in position-momentum space and not in position-velocity space so that care should be exercised when comparing Eq. (69) with other notations.

V. SUMMARY

A modified Boltzmann equation has been derived for the Wigner distribution function for the general case in which molecules have degenerate internal states. This is Eq. (68). The usual quantum-mechanical Boltzmann equation is obtained as a special case [Eq. (69)]. The approximations and assumptions involved in the derivation of Eq. (68) are summarized as follows.

Besides the usual very good assumption that the potential of interaction in a gas is the sum of the pairs of interaction between molecules, the first main assumption that is made is that the Boltzmann property, Eq. (3), holds almost everywhere. This may be justified physically by restricting the gas to be dilute, that is, the density of the gas should be low enough so that each molecule essentially is independent of every other molecule in the gas. Further, it has been shown[23,24] that this property is consistent with the classical Boltzmann equation and so may be assumed reasonably to be true here also. The restriction to dilute gases is also the justification for using the binary collision approximation to simplify Eq. (7) to Eq. (9).

The binary collision problem is solved then by the aid of the formal scattering theory of Lippmann and Schwinger in Sec. III where neglect of the difference between $\rho^{(1)}(1_{t-t_0};t)$ and $\rho^{(1)}(1;t)$ is discussed quite fully. This results in Eq. (34). In order to proceed further, another assumption must be made. This is that the density matrix $\rho^{(1)}$ is approximately diagonal in the energy, physical arguments being introduced in

[29] See, e.g., R. G. Sachs, *Nuclear Theory* (Addison-Wesley Publishing Company, Inc., Reading, Massachusetts, 1953), p. 289.

Sec. IV [Eq. (59)] that this should be so. Note that this property of $\rho^{(1)}$ is assumed on both sides of Eq. (34). The physical argument for this property of $\rho^{(1)}$ first of all states that $\rho^{(1)}$ is diagonal in internal state energy and, secondly, is approximately diagonal in linear momentum because of the assumed near homogeneity of the gas. This latter is considered as one of the usual restrictive conditions of applicability of the Boltzmann equation. Furthermore, it is shown in the derivation of Eq. (68) that this property is reproduced by Eq. (61). That is, by assuming the property for the Wigner distribution function f on the right side of Eq. (61), this equation implies that f on the left side also is nearly spatially homogeneous. This is the same type of argument that has been used to prove the consistency of the Boltzmann property.

A possible alternative to the physical arguments just given, is to time average Eq. (34) in much the same way as Kirkwood[5] does, this giving an approximate energy diagonalization. If the time T over which the averaging is done is of the magnitude

$$T \simeq 2\mu a^2/\hbar, \tag{71}$$

where μ is the reduced mass, and a is the cell size of Sec. IV, then $\rho^{(1)}$ could still be nondiagonal in [p] [Eqs. (54–55)] without inconsistencies. With the reproducibility of the slow position dependence of f (approximate linear momentum diagonality of $\rho^{(1)}$), this would necessitate an approximate internal energy diagonalization. Consequently, if the internal energy states are further apart than this limit, then internal energy diagonalization also will be reproducible.

Lastly, the derivation of Eq. (68) involves the assumption that the matrix elements of the Lippmann-Schwinger t matrix are insensitive to momentum differences of the magnitude of $\hbar/a$. This is reasonable physically, provided that a (the cell size of Sec. IV) is large in comparison to the range of the intermolecular potential. Moreover, it is necessary to neglect momentum differences of the order of $\hbar/a$ in the Wigner distribution at one point in the derivation.

ACKNOWLEDGMENTS

The author would like to acknowledge the financial support of the National Research Council of Canada during the course of this research. Thanks are also due to Dr. Opechowski of the Physics Department of the University of British Columbia for several interesting discussions on this paper and to Dr. McDowell of the Chemistry Department for comments on the manuscript.

Forbidden Band Systems in Nitrogen. III. The $Y\ ^3\Sigma_u^- \leftarrow X\ ^1\Sigma_g^+$ System in Absorption*

P. G. WILKINSON

Laboratory of Molecular Structure and Spectra, Department of Physics, The University of Chicago, Chicago 37, Illinois

(Received October 9, 1959)

Four bands of the $Y\ ^3\Sigma_u^- \leftarrow X\ ^1\Sigma_g^+$ system of nitrogen have been observed in absorption in a path of 3.4 meter-atmospheres at 1518 A (0–0), 1484 A (1–0), 1453 A (2–0) and 1423 A (3–0). These bands consist of an unresolved Q branch (^QQ, ^QP, ^QR), and ^SR and ^OP branches.

From a comparison of the experimental and calculated intensity distribution, it is shown that the upper state is $^3\Sigma_u^-$ rather than the alternative assignment of $^3\Delta_u$.

It is further shown that the $Y\ ^3\Sigma_u^-$ state is identical with the upper state of certain infrared bands recently found in the active nitrogen afterglow. Those bands are thereby identified as $Y\ ^3\Sigma_u^- \rightarrow B\ ^3\Pi_g$. The upper state was designated "Y" by Kistiakowsky and Warneck.

The constants of $Y\ ^3\Sigma_u^-$ as obtained here are: $\omega_e = 1517.6_9$ cm^{-1}; $\omega_e x_e = 12.2_2$ cm^{-1}; $B_e = 1.472$ cm^{-1}; $\alpha_e = 0.016_1$ cm^{-1}; $T_{00} = 65850.6$ cm^{-1}; $r_e = 1.278_8$ A.

The transition $Y\ ^3\Sigma_u^- \leftarrow X\ ^1\Sigma_g^+$ receives intensity from perturbations of $Y\ ^3\Sigma_u^-$ by $^1\Sigma_u^+$ and $^1\Pi_u$ states lying at higher energies.

I. INTRODUCTION

THE following forbidden band systems of nitrogen have now been observed:[1] the Vegard-Kaplan bands ($A\ ^3\Sigma_u^+ - X\ ^1\Sigma_g^+$); the Lyman-Birge-Hopfield bands ($a\ ^1\Pi_g - X\ ^1\Sigma_g^+$); the $C\ ^3\Pi_u - X\ ^1\Sigma_g^+$ system; the $a'\ ^1\Sigma_u^- - X\ ^1\Sigma_g^-$ system; and the new system reported here, $Y\ ^3\Sigma_u^- - X\ ^1\Sigma_g^+$. All have been obtained in absorption, and most of them (some very recently) in emission.[2] The $^3\Sigma_u^-$ state is here identified with the upper state of a system observed in the nitrogen afterglow, $Y\ ^3\Sigma_u^- \rightarrow B\ ^3\Pi_g$ ("Y" bands.[3,4] Very recently the 5—1 band of the $Y-B$ system has been observed under high resolution,[5] and a rotational analysis obtained. In the present work the 0—0, 1—0, 2—0, and and 3–0 bands of $Y-X$ were observed in absorption under high resolution; a discussion of these bands follows.

II. EXPERIMENTAL

The instrument used was a 21-ft vacuum spectrograph; the spectra were obtained in the fourth order of the grating employing a krypton light source as the absorption background. Nitrogen was flowed through the spectrograph during the exposure at pressures of 130 and 300 mm. Further experimental details are contained in a previous paper.[1]

The observed lines are unusually broadened. This was first thought to be pressure broadening; it was later found that it was partly instrumental in origin. When the instrument is completely evacuated, considerable strain is induced in various components; when gas is introduced, a partial relief of strain occurs which causes a shift of the spectral lines by about 10–15 μ. This shift is not instantaneous, but takes place slowly; the result is an increased line width when spectra are taken during the shift. The exact source of the mechanical movement is at present unknown; if it can be located and corrected, improved photographs will be possible. However, it is thought that the present data are of sufficient interest to report.

The absorption lines are measured on a Gaertner comparator equipped with a photometric setting device[6] at the Argonne National Laboratory. The absolute accuracy of the wavelength measurement is estimated to be ± 0.003 A (equivalent to ± 0.15 mm^{-1}); the relative accuracy is ± 0.0003 A (equivalent to ± 0.015 cm^{-1}) on single lines of medium intensity.

III. RESULTS

(A) General

The 1–0 band at 1484 A is the only one which is well developed and not overlapped by stronger band systems. The others are either badly overlapped or are very weak or both. A microphotometer tracing of the 1–0 band is shown in Fig. 1.

The observed wave numbers of all the bands, along with the rotational assignment and intensities (in parentheses) are given in Table I.

Two electronic states of electron configuration $\pi_u^3 \sigma_g\ ^2\pi_g$ are expected to lie near 70 000 cm^{-1}. These are $^3\Sigma_u^-$ and $^3\Delta_u$.[7] Under low resolution, the transitions $^3\Sigma_u^- - {}^1\Sigma_g^+$ and $^3\Delta_u - {}^1\Sigma_g^+$ might be expected to look somewhat alike; the former would consist of five branches and the latter, nine branches.

* This work was assisted by the Geophysics Research Directorate of the Air Force Cambridge Research Center, Air Research and Development Command under Contract AF19(604)-3478 with the University of Chicago.

[1] A literature survey is given in a previous paper. See P. G. Wilkinson and R. S. Mulliken, J. Chem. Phys. 31, 674 (1959).

[2] M. Ogawa and Y. Tanaka, J. Chem. Phys. (to be published).

[3] Le Blanc, Tanaka, and Jursa, J. Chem. Phys. 28, 979 (1958).

[4] K. D. Bayes and G. B. Kistiakowsky, J. Chem. Phys. 29, 949 (1958).

[5] P. K. Carroll and H. E. Rubalcava, Nature 184, 119 (1959).

[6] M. Fred and F. S. Tomkins, J. Opt. Soc. Am. 41, 641 (1951).

[7] R. S. Mulliken, *The Threshold of Space* (Pergamon Press, New York, 1957), p. 169.

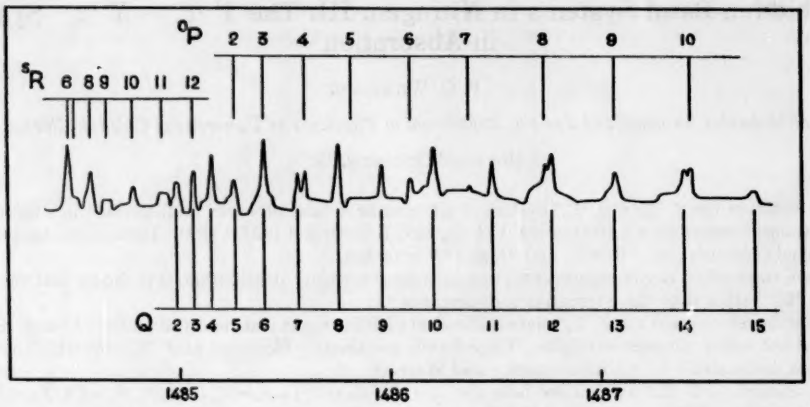

FIG. 1. Microphotometer tracing of the 1–0 absorption band of the $Y\,^3\Sigma_u^- \leftarrow X\,^1\Sigma_g^+$ transition.

TABLE I. Wave numbers in the $Y\,^3\Sigma_u^- \leftarrow X\,^1\Sigma_g^+$ system.

1–0 Band

J	Q(obs.)	Q(calc.)[b]	^{S}R(obs.)	^{S}R(calc.)[c]
2	67340.62(11)	67340.72		
3	337.27(15)[a]	337.49		
4	332.98(22)	333.15	67364.74(7)[a]	67365.02
5	327.77(11)	327.72	364.66(6)[a]	365.40
6	321.21(28)[a]	321.21	364.14(9)[a]	364.68
7	313.61(14)[a]	313.62	362.49(5)	362.87
8	304.86(26)	304.91	359.40(15)	359.99
9	295.02(18)	295.17	355.45(4)	356.01
10	284.33(19)	284.31	350.45(9)	350.95
11	272.43(16)	272.38	343.91(3)	344.81
12	259.42(17)	259.36	337.27(15)[a]	337.58
13	245.27(12)[a]	245.25		
14	230.10(14)	230.05		
15	214.26(5)	213.78		
16	196.40(10)	196.41		

J	^{O}P (obs.)	^{O}P (calc.)[d]
2	67327.27(8)[a]	67332.06
3	321.21(6)[a]	323.02
4	312.01(10)	312.89
5		
6	288.73(12)	289.37
7	277.03(9)	275.98
8	260.70(16)	261.51
9	245.27(13)[a]	245.96
10	228.94(15)	229.32

2–O band

J	$Q(J)$	$^{S}R(J)$	$^{O}P(J)$
2		68829.3(6)[a]	
3		831.4(58)[a]	68789.8(150)[a]
4		834.0(90)	780.9(49)[a]
5		833.1(78)	768.6(45)
6	68789.8(150)[a]	831.4(58)[a]	757.0(100)
7	780.9(49)[a]	829.3(6)[a]	728.8(17)
8	772.3(45)		713.0(19)
9	762.0(123)[a]		695.9(30)[a]
10	751.1(53)		678.5(25)[a]
11		809.4(20)	659.1(20)[a]
12	727.5(25)		
13	710.7(17)		
14	695.9(30)[a]	783.4(65)	
15	678.5(25)[a]	773.8(88)	
16	659.1(20)[a]	762.0(123)[a]	
17		747.0(44)	
18		732.9(24)	

3–O band

J	$Q(J)$	$^{S}R(J)$	$^{O}P(J)$
0		70264.52(27)[a]	
1	70256.21(35)	269.23(62)[a]	
2	253.50(103)	272.72(51)[a]	
3	251.23(38)[a]	274.82(72)[a]	70236.26(15)
4	245.56(62)	276.19(47)	225.22(73)[a]
5	239.92(43)	277.33(62)	215.80(60)[a]
6	233.01(66)[a]	274.82(72)	201.42(32)
7	225.22(73)[a]	272.71(51)	187.65(19)
8	215.80(60)[a]	269.23(62)	172.90(34)
9	205.56(40)	264.52(27)[a]	156.93(21)
10	194.01(60)	258.47(38)[a]	139.86(33)
11	181.42(35)	251.23(38)[a]	122.10(28)
12	167.59(51)	243.86(27)	
13	152.82(33)	233.01(66)[a]	
14	136.59(39)	228.61(30)	
15	119.79(22)		
16		214.22(19)	

[a] Blended line.

[b] $Q(J)=67344.00-0.5426J(J+1)$.

[c] $^{S}R(J)=67352.70+5.2512J-0.5426J^2$.

The calculated wave numbers for the ^{S}R and ^{O}P branches are all larger than the observed wave numbers because the rotational constants were obtained from the blended Q branch.

[d] $^{O}P(J)=67346.89-0.6331J-0.5426J^2$.

(B) Rotational Analysis

The F_1, F_2, and F_3 sublevels of a $^3\Sigma$ or $^3\Delta$ (case b) state correspond to $J=N+1$, N, $N-1$; for small N, the F_1 and F_3 levels lie close together and considerably below F_2. According to Schlapp,[8] only the F_2 levels of a $^3\Sigma$ state and only the mean of the three levels of a $^3\Delta$ state obey the standard simple formula,

$$F(J)=BJ(J+1)-DJ^2(J+1)^2. \quad (1)$$

In a $^3\Sigma-{}^1\Sigma$ transition, only the ^QQ branch involves F_2. Because of the excessive instrumental broadening, the triplet splitting was not observed, and the three branches ^QQ, ^QP, and ^QR were blended into one (hereafter referred to as Q). The rotational analysis was carried out using this blended Q branch as follows. The even and odd numbered lines could be readily identified from the intensity alternation, since the strong lines in each branch are blended as are also the weak lines (Fig. 1), and a preliminary assignment of the quantum numbering was made. This numbering was varied by units of two, until a plot of $Q(J)$ against $J(J+1)$ gave a straight line. A preliminary value of ν_0 was obtained by extrapolating to $J(J+1)=0$. From the accurately known rotational constants of $X\,{}^1\Sigma_g^+$,[9,10] the following function was calculated:

$$B_v'(J)-D_v'J(J+1)=[Q(J)-\nu_0+B_0''J(J+1) -D_0''J^2(J+1)^2]/J(J+1). \quad (2)$$

The resulting function was then plotted against $J(J+1)$; the intercept gave B_v' and the slope, D_v'. A more precise value of ν_0 was then obtained by plotting $Q(J)+(B_v'-B_0'')J(J+1)$ against $J(J+1)$. The function (2) was then recalculated to obtain the final value of B_v'. The resulting rotational constants, band origins, and ΔG values are given in Table II. These B_v' values are not the accurate constants of the $F_2(J)$ levels, but are slightly in error due to blends of ^QQ with ^QP and ^QR. However, they are sufficiently precise to permit identification of the lines in the ^OP and ^SR branches. Since ^OP involves only F_1 levels, and ^SR only F_3 levels, the calculated and observed wave numbers of ^OP and ^SR do not agree exactly but show a small defect. From this defect one can estimate that the separation between ^QQ and $^QP+{}^QR$ (F_2 and F_1, F_3) is about 1.2 cm^{-1}; this is approximately equal to $\lambda+\frac{1}{2}\gamma$.[11]

(C) Rotational Intensity Distribution

The intensity distribution to be expected in an absorption band may be expressed:

$$I_{abs}=\nu K(\tfrac{1}{2})^n S_J \exp-[B_0''J(J+1)hc/kT] \quad (3)$$

where ν is the frequency of the transition and is essentially constant during a transition, K is a constant, and n is 0 or 1 for even and odd J, respectively. In the present case, $B_0''=1.9898$ cm^{-1}, and $T=300°$K; S_J has been calculated by Schlapp[12] for both $^3\Sigma^-{}-{}^1\Sigma$ and $^3\Delta-{}^1\Sigma$ transitions as follows:

(1). $^3\Sigma^-{}-{}^1\Sigma^+$

Branch	S_J
^QQ	$2A^2(2J+1)$
^QR	$[2A^2(J+1)^2+B^2J^2]/(2J+1)$
^QP	$[2A^2J^2+B^2(J+1)^2]/(2J+1)$
^SR	$[2A^2+B^2]J(J+1)/(2J+1)$
^OP	$[2A^2+B^2]J(J+1)/(2J+1)$ (4)

where A and B are constants related to the interaction of $^3\Sigma^-$ with $^1\Pi$, and $^1\Sigma^+$ states, respectively.

(2). $^3\Delta$ (case b)$-{}^1\Sigma^+$

Branch	S_J
^SR	$(J+2)(J+3)/(2J+1)$
^RQ	$(J+2)(J+3)/J$
^QP	$(J+1)(J+2)(J+3)/J(2J+1)$
^RR	$(J-2)(J+3)/(J+1)$
^QQ	$(J-2)(J+3)(2J+1)/J(J+1)$
^PP	$(J-2)(J+3)/J$
^QR	$J(J-1)(J-2)/(J+1)(2J+1)$
^PQ	$(J-1)(J-2)/(J+1)$
^QP	$(J-2)(J-2)/(2J+1)$ (5)

If we choose $B^2=8A^2$, the theoretical intensity distribution in a $^3\Sigma^-{}-{}^1\Sigma^+$ transition may be computed and this is shown graphically in Fig. 2 for even J. The intensities of ^QQ, ^QP, and ^QR are very nearly equal, and these have been added to obtain the curve for Q in the figure.

TABLE II. Band origins, rotational constants and ΔG values of the $Y\,{}^3\Sigma_u^-\leftarrow X\,{}^1\Sigma_g^+$ system (cm^{-1}).

v'	B_v'	ν_0	$\Delta G_{v'+\frac{1}{2}}$	ν_{QH}[a]
0		65850.6[c]		65850.4
			1493.2	
1	1.448$_2$	67343.85		67344.1
			1468.6	
2	1.432	68812.5		68815.8
			1444.6	
3	1.416	70257.1		70265.5
5	1.381[b]			

[a] M. Ogawa and Y. Tanaka, J. Chem. Phys. (to be published). The wave number given is that of the Q head.
[b] Private communication from Dr. P. K. Carroll.
[c] Calculated from the Q head.

[8] R. Schlapp, Phys. Rev. **51**, 342 (1937).
[9] B. P. Stoicheff, Can. J. Phys. **32**, 630 (1954).
[10] P. G. Wilkinson, Astrophys. J. **126**, 1 (1957).
[11] G. Herzberg, *Spectra of Diatomic Molecules* (D. Van Nostrand Company, Inc., Princeton, New Jersey, 1950), p. 223.
[12] R. Schlapp, Phys. Rev. **39**, 806 (1932).

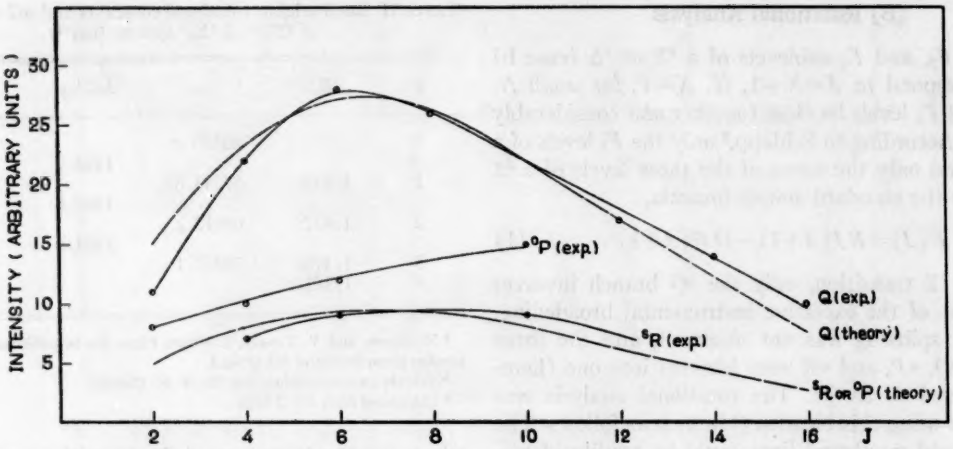

FIG. 2. A comparison of the theoretical intensity distribution (dashed curve) with the approximate experimental intensity distribution (solid curve) in the 1−0 band of the $Y\,{}^3\Sigma_u^- \rightarrow X\,{}^1\Sigma_g^+$ system.

From the formula for S_J (Eq. 4), the intensity distribution should be the same for both ${}^sR$ and ${}^oP$ branches. The experimental intensities were obtained only roughly from microphotometer traces, and these are also shown in Fig. 2. If the experimental and theoretical curves for Q are adjusted to match at the peak intensity ($J=7$), the experimental and theoretical intensities are in rough agreement for ${}^sR$ and ${}^oP$. A relation greatly different from $B^2=8A^2$ (such as $B^2=2A^2$) produces a quite different intensity distribution. It is to be noted that in the analogous bands of CO,[13] $e\,{}^3\Sigma^- - X\,{}^1\Sigma^+$, $B^2=2A^2$ (See also Sec. D).

For a ${}^3\Delta_u$ (case a) $-{}^1\Sigma_g^+$ transition, only simple P, R and Q branches would be observed. Since P and R branches have not been found, we need only consider case b. From Eqs. (3) and (5), the intensity distribution in each of the nine branches may be computed. It was found that the ${}^oP$ branch would be extremely weak (about 7% of the Q branch), and would probably be unobservable; the ${}^sQ$ branch would be very strong (even stronger than the Q at low J). The ${}^sR$ branch would be intermediate in intensity (about 30% of the Q). Since, experimentally, ${}^oP$ is found to be quite strong (even stronger than ${}^sR$), and no ${}^sQ$ branch is found at all, it seems certain that the transition observed is $Y\,{}^3\Sigma_u^- \leftarrow X\,{}^1\Sigma_g^+$.

Very recently, Carroll and Rubalcava[5] have obtained a rotational analysis of the 5-1 band of the $Y-B$ system. They conclude that state Y is also of species ${}^3\Sigma_u^-$ (See Sec. IV and Table II).

Furthermore, certain combination relations must hold:

$$ {}^sR(J-1)-{}^qP(J+1)={}^qR(J-1)-{}^oP(J+1) $$
$$ =\Delta_2F''(J) \quad (6) $$

These have been obtained for a few J values, and are collected in Table IV. Since the Q branches were unresolved, some errors are to be expected; on the whole, the agreement of the combination relations with the known $\Delta_2F''(J)$ values is satisfactory.

D. Mixing of $Y\,{}^3\Sigma_u^-$ with ${}^1\Pi_u$ and ${}^1\Sigma_u^+$ States

In a previous paper,[1] the total transition probability of $Y\,{}^3\Sigma_u^- \leftarrow X\,{}^1\Sigma_g^+$ was estimated to be $15\cdot10^{-6}$.[14] The intensity of the ${}^qQ$ branch is about 20% of the total; from this, the constants A and B may be estimated to be about $1.2\cdot10^{-3}$ and $3.4\cdot10^{-3}$, respectively.

All of the components (F_1, F_2, and F_3) of $Y\,{}^3\Sigma_u^-$ can interact with neighboring ${}^1\Pi_u$ states, thus causing Y

TABLE III. Rotational and vibrational constants of the $Y\,{}^3\Sigma_u^-$ state (cm^{-1}).

T_{00}	ω_e	$\omega_e x_e$	B_e	α_e	r_e (A)
65850.6_6	1517.6_9[a]	12.2_2[a]	1.472	0.016_1	1.278_8

[a] M. Ogawa and Y. Tanaka, J. Chem. Phys. (to be published) give $\omega_e=1515.7cm^{-1}$, $\omega_e x_e=11.00\ cm^{-1}$, based on band head data.

[13] G. Herzberg and T. J. Hugo, Can. J. Phys. 33, 757 (1955).

TABLE IV. Comparison of $\Delta_2F''(J)$ values obtained from the 1–0 band of the $Y-X$ system, and those obtained from accurately known rotational constants of $X\,{}^1\Sigma_g^+$.

J	${}^sR(J-1)-{}^qP(J+1)$	${}^qR(J-1)-{}^oP(J+1)$	$\Delta_2F''(J)$[a]
3		28.61	27.84
5	42.93	44.25	43.70
6	51.05	50.74	51.59
7	59.28	60.51	59.47
8	67.47	67.71	67.34
9	75.07	75.92	75.17
10	83.02		82.98
11	91.03		90.75
12	98.64		98.49
13	107.17		106.19

[a] $\Delta_2F''(J)=7.9592(J+\frac{1}{2})-5.12\cdot10^{-5}(J+\frac{1}{2})^3$.

[14] In reference 1, state Y was referred to as B'.

to take on some of the properties of the latter; in addition, the F_1 and F_3 components can interact with neighboring $^1\Sigma_u^+$ states and, likewise, take on some of the properties of $^1\Sigma_u^+$ states. From the experimental values of A and B (above), the interactions with $^1\Sigma_u^+$ states are somewhat stronger than the interactions with $^1\Pi_u$ states. These interactions contribute to the intensity of the $Y\,^3\Sigma_u^- \leftarrow X\,^1\Sigma_g^+$ transition, and help to make possible the observation of that band system.

The nearest $^1\Pi_u$ and $^1\Sigma_u^+$ states with electron configurations similar to the $\sigma_u{}^2\Pi_u{}^3\sigma_g\,{}^3\Pi_g$ configuration of $Y\,^3\Sigma_u^-$ are a predicted $^1\Pi_u$ (at about 98 000 cm^{-1}) with a configuration $\sigma_u\,{}^2\pi_u{}^3\sigma_g\,{}^2\pi_g$. The mixing of $^1\Sigma_u^+$ with $Y\,^3\Sigma_u^-$ should presumably be stronger than that of $^1\Pi_u$ with $^3\Sigma_u^-$ for two reasons: (1), $b'\,^1\Sigma_u^+$ has exactly the same electron configuration as $Y\,^3\Sigma_u^-$, and (2), the $b'-X$ transition is known to be among the strongest transitions (predicted to be $V-N$ in type) in nitrogen.

It would seem that the interactions contributing to the intensity of the $Y-X$ bands are due not to just one $^1\Pi_u$ state and to just one $^1\Sigma_u^+$ state, but rather to many such states in the region above 98 000 cm^{-1}, both observed and predicted.[7] However, it appears unlikely that these states which are so much higher than $Y\,^3\Sigma_u^-$ could quantitatively account for the observed intensity of $Y \leftarrow X$. A similar difficulty exists in attempting to account for the observed intensity of the $a'\,^1\Sigma_u^- \leftarrow X\,^1\Sigma_g^+$ transition[1] which supposedly gains intensity by interaction with $^1\Pi_u$ states.

IV. IDENTIFICATION OF THE "Y" BANDS

Kistiakowsky and collaborators[4,15] and earlier Brook[16] and Le Blanc, Tanaka, and Jursa[3] obtained a new emission system which Kistiakowsky *et al.* called "Y" bands, in the afterglow of active nitrogen, and LBTJ identified the lower state as $B\,^3\Pi_g$. The nature of the upper state was unknown, but believed to be either $^3\Sigma_u^-$ or $^3\Delta_u$; in addition, the vibrational numbering was in doubt at first; e.g., the band at 12 381 cm^{-1} given by LBTJ was listed as $(n+0)$, 0. Bayes and Kistiakowsky[4] obtained the Y bands also with $N_2{}^{15}$ and were able to show that most probably n is equal to 4. Using the known T_{00} of $B\,^3\Pi_g$ (59 314 cm^{-1}), and 12381 cm^{-1} for Y (4–0), the wavelengths of the band heads to be expected in absorption from the ground state of nitrogen to the upper state of the Y bands are: 0–0, 1518.9 A; 1–0, 1485.0; 2–0, 1453.2; 3–0, 1423.2 A. These are in close agreement with the band origins found in the present work (1518.59 A, 1484.916 A, 1453.224 A, and 1423.344 A), and with those calculated from the Ogawa and Tanaka emission system,[2] showing that the upper state of the Y bands is indeed $Y\,^3\Sigma_u^-$. Carroll and Rubalcava[5] very recently obtained the 5–1 band with $N_2{}^{14}$ and $N_2{}^{15}$, and showed that state Y is $^3\Sigma_u^-$ in type and also that $n=4$. It is of interest also that Kostikov and Megrelishvili[17] observed the Y 7–1 and Y 6–0 bands in the twilight sky spectrum.

The band structure of the Y bands can be accurately predicted. It turns out that they should have an appearance almost exactly like that of the first positive group ($B\,^3\Pi_g \rightarrow A\,^3\Sigma_u^+$), except that they should be red-shaded instead of violet-shaded. This is due to the fact that the B_e values for $Y\,^3\Sigma_u^-$ and $A\,^3\Sigma_u^+$ are very nearly equal (the two states have the same electron configuration). In a published photograph,[3] both the Y bands and the first positive bands are shown on the same spectrogram. The similarity between the two systems, except for the reversal of the direction of shading, is remarkable and supports the identification of the Y bands as $Y\,^3\Sigma_u^- \rightarrow B\,^3\Pi_g$.

V. DISCUSSION

As Schlapp[12] has pointed out, the selection rule that Σ^+ does not combine with Σ^- does not hold for intercombinations. Therefore, the $Y\,^3\Sigma_u^- \leftarrow X\,^1\Sigma_g^+$ transition would be expected to be about as strong as the Vegard-Kaplan bands ($A\,^3\Sigma_g^+ \leftarrow X\,^1\Sigma_g^+$). In a previous paper,[1] the transition probabilities of these are listed. For the $A-X$ system a value of $2.8\cdot10^{-6}$ was obtained; for the present transition, this is $1.5\cdot10^{-6}$.

All nitrogen electronic states of electron configuration $\pi_u{}^3\sigma_g\,{}^2\pi_g$ have now been observed and precisely located in energy except $^3\Delta_u$. These states are $A\,^3\Sigma_u^+$, $a'\,^1\Sigma_u^-$, $Y\,^3\Sigma_u^-$, $w\,^1\Delta_u$ and $b'\,^1\Sigma_u^+$.[7] The molecular constants are also known with considerable accuracy. Exactly why $^3\Delta_u$ is as yet unobserved is not clear. However, a transition to $^3\Delta_u$ would receive intensity by interaction only with the $^1\Pi_u$ group of states above about 98,000 cm^{-1}. The intensity of the transition $^3\Delta_u \leftarrow X\,^1\Sigma_g^+$ may be just too low to observe in the present experiments.

The $Y-X$ transition in nitrogen is analogous to the $e\,^3\Sigma^- - X\,^1\Sigma^+$ system of carbon monoxide.[13] The bands also are very similar in appearance and are of about equal intensity.

ACKNOWLEDGMENT

I am very grateful to Professor R. S. Mulliken and Dr. G. Herzberg for helpful discussions during the course of this research. I am especially indebted to Dr. M. Ogawa, Dr. Y. Tanaka, and Dr. P. K. Carroll for showing me their emission data in advance of publication. I am also grateful to Dr. M. Fred and Dr. F. Tomkins of the Argonne National Laboratory for permission to use their photoelectric comparator.

Note added in proof.—Dr. P. K. Carroll pointed out in a private communication that he and N. D. Sayers [Proc. Phys. Soc. **66**, 1138 (1953)] had observed one band of the $Y-B$ system although no assignment was made at that time. Furthermore, it is now suggested here, in accordance with the nomenclature recommended by Dr. Carroll, that state $Y\,^3\Sigma_u^-$ be called $B'\,^3\Sigma_u^-$.

[15] G. B. Kistiakowsky and P. Warneck, J. Chem. Phys. **27**, 1417 (1957).

[16] M. Brook, Science Report No. 2, Contract AF19(122)–453 of U. S. Air Force Geophysics Directorate with UCLA.

[17] I. A. Khostikov and T. G. Megrelishvili, Nature **183**, 811 (1959).

Volumes of Activation. II. Pressure Dependence of Activation Parameters

ROBERT W. KEYES

Westinghouse Research Laboratories, Pittsburgh 35, Pennsylvania

(Received October 15, 1959)

The relation between activation volume and activation energy of diffusive processes which was previously proposed is integrated to show how the activation free energy depends on the volume of the solid. The result is shown to be in agreement with the data of Nachtrieb *et al.* on the pressure dependence of the diffusion constant of sodium.

I. INTRODUCTION

IN a recent paper,[1] hereafter referred to as I, the author has shown that measurements of the activation volumes for diffusive processes in solids can be approximately related to the activation energies of the same processes by the equation

$$\Delta V^* = k\beta \Delta X^*. \tag{1}$$

Here ΔX^* is the activation energy, β is the isothermal compressibility of the substance in which the diffusion takes place, and k is a dimensionless numerical constant. The value of k which gave the best representation of most of the data was 4. It was also shown in I that several models in which macroscopic concepts are used to describe the atomic processes which cause diffusion lead to the relation given by Eq. (1). Additional justification of Eq. (1) has been given by Lawson.[2]

The activation energy ΔX^*, which appears in Eq. (1), was not defined precisely in I; in the discussions of models of atomic processes the various thermodynamic parameters which might be referred to as "activation energy," such as activation enthalpy and Gibbs free energy of activation, were regarded as equivalent quantities, and the symbol ΔH was used to represent them. The value of ΔX^* which was used to compare Eq. (1) with experimental results was that appropriate to a representation of the temperature dependence of the diffusive process in question by an Arrhenius equation at a pressure of one atmosphere. This approach was satisfactory, because Eq. (1) was intended to apply to a wide variety of diffusive processes and models, and was given a partially empirical justification.

The purpose of this note is to compare Eq. (1) with a case in which ΔV^* and β can be varied appreciably in a single substance. The only such case for which we are aware that data are available is that of self-diffusion in sodium. The effect of pressure on the diffusion constant has been measured by Nachtrieb *et al.*[3] to pressures of 12 000 kg/cm². These authors found that ΔV^* changed by a factor of about 1.5 in this pressure range. The compressibility has been measured by Bridgman,[4] who finds that β varies by a factor 1.7 in the same range. The desired comparison requires that a more accurate definition of ΔX^* be given first.

II. IDENTIFICATION OF ΔX^*

The meaning of the ΔX^* of Eq. (1) can be seen clearly in those cases in which Eq. (1) was justified by the application of thermodynamics to models of an atomic defect based on macroscopic concepts.[1,5,6] The strain energy model is the best known example.[5,6] The theory for these cases[1,6] shows that the quantity which has the value $k\beta$ is $(\partial V/\partial \epsilon)_{P,T}$, where ϵ is the work done on the crystal by the forces which are invoked to create the defect. As is seen from the fact that the derivative is taken at constant P and T, ϵ is isobaric, isothermal work. The isobaric, isothermal work, however, is the Gibbs free energy of activation for formation of the defect.[5] The Gibbs free energy of activation will be denoted here by ΔG^*. Thus Eq. (1) should be written

$$\Delta V^* = k\beta \Delta G^*. \tag{2}$$

(This ΔG^* is called ΔF by Nachtrieb *et al.*[3])

Nachtrieb, Resing, and Rice,[7] and Rice and Nachtrieb[8] have shown that the effect of pressure on diffusion can be represented by an equation which is similar in form to Eqs. (1) and (2), namely,

$$\Delta V^*/\Delta H^* = \Delta V_m/\Delta H_m.$$

Here the subscript m designates melting parameters. The similarity between Eq. (2) and the result of Nachtrieb and Rice[7,8] has implications which we intend to explore in future work.

III. COMPARISON WITH THE DATA

Now we wish to compare Eq. (2) with the data of Nachtrieb *et al.*[3] who have measured ΔG^* at six pressures in the range 0 to 12 000 Kg/cm. ΔV^* can be found from the data by the relationship

$$\Delta V^* = (\partial \Delta G^*/\partial P)_T. \tag{3}$$

[1] R. W. Keyes, J. Chem. Phys. **29**, 467 (1958).
[2] A. W. Lawson, J. Chem. Phys. **30**, 1114 (1959).
[3] Nachtrieb, Weil, Catalano, and Lawson, J. Chem. Phys. **20**, 1189 (1952).
[4] P. W. Bridgman, Proc. Natl. Acad. Sci. U. S. **21**, 109 (1935).
[5] C. Zener in *Imperfections in Nearly Perfect Crystals* (John Wiley & Sons, Inc., New York, 1952), pp. 289–316.
[6] R. W. Keyes, Acta Metallurgica **6**, 611 (1958).
[7] Nachtrieb, Resing, and Rice, J. Chem. Phys. **31**, 135 (1959).
[8] S. A. Rice and N. H. Nachtrieb, J. Chem. Phys. **31**, 139 (1959).

The differentiation indicated in Eq. (3) is most conveniently performed by drawing a smooth curve through the data and differentiating this curve. Because of the normal experimental errors, however, there is some flexibility in the way this curve is drawn. This flexibility is magnified in the derived values of ΔV^*. Therefore we will compare the experimental values of ΔG^* directly with an integrated form of Eqs. (2) and (3).

In order to derive the desired integrated relationship, we recall the definition of β,

$$\beta \equiv -(1/V)(\partial V/\partial P)_T. \tag{4}$$

Here V is the volume of the crystal. Combination of Eqs. (2), (3) and (4) yields

$$(1/\Delta G^*)(\partial \Delta G^*/\partial P)_T = -k(1/V)(\partial V/\partial P)_T, \tag{5}$$

which is readily integrated to give

$$\log(\Delta G^*/\Delta G_0) = -k \log(V/V_0). \tag{6}$$

Here the subscript 0 has been introduced to designate values of the parameters at $P=0$.

The comparison of Eq. (6) with the experimental results is given in Table I. The first column of the table lists the pressures at which the diffusion coefficient D was measured by Nachtrieb *et al.*[3] and the second column gives their values for $\log_{10}(D/\gamma a^2 \nu)$. This logarithm is ΔG^*, except for a pressure-independent factor. The third column gives the values of V/V_0, taken from the work of Bridgman.[4] The value of k as calculated from Eq. (6) is given in the fourth column. The implication of the previous discussion is that these values should all be the same. It is seen that this is approximately true and that the deviations of the derived values of k from constancy are of the type which would arise from experimental uncertainty, and contain no systematic trend.

The representation of the data by Eq. (6) is also illustrated in Fig. 1, in which an average value of k,

TABLE I. A comparison of the pressure dependence of the diffusion constant of sodium with Eq. (6).

P (Kg/cm)²	$\log_{10}(D/\gamma a^2 \nu)$	V/V_0	$-\dfrac{\log_{10}(G^*/G_0^*)}{\log_{10}(V/V_0)} (=k)$
1	−4.701	1.0000	...
4 030	−5.343	0.9444	2.238
7 970	−5.750	0.9023	1.959
8 060	−5.796	0.9013	2.015
8 550	−5.963	0.8968	2.183
12 000	−6.329	0.8668	2.080

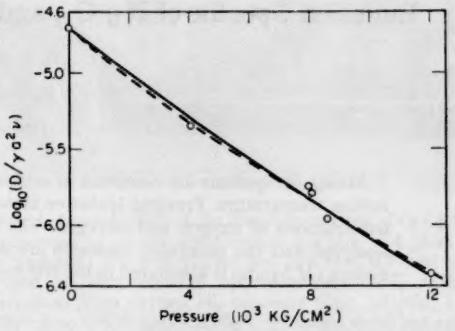

FIG. 1. The pressure dependence of the free energy of activation for self-diffusion in sodium. The experimental points and the dotted line are taken from Nachtrieb *et al.*[3]; the solid line represents the fit of Eq. (6) to the data.

$k=2.095$, determined from Table I, has been used to calculate ΔG^* from Eq. (6). The result of the calculation is shown by the solid line, and, for comparison, the curve drawn by Nachtrieb *et al.* (their Fig. 4) is shown by a dotted line. It is seen that the curves are quite close to one another, and that both represent the data quite well.

It should be pointed out that our curve is actually a two-parameter fit to the data, since we have chosen ΔG^* so that the calculated curve passes through the experimental point at $P=0$ and have determined k from Table I. The data obtained in most studies of the pressure dependence of diffusion constants cover only ranges of pressures in which ΔG^* is a linear function of P. A two-parameter fit to the data in such cases is trivial. In the case considered here it is significant, and constitutes a demonstration of the utility of Eqs. (2) and (6). The parameters of Eq. (6) can, however, be determined from accurate data in the linear or low-pressure range. Thus Eq. (6) can be used to extrapolate diffusion measurements from the linear range to the full pressure range for which the volume is known.

IV. CONCLUSIONS

The important points presented in this paper are: (1) The appropriate thermodynamic function to use for the "activation energy" in calculating the volume according to the method of I is the activation Gibbs free energy. (2) Equation (2) can be integrated to give Eq. (6). (3) The experimental results of Nachtrieb *et al.*[3] on the pressure dependence of self-diffusion in sodium can be represented by Eq. (6). (4) Equation (6) furnishes a reasonable method for extrapolating the pressure dependence of a diffusive process to higher pressures.

THE JOURNAL OF CHEMICAL PHYSICS VOLUME 32, NUMBER 4 APRIL, 1960

Emission Spectra of N_2, O_2, and NO Molecules Trapped in Solid Matrices*

H. P. Broida and M. Peyron†

National Bureau of Standards, Washington, D. C.

(Received October 12, 1959)

Molecular systems are observed in emission in solid products from a gas discharge trapped at liquid helium temperature. Previous tentative molecular assignments have been checked with the help of isotopic substitutions of oxygen and nitrogen. The Herzberg system (A bands) of oxygen ($A\,^3\Sigma_u^+ - X\,^3\Sigma_g^-$) is analyzed and the molecular constants are derived for a molecule trapped in a nitrogen matrix. Another system (M bands) is attributed to the NO molecule ($^4\Pi - X\,^2\Pi$).

INTRODUCTION

SEVERAL molecular band systems observed in products from a gas discharge trapped at liquid helium temperature have been described previously.[1,2] Most of these systems also have been observed in emission from solidified gases (nitrogen and rare gases) subjected to electron and ion bombardment.[3-5] Tentative identifications have been made on the basis of the gases used and by comparison of wavelengths and intensities in the solid with values in the gas. Since further evidence was needed for more certainty in some of the identifications, nitrogen and oxygen isotopes have been used.

The aim of this paper is primarily to present new results, but earlier measurements are included occasionally for completeness. Spectra have been obtained by condensing products from a gas discharge on a surface cooled to 4.2°K.[1,2] Special attention has been given to the numbering of the bands for this is one of the main results coming from isotopic substitution. The accuracy of the frequency measurements ($\sim$5 cm^{-1}) is limited by the diffuseness of the bands.

PRESENT STATUS OF THE BAND ASSIGNMENT

Previous studies[1,2] have shown that six different molecular systems appear in emission in solidified gases at liquid helium temperatures. After isotopic substitution and further experimental investigation, the present status of the band assignments may be summarized as follows:

(1) The A band system which was attributed incorrectly to the $^5\Sigma - A\,^3\Sigma_u^+$ transition of the nitrogen molecule,[1,6] is due to the $A\,^3\Sigma_u^+ - X\,^3\Sigma_g^-$ transition of the oxygen molecule. The influence of oxygen concentration on the band intensity is very marked. The isotopic shift, and intensity distribution, and the vibrational constants derived from the experimental data fit well with the lower state of the transition.

(2) The $D(NO_\beta)$ system has been observed to shift after isotopic substitution of both nitrogen and oxygen. The extent of the shifts as measured on a few bands is consistent with the proposed identification. The $E(NO_\gamma)$ system has been observed to shift with oxygen isotopic substitution. No nitrogen isotopic substitution has been made. Since this system has the same appearance as in the gas phase,[1] there is no doubt about its identification.

(3) The B bands, attributed to NO_2,[1] have been observed to shift after isotopic substitution of oxygen. Whether or not they shift after nitrogen substitution is still unknown because the bands are very broad (700 cm^{-1}). In any case the shift is considerably smaller than after the oxygen substitution.

(4) The Vegard-Kaplan system of nitrogen is emitted in solids containing rare gases with a fairly large amount of nitrogen. This system also is observed very weakly in pure nitrogen. It is attributed to the $A\,^3\Sigma_u^+ - X\,^1\Sigma_g^+$ transition of the nitrogen molecule.[2,3] The only new result is the observation of the shift of the bands with isotopic substitution of nitrogen in a manner consistent with the identification.

(5) The M bands appear in solids containing argon with traces of nitrogen and oxygen. They had been attributed tentatively to N_2,[2] but it is known now that the emitting molecule is NO, probably the $^4\Pi - X\,^2\Pi$ transition. Controlled traces of oxygen in argon are observed to increase their intensity. Isotropic substitution of oxygen shows that the emitting molecule contains only one atom of oxygen. Every effort to increase the band intensity by controlled addition of N_2, C, and H_2 has been in vain. However addition of isotopic nitrogen shows that this element is the other atom of the emitter.

INDIVIDUAL BAND SYSTEMS

(1) Herzberg System of Oxygen ($A\,^3\Sigma_u^+ - X\,^3\Sigma_g^-$)

This system has been observed both in argon or in nitrogen containing traces of oxygen (less than 10%).

* This research was performed under the National Bureau of Standards Free Radicals Research Program supported by the Department of the Army.

† Now at the Institut National des Sciences Appliquées, Lyon, France.

[1] A. M. Bass and H. P. Broida, Phys. Rev. **101**, 1740 (1956).

[2] M. Peyron and H. P. Broida, J. Chem. Phys. **30**, 139 (1959).

[3] The most important Vegard publications are listed in references 1 and 2.

[4] E. M. Hörl, J. Mol. Spectroscopy **3**, 425 (1959).

[5] L. J. Schoen and R. E. Rebbert, J. Mol. Spectroscopy **3**, 417 (1959).

[6] C. M. Herzfeld and H. P. Broida, Phys. Rev. **101**, 606 (1956).

TABLE I. The Herzberg bands of O_2 as observed in a solid containing 1% oxygen and 99% nitrogen.

	$O^{16}O^{16}$		$O^{16}O^{18}$		$O^{18}O^{18}$	
v', v''	λ(A)	ν(cm^{-1})	λ(A)	ν(cm^{-1})	λ(A)	ν(cm^{-1})
0, 3	3396.7	29 471				
0, 4	3571.0	27 981	3550.1	28 160		
0, 5	3769.4	26 522	3738.7	26 740		
0, 6	3985.5	25 086	3946.3	25 333	3905.9	25 595
0, 7	4223.5	23 667	4173.2	23 956	4122.5	24 250
0, 8	4488.6	22 271	4424.5	22 595	4360.4	22 927
0, 9	4781.8	20 907	4702.2	21 261	4622.7	21 626
0, 10	5112.3	19 555	5013.4	19 941	4915.3	20 339
0, 11	5482.6	18 234	5361.1	18 648		
0, 12	5906.9	16 925	5752.9	17 378		
0, 13	6390.5	15 644				

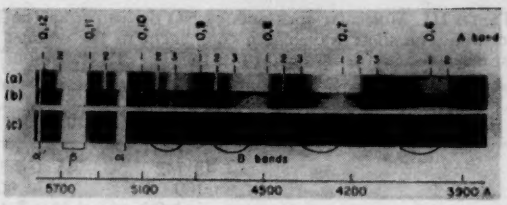

FIG. 1. Isotopic shift of the Herzberg system of O_2 (A bands) as observed in an oxygen-nitrogen mixture. $f/4$ glass prism spectrograph; 103 a–F plates; gas flow rate 0.3 cm^3/sec. (a) Oxygen 18 concentration approximately 0.5% with contamination from oxygen 16; exposure time, 10 min; 1 refers to O_2^{16}, 2 to $O^{16}O^{18}$ and 3 to O_2^{18}. (b) Same as (a) but exposure time 3 min. (c) 1% oxygen 16 in nitrogen; exposure time 3 min.

It also has been observed in krypton and xenon.[7] Table I gives a complete list of wavelength measurements for the molecules O_2^{16}, $O^{16}O^{18}$, and O_2^{18} as observed in a solid containing about 1% of O_2^{18}. The oxygen used contained 98% of O_2^{18} (from the manufacturer's analysis). Contamination from handling gave a sufficient amount of $O^{16}O^{18}$ molecules to observe the corresponding bands with a fairly great intensity. Measurements from the O_2^{16} molecule also are new. They are consistent with the previous measurements[1] except in the near ultraviolet region where the $f/1.5$ grating instrument[8] gives better dispersion. The wavelengths of the bands corresponding to the O_2^{18} and $O^{16}O^{18}$ molecules have been measured on the same plate. The three sets of bands are shown in Fig. 1.

The constants a, b, and c of the three-parameter equation $\nu = a - bv + cv^2$ have been computed with the help of the least squares method and the results for the three sets of bands are listed in Table II. In the same table are listed also the constants ω_e and $\omega_e x_e$ derived from a, b, and c. Also experimental and calculated ρ^2 (the ratio of the reduced mass of the ordinary molecule to the reduced mass of the isotopic molecule) values are presented. This ratio may be computed either from ω_e values or from $\omega_e x_e$ values. The results agree very well, taking into account the estimated error, and giving further support to the experimental ω_e and $\omega_e x_e$ values.

The data also show that there is only a relatively small change of the vibrational constants when the molecule is trapped in the solid. On the other hand there is a red shift of ν_{00} of about 945 cm^{-1}.

(2) NO_β System

Table III, obtained from the results of Bass and Broida,[1] shows the vibrational constants of the various states of NO involved and compares them to their values in the gas phase. ω_e and $\omega_e x_e$ ($B^2\Pi$) should not be taken too seriously since they are supported only by three weak bands coming from upper state vibrational levels.

Here again, there are only small changes of the molecular constants of the molecule when it is trapped in the solid.

(3) NO_γ System

This system exhibits rotational lines and no shift as compared to the gas phase.[1] It very probably is emitted from a gas glow immediately surrounding the solid.

TABLE II. Molecular constants of the O_2 molecule derived from the Herzberg band system.

Constants	O_2^{16} solid (cm^{-1})	$O^{16}O^{18}$ solid (cm^{-1})	O_2^{18} solid (cm^{-1})	O_2^{16} gas[a] (cm^{-1})
$a = \nu_{00}$	34 055 ±30	34 073 ±37	34 067 ±60	35 000 ±.4
b	1563 ±8	1521 ±10	1471 ±16	1564.9 ±0.1
c	11.3±0.5	10.8±0.6	9.9±1.0	11.33±0.006
$\omega_e(X\,^3\Sigma_g^-)$	1574	1532	1481	1576.2
$\omega_e x_e(X\,^3\Sigma_g^-)$	11.3	10.8	9.9	11.33
ρ^2 (from ω_e)		0.947±0.006	0.885±0.006	
ρ^2 (from $\omega_e x_e$)		0.956±0.05	0.876±0.05	
ρ^2 (calculated value)		0.944	0.889	

[a] The gas values of the constants have been calculated using Herzberg's [G. Herzberg, Can. J. Phys. 30, 185 (1952)] calculated values for the vibrational transitions 0,4 through 0,14, with the vibrational numbering changed by one unit [H. P. Broida and A. G. Gaydon, Proc. Roy. Soc. (London) A222, 181 (1954)]. These values have been fitted to a three-parameter equation and processed the same way as the experimental frequencies.

[7] L. J. Schoen and H. P. Broida, J. Chem. Phys. (to be published).
[8] Peyron, Hörl, Brown, and Broida, J. Chem. Phys. 30, 1304 (1959).

TABLE III. Molecular constants of NO derived from the NO_β spectrum. The short wavelength component of the doublet has been measured and is assumed to be the $^2\Pi_{\frac{1}{2}}-{}^2\Pi_{\frac{1}{2}}$ transition.

State	Constant	Solid (cm^{-1})	Gas[a] (cm^{-1})
$B\,^2\Pi_{\frac{1}{2}}$	ν_{00}	45 742	45 486.1
	ω_e	1007.5 ?	1036.96
	$\omega_e x_e$	4.0 ?	7.60
$X\,^2\Pi_{\frac{1}{2}}$	ω_e	1917.4	1904.03
	$\omega_e x_e$	14.0	13.97

[a] G. Herzberg, *Molecular Spectra and Molecular Structure* (D. Van Nostrand Company, Inc., Princeton, New Jersey, 1957).

TABLE IV. Vegard-Kaplan band system of N_2 observed in a solid containing 3% nitrogen and 97% argon.

	N_2^{14}		N_2^{15}	
v', v''	λ(A)	ν(cm^{-1})	λ(A)	ν(cm^{-1})
0, 5	2613.0	38 259	2586.5	38 651
0, 6	2770.9	36 079	2736.6	36 531
0, 7	2947.0	33 923	2902.0	34 449
0, 8	3144.0	31 797	3087.1	32 383
0, 9	3366.9	29 692	3295.0	30 343
0, 10	3618.3	27 629	3528.6	28 332
1, 8	3008.5	33 229	2960.7	33 766
1, 9	3211.3	31 131	3150.5	31 732
1, 10	3439.8	29 063	3363.2	29 725
1, 11	3699.2	27 025	3603.2	27 745
1, 12	3998	25 005	3875	25 799
2, 10	3281.3	30 467		
2, 11	3516.9	28 426	3435.4	29 100
2, 12	3784.6	26 415	3682.2	27 150
2, 13	4090	24 443	3965	25 214

TABLE V. Molecular constants of N_2 (in solid argon) derived from the Vegard-Kaplan system and isotope effect ($\rho^2_{calc}=0.933$).

State	Constants	N_2^{14}(solid) (cm^{-1})	N_2^{15}(solid) (cm^{-1})	N_2^{14}(gas)[a] (cm^{-1})	ρ^2(solid)
	ν_{00}	49 619	49 609	49 756.5	
$A\,^3\Sigma_u^+$	ω_e	1 460.0	1 420.5	1 460.37	0.947
	$\omega_e x_e$	13.5	16.5 ?	13.89	
$X\,^1\Sigma_g^+$	ω_e	2 358.5	2 272.2	2 359.61	0.927
	$\omega_e x_e$	14.5	13.2	14.46	0.910

[a] G. Herzberg, *Molecular Spectra and Molecular Structure* (D. Van Nostrand Company, Inc., Princeton, New Jersey (1957).

TABLE VI. The *M* band system of NO observed in a 1% oxygen and 99% argon mixture (with unknown amount of nitrogen impurity).

	O_2^{16}		O_2^{18}	
v', v''	λ(A)	ν(cm^{-1})	λ(A)	ν(cm^{-1})
0, 4	3262.8	30 640	3241.9	30 837
0, 5	3462.3	28 874	3434.1	29 111
0, 6	3682.9	27 145	3645.6	27 423
0, 7	3929.9	25 439	3880.8	25 761
0, 8	4206.7	23 765	4144.3	24 123
0, 9	4520.0	22 118	4440.5	22 514
0, 10	4877.8	20 495	4776.9	20 928

(4) *B* Bands (NO_2 ?)

These bands are observed in nitrogen-oxygen mixtures (less than 5% of oxygen). They have a very diffuse appearance and are extremely broad, extending in some cases 50 to 100 A.[2] One additional band has been observed at 4985 A (20 055 cm^{-1}). The shift, after isotopic substitution of oxygen, has been observed for the four longer wavelength bands. It is fairly constant with an average of 400 cm^{-1}.

(5) The Vegard-Kaplan System of Nitrogen ($A\,^3\Sigma_u^+-X\,^1\Sigma_g^+$)

New measurements in a 3% nitrogen 97% argon mixture are presented in Table IV, both for N_2^{14} and N_2^{15}. These values are consistent with the numbers presented in reference 2 for a 5% nitrogen, 95% argon mixture. The shorter wavelength head has been measured for each double-headed band.

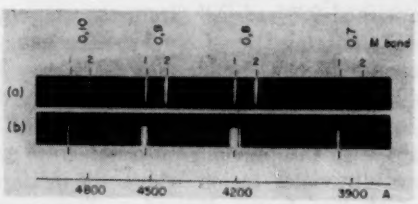

FIG. 2. Isotopic shift of NO (*M* bands) as observed in an oxygen-argon mixture. (a) Oxygen 18 concentration approximately 0.5% with contamination from oxygen 16; exposure time 4 min; 1 refers to O^{16} and 2 to O^{18}. (b) 1% oxygen 16 in nitrogen; exposure time 3 min and 25 min.

The molecular constants for N_2^{14} and N_2^{15} and the ρ^2 values are listed in Table V. The experimental isotope effect is reasonably consistent with the calculated one, except for $\omega_e x_e$ ($A^3\Sigma_u^+$) where the experimental data are not sufficient to provide enough accuracy for the molecular constant.

(6) The *M* Bands

Table VI lists the observed wavelengths for this system in argon (containing unknown traces of nitrogen as an impurity) in which 1% oxygen (O_2^{16} or O_2^{18}) was added. A photograph of the spectra is presented in Fig. 2. The two sets of bands show that a single atom of oxygen is in the molecular emitter. There is an approximately constant difference of 14 cm^{-1} between the new measurements and the previous ones.[2] This is because the higher dispersion used this time shows a diffuse head on the short wavelength side of the bands; the head has been measured instead of the center of the band. When spectra from a mixture of the same argon, 0.5% of O_2^{16} and 0.5% of N_2^{15} were photographed, two sets of bands were observed, showing that the other atom of the diatomic emitter is nitrogen. The frequency shifts of four bands belonging to $N^{15}O^{16}$ are in qualitative agreement with the calculated one.

TABLE VII. Molecular constants of NO derived from the analysis of the M bands ($\rho^2_{calc}=0.948$).

Constants	Molecules			ρ^2 solid
	$N^{14}O^{16}$ solid (cm^{-1})	$N^{14}O^{18}$ solid (cm^{-1})	$N^{14}O^{16}$ gas[a] (cm^{-1})	
$a=\nu_{00}$	37 965 ±25 (4.7 ev)	37 981 ±45	(4.5 ev)[b]	
b	1888.4 ±8	1841.2 ±14		
c	14.15±0.6	13.61±1.0		
ω_e ($X\,^2\Pi$)	1902.5	1854.8	1904.03	0.951±0.005
$\omega_e x_e$ ($X\,^2\Pi$)	14.16	13.61	13.97	0.961±0.07

[a] G. Herzberg, *Molecular Spectra and Molecular Structure* (D. Van Nostrand Company, Inc., Princeton, New Jersey, 1957).
[b] From Mulliken [R. S. Mulliken, Rev. Modern Phys. 4, 1 (1932)].

The best set of molecular constants obtained for the molecule is presented in Table VII as well as the experimental ρ^2 value. This value compares very well with the calculated ρ^2 for a NO molecule. Furthermore Mulliken[9] predicted a $^4\Pi$ electronic state of the NO molecule approximately 4.5 ev above the ground state which fits well with the approximately 4.7 ev observed for the upper state of the M bands.

SOME REMARKS ABOUT EXCITATION PROCESSES

In the present state of the work it is impossible to know with any certainty the excitation processes of the emitting species. However, during the development of this work, some experimental facts have been noticed, which might help to understand the phenomena.

At this point, one must recall that the origin of the energy in the solid is still very doubtful. Nitrogen, and possibly O atoms are trapped in the solid for long periods of time.[8] Evidence of this fact is given by the emission of atomic lines during the warm-up period of the solid, several hours after the deposition from the gas discharge has been stopped. However, atom concentrations are very low; several different measurements give an upper limit of the order of 0.1% of the total number of particles.[10] There is evidence that the atomic species are not trapped in an excited state but that they are reexcited when the solid loses its rigidity and the atoms move and recombine. However, the low concentration of atoms makes a three-body process very improbable. There is no evidence that electronically excited molecules are trapped for long periods of time, and the origin of the excitation energy is probably in the recombination of atoms.

(1) Herzberg System

This system is observed during deposition, but has been observed only once, very weakly, during the warm-up period. It appears when the oxygen is added downstream from a nitrogen discharge as well as when the oxygen is premixed before the discharge. The excitation energy does not seem to come from the nitrogen atom recombination, since the glow is not observed during the warm-up period. The oxygen molecules probably are excited in the gas phase by exchange of energy with excited N_2 molecules or with the help of the same process responsible for the excitation of N_2 molecules in the gas afterglow. It is possible that a N_2 molecule could be excited to the $A^3\Sigma_u^+$ state in the gas phase and, due to its relatively long lifetime in the gas (0.07 sec),[11] not radiate until it is in the solid.

(2) NO_β System

This system also is observed in the gas afterglow of nitrogen-oxygen mixtures. It has been observed only when oxygen is premixed with nitrogen and only during deposition. The transition $B\,^2\Pi - X\,^2\Pi$ is allowed, and one cannot expect the lifetime of the excited NO molecule made in the gas to be very long. This lifetime is certainly shorter than the transfer time to the solid (about 10^{-2} sec). This implies that the species must be excited in the solid, yet it is difficult to understand why this spectrum does not appear during the warm-up period.

(3) B Bands System

This system occurs along with the A bands in nitrogen-oxygen mixtures. It is very intense at the end of the warm-up period (around 30°K), giving a blue color to the solid.[2]

(4) Vegard-Kaplan System

These bands are very weak in pure nitrogen, but become extremely intense in mixtures of nitrogen with argon, neon, krypton, and hydrogen. It is not implausible to think that the recombination of atoms gives an excited nitrogen molecule responsible for this emission. But an explanation for the weakness of the emission in pure nitrogen is needed. It is possible that in this case the excited molecules ($A^3\Sigma_u^+$) lose their energy by direct transfer to neighbors until a nitrogen atom is excited on the way. In case of dilution by a rare gas such an energy transfer may not be possible.

[9] R. S. Mulliken, Revs. Modern Phys. 4, 1 (1932).
[10] B. J. Fontana, J. Chem. Phys. 31, 148 (1959).
[11] Bills, Carleton, and Oldenberg, Communication at the IV Meeting of Molecular Spectroscopy, Bologna (1959).

Dependence upon Volume of Nuclear Quadrupole Interactions in Crystals*

R. A. BERNHEIM† AND H. S. GUTOWSKY

Noyes Chemical Laboratory, University of Illinois, Urbana, Illinois

(Received September 23, 1959)

The electric quadrupole splitting of the Na^{23} nuclear magnetic resonance has been measured in single crystals as a function of pressure and temperature for $NaNO_3$, and as a function of temperature for $NaBrO_3$. It is found that the electric field gradient at the sodium nuclei varies as $V^{-3.5}$ in $NaNO_3$ and as $V^{-2.0}$ in $NaBrO_3$. These results, together with the previously reported $V^{-1.9}$ dependence for Na^{23} in $NaClO_3$, are compared with theoretical values computed from point charge models for the crystal lattices. It is concluded that the large volume dependence in $NaNO_3$ arises from the anisotropic thermal expansion and compressibility of the hexagonal crystal plus the retention of size and configuration of the NO_3^- group. The experimental results for $NaClO_3$ can be explained in the same manner, assuming a rigid ClO_3^- group; however, this model does not account for the V^{-2} dependence of the Na^{23} quadrupole coupling observed in $NaBrO_3$. The assumed rigidity of the ClO_3^- group is supported by the small volume dependence, $V^{-0.10}$, found for the Cl^{35} quadrupole coupling in $NaClO_3$, and also by calculations of the interionic contribution to the field gradient at the chlorine nuclei in $NaClO_3$ and $KClO_3$.

1. INTRODUCTION

THE present work is a continuation of earlier studies of the dependence upon volume of electric field gradients in crystals.[1,2] Kushida *et al.*[1] have measured the effects of temperature and pressure upon nuclear pure quadrupole resonance frequencies and found that the nuclear electric quadrupole interaction varies as $V^{-0.96}$ for Cu^{63} in Cu_2O and as $V^{-0.025}$ for Cl^{35} in $KClO_3$. Similar measurements of the quadrupole splitting of the Na^{23} nuclear magnetic resonance in $NaClO_3$ gave a $V^{-1.9}$ dependence. The volume dependence observed for the quadrupole interaction results from the volume dependence of the electric field gradient, eq, at the nucleus, inasmuch as the interaction energy or coupling constant, ν cps, is given by the

$$\nu = e^2Qq/h, \tag{1}$$

where Q, the nuclear quadrupole moment, as well as the electronic charge e, are constants.

If an assembly of charges produces an electric field with axial symmetry, the electric field gradient at a point on the axis may be expressed as

$$eq = \sum_j e_j(3\cos^2\theta_j - 1)/r_j^3, \tag{2}$$

where the summation is over all charges e_j present at distance r_j from the point, and θ_j is the angle between r_j and the symmetry axis of eq. Inspection of Eq. (2) shows that an isotropic volume change would produce an r^{-3} or V^{-1} change in eq and thus, in the observed coupling constant ν. The crystals in question here have field gradients with axial symmetry at the nuclei observed, except for a small asymmetry ($\eta = 0.006$) at the chlorine in $KClO_3$.[3] Therefore, Eq. (2) is an appropriate, idealized model for the volume dependence of eq. On this basis, the volume dependences reported previously are anomalous with the exception of that for Cu^{63} in Cu_2O.

The fact that eq in Cu_2O has nearly a V^{-1} dependence is strong evidence that solid Cu_2O has a completely ionic structure.[1] Moreover, the very small dependence, $V^{-0.025}$, observed for Cl^{35} in $KClO_3$ is consistent with the view that a volume change affects the distance between the K^+ and ClO_3^- ions but leaves the ClO_3^- ion unchanged in size and configuration.[1] The field gradient at the chlorine nucleus is due primarily to the electron distribution in the ClO_3^- ion, which is relatively unaffected by changes in molar volume. Presumably, only the small contribution of the crystalline field to eq at the Cl nucleus could have a V^{-1} dependence.

The cause of the $V^{-1.9}$ dependence found for Na^{23} in $NaClO_3$ is not quite as obvious as that for the very small dependence for Cl^{35} in the ClO_3^- ion. It was suggested[2] that anisotropic changes in the interionic distances attending a volume change might be responsible, as it is for the Cl^{35}, but there was insufficient evidence to settle the question. Further work was indicated and we have extended the experimental observations to include the volume dependence for Na^{23} in $NaBrO_3$ and in $NaNO_3$, and for Cl^{35} in $NaClO_3$. The observations on $NaBrO_3$ and $NaClO_3$ were made in order to obtain data for Na^{23} in different compounds having the same crystal structure. $NaNO_3$ was studied because of its different, noncubic crystal structure and known anisotropic thermal expansion and compressibility. Calculations of the field gradients as a function of volume are necessary for a quantitative understand-

* Assisted by the Office of Naval Research. Taken in main from the Ph.D. thesis of R. A. Bernheim, University of Illinois (1959).

† Du Pont Teaching Fellow in Chemistry. Now at Department of Chemistry, Columbia University, New York.

[1] Kushida, Benedek, and Bloembergen, Phys. Rev. **104**, 1364 (1956).

[2] H. S. Gutowsky and G. A. Williams, Phys. Rev. **105**, 464 (1957). See also prior work cited there.

[3] T. P. Das and E. L. Hahn, "Nuclear quadrupole resonance spectroscopy" in *Solid State Physics*, edited by F. Seitz and D. Turnbull (Academic Press Inc., New York, 1958), Suppl. 1.

ing of the effects observed. We have made such calculations using a point charge model for the ionic lattice with the assumption that the XO_3^- groups (X=Cl, Br, N) retain their configuration while the distances between the Na^+ (or K^+) and XO_3^- change.[4] Comparison of the calculated and experimentally derived effects suggests that such studies will improve our understanding of crystal structure.

2. EXPERIMENTAL PROCEDURE AND RESULTS

The stainless steel pressure bomb,[2] the magnetic resonance apparatus and cryostat,[5] and most of the methods[2] used in these experiments have been described previously. Heavy white mineral oil was used as the hydraulic fluid in the pressure experiments. The single crystals of $NaBrO_3$ and $NaNO_3$ were obtained, respectively, from Dr. D. W. McCall of the Bell Telephone Laboratories, and the Harshaw Chemical Company. The quantities needed to complement the data from earlier experiments were the temperature coefficients of the Na^{23} coupling constant in $NaBrO_3$ and $NaNO_3$ and the pressure coefficient in $NaNO_3$. Because of the weak Na^{23} quadrupole coupling in these compounds, the quadrupolar splitting of the Na^{23} nuclear magnetic resonance was used to measure e^2qQ/h at different pressures and temperatures. The field of the permanent magnet used was about 6300 gauss.

The orientation of the $NaBrO_3$ crystal, and the measurements on it were performed in the same manner as for $NaClO_3$.[2] The temperature dependence of the Na^{23} coupling was measured at atmospheric pressure between −196° and 84°C. The thermal coefficient

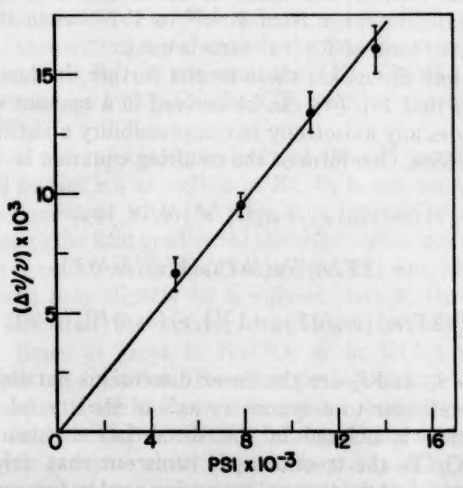

FIG. 1. Dependence upon pressure of the electric quadrupole splitting of the Na^{23} nuclear magnetic resonance absorption in a single crystal of $NaNO_3$ at room temperature.

TABLE I. The effects of temperature and pressure upon the Na^{23} quadrupole coupling observed in some ionic crystals at atmospheric pressure and 25°C.

Compound	$(1/T)(\Delta\nu/\nu)$	$(1/P)(\Delta\nu/\nu)$
$NaClO_3$[a]	-4.2×10^{-4} deg^{-1}	7.7×10^{-6} kg^{-1} cm^2
$NaBrO_3$	−2.2	6.0[b]
$NaNO_3$	−7.75[b]	17.2

[a] From reference 2.
[b] See also reference 9.

$(1/T)\Delta\nu/\nu$ increases somewhat in magnitude at higher temperatures, as is customary for most crystals.[3] The value at 25°C was found to be $-(3.2\pm0.2)\times10^{-4}$ deg^{-1}.

The crystal structure of $NaNO_3$ is rhombohedral, but it can also be described as hexagonal.[6,7] There are two molecules per unit cell, both having the same symmetry axis which is along the Na—N direction. Consequently, there are only three transitions in the Na^{23} resonance for an arbitrary orientation of the crystal.[8] The NO_3^- groups are planar and perpendicular to the symmetry axis. In observing fractional changes in e^2qQ, it is desirable to orient the crystal so that the outer "satellite" transitions have the maximum separation from the central transition. In this event, a change in e^2qQ causes a maximum change in the position of the satellites. Equations describing the angular dependence of the quadrupole splitting have been presented elsewhere.[2,8]

The $NaNO_3$ crystal was of such a shape that the optimum orientation and filling factor of the sample coil could not be achieved simultaneously. Therefore, with the filling factor a maximum, the crystal was rotated in the magnetic field H_0 until a maximum splitting of the Na^{23} resonance was obtained. The orientation of the field gradient axis with respect to H_0 was determined from the separation between a satellite and the central component, and the value of 334 kc/sec for e^2qQ/h at atmospheric pressure and room temperature obtained by Pound.[8]

The quadrupole splitting of the Na^{23} resonance was measured in $NaNO_3$ at four temperatures between room temperature and 70°C. The resulting value for $(1/T)\Delta\nu/\nu$ at 25°C and atmospheric pressure is $-(7.75\pm0.5)\times10^{-4}$ deg^{-1}, which agrees with the more extensive measurements made recently by Andrew.[9] The pressure dependence of the Na^{23} quadrupole coupling observed in $NaNO_3$ at room temperature is shown in Fig. 1. The result for $(1/P)\Delta\nu/\nu$ at atmospheric pressure is 17.2×10^{-6} kg^{-1} cm^2. The various results obtained in these experiments, together with those reported previously[2,9] for the Na^{23} quad-

[4] While our work was in progress, R. Bersohn [J. Chem. Phys. 29, 326 (1958)] reported similar, less detailed, calculations for $NaClO_3$ which support this model.
[5] Gutowsky, Meyer, and McClure, Rev. Sci. Instr. 24, 644 (1953).
[6] R. W. G. Wyckhoff, *Crystal Structures* (Interscience Publishers, Inc., New York, 1957).
[7] P. E. Tahvonen, Ann. Acad. Sci. Fennicae Ser. AI 42 (1947).
[8] R. V. Pound, Phys. Rev. 79, 685 (1950).
[9] Eades, Hughs, and Andrew, Proc. Phys. Soc. 71, 1019 (1958).

TABLE II. Compressibility, coefficient of thermal expansion, and the temperature coefficient of the Raman lattice frequencies for $NaClO_3$, $NaBrO_3$, and $NaNO_3$, at atmospheric pressure and 25°C.

	$NaClO_3$	$NaBrO_3$	$NaNO_3$
β	4.0×10^{-6} kg^{-1} cm^2 [a]	3.0×10^{-6} kg^{-1} cm^2 [a,c]	3.85×10^{-6} kg^{-1} cm^2 [e]
$\beta_{\|\|}$	...	...	2.44[e]
$\beta_\perp$	...	...	0.709[e]
α	1.32×10^{-4} deg^{-1} [a]	1.28×10^{-4} deg^{-1} [a]	1.56×10^{-4} deg^{-1} [f,g]
$\alpha_{\|\|}$	...	...	1.18[f]
$\alpha_\perp$	...	...	0.104[f]
$(1/\nu_l)(\partial\nu_l/\partial T)_P$	-2.5×10^{-4} deg^{-1} [b]	-2.5×10^{-4} deg^{-1} [d]	-2.66×10^{-4} deg^{-1} [h]

[a] S. S. Sharma, Proc. Indian Acad. Sci. **31A**, 83 (1950).
[b] C. S. Kumari, Proc. Indian Acad. Sci. **31A**, 348 (1950).
[c] W. P. Mason, Phys. Rev. **70**, 529 (1946).
[d] See text.
[e] P. W. Bridgeman, Proc. Am. Acad. Arts Sci. **64**, 51 (1929).
[f] Reference 7.
[g] F. C. Kracek, J. Am. Chem. Soc. **53**, 2609 (1931).
[h] T. M. K. Nedungadi, Proc. Indian Acad. Sci. **8A**, 397 (1938).

rupole coupling in ionic crystals are summarized in Table I.

3. ANALYSIS OF THE EXPERIMENTAL DATA

In general, the quadrupole coupling observed in a solid is a function of several variables, some of which are related. For the present purposes, we may consider the quadrupole coupling constant ν to be a function of the molar or unit cell volumes, the temperature and the molecular torsional oscillations or lattice frequencies, ν_l. Thus, we write

$$\nu=f(\nu_l, V, T), \tag{3}$$

and the functional dependence upon volume can be obtained by an appropriate separation of variables. This separation of variables has been discussed[1,2] and will not be repeated here. Upon solution for the volume dependence of ν, the following relationship is found

$$\alpha(V/\nu)(\partial\nu/\partial V)_{T,\nu_l}=(2T/\nu_l)(\partial\nu_l/\partial T)_P(1/V)(\partial\nu/\partial T)_P$$
$$+[(2T/\nu_l)(\partial\nu_l/\partial T)_P-1](1/\nu)(\partial\nu/\partial P)_T(\alpha/\beta). \tag{4}$$

In order to simplify our notation, we have represented by the one symbol ν_l *all* the lattice frequencies which affect ν. It should be understood that in equations such as Eq. (4), one must take a summation over l of terms in ν_l.

In order to evaluate the volume dependence, it is seen that in addition to the observed pressure and temperature coefficients of ν, one needs experimental values for α, the cubical coefficient of thermal expansion; β, the compressibility; and for $(1/\nu_l)(\partial\nu_l/\partial T)_P$, the temperature coefficient of the lattice frequencies, which is obtained from Raman effect studies of the crystalline solid. Values of the last three quantities are summarized in Table II for $NaClO_3$, $NaBrO_3$ and $NaNO_3$. The temperature coefficient for the Raman frequencies in $NaBrO_3$ is not known; in Table II it was given the same value as that reported for $NaClO_3$ because of the small difference in this quantity for $NaClO_3$ and $NaNO_3$. The thermal expansion and compressibility of $NaNO_3$ are anisotropic and the linear components are listed along with the cubical values. The subscripts $||$ and $\perp$ denote the linear components parallel and perpendicular, respectively, to the hexagonal axis of the crystal. In employing Eq. (4) to obtain $(V/\nu)(\partial\nu/\partial V)_{T,\nu_l}$, the differential form of the volume dependence, it is necessary to know only the cubical coefficients of the compressibility and thermal expansion. All cases now known of the volume dependence of quadrupole coupling constants, obtained in this manner, are listed in Table III. The volume dependences range from $V^{-0.025}$ to $V^{-3.8}$, when the integrated form of Eq. (4) for ν is used.

Before discussion these results further, it should be noted that Eq. (4) can be derived in a manner which includes any anisotropy in compressibility and thermal expansion. One form of the resulting equation is

$$\alpha_{||}(l_{||}/\nu)(\partial\nu/\partial l_{||})_{T,\nu_l}+\alpha_\perp(l_\perp/\nu)(\partial\nu/\partial l_\perp)_{T,\nu_l}$$
$$=(2T/\nu_l)(\partial\nu_l/\partial T)_P(1/\nu)(\partial\nu/\partial T)_P$$
$$+[(2T/\nu_l)(\partial\nu_l/\partial T)_P-1](1/\nu)(\partial\nu/\partial P)_T(\alpha/\beta), \tag{5}$$

where $l_{||}$ and $l_\perp$ are the linear dimensions parallel and perpendicular to a symmetry axis of the crystal. This equation is utilized in the theoretical discussion of $NaNO_3$. In the treatment, it turns out that only the anisotropy of the thermal expansion need be known, and it is fortunate that some very accurate measurements have been made of this quantity.[10] The "bulk" compressibility and thermal expansion of $NaClO_3$ and $NaBrO_3$ are isotropic since both have cubic unit cells.

[10] J. B. Austin and R. H. H. Pierce, Jr., J. Am. Chem. Soc. **55**, 661 (1933).

Na^{23} Coupling

$NaClO_3$ and $NaBrO_3$ are isomorphous and the Na^{23} quadrupole coupling differs by only about 5 percent in the two compounds.[2] Therefore, one would expect the volume dependence of the coupling to be similar and indeed it is, being $V^{-1.9}$ in $NaClO_3$ and $V^{-2.0}$ in $NaBrO_3$. The results for $NaNO_3$ proved to be more interesting. When the appropriate quantities in Tables I and II were combined in Eq. (4), the Na^{23} coupling in $NaNO_3$ was found to be proportional to $V^{-3.8}$. This is an even more violent departure from the idealized V^{-1} dependence than that found in $NaClO_3$ and $NaBrO_3$. This unusually large volume dependence for a compound in which the bulk volume change is anisotropic suggested that anisotropic changes in the interionic distances are responsible for the deviations from a V^{-1} dependence of the Na^{23} coupling observed in $NaClO_3$ and $NaBrO_3$ as well as in $NaNO_3$. The remainder of this paper is devoted mainly to investigating whether such is indeed the case.

Cl^{35} Coupling

Kushida *et al.*[1] have reported previously that the Cl^{35} coupling constant in $KClO_3$ varies as $V^{-0.025}$. It is interesting to see how a change in the cation affects this relatively small volume dependence. We have not made a systematic study of the chlorates; however, sufficient experimental data are available in the literature for the volume dependence to be evaluated for the Cl^{35} coupling in $NaClO_3$, and the result seems well worth discussing. The pressure coefficient[11] of the Cl^{35} coupling constant in $NaClO_3$ is 0.93×10^{-6} kg^{-1} cm^2 and the temperature coefficient[12] is -1.4×10^{-4} deg^{-1}. This information, together with the data given in Table II, yields via Eq. (4) the result that $(V/\nu)(\partial\nu/\partial V)_{T,\nu_l}=-0.10$, or $\nu\propto V^{-0.10}$, for the Cl^{35} coupling constant in $NaClO_3$.

That the volume dependence of the Cl^{35} coupling is small in $NaClO_3$ as well as in $KClO_3$ is not surprising. It is consistent with the view that the major contribution to the field gradient at the chlorine nucleus comes from the electron distribution in the ClO_3^- ion, which is affected only slightly by a volume change. However, the fact that the volume dependence is nonetheless four times as great in $NaClO_3$ as in $KClO_3$ merits further consideration. The most probable cause of this difference is the difference in crystal structure of the two compounds.[6,13,14] $KClO_3$ belongs to the monoclinic crystal system, while $NaClO_3$ is cubic. The ClO_3^- groups have very nearly the same size and shape in the two compounds.

TABLE III. The experimentally determined volume dependence of the electric quadrupole coupling constant for various nuclear species in ionic solids, at atmospheric pressure and 25°C.

Compound	Nucleus	Volume dependence
$KClO_3$	Cl^{35}	$V^{-0.025}$ [a]
$NaClO_3$	Cl^{35}	$V^{-0.10}$
Cu_2O	Cu^{63}	$V^{-0.96}$ [a]
$NaClO_3$	Na^{23}	$V^{-1.9}$ [b]
$NaBrO_3$	Na^{23}	$V^{-2.0}$
$NaNO_3$	Na^{23}	$V^{-3.8}$

[a] Reference 1.
[b] Reference 2.

The different volume dependence of the Cl^{35} coupling in the two chlorates could also arise, at least in part, from different interionic contributions to the field gradient. This possibility is suggested by the observation[15] that the Cl^{35} coupling constant is larger in $NaClO_3$, 59.84 Mc/sec at room temperature, than in $KClO_3$, 56.17 Mc/sec. In order to investigate the question and also to provide a check on our model for the Na^{23} volume dependence, we have calculated the interionic contribution to the field gradient at the chlorine nuclei in the two compounds.

4. CALCULATION OF FIELD GRADIENTS IN IONIC CRYSTALS

There are two more or less separate phases to a quantitative, theoretical investigation of the volume dependence of quadrupole coupling constants. First, a model is assumed for the charge distribution in the lattice and calculations are made of the resulting electric field gradient at the nuclear species in question, using lattice parameters for some particular temperature and pressure, usually NTP. If the result agrees with the experimentally determined field gradient, or if some reasonable modification can be made in the model to produce agreement, then the calculations are repeated changing the internuclear distances and molar volume in some systematic fashion.

In our calculations we assume a point charge model for the ionic lattice. There is the problem of the charge distribution on the XO_3^- ions; this, we treat as a parameter to be determined by comparison with experiment. For this model, is is relatively easy to calculate field gradients produced by charges external to the atom or ion in question. However, the electron distribution within the atom or ion is itself polarized by the externally developed field gradient. The resultant enhancement or diminution of the coupling constant is described by the shielding parameter,[16–19] γ_∞, according to the equation for an axially symmetric field,

$$e^2qQ/h=(eQ/h)(1-\gamma_\infty)\phi_{zz}, \qquad (6)$$

[11] Benedek, Bloembergen, and Kushida, Bull. Am. Phys. Soc., Ser. II **1**, 11 (1956).
[12] T. C. Wang, Ph.D. thesis, Columbia University, 1955 (unpublished).
[13] C. Aravindakshan, Z. Krist. **111**, 35 (1958).
[14] H. Zeldes and R. Livingston, J. Chem. Phys. **26**, 1102 (1957).
[15] Wang, Townes, Schawlow, and Holden, Phys. Rev. **86**, 809 (1952).
[16] T. P. Das and R. Bersohn, Phys. Rev. **102**, 733 (1956).
[17] Foley, Sternheimer, and Tycho, Phys. Rev. **93**, 734 (1954).
[18] R. Sternheimer and H. Foley, Phys. Rev. **102**, 731 (1956).
[19] E. G. Wikner and T. P. Das, Phys. Rev. **109**, 360 (1958).

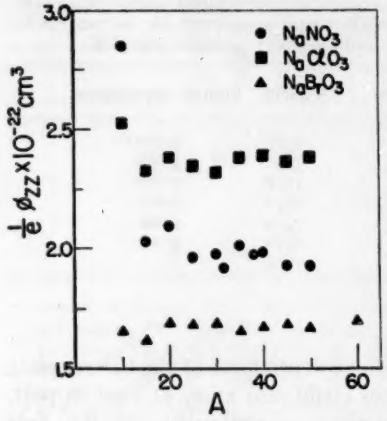

FIG. 2. The field gradients calculated at the sodium nuclei in $NaNO_3$, $NaClO_3$, and $NaBrO_3$ by means of Eq. (7), plotted as a function of the radius, R, over which the summation extended. The charge on the X atom, where X=N, Cl, and Br, was assumed to be zero for purposes of comparison.

where ϕ_{zz} is the direct contribution to the field gradient along the z axis, from all charges external to the atom or ion. We shall calculate ϕ_{zz} and assume that γ_∞ is independent of volume.

Field Gradients at Na in $NaXO_3$ Compounds

Calculation of ϕ_{zz}

The field gradients at the sodium atoms in $NaClO_3$, $NaBrO_3$ and $NaNO_3$ have been calculated by Bersohn[4] who also used a point charge model. His calculations have been repeated and extended. From Eq. (2), we can write

$$\phi_{zz}=\sum_j e_j\sum_i[(3\cos^2\theta_{iz}-1)/r_i^3] \qquad (7)$$

where the inner summation is over all atoms i of type j with a point charge e_j. For the $NaXO_3$ compounds, it was assumed that $e_{Na}=+e$, $e_X=ze$, and $e_O=-(1+z)e/3$, so that the charge distribution in the XO_3^- group is represented by a single parameter, z, the charge on the X atom. In accordance with the conditionally convergent properties of Eq. (7), the inner summations were performed over a sphere of radius R by means of the University of Illinois digital computer, the Illiac.[20] The convergence was examined directly by repeating the computation for different values of R, as shown in Fig. 2 for the three compounds. It is seen that the values for the field gradients converge at $R\cong50$ A.

The summations obtained for the different types of atoms are given in Table IV for $NaNO_3$ and in Table V for $NaClO_3$ and $NaBrO_3$. In the case of $NaNO_3$, the six O atoms in the unit cell contribute equally to the field gradient at Na^I, as do the two N atoms. Therefore, summations were made for only one atom of each type, and the total external field gradient experienced by the sodium atoms in $NaNO_3$ was found by multiplying the results in Table IV, for $R=50$ A, by the number of atoms of each type. The result is

$$\phi_{zz}(\text{at Na in } NaNO_3)=(0.01957-0.02687z_N)\times e\times10^{24}\text{ cm}^{-3}. \qquad (8)$$

The summations in Table V, for $R=50$ A, lead to the following result for $NaClO_3$:

$$\phi_{zz}(\text{at Na in } NaClO_3)=(-0.02004+0.01202z_{Cl})\times e\times10^{24}\text{ cm}^{-3}; \qquad (9)$$

and to the following, for $NaBrO_3$, for $R=60$ A

$$\phi_{zz}(\text{at Na in } NaBrO_3)=(-0.01701+0.02282z_{Br})\times e\times10^{24}\text{ cm}^{-3}. \qquad (10)$$

Equation (9) for $NaClO_3$ is derived from the recently refined structural parameters listed in Table V. The lattice sums for the old parameters give the following:

$$\phi_{zz}(\text{at Na in } NaClO_3)=(-0.02380+0.00799z_{Cl})\times e\times10^{24}\text{ cm}^{-3}. \qquad (11)$$

The high sensitivity of ϕ_{zz} to the lattice parameters is shown by comparison of this equation with Eq. (9). A 20% change in ϕ_{zz} results from changes in the lattice parameters of only about one percent. In this comparison, it was assumed that the convergence of the lattice sums shown in Fig. 2 for the unrefined structure applied to the refined structure, for which only the sums for $R=50$ A were calculated.

Estimations of z_X

Equation (6) can be combined with Eqs. (8) to (10) to calculate z_X, the effective charge on the X atom, provided that values are known for the coupling constants; for the Na^{23} quadrupole moment, Q_{23}; and for the shielding factor, γ_∞, of the sodium nucleus in the $NaXO_3$ compounds. Of these quantities, the Na^{23} quadrupole coupling constants are obtained most directly and accurately from experiment. The value in $NaNO_3$ is 334 kc/sec,[8] and in $NaClO_3$ and $NaBrO_3$, 779 kc/sec and 842 kc/sec, respectively.[2] These coupling constants may be either positive or negative, so that when the values are substituted in Eqs. (6) and (8)–

TABLE IV. Contributions to the electric field gradient at Na^I in $NaNO_3$,[a] calculated for $R=50$ A.

Atom	Coordinates	Field gradient per unit charge
Na^I	$\frac{1}{2}, \frac{1}{2}, \frac{1}{2}$	$-0.01601\times e\times10^{24}$ cm^{-3}
Na^{II}	$\frac{1}{2}, \frac{1}{2}, \frac{1}{2}$	0.03257
N	0, 0, 0	−0.01494
O	$u, u, 0$	−0.00150

[20] We are indebted to the Digital Computer Laboratory and its staff for their assistance.

[a] The NTP crystal parameters used in the calculations were taken from reference 7; they are $a=6.3108$ A, $\alpha=47°16'$, $u=0.242$.

TABLE V. Contributions to the electric field gradient at Na^I in $NaClO_3$ and $NaBrO_3$.

Atom	Coordinates	Field gradient per unit charge, in units of $e\times10^{24}$ cm^{-3} $NaClO_3$[a] $R=50$ A	$NaClO_3$[b] $R=50$ A	$NaBrO_3$[a] $R=60$ A
Na^I	u, u, u	0	0	0
Na^{II}	$u+\frac{1}{2}, \frac{1}{2}-u, \bar{u}$	−0.00315	−0.00326	−0.00373
Cl^I, Br^I	v, v, v	0.01539[c]	0.01581	0.02139
Cl^{II}, Br^{II}	$v+\frac{1}{2}, \frac{1}{2}-v, \bar{v}$	0.00232	0.00215	0.00242
O^I	x, y, z	0.00026	0.00051	−0.00054
O^{II}	$x+\frac{1}{2}, \frac{1}{2}-y, \bar{z}$	−0.00778[c]	−0.00674	−0.00302
O^{III}	$\bar{x}, y+\frac{1}{2}, \frac{1}{2}-z$	0.00956	0.00850	0.00420
O^{IV}	$\frac{1}{2}-x, \bar{y}, z+\frac{1}{2}$	0.01232	0.007980	0.00518
a_0		6.555 A	6.5755 A	6.689 A
u		0.064	0.0659	0.075
v		0.417	0.4168	0.405
x		0.303	0.3052	0.258
y		0.592	0.5921	0.614
z		0.500	0.4936	0.480

[a] Crystal structure from reference 6.
[b] Crystal structure according to Bower, Sparks, and Trueblood (personal communication from K. Trueblood). Lattice constant from Swanson and Fuyat, Natl. Bur. Standards Circular No. 539, 3, 51 (1954).
[c] These lattice sums differ by a significant amount from the corresponding values given in reference 4. Recalculations of the field gradient in $NaClO_3$ by R. Bersohn (personal communication) gave new values agreeing with those listed here.

(10) for $NaNO_3$, $NaClO_3$, and $NaBrO_3$, respectively, we obtain

$$(e^2/h)(0.01957-0.02687z_N)10^{24}(1-\gamma_\infty)_{Na}+Q_{23}=\pm334\times10^3$$

$$(e^2/h)(-0.02004+0.01202z_{Cl})10^{24}(1-\gamma_\infty)_{Na}+Q_{23}=\pm779\times10^3$$

$$(e^2/h)(-0.01701+0.02282z_{Br})10^{24}(1-\gamma_\infty)_{Na}+Q_{23}=\pm842\times10^3. \quad (12)$$

The nuclear quadrupole moment of Na^{23} has been determined from atomic beam measurements[21] on sodium atoms in a $3\,^2P_{\frac{1}{2}}$ state, using a Sternheimer correction factor[22] of C=0.97. Of the two values, +0.100 and −0.836 barn, which result from the two possible assignments of the transitions observed in the atomic beam experiments, the former is most likely on theoretical grounds.[21] Recently, a new correction factor, C=0.805, has been calculated[23]; the resulting two values for Q_{23} are $+0.087\pm0.010$ and -0.732 ± 0.024 barn. Of these, the positive value, +0.087 barn, seems to be most likely for the same reasons given[21] in discussing the original values derived from C=0.97. However, both new values were used in computing z_X to ascertain whether additional support could be found for the choice $Q_{23}=0.087$. The best available value of γ_∞ for Na^{23} appears to be −4.53, which was calculated for a free Na^+ by a variational method.[16] This value of γ_∞ was substituted in Eq. (12) and z_X was calculated for each choice of Q_{23} for both positive and negative coupling constants. The results are summarized in Table VI.

In the XO_3^- groups, oxygen is more electronegative than N, Cl, and Br, which would tend to make the X atoms positive with respect to O. However, because of the net negative charge on the XO_3^- groups, and its tendency to concentrate on the outside of the ion, one would expect that X would nonetheless have a small negative charge, or at most a very small positive charge. On this basis, the only reasonable value of z_X in Table VI is $z_N=-0.001$ for $Q_{23}=0.087$ and a positive coupling constant in $NaNO_3$. Unfortunately, there are several possible causes of the unreasonably large values for z_{Cl} and z_{Br}. The point charge model used in calculating ϕ_{zz} is an idealization whose inadequacies have been commented upon previously.[24] Also, the value of ϕ_{zz} is very sensitive to the structural parameters, which are not known as accurately for $NaBrO_3$ as for $NaClO_3$ and $NaNO_3$. Finally, the value of γ_∞ for Na^+ in a solid will differ from the free ion value[24] used in the calculations, because of changes in excitation energies and the presence of overlap and covalency effects.

Variations in γ_∞ may contribute to the apparent difference between z_N, and z_{Cl} and z_{Br}. In $NaNO_3$, the Na^+ is equidistant from the two nearest N atoms on the symmetry axis; but this not the case for Na^+ in the chlorate and bromate. Therefore, different values of γ_∞ may be required for the different compounds.

Calculation of z_{Cl} from the Cl^{35} Quadrupole Coupling Constant

Although we lack enough data to explore in detail the possibilities mentioned in the preceding paragraph, it is possible to make an independent estimate of z_{Cl}

[21] Pearl, Rabi, and Senitzky, Phys. Rev. 98, 611 (1955).
[22] R. M. Sternheimer, Phys. Rev. 95, 736 (1954).
[23] R. M. Sternheimer, Phys. Rev. 105, 158 (1957).
[24] M. H. Cohen and F. Reif, Solid State Physics 5, 321 (1957).

TABLE VI. Values of the effective charge, z_X, in the $NaXO_3$ salts, derived by means of Eq. (12), for the two possible values of Q_{23}, the Na^{23} quadrupole moment; using the calculated field gradients ϕ_{zz}, the coupling constants observed for Na^{23}, and the calculated value of -4.53 for γ_∞ in Na^+.

Salt	e^2Qq/h	z_X for $Q_{23}=0.087$ barn	z_X for $Q_{23}=-0.732$ barn
$NaNO_3$	+334 kc/sec	−0.001	0.82
	−334	1.47	0.64
$NaClO_3$	+779	5.54	1.21
	−779	−2.20	2.13
$NaBrO_3$	+842	2.88	0.48
	−842	−1.45	1.01

from the Cl^{35} quadrupole coupling constant observed in $NaClO_3$. Bersohn was discouraged from doing this because of the necessity for very accurate bond angles in the XO_3^- group.[4] However, the recent refinement of the structural parameters for $NaClO_3$ makes it of interest to estimate z_{Cl} using the extension of the Townes and Dailey[25] method described by Das and Hahn.[26]

Details of the calculation will not be given because they are identical with the earlier work[26] except for the angle, θ, between the C_{3v} axis and the Cl—O bond of the ClO_3^- group. The recent structural determination[27] gives a value of 107.4° for the O—Cl—O angle, which corresponds to $\theta=111.5°$. With this value for θ and with the same assumptions as before,[26] namely that q_{zz} (at Cl in ClO_3^-) is negative and is entirely caused by p electrons on the chlorine, the ionic character of the Cl—O bond is found to be $I=-0.21$, where the negative sign indicates a shift of electron density toward the chlorine. The valence shell around the chlorine consists of two electrons from the lone pair orbital, plus $1-I$ electrons from each Cl—O bond, so z_{Cl} would have to be +1.37. The standard deviation in the determination of the O—Cl—O angle[27] is ±1.5°, which puts limits of +1.22 and +1.55, respectively, on z_{Cl}. This large separation of charge over the small structure of the chlorate ion is surprising. It requires that γ_∞ for Na^+ be unreasonably large, about −71, for the preferred value of Q_{23}, 0.087 barn, compared with the calculated value[16] $\gamma_\infty=-4.5$ for the free ion.

The calculation assumes that the ClO_3^- ion is free, while in actuality it is surrounded by other ions in the crystal, the nearest neighbors being Na^+ ions. It is likely that the nearby ions will polarize the negative charge cloud of the ClO_3^- ion and thereby affect the hybridization of the orbitals in the ClO_3^- ion. In fact, a 4% increase in s character of each Cl—O bond, accompanied by a 12% decrease in s character of the lone pair orbital, will give a neutral charge on the chlorine *via* the Townes and Dailey routine. The effects of d hybridization and double bond character have also been neglected. Similar considerations apply to $NaBrO_3$. We conclude that the charge distribution within a polyatomic ion such as ClO_3^- in a crystalline environment cannot be determined very well by this method.

[25] C. H. Townes and B. P. Dailey, J. Chem. Phys. **17**, 782 (1949).
[26] Reference 3, pp. 153–154, Eq. (7.52).

Comparison of the Nitrate with the Halates

One would like to have an explanation of why the point charge model works well for $NaNO_3$, while poor results are obtained for $NaClO_3$ and $NaBrO_3$. The main difference between the XO_3^- ions of the two groups is that in the halate compounds there is a lone pair orbital which is occupied by two electrons, while in the nitrate case this orbital is empty. Since the orbital lies on the symmetry axis and points toward the sodium, overlap effects might be expected to occur in the halates. Charge transfer involving the lone pair orbital would also be more probable in the case of the halates.

In the succeeding discussion, it will be seen that the point charge model and the charge distribution derived from Eq. (12) for $NaNO_3$ provides a reasonable interpretation of the experimental results for the crystal. However, the model certainly needs further investigation for the halate compounds even though the situation can be improved by adjusting the values of γ_∞ and z_X for these compounds.

Volume Dependence of Field Gradients at Na

In order to obtain from Eq. (7) a theoretical volume dependence of ϕ_{zz} other than V^{-1}, anisotropic changes must occur in the interionic distances, r_i. Two types of anisotropy are possible: (a) Anistotropic changes in the unit cell dimensions, and (b) anisotropic changes in the atomic positions within the unit cell. $NaClO_3$ and $NaBrO_3$ have cubic unit cells,[6] so only type (b) anisotropy can occur. However, $NaNO_3$ can be described as hexagonal,[6,7] its unit cell expands anisotropically, and type (a) as well as type (b) anisotropy must be considered.

$NaNO_3$

Two models were investigated for $NaNO_3$. In the first of these, an "homogeneous" model, it is assumed that the atomic positions change in proportion to the anisotropic changes in the unit cell dimensions. The second, an "inhomogeneous" model, assumes that the size and shape of the NO_3^- group are unaffected while the other atomic positions change in proportion to the unit cell dimensions. The general procedure in making the analysis is the following. By combining Eqs. (4) and (5), we obtain the relationship,

$$\alpha_{||}(l_{||}/\nu)(\partial\nu/\partial l_{||})_{T,\nu_l}+\alpha_\perp(l_\perp/\nu)(\partial\nu/\partial l_\perp)_{T,\nu_l} =\alpha(V/\nu)(\partial\nu/\partial V)_{T,\nu_l}. \quad (13)$$

Moreover, if γ_∞ is independent of volume, we can assert from Eqs. (1) and (6) that

$$(1/\nu)(\partial\nu/\partial l_{||})_{T,\nu_l}=(1/\phi_{zz})(\partial\phi_{zz}/\partial l_{||})$$

and

$$(1/\nu)(\partial\nu/\partial l_\perp)_{T,\nu_l}=(1/\phi_{zz})(\partial\phi_{zz}/\partial l_\perp). \quad (14)$$

Upon substituting Eq. (14) in Eq. (13), we find that

$$(\alpha_{||}/\alpha)(l_{||}/\phi_{zz})(\partial\phi_{zz}/\partial l_{||})+(\alpha_\perp/\alpha)(l_\perp/\phi_{zz})(\partial\phi_{zz}/\partial l_\perp)$$
$$=(V/\nu)(\partial\nu/\partial V)_{T,\nu_l}. \quad (15)$$

The left-hand side of Eq. (15) can be evaluated from the known anisotropic and cubical expansion coefficients together with computed values of $\partial\phi_{zz}/\partial l_{||}$ and $\partial\phi_{zz}/\partial l_\perp$ for the sodium atoms. This procedure amounts to a "weighting" of the two contributions to $\partial\phi_{zz}/\partial V$, by their thermal expansion coefficients. In the calculations, the hexagonal description of $NaNO_3$ is used; the hexagonal c axis is designated as $l_{||}$ and the hexagonal a axis as $l_\perp$. ϕ_{zz} is calculated for independent variations in $l_{||}$ and $l_\perp$. It should be noted that changing $l_\perp$ affects the hexagonal faces of the unit cell, and is thus a change in two dimensions rather than a linear change. The results of the calculations are shown in Fig. 3 where ϕ_{zz} is plotted as a function of the fractional change in l for the terms that are independent of z_N. A like graph, not shown here, results from the terms dependent upon z_N. In the figure, $\Delta_{||}$ and $\Delta_\perp$ refer to the dependence of ϕ_{zz} upon homogeneous changes in all atomic positions as $l_{||}$ and $l_\perp$ are changed. For the inhomogeneous model, only $(\partial\phi_{zz}/\partial l_\perp)'\equiv\Delta_\perp'$ differs from the value for the other model. The reason is that the NO_3^- group is planar and perpendicular to $l_{||}$; its dimensions are not changed in either model by a change in $l_{||}$.

The slopes of the curves at $\Delta l/l^0=0$ in Fig. 3 give the dependence of ϕ_{zz} upon $l_{||}$ and $l_\perp$ at NTP for the two

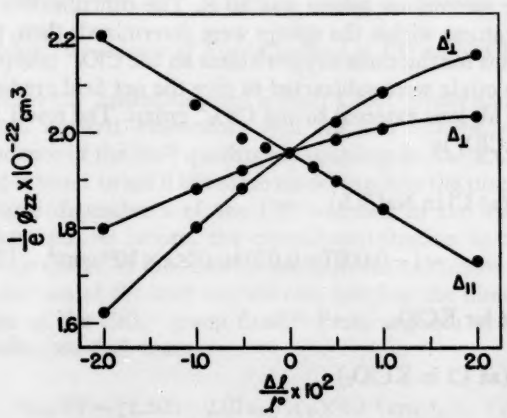

FIG. 3. The field gradient calculated at the sodium nuclei in $NaNO_3$ by means of Eq. (7), plotted as a function of the lattice parameters. $\Delta_{||}$ and $\Delta_\perp$ indicate homogeneous changes in atomic positions along the hexagonal c and a axes, respectively. $\Delta_\perp'$ indicates a similar change along the hexagonal a axis except that the NO_3^- group retains its size and configuration. Only the terms independent of z_N are included in the values for ϕ_{zz} given in this figure.

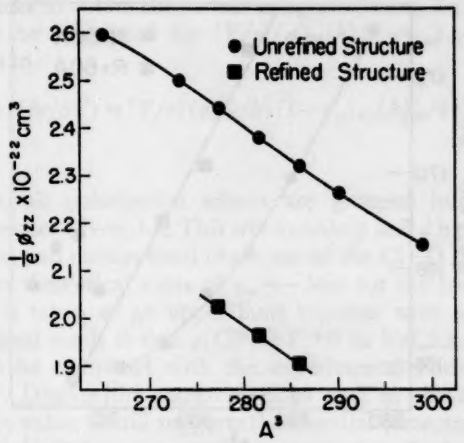

FIG. 4. The field gradient calculated at the sodium nuclei in $NaClO_3$ by means of Eq. (7), plotted as a function of the volume of the cubic unit cell. It was assumed in the calculations that the ClO_3^- group retains its size and configuration while the other atomic positions change homogeneously. Only the terms independent of z_{Cl} are included in the values for ϕ_{zz} given in this figure.

models. The results, including the terms in z_N are as follows:

$$(l_{||}/\phi_{zz})(\partial\phi_{zz}/\partial l_{||})$$
$$=(-0.114-0.134z_N)/(0.0196-0.0269z_N)$$
$$(l_\perp/\phi_{zz})(\partial\phi_{zz}/\partial l_\perp)$$
$$=(0.0636+0.196z_N)/(0.196-0.0269z_N)$$
$$(l_\perp/\phi_{zz})(\partial\phi_{zz}/\partial l_\perp)'$$
$$=(0.143+0.278z_N)/(0.0196-0.0269z_N). \quad (16)$$

If these values, together with the coefficients of thermal expansion, are used in Eq. (15), and the charge z_N is set equal to zero as surmised from Eq. (12), we find that $\nu\propto V^{-4.2}$ for the homogeneous model with atomic positions changing in proportion to the unit cell parameters. If the NO_3^- group retains its size and shape, we find that $\nu\propto V^{-3.9}$, which is in better agreement with the experimental value of $\nu\propto V^{-3.8}$ for the Na^{23} coupling constant.

$NaClO_3$ *and* $NaBrO_3$

For these compounds, ϕ_{zz} was calculated as a function of the cubic unit cell volume, assuming that the XO_3^- group retains its size and configuration while the other atomic positions change homogeneously. The results for the terms independent of z_{Cl} in $NaClO_3$ are shown in Fig. 4 for both the unrefined and refined structures. For the refined structure, the extrenal field gradient at the sodium atoms, including the terms in z_{Cl}, is given as the following function of volume,

$$(V/\phi_{zz})(\partial\phi_{zz}/\partial V)$$
$$=(0.0420-0.0085z_{Cl})/(-0.0200+0.0120z_{Cl}). \quad (17)$$

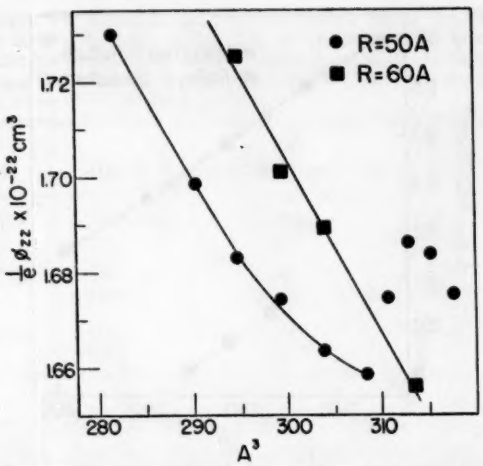

FIG. 5. The field gradient calculated at the sodium nuclei in $NaBrO_3$ by means of Eq. (7), plotted as a function of the volume of the cubic unit cell. It was assumed in the calculations that the BrO_3^- group retains its size and configuration while the other atomic positions change homogeneously. Only the terms independent of z_{Br} are included in the values for ϕ_{zz} given in this figure. The discontinuity in ϕ_{zz} at large unit cell volumes, for $R=50$ A, is due to convergence effects.

Substitution of the experimental $V^{-1.9}$ dependence in Eq. (17) leads to a value for z_{Cl} of -0.28, which is consistent with our assumption of only a small amount of charge on the chlorine. For the unrefined $NaClO_3$ structure, the dependence of the field gradient upon volume is

$$(V/\phi_{zz})(\partial\phi_{zz}/\partial V)$$
$$=(0.0428+0.0030z_{Cl})/(-0.0238+0.0080z_{Cl}). \quad (18)$$

In this case, a charge of $z_{Cl}=+0.2$ is required to fit the experimental $V^{-1.9}$ dependence, which indicates the sensitivity of the parameters to small changes in crystal structure.

The results for the terms independent of z_{Br} in $NaBrO_3$ are shown in Fig. 5. The summations in ϕ_{zz} for a sphere of radius $R=50$ A exhibit a discontinuity at larger volumes, apparently because of convergence effects. Therefore, some of the points were recalculated for $R=60$ A. The slope of the ϕ_{zz} *vs* V plot is somewhat different at the larger R, and the discontinuity no longer appears. The slope of the terms dependent on z_{Br} did not change in the recalculation. The total volume dependence, for an R of 60 A, is

$$(V/\phi_{zz})(\partial\phi_{zz}/\partial V)$$
$$=(0.0083-0.0299z_{Br})/(-0.0170+0.0228z_{Br}). \quad (19)$$

In order for this equation to match the experimental result that $\nu \propto V^{-2.0}$, it is necessary to have $z_{Br}=1.6$. This value is much larger than those considered feasible in connection with Eq. (12) and the fitting of the Na^{23} coupling constants observed in $NaClO_3$ and $NaBrO_3$ at NTP. Clearly, something is the matter. The point charge model may be worse for $NaBrO_3$ than for $NaClO_3$; the structural parameters for $NaBrO_3$ may not be known with sufficient accuracy for our calculations; or else a rigid BrO_3^- group is not the correct model for the volume changes. The latter possibility could perhaps be checked by a study of the Br^{81} coupling constant, as a function of volume.

Field Gradients at Cl in $NaClO_3$ and $KClO_3$

Calculation of Interionic Contribution to ϕ_{zz}

In the application discussed above of the Townes and Dailey treatment[25] to the ClO_3^- group in order to estimate z_{Cl}, the approximation was made that the coupling constant observed for Cl^{35} in solid $NaClO_3$ is the same as for the free ClO_3^- ion. The approximation is supported by the small volume dependence of the chlorine coupling constant in $NaClO_3$ and $KClO_3$. This point, as well as the internal consistency of our calculations, can be explored further by calculating the crystalline field contribution to the gradient at the chlorine.

Such calculations were made for $NaClO_3$ and $KClO_3$ using the refined crystal structures for both of these compounds.[27] The lattice sums were performed as before except that the Cl nucleus was taken as the origin. The chlorine nucleus in $NaClO_3$ lies on an axis of symmetry, the same as that for the Na^+ ion. In $KClO_3$ there is a slight asymmetry, $\eta=0.006$, in the field gradient. The z principal axis of the field gradient, for which the summation was made, has been determined experimentally[14] to lie in the *ac* plane of the monoclinic unit cell, at an angle of 57.5° with the *c* axis. This axis does note quite coincide with the axis of the ClO_3^- group, which also lies in the *ac* plane but at an angle of 59.2° from *c*.[27] In both $NaClO_3$ and $KClO_3$, the summation sphere was 50 A. The contributions of all atoms within the sphere were determined; then, the terms for the three oxygen atoms on the ClO_3^- group at the origin were subtracted to give the net field gradient for all ions external to the ClO_3^- group. The result for $NaClO_3$ is

$$\phi_{zz}(\text{at Cl in } NaClO_3)$$
$$=(-0.0087-0.0293z_{Cl})\times e\times 10^{24}\ \text{cm}^{-3}, \quad (20)$$

and for $KClO_3$,

$$\phi_{zz}(\text{at Cl in } KClO_3)$$
$$=(-0.0201-0.0625z_{Cl})\times e\times 10^{24}\ \text{cm}^{-3}. \quad (21)$$

If we assume that $z_{Cl}=1.37$ is the correct value for both $NaClO_3$ and $KClO_3$ and introduce values of

[27] See reference b in Table V.

-0.085 barn[4] and $+1$ for the Q and $(1-\gamma_\infty)$ of Cl^{35}, respectively, we find from Eqs. (6), (20), and (21) that the crystalline field contribution to the Cl^{35} coupling is $+0.14$ and $+0.31$ Mc/sec for $NaClO_3$ and $KClO_3$. These values are to be compared with the observed[15] total coupling constants of 59.84 and 56.17 Mc/sec, respectively, both of which are presumably positive.[26] The use of $+1$ for $(1-\gamma_\infty)$ requires that γ_∞ be zero, which would indeed be the case if we were dealing with a free ClO_3^- ion. This follows from the use of the experimental O—Cl—O angle to determine via the Townes and Dailey route[25] the bond hybridization and thence the value of 1.37 used for z_{Cl}. In effect, this procedure fixes the electronic wave function of the ClO_3^- ion. Polarization of the ClO_3^- ion by the crystalline field not only makes $\gamma_\infty \neq 0$ but also complicates the relation between z_{Cl} and the bond angles. In any case, the results support our previous assumption that the crystalline field contribution to the coupling is small compared with the intra-ClO_3^- contribution.

There is still the question as to why the Cl coupling is larger in the $NaClO_3$ than in $KClO_3$. However, both the crystalline and the intra-ClO_3^- field gradient are very sensitive to z_{Cl}. Polarization of the ClO_3^- ion by its crystal environment could produce a different charge distribution and a different effective $(1-\gamma_\infty)_{Cl}$ in the two chlorates and account for the discrepancy. If this is the case, the polarization need have only a small dependence upon volume in order to maintain consistency with the experimental findings. If instead of 1.37 for z_{Cl}, we use the -0.28 value which fits the volume dependence of the sodium coupling in $NaClO_3$, the sign of the crystalline field contribution to ϕ_{zz} for Cl is changed but the magnitude is still very small and the preceding qualitative discussion still applies even if one uses for γ_∞ the large value of -56.6 calculated for the free Cl^- ion.

Volume Dependence of Field Gradient at Cl^{35} *in* $NaClO_3$

Since the assumptions of a rigid ClO_3^- group and a $z_{Cl} \cong 0$ account reasonably well for the volume dependence of the Na^{23} quadrupole coupling in $NaClO_3$, it is of interest to see if the same model predicts the proper volume dependence of the Cl^{35} coupling in the same compound. As before, the crystal contribution to the field gradient at the chlorine nucleus was calculated as a function of the unit cell volume, keeping the dimensions of the ClO_3^- group fixed.[28] From a graph of the results, we find that

$$\partial\phi_{zz}/\partial V = (1.506 - 2.01 z_{Cl}) \times e \times 10^{-4}\ \text{cm}^{-6}. \quad (22)$$

[28] In changing the volume of the unit cell while keeping the dimensions of the XO_3^- group fixed, one point on the XO_3^- group must be considered as "attached" to the unit cell. The anisotropic changes in interatomic positions depend to some extent upon the choice of this point. In all of the calculations described here, the point of attachment was taken to be the X nucleus.

In order to obtain the correct integrated form, Eq. (22) must be multiplied by $(V/\nu)(eQ_{35}/h)(1-\gamma_\infty)_{Cl}$; this leads to

$$(V/\nu)(\partial\nu/\partial V) = (V/\nu)(eQ_{35}/h)(1-\gamma_\infty)_{Cl}(\partial\phi_{zz}/\partial V). \quad (23)$$

Here, all polarization effects are grouped into the parameter $(1-\gamma_\infty)_{Cl}$. This will include p and d hybridization and double bond character of the Cl—O bonds. If the theoretical value of $\gamma_\infty = -56.6$ for the free Cl^- ion[4] is taken as an upper limit together with $z_{Cl} \cong 0$, the final result is that $\nu(Cl^{35}) \propto V^{-0.12}$ in $NaClO_3$. This is to be compared with the experimental finding of $V^{-0.1}$. Despite the approximations used to obtain the above value, it still supports the essential correctness of the rigid ClO_3^- group model because of the high sensitivity of the intra-ClO_3^- chlorine coupling to changes in bond angles.

The volume dependence of the Cl^{35} coupling in $KClO_3$ was not calculated theoretically because it is not known how the orientation of the principal axes of the field gradient change with a change in volume.

Throughout the discussion in this work, the question of the charge distribution within the chlorate and bromate ions has not been satisfactorily solved. In the case of $NaNO_3$ a neutral charge on the nitrogen gave consistent results for both the field gradient at the sodium and for the volume dependence of the Na^{23} coupling. In $NaClO_3$ three independent estimates of z_{Cl} could be made which differed widely from one another. The value of $z_{Cl} = -0.28$ obtained from the volume dependence of the Na^{23} coupling in $NaClO_3$ was the only one of the three that approached the expected neutral charge on the chlorine.

5. CONCLUSION

Although the approximations and assumptions made in our analysis leave much to be desired, the results show that anisotropic changes in atomic positions are the main source of the deviations observed from a V^{-1} dependence for quadrupole coupling constants in solids. Studies of this nature reflect in a very sensitive fashion the structural changes in a crystal. The chief difficulty encountered is that the observed quantities are insufficient to determine all of the several parameters which govern the quadrupole coupling. The seriousness of this problem is reduced if more than one quadrupole constant can be observed in the same crystal, as in the case of $NaClO_3$.

Also, it is apparent that very accurate measurements of crystal parameters are necessary if quadrupole coupling data are to be of maximum usefulness in investigating the electronic structure of solids. For example, if there were available precise crystal data as a function of temperature and pressure for the crystals studied here, it would be possible to draw some conclusions about the point-charge model and charge distribu-

tions rather than about the volume dependence of the atomic positions. The cause might be found of the apparent large variation in $(1-\gamma_\infty)_{Na^+}$ needed to explain the coupling in the $NaXO_3$ compounds.

A last point concerns the calculation of the lattice sums. Our results for ϕ_{zz} as a function of the radius of summation confirm Bersohn's result[4] that the field gradients in ionic crystals are of long-range origin. This makes the calculations lengthy. However, high-speed computers are becoming increasingly available, and general programs can be developed without great difficulty for calculating the field gradient in an arbitrary direction for a crystal of arbitrary type.

ACKNOWLEDGMENTS

We are very grateful to Dr. Geneva Belford for the excellent Illiac routine used in computing the lattice sums and to Professor K. Trueblood for sending us his x-ray results on $NaClO_3$ and $KClO_3$ prior to publication. Also, we are indebted to Professor R. Bersohn and Martin Karplus for a number of helpful communications and discussions.

THE JOURNAL OF CHEMICAL PHYSICS VOLUME 32, NUMBER 4 APRIL, 1960

Ligand-Field Theory of Linear Gaseous Molecules Involving the First Transition Series Elements*

ROBERT A. BERG AND OKTAY SINANOGLU†

Department of Chemistry and Lawrence Radiation Laboratory, University of California, Berkeley, California

(Received November 5, 1959)

The diatomic and linear triatomic molecules such as the oxides and halides of the "iron-group" elements are of importance in high temperature systems. Although the various high symmetry compounds of these elements, e.g., the solid oxides, hydrated complexes, etc., are sufficiently understood in terms of the present ligand-field theory, no semiquantitative schemes have been utilized to understand and predict the spectroscopic and thermal properties of their simple, gaseous molecules. In this article, the observed dissociation energy vs atomic number curves for the linear gaseous oxides and the halides of the first transition series are compared with the corresponding energy curves of the solid oxides and the halides, and the similarities are pointed out. It is shown that the double maximum stabilization curves observed in the gaseous molecules as well can be understood in terms of the splitting of the (3*d*) shell of the transition atoms in a linear ($C_{\infty v}$ or $D_{\infty h}$ symmetry) ligand field with two independent splitting parameters, one of which is small. A method for predicting the low-lying molecular spectral states is developed. The energies of the states depend on the splitting parameters and the electron interactions. The parameters are estimated from the first portion of the thermal data and used only for these elements. The electron interaction energy is obtained from the spectral terms of free atoms (ions). Unlike the case in the high symmetry applications, this procedure here takes into account "electronic correlation" (configuration interaction) effects. The generality of the treatment is revealed by comparing the results of the simple ionic and covalent models with those of the molecular orbital method. Calculations of spectral states are made for ScO, TiO, VO, and CrO, and experimental data are discussed.

DIATOMIC and linear triatomic gaseous molecules involving metals of the first transition series are of chemical and astrophysical interest. However there are no simple ways of predicting their spectroscopic states or dissociation energies. The usual semiempirical molecular orbital method[1] has been applied to correlate spectral data of homonuclear and heteronuclear molecules of the first three periods; by analogy one can treat the states of similar heavier gaseous species when sufficient data exist for comparison. The success of this method has been due to two favorable circumstances; first, as in the atomic case, light molecules have fewer low-lying states and have less complicated states than heavy molecules; second, the light molecules have been subjected to a great deal of spectral investigation and analysis. As a result it has been possible to draw empirical correlation diagrams showing the crossing points of the energy levels in going from the "separated atoms" to the "united atom" configurations. Neither of these circumstances obtains for the gaseous species of the first transition series. The spectral data,[2] as is well known, are quite incomplete and many of the observed transitions remain unanalyzed because of their complexity. Even the ground states of the molecules are not established. The unfilled inner shells characteristic of the transition metals cause the greatest difficulty in applying a molecular orbital model, particularly in heteronuclear molecules such as oxides or halides.

The variation with atomic number of the heats of dissociation of the gaseous transition-metal compounds also shows interesting features (Figs. 1 and 2).[3] If bonding occurs among the outer electrons of the

* This work was carried out under the auspices of the U.S. Atomic Energy Commission.

† Lawrence Radiation Laboratory Postdoctoral Fellow, 1959–1960.

[1] G. Herzberg, *Spectra of Diatomic Molecules* (D. Van Nostrand Company, Inc., Princeton, New Jersey, 1950), Chap. 6.

[2] *Données Spectroscopiques Concernant Les Molécules Diatomiques*, edited by B. Rosen (Hermann et Cie, Paris, 1951).

[3] Leo Brewer (private communication).

atoms one would expect for either covalent or ionic bonding a smooth, continuous variation in heats. In all cases for which data are available double-humped curves are obtained. Similar anomalous variations of binding energies have been observed for metals,[4] for a wide range of solid compounds[4] and for complexes in solution.[5]

For many years ligand-field theory has been used to explain the magnetic and spectral properties of complexes in solution. Recently Orgel[6] and, independently, Griffith[7] have applied ligand-field theory to solids and to aqueous complexes involving transition metals to explain the observed variation in stabilities across the periodic table. In the presence of electrostatic fields of symmetry commonly found in solid compounds and in complexes in solution, the five $3d$ orbitals of the first transition series metals lose their degeneracy, and in octahedral or tetrahedral fields, for example, they are split into two sublevels. The binding energy E will reflect the d-orbital splitting and may be understood as having three components,[6,7]

$$E = P' + \lambda\Delta + p. \qquad (1)$$

P' represents the energy required to transform the free transition-metal atom into its valence state, the state in which presumably it exists in a compound. For example, in ionic compounds P' is the ionization potential with respect to the free atoms. Δ represents the difference in energy between the two d sublevels in the ligand field. The first transition group elements display the properties of intermediate field splitting, in which the field splitting is large compared to spin-orbit coupling (which is neglected),[7] but comparable to the term separations in the free atom. p represents that part of the energy which is not very sensitive to the value of λ—for example, the Coulomb attractive energy in an ionic molecule—and it will vary in some regular way across the periodic table.

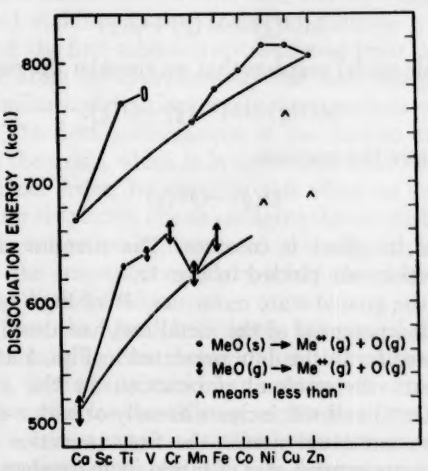

FIG. 1. Dissociation energies of solid and gaseous diatomic oxides.

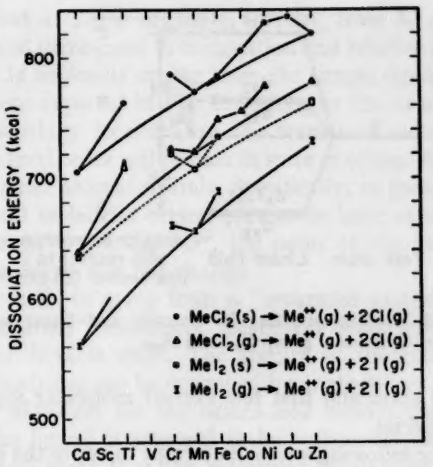
DISSOCIATION ENERGY (kcal)
800
700
600
500
• MeCl₂(s) → Me⁺⁺(g) + 2Cl(g)
▲ MeCl₂(g) → Me⁺⁺(g) + 2Cl(g)
• MeI₂(s) → Me⁺⁺(g) + 2I(g)
‡ MeI₂(g) → Me⁺⁺(g) + 2I(g)
Ca Sc Ti V Cr Mn Fe Co Ni Cu Zn

FIG. 2. Dissociation energies of solid and gaseous chlorides and iodides.

This model has been used to explain the variation in binding energies for the whole spectrum of bond types, from metallic bonding to complex bonding in solution.[6,7] In metals, the d electrons are delocalized; Δ is not important. The variation in bond energies depends on P'. In complexes which are of Pauling's "ionic" type,[8] P' is zero with respect to the free ion and Δ plays the dominant role. In all cases, however, a minimum is predicted at Mn, producing the characteristic double-humped curve.

The binding energies of the solid oxides and halides of the first transition series exhibit the double minimum behavior, as is shown in Figs. 1 and 2. According to the theory[6,7] outlined in the foregoing the variation is due to the ligand-field (i.e., Δ) effect. However it is quite striking that the stabilizations of these solids are very similar, both in magnitude and variation with Z, to those observed for the corresponding gaseous species in Figs. 1 and 2. This similarity might suggest that in both cases the stabilization is due to an essentially atomic quantity such as P', as is the case with metals,[7] rather than to a symmetry-dependent ligand field. On the other hand, we might willfully set aside this possibility and consider whether the trend in dissociation energies of the gaseous molecules could be explained within the framework of the ligand-field theory. We shall show that this may indeed be the case; then going one step further we may make full use of this framework toward a crude prediction of the spectroscopic

[4] O. Krikorian, *High Temperature Studies* UCRL-2888 (1955); L. Brewer and O. Krikorian, J. Electrochem. Soc. **103**, 38, 701 (1956).

[5] M. Calvin and N. Melchior, J. Am. Chem. Soc. **70**, 3270 (1948); L. E. Orgel, J. Chem. Soc. **1952**, 4756; H. Irving and R. J. P. Williams, *ibid.*, 3192.

[6] L. E. Orgel, J. Chem. Phys. **23**, 1819 (1955).

[7] J. S. Griffith, J. Inorg. & Nuclear Chem. **2**, 1, 229 (1956); **3**, 15 (1956).

[8] L. Pauling, *The Nature of the Chemical Bond* (Cornell University Press, Ithaca, New York, 1940), p. 37.

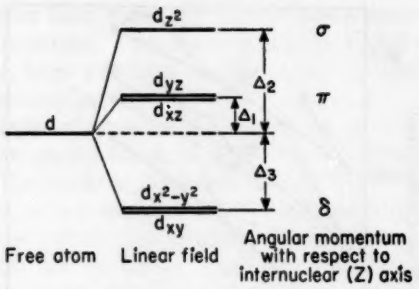

FIG. 3. d-orbital splitting in diatomic and linear triatomic molecules. Symmetry group $C_{\infty v}$ and $D_{\infty h}$.

ground state and first few excited molecular states of these species.

In the following we shall attempt to apply the ligand-field theory as used by Griffith and Orgel[6,7] to the oxide, halide, etc. gaseous molecules of the first transition group toward some understanding of their spectroscopic and energy properties. We shall in addition consider the simple molecular orbital and valence-bond pictures of these molecules and discuss the relations between the various approaches.

Let us first give a description of a molecule such as $MO(g)$ or linear $MCl_2(g)$ strictly in terms of the usual ligand-field theory, assuming that all the bonding or charge-transfer effects involve the outer $4s$ and $4p$ orbitals of the metal atom and that the $(3d)^n$ subshell remains essentially as in the free ion. Later we shall consider the complications that would arise from various types of bonding and consider the result of a general molecular orbital treatment. We assume, for the moment, that the gas molecule is ionic ($M^{++}O^{--}$) and the ligand field seen by the $(3d)^n$ subshell is comparable in strength to the solid. In diatomic and linear triatomic molecules (symmetry group $C_{\infty v}$ or $D_{\infty h}$) the $3d$ levels of the metal atom will split into three subshells, as in Fig. 3.

The naming of the orbitals assumes that the z axis lies along the internuclear axis. The splitting is subject to the following constraint,[9]

$$2\Delta_3=2\Delta_1+\Delta_2, \tag{2}$$

and so there are only two independent splitting parameters. The splitting pattern, which can be derived from group theory, is due to the spatial properties of the d-orbitals, which are of two types. Three (d_{xy}, d_{zx}, d_{yz}) have charge densities between the Cartesian coordinate axes and two ($d_{z^2-y^2}$, d_{z^2}) have charge densities along the axes. If we imagine bringing the charge cloud associated with another atom along the internuclear (z) axis into the neighborhood of an atom with stable d orbitals, d_{z^2} will feel most strongly the coulomb repulsion and as a result its energy will increase. $d_{x^2-y^2}$ and d_{xy} will be least affected by the presence of negative charge along the z axis, while d_{zx} and d_{yz} will experience moderate repulsion. In this way the main features of the splitting diagram presented in Fig. 3 are explained.

If localized $3d$ orbitals and intermediate field strength as defined above are assumed, the $3d$ sublevels will not be overlapped by any other energy levels in the molecule. Then, the splitting scheme is more general than it is strictly for the $M^{++}O^{=}$ structure. Mixing with other configurations, such as $M^{+}O^{-}$ or MO, will give qualitatively the same result so long as these effects are confined to the $4s$ and $4p$ electrons of the metal. This is because the electron cloud of the ligand will remain symmetrically disposed about the internuclear axis and will continue to provide a field of $C_{\infty v}$ symmetry.

In a general molecular orbital treatment one would combine the $2p$ electrons of O with the metal $4s$, $4p$, and $3d$ electrons of the same symmetry. Because there are more available orbitals on the metal than can be used to bond with O there will be several anti- and nonbonding orbitals in addition to the nonbonding $3d$ orbitals. This is in contrast to the situation with high (tetrahedral or octahedral) coordination,[10] in which the only nonbonding orbital is $3d$, which is thus obviously the lowest orbital available for $3d$ electrons in a complex or compound. Although the situation in the gaseous species is somewhat more ambiguous, the molecular orbitals for that case can be reasonably ordered so as to give the same qualitative result as the ligand-field splitting.

We can now apply energy considerations to the shape of the graph of dissociation energies. Although we are ultimately interested in dissociations of the type

$$MO(g)\rightarrow M(g)+O(g) \tag{3}$$

the ionic model suggests that we consider the reaction

$$MO(g)\rightarrow M^{++}(g)+O(g). \tag{4}$$

We ignore the reaction

$$O(g)\rightarrow O^{=}(g) \tag{5}$$

because its effect is constant. The energies of these dissociations are plotted in Fig. 1.

For the ground-state molecules, P' of Eq. (1) is the ionization potential of the metal and has already been accounted for in the data presented in Figs. 1 and 2. p represents the coulomb interaction in the case of ($M^{++}O^{--}$) and will increase linearly or with a slightly negative curvature across the first transition series. In the more general case of mixed ionic-covalent bonding as in $M^{+}O^{-}$, P' may still be retained as the total ionization potential, whereas the effect of $4s-4p$ bonding may be incorporated into p since this will vary uniformly with Z. From the nature of the field splitting we expect a double-humped curve with maxima at $d^2(Ti^{++})$ and $d^7(Co^{++})$ and minima at $d^0(Ca^{++})$, $d^5(Mn^{++})$, and $d^{10}(Zn^{++})$. For the solids (Figs. 1

[9] See, for example, H. A. Bethe, Ann. Physik (5) 3, 182–188 (1929).

[10] J. W. Linnett, Discussions Faraday Soc. 26, 7 (1958).

and 2) octahedral splitting will produce maxima at d^3 and d^8. The data are not sufficiently complete to illustrate this difference between the two cases; however there is nothing in the data which contradicts that assumption. We cannot hope to evaluate Δ_1, Δ_2, and Δ_3 for the gaseous case from the rather limited data. Furthermore, Williams[11] observes that even in an octahedral field the single splitting parameter is not constant for all the transition metals. However we can attempt a rough approximation of Δ_3 from Ca, Sc, and Ti points and of Δ_1 from V and Cr points. The ligand-field splitting is taken as the difference from the smooth base curve. For the gaseous diatomic oxides

$$\Delta_3 \sim 35 \text{ kcal}, \qquad \Delta_1 \sim 10 \text{ kcal}.$$

The value of Δ_3 has been obtained from only two points; Δ_1, from two independent differences, is about constant, so that the variation of splitting parameters between the first few neighboring elements is apparently small. Furthermore, these splitting parameters which have been approximated from the thermodynamic data for the first few transition oxides will be applied later only to these *same* species. Since Δ_1 is small the ligand-field result has been reduced to essentially one independent parameter for the first few transitions elements, as in the octahedral field in the solid. For the solid[7] we obtain

$$\tfrac{4}{9}\Delta \sim 20 \text{ kcal}$$

where Δ is the energy difference between the $2d$ sublevels in the octahedral field. This corresponds to Δ_3 in the gaseous case and is comparable in magnitude. Under the restriction that Ca, Mn, and Zn must show zero field stabilization any d-orbital splitting schemes for which the first sublevels are depressed from those of the free atom by approximately the same energy will show similar stabilizations in the first portions of each hump. The field stabilizations in the halides are less than in the oxide, which is in agreement with the spectrochemical series. Interpreting this effect on an ionic model, for simplicity, one can imagine that in the halides only one $4s$ electron is transferred to the ligand, leaving one on the transition metal to shield the d electrons from the ligand field.

Now that the ligand-field theory has proved suitable for rationalizing the behavior of the dissociation energies, it seems worthwhile to extend the model to try to account for the order of electronic states in the molecule, as was suggested earlier in the introduction.

The ground molecular state is determined by the order of available orbitals in the ligand field. In the general molecular orbital treatment mentioned in the foregoing it is found that the bonding orbitals (σ and Π) are filled by the valence electrons associated with the ligand (oxygen) and the outer $4s$ shell of the transition metal. The first orbitals available for $3d$ electrons are a group of three nonbonding orbitals of designation δ, Π. and σ. These originate, in part, from $3d$ atomic levels and correspond in designation and relative energy to the $3d$ sublevels arising from the simple ligand-field treatment depicted in Fig. 3. So long as the $3d$ orbitals are essentially localized on the transition metal, the energy level order will remain in spite of charge transfer in the outer atomic orbitals. Specifically, in going from a general molecular orbital picture to ionic structures such as M^+O^- or $M^{++}O^{=}$, the order of the inner $3d$ electron levels will not change.

Of course, in going from a "separated atoms" to a "united atom" framework the energy levels will cross in unpredictable ways. The spectra of the transition metal hydrides can be described by analogy to a united atom.[1] However for the oxides and halides discussed here the ligand is assumed to be sufficiently far from the metal atom that the molecular orbitals have not altered from the "separated atoms" case. This is a restatement of our previous assumption of localized $3d$ orbitals.

Because it is so convenient to use an ionic model for purposes of description we will relate the molecular orbitals of the gaseous molecule to the ionic structure $M^{++}O^{=}$. However, it should be noted that the result is not limited to an ionic model. For that structure, then, we consider $O^{=}$ produced in a ^1S state. Since a spherically symmetric state makes no contribution to net angular momentum or spin we can identify the angular momentum designations of the transition metal orbitals in the $C_{\infty v}$ splitting scheme as those of the molecular orbitals of the diatomic molecule. We are specifically interested in the $3d$ transition-metal orbitals.

Molecular states are obtained by assigning the d-electrons to the lower d sublevels of Fig. 3. We represent the electron configuration as in the following example of a TiO state: 2^+-2^+ refers to the configuration with two d electrons in δ orbitals with angular momenta opposed and spins parallel. The resultant state is $^3\Sigma$. In this way, the designations of all possible low-lying states can be obtained.

The next problem is to arrange the molecular states in order of their energies. There are two separate contributions to the energy of a state: a ligand-field term, and the energy of electron interaction, commonly called "pairing energy,"[6,7] although it includes terms in addition to those due to electron-spin pairing. The ligand-field energy is given in terms of Δ. We assume that the electron interaction, or pairing energy, is approximately the same as in the free atom (ion) and can be obtained from the free atom (ion) terms,[12] neglecting the mixing of some of the free ion terms that would arise from the polarization of the $3d$ orbitals by the ligand field. If the ligand-field splitting energy of the $3d$ orbitals is considered as being of the first order, then the polarization effect is given by second-order perturbation and will be ignored. There is no one-to-one corre-

[11] R. J. P. Williams, Discussions Faraday Soc. **26**, 125 (1958).

[12] C. E. Moore, "Atomic Energy Levels," Natl. Bur. Standards Circ. **467**, 1949.

TABLE I. First few predicted states of diatomic oxides and their energies.

Molecule	d-electron configuration	State designation	Energy[a]	Energy (cm^{-1})	Ground state (?)
ScO	2^+	$^2\Delta$	...	0.00	X
	1^+	$^2\Pi$	$\Delta_3+\Delta_1=\Delta$	Δ(~16 000)	
	0^+	$^2\Sigma$	$\Delta_3+\Delta_2$	~30 000	
TiO	2^+-2^+	$^3\Sigma$	...	0.00	X
	2^+-1^+	$^3\Pi$	Δ	Δ(~16 000)	
	$2^+\ 1^+$	$^3\Phi$	Δ	Δ	
	2^+-2^-	$^1\Sigma$	$^1D-{}^3F$	~8300	
	$2^+\ 2^-$	$^1\Gamma$	$^1G-{}^3F$	~14 200	
VO	$2^+-2^+\ 1^+$	$^4\Pi$	...	0.00	
	$2^+\ 1^+-1^+$	$^4\Delta$	Δ	Δ	
	$2^+-2^+\ 2^-$	$^2\Delta$	$(^3G-{}^4F)-\Delta$	~11 700$-\Delta$	X
	$2^+-2^+\ 1^-$	$^2\Pi$	$^2P-{}^4F$	~11 000	
	$2^+-1^+-1^-$	$^2\Sigma$	$(^2P-{}^4F)+\Delta$	~11 000$+\Delta$	
CrO	$2^+-2^+\ 1^+-1^+$	$^5\Sigma$	...	0.00	X
	$2^+-2^+-1^+\ 0^+$	$^5\Pi$	$\Delta_3-\Delta_1=\Delta'$	Δ'(~14 000)	
	$2^+-2^+\ 2^--1^+$	$^3\Pi$	$(^3P-{}^5\Delta)-\Delta$	~16 800$-\Delta$	X
	$2^+-2^+-2^--1^+$	$^3\Phi$	$(^3H-{}^5\Delta)-\Delta$	~17 000$-\Delta$	X
	$2^+-2^+-1^-\ 0^+$	$^3\Pi$	$(^3P-{}^5D)+\Delta'$	~16 800$+\Delta'$	
	$2^+-2^+\ 2^--1^-$	$^1\Pi$	$(^1F-{}^5D)-\Delta$	~41 000$-\Delta$	
	$2^+-2^+-2^--1^-$	$^1\Phi$	$(^1F-{}^5D)-\Delta$	~41 000$-\Delta$	
	$2^+-2^+\ 1^-\ 0^-$	$^1\Pi$	$(^1F-{}^5D)+\Delta'$	~39 000$+\Delta'$	

[a] Electron interaction energies are obtained from the observed[13] term values of the free ions, M^{++}.

spondence between states of atoms and of molecules with the same number of d electrons. Any one molecular state with resultant angular momentum Λ corresponds to all these atomic (free ion) states of the same spin that have a component of angular momentum $M_L=\Lambda$. The pairing energy difference between two molecular states of configuration $(3d)^n$ is taken as the difference in energy between the lowest atomic (ionic) $(3d)^n$ terms with the same spin and with M_L, respectively. For multiplet atomic states the center of energy is taken.

This device corresponds to a calculation of configuration interaction among all states of the molecule with the same angular momentum designation Λ. The same situation obtains in the free ion and the result of the corresponding "calculation" is, indeed, given by the separation of the ionic term values. Furthermore, the difference in ionic terms gives not only the "spin pairing" energy but a complete electron interaction energy of $(3d)^n$, including electron correlation.

This simplification in calculation, which results from the direct relation between the molecular Λ and M_L of the atom, is not possible in octahedral or tetrahedral fields. For those cases,[6,7] individual coulomb and exchange integrals must be determined and essentially configuration interaction neglected.

The results of calculations of low-lying molecular states of the diatomic gaseous oxides are given in Table I. We have attempted to define only the ground state and first few excited states. Higher excitation would involve orbitals other than those of the $3d$ electrons. The tabulation is limited to the first four transition series oxides, which are the species for which values of the splitting parameters Δ_3 and Δ_1 have already been approximated. Of course the method could readily be extended to other members of the transition series oxides and to diatomic halides, if Δs were available for them. The states of ScO with one d electron are the simplest to determine, and the number and complexity of low-lying states increase as more d electrons are added. However, because of the selection rules for molecular transitions, few transitions among the low-lying levels of any one species would be possible. In Table II some of the observed transitions are listed. The state that is presumably the ground state is indicated by X. In the following paragraphs we will consider these observations in light of the predictions of the theory developed in the foregoing.

TABLE II. First few observed transitions in the oxides.[a]

Molecule	Observed transitions	Observed energy difference (cm^{-1})
ScO	$A\ ^2\Pi \rightleftarrows X\ ^2\Sigma$	16 500
	$B\ ^2\Sigma \rightleftarrows X\ ^2\Sigma$	20 650
TiO	Neglecting singlet states:	
	$B\ ^3\Sigma \rightleftarrows X\ ^3\Pi$	14 200
	$C\ ^3\Pi \rightleftarrows X\ ^3\Pi$	19 500
VO	$(^2\Delta) \rightleftarrows X\ (^2\Delta)$	17 500
CrO	$A\ ^5\Pi \rightleftarrows X\ ^5\Pi$[b]	16 600

[a] Data from *Données Spectroscopiques Concernant Les Molécules Diatomiques* edited by B. Rosen (Hermann et Cie, Paris, 1951).

[b] See also M. Ninomiya, J. Phys. Soc. Japan **10**, 829 (1955).

[13] Footnote 1, Chap. 5.

For ScO, the observed $^2\Pi \rightleftarrows {}^2\Sigma$ transition may arise from the first two predicted excited states. However, in that case, the order of relative energy is reversed; $^2\Pi$ would be lower. The differences between $^2\Sigma \rightarrow {}^2\Pi$ and $^2\Pi \rightarrow {}^2\Sigma$ are slight[13]—different rotational lines would be missing at the beginning of the rotational branches in the two cases. Also there would be differences in relative intensities of the branches. Accurate analysis would require high dispersion and careful study of levels of low rotational quantum number. It is possible that the $^2\Pi \rightleftarrows X\ ^2\Sigma$ transitions observed in BO and AO, which do not have unfilled inner shells, have served as misleading clues in the assignment of the ScO spectrum.

The $^3\Sigma \rightleftarrows {}^3\Pi$ transition of TiO may correspond to the first two predicted states. However, again the order of levels would have to be reversed and for the same reasons as given above for ScO. $^3\Sigma$ would be lower.

The parentheses in Table II for the states of VO indicate that their true designation is highly in question. However, one of the $^2\Delta$ may correspond to the predicted ground state $^2\Delta$. A quartet transition ($^4\Delta \rightleftarrows {}^4\Pi$) would also be expected in the visible region as well as another doublet transition ($^2\Sigma \rightleftarrows {}^2\Pi$).

We would expect $^5\Pi \rightleftarrows X\ ^5\Sigma$ for CrO instead of $^5\Pi \rightleftarrows X\ ^5\Pi$. In addition we would expect low-lying triplet and singlet states with transitions $^1\Pi - {}^1\Pi$ and $^3\Pi - {}^3\Pi$ in the range of 3000 A.

From these few comparisons it is apparent that at present the spectroscopic data are not sufficiently complete nor are the available analyses sufficiently reliable for a meaningful comparison with the predictions of the model presented in the foregoing. The model has many limitations; nevertheless it is hoped that as data become available they might serve as a useful guide to correlate spectroscopic information. Eventually it may be possible to obtain the stabilization energies along the transition series from the splitting parameters obtained from the spectral terms, and thus have a means for interpolating and filling in missing thermodynamic data.

ACKNOWLEDGMENTS

We are indebted to Professor Leo Brewer and Professor Kenneth Pitzer for helpful discussions during the course of this work. Professor Brewer also provided the data presented in Figs. 1 and 2 prior to publication.

THE JOURNAL OF CHEMICAL PHYSICS VOLUME 32, NUMBER 4 APRIL, 1960

Infrared Spectra of Alkyldiboranes. I. Monomethyldiboranes

WALTER J. LEHMANN,* CHARLES O. WILSON, JR.,† AND I. SHAPIRO*

Research Laboratory, Olin Mathieson Chemical Corporation, Pasadena, California

(Received October 14, 1959)

The infrared spectra of five isotopic derivatives of monomethyldiborane ($CH_3B_2{}^{10}H_5$, $CH_3B_2H_5$, $CH_3B_2D_5$, $CD_3B_2H_5$, and $CD_3B_2D_5$) are analyzed and frequency assignments are made through correlation with trimethylborane and terminally substituted B_2H_5D and B_2D_5H.

INTRODUCTION

In an earlier paper[1] we discussed the effects on the vibrational spectrum of diborane when deuterium was substituted for protium; spectra of B_2H_5D and B_2D_5H were obtained by use of compensation techniques. The present paper is the first of a series dealing with the consequences of alkyl substitution in diborane. Even though the alkyl groups add complexity by introducing vibrations internal to the alkyl groups, the problem as a whole is somewhat simplified by the absence of bridge substitution.

In the first article of the series we have analyzed the infrared spectra of five isotopic derivatives of monomethyldiborane and have made general frequency assignments. Subsequent papers will deal in a similar manner with the spectra of other methyl- and ethyldiboranes. This work not only will provide analytical standards, but the identification and assignment of characteristic bands will assist ultimately in elucidating structures of more complex boron-carbon compounds.

EXPERIMENTAL

The various monomethyldiboranes ($CH_3B_2{}^{10}H_5$, $CH_3B_2H_5$, $CH_3B_2D_5$, $CD_3B_2H_5$ and $CD_3B_2D_5$) were prepared by circulating, for *ca* four hours in standard high-vacuum apparatus, mixtures (*ca* 10:1 molar ratio) of the appropriate isotopic species of diborane and trimethylborane through a glass coil at 95°C. Monomethyldiborane was then separated from the product mixture (containing all species ranging from mono- to some tetramethyldiborane) by distillation through a trap at −135°C and condensation at −145°C. This purification process was repeated several times.

Mass spectrometric analysis and careful scrutiny of the infrared spectra of the purified compounds indicated negligible impurities, consisting mostly of minute traces of diborane (e.g., shoulders at 971 and 1181 cm^{-1}) and of 1,2-dimethyldiborane (e.g., 917 cm^{-1}), formed by the disproportionation of monomethyldiborane. The rate of disproportionation is such that within fifteen minutes at room temperature traces of these products are detectable as small pips or shoulders in the infrared spectrum.

The infrared spectra were recorded on a Perkin-Elmer Model 21 spectrophotometer equipped with sodium chloride optics. The spectra of four of the compounds, all with isotopically normal boron, are reproduced in Fig. 1. Table I is a list of their measured absorption peaks as well as those of $CH_3B_2{}^{10}H_5$. Intensities were obtained for each band by dividing the value of $\log_{10}I_0/I$ (i.e., the optical density, or absorbance) by the cell length in centimeters and by the pressure in millimeters and multiplying by 10^5. Both 5-cm and 10-cm cells were used; for uniformity reported pressures have been adjusted to correspond to 5-cm path lengths. Because of overlapping bands and because some of the pressures were determined only approximately, the reported intensities are semiquantitative.

In the following discussion, the designations "A" to "E" will be used for the compounds (see heading of Table I).

DISCUSSION

Group Frequencies

Comparison of the four reproduced spectra will quickly yield clues as to which fragment of each molecule is responsible for each particular absorption. Bands caused by vibrations of the $-B_2H_5$ fragment appear exclusively in the spectra of "B" and "D", while $-CH_3$ bands occur only in the "B" and "C" spectra; in an analogous manner the $-B_2D_5$ and $-CD_3$ absorptions are determined (see Fig. 2).

Further checks on the $-B_2H_5$ and $-B_2D_5$ assignments can be obtained from examination of the spectra of the partially deuterated diboranes (B_2H_5D and B_2D_5H),[1] the monoethyldiboranes,[2] and the halodiboranes (B_2H_5Cl and B_2H_5Br).

On the whole, this correlation is fairly straightforward. The group assignments are indicated by numbers in Fig. 1 ([1] for $-B_2H_5$, [2] for $-B_2D_5$, [3] for $-CH_3$, and [4] for $-CD_3$).

Molecular Symmetry

The only symmetry element in monomethyldiborane is a plane through the carbon, the two borons, and the terminal hydrogens (i.e., perpendicular to the BH_2B

* Present address: Hughes Tool Company, Aircraft Division, Culver City, California.

† Present address: National Engineering Science Company, Pasadena, California.

[1] Lehmann, Ditter, and Shapiro, J. Chem. Phys. **29**, 1248 (1958); also see W. J. Lehmann and J. F. Ditter, J. Chem. Phys. **31**, 549 (1959).

[2] Lehmann, Wilson, and Shapiro, J. Chem. Phys. (submitted).

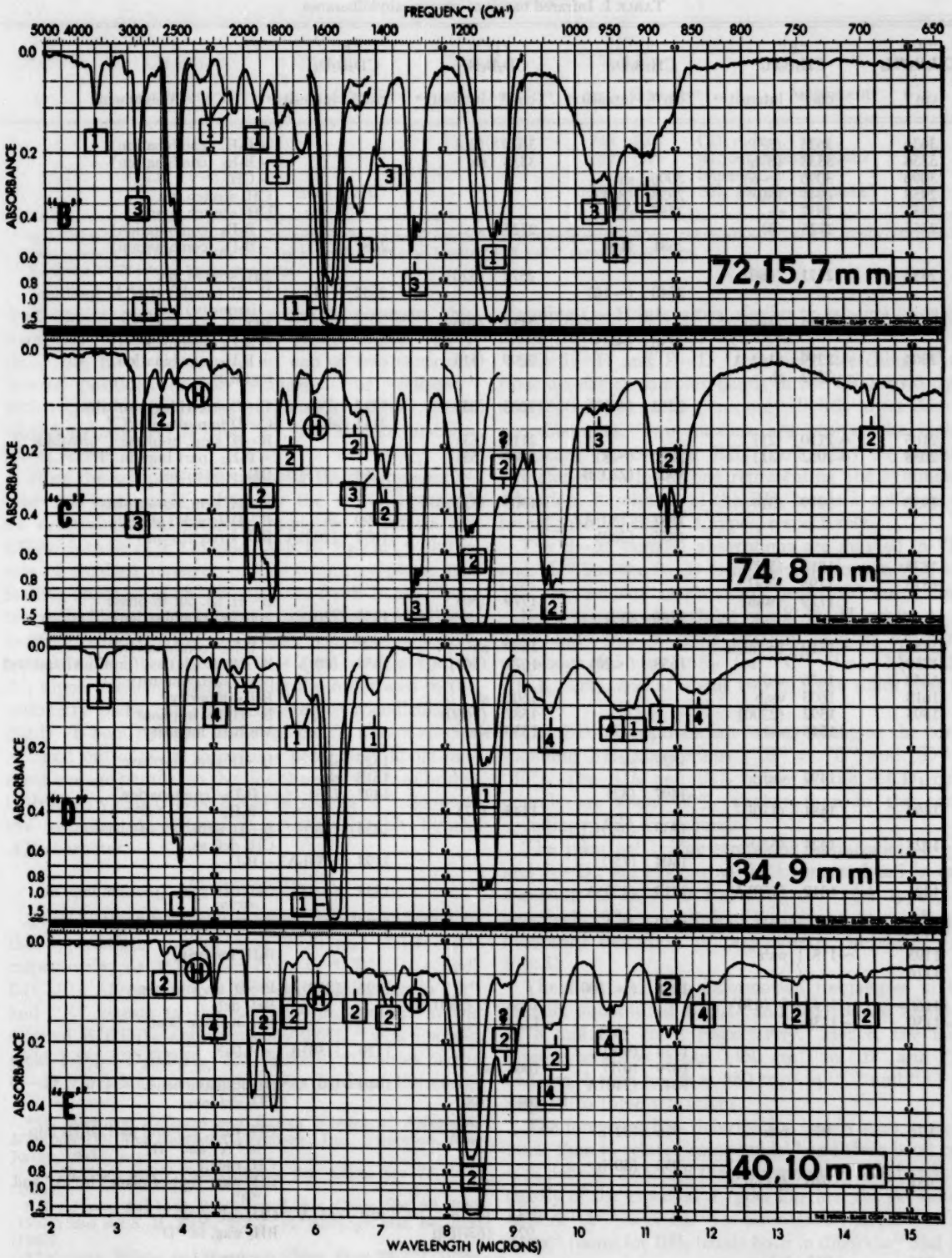

FIG. 1. Infrared spectra of gaseous monomethyldiboranes; pressures reported for 5-cm cells: "B" $CH_3B_2H_5$; "C" $CH_3B_2D_5$; "D" $CD_3B_2H_5$; "E" $CD_3B_2D_5$; [1] —B_2H_5 bands; [2] —B_2D_5 bands; [3] —CH_3 bands; [4] —CD_3 bands; (H) Protium-impurity bands.

TABLE I. Infrared bands of monomethyldiboranes

"A" $CH_3B_2{}^{10}H_5$	"B" $CH_3B_2H_5$		"C" $CH_3B_2D_5$		"D" $CD_3B_2H_5$		"E" $CD_3B_2D_5$		
cm^{-1}	cm^{-1}	intensity[a]	cm^{-1}	intensity[a]	cm^{-1}	intensity[a]	cm^{-1}	intensity[a]	Assignment[b]
3636	3623	(27)			3610	(20)			$-B_2H_5$ (combination)
3356	3333	(3)b			3333	sh			$-B_2H_5$ (combination)
3096	3096	(~5)	3096	sh					$-CH_3$
2958	2941	(80)	2958	(86)					CH_3 stretch. as.
2857	2857	sh	2857	sh					CH_3 stretch. sym.
2755	2725	(3)			2725	w			$-B_2D_5$ (combination)
			2681	(19)			2681	(11)	$-B_2D_5$ (combination)
2584	2571	(480)			2571	(320)			BH_2 stretch. as.
			2540	(~16)			2532	(14)	B—H (single) stretch. (protium impurity)
2519	2513	(580)			2513	(400)			BH_2 stretch. sym.
			2336	(~5)					$-B_2D_5$ (combination)
2304	2299	(14) A?			2299	(11)			$-B_2H_5$ (combination)
	2262	sh							impurity
			2212	(~10)	2208	(65)	2212	(50)	C—D stretching; probable
							2141	sh	C—D impurity in "C"
2105	~2110	(21)			2114	(53)			B—H′ sym. in-phase ("breathing")
2053	~2062	(31)	2070	(~8)	2049	(55)			$-B_2H_5$ (part imp. in "B")
			1965	(220)B			1968	(175)B?	BD_2 stretch. as.
1930	1919	(31)			1905	(52)vb			B—H′ sym. out-of-phase
			1887	(180)A?			~1890	sh	B—D (single) stretch.
			1855	(300)			1852	(200)A	BD_2 stretch. sym.
1833	1815	(39i)							
1813	1793	(36i)							
	1779	wsh			1779	(59)			B—H′ as. out-of-phase
			1760	(38)			1757	(20)	$-B_2D_5$ (combination)
1745	~1710	(~60)b			1689	sh			$-B_2H_5$ (combination)
1730			1658	(~20)	1672	(56)	1653	(20)b	B—H′ (single) as. (protium impurity)
1658	1656	wsh							prob. B_2H_6 impurity
1618	1605	vssh			1600	sh			B_2H_6 impurity?
1595	1592	(2300)			1587	(1650)			B—H′ as. in-phase
	1546	wsh			1550	sh			$Me_2B_2H_4$ impurity
			1527	sh			1527	sh	B—D′ sym. in-phase
	1497	wsh					1515	sh	
			1497	(32)			1492	(30)	$-B_2D_5$ (combination)
1492	1481	(110i)			1443	(47)			$-B_2H_5$
			1433	(67i)C			1435	(55i)	B—D′ sym. out-of-phase
1428	1424	(57i)							CH_3 def. as.
			1404	(75i)			1393	(65)bA?	$-B_2D_5$
1321	1319	(150)A	1319	(250)A			1333	(~25)	CH_3 def. sym. (protium imp. in "E"?)
			~1240	wbsh			~1255	wbsh	B—D′ as. out-of-phase?
1195	~1181	wsh							B_2H_6 impurity
1176									
			1188	(~1200)A			1192	(1350)A?	B—D′ as. in-phase
1160—	1143—	(650)			1168—	(530)			BH_2 def.
—1150	—1130				—1153				BH in-plane bend
			1124	(90i)			1120	(150)A	$-B_2D_5$?
			1079	(67i)	1066	sh			
			1042	(240)A			1040	(80)A?	BD in-plane bend.
					1045	(68)			CD_2 def. as.
976	971	bsh	976	(32)b					CH_3 rock. (?) and part. B_2H_6 imp. in "A" and "B"
			952	(30)b					CH_3 rock.?
951	946	(117)C							BH_2 wag. (out-of-plane) in "A" and "B"
					943	(65)b	950	(63)A	CD_2 def. sym.
					923	(63i)pip			BH_2 wag. in "D"
926	917	bsh							$(MeBH_2)_2$ imp.
913	901	(60)			909	sh			BH out-of-plane bend.
893	887	sh							
			883	(130)A			880	(90)A	BD_2 def.

TABLE I.—*Continued.*

"A" $CH_3B_2{}^{10}H_5$	"B" $CH_3B_2H_5$		"C" $CH_3B_2D_5$		"D" $CD_3B_2H_5$		"E" $CD_3B_2D_5$		
cm^{-1}	cm^{-1}	intensity[a]	cm^{-1}	intensity[a]	cm^{-1}	intensity[a]	cm^{-1}	intensity[a]	Assignment[b]
					853	(44)B?	840	(60)	CD_3 rock.
							750	(57)	BD out-of-plane bend.? impurity
	730	(~3)b							
			696	(27)C			696	(55)	BD_2 wag. (out-of-plane)

[a] Approximate intensities expressed as absorbance×10[3] divided by cell length in cm and sample pressure in mm. Abbreviations: w, weak; s, strong; sh, shoulder; b, broad; v, very; i, apparent intensity increased by overlap with other band(s); A, B, and C, apparent band types.
[b] B—H′ and B—D′ refer to bridge stretchings.

ring)—point group[3] C_s. The molecule possesses this symmetry whether the methyl group rotates freely about the B—C bond, or is in one of two sterically favored positions (either "staggered" or "eclipsed" with respect to the nearby terminal hydrogen). Both vibrational species, A' and A'', are Raman and infrared active.

Using the accepted dimensions of the diborane molecule[4] and reasonable values for the B—C distance,[5] we determined the principal moments of inertia for $CH_3B_2H_5$ to be 21.6, 113, and 131×10^{-40} g cm², with the axis of smallest moment in the symmetry plane and making an angle of 28° 25′ with the B—B bond. Thus, the molecule is an asymmetric top. Change of dipole moment parallel to the minor axis (i.e., approximately along the B—B bond) produces *A*-type bands of species A'; dipole moment change along the other axis in the symmetry plane (i.e., approximately perpendicular to the B—B bond) results in *B*-type bands, also of species A'; and out-of-plane vibrations producing dipole moment change parallel to the line through the two bridge hydrogens yields *C*-type bands of species A''. Some of the in-plane, A', vibrations actually exhibit hybrid *AB* character.

Assignments

The C—H and C—D stretching bands are found in the appropriate spectra near 2950 and 2210 cm^{-1}, respectively, *ca* 1% lower than in [6] $B(CH_3)_3$ and[7] $B(CD_3)_3$. Absence of any 2950 cm^{-1} absorption in "D" and "E" attests to the low protium content in the original $B(CD_3)_3$, approximately 0.5%[7,8] which would yield 1.5% $CD_2HB_2H_5$. The relative intensities of the C—D vibrations are roughly two-thirds of the corresponding C—H intensities, similar to relative intensity ratios for $B(CH_3)_3$ and $B(CD_3)_3$.

The B—H and B—D (terminal) stretching vibrations appear as complex bands in the 2500–2600 cm^{-1} and 1850–1970 cm^{-1} regions, only slightly lower than in the diboranes. Two maxima are visible, the higher frequency representing BH_2 (and BD_2) asymmetric stretching, the lower one representing the symmetric vibration. Resolution of the BD_2 bands is sufficient to reveal them as *B* and *A* types, respectively.

The B—H (single) absorptions are masked in "B" and "D" but the B—D (single) vibrations in "C" and "E" are evident as shoulders near 1890 cm^{-1}. Both $-B_2D_5$ compounds exhibit weak B—H peaks at *ca* 2540 cm^{-1} due to some protium content estimated at about 0.5 to 0.6% for "C" (i.e., 2.5 to 3% $CH_3B_2D_4H$), and at about two to three times that for "E".

The BD_2 absorptions are half as strong as the corresponding BH_2 absorptions ("B" *vs* "C" and "D" *vs* "E"). The BH_2 and BD_2 bands in the $-CD_3$ compounds are about 30% weaker than in the corresponding $-CH_3$ compounds.

The principal bridge stretching frequencies, B—H′ and B—D′, are evident as the strongest band in each spectrum at *ca* 1590 and 1190 cm^{-1} (*A* type), respectively. These vibrations correspond to ν_{17} (b_{2u}) in diborane,[1] described as "asymmetric, in-phase" (see Fig. 3).

The BH_2 and BD_2 deformation frequencies in terminally substituted B_2H_5D and B_2D_5H are found at 1178 and 898 cm^{-1}, respectively.[1] Hence, the fairly intense bands at about 1150 cm^{-1} in "B" and "D" and the *A*-type bands at 880 cm^{-1} in "C" and "E" are asigned to these vibrations.

The foregoing BH_2 deformation bands seem more intense than in related compounds[1,9] and their band type is ill defined, although the corresponding BD_2 bands are clearly of the expected *A* type. Further, the B^{10}-isotope shift in "A" (*ca* 20 cm^{-1}) is considerably larger than the 4 cm^{-1} found for BH_2 bands both in diborane[10] and 1,1-

[3] G. Herzberg, *Infrared and Raman Spectra of Polyatomic Molecules* (D. Van Nostrand Company, Inc., Princeton, New Jersey, 1945).
[4] K. Hedberg and V. Schomaker, J. Am. Chem. Soc. **73**, 1482 (1951).
[5] H. A. Levy and L. O. Brockway, J. Am. Chem. Soc. **59**, 2085 (1937); also see S. H. Bauer and J. M. Hastings, *ibid.* **64**, 2686 (1942).
[6] Lehmann, Wilson, and Shapiro, J. Chem. Phys. **28**, 777 (1958).
[7] Lehmann, Wilson, and Shapiro, J. Chem. Phys. **31**, 1071 (1959).
[8] Lehmann, Wilson, and Shapiro, J. Inorg. & Nuclear Chem. **11**, 91 (1959).
[9] Lehmann, Wilson, and Shapiro, J. Chem. Phys. (to be published).
[10] R. C. Lord and E. Nielsen, J. Chem. Phys. **19**, 1 (1951).

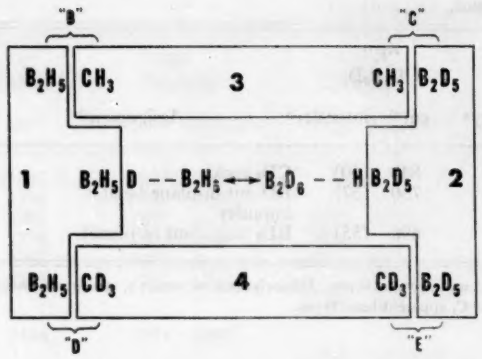

FIG. 2. Schematic comparison of some mono-substituted diboranes.

dialkyldiboranes.[9] We conclude that the BH_2 deformations are overlapped by intense BH in-plane bending bands, found between 1110 and 1140 cm^{-1} in 1,2-dialkyl- and trialkyldiboranes[9] and exhibiting B^{10} shifts of about 20 cm^{-1}.

The corresponding BD bending mode is assigned to the strong *A*-type band at 1042 cm^{-1} in "C" and "E" (1079 and 1073 cm^{-1} in B_2H_5D and B_2D_5H).

Comparison with trimethylborane[6] immediately identifies the *A*-type bands at 1320 cm^{-1} as the CH_3 symmetric deformations. The ratios of CH_3 to CD_3 frequencies for this type of vibration in a number of compounds are about 1.30 or higher.[7] Hence, the CD_3 symmetric deformations in "D" and "E" are expected at about 1000 cm^{-1} or slightly below. Suitable bands are observed at about 950 cm^{-1} (ratio of 1.39). In "E", this is a clean *A*-type band; in "D", it has a more complex shape, indicating superposition of several vibrations.

The remaining fairly intense band in spectrum "B" is a sharp *C*-type band at 946 cm^{-1}, which is interpreted as BH_2 wagging (out-of-plane). B_2H_6 and B_2H_5D contain analogous *C*-type bands at 973 and 941 cm^{-1}, respectively. Diborane and "A" both exhibit identical B^{10} shifts of 5 cm^{-1} for this band. In "D" this absorption is superimposed on the CD_3 symmetric deformation band and is probably responsible for the pip at 923 cm^{-1}. The corresponding BD_2 wagging modes (720 cm^{-1} in B_2D_6, 730 cm^{-1} in B_2D_5H) are found as weak bands at 696 cm^{-1} in "C" and "E".

The CH_3 asymmetric deformation vibrations are assigned to 1440–60 cm^{-1} in trimethylborane.[6,7] That broad infrared band exhibits a B^{10} shift of *ca* 20 cm^{-1}. Accordingly, the 1424 cm^{-1} band in "B" (1428 cm^{-1} in "A") is assigned to a CH_3 asymmetric deformation. Two of these vibrations are expected, one for each symmetry species. (In the related propene molecule[11] these vibrations are assigned to 1448 and 1472 cm^{-1}.) Possibly, the other band is masked near 1480 cm^{-1}. In "C" both these bands are masked by $-B_2D_5$ vibrations.

The corresponding CD_3 vibrations in $B(CD_3)_3$ are found[7] at 1070 cm^{-1}. Hence, we assign the odd-shaped band at 1045 cm^{-1} in "D" to the CD_3 asymmetric deformation. In "E" this absorption again is masked by the BD bending band. (We can come to no other conclusion, even though the 1040 cm^{-1} band in "E" is relatively weak.)

Only a number of weaker bands remain to be assigned. Through the comparison technique described in the previous section on Group Frequencies, a number of weak bands in the 1600 to 2500 cm^{-1} region have been assigned as $-B_2H_5$ vibrations. These then must be either B—H′ stretchings (see Fig. 3) or combination and overtone bands.

In terminally substituted B_2H_5D, the symmetric in-phase (i.e., the "breathing") vibration has been assigned[1] to 2128 cm^{-1}, the symmetric out-of-phase to *ca* 1900, and the asymmetric out-of-phase to *ca* 1760 cm^{-1}. In the monomethyldiboranes, it has been possible to assign these vibrational modes to quite similar values (see Table I). Further support for these assignments is obtained from the B^{10} shifts, which are compatible with those[10,12] for $B_2{}^{11}H_6 \rightarrow B_2{}^{10}H_6$.

In a like manner the B—D′ symmetric in-phase and out-of-phase bands (in "C" and "E") are assigned to 1527 and 1435 cm^{-1}, respectively. The weak shoulders near 1250 cm^{-1} might conceivably represent the B—D′ asymmetric out-of-phase vibrations.

The bands at *ca* 1655 cm^{-1} in the spectra of the boron-deuterated compounds "C" and "E" were observed to vary with the protium content, as determined by the 2540 cm^{-1} absorptions. These bands, located between the B—H′ asymmetric out-of-phase and asymmetric in-phase frequencies, represent the asymmetric stretching of the single B—H′ in the partially deuterated B(HD)B bridge. The present case beautifully corroborates the assignment[1] of the B—H′ (single) vibration to 1710 and 1700 cm^{-1} in bridge-substituted B_2H_5D and B_2D_5H. The corresponding B—D′ (single) band (1232 cm^{-1} in B_2D_5H) is probably too weak and too near the strong B—D′ (asymmetric in-phase) to be discernible.

Three expected types of fundamental vibrations have

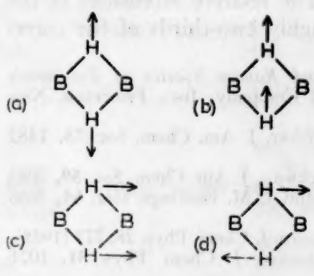

FIG. 3. The bridge stretching (B—H′) vibrations: (a) symmetric in-phase; (b) symmetric out-of-phase; (c) asymmetric in-phase; (d) asymmetric out-of-phase.

[11] E. B. Wilson, Jr., and A. J. Wells, J. Chem. Phys. **9**, 319 (1941); also see reference 3, p. 355.

[12] R. C. Taylor and A. R. Emery, Spectrochim. Acta **10**, 423 (1958).

not yet been assigned, B—C (single) stretching, one or two methyl rocking modes, and BH out-of-plane bending. The B—C vibration is anticipated somewhere in the 900 to 1100 cm^{-1} range, but no clear-cut assignment is found.

Methyl rocking modes in $B(CH_3)_3$ occur in the 860–970 cm^{-1} range, the latter value being an infrared active out-of-plane frequency. Possibly, the broad shoulder at 971 cm^{-1} in "B" and the weak 952–976 cm^{-1} bands in "C" represent such vibrations. Both of these assignments for the rocking modes are compatible with a CD_3 shift to *ca* 850 cm^{-1} in "D" and "E" [870 cm^{-1} in $B(CD_3)_3$]. The apparent *B*-type character of the CD_3 bands indicates in-plane rocking modes.

Out-of-plane bending BH and BD modes have been assigned to the 900–920 and 770 cm^{-1} regions, respectively, for dialkoxyboranes,[13,14] $HB(OR)_2$. Hence, the 901–913 cm^{-1} absorptions in "A", "B" and "D" are assigned to such BH out-of-plane bending. For the corresponding BD motion, only 750 cm^{-1} is available in "E", and no suitable band is found in "C".

[13] Lehmann, Onak, and Shapiro, J. Chem. Phys. **30**, 1215 (1959).
[14] Lehmann, Weiss, and Shapiro, J. Chem. Phys. **30**, 1222, 1226 (1959).

THE JOURNAL OF CHEMICAL PHYSICS VOLUME 32, NUMBER 4 APRIL, 1960

Lattice Dynamics and Heat Capacity of Indium

L. J. SLUTSKY AND ANN LIVINGSTON

Department of Chemistry, University of Texas, Austin, Texas

(Received October 19, 1959)

The frequency distribution spectrum of the normal modes of vibration for a noncentral force model of indium has been approximated by a root-sampling technique. Interactions between an atom and its first and second-nearest neighbors were considered, the interatomic force constants being evaluated from the room-temperature elastic constants of indium. The calculated specific heat of indium from 4° to 80°K is in fairly good agreement with experiment.

I. INTRODUCTION

BORN and Begbie[1] have developed a method for relating the parameters of a noncentral interatomic lattice force model to the adiabatic elastic constants of a crystal. In the case of indium, which has a body-centered tetragonal (primitive monoclinic) lattice, six independent interatomic force constants are required to describe the interactions of an atom with its nearest and second-nearest neighbors. If interactions with more distant neighbors are neglected, these force constants may be evaluated from the six independent elastic constants of indium. In this paper Born's formulas are evaluated explicitly for the case of a body-centered tetragonal lattice and an approximate calculation of the vibrational frequency distribution function for indium is made using force constants derived from Winder and Smith's[2] measurement of the elastic constants of indium.

II. FORCE MODEL

The coordinate systems pertinent to a discussion of this problem are illustrated schematically in Fig. 1, in which $\mathbf{x}_1$, $\mathbf{x}_2$, and $\mathbf{x}_3$ are the unit vectors of a cartesian system, $\mathbf{a}_1$, $\mathbf{a}_2$, and $\mathbf{a}_3$ represent the base vectors of the monoclinic lattice, and $\mathbf{b}_1$, $\mathbf{b}_2$, and $\mathbf{b}_3$ are the base vectors of the reciprocal lattice.

The equilibrium position of any atom may be designated by the vector $\mathbf{r}(l)=l_1\mathbf{a}_1+l_2\mathbf{a}_2+l_3\mathbf{a}_3$ with the l's integers. The atom whose position is chosen to be the origin is called atom 0. A list of the values of l_1, l_2, and l_3 for the nearest and second-nearest neighbors of atom 0 is given in Table I.

The displacement of an atom from its equilibrium position is specified by the vector $\mathbf{u}(l)=u_1(l)\mathbf{x}_1+u_2(l)\mathbf{x}_2+u_3(l)\mathbf{x}_3$ and the interatomic force constants Φ_{ab} are defined as the partial derivatives of the lattice potential energy Φ with respect to the components of $\mathbf{u}$:

$$\Phi_{ab}(l-l')=\partial^2\Phi/\partial u_a(l)\,\partial u_b(l')=\Phi_{ba}(l'-l). \quad (1)$$

Relations between the various interatomic force constants are provided by a consideration of how the quantities $\Phi_{ab}(l-l')$ transform under the symmetry operations of the lattice point group. In the case of indium, a sufficient set of operations is reflection in the x_2x_3 plane (T_1), reflection in the $x_1=x_2$ plane (T_2), reflection in the x_1x_2 plane (T_3), and a symmetry center at the origin (T_4).

In this application of Born and Begbie's method arbitrary matrices $\Phi(1)$ and $\Phi(3)$ are assumed for the

[1] G. H. Begbie and M. Born, Proc. Roy. Soc. (London) **A188**, 179 (1946); G. H. Begbie, *ibid.* **A188**, 189 (1946).
[2] D. R. Winder and C. S. Smith, J. Phys. Chem. Solids **4**, 128 (1958).

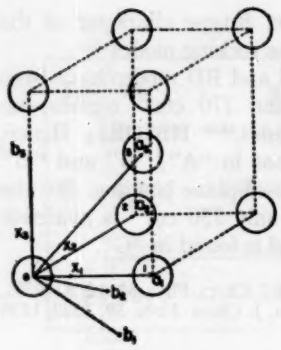

FIG. 1. The body-centered tetragonal unit cell. The base vectors of the cartesian coordinate system (x's), of the monoclinic lattice (a's), and of the reciprocal lattice (b's) are shown as are a few neighbors of atom 0.

interaction of atom 0 with atoms 1 and 3. Since the vector $\mathbf{r}(1)$ is not affected by T_1 or T_3, $\mathbf{T}_1^{-1}\Phi(1)\mathbf{T}_1=\Phi(1)$ and $\mathbf{T}_3^{-1}\Phi(1)\mathbf{T}_3=\Phi(1)$. It therefore is required that the off-diagonal elements of $\Phi(1)$ be zero and we may write

$$\Phi(1)=\begin{vmatrix}-\alpha & 0 & 0\\ 0 & -\omega & 0\\ 0 & 0 & -\beta\end{vmatrix}=\Phi(\bar{1}). \tag{2}$$

Similarly, $\mathbf{r}(3)$ is not changed by T_2. Equation (1) and the relation $\mathbf{T}_2^{-1}\Phi(3)\mathbf{T}_2=\Phi(3)$ require that $\Phi(3)$ be of the form

$$\Phi(3)=\begin{vmatrix}-\gamma & -\lambda & -\epsilon\\ -\lambda & -\gamma & -\epsilon\\ -\epsilon & -\epsilon & -\mu\end{vmatrix}=\Phi(\bar{3}). \tag{3}$$

The force constant matrices for the remaining neighbors of atom 0 may be calculated from $\Phi(1)$ and $\Phi(3)$:

$$\begin{aligned}
\Phi(2)&=\mathbf{T}_2^{-1}\Phi(1)\mathbf{T}_2=\begin{vmatrix}-\omega & 0 & 0\\ 0 & -\alpha & 0\\ 0 & 0 & -\beta\end{vmatrix}=\Phi(\bar{2})\\
\Phi(4)&=\mathbf{T}_1^{-1}\Phi(3)\mathbf{T}_1=\begin{vmatrix}-\gamma & \lambda & \epsilon\\ \lambda & -\gamma & -\epsilon\\ \epsilon & -\epsilon & -\mu\end{vmatrix}=\Phi(\bar{4})\\
\Phi(6)&=\mathbf{T}_3^{-1}\Phi(4)\mathbf{T}_3=\begin{vmatrix}-\gamma & \lambda & -\epsilon\\ \lambda & -\gamma & \epsilon\\ -\epsilon & \epsilon & -\mu\end{vmatrix}=\Phi(\bar{6})\\
\Phi(5)&=\mathbf{T}_1^{-1}\Phi(6)\mathbf{T}_1=\begin{vmatrix}-\gamma & -\lambda & \epsilon\\ -\lambda & -\gamma & \epsilon\\ \epsilon & \epsilon & -\mu\end{vmatrix}=\Phi(\bar{5}).
\end{aligned} \tag{4}$$

The requirement that the potential energy Φ not be affected by a translation of the lattice as a whole may be expressed[3]

$$\sum_l \Phi_{ab}(l)=0. \tag{5}$$

Thus $\Phi(0)$ may readily be calculated from Eqs. (2)–(5):

$$\Phi(0)=\begin{vmatrix}2(\alpha+\omega+4\gamma) & 0 & 0\\ 0 & 2(\alpha+\omega+4\gamma) & 0\\ 0 & 0 & 4(\beta+2\mu)\end{vmatrix}. \tag{6}$$

III. SECULAR EQUATION

In the Born-von Kármán theory of lattice vibrations the normal modes of a crystal are described as traveling waves with frequencies ν determined by a secular equation

$$|\,C_{ab}(\mathbf{y})-4\pi^2M\nu^2\mathbf{I}\,|=0, \tag{7}$$

where M is the mass of an atom, $\mathbf{I}$ is the 3×3 unit matrix, and $\mathbf{y}=y_1\mathbf{b}_1+y_2\mathbf{b}_2+y_3\mathbf{b}_3$ is a vector along the direction of propagation of the wave with magnitude equal to the reciprocal of the wavelength. The elements of the secular determinant are given by the relation[3]

$$C_{ab}(\mathbf{y})=\sum_l \Phi_{ab}(l)\exp[2\pi i(l_1y_1+l_2y_2+l_3y_3)]. \tag{8}$$

Thus

$$\begin{aligned}
C_{11}(\mathbf{y})&=2[(\alpha+\omega+4\gamma)-\alpha C_1-\omega C_2-\gamma(C_3+C_{1-3}\\
&\qquad+C_{1+2-3}+C_{2-3})]\\
C_{12}(\mathbf{y})&=2\lambda(C_{1-3}+C_{2-3}-C_3-C_{1+2-3})=C_{21}(y)\\
C_{13}(\mathbf{y})&=2\epsilon(C_{1-3}+C_{1+2-3}-C_{2-3}-C_3)=C_{31}(y)\\
C_{22}(\mathbf{y})&=2[(\alpha+\omega+4\gamma)-\omega C_1-\alpha C_2\\
&\qquad-\gamma(C_3+C_{1-3}+C_{1+2-3}+C_{2-3})]\\
C_{23}(\mathbf{y})&=2\epsilon(C_{2-3}-C_{1-3}-C_3+C_{1+2-3})=C_{32}(y)\\
C_{33}(\mathbf{y})&=4(\beta+2\mu)-2\beta(C_1+C_2)\\
&\qquad-2\mu(C_3+C_{1-3}+C_{1+2-3}+C_{2-3}),
\end{aligned}$$

TABLE I. Position designations for the neighbors of atom 0.

l	l_1	l_2	l_3	l	l_1	l_2	l_3
0	0	0	0	5	−1	−1	1
1	1	0	0	6	0	−1	1
2	0	1	0	7	0	0	−1
1	−1	0	0	4	1	0	−1
2	0	−1	0	5	1	1	−1
3	0	0	1	6	0	1	−1
4	−1	0	1				

[3] M. Born and K. Huang, *Dynamical Theory of Crystal Lattices* (Oxford University Press, New York, 1954).

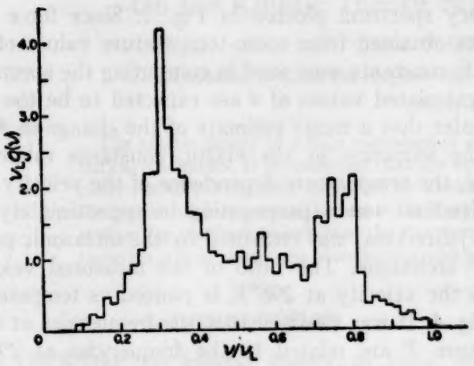

FIG. 2. The frequency distribution spectrum $g(\nu)$ for a tensor-force model of indium.

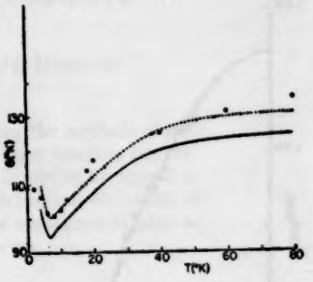

FIG. 3. The equivalent Debye θ vs temperature for indium. Solid circles (●) represent the experimental values. The solid curve is calculated from the spectrum shown in Fig. 2, the dotted curve is corrected for the temperature dependence of the elastic constants.

where $C_1=\cos 2\pi y_1$, $C_2=\cos 2\pi y_2$, $C_3=\cos 2\pi y_3$, $C_{1-3}=\cos 2\pi(y_1-y_3)$, $C_{2-3}=\cos 2\pi(y_2-y_3)$, and $C_{1+2-3}=\cos 2\pi(y_1+y_2-y_3)$.

IV. ELASTIC CONSTANTS

In the limit of very long waves (small $|\mathbf{y}|$) Eq. (7) must be identical with the elastic secular equation. Relations between the elastic constants and the interatomic force constants may thus be obtained by expanding the lattice dynamical secular equation in powers of the components of $\mathbf{y}$, retaining only quadratic terms, and comparing the result with the elastic secular determinant. Since the elastic constants are defined in terms of a cartesian coordinate system it will be convenient to write y in terms of cartesian base vectors as $\mathbf{y}=Y_1\mathbf{x}_1+Y_2\mathbf{x}_2+Y_3\mathbf{x}_3$ where

$$y_1=aY_1 \qquad y_2=aY_2 \qquad y_3=[cY_3+a(Y_1+Y_2)]/2, \quad (9)$$

a and c being the lattice constants of the body-centered tetragonal unit cell.

When the indicated expansion is performed, we obtain for the long-wave form of the lattice dynamical secular equation

$$\begin{vmatrix} a^2(\alpha+\gamma)Y_1^2+a^2(\omega+\gamma)Y_2^2+c^2\gamma Y_3^2-M\nu^2 & 2a^2\lambda Y_1Y_2 & 2ac\epsilon Y_1Y_3 \\ 2a^2\lambda Y_1Y_2 & a^2(\omega+\gamma)Y_1^2+a^2(\alpha+\gamma)Y_2^2+c^2\gamma Y_3^2-M\nu^2 & 2ac\epsilon Y_2Y_3 \\ 2ac\epsilon Y_1Y_3 & 2ac\epsilon Y_2Y_3 & a^2(\beta+\mu)(Y_1^2+Y_2^2)+c^2\mu Y_3^2-M\nu^2 \end{vmatrix}=0. \quad (10)$$

The elastic secular equation is

$$\begin{vmatrix} c_{11}Y_1^2+c_{66}Y_2^2+c_{44}Y_3^2-\rho\nu^2 & (c_{12}+c_{66})Y_1Y_2 & (c_{13}+c_{44})Y_1Y_3 \\ (c_{12}+c_{66})Y_1Y_2 & c_{66}Y_1^2+c_{11}Y_2^2+c_{44}Y_3^2-\rho\nu^2 & (c_{13}+c_{44})Y_2Y_3 \\ (c_{13}+c_{44})Y_1Y_3 & (c_{13}+c_{44})Y_2Y_3 & c_{44}(Y_1^2+Y_2^2)+c_{33}Y_3^2-\rho\nu^2 \end{vmatrix}=0, \quad (11)$$

where ρ is the density. After dividing Eq. (10) by the volume per atom $(a^2c/2)$ and comparing with Eq. (11), the following relations between the elastic constants and force constants are obtained:

$$c_{11}=2(\alpha+\gamma)/c, \qquad c_{33}=2c\mu/a^2,$$
$$c_{44}=2c\gamma/a^2=2(\beta+\mu)/c,$$
$$c_{66}=2(\omega+\gamma)/c, \qquad c_{12}=2(2\lambda-\gamma-\omega)/c,$$
$$c_{13}=(2/a)[2\epsilon-(c\gamma/a)].$$

The elastic constants,[2] in units of 10^{11} dynes/cm^2 are: $c_{11}=4.45$, $c_{12}=3.95$, $c_{13}=4.05$, $c_{33}=4.44$, $c_{44}=0.655$, and $c_{66}=1.22$. The force constants in dynes/cm are: $\alpha=10\,988$, $\omega=2314$, $\gamma=698$, $\beta=-3114$, $\epsilon=3816$, $\lambda=6382$, $\mu=4732$.

V. FREQUENCY SPECTRUM AND HEAT CAPACITY

The frequency distribution function $g(\nu)$ is so defined that $g(\nu)d\nu$ is the number of normal modes of vibration with frequencies in the interval between ν and $\nu+d\nu$. The frequency distribution may be approximated by solving Eq. (7) at a mesh of points evenly distributed throughout the reduced Brillouin zone and determining the number of roots that lie within given frequency intervals. The histogram shown in Fig. 2 was constructed from solutions of the secular equation at 800 points in the portion of the Brillouin zone which

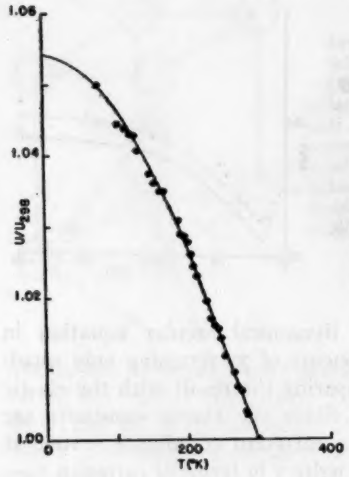

FIG. 4. Variation with temperature of the velocity (U) of a longitudinal elastic wave in indium.

cannot be further reduced by the symmetry operations of the lattice point group.

The lattice contribution to the constant-volume heat capacity may be computed from the relation

$$C_v = k\int_0^{\nu_L} g(\nu)\,(h\nu/kT)^2 \times\{\exp(h\nu/kT)\,d\nu/[\exp(h\nu/kT)-1]^2\}, \quad (12)$$

where ν_L is the maximum vibrational frequency. A comparison between calculated and experimental[4,5] heat capacities in the form of a plot of θ, the equivalent Debye temperature, vs temperature is given in Fig. 3. The solid curve in Fig. 3 is calculated from the frequency spectrum plotted in Fig. 2. Since force constants obtained from room-temperature values of the elastic constants were used in computing the spectrum, the calculated values of θ are expected to be too low. In order that a rough estimate of the change in θ due to the variation in the elastic constants might be made, the temperature dependence of the velocity of a longitudinal wave (propagating in approximately the [100] direction) was measured by the ultrasonic pulse-echo[6] technique. The ratio of the measured velocity U to the velocity at 298°K is plotted vs temperature in Fig. 4. It was assumed that the frequencies at temperature T are related to the frequencies at 298°K by $\nu_T/\nu_{298}=U_T/U_{298}$. Therefore the heat capacity at T calculated with Eq. (12) and the spectrum derived from 298°K values of the elastic constants will actually correspond to the heat capacity at a temperature $T'=T(U_T/U_{298})$. If the calculated values of θ are "corrected" as outlined in the foregoing the dotted curve in Fig. 3 is the result. The estimated value of U_0/U_{298} is 1.055 ± 0.015, the effect of the correction is thus to increase θ by about 5% in the temperature range plotted in Fig. 3.

The calculated θ vs T curves are in fairly good agreement with the experimental results above 4°K. Since the root sampling is certainly not sufficient to characterize the extreme low-frequency end of the spectrum, where there are comparatively few roots, the lattice heat capacity at very low temperatures can not be calculated. Otherwise it appears that the Born and Begbie model with first and second-nearest neighbor interactions gives a good account of the temperature dependence of the lattice heat capacity of indium.

[4] J. R. Clement and E. H. Quinnell, Phys. Rev. **92**, 258 (1953).
[5] K. Clusius and L. Schachinger, Z. angew. Phys. **4**, 442 (1952).
[6] H. B. Huntington, Phys. Rev. **72**, 321 (1947).

On the Kinetic Theory of a Fluid Composed of Rigid Spheres*

JAMES T. O'TOOLE AND JOHN S. DAHLER

Department of Chemical Engineering, University of Minnesota, Minneapolis 14, Minnesota

(Received September 22, 1959)

The kinetic theory of a fluid composed of rigid sphere molecules is studied by using the methods of statistical mechanics. It is confirmed that the equation of change for the singlet distribution function has precisely the form originally suggested by Enskog on the basis of intuitive arguments involving an appeal to the notion of forward and inverse collisions. The formal derivation of the hydrodynamical equations of motion for the fluid reveals that the flux tensors for the rigid sphere fluid are of the same general form as those for a fluid composed of molecules which interact according to nonimpulsive forces.

I. INTRODUCTION

ALTHOUGH the kinetic theory of rigid spheres has been the subject of many investigations, the mathematical methods employed in these studies have invariably suffered from a lack of rigor. In particular, the equation of change for the singlet distribution function and the hydrodynamical equations have usually been obtained by the use of methods which are truly applicable only if the molecular interactions can be represented by continuous functions. The results presented here illustrate that a more rigorous approach to this problem can be developed. It is also shown that the "collisional transfer" contributions to the fluxes of momentum and energy derived by Irving and Kirkwood[1] for molecules with continuous potentials of interaction retain their validity in the case of the rigid sphere fluid.

In the next section we shall consider the derivation of the equation of change for the singlet distribution function. It is established that this equation has precisely the same form as that which one would derive from the conceptually simpler but more questionable mathematical methods originally applied to this problem by Enskog.[2] In Sec. III we derive the equations of hydrodynamics and obtain explicit representations for the fluxes appropriate to the rigid sphere fluid.

II. EQUATION OF CHANGE FOR THE SINGLET DISTRIBUTION FUNCTION

Let us now consider a system composed of N identical rigid spheres, each of diameter σ and of mass m. This system is enclosed by a container of volume V. To avoid the introduction of surface effects we shall eventually assume that V and N become arbitrarily large in such a way that the average number density N/V remains finite.

The Gibbsian *specific* distribution function for the system will be denoted by

$$F^{(N)}(\mathbf{R}^N, \mathbf{p}^N; t) = F^{(N)}(\mathbf{R}_1, \mathbf{p}_1; \cdots; \mathbf{R}_N, \mathbf{p}_N; t)$$

where $\mathbf{R}_i$ and $\mathbf{p}_i$ are, respectively, the position vector and momentum of the ith sphere. Now if the molecular interactions were continuous functions of the position vectors, $F^{(N)}$ would itself be a continuous function having singularities only on the set of zero measure where two of the $\mathbf{R}_i$'s had identical values. However, in the case of rigid spheres $F^{(N)}$ is zero on the set of finite measure where $R_{ij} = |\mathbf{R}_i - \mathbf{R}_j| < \sigma$ for any pair of indices $i \neq j$. At the boundaries of this set $F^{(N)}$ is discontinuous having a finite value on the surface and zero value within. Thus, there is a considerable difference in the behavior of $F^{(N)}$ for the rigid sphere fluid (and indeed for any interaction potential incorporating a rigid core) and that for a fluid whose molecules interact according to continuous potential functions. In what follows we shall consider these differences in great detail and illustrate in what ways they necessitate the introduction of mathematical techniques different from those used in the case of continuous potentials of interaction.

Of particular importance in the kinetic theory is the equation of change for

$$F^{(1)}(\mathbf{R}_1, \mathbf{p}_1; t) = \int^V \cdots \int^V F^{(N)}(\mathbf{R}^N, \mathbf{p}^N; t)\, d\mathbf{R}_2 d\mathbf{p}_2 \cdots d\mathbf{R}_N d\mathbf{p}_N. \quad (1)$$

the singlet distribution function specific to a particular one of the N molecules (in this case the first). The temporal derivative of this function can be written in the form

$$\frac{\partial F^{(1)}(\mathbf{R}_1, \mathbf{p}_1; t)}{\partial t} = \lim_{\tau \to 0} (1/\tau) \int^V \cdots \int^V [F^{(N)}(\mathbf{R}^N, \mathbf{p}^N; t+\tau) - F^{(N)}(\mathbf{R}^N, \mathbf{p}^N; t)]\, d\mathbf{R}_2 d\mathbf{p}_2 \cdots d\mathbf{R}_N d\mathbf{p}_N$$
$$= \lim_{\tau \to 0} (1/\tau) \int^V \cdots \int^V [F^{(N)}(\mathbf{R}_0^N, \mathbf{p}_0^N; t) - F^{(N)}(\mathbf{R}^N, \mathbf{p}^N; t)]\, d\mathbf{R}_2 d\mathbf{p}_2 \cdots d\mathbf{R}_N d\mathbf{p}_N, \quad (2)$$

* This work was supported in part by the National Science Foundation and in part by the National Aeronautics and Space Administration.

[1] J. H. Irving and J. G. Kirkwood, J. Chem. Phys. 18, 817 (1950).

[2] S. Chapman and T. G. Cowling, *The Mathematical Theory of Non-uniform Gases* (Cambridge University Press, New York, 1939), Chap. 16. See also, F. C. Collins and H. Raffel, J. Chem. Phys. 22, 1728 (1954); H. C. Longuet-Higgins and J. A. Pople, *ibid.* 25, 884 (1956); J. S. Dahler, *ibid.* 27, 1428 (1957), and S. T. Choh (thesis, University of Michigan, 1958).

where $\mathbf{R}_0^N$, $\mathbf{p}_0^N$ is that state of the system at time t which dynamically evolves to $\mathbf{R}^N$, $\mathbf{p}^N$ at the later time $t+\tau$. From the properties of contact transformations it follows that the Jacobian, $\partial(\mathbf{R}^N, \mathbf{p}^N)/\partial(\mathbf{R}_0^N, \mathbf{p}_0^N)$, has the value unity. The equality of $F^{(N)}(\mathbf{R}^N, \mathbf{p}^N; t+\tau)$ and $F^{(N)}(\mathbf{R}_0^N, \mathbf{p}_0^N; t)$ is a direct consequence of this and the fact that no mechanism exists by which members can either be lost or gained from the ensemble representative of the dynamical system under consideration.

To conduct the integration of the right-hand side of (2) one can now proceed in a stepwise manner considering separately those contributions to the integral which arise from: (i) no collisions among *any* of the N molecules during the interval $(t, t+\tau)$; (ii) collisions involving a single pair of the molecules during $(t, t+\tau)$; (iii) the successive collisions of a particular molecule with two (or more) others during the interval; (iv) two (or more) binary encounters involving four (or more) distinctly different molecules; (v) more complicated events involving several molecules.† Each of these collisional classifications can, as we shall now demonstrate, be associated with a particular portion of the range over which the right-hand side of (2) is to be integrated. For example let us consider a state $\mathbf{R}^N$, $\mathbf{p}^N$ at t so defined that during the previous interval of time τ only molecules i and j can have suffered a mutual collisional encounter. If this encounter terminated at $t+s^+$ where $0<s<\tau$, then at that moment the two molecules of interest must have been in the state $(\mathbf{R}_i', \mathbf{p}_i; \mathbf{R}_j', \mathbf{p}_j)$ where

$$\mathbf{R}_i' = \mathbf{R}_i - (\mathbf{p}_i/m)(\tau - s), \tag{3}$$

$$\mathbf{R}_j' = \mathbf{R}_i' + \sigma\mathbf{k}_{ji} = \mathbf{R}_j - (\mathbf{p}_j/m)(\tau - s),$$

and $\mathbf{k}_{ji}$ is the unit vector directed along the line of molecular centers from i to j at their moment of contact. It should also be noted that if the two completed their collision at $t+s^+$ then $\mathbf{k}_{ji}\cdot(\mathbf{p}_j-\mathbf{p}_i)>0$ since otherwise they would be proceeding toward one another. For fixed values of $\mathbf{R}_i$, $\mathbf{p}_i$, and $\mathbf{p}_j$ the range of $\mathbf{R}_j$ values associated with (ij) collisions completed in the interval $(t+s, t+s+ds)$ with the direction of the line of centers in the element $(\mathbf{k}_{ji}, \mathbf{k}_{ji}+\mathbf{dk}_{ji})$ is easily shown to equal

$$\mathbf{dR}_j = (\sigma^2/m)\mathbf{k}_{ji}\cdot(\mathbf{p}_j-\mathbf{p}_i)\mathbf{dk}_{ji}ds$$

$$[0<s<\tau; \mathbf{k}_{ji}\cdot(\mathbf{p}_j-\mathbf{p}_i)>0],$$

where the element of solid angle $\mathbf{dk}_{ji}$ may be written in the form $\sin\theta d\theta d\phi$ with θ and ϕ as the polar and equatorial angles of $\mathbf{k}_{ji}$ relative to $(\mathbf{p}_j-\mathbf{p}_i)$ as the polar direction. Simple dynamical considerations reveal that at the beginning of the interval $(t, t+\tau)$ the two molecules were in the state $(\mathbf{R}_{i0}, \mathbf{p}_{i0}; \mathbf{R}_{j0}, \mathbf{p}_{j0})$ where

$$\mathbf{R}_{i0} = \mathbf{R}_i' - (\mathbf{p}_{i0}/m)s,$$

$$\mathbf{p}_{i0} = \mathbf{p}_i + \mathbf{k}_{ji}\mathbf{k}_{ji}\cdot(\mathbf{p}_j-\mathbf{p}_i),$$

$$\mathbf{R}_{j0} = \mathbf{R}_{i0} + \sigma\mathbf{k}_{ji} - (\mathbf{p}_{j0}-\mathbf{p}_{i0})s/m,$$

$$\mathbf{p}_{j0} = \mathbf{p}_j - \mathbf{k}_{ji}\mathbf{k}_{ji}\cdot(\mathbf{p}_j-\mathbf{p}_i). \tag{4}$$

Therefore, the contribution to the right-hand side of (2) due to isolated binary encounters between molecules i and j (neither of which is 1) is given by

$$\lim_{\tau\to 0}(\sigma^2/m\tau)\int^{V_i(\tau)}\cdots\int\mathbf{k}_{ji}\cdot(\mathbf{p}_j-\mathbf{p}_i)\mathbf{dk}_{ji}\mathbf{dR}_i\mathbf{dp}_i\mathbf{dp}_j\int^{V_2(\tau)}\cdots\int^{V_N(\tau)}\mathbf{dR}^{N-1-i-j}\mathbf{dp}^{N-1-i-j}$$

$$\{\mathbf{k}_{ji}\cdot(\mathbf{p}_j-\mathbf{p}_i)>0\}$$

$$\times\int_0^\tau ds\{F^{(N)}(\mathbf{R}_0^{N-i-j}, \mathbf{p}_0^{N-i-j}; \mathbf{R}_{i0}, \mathbf{p}_{i0}; \mathbf{R}_{j0}, \mathbf{p}_{j0}; t)$$

$$-F^{(N)}(\mathbf{R}^{N-i-j}, \mathbf{p}^{N-i-j}; \mathbf{R}_i, \mathbf{p}_i; \mathbf{R}_i+\sigma\mathbf{k}_{ji}+[(\mathbf{p}_j-\mathbf{p}_i)s/m], \mathbf{p}_j; t)\}, \tag{5}$$

where $V_n(\tau)$ is that portion of V where molecule n does not collide during $(t, t+\tau)$ with any of the molecules following it in the integration sequence. Because of the manner in which this term has been constructed the momenta $\mathbf{p}_{n0}(n\neq i, j)$ are just equal to the corresponding $\mathbf{p}_n$'s and $\mathbf{R}_{n0}=\mathbf{R}_n-(\mathbf{p}_n/m)\tau$. In the limit of $\tau\to 0$ the

† No mention has been made of collisions between the molecules and the boundaries of V. Although these surface contributions to $\partial F^{(1)}(\mathbf{R}_1, \mathbf{p}_1; t)/\partial t$ are simple to calculate, they should be of importance only if we wish to determine the behavior of $F^{(1)}$ for a molecule lying very near the boundaries or if the dimensions of V are such that Knudsen flow occurs. Neither of these situations are of particular interest to us here and so the surface effects are neglected.

s integration simply introduces a multiplicative factor of τ into the integrand of (5) and this term reduces to

$$(\sigma^2/m)\int \mathbf{k}_{ji}\cdot(\mathbf{p}_j-\mathbf{p}_i)\,d\mathbf{k}_{ji}\int^{V_2}\cdots\int^{V_N} d\mathbf{R}^{N-1-j}d\mathbf{p}^{N-1}$$

$$\{\mathbf{k}_{ji}\cdot(\mathbf{p}_j-\mathbf{p}_i)>0\}$$

$$\times[F^{(N)}(\mathbf{R}^{N-i-j},\,\mathbf{p}^{N-i-j};\,\mathbf{R}_i,\,\mathbf{p}_{i0};\,\mathbf{R}_i+\sigma\mathbf{k}_{ji},\,\mathbf{p}_{j0};\,t)-F^{(N)}(\mathbf{R}^{N-i-j},\,\mathbf{p}^{N-i-j};\,\mathbf{R}_i,\,\mathbf{p}_i;\,\mathbf{R}_i+\sigma\mathbf{k}_{ji},\,\mathbf{p}_j;\,t)]$$

$$=(\sigma^2/m)\int^{V_i}\cdots\int \mathbf{k}_{ji}\cdot(\mathbf{p}_j-\mathbf{p}_i)\,d\mathbf{k}_{ji}d\mathbf{R}_i d\mathbf{p}_i d\mathbf{p}_j[F^{(3)}(\mathbf{R}_1,\,\mathbf{p}_1;\,\mathbf{R}_i,\,\mathbf{p}_{i0};\,\mathbf{R}_i+\sigma\mathbf{k}_{ji},\,\mathbf{p}_{j0};\,t)$$

$$\{\mathbf{k}_{ji}\cdot(\mathbf{p}_j-\mathbf{p}_i)>0\}$$

$$-F^{(3)}(\mathbf{R}_1,\,\mathbf{p}_1;\,\mathbf{R}_i,\,\mathbf{p}_i;\,\mathbf{R}_i+\sigma\mathbf{k}_{ji},\,\mathbf{p}_j;\,t)]. \quad (6)$$

where $F^{(3)}$ is the (specific) triplet distribution function‡ and $V_n=\lim_{\tau\to 0}V_n(\tau)=V$. §

The analysis presented here can also be applied to the situation where one of the molecules involved in the collision is 1 itself. Combining all of the contributions to $\partial F^{(1)}(\mathbf{R}_1,\,\mathbf{p}_1;\,t)/\partial t$ arising from isolated binary collisions we then obtain

$$(\sigma^2/m)\sum_{j=2}^{N}\int\cdots\int \mathbf{k}_{j1}\cdot(\mathbf{p}_j-\mathbf{p}_1)\,d\mathbf{k}_{j1}d\mathbf{p}_j[F^{(2)}(\mathbf{R}_1,\,\mathbf{p}_{10};\,\mathbf{R}_1+\sigma\mathbf{k}_{j1},\,\mathbf{p}_{10};\,t)-F^{(2)}(\mathbf{R}_1,\,\mathbf{p}_1;\,\mathbf{R}_1+\sigma\mathbf{k}_{j1},\,\mathbf{p}_j;\,t)]$$

$$\{\mathbf{k}_{j1}\cdot(\mathbf{p}_j-\mathbf{p}_1)>0)\}$$

$$+(\sigma^2/m)\sum_{N\geq j>i>1}\sum\int\cdots\int \mathbf{k}_{ji}\cdot(\mathbf{p}_j-\mathbf{p}_i)\,d\mathbf{R}_i d\mathbf{p}_i d\mathbf{p}_j d\mathbf{k}_{ji}[F^{(3)}(\mathbf{R}_1,\,\mathbf{p}_1;\,\mathbf{R}_i,\,\mathbf{p}_{i0};\,\mathbf{R}_i+\sigma\mathbf{k}_{ji},\,\mathbf{p}_{j0};\,t)$$

$$\{\mathbf{k}_{ji}\cdot(\mathbf{p}_j-\mathbf{p}_i)>0\}$$

$$-F^{(3)}(\mathbf{R}_1,\,\mathbf{p}_1;\,\mathbf{R}_i,\,\mathbf{p}_i;\,\mathbf{R}_i+\sigma\mathbf{k}_{ji},\,\mathbf{p}_j;\,t)]. \quad (7)$$

It is easily verified that none of the more complex collisional events provide finite contributions to the right-hand side of (2). Thus, in the case of two successive encounters involving the same molecule or of two isolated binary encounters, *two* timelike intergrations enter into the calculation of contributions to the right-hand side of (2); for small values of τ each of these integrations introduces a multiplicative factor of τ into the integrand. Therefore, a net contribution of order τ is obtained which vanishes in the limit of $\tau\to 0$. The physical significance of this is that during an infinitesimal interval of time only isolated binary encounters (of zero duration) can possibly occur since all other collisional events require a finite time for their completion.

We consequently arrive at the conclusion that the only contributions to the right-hand side of (2) are the binary collision terms given by (7) and the "noncollision contribution."

$$\lim_{\tau\to 0}\tau^{-1}\int^{V_2(\tau)}\cdots\int^{V_N(\tau)}[F^{(N)}(\mathbf{R}_0^N,\,\mathbf{p}_0^N;\,t)-F^{(N)}(\mathbf{R}^N,\,\mathbf{p}^N;\,t)]\,d\mathbf{R}^{N-1}d\mathbf{p}^{N-1}$$

$$=\lim_{\tau\to 0}\tau^{-1}\int^{V_2(\tau)}\cdots\int^{V_N(\tau)}[F^{(N)}(\mathbf{R}^N-\mathbf{p}^N\tau/m,\,\mathbf{p}^N;\,t)-F^{(N)}(\mathbf{R}^N,\,\mathbf{p}^N;\,t)]\,d\mathbf{R}^{N-1}d\mathbf{p}^{N-1}. \quad (8)$$

---

‡ In general, the n-particle distribution function specific to molecules $1, 2\cdots n$ is defined by

$$F^{(n)}(\mathbf{R}^n,\,\mathbf{p}^n;\,t)=\int^{V}\cdots\int^{V}F^{(N)}(\mathbf{R}^N,\,\mathbf{p}^N;\,t)\,d\mathbf{R}^{N-n}d\mathbf{p}^{N-n}.$$

§ It can be verified that $\{V-V_2(\tau),\cdots,\,V-V_N(\tau)\}$ is composed of order τ terms arising from the isolated binary collision regions, order τ^2 terms due to successive or separate binary encounters, etc.

In $\{V_2(\tau)\cdots V_N(\tau)\}$, $F^{(N)}$ is a continuous function of its spatial variables. We may therefore expand $F^{(N)}(\mathbf{R}^N-\mathbf{p}^N\tau/m, \mathbf{p}^N; t)$ in a Taylor series about $\mathbf{R}^N$, $\mathbf{p}^N$ and then retain only the first two terms as $\tau\to 0$ to obtain,

$$-\int^V\cdots\int^V(\mathbf{p}_1/m)\cdot\nabla_{\mathbf{R}_1}F^{(N)}(\mathbf{R}^N, \mathbf{p}^N; t)\,d\mathbf{R}^{N-1}d\mathbf{p}^{N-1}$$

$$-\sum_{j=2}^{N}\int^V\cdots\int^V(\mathbf{p}_j/m)\cdot\nabla_{\mathbf{R}_j}F^{(N)}(\mathbf{R}^N, \mathbf{p}^N; t)\,d\mathbf{R}^{N-1}d\mathbf{p}^{N-1}. \tag{9}$$

These very same integrals do, of course, appear in the equation of change for the singlet distribution function of a fluid whose molecules interact according to continuous potentials. For systems of this sort $F^{(N)}$ is continuous and differentiable everywhere except on a set of measure zero and so in that term of (9) involving differentiation with respect to $\mathbf{R}_1$ the order of integration and differentiation can be reversed to yield the simple result, $-(\mathbf{p}_1/m)\cdot\nabla_{\mathbf{R}_1}F^{(1)}(\mathbf{R}_1, \mathbf{p}_1; t)$. Furthermore, the divergence theorem can be used to transform the terms involving differentiation with respect to $\mathbf{R}_j$ $(j\neq 1)$ into integrals over the surface of V. Then if these surface contributions are assumed to be negligible, i.e., if $V\to\infty$, (9) reduces to the single "streaming term," $-(\mathbf{p}_1/m)\cdot\nabla_{\mathbf{R}_1}F^{(1)}(\mathbf{R}_1, \mathbf{p}_1; t)$.

For rigid spheres it is necessary to proceed more cautiously since $F^{(N)}$ is discontinuous at the surface $R_{ij}=\sigma$ (for all $i\neq j$). Thus, in (9) the integrations with respect to $\mathbf{R}_2, \cdots, \mathbf{R}_N$ extend only over the regions where $R_{ij}\geq\sigma$ for all $i\neq j$. To perform the integration of the first term in (9) we transform to the variables $\mathbf{R}_1, \mathbf{R}_{21}, \cdots, \mathbf{R}_{N1}$ where $\mathbf{R}_{j1}=\mathbf{R}_j-\mathbf{R}_1$, and integrate over the regions where the integrand is continuous. As a result of this change of variables the gradient operator $\nabla_{\mathbf{R}_1}$ becomes

$$\nabla_{\mathbf{R}_1}-\sum_{j=2}^{N}\nabla_{\mathbf{R}_{j1}}.$$

In the limit $V\to\infty$, $\nabla_{\mathbf{R}_1}$ commutes with the integration operations and the integral consequently assumes the form

$$-(\mathbf{p}_1/m)\cdot\nabla_{\mathbf{R}_1}\int\cdots\int_{\{R_{ij}\geq\sigma\}}F^{(N)}(\mathbf{R}_1, \mathbf{R}_1+\mathbf{R}_{21}, \cdots, \mathbf{R}_1+\mathbf{R}_{N1}, \mathbf{p}^N; t)\,d\mathbf{R}_{21}\cdots d\mathbf{R}_{N1}d\mathbf{p}^{N-1}$$

$$+\sum_{j=2}^{N}\int\cdots\int(\mathbf{p}_1/m)\cdot\nabla_{\mathbf{R}_{j1}}F^{(N)}(\mathbf{R}_1, \mathbf{R}_1+\mathbf{R}_{21}, \cdots, \mathbf{R}_1+\mathbf{R}_{N1}; \mathbf{p}^N; t)\,d\mathbf{R}_{21}\cdots d\mathbf{R}_{N1}d\mathbf{p}^{N-1}. \tag{10}$$

In the first term of this expression the original variables of integration can now be reintroduced while in the second the divergence theorem can be employed to obtain integrals over the surfaces $\mathbf{R}_{j1}=\sigma\mathbf{k}_{j1}$. As a result of these operations we obtain in place of (10) the expression,

$$-(\mathbf{p}_1/m)\cdot\nabla_{\mathbf{R}_1}F^{(1)}(\mathbf{R}_1, \mathbf{p}_1; t)-(\sigma^2/m)\sum_{j=2}^{N}\iint\mathbf{k}_{j1}\cdot\mathbf{p}_1F^{(2)}(\mathbf{R}_1, \mathbf{p}_1; \mathbf{R}_1+\sigma\mathbf{k}_{j1}, \mathbf{p}_j; t)\,d\mathbf{k}_{j1}d\mathbf{p}_j. \tag{11}$$

The second term in (9) will be readily identified as the sum of: (a) $(N-1)$ surface integrals arising from contacts between molecule 1 and the remaining $(N-1)$ members of the system; and (b) $(N-1)(N-2)$ surface integrals due to contacts between the various molecular pairs (ij), neither of which is 1. Thus the second term of (9) can be written as

$$(\sigma^2/m)\sum_{j=2}^{N}\iint\mathbf{k}_{j1}\cdot\mathbf{p}_jF^{(2)}(\mathbf{R}_1, \mathbf{p}_1; \mathbf{R}_1+\sigma\mathbf{k}_{j1}, \mathbf{p}_j; t)\,d\mathbf{k}_{j1}d\mathbf{p}_j$$

$$+(\sigma^2/m)\sum_{N\geq j>i>1}\sum\int\cdots\int\mathbf{k}_{ji}\cdot(\mathbf{p}_j-\mathbf{p}_i)F^{(3)}(\mathbf{R}_1, \mathbf{p}_1; \mathbf{R}_i, \mathbf{p}_i; \mathbf{R}_i+\sigma\mathbf{k}_{ji}, \mathbf{p}_j; t)\,d\mathbf{k}_{ji}d\mathbf{p}_id\mathbf{p}_jd\mathbf{R}_i. \tag{12}$$

The integration of these terms is now separated into integrals over the two hemispheres, $\mathbf{k}_{ji}\cdot(\mathbf{p}_j-\mathbf{p}_i)>0$ and $\mathbf{k}_{ji}\cdot(\mathbf{p}_j-\mathbf{p}_i)<0$. Then when the signs of the $\mathbf{k}$ vectors are reversed in the second of these integrals, the

total contribution of the "noncollision" term (9) becomes

$$-(\mathbf{p}_1/m)\cdot\nabla_{\mathbf{R}_1}F^{(1)}(\mathbf{R}_1,\mathbf{p}_1;t)+(\sigma^2/m)\sum_{j=2}^{N}\int\cdots\int_{\{\mathbf{k}_{j1}\cdot(\mathbf{p}_j-\mathbf{p}_1)>0\}}\mathbf{k}_{j1}\cdot(\mathbf{p}_j-\mathbf{p}_1)[F^{(2)}(\mathbf{R}_1,\mathbf{p}_1;\mathbf{R}_1+\sigma\mathbf{k}_{j1},\mathbf{p}_j;t)$$

$$-F^{(2)}(\mathbf{R}_1,\mathbf{p}_1;\mathbf{R}_1-\sigma\mathbf{k}_{j1},\mathbf{p}_j;t)]d\mathbf{k}_{j1}d\mathbf{p}_j+(\sigma^2/m)\sum_{N\geq i>1}\sum\int\cdots\int_{\{\mathbf{k}_{ji}\cdot(\mathbf{p}_j-\mathbf{p}_i)>0\}}\mathbf{k}_{ji}\cdot(\mathbf{p}_j-\mathbf{p}_i)$$

$$\times[F^{(3)}(\mathbf{R}_1,\mathbf{p}_1;\mathbf{R}_i,\mathbf{p}_i;\mathbf{R}_i+\sigma\mathbf{k}_{ji},\mathbf{p}_j;t)-F^{(3)}(\mathbf{R}_1,\mathbf{p}_1;\mathbf{R}_i,\mathbf{p}_i;\mathbf{R}_i-\sigma\mathbf{k}_{ji},\mathbf{p}_j;t)]d\mathbf{k}_{ji}d\mathbf{R}_id\mathbf{p}_id\mathbf{p}_j. \quad (13)$$

To obtain the final form of the equation of change for $F^{(1)}(\mathbf{R}_1,\mathbf{p}_1;t)$ this expression must now be added to (7). When this is done the terms involving $F^{(2)}(\mathbf{R}_1,\mathbf{p}_1;\mathbf{R}_1+\sigma\mathbf{k}_{j1},\mathbf{p}_j;t)$ and $F^{(3)}(\mathbf{R}_1,\mathbf{p}_1;\mathbf{R}_i,\mathbf{p}_i;\mathbf{R}_i+\sigma\mathbf{k}_{ji},\mathbf{p}_j;t)$ cancel, so that

$$[(\partial/\partial t)+(\mathbf{p}_1/m)\cdot\nabla_{\mathbf{R}_1}]F^{(1)}(\mathbf{R}_1,\mathbf{p}_1;t)$$

$$=(\sigma^2/m)\sum_{j=2}^{N}\iint_{\{\mathbf{k}_{j1}\cdot(\mathbf{p}_j-\mathbf{p}_1)>0\}}\mathbf{k}_{j1}\cdot(\mathbf{p}_j-\mathbf{p}_1)[F^{(2)}(\mathbf{R}_1,\mathbf{p}_{1'};\mathbf{R}_1+\sigma\mathbf{k}_{j1},\mathbf{p}_j;t)-F^{(2)}(\mathbf{R}_1,\mathbf{p}_1;\mathbf{R}_1-\sigma\mathbf{k}_{j1},\mathbf{p}_j;t)]d\mathbf{k}_{j1}d\mathbf{p}_j$$

$$+(\sigma^2/m)\sum_{N\geq i>1}\sum\int\cdots\int_{\{\mathbf{k}_{ji}\cdot(\mathbf{p}_j-\mathbf{p}_i)>0\}}\mathbf{k}_{ji}\cdot(\mathbf{p}_j-\mathbf{p}_i)[F^{(3)}(\mathbf{R}_1,\mathbf{p}_1;\mathbf{R}_i,\mathbf{p}_{i'};\mathbf{R}_i+\sigma\mathbf{k}_{ji},\mathbf{p}_{j'};t)$$

$$-F^{(3)}(\mathbf{R}_1,\mathbf{p}_1;\mathbf{R}_i,\mathbf{p}_i;\mathbf{R}_i-\sigma\mathbf{k}_{ji},\mathbf{p}_j;t)]d\mathbf{k}_{ji}d\mathbf{p}_id\mathbf{R}_id\mathbf{p}_j. \quad (14)$$

Although the first integral on the right-hand side of (14) describes the rate of change of $F^{(1)}(\mathbf{R}_1,\mathbf{p}_1;t)$ due to binary encounters directly involving molecule 1, the second pertains to collisional events which in no way modify the state of this molecule. Therefore, we should expect this term to be identically zero. To establish that this is so we separate the second integral into two parts, one involving

$$F^{(3)}(\mathbf{R}_1,\mathbf{p}_1;\mathbf{R}_i,\mathbf{p}_{i'};\mathbf{R}_i+\sigma\mathbf{k}_{ji},\mathbf{p}_{j'};t)$$

and the other

$$F^{(3)}(\mathbf{R}_1,\mathbf{p}_1;\mathbf{R}_i,\mathbf{p}_i;\mathbf{R}_i-\sigma\mathbf{k}_{ji},\mathbf{p}_j;t).$$

In the first of these two integrals we next transform the variables of integration from $\mathbf{p}_i$, $\mathbf{p}_j$ to $\mathbf{p}_{i'}$, $\mathbf{p}_{j'}$ [from (4) the Jacobian of this transformation is equal to -1] and change the variable of integration $\mathbf{k}_{ji}$ to $-\mathbf{k}_{ji}$.

If the labels of the pre- and postcollisional momenta are then interchanged and use is made of the dynamical result $\mathbf{k}_{ji}\cdot(\mathbf{p}_j-\mathbf{p}_i)=-\mathbf{k}_{ji}\cdot(\mathbf{p}_{j'}-\mathbf{p}_{i'})$ one sees that the two portions of the second integral on the right-hand side of (14) cancel one another.

Now, in the statistical theory one is concerned not with the specific distribution functions but with the *generic* distribution functions,

$$f^{(1)}(\mathbf{R},\mathbf{p};t)=\sum_{i=1}^{N}\iint\delta(\mathbf{R}_i-\mathbf{R})\delta(\mathbf{p}_i-\mathbf{p})F^{(1)}(\mathbf{R}_i,\mathbf{p}_i;t)d\mathbf{R}_id\mathbf{p}_i \quad (15)$$

and

$$f^{(2)}(\mathbf{R},\mathbf{p};\mathbf{R}'',\mathbf{p}'';t)=\sum_{N\geq j>i>1}\sum\int\cdots\int\delta(\mathbf{R}_i-\mathbf{R})\delta(\mathbf{p}_i-\mathbf{p})\delta(\mathbf{R}_j-\mathbf{R}'')\delta(\mathbf{p}_j-\mathbf{p}'')$$

$$\times F^{(2)}(\mathbf{R}_i,\mathbf{p}_i;\mathbf{R}_j,\mathbf{p}_j;t)d\mathbf{R}_id\mathbf{p}_id\mathbf{R}_jd\mathbf{p}_j, \quad (16)$$

which represent the probabilities of occupation of the prescribed dynamical state(s) by *any* suitable subset of the N molecules belonging to the system. From these definitions and (14) it follows that the equation of change for the singlet generic distribution function is

$$[(\partial/\partial t)+(\mathbf{p}/m)\cdot\nabla_{\mathbf{R}}]f^{(1)}(\mathbf{R},\mathbf{p};t)$$

$$=(\sigma^2/m)\iint_{\{\mathbf{k}\cdot(\mathbf{p}_1-\mathbf{p})>0\}}\mathbf{k}\cdot(\mathbf{p}_1-\mathbf{p})[f^{(2)}(\mathbf{R},\mathbf{p}';\mathbf{R}+\sigma\mathbf{k},\mathbf{p}_1';t)-f^{(2)}(\mathbf{R},\mathbf{p};\mathbf{R}-\sigma\mathbf{k},\mathbf{p}_1;t)]d\mathbf{k}d\mathbf{p}_1. \quad (17)$$

Here, of course, the subscripts on the variables are simply notational devices and do not refer to the states of specific molecules. The primed and unprimed variables are related to one another in the manner,

$$\mathbf{p}'=\mathbf{p}+\mathbf{k}\mathbf{k}\cdot(\mathbf{p}_1-\mathbf{p}),$$
$$\mathbf{p}_1'=\mathbf{p}_1-\mathbf{k}\mathbf{k}\cdot(\mathbf{p}_1-\mathbf{p}). \quad (18)$$

According to (17) the rate of change of the singlet distribution function can be determined only if the pair function is already known. Hence, (17) simply provides a relationship between these two functions and in no way represents a closed mathematical system which can be solved for $f^{(1)}(\mathbf{R}, \mathbf{p}; t)$. It is at this point in the statistical theory where the need for additional information concerning the relationship between the pair and singlet distribution functions invariably arises. Since no rigorous mathematical demonstration of such a relationship has yet been reported, the desired information must be obtained by appeal to physical intuition. The usual result of this intuitive approach is the "assumption of molecular chaos" which states that prior to a particular binary encounter the momenta of the two colliding molecules are completely uncorrelated. At low densities there should, indeed, be very little chance that the states of two such molecules are correlated by the past few encounters which they have suffered. However, at high densities there is a much greater probability that the dynamical states of the two molecules in question will be coupled by the past few collisional encounters in which they have taken part. This coupling may be due to the occurrence of prior binary encounters between these very same two molecules or to chains of collisional events which involve others as well.

A mathematical statement of this assumption is that for a state $(\mathbf{R}_1, \mathbf{p}_1; \mathbf{R}_2, \mathbf{p}_2)$ which *precedes* a binary encounter,

$$F^{(2)}(\mathbf{R}_1, \mathbf{p}_1; \mathbf{R}_2, \mathbf{p}_2; t) = \chi(\mathbf{R}_1, \mathbf{R}_2) F^{(1)}(\mathbf{R}_1, \mathbf{p}_1; t) F^{(1)}(\mathbf{R}_2, \mathbf{p}_2; t). \quad (19)$$

Here χ is a correlation function dependent only upon the locations of the two molecules and not upon their momenta. The form of Eq. (19) is very suggestive since it is precisely analogous to the relationship used in equilibrium statistical mechanics to define the radial distribution function, $g(\mathbf{R}_1, R_{21})$. Our present lack of theoretical information concerning the nonequilibrium spatial correlation function $\chi(\mathbf{R}_1, \mathbf{R}_2)$ suggests that we provisionally identify it with the equilibrium value of the radial distribution function appropriate to the local thermodynamical state of the fluid.

Now, before the chaos assumption [in the form of Eq. (19)] can be introduced into (17) we must be certain that the dynamical states involved refer to *pre-* rather than to postcollisional configurations, for otherwise little justification either theoretical or intuitive could be advanced in its defense. It is easily verified that the arguments of the pair functions appearing in (17) do indeed refer to precollision states, $(\mathbf{R}, \mathbf{p}'; \mathbf{R}+\sigma\mathbf{k}, \mathbf{p}_1')$ being the immediate precursor to the postcollisional configuration $(\mathbf{R}, \mathbf{p}; \mathbf{R}+\sigma\mathbf{k}, \mathbf{p}_1)$, and $(\mathbf{R}, \mathbf{p}; \mathbf{R}-\sigma\mathbf{k}, \mathbf{p}_1)$ the precursor to $(\mathbf{R}, \mathbf{p}'; \mathbf{R}-\sigma\mathbf{k}, \mathbf{p}_1')$. The corresponding portions of the integral appearing in (17) may, therefore, be interpreted as the collisional rates of gain and loss, respectively, to $f^{(1)}(\mathbf{R}, \mathbf{p}; t)$. It is worthy of notice that these arguments would have failed had the two pair distribution functions in (17) been evaluated at the same point, $(\mathbf{R}, \mathbf{R}+\sigma\mathbf{k})$, in pair configuration space. One is therefore inclined to doubt the validity of Dahler's[3] equation of change which differs from (17) in that the spatial coordinates of both pair d.f.'s are identical. In fact it can be shown that although his original derivation was erroneous, the correct application of his method results in an equation which is identical to (17).

As a consequence of these arguments we conclude that the Boltzmann equation for the rigid sphere fluid should be that originally proposed by Enskog,

$$[(\partial/\partial t)+(\mathbf{p}/m)\cdot\nabla_{\mathbf{R}}]f^{(1)}(\mathbf{R}, \mathbf{p}; t) = (\sigma^2/m)g(\mathbf{R}, \sigma) \iint_{\{\mathbf{k}\cdot(\mathbf{p}_1-\mathbf{p})>0\}} \mathbf{k}\cdot(\mathbf{p}_1-\mathbf{p})[f^{(1)}(\mathbf{R}, \mathbf{p}'; t)f^{(1)}(\mathbf{R}+\sigma\mathbf{k}, \mathbf{p}_1'; t) - f^{(1)}(\mathbf{R}, \mathbf{p}; t)f^{(1)}(\mathbf{R}-\sigma\mathbf{k}, \mathbf{p}_1; t)]\mathbf{dk}d\mathbf{p}_1 \quad (20)$$

Before proceeding to the derivation of the hydrodynamical equations let us examine some of the more noteworthy features of the development given in the foregoing. It will be observed that our final result, Eq. (14) or (17) could have been obtained more directly had we made use of the conditions

$$F^{(2)}(\mathbf{R}_1, \mathbf{p}_{10}; \mathbf{R}_1+\sigma\mathbf{k}_{j1}, \mathbf{p}_{j0}; t) = F^{(2)}(\mathbf{R}_1, \mathbf{p}_1; \mathbf{R}_1+\sigma\mathbf{k}_{j1}, \mathbf{p}_j; t); \quad \text{if} \quad \mathbf{k}_{j1}\cdot(\mathbf{p}_j-\mathbf{p}_1)>0, \quad (21)$$

and

$$F^{(3)}(\mathbf{R}_1, \mathbf{p}_1; \mathbf{R}_i, \mathbf{p}_{i0}; \mathbf{R}_i+\sigma\mathbf{k}_{ji}, \mathbf{p}_{j0}; t) = F^{(3)}(\mathbf{R}_1, \mathbf{p}_1; \mathbf{R}_i, \mathbf{p}_i; \mathbf{R}_i+\sigma\mathbf{k}_{ji}, \mathbf{p}_j; t); \quad \text{if} \quad \mathbf{k}_{ji}\cdot(\mathbf{p}_j-\mathbf{p}_i)>0. \quad (22)$$

[3] J. S. Dahler, J. Chem. Phys. **30**, 1447 (1959).

for with these conditions the "collisional contribution" to $\partial F^{(1)}(\mathbf{R}_1, \mathbf{p}_1; t)/\partial t$ given by (7) vanishes identically and the "noncollisional contributions" represented by (13) became equal to the sum of $-(\mathbf{p}_1/m)\cdot\nabla_{\mathbf{R}_1}F^{(1)}(\mathbf{R}_1, \mathbf{p}_1; t)$ and the terms appearing on the right-hand side of (14). Although no necessity for the introduction of these conditions arose in our derivation, there would nevertheless seem to be very strong arguments in favor of their validity. Thus, the statement of (21) and (22) is that the distribution function is invariant for the contact transformation associated with the evolution of the system during the interval of zero duration within which a binary collisional encounter takes place. We observe that while the duration of this event is zero, the requirement that $\mathbf{k}_{ji}\cdot(\mathbf{p}_j-\mathbf{p}_i)$ and $\mathbf{k}_{j1}\cdot(\mathbf{p}_j-\mathbf{p}_1)$ be nonnegative implies that the "direction of time" is positive, the states appearing on the left-hand sides of (21) and (22) being the immediate *pre*cursors of those on the right. If these conclusions are accepted then there would seem to be little reason to favor one method of derivation over the other.

These remarks suggest the the equation of change for $F^{(1)}$ could have been obtained in a still more direct manner. Thus, in the case of rigid spheres let us replace the Liouville equation with the simple diffusion equation

$$\partial F^{(N)}/\partial t+\sum_{i=1}^{N}(\mathbf{p}_i/m)\cdot\nabla_{\mathbf{R}_i}F^{(N)}=0,$$

where the collisional terms are now replaced by the boundary condition that $F^{(N)}$ be zero whenever $R_{ij}<\sigma$ for any pair of indices $i\neq j$. The integral contraction of this diffusion equation can then be accomplished in precisely the same manner as we have previously outlined to yield just those terms given by (13) and which, according to the conditions (21) and (22), may be rewritten in the form (14) In many ways this procedure is the most natural since it stresses the role of molecular collisions as sinks and sources of molecular pairs in the prescribed dynamical states. In particular, it is seen that the sources and sinks in singlet space are related to the passage (in pair space) of molecular pairs across the boundary surfaces, $R_{ij}=\sigma$.

III. HYDRODYNAMICAL EQUATIONS AND FLUXES

From (17) it is now a simple matter to derive the hydrodynamical equations and to find explicit representations for the fluxes of momentum and energy. We consider a function $\psi_i=\psi(\mathbf{p}_i)$ which is dependent only upon the linear momentum of the ith molecule. Then, multiplying (17) by $\psi(\mathbf{p})$ and integrating with respect to $\mathbf{p}$ we obtain

$$(\partial/\partial t)\int\psi(\mathbf{p})f^{(1)}(\mathbf{R}, \mathbf{p}; t)\,\mathbf{dp}+\nabla_{\mathbf{R}}\cdot\int(\mathbf{p}/m)\psi(\mathbf{p})f^{(1)}(\mathbf{R}, \mathbf{p}; t)\,\mathbf{dp}=\Theta(\mathbf{R}, t), \tag{23}$$

where

$$\Theta(\mathbf{R}, t)=(\sigma^2/m)\iiint_{\{\mathbf{k}\cdot(\mathbf{p}_1-\mathbf{p})>0\}}\mathbf{k}\cdot(\mathbf{p}_1-\mathbf{p})[f^{(2)}(\mathbf{R}, \mathbf{p}'; \mathbf{R}+\sigma\mathbf{k}, \mathbf{p}_1'; t)-f^{(2)}(\mathbf{R}, \mathbf{p}; \mathbf{R}-\sigma\mathbf{k}, \mathbf{p}_1; t)]\psi(\mathbf{p})\,\mathbf{dk}\mathbf{dp}\mathbf{dp}_1. \tag{24}$$

Just as in the usual deduction of Enskog's equations of change|| one now seeks to symmetrize the integrand of $\Theta(\mathbf{R}, t)$. In the first term of this integral we transform from the unprimed to primed variables of integration, replace $\mathbf{k}$ by $-\mathbf{k}$, and then interchange the roles of the primed and unprimed variables to obtain

$$\Theta(\mathbf{R}, t)=(\sigma^2/m)\iiint_{\{\mathbf{k}\cdot(\mathbf{p}_1-\mathbf{p})>0\}}\mathbf{k}\cdot(\mathbf{p}_1-\mathbf{p})[\psi(\mathbf{p}')-\psi(\mathbf{p})]f^{(2)}(\mathbf{R}, \mathbf{p}; \mathbf{R}-\sigma\mathbf{k}, \mathbf{p}_1; t)\,\mathbf{dk}\mathbf{dp}\mathbf{dp}_1. \tag{25}$$

From this it follows that for the choice of $\psi=m$, (23) will reduce to the familiar equation of continuity,

$$(\partial\rho/\partial t)+\nabla\cdot[\rho\mathbf{u}]=0, \tag{26}$$

where

$$\mathbf{u}=\rho^{-1}\int\mathbf{p}f^{(1)}(\mathbf{R}, \mathbf{p}; t)\,\mathbf{dp}$$

|| For example, see Hirschfelder, Curtiss, and Bird, *The Molecular Theory of Gases and Liquids* (John Wiley & Sons, Inc., New York, 1954), Chap. 7.

is the statistical analog to the hydrodynamical stream velocity and

$$\rho(\mathbf{R}, t) = m\int f^{(1)}(\mathbf{R}, \mathbf{p}; t)\,\mathbf{dp}$$

is the mass density.

To derive the other hydrodynamical equations a further modification of $\Theta(\mathbf{R}, t)$ is required. To this end we now interchange the roles of the variables $\mathbf{p}$ and $\mathbf{p}_1$ and utilize the symmetry property $f^{(2)}(\mathbf{R}, \mathbf{p}; \mathbf{R}'', \mathbf{p}''; t) = f^{(2)}(\mathbf{R}'', \mathbf{p}''; \mathbf{R}, \mathbf{p}; t)$. Then by changing the variable $\mathbf{k}$ to $-\mathbf{k}$ and reversing the roles of the primed and unprimed variables we find that

$$\Theta(\mathbf{R}, t) = (\sigma^2/m) \iiint_{\{\mathbf{k}\cdot(\mathbf{p}_1-\mathbf{p})>0\}} \mathbf{k}\cdot(\mathbf{p}_1-\mathbf{p})[\psi(\mathbf{p}_1')-\psi(\mathbf{p}_1)] f^{(2)}(\mathbf{R}+\sigma\mathbf{k}, \mathbf{p}; \mathbf{R}, \mathbf{p}_1; t)\,\mathbf{dkdpdp}_1. \tag{27}$$

Since the only functions ψ with which we shall be concerned are summational invariants satisfying the equation $\psi(\mathbf{p})+\psi(\mathbf{p}_1)=\psi(\mathbf{p}')+\psi(\mathbf{p}_1')$, (25) and (27) can be combined to yield

$$\Theta(\mathbf{R}, t) = -(\sigma^2/2m) \iiint_{\{\mathbf{k}\cdot(\mathbf{p}_1-\mathbf{p})<0\}} \mathbf{k}\cdot(\mathbf{p}_1-\mathbf{p})[\psi(\mathbf{p}')-\psi(\mathbf{p})] \times[f^{(2)}(\mathbf{R}, \mathbf{p}; \mathbf{R}+\sigma\mathbf{k}, \mathbf{p}_1; t)-f^{(2)}(\mathbf{R}-\sigma\mathbf{k}, \mathbf{p}; \mathbf{R}, \mathbf{p}_1; t)]\mathbf{dkdpdp}_1. \tag{28}$$

The difference of pair distribution functions appearing within the integral may then be written as

$$\begin{aligned}[f^{(2)}(\mathbf{R}, \mathbf{p}; \mathbf{R}+\sigma\mathbf{k}, \mathbf{p}_1; t)-f^{(2)}(\mathbf{R}-\sigma\mathbf{k}, \mathbf{p}; \mathbf{R}, \mathbf{p}_1; t)] &= \nabla_{\mathbf{R}}\cdot\{\sigma\mathbf{k}[1-(\sigma/2)\mathbf{k}\cdot\nabla_{\mathbf{R}}+\cdots+(1/n!)(-\sigma\mathbf{k}\cdot\nabla_{\mathbf{R}})^{n-1}+\cdots]f^{(2)}(\mathbf{R}, \mathbf{p}; \mathbf{R}+\sigma\mathbf{k}, \mathbf{p}_1; t)\} \\ &= \nabla_{\mathbf{R}}\cdot\left[\sigma\mathbf{k}\int_0^1 f^{(2)}(\mathbf{R}-\alpha\sigma\mathbf{k}, \mathbf{p}; \mathbf{R}-\alpha\sigma\mathbf{k}+\sigma\mathbf{k}, \mathbf{p}_1; t)\,d\alpha\right],\end{aligned} \tag{29}$$

the last form being due to Irving and Kirkwood.[1]

Substituting (29) into (28) we finally obtain the result $\Theta(\mathbf{R}, t) = -\nabla_{\mathbf{R}}\cdot\Psi(\mathbf{R}, t)$ where

$$\Psi(\mathbf{R}, t) = -(\sigma^3/2m) \iiint_{\{\mathbf{k}\cdot(\mathbf{p}_1-\mathbf{p})<0\}} \mathbf{kk}\cdot(\mathbf{p}_1-\mathbf{p})[\psi(\mathbf{p}')-\psi(\mathbf{p})] \times[1-(\sigma/2)\mathbf{k}\cdot\nabla_{\mathbf{R}}+\cdots+(1/n!)(-\sigma\mathbf{k}\cdot\nabla_{\mathbf{R}})^{n-1}+\cdots]f^{(2)}(\mathbf{R}, \mathbf{p}; \mathbf{R}+\sigma\mathbf{k}, \mathbf{p}_1; t)\,\mathbf{dkdpdp}_1, \tag{30}$$

may be interpreted as the "collisional transfer" contribution to the flux of the property ψ. This contribution, originally discovered by Enskog, is associated with the instantaneous collisional transfer of the property ψ from one of the colliding molecules to the other.

When ψ is chosen equal to the particle momentum, $\mathbf{p}$, Eqs. (23) and (30) reduce to

$$(\partial/\partial t)[\rho\mathbf{u}]+\nabla_{\mathbf{R}}\cdot[\rho\mathbf{uu}+\mathbf{p}]=0, \tag{31}$$

where $\mathbf{p}=\mathbf{p}_K+\mathbf{p}_U$ is the fluid pressure tensor defined as the sum of a kinetic contribution,

$$\mathbf{p}_K=(1/m)\int(\mathbf{p}-m\mathbf{u})(\mathbf{p}-m\mathbf{u})f^{(1)}(\mathbf{R}, \mathbf{p}; t)\,\mathbf{dp}, \tag{32}$$

and the collisional transfer contribution,

$$\mathbf{p}_U=(\sigma^3/2m) \iiint_{\{\mathbf{k}\cdot(\mathbf{p}_1-\mathbf{p})<0\}} \mathbf{k}\cdot\mathbf{k}(\mathbf{p}_1-\mathbf{p})(\mathbf{p}'-\mathbf{p})[1-(\sigma/2)\mathbf{k}\cdot\nabla_{\mathbf{R}}+\cdots]f^{(2)}(\mathbf{R}, \mathbf{p}; \mathbf{R}+\sigma\mathbf{k}; \mathbf{p}_1; t)\,\mathbf{dkdpdp}_1. \tag{33}$$

In the event that ψ is equal to the kinetic energy of a molecule, $p^2/2m$, we obtain from (23) and (30) the equation of energy balance,

$$(\partial/\partial t)E+\nabla_{\mathbf{R}}\cdot[\mathbf{u}E+\mathbf{q}+\mathbf{p}\cdot\mathbf{u}]=0 \tag{34}$$

where

$$E(\mathbf{R},t)=\int(p^2/2m)f^{(1)}(\mathbf{R},\mathbf{p};t)\,\mathbf{dp} \tag{35}$$

represents the local density of energy and the heat flux, $\mathbf{q}=\mathbf{q}_K+\mathbf{q}_V$, is the sum of kinetic and collisional transfer contributions given by

$$\mathbf{q}_K=(1/2m^2)\int(\mathbf{p}-m\mathbf{u})(\mathbf{p}-m\mathbf{u})^2 f^{(1)}(\mathbf{R},\mathbf{p};t)\,\mathbf{dp} \tag{36}$$

and

$$\mathbf{q}_V=(\sigma^3/2m^2)\iiint_{\{\mathbf{k}\cdot(\mathbf{p}_1-\mathbf{p})<0\}}\mathbf{kk}\cdot(\mathbf{p}_1-\mathbf{p})[|\,\mathbf{p}'-m\mathbf{u}\,|^2-|\,\mathbf{p}-m\mathbf{u}\,|^2][1-(\sigma/2)\mathbf{k}\cdot\nabla_{\mathbf{R}}+\cdots]$$
$$\times f^{(2)}(\mathbf{R},\mathbf{p};\mathbf{R}+\sigma\mathbf{k},\mathbf{p}_1;t)\,\mathbf{dkdpdp}_1. \tag{37}$$

The collisional transfer portions of the pressure tensor and of the heat flux (33) and (37) are precisely analogous to those derived by Irving and Kirkwood for molecular systems with continuous potentials of interaction. To obtain representations of these fluxes similar to those first proposed by Enskog we can employ dynamical considerations to replace $(\mathbf{p}'-\mathbf{p})$ in (33) by $\mathbf{kk}\cdot(\mathbf{p}_1-\mathbf{p})$ and $[|\,\mathbf{p}'-m\mathbf{u}\,|^2-|\,\mathbf{p}-m\mathbf{u}\,|^2]$ in (37) by

$$\mathbf{kk}\cdot(\mathbf{p}_1-\mathbf{p})\cdot(\mathbf{p}_1+\mathbf{p}-2m\mathbf{u}).$$

Next we observe that to terms of order σ,

$$[1-(\sigma/2)\mathbf{k}\cdot\nabla_{\mathbf{R}}+\cdots]f^{(2)}(\mathbf{R},\mathbf{p};\mathbf{R}+\sigma\mathbf{k},\mathbf{p}_1;t)\cong f^{(2)}(\mathbf{R}-(\sigma\mathbf{k}/2),\mathbf{p};\mathbf{R}+(\sigma\mathbf{k}/2),\mathbf{p}_1;t).$$

Consequently, (33) and (37) may be written in the alternate forms,

$$\mathbf{p}_V=(\sigma^3/2m^2)\iiint_{\{\mathbf{k}\cdot(\mathbf{p}_1-\mathbf{p})<0\}}\mathbf{kkkk}:(\mathbf{p}_1-\mathbf{p})(\mathbf{p}_1-\mathbf{p})f^{(2)}(\mathbf{R}-\sigma\mathbf{k}/2,\mathbf{p};\mathbf{R}+\sigma\mathbf{k}/2,\mathbf{p}_1;t)\,\mathbf{dkdpdp}_1, \tag{38}$$

and

$$\mathbf{q}_V=(\sigma^3/2m^2)\iiint_{\{\mathbf{k}\cdot(\mathbf{p}_1-\mathbf{p})<0\}}\mathbf{kkkk}:(\mathbf{p}_1-\mathbf{p})(\mathbf{p}_1-\mathbf{p})(\mathbf{p}_1+\mathbf{p}-2m\mathbf{u})f^{(2)}(\mathbf{R}-\sigma\mathbf{k}/2,\mathbf{p};\mathbf{R}+\sigma\mathbf{k}/2,\mathbf{p}_1;t)\,\mathbf{dkdpdp}_1. \tag{39}$$

Finally, if use is made of the chaos assumption, we can replace the pair distribution functions appearing in (38) and (39) by

$$f^{(1)}(\mathbf{R}-(\sigma\mathbf{k}/2),\mathbf{p};t)f^{(1)}(\mathbf{R}+(\sigma\mathbf{k}/2),\mathbf{p}_1;t)g(\mathbf{R},\sigma)$$

and thereby obtain Enskog's expressions for the collisional transfer contributions to the fluxes of momentum and energy. As mentioned previously there is great reason to doubt the validity of the chaos assumption at high fluid densities and so its use in simplifying the calculation of transport properties should be viewed as a provisional device which one eventually hopes to replace by a more rigorous and accurate theory.

VI. CONCLUDING REMARKS

Shortly after this article was submitted for publication two other studies of the rigid sphere fluid were reported. Consequently, it would now seem appropriate to devote some additional space to the comparison of these investigations with that which has been presented here.

Hollinger[4] has derived Eq. (17) by the use of techniques which closely resemble those we have described and which, in particular, involve the imposition upon the distribution functions of conditions similar to our (21) and (22). In general his conclusions concerning

[4] H. B. Hollinger (thesis, University of Wisconsin, August, 1959).

both the equation of change for the singlet d.f. and the hydrodynamical equations are in agreement with ours.

On the other hand, Rice, Kirkwood, Ross, and Zwanzig[5] have derived an equation of change for $f^{(1)}$ which differs from (17) in that the pair distribution functions appearing within the integrand are both evaluated at the *same* point in pair configuration space. This equation is identical to that proposed by Dahler.[3] One effect of this modification is to negate our interpretation of the right-hand side of (17) in terms of direct and inverse encounters. Were this modified equation of change correct, then the physical argument of chaos which we have used to rationalize the factorization of the pair distribution function, cf (19), could no longer be trusted. From a physical point of view, the concepts of direct and inverse collisions and of chaos are so very plausible that we might choose to defend our results on that basis alone. However, a less emotional and at once more rigorous argument in favor of our approach can be advanced on purely mathematical grounds. To illustrate this we must first emphasize that although the mathematical techniques of Rice, Kirkwood, Ross, and Zwanzig are quite different from ours, both methods result in the same "collisional contribution" to the equation of change. The distinction between the two approaches can therefore be traced to the different ways in which the integral contraction of the streaming terms,

$$\sum_{i=1}^{N}(\mathbf{p}_i/m)\cdot\nabla_{\mathbf{R}_i}F^{(N)},$$

is accomplished. Our method of calculation was forced upon us by the fact that in the case of rigid sphere interactions $F^{(N)}$ is a discontinuous function of its spatial arguments. However, Rice, Kirkwood, Ross, and Zwanzig first performed these integrations for a continuous potential of interaction and *then* considered the form of the resulting equation in the limit that the pair potential tends to the discontinuous rigid sphere interaction. It is this procedure which we question for in the limit $F^{(N)}$ will behave like a step function in the neighborhood of the points $R_{ij}=\sigma$. Therefore, the gradients $\nabla_{\mathbf{R}_{ij}}F^{(N)}$ exhibit delta singularities which are easily shown to provide just those terms which distinguish our result from that obtained by Rice *et al.* A detailed examination of the rigid sphere limit and of the relationship between this rather pathological case and that of softer potentials is nearing completion and will be communicated at a future date.

[5] Rice, Kirkwood, Ross, and Zwanzig, J. Chem. Phys. **31**, 575 (1959).

ACKNOWLEDGMENTS

The authors take this opportunity to acknowledge the very stimulating correspondence with Stuart A. Rice which contributed much to the success of this investigation.

THE JOURNAL OF CHEMICAL PHYSICS VOLUME 32, NUMBER 4 APRIL, 1960

Steady-State Studies by EPR on the Photodissociation of Some Alkyl Hydroperoxides

L. H. PIETTE

Instrument Division, Varian Associates, Palo Alto, California

AND

W. C. LANDGRAF

Department of Chemistry, Stanford University, Stanford, California

(Received November 12, 1959)

A new steady-state method for studying dynamic photochemical processes by EPR is discussed. The EPR spectra of some photolysed alkyl hydroperoxides are obtained and the free radical intermediates identified as alkoxy radicals.

Recombination rate constants of $\sim 10^6$ liters/mole sec were obtained with activation energies of ~ 4 kcal. A new EPR spectrometer with improved sensitivity capable of photoirradiation *in situ* and variable temperatures is discussed.

INTRODUCTION

IN the past, photochemists[1] had to rely upon product analysis and quantum yield determinations in order to obtain rate data and subsequent mechanisms for free radical formation and decay in the photolysis of simple organic molecules. More recently, trapping and flashing techniques[2–5] have been developed to study directly the unstable intermediates formed by either thermal or photolytic methods. These techniques, however, merely ascertain the presence of these intermediates and only in a few limited cases where the band spectra can be interpreted are the intermediates unequivocally identified as free radicals. Rate studies of such dynamic systems normally require rapid scanning devices.

It is now possible to utilize EPR techniques to study these dynamic photochemical processes. EPR is an especially advantageous approach since it will only respond to systems containing unpaired electrons such as free radicals, which are thought to be the intermediates formed. Using a highly sensitive EPR spectrometer it is now possible to conduct direct ultraviolet irradiations *in situ* and simultaneously measure the steady-state concentration of the free radical intermediates formed. The identification of these free radical intermediates can very often be inferred from their characteristic hyperfine patterns. Establishing sufficient steady-state concentrations that are observable can be achieved by suitable adjustment of the rate of formation and/or the rate of decay of these intermediates. The decay rate is the simplest parameter to adjust and is accomplished by a simple temperature variation.

The above technique has been applied to the study of the photochemical decomposition of primary, secondary, and tertiary hydroperoxides. The steady-state free radical intermediates in each case have been identified and their rates of decay measured at various temperatures.

EXPERIMENTAL PROCEDURE

The EPR spectrometer used was a Varian V-4500 equipped with the V-4560 100-kc field modulation system. The 100-kc field modulation improved the sensitivity of the spectrometer a factor of 16 over that of the 400-cps instrument. This enhancement of sensitivity was essential in observing the *n*-butyl hydroperoxide steady-state intermediate. The cavity used in these experiments contained radiation slots which permitted the entry of ultraviolet energy with negligible effects on the cavity microwave properties. See Fig. 1. The cavity contains special sample ports which permit the insertion of an 11-mm o.d. open-ended quartz Dewar insert.

Temperature variation and control were achieved by using a simple heat exchanger system. Dry nitrogen was passed through a copper coil immersed in liquid nitrogen and conducted through a Vycor transfer tube, with contained heater, to the quartz Dewar insert. The cooling gas passes around the quartz sample tube and is exhausted through the top of the cavity Dewar (see Fig. 2). Temperature control was achieved by varying the flow rate of the cooling gas and controlling the heater current.

The uv source was a GE medium-pressure mercury lamp, H85C3. The uv radiation was focused on the cavity slots by means of an aluminized parabolic mirror. The entire system was contained in an aluminum box with an attached aluminum leaf shutter so that the light could be rapidly extinguished. Rapid decay rates were measured with a Sanborn Model No. 151 recorder. The hyperfine splittings were measured, using a proton resonance spectrometer.

The hydroperoxides were prepared by the method of Mosher and Williams[6] and purified, first by reaction with 40% aqueous potassium hydroxide, followed by

[1] See C. Walling, *Free Radicals in Solution* (John Wiley & Sons, Inc., New York, 1957), p. 539.
[2] G. N. Lewis and M. Kasha, J. Am. Chem. Soc. **66**, 2100 (1944).
[3] M. Kasha, Chem. Revs. **41**, 401 (1947).
[4] R. G. W. Norrish and G. Porter, Nature **164**, 658 (1949).
[5] L. Bateman, Quart. Revs. **8**, 147 (1954).
[6] H. S. Mosher and H. Williams, J. Am. Chem. Soc. **76**, 2984 (1954).

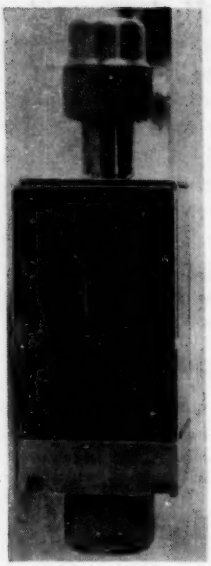

FIG. 1. 100-kc field modulation microwave cavity with slots for direct photo irradiation.

an extraction with ether, then by neutralization and reextraction with ether. They were dried over $MgSO_4$ and distilled at 0.5 mm pressure.

Approximately 0.1 cc of sample was placed in a 4-mm o.d. quartz tube which had been previously tested for irradiation damage by uv; then degassed in a vacuum line several times.

RESULTS AND DISCUSSION

Electron resonance spectra of the steady-state free radicals produced in the photolysis of *n*-butyl, *sec*-butyl, and *t*-butyl hydroperoxide are illustrated in Fig. 3. The GE H85C3 lamp that was used has an output of 0.07 watts at 2537 A and 0.02 watts at 2200–2300A. The energy at these wavelengths is capable of rupturing most of the bonds in the molecule and the signal observed is due to those free radicals that are the least reactive or the easiest to produce.

From simple bond energy considerations alone, the photo-induced dissociation would be expected to take place at the O—O bond, yielding the alkoxy and the hydroxy radical. The possible formation of alkyl R· and $\cdot HO_2$ radicals by rupture at the C—O bond cannot be ignored completely. Ingram *et al.*[7] have produced hydroxyl alkyl radicals

$$(CH_3-\dot{C}(OH)-CH_3)$$

at 77°K in peroxide-alcohol solutions as a result of uv irradiation. The possible production of peroxy ROO· and hydrogen radicals cannot be ignored either, even though the bond energy of the O—H bond is greater. If alkyl radicals are formed in the steady state, the *n*-butyl radical $CH_3CH_2CH_2CH_2\cdot$ so formed would be expected to give a hyperfine pattern of possibly three lines, each of which is further split into three more lines, for a total nine-line pattern, or, alternatively, if the α and β methylene protons are equivalent (α and β to the oxygen in the hydroperoxide), five equally spaced lines would be obtained. The *sec*-butyl alkyl radicals $CH_3\dot{C}HCH_2CH_3$ could possibly yield seven equally spaced lines as a result of the coupling with the five equivalent β carbon protons and the proton on the α carbon. Finally, the *t*-butyl radical

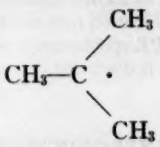

could conceivably give a 10-line pattern as a result of the coupling with all nine equivalent β protons. In each case the expected hyperfine coupling in these alkyl radicals would be 20 to 30 gauss, as has been observed for alkyl radicals stabilized by other techniques.[8–10] If alkoxy radicals RO· are formed in each case, however, it would be expected that the unpaired electron density at the α and β carbons would be attenuated by the oxygen and would therefore have a reduced value

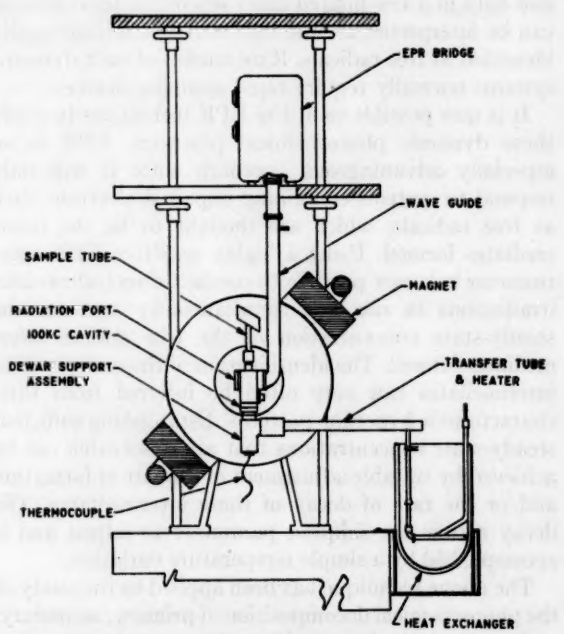

FIG. 2. Temperature flow apparatus for varying and controlling the temperature over the sample. System is shown as would be assembled in the magnet.

[7] J. F. Gibson, D. J. E. Ingram, M. C. R. Symons, and M. Townsend, Trans. Faraday Soc. **53**, 914 (1957).

[8] W. Gordy and H. Shields, Proc. Natl. Acad. Sci. U.S. **41**, 983 (1955).

[9] B. Smaller and M. S. Matheson, J. Chem. Phys. **28**, 1169 (1958).

[10] R. S. Alger, T. H. Anderson, and L. A. Webb, J. Chem. Phys. **30**, 695 (1959).

at the α carbon proton and a negligible value at the β carbon. The attenuation at the α carbon could conceivably be an order of magnitude and as a consequence a simple triplet would be anticipated for the *n*-butoxy, a doublet for the *sec*-butoxy, and a single line for the *t*-butoxy radical, with coupling constants of 2 to 3 gauss. If peroxy radicals ROO· were formed in each case, the unpaired electron density at the α carbons might be further attenuated by the second oxygen another order of magnitude and no hyperfine interaction with any of the protons on the α or β carbons would be resolved.

A triplet has been observed with a hyperfine coupling of 3.5 gauss for the *n*-butyl case, a doublet of 2.8 gauss for the *sec*-butyl, and a single line for the *t*-butyl; therefore, these steady-state free radicals are identified as the alkoxy radicals. A resonance for the hydroxy radical which would have been produced simultaneously with the alkoxy radical was not observed. It would be expected that the lifetime of the hydroxy radical is far too short at the temperatures at which these experiments were conducted, and hence would not be observed.

In order to decrease the decay rate of the *n*-butoxy radicals sufficiently to create an observable steady-state concentration it was necessary to operate at temperatures in the vicinity of 175°K. The *sec*-butoxy radicals require temperatures below 230°K and *t*-butoxy radicals require temperatures below 273°K. These steady-state temperatures reflect the decreased rate of recombination of these radicals, i.e., *n*-butoxy> than *sec*-butoxy> than *t*-butoxy.

Rate studies of the decay process were made on the three free radicals observed by merely measuring the time rate of decay of these signals when the uv lamp was extinguished. Figure 4 represents typical decay curves. Satisfactory decay curves that could be analyzed were obtained only for the secondary and *t*-butoxy radicals. The signal-to-noise ratio was too poor for the *n*-butoxy radical to get a reliable decay curve; however, the half-lives, $t_{\frac{1}{2}}$, could be measured for all three cases.

The decay curves were found to fit a second-order dependence very nicely, and this was checked by varying the initial steady-state concentration by two or threefold. Table I gives the second-order rate constants for the decay process where k_t refers to the reaction

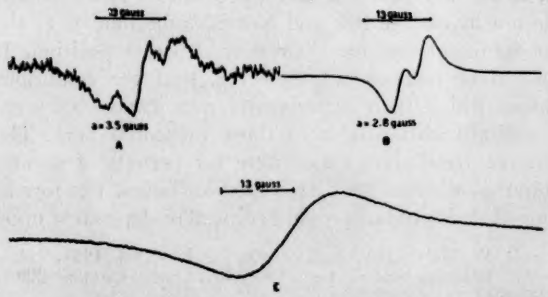

FIG. 3. (A) Steady-state *n*-butoxy free radical produced by uv irradiation at $T=183°K$, a=hyperfine coupling. (B) Steady-state *sec*-butoxy free radical at $T=203°K$, a=hyperfine coupling. (C) Steady-state *t*-butoxy free radical at $T=270°K$. No hyperfine observed. In each case the center of resonance did not deviate from $g=2.003$ for DPPH.

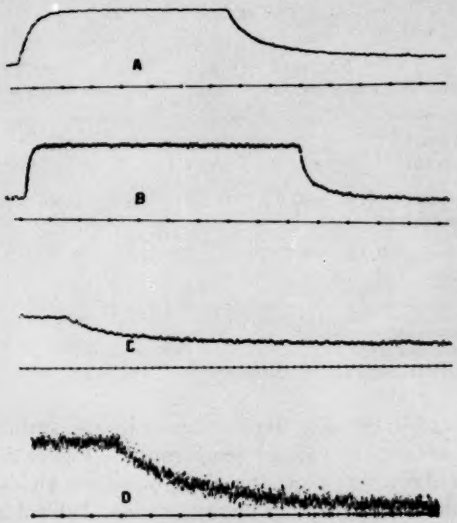

FIG. 4. (A) Decay curve for the *sec*-butoxy radical at $T=-75°C$. The curve shows the rise time as (1) far left, the light is turned on, (2) the steady-state is attained, (3) the light is then extinguished, and (4) the subsequent decay curve on the right is obtained. The X axis is graduated in 1 sec intervals. (B) Decay curve for *sec*-butoxy radical at $T=-40°C$. (C) Decay curve for *t*-butoxy radical at $T=-20°C$. X-time scale has been changed. (D) Decay curve for *t*-butoxy radical at $T=22°C$.

$$2\mathrm{RO}\cdot \xrightarrow{k_t} \text{diamagnetic products.} \qquad (1)$$

Alternatively, these rate constants can also be obtained from the steady-state condition which can be represented for the simple second-order case, as,

$$d(\mathrm{RO}\cdot)/dt=-k_t(\mathrm{RO}\cdot)^2+U, \qquad (2)$$

where U=the rate of formation of free radicals as determined by the lamp intensity. The steady-state condition implies that $d(\mathrm{RO}\cdot)/dt=0$, and Eq. (2) reduces to $U=k_t(\mathrm{RO}\cdot)_s^2$ where $(\mathrm{RO}\cdot)_s$=the steady-state concentration. Knowing U and measuring the steady-state concentration, one can determine the rate constant for the decay process. The steady-state concentration can be measured by comparing the first moment of the resonance lines of the sample with the first moment of a single line obtained from the eight-line spectrum of VO^{++} in a known concentration of aqueous vanadyl sulfate in 5N HCl. Moment comparisons of free radical lines with the lines of the stable VO^{++} are probably only accurate to within 20%. U, the rate of formation of the free radicals as determined by the lamp intensity, was obtained by lowering the temperature to a value at which the decay rate was negligible and measuring the time necessary to produce a certain concentration of free radicals.

TABLE I.

Compound	$k_t \times 10^{-8}$ moles sec/liter	$t_{\frac{1}{2}}$, sec	E_a, kcal/mole	$\nu^a \times 10^{-8}$ moles sec/liter
n-butyl hydroperoxide		0.1 (−90°C)		
sec-butyl hydroperoxide	4.9 (−40°C)	0.25	4±[b]	6.4 (−40°C)
t-butyl hydroperoxide	0.16 (−9°C)	3	4±[c]	1.2 (−9°C)

[a] Arrhenius frequency factor.
[b] Temperature range for E_a measurement was −40 to −85°C.
[c] Temperature range for E_a measurement was −5 to +22°C.

Activation energies were obtained by measuring the rate constants at various temperatures. Figure 5 is a typical Arrhenius plot, the slope of which yields the activation energy for the decay process. Table I gives these activation energies for the secondary and tertiary radical decay.

Bell[11] and Norrish *et al.*[12] have studied the thermal and photodissociation of *t*-butyl hydroperoxide, respectively. From product analysis and quantum yields

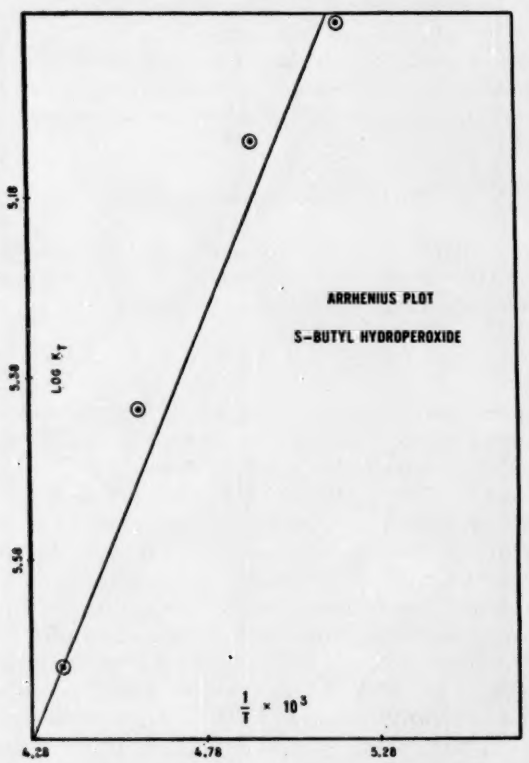

FIG. 5. Arrhenius plot for *sec*-butoxy free radical. The slope of the line is equal to E_a/RT.

[11] E. R. Bell, J. H. Raley, F. F. Rust, F. H. Seubold, Jr., and W. E. Vaughn, Discussions Faraday Soc. **10**, 242 (1951).
[12] J. T. Martin and R. G. W. Norrish, Proc. Roy. Soc. (London) **220A**, 322 (1953).

obtained for continuous irradiations, they both have arrived at a similar type of mechanism for the production and decay of the free radical intermediate. They suggest the following mechanism:

$$\mathrm{RO}\cdot + \mathrm{ROOH} \xrightarrow{k_p} \mathrm{ROO}\cdot + \mathrm{ROH}$$

$$2\mathrm{ROO}\cdot \xrightarrow{k_t'} 2\mathrm{RO}\cdot + \mathrm{O_2}.$$

They do not indicate a chain-terminating step, which must be a radical recombination. Their mechanism indicates that the most important process is proton abstraction by the alkoxy radical. Typical activation energies for such proton abstraction processes have been measured by others[13,14] and are reported to be 5–8 kcal. Rate constants of such reactions for simple hydrocarbons are reported to be $k_p = 0.5$ to 10 liters/mole sec. Free radical recombinations for peroxy radicals, however, are reported by these same authors to have activation energies of 2–5 kcal and rate constants $k_t' = 10^4$ to 10^6 liters/mole sec.

FIG. 6. Spectrum obtained from 10-min uv irradiation of *sec*-butyl hydroperoxide at 77°K.

It seems reasonable therefore from the obtained activation energies of 4 kcal and rate constants of $\sim 10^5$ liters/mole sec that the dominant reaction occurring in the decay process is the simple recombination of two alkoxy radicals to form the dialkyl peroxide,

$$2\mathrm{RO}\cdot \xrightarrow{k_t} \mathrm{ROOR}. \qquad (4)$$

The fact that the free radical signal decayed without the simultaneous growth of another signal due to a different free radical[15] seems to substantiate the conclusion that only the terminating step of radical recombination is taking place.

Dialkyl peroxides have been isolated as decomposition products in the decomposition of both *t*-butyl hydroperoxide and cumene hydroperoxide.[16] These results do not invalidate Bell and Norrish's mechanism as the predominant one for their over-all decomposition. It should be pointed out, however, that the conditions under which their experiments were conducted were drastically different from those presented here. The present irradiation times were for periods of several minutes, whereas they irradiated for hours. The formation of their products could very well be dependent upon

[13] H. W. Melville and S. Richards, J. Chem. Soc. **1954**, 944.
[14] L. Bateman and G. Gee, Proc. Roy. Soc. (London) **220A**, 322 (1953).
[15] A different free radical could be observed only if it had a different *g* value or hyperfine pattern, but could be definitely inferred to exist if the decay curves were more complicated than simple second order.
[16] J. W. L. Fordham and H. W. Williams, Can. J. Research **B27**, 943 (1949).

secondary reactions, whereas the formation of our products would probably be dependent only upon the direct recombination of the free radicals formed in the steady state. It is further expected that the rates being measured here are comparable to the rates of diffusion for the larger alkoxy free radicals.

At the low temperatures of these experiments (i.e., 175°K) the hydroperoxides are glassy in nature and therefore have an appreciable viscosity. It is expected then that the decay rates observed are diffusion-controlled, a fact that seems to be substantiated by a comparison of the decay rates of the bulkier *t*-butoxy radicals with the *n*-butoxy. The rates of recombination increase with decreasing complexity of the molecules, which is more consistent with a diffusion mechanism than it is with a difference in chemical reactivity for the three radicals.

Results obtained from continuous irradiations at 77°K seem to support Bell and Norrish's contention of free radicals other than the alkoxy being formed as a result of secondary reactions. There is no decay of the free radicals formed at 77°K when the uv source is extinguished. Figure 6 shows the spectrum obtained for the continuous irradiation at 77°K; it can be seen that the predominant species is still the alkoxy radical, although its hyperfine pattern has been smeared out, probably by the anisotropic term of the hyperfine interaction. It can also be seen from this spectrum that other free radicals have been produced with more complex hyperfine patterns.

Further experiments are under way on the temperature kinetics of these more reactive species stabilized at 77°K and on the effects of solvents on the recombination rates of the alkoxy radicals.

THE JOURNAL OF CHEMICAL PHYSICS VOLUME 32, NUMBER 4 APRIL, 1960

Experimental Oscillator Strength of the Comet-Tail System of CO^+

R. G. BENNETT AND E. W. DALBY

Radiation Physics Laboratory, Engineering Dept., E. I. du Pont de Nemours & Co., Inc.

(Received December 7, 1959)

The radiative lifetimes ($\tau_{v'}$) of the upper electronic state of the comet-tail bands of CO^+ have been measured. There is an appreciable variation (about 50%) of $\tau_{v'}$ with v', the upper electronic state vibrational quantum number. By using an average $\tau = (2.6)10^{-6}$ sec, and an average frequency corresponding to 4200 A an oscillator strength $f = (2.2 \pm 0.5)10^{-3}$ is calculated. The uncertainty arises largely because of the observed lifetime variation with v'.

INTRODUCTION

THE most prominent bands in the spectrum of comet tails are the $A\ ^2\Pi \rightarrow X\ ^2\Sigma$ transitions of CO^+ (often referred to as the "comet-tail" system). These bands, in common with others found in cometary spectra, are thought to arise through a resonance fluorescence excited by sunlight.[1] In order to proceed from the observed emission intensity to a calculation of the CO^+ concentration, it is necessary to know the oscillator strength for the transition. Until the present, no accurate experimental or theoretical values have been obtained for this quantity. This paper describes an experimental determination of the oscillator strength of the CO^+ comet-tail bands. This work was also stimulated by the hope that sufficiently accurate measurements on individual bands of this extensive system might provide information on the possible variation of the electronic dipole transition integral with vibrational quantum number.[2]

The experimental method has been described in detail in an earlier paper,[3] which reported a measurement of the f value of the first negative system of N_2^+. In short, the electronic transition of interest is excited by electron bombardment of a suitably chosen parent molecule. The electron beam is then turned off, and the light output measured as a function of time to yield the radiative lifetime of the upper electronic state. From this radiative lifetime for spontaneous emission the oscillator strength is calculated using the theory first developed by Einstein.[4]

RESULTS

The emission spectra obtained from the bombardment of CO, at a pressure of 3 μ, by 200-ev electrons, are shown in Figs. 1–2. The first spectrum was recorded with a small Bausch and Lomb grating monochromator using a DuMont K1306 (uv sensitive) photomultiplier detector. The second spectrum, which was taken with a Hilger medium quartz spectrograph, exhibits the same bands under greater resolving power.

[1] G. Herzberg, *Molecular Spectra and Molecular Structure. I. Diatomic Molecules* (D. Van Nostrand Co., Inc., Princeton, New Jersey, 1950), p. 485.

[2] R. W. Nicholls, Proc. Phys. Soc. (London) **A69**, 741 (1956); L. V. Wallace and R. W. Nicholls, J. Atmospheric and Terrest. Phys. **7**, 101 (1955).

[3] R. G. Bennett and F. W. Dalby, J. Chem. Phys. **31**, 434 (1959).

[4] A. Einstein, Physik. Z. **8**, 121 (1917).

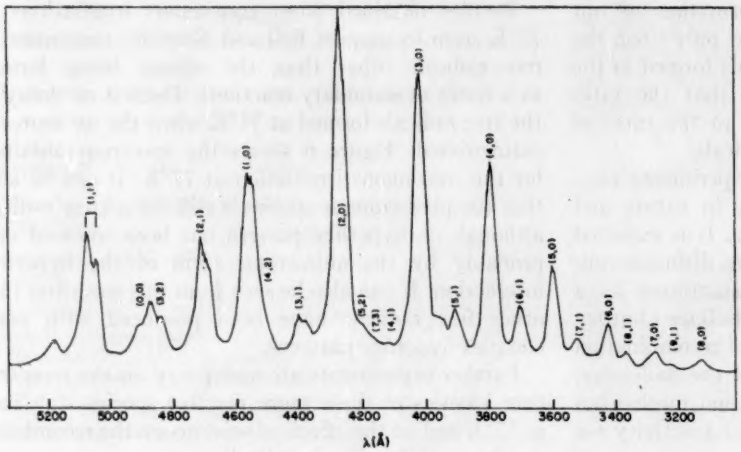

FIG. 1. Emission spectrum observed from CO excited by 200-ev electrons. The bands are identified with the "comet-tail" system of CO^+. A small Bausch and Lomb grating monochromator was used.

All the prominent spectral features agree both in wavelength and relative intensity with the well-known bands in the comet-tail system of $CO^+(A\ ^2\Pi \rightarrow X\ ^2\Sigma)$. The intercombination system $B \rightarrow A$ of CO^+ is discernible but very weak.

The lifetimes against spontaneous emission were measured for several vibrational bands. Figure 3 shows, on a semilog plot, the emission intensity for the (2, 0) band as a function of time after the excitation source is turned off. In Table I, the results of similar experiments on several vibrational levels are recorded. At least eight independent runs were made on each band. The quoted error is the statistical deviation between such runs. The electron energy used in the experiments was 185 ev.

It was found that the lifetimes are independent of CO pressure, over the range 0.2 μ to 6 μ. Thus, the possible perturbing effects on the radiative lifetime of collision quenching or trapping of resonance radiation can be ruled out. The possibility exists that the measured lifetime is not that of the $A\ ^2\Pi$ state, but is determined by a cascading transition from a higher electronic state. Since the Baldet-Johnson intercombination system $(B \rightarrow A)$ is weak (Fig. 2) in comparison to the comet-tail bands studied, it follows that any influence on the measured lifetimes due to cascading from the B state may be neglected. There are no known higher electronic states which combine with the A state of CO^+. Moreover, it is to be expected that the excitation probability under electron bombardment decreases significantly for the higher excited states.[5] If some cascading does exist, it might be possible to observe an effect on the measured lifetime by changing the duration of the electron beam pulse. Thus, if the initial state in the cascade and the A state have different lifetimes, then the relative excitation of these two levels may depend on the excitation duration. There was no effect on the measured lifetime when the electron beam pulse duration was changed from $2.4(10^{-7})$ sec to $3(10^{-6})$ sec. The photomultiplier "on-

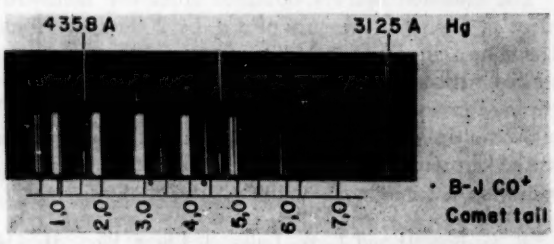

FIG. 2. The spectrum taken with a Hilger medium quartz spectrograph.

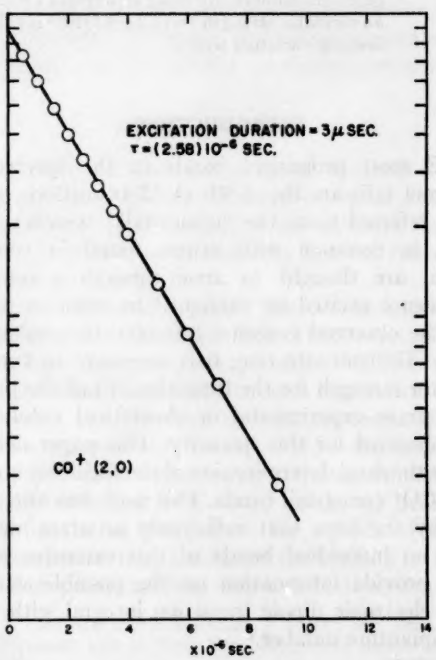

FIG. 3. Semilogarithmic plot of the free decay of light associated with the (2, 0) $A \rightarrow X$ transition of CO^+.

[5] H. S. W. Massey and E. H. S. Burhop, *Electronic and Ionic Impact Phenomena* (Oxford University Press, New York, 1956).

time" was 10^{-7} sec in both cases. The considerations mentioned above, taken together with the strict single-exponential nature of the decay curve (Fig. 3) make it unlikely that cascading is an important effect.

The individual vibrational levels were isolated by use of interference filters. The filters were chosen so that their wavelength of maximum transmission was within 15 A of the emission maximum studied. For light incident perpendicularly to the plane of the filter, the full width of each transmission band at half-maximum transmission is approximately 100 A. The band pass is not always sufficiently small to completely isolate individual CO^+ bands and some mixing occurs.

DISCUSSION

The spontaneous transition probability A, for transitions between vibrational levels v', v'' of the electronic states n, m having degeneracy d_n, d_m can be written,

$$A_{mn\,v'v''}=(64\pi^4e^2/3hc^3)\,(1/d_n)\nu^3\,|\,R_e^{mn}\,|^2\,|\,R_{\rm vib}^{v'v''}\,|^2, \quad (1)$$

where ν is the frequency of the transition, $|\,R_e^{mn}\,|^2$ is the electronic transition moment, and $|\,R_{\rm vib}^{v'v''}\,|^2$ is the Franck-Condon factor. (Some authors use $q_{v'v''}$ for the Franck-Condon factor.) The radiative lifetime for the v' vibrational level ($\tau_{v'}$), is then

$$(1/\tau_{v'})=(64\pi^4e^2/3hc^3)\,(1/d_n)\sum_{v''}\nu_{v'v''}{}^3\,|\,R_e^{mn}\,|^2\,|\,R_{\rm vib}^{v'v''}\,|^2 \quad (2)$$

The Franck-Condon factors satisfy the sum rule

$$\sum_{v''}|\,R_{\rm vib}^{v'v''}\,|^2=1, \quad \text{for all } v'. \quad (3)$$

It follows from Eq. (2) that for an extensive band system embracing a large frequency range, $\tau_{v'}$ would be expected to vary appreciably because of the ν^3 factor. Table I shows that there is indeed an appreciable variation (about 50%) in $\tau_{v'}$ with v'. Moreover, qualitatively, the dependence of $\tau_{v'}$ with frequency ν is in the expected direction, the levels arising from higher values of v' having the shorter lifetimes. However, for a quantitative comparison one needs rather complete Franck-Condon factors, which are unfortunately not available.[6] These factors would be difficult to evaluate because accurate vibrational wave functions for the high vibrational levels would be very complex.

TABLE I. Radiative lifetimes measured for various CO^+ comet-tail bands.

(v', v'')	τ (μsec)[a]
1, 0	2.61±0.20
1, 1	2.95±0.22
2, 0	2.48±0.21
2, 1	2.74±0.21
3, 0	2.36±0.15
4, 0	2.22±0.13
5, 0	2.11±0.13

[a] The error quoted is probable error, including only statistical uncertainty determined in each case by a series of at least eight measurements.

The interesting question as to whether or not the electronic transition moment is constant, independent of vibration, as was assumed in the treatment above, cannot at present be answered. The predominant variation of the τ's with v' is due to the variation in the frequency and without complete, accurate Franck-Condon factors one cannot determine if an additional variation due to changes in $|\,R_e^{mn}\,|^2$ occurs.

To determine an oscillator strength from the lifetime measurements, we take an average frequency corresponding to 4200 A and $\tau=(2.6)10^{-6}$ sec for the average lifetime. The oscillator strength, f, is given by

$$f=(mc^3/8\pi^2e^2\nu^2\tau)\,(d_n/d_m)=(2.2)10^{-3}.$$

The limitation upon the accuracy of this value, about ±25%, arises because ν^3 varies significantly across the band system.

When accurate, complete Franck-Condon factors become available the errors in this oscillator strength can be reduced to less than 10%. At the same time, small variations in the dipole transition moment as a function of vibrational quantum number can be determined.

[6] Jarmain, Fraser, and Nicholls, Astrophysical J. 122, 55 (1955).

Ground State Electronic Wave Function of Methane

R. K. NESBET

Department of Physics, Boston University, Boston, Massachusetts

(Received November 4, 1959)

An approximate electronic wave function for the ground state of CH_4, in the equilibrium nuclear configuration, has been obtained by a variational calculation. Approximate Hartree-Fock molecular orbitals are expanded as linear combinations of a set of basis orbitals of the form $f(x, y, z)\exp(-ar^2)$ centered on carbon and hydrogen. Five independent s orbitals and two p orbitals on carbon are combined with one simple Gaussian orbital on each hydrogen nucleus. The parameters specifying these orbitals were obtained by preliminary variational calculations on the carbon atom. Correlation effects due to all possible Slater determinants constructed from these orbitals are calculated by a perturbation method. Parallel calculations with the same orbitals were carried out on the ^3P ground state of carbon. Calculated ionization potential and dissociation energy are compared with experimental values.

I. INTRODUCTION

THIS paper describes an *ab initio* calculation of the ground state electronic wave function of CH_4 in the equilibrium nuclear configuration. The principal results obtained are calculated values of the ionization potential and cohesive energy of the molecule. This is the first calculation, on a molecule other than H_2, which includes a treatment of the correlation energy that can be compared with the atomic calculations of Boys and his collaborators.[1] Because of the great practical difficulty in carrying out calculations on a polyatomic molecule, it was not feasible to attempt to obtain the internuclear potential energy surface needed to calculate vibrational frequencies. This would require a series of electronic wave function calculations similar to that described here, but carried out to greater accuracy. It is hoped that the present work will serve as a model for more accurate calculations in the future.

The general method used is that proposed by Boys,[2] with modifications which emphasize a preliminary Hartree-Fock self-consistent field calculation as described in an earlier paper.[3] The principal numerical work separates into three distinct stages of calculation.

In the first stage, matrix elements of all operators in the many-electron Hamiltonian must be obtained as integrals over a set of orbitals (one-electron wave functions) which are chosen for their analytic simplicity. Orbitals of this basis set have no physical significance in themselves, but the self-consistent Hartree-Fock orbitals are expanded as linear combinations of them. On following the original proposal by Boys,[2] the basis orbitals used in the present work are Gaussian exponential functions ($\exp -ar^2$) centered on each of the nuclei in the molecule, multiplied by polynomials in the Cartesian coordinates (x, y, z). The special methods developed to evaluate the necessary molecular integrals will be described in another paper.[4] Some details pertinant to the present work are given in Sec. II.

The second major stage of calculation is an approximate Hartree-Fock calculation in the matrix representation of the basis set of orbitals. This method was originally proposed by Roothaan[5] and by Hall.[6] It has been generalized to deal with open shell configurations and adapted for the use of automatic digital computers by the author.[3,7] Approximate Hartree-Fock calculations by this method, carried out for the carbon atom and for CH_4, are described in Sec. III.

The third stage of calculation is a calculation of the correlation energy by the method of superposition of configurations. This was carried out for both carbon and CH_4 and is described in Sec. IV.

II. CALCULATION OF INTEGRALS OVER SYMMETRY ORBITALS

As shown by Boys[2] all matrix elements of the operators in the many-electron Hamiltonian for a molecule can be evaluated in closed form for a basis of orbitals of the form

$$\eta_{aA}=x_A{}^l y_A{}^m z_A{}^n \exp(-ar_A{}^2), \qquad (1)$$

where $x_A=x-A_x$, etc., and $\mathbf{A}$ is the vector position of any nucleus with respect to an arbitrary origin of coordinates. Here l, m, n are positive integers and a is any positive number.

Formulas for all necessary integrals for simple Gaussian functions $\exp(-ar_A{}^2)$ have been derived by Boys, who points out that integrals for the more complicated functions of Eq. (1) can be obtained by differentiating with respect to parameters. This procedure was used for the present work, except that one-center integrals were obtained by another method, based on recurrence formulas. The integrals were evaluated on the EDSAC digital computer. Details of

[1] S. F. Boys, Proc. Roy. Soc. (London) **A201**, 125 (1950); **A217**, 136, 235 (1953); M. J. M. Bernal and S. F. Boys, Phil. Trans. Roy. Soc. (London) **A245**, 139 (1952); S. F. Boys and V. E. Price, *ibid.* **A246**, 57 (1954).

[2] S. F. Boys, Proc. Roy. Soc. (London) **A200**, 542 (1950).

[3] R. K. Nesbet, Proc. Roy. Soc. (London) **A230**, 312 (1955).

[4] R. K. Nesbet, J. Chem. Phys. (to be published).

[5] C. C. J. Roothaan, Revs. Modern Phys. **23**, 69 (1951).

[6] C. G. Hall, Proc. Roy. Soc. (London) **A205**, 541 (1951).

[7] R. K. Nesbet, Ph.D. Dissertation, University of Cambridge (1954); Quarterly Progress Rept.; Solid State and Molecular Theory Group, M.I.T. (October 15, 1955), pp. 4–8 (unpublished).

special methods developed for the calculation of integrals will be given in another paper.[4]

Since the equilibrium nuclear framework of CH_4 is tetrahedral, it is convenient wherever possible to work with orbitals (one-electron wave functions) that transform as basis functions for irreducible representations of the tetrahedral group. Such orbitals will be called *symmetry orbitals*, whether or not they have any close relationship to the Hartree-Fock self-consistent orbitals, following the terminology of Hall and Lennard-Jones.[8] Since the Hartree-Fock orbitals for the electronic ground state have this property, they can be expanded as linear combinations of symmetry orbitals made up from functions of the basis set (which are centered on individual atoms). None of the operators in the Hamiltonian has matrix elements connecting symmetry orbitals with different transformation properties, and the matrix elements of these operators are the same for all members of a basis for a degenerate irreducible representation. These properties greatly reduce the dimensions of matrices which must be diagonalized in the Hartree-Fock calculation, and cause the reduced matrices to be identical in sets for each degenerate representation.

In the specific coordinate system chosen to describe the tetrahedral ground state of CH_4, the nuclei are located as follows:

$$\begin{aligned} &\mathrm{C} \quad (0,0,0)\\ &\mathrm{H}_a \quad (t,t,t)\\ &\mathrm{H}_b \quad (t,-t,t)\\ &\mathrm{H}_c \quad (-t,t,-t)\\ &\mathrm{H}_d \quad (-t,-t,t), \end{aligned} \tag{2}$$

where t is half the edge of a cube centered on the carbon nucleus. The observed CH distance[9] is 1.0936 A, equal to 2.0665 atomic units. Hence, the distance t is 1.19309 atomic units.

This nuclear framework is carried into itself by operations of the tetrahedral point group T_d. The character table of T_d is given by Eyring, Walter, and Kimball.[10] There are two nondegenerate irreducible representations of this group, A_1 and A_2, a doubly degenerate irreducible representation E, and two triply degenerate irreducible representations T_1 and T_2. In the coordinate system of Eq. (2), real spherical harmonics belong to the following irreducible representations of T_d:

$$\begin{aligned} &s \quad \epsilon A_1\\ &p_x,\ p_y,\ p_z \quad \epsilon T_2\\ &d_{3z^2-r^2},\ d_{x^2-y^2} \quad \epsilon E\\ &d_{xy},\ d_{xz},\ d_{yz} \quad \epsilon T_2 \end{aligned} \tag{3}$$

The irreducible representation matrices for T_d will be chosen so that the real spherical harmonics are typical of particular symmetry species (i.e., transform as basis functions for these irreducible representations). Then if $\sim$ is read "transforms as," the notation for symmetry orbitals adopted here is such that

$$\begin{aligned} &a_1 \sim s \quad \epsilon A_1\\ &e_1 \sim d_{3z^2-r^2};\ e_2 \sim d_{x^2-y^2} \quad \epsilon E\\ &t_{2x} \sim p_x,\ d_{xy};\ t_{2y} \sim p_y,\ d_{xz};\ t_{2z} \sim p_z,\ d_{xy} \quad \epsilon T_2. \end{aligned} \tag{4}$$

Any function invariant under the rotations of T_d but antisymmetrical under reflection in a plane of symmetry belongs to A_2 and will be designated by a_2. Basis functions for T_1 transform like those of T_2 under rotation but have opposite sign under reflection.

The EDSAC programs for evaluating the two-electron integrals (which depend on four orbitals from the basis set) were constructed separately for each of four possible cases. These cases differ according to whether the four orbitals are centered on a single point, on points lying on a straight line, on points lying in a plane, or on four unrelated points. The number of parameters needed to specify a particular integral varies among these cases, and the higher symmetry of the one-center and two-center integrals can be used to simplify the integral formulas. In fact, the one-center integrals are evaluated by an entirely different method from the others.

A different coordinate system was used for each of the three other types of integrals. For two-center integrals, C and H_a were taken to lie on a straight line at $\zeta_C=0$ and $\zeta_H=2.0665$ atomic units. The two directions orthogonal to ζ are ξ and η. Integrals in the standard coordinate system, Eq. (2), are obtained by choosing specific directions for ξ and η and transforming the calculated integrals (for orbitals such as p_ξ, p_η). The real spherical harmonics used transform as follows:

$$\begin{aligned} &p_\zeta=(\tfrac{1}{3})^{\frac{1}{2}}(p_z+p_x+p_y) \quad \text{or} \quad p_z=(\tfrac{1}{3})^{\frac{1}{2}}p_\zeta+(\tfrac{2}{3})^{\frac{1}{2}}p_\xi\\ &p_\xi=(\tfrac{1}{6})^{\frac{1}{2}}(2p_z-p_x-p_y) \quad \text{or} \quad p_x=(\tfrac{1}{3})^{\frac{1}{2}}p_\zeta-(\tfrac{1}{6})^{\frac{1}{2}}p_\xi+(\tfrac{1}{2})^{\frac{1}{2}}p_\eta\\ &p_\eta=(\tfrac{1}{2})^{\frac{1}{2}}(p_x-p_y) \qquad\qquad\quad p_y=(\tfrac{1}{3})^{\frac{1}{2}}p_\zeta-(\tfrac{1}{6})^{\frac{1}{2}}p_\xi-(\tfrac{1}{2})^{\frac{1}{2}}p_\eta. \end{aligned} \tag{5}$$

Two coordinate systems were used for three-center (planar) integrals. For integrals involving carbon orbitals and two different hydrogen orbitals the nuclei were located in a (ζ', ξ') plane, at the three points C(0, 0); H(1.1930944, $\pm$1.6872903). For integrals

[8] G. G. Hall and J. E. Lennard-Jones, Proc. Roy. Soc. (London) **A202**, 155 (1950); J. E. Lennard-Jones, *ibid.* **A198**, 1, 14 (1949).

[9] G. Herzberg, *Infrared and Raman Spectra of Polyatomic Molecules* (D. Van Nostrand Co., Inc., Princeton, New Jersey, 1945), p. 439.

[10] H. Eyring, J. Walter, and G. E. Kimball, *Quantum Chemistry* (John Wiley & Sons, Inc., New York, 1944), p. 388.

TABLE I. Parameters for normalized basis orbitals $N_a f(x, y, z) \exp(-ar^2)$.

Orbital	Atom	$f(x, y, z)$	a	N_a
η_1	C	$(1/4\pi)^{\frac{1}{2}}$	68.32339	60.0401943
η_2	C	$(1/4\pi)^{\frac{1}{2}}$	12.87507	17.1722496
η_3	C	$(1/4\pi)^{\frac{1}{2}}$	2.46240	4.9663117
η_4	C	$(1/4\pi)^{\frac{1}{2}}r^2$	1.93365	8.2735353
η_5	C	$(1/4\pi)^{\frac{1}{2}}r^2$	0.50613	0.7924810
η_6	C	$(3/4\pi)^{\frac{1}{2}}(x, y, z)$	0.17976	0.3414707
η_7	C	$(3/4\pi)^{\frac{1}{2}}(x, y, z)$	1.21210	3.7102795
η_8	H	$(3/4\pi)^{\frac{1}{2}}$	0.28294	0.9801402

involving three different hydrogen orbitals the nuclei were in a (ζ'', ξ'') plane at points $H_0(-1.7293781, 0)$; $H(1.1930944, \pm 1.6872903)$.

The real spherical harmonics in this system are related to the real harmonics in the standard reference frame by

$$\begin{aligned} p_{\zeta'} &= p_z & p_z &= p_{\zeta'} \\ p_{\xi'} &= -(\tfrac{1}{2})^{\frac{1}{2}}(p_x + p_y) \quad \text{or} & p_x &= (\tfrac{1}{2})^{\frac{1}{2}}(-p_{\xi'} + p_{\eta'}) \\ p_{\eta'} &= (\tfrac{1}{2})^{\frac{1}{2}}(p_x - p_y) & p_y &= -(\tfrac{1}{2})^{\frac{1}{2}}(p_{\xi'} + p_{\eta'}). \end{aligned} \tag{6}$$

None of the integrals calculated in the (ζ'', ξ'') plane was dependent on orientation, so no transformation was required.

Given integrals between basic orbitals, with all real spherical harmonics on carbon (p_x, p_y, p_z) referred to the standard reference frame, values of integrals were required for symmetry orbitals constructed from orbitals centered on the hydrogen nuclei. Only orbitals spherically symmetric about each hydrogen nucleus were considered. Let four such orbitals, equivalent except for their location on the different nuclei of Eq. (2) be denoted by $\eta_a, \eta_b, \eta_c, \eta_d$.

In the present calculations, five s orbitals and two independent p orbitals of the basis set were centered on carbon. By the choice of coordinate system made, these are already symmetry orbitals of the tetrahedral group, and can be denoted by

$$1a_1, \cdots, 5a_1 \quad \text{and} \quad 6l_{2x}, 6l_{2y}, \cdots, 7l_{2z}. \tag{7}$$

The symmetry orbitals constructed from basis orbitals on hydrogen are:

$$\begin{aligned} 0a_1 &= A = \tfrac{1}{4}(\eta_a + \eta_b + \eta_c + \eta_d) \\ 8l_{2x} &= X = \tfrac{1}{4}(\eta_a + \eta_b - \eta_c - \eta_d) \\ 8l_{2y} &= Y = \tfrac{1}{4}(\eta_a - \eta_b + \eta_c - \eta_d) \\ 8l_{2z} &= Z = \tfrac{1}{4}(\eta_a - \eta_b - \eta_c + \eta_d). \end{aligned} \tag{8}$$

These orbitals are not normalized, but are of course orthogonal. The inverse transformation is

$$\begin{aligned} \eta_a &= A + X + Y + Z \\ \eta_b &= A + X - Y - Z \\ \eta_c &= A - X + Y - Z \\ \eta_d &= A - X - Y + Z. \end{aligned} \tag{9}$$

These orbitals are normalized.

Integrals between the symmetry orbitals are linear combinations of integrals calculated between hydrogen orbitals, referred to the standard coordinate system. These linear transformations and the inverse transformations were derived, expressed in terms of linearly independent integrals only. The inverse transformations were carried out to check the direct transformations and incidentally to check that all possible integrals had been calculated.

These transformations were carried out on a desk calculator. With the necessary checks against random errors, these manual calculations required a greater amount of time than the total spent on the rest of the calculation on CH_4, programed for EDSAC.

III. APPROXIMATE HARTREE-FOCK CALCULATIONS

Since any antisymmetric many-electron wave function can be expressed as a linear combination of Slater determinants, it is convenient in solving Schrödinger's equation by perturbation or variational methods to obtain as a zeroth order approximation a single Slater determinant of stationary energy. When expressed analytically, this condition can be shown to be equivalent to the statement that the occupied orbitals of this Slater determinant should satisfy the Hartree-Fock integro-differential equations.[11] Because of the great practical difficulty in solving such equations for the electronic orbitals of molecules, it is convenient to approximate these orbitals by linear combinations of simple analytic functions centered on each atomic nucleus in the molecule. It can be shown that the equations satisfied by the coefficients in such linear combinations are just the matrix representation of the Hartree-Fock equations in a basis of the arbitrarily chosen analytic atomic orbitals.[5,6] This method can be used for open shell systems (such as the carbon atom ground state) by the method of symmetry and equivalence restrictions,[3] which was devised to make such matrix Hartree-Fock calculations possible in terms of iterated homogeneous linear eigenvalue equations.

Once the integrals over basic orbitals, matrix elements of the operators in the many-electron Hamilton, have been expressed in terms of symmetry orbitals, as discussed in Sec. II, above, standard digital computer programs can be used for the actual approximate Hartree-Fock calculations. These programs, which were originally written for the present calculations on the EDSAC, have been rewritten twice without major modifications in their structure, and will be described in detail elsewhere.[7] Because of the use of the method of symmetry and equivalence restrictions, these programs can be used for calculations on either closed shell or open shell systems.

Results of calculations on the carbon atom are summarized in Tables I and II. A series of preliminary

[11] V. Fock, Z. Phys. **61**, 126 (1930); **81**, 195 (1933); P. A. M. Dirac, Proc. Cambridge Phil. Soc. **26**, 376 (1930).

TABLE II. One-electron energies ϵ_i and coefficients x_{ia} for orthonormal self-consistent orbitals ϕ_i of C(^3P) expressed as linear combinations of normalized atomic basis orbitals η_a.

ϕ_i	ϵ_i	x_{i1}	x_{i2}	x_{i3}	x_{i4}	x_{i5}
$1s$	−11.24461 au	0.15570	0.55379	0.49645	−0.09719	0.02240
$2s$	−0.81993	−0.03814	−0.14808	−0.01221	0.39489	0.74469
$3s$	2.12392	0.06295	0.20176	0.05942	−1.08981	0.87028
$4s$	12.89106	−0.10210	−1.24753	2.06145	−1.47341	0.34833
$5s$	91.60010	1.36267	−1.51815	0.93828	−0.51550	0.10558
	ϵ_i	x_{i6}	x_{i7}			
$2p$	−0.37132	0.76752	0.41784			
$3p$	1.10492	−0.75366	0.99121			

calculations were carried out on the single determinant wave function

$$\det(1s)^2(2s)^2(2p_z)^2, \tag{10}$$

which has a closed shell configuration with respect to the axial group, and thus does not require the variational constraint of equivalence restriction.[12] This wave function is actually a linear combination of ^1S and ^1D, and is not by itself an approximation to a steady state of carbon. These preliminary calculations were used to determine values of the parameters (the constants in the exponent) of the basic orbitals of the Gaussian class centered on carbon, by calculating a Hartree-Fock energy for each choice of parameters, and minimizing this by the method of steepest descents. Final values of the parameters are listed in Table I. Since each value of this energy function represented a major calculation, it was not possible to carry out more than a few cycles in the variation of the set of seven independent exponents. However, any further improvement in the calculated Hartree-Fock energy with the same number of Gaussian orbitals should be small compared with the effect of adding another orbital to the set.

The Hartree-Fock energy calculated for the wave function, Eq. (10), with the parameters listed in Table I was −36.99052 au, compared with an experimental energy [a weighted average $\frac{2}{3}E(^1D)+\frac{1}{3}E(^1S)$] of −37.792 au.[13] The one-electron energies obtained as eigenvalues of the approximate Hartree-Fock operator were

$$\begin{aligned}\epsilon(1s)&=-11.25138 \text{ au}\\ \epsilon(2s)&=-0.72321\\ \epsilon(2p)&=-0.29927.\end{aligned} \tag{11}$$

These may be compared with the appropriately weighted average of the one-electron energies obtained in a numerical Hartree-Fock calculation of the lowest ^1D and ^1S states of carbon by Jucys[14]:

$$\begin{aligned}\epsilon(1s)&=-11.362 \text{ au}\\ \epsilon(2s)&=-0.7295\\ \epsilon(2p)&=-0.3580.\end{aligned} \tag{12}$$

[12] R. K. Nesbet, Phys. Rev. **109**, 1017 (1958).
[13] C. E. Moore, *Atomic Energy Levels* [National Bureau of Standards (U.S.), 1949], Circular 476, Vol. I.
[14] A. Jucys, Proc. Roy. Soc. (London) **A173**, 59 (1939).

The same basis orbitals were used for a similar calculation of the ^3P ground state wave function of carbon. Expressed in terms of real spherical harmonics a single Slater determinant Φ_0 can be constructed, which is a ^3P eigenfunction of the total angular momentum operators L^2 and S^2. In a convenient notation, with the antisymmetrizing operator to be understood, and spatial orbitals with $\alpha(m_s=+\frac{1}{2})$ spin factors written to the left of a comma, spatial orbitals with $\beta(m_s=-\frac{1}{2})$ written to the right, this is

$$\Phi_0=1s2s2p_x2p_y,\ 1s2s. \tag{13}$$

Since this function is not invariant under spin transformations nor under spatial rotations, the method of symmetry and equivalence restrictions[3] was used in the approximate matrix Hartree-Fock calculation. In the present case, this meant that at each iteration of the self-consistent calculation only those matrices of the one-electron Hamiltonian were diagonalized which represented matrix elements between orbitals of the symmetry species $s\alpha$ or of the symmetry species $p_z\alpha$. Matrix elements between orbitals of symmetry species $s\beta$ would be different from those for $s\alpha$.

The special configuration interaction matrix elements due to this equivalence restriction[3] were found to lead to negligible effects in this case. This indicates that the error introduced by using the method of symmetry and equivalence restrictions, rather than the traditional Hartree-Fock method (in a comparable matrix representation), was negligible.

Results of this approximate Hartree-Fock calculation on C(^3P) are given in Table II.

The ground state electronic wave function of methane is approximated by a single Slater determinant

$$\left.\begin{aligned}\Phi_0&=1a_12a_11l_{2x}1l_{2y}1l_{2z},\ 1a_12a_11l_{2x}1l_{2y}1l_{2z}\\ &=\det(1a_1)^2(2a_1)^2(1l_2)^6\end{aligned}\right\} \tag{14}$$

Here, the l_2 orbitals of lowest energy are numbered $1l_2$ although they correspond to the $2p$ orbital of carbon. Since Φ_0 is invariant under spin transformations and operations of the tetrahedral point group T_d, this is a closed-shell configuration and no special restrictions are needed in the Hartree-Fock calculation.

Results of an approximate Hartree-Fock calculation, using the basis orbitals centered on carbon listed in

TABLE III. One-electron energies ϵ_i and coefficients x_{ia} for orthonormal self-consistent orbitals ϕ_i of $CH_4(^1A_1)$ expressed as linear combinations of basis symmetry orbitals. The symmetry orbitals constructed from atomic orbitals on hydrogen are defined by Eq. (8); those on carbon are the same as the atomic basis orbitals of Table II.

ϕ_i	ϵ_i	x_{i1}	x_{i2}	x_{i3}	x_{i4}	x_{i5}	x_{i6}
$1a_1$	−11.22842 au	−0.15583	−0.55335	−0.49862	0.09782	−0.03575	0.02346
$2a_1$	−1.01218	−0.03142	−0.12343	−0.04907	0.26920	0.45854	0.66874
$3a_1$	0.37519	0.02729	0.09671	−0.15253	−0.49136	−1.42860	2.93737
$4a_1$	2.47421	−0.06199	−0.20472	−0.13367	1.00921	−1.60337	1.51840
$5a_1$	13.10282	0.10227	1.25188	−2.10731	1.50314	−1.61037	0.45499
$6a_1$	91.72376	−1.36353	1.52542	−0.95946	0.52822	−0.18137	0.13171
	ϵ_i	x_{i6}	x_{i7}	x_{i8}			
$1l_2$	−0.53246	0.41751	0.30803	1.05645			
$2l_2$	0.35993	−1.58860	−0.17367	3.86624			
$3l_2$	1.09381	−0.87135	1.01654	0.48428			

TABLE IV. Symmetrized functions Ψ_ν, orthonormal linear combinations of Slater determinants for $C(^3P)$. A single normalized Slater $\det\phi_i\alpha\ \phi_j\alpha\ \phi_k\alpha\ \phi_l\alpha\ \phi_m\beta\ \phi_n\beta$ is symbolized by $(i\,j\,k\,l,\,m\,n)$. $\Psi_0=\Phi_0$, the Hartree-Fock determinantal function. Orbital $2p_x$ is denoted by 2_x, etc. The orbitals are those of Table II.

ν	Formula
0	$(1\,2\,2_x\,2_y,\,1\,2)$
1	$(1\,2_z\,2_x\,2_y,\,1\,2_z)$
2	$(\frac{1}{2})\{(1\,2\,3_x\,2_y,\,1\,3)+(1\,2\,3\,2_y,\,1\,3_x)+(1\,2\,2_x\,3_y,\,1\,3)+(1\,2\,2_x\,3,\,1\,3_y)\}$
3	$(1\,2\,3_z\,3_y,\,1\,2)$
4	$(\frac{1}{2})^{\frac{1}{2}}\{(1\,3_z\,2_x\,2_y,\,1\,3_z)+(1\,3_z\,2_x\,2_y,\,1\,3_z)+(1\,3_y\,2_x\,2_y,\,1\,3_y)\}$
5	$(1\,3\,2_x\,2_y,\,1\,3)$
6	$(1/12)^{\frac{1}{2}}\{3(1\,2_z\,2_x\,2_y,\,1\,3_z)+(1\,3_z\,2_x\,2_y,\,1\,2_z)+(1\,3_z\,2_z\,2_x,\,1\,2_y)+(1\,3_z\,2_y\,2_z,\,1\,2_x)\}$
7	$(\frac{1}{2})\{(1\,3\,3_x\,2_y,\,1\,2)+(1\,2\,3\,3_x,\,1\,2_y)+(1\,3\,2_x\,3_y,\,1\,2)+(1\,2\,3_y\,3,\,1\,2_x)\}$
8	$(3\,2\,2_x\,2_y,\,3\,2)$
9	$(\frac{1}{2})^{\frac{1}{2}}\{(1\,4\,2_x\,2_y,\,4\,2)+(4\,2\,2_x2_y,\,1\,4)\}$

Table I, and symmetry orbitals constructed from a single Gaussian function centered on each hydrogen nucleus, as discussed in Sec. II, are given in Table III.

IV. SUPERPOSITION OF CONFIGURATIONS

The method of superposition of configurations is a variational approximation to a steady-state solution of Schrödinger's equation by the Ritz procedure. Matrix elements of the many-particle Hamiltonian are evaluated between all functions of an orthonormal basis set of Slater determinants. If this matrix is diagonalized the eigenvectors correspond to expansions of eigenfunctions as linear combinations of the basis functions, and the matrix eigenvalues converge to energy eigenvalues of the Hamiltonian as the basis is expanded to become complete.

This method has been used by Boys and his collaborators[1] to obtain the most accurate electronic wave functions currently available for many-electron atoms.

Because of the large number of independent basis orbitals used in the present work, the number of orthonormal Slater determinants that could be constructed from these is extremely large. For CH_4, this number is the number of combinations of 30 objects taken ten at a time, if the spin and spatial symmetries are not taken into account. Even if only the fully symmetrical singlet states are considered, there are still several thousand that could be constructed.

This situation is enormously simplified by the use of Brillouin's theorem, which holds for the approximate Hartree-Fock functions obtained in the first stages of the present calculations,[15,3] and by use of the second order perturbation theory. Brillouin's theorem limits the excited configurations that contribute in the second order of perturbation theory to those obtained by replacing two orbitals in the Hartree-Fock function, except for some additional configurations due to equivalence and symmetry restrictions in open shell cases.[3] The use of perturbation theory is justified *a posteriori* in the present work by the smallness of the second order energy effects calculated.

In the procedure used, it was not necessary to evaluate matrix elements between symmetrized combinations of Slater determinants unless matrix elements between particular determinants in these symmetrized functions were sufficiently large to give a nonnegligible contribution to the energy. This could very rapidly be

[15] L. Brillouin, *Les Champs Self-Consistent de Hartree et de Fock* (Hermann & Cie., Paris, France, 1934), No. 159 in series: Actualités Scientifiques et Industrielles.

TABLE V. Symmetrized functions Ψ_ν, orthonormal linear combinations of Slater determinants for $CH_4(^1A_1)$. Doubly occupied orbitals are grouped together, thus $(1\,2)^2(i\,j,\,k\,l) = (1\,2\,i\,j,\,1\,2\,k\,l)$, and singlet spin operators are defined as follows:

$\mathcal{S}_0(i,\,j) = (\frac{1}{2})^{\frac{1}{2}}[(i,\,j)+(j,\,i)]$,

$\mathcal{S}_1(i\,j,\,k\,l) = (1/12)^{\frac{1}{2}}[2(i\,j,\,k\,l)+(k\,j,\,i\,l)+(l\,j,\,k\,i)+(i\,k,\,j\,l)+(i\,l,\,k\,j)+2(k\,l,\,i\,j)]$,

$\mathcal{S}_2(i\,j,\,k\,l) = (\frac{1}{2})[(k\,j,\,k\,l)-(l\,j,\,k\,i)-(i\,k,\,j\,l)+(k\,l,\,i\,j)]$.

Otherwise the notation is the same as that of Table IV. The orbitals are those of Table III.

ν	Formula
0	$(1\,2\,1_x\,1_y\,1_z)^2$
1	$(\frac{1}{3})^{\frac{1}{2}}\{(1\,2)^2[(1_y)^2\mathcal{S}_1(1_x\,3_z,\,3_x\,1_z)+(1_z)^2\mathcal{S}_1(1_y\,3_x,\,3_y\,1_x)+(1_x)^2\mathcal{S}_1(1_z3_y,\,3_z\,1_y)]\}$
2	$(\frac{1}{3})^{\frac{1}{2}}\{(1\,2)^2[(1_x\,1_y\,3_z)^2+(3_x\,1_y\,1_z)^2+(1_x\,3_y\,1_z)^2]\}$
3	$(\frac{1}{3})^{\frac{1}{2}}\{(1\,2)^2[(1_y)^2\mathcal{S}^2(1_x\,2_z,\,2_x\,1_z)+(1_z)^2\mathcal{S}_2(1_y\,2_x,\,2_y\,1_x)+(1_x)^2\mathcal{S}_2(1_z\,2_y,\,2_z\,1_y)]\}$
4	$(1/6)^{\frac{1}{2}}\{(1\,2)^2[(1_y)^2\mathcal{S}_1(1_x\,2_z,\,3_x\,1_z)+(1_z)^2\mathcal{S}_1(1_y\,2_z,\,3_y\,1_z)+(1_x)^2\mathcal{S}_1(1_z\,2_y,\,3_z\,1_y)+(1_y)^2\mathcal{S}_1(2_x\,1_z,\,1_x\,3_z)+(1_z)^2\mathcal{S}_1(2_y\,1_x,\,1_y\,3_x)+(1_x)^2\mathcal{S}_1(2_z\,1_y,\,1_z\,3_y)]\}$
5	$(\frac{1}{3})^{\frac{1}{2}}\{(1\,2)^2[(1_y)^2\mathcal{S}_1(1_x\,3,\,2_y\,1_z)+(1_z)^2\mathcal{S}_1(1_y\,3,\,2_z\,1_x)+(1_x)^2\mathcal{S}_1(1_z\,3,\,2_x\,1_y)]\}$
6	$(\frac{1}{3})^{\frac{1}{2}}\{(1\,2)^2[(1_y)^2\mathcal{S}_2(1_x\,3_z,\,3_x\,1_z)+(1_z)^2\mathcal{S}_2(1_y\,3_x,\,3_y\,1_x)+(1_x)^2\mathcal{S}_2(1_z\,3_y,\,3_z\,1_y)]\}$
7	$(\frac{1}{3})^{\frac{1}{2}}\{(1\,2)^2[(1_x\,1_y\,3)^2+(3\,1_y\,1_z)^2+(1_x\,3\,1_z)^2]\}$
8	$(\frac{1}{3})^{\frac{1}{2}}\{(1\,2)^2[(1_y\,1_z)^2\mathcal{S}_0(2_x,\,3_x)+((1_z\,1_x)^2\mathcal{S}_0(2_y,\,3_y)+(1_x\,1_y)^2\mathcal{S}_0(2_z,\,3_z)]\}$
9	$(2\,1_x\,1_y\,1_z)^2\mathcal{S}_0(6,\,5)$
10	$(\frac{1}{3})^{\frac{1}{2}}\{(1\,2)^2[(2_x\,1_y\,1_z)^2+(1_x\,2_y\,1_z)^2+(1_x\,1_y\,2_z)^2]\}$
11	$(6\,2\,1_x\,1_y\,1_z)^2$
12	$(\frac{1}{3})^{\frac{1}{2}}\{(1\,2)^2[(1_y)^2\mathcal{S}_1(1_x\,2_z,\,2_x\,1_z)+(1_z)^2\mathcal{S}_1(1_y\,2_x,\,2_y\,1_x)+(1_x)^2\mathcal{S}_1(1_z\,2_y,\,2_z\,1_y)]\}$
13	$(\frac{1}{3})^{\frac{1}{2}}\{(1\,1_x\,1_y\,1_z)^2[(3_x)^2+(3_y)^2+(3_z)^2]\}$
14	$(1\,3\,1_x\,1_y\,1_z)^2$
15	$(\frac{1}{3})^{\frac{1}{2}}\{(1\,1_x\,1_y\,1_z)^2[(2_x)^2+(2_y)^2+(2_z)^2]\}$
16	$(\frac{1}{3})^{\frac{1}{2}}\{(1\,2)^2[(1_y)^2\mathcal{S}_2(1_x\,3,\,2_y\,1_z)+(1_z)^2\mathcal{S}_2(1_y\,3,\,2_z\,1_x)+(1_x)^2\mathcal{S}_2(1_z\,3,\,2_x\,1_y)]\}$
17	$(1\,1_x\,1_y\,1_z)^2\mathcal{S}_0(4,\,3)$
18	$(1/6)^{\frac{1}{2}}\{(1\,2)^2[(1_y)^2\mathcal{S}_2(1_x\,2_z,\,3_x\,1_z)+(1_z)^2\mathcal{S}_2(1_y\,2_x,\,3_y\,1_z)+(1_x)^2\mathcal{S}_2(1_z\,2_y,\,3_z\,1_y)+(1_y)^2\mathcal{S}_2(2_x\,1_z,\,1_x\,3_z)+(1_z)^2\mathcal{S}_2(2_y\,1_x,\,1_y\,3_z)+(1_x)^2\mathcal{S}_2(2_z\,1_y,\,1_z\,3_y)]\}$
19	$(1\,4\,1_x\,1_y\,1_z)^2$

estimated, since to second order the energy correction is a ratio of the square of a two-electron integral (these were tabulated in the basis of self-consistent orbitals) to an energy difference approximated by a difference of one-electron energies for the four orbitals involved.

The formulas for matrix elements between symmetrized functions (^3P for carbon and $^1A_1$ for CH_4) were obtained by direct methods, and could be checked by simpler techniques devised later.[16] The symmetrized functions which contributed more than 0.0005 au to the energy for carbon or CH_4 are listed in Table IV and Table V. The approximate eigenvectors and energy contributions to second order are given in Table VI and Table VII for these functions.

It should be emphasized that these tables include contributions to the total energy from *all* configurations of the several thousand of the correct symmetry that contribute more than 0.0005 au in either case. None of the matrix elements specifically due to equivalence restriction in the calculation on $C(^3P)$ contributed an energy as great as this.

[16] R. K. Nesbet, Ann. Phys. 3, 397 (1958).

V. DISCUSSION OF RESULTS

The calculated electronic energies of $C(^3P)$ and CH_4 are compared in Table VIII. The nuclear repulsion energy at the assumed internuclear distances is 13.39184 au. Binding energy is calculated relative to the calculated energy of $C(^3P)$ and the energy of isolated hydrogen atoms is obtained by a variational calculation with a single Gaussian orbital. This is -0.42441 au for each hydrogen, to be compared with a true nonrelativistic energy of -0.500 au.

In the Hartree-Fock approximation the calculated energy of $C(^3P)$ is 97.9% of the observed value, and is 98.0% when configuration interaction is included. By comparison, the hydrogen energy calculated with the best single Gaussian orbital is only 83.5% of the true value, and no configuration interaction is possible. The use of only a single Gaussian on hydrogen may be an important source of the errors in the calculated binding energy and ionization potential of CH_4.

A calculation on O_2 was carried out by Meckler, who used only a single Gaussian orbital for each atomic

TABLE VI. Configuration interaction for $C(^3P)$. Second order perturbation calculation in terms of the symmetrized many-electron functions of Table IV. Here, $H_{\nu 0}=(\nu|H|0)$, $\Delta_\nu=(\nu|H|\nu)-(0|H|0)$. To second order in the energy, the coefficient of Ψ_ν in the approximate wave function Ψ is $c_\nu=-H_{\nu 0}/\Delta_\nu$, and the energy correction due to Ψ_ν is $c_\nu H_{\nu 0}=-H_{\nu 0}^2/\Delta_\nu$.

ν	$H_{\nu 0}$	Δ_ν	c_ν	$c_\nu H_{\nu 0}$
0	$H_{00}=-37.06596$ au		1.00000	...
1	0.10401	0.79756	−0.13041	−0.01356
2	−0.13453	3.45342	0.03895	−0.00524
3	0.08387	2.13215	−0.03934	−0.00330
4	0.08801	2.85269	−0.03085	−0.00272
5	0.10269	4.71123	−0.02180	−0.00224
6	0.05488	1.81807	−0.03019	−0.00166
7	−0.06313	3.45985	0.01825	−0.00155
8	0.12069	26.86953	−0.00449	−0.00054
9	−0.13445	34.76957	0.00387	−0.00052
			Total energy correction	−0.03133 au

TABLE VII. Configuration interaction for $CH_4(^1A_1)$, in terms of the symmetrized many-electron functions of Table V. The notation is the same as that of Table VI.

ν	$H_{\nu 0}$	Δ_ν	c_ν	$c_\nu H_{\nu 0}$
0	$H_{00}=-52.49395$ au		1.00000	...
1	0.22493	2.49679	−0.09009	−0.02026
2	0.17270	2.56123	−0.06743	−0.01164
3	−0.09508	1.25031	0.07604	−0.00723
4	−0.11330	1.96033	0.05780	−0.00655
5	0.06220	1.22901	−0.05061	−0.00315
6	0.08702	2.48702	−0.03499	−0.00304
7	0.06088	1.28263	−0.04747	−0.00289
8	−0.06512	1.77110	0.03677	−0.00239
9	−0.50170	122.11690	0.00411	−0.00206
10	0.04965	1.20468	−0.04121	−0.00205
11	0.62429	199.98823	−0.00312	−0.00195
12	0.04591	1.21865	−0.03767	−0.00173
13	0.07379	3.36452	−0.02193	−0.00162
14	0.05376	2.19216	−0.02452	−0.00132
15	0.04906	2.19792	−0.02232	−0.00109
16	−0.03591	1.20322	0.02985	−0.00107
17	−0.05548	4.07486	0.01362	−0.00076
18	−0.03451	1.79465	0.01923	−0.00066
19	0.06102	6.01608	−0.01014	−0.00062
			Total energy correction	−0.07208 au

TABLE VIII. Summary of results.

Calculated electronic energy of CH_4, Hartree-Fock approximation	−52.49395 au
Configuration interaction correction	−0.07208
Calculated electronic energy of $C(^3P)$, Hartree-Fock approximation	−37.06596
Configuration interaction correction	−0.03133
Energy of H atoms, calculated with single Gaussian orbitals	−1.69764
Nuclear repulsion	13.39184
Zero-point energy, from observed vibration frequencies[a]	0.04409
Calculated binding energy (1 au = 27.205 ev)	0.33517 au = 211 kcal/mole
Observed binding energy[b]	392.216, 358.27, or 346.764 kcal/mole.

[a] D. M. Dennison, Revs. Modern Phys. **12**, 175 (1940).
[b] See reference 19.

orbital.[17] Since this necessarily limits the total energy to roughly 85% of its true value, such a calculation is probably too crude to give any reliable information about properties of the molecule. Even the present calculations, although much more accurate than this, do not compare favorably with the total energies obtained in atomic Hartree-Fock calculations of 99.5 or 99.6% of experimental values. This suggests that considerably more Gaussian basis orbitals will have to be used before high accuracy can be achieved in molecular calculations.

The first ionization potentials, calculated as one-electron energies in the Hartree-Fock approximation, are

	Calculated	Observed
$C(^3P)$	0.37132 au = 10.102 ev	11.264 ev[13]
CH_4	0.53246 au = 14.486 ev	13.04 ev.[18]

(15)

The absolute binding energy of CH_4 is known experimentally only with respect to the heat of vaporization of graphite, $L(C)$. Glockler[19] obtains three possible values of the binding energy (atomic heat of formation), corresponding to three possible values of $L(C)$. These are

$$\begin{aligned} L(C)&=169.75 \text{ kcal}; \quad \text{B.E.}(CH_4)=392.216 \text{ kcal} \\ &=135.8 \text{ kcal} \qquad\quad =358.27 \text{ kcal} \\ &=124.3 \text{ kcal} \qquad\quad =346.764 \text{ kcal.} \end{aligned} \tag{16}$$

In an empirical study of the properties of other hydrocarbons Glockler finds that $L(C)=169.75$ kcal gives the most consistent agreement with the data considered. The data do not positively exclude the other two values.

The binding energy of CH_4 obtained by the present calculation is

$$\text{B.E.}=0.33517 \text{ au}=211 \text{ kcal}. \tag{17}$$

The calculation is clearly not accurate enough to distinguish among the three empirical values given. Even if the calculated binding energy were within the range of possible empirical values, it would still be very difficult to justify any choice of $L(C)$. It would have to be established that the result was insensitive to any arbitrary restrictions imposed, such as the inaccurate expansion of the 1s orbital. The calculated binding energy would have to be stable under an increase in the number of basis orbitals.

A calculation on CH_4 by Buckingham, Massey, and Tibbs,[20] a Hartree self-consistent field calculation with a spherically averaged potential due to the hydrogen nuclei, obtained a binding energy of nearly 400 kcal. A numerical error has been found in this work and the

[17] A. Meckler, J. Chem. Phys. **21**, 1750 (1953).
[18] R. E. Honig, J. Chem. Phys. **16**, 105 (1948).
[19] G. Glockler, J. Chem. Phys. **21**, 1242 (1953).
[20] R. A. Buckingham, H. S. W. Massey, and S. R. Tibbs, Proc. Roy. Soc. (London) **A178**, 119 (1941).

actual calculated total energy gives essentially no binding energy for the molecule.[21]

The present calculations have shown that configuration interaction is a relatively small effect in $C(^3P)$ and CH_4. The energy due to configuration interaction is an additive correction to the Hartree-Fock energy, in the second order of perturbation theory, and is very much smaller than the Hartree-Fock energy. Hence, the relative accuracy needed in the configuration interaction calculation is very much smaller than in the Hartree-Fock calculation, for the same margin of error in calculating the total energy. For this reason, the present calculation with Gaussian orbitals probably provides a very good estimate of the total correlation energy (due to configuration interaction) because of the large number of independent orbitals used. At the same time, the small relative error in the Hartree-Fock energy (approximately 2%) leads to the same percentage error in the total energy, and this is an absolute error that is large compared with the binding energy.

It is interesting to compare these results with the most accurate calculation reported on a molecule isoelectronic with CH_4. This is a calculation on HF by Karo and Allen.[22] They used Hartree-Fock atomic orbitals, but otherwise followed the general procedure of the present work. The choice of basis orbitals of Karo and Allen assured that their calculated total electronic energy should be in the range of accuracy of atomic Hartree-Fock calculations (about 99.5% of experimental). However, since the number of basis orbitals is very small, in fact the minimum number required to describe the separated atoms, the polarization and redistribution of charge in the atoms in their molecular environment can be represented only to a limited extent. Moreover, the number of higher configurations available for a configuration interaction calculation is severely limited. These remarks apply with equal force to earlier molecular calculations using simple analytic atomic orbitals, which are usually referred to as LCAO (linear combination of atomic orbitals) calculations.

The present calculation is complementary to these LCAO calculations, in that a large number of basis orbitals are available and the variation of their coefficients in the self-consistent molecular orbitals can represent such effects as polarization of the atomic orbitals in the molecule, but the total energy is not comparable with atomic Hartree-Fock energies. As mentioned above, this does not necessarily affect the reliability of the present calculation of correlation energy.

Karo and Allen obtain a molecular binding energy of approximately one-third the experimental value. The present calculation on CH_4 obtains a binding energy of approximately half the experimental value (Table VIII). The calculated correlation energy difference between molecule and separated atoms is small compared with the error in calculated binding energy. From the argument given above, it cannot be expected that any more accurate calculation of the correlation energy will give a significantly greater effect. For this reason, it is to be expected that the bulk of the discrepancy between calculated and experimental binding energies will be obtained only through more accurate *molecular* Hartree-Fock calculations. Since Karo and Allen have already used the most accurate single orbitals possible for the separated atoms, it is clear that a greater number of independent atomic basis orbitals must be used, as has been done in the calculations described here.

[21] C. Carter, Proc. Roy. Soc. (London) **A235**, 321 (1956).
[22] A. Karo and L. C. Allen, J. Chem. Phys. **31**, 968 (1959).

VI. CH BOND ORBITAL IN METHANE

The orbitals of a single Slater determinant are defined only up to a unitary transformation. Lennard-Jones[8,23] has emphasized the importance of such transformations in the molecular orbital theory, by transforming occupied Hartree-Fock self-consistent orbitals into orbitals that are more strongly localized, concentrated in a particular region of the molecule or oriented in a particular direction. This idea has been applied to various problems in the theory of chemical valency.[23]

One particular type of transformation emphasized by Lennard-Jones and his school is a transformation to orbitals that are spatially equivalent and permute among themselves under operations of the molecular symmetry group. Such transformations can be analyzed by group theoretical methods.[24] Methane has frequently been described in terms of equivalent orbitals, considered as electron distributions in a CH bond, based on the intuitive concept of a chemical valence bond rather than the more abstract analysis of Lennard-Jones and his collaborators. This abstract analysis provides a necessary link between the Hartree-Fock method, which allows configuration interaction to be treated as a generally small perturbation, and the descriptive language of practical chemistry.

The molecular orbitals for CH_4 given in Table III are normalized and mutually orthogonal. In terms of these, the normalized equivalent orbital in the direction $C—H_a$ is

$$\chi_a = \tfrac{1}{2}(2a_1 + 1t_{2x} + 1t_{2y} + 1t_{2z}),$$

if the orbital $1a_1$ is considered to be purely a carbon inner shell orbital, not entering into the valence bond. Three other equivalent orbitals of an orthonormal set are obtained from χ_a by operations of the tetrahedral symmetry group.

[23] G. G. Hall and J. E. Lennard-Jones, Proc. Roy. Soc. (London) **A205**, 357 (1951); J. E. Lennard-Jones and J. A. Pople, *ibid.* **A202**, 166 (1950); J. A. Pople, *ibid.* **A202**, 323 (1950); G. G. Hall, *ibid.* **A205**, 541 (1951); **A213**, 113 (1952).
[24] G. G. Hall, Proc. Roy. Soc. (London) **A202**, 336 (1950).

Expressed as a linear combination of basis orbitals,

$$\begin{aligned}
\chi_a = &-0.94333 \quad \exp(-68.32339r^2)\\
&-1.05976 \quad \exp(-12.87507r^2)\\
&-0.12185 \quad \exp(-2.46240r^2)\\
&+1.11361 \quad r^2\exp(-1.93365r^2)\\
&+0.18169 \quad r^2\exp(-0.50613r^2)\\
&+0.21385 \quad z_a\exp(-0.17976r^2)\\
&+1.71429 \quad z_a\exp(-1.21210r^2)\\
&+0.47023 \quad \exp(-0.28294r_A^2)\\
&-0.04750 \quad \exp(-0.28294r_B^2)\\
&-0.04750 \quad \exp(-0.28294r_C^2)\\
&-0.04750 \quad \exp(-0.28294r_D^2). \qquad (18)
\end{aligned}$$

Here, z_a is distance parallel to C—H_a, measured from the carbon nucleus, and $r_A, \cdots, r_D$ are distances measured from the hydrogen nuclei. The centroid of χ_a^2 lies in the line through C and H_a with coordinate

$$z_a = 1.34373a_0,$$

where $a_0 = 0.5292\times10^{-8}$ cm is the atomic unit of length.

ACKNOWLEDGMENTS

The author is indebted to Dr. S. F. Boys, who suggested this project, supervised and encouraged it through its completion, and provided many of the detailed techniques required for various aspects of this work. He is also indebted to the University Mathematical Laboratory, Cambridge, for the use of the EDSAC digital computer, and to the National Science Foundation (U.S.) for the grant of a Predoctoral Fellowship.

This work was completed in the Theoretical Chemistry Department at the University of Cambridge and forms part of the author's doctoral dissertation.[7]

THE JOURNAL OF CHEMICAL PHYSICS VOLUME 32, NUMBER 4 APRIL, 1960

Anomalous Faraday Dispersion of O_2

JON T. HOUGEN*

Mallinckrodt Chemical Laboratory, Harvard University, Cambridge 38, Massachusetts

(Received October 26, 1959)

The Verdet constant of O_2, in contrast to that of other colorless molecules, is not approximately proportional to ν^2 in the visible, near ultraviolet, and near infrared spectral regions. It is shown below that the inability of early theoretical treatments to explain the observed frequency dependence can be overcome by including in the Hamiltonian for the problem the interaction of the spin magnetic moment of the O_2 molecule with the magnetic field of the light wave being propagated through the sample cell. This corresponds to considering *magnetic* dipole transitions as well as *electric* dipole transitions in the absorption spectrum. An expression is obtained which fits the oxygen data to 1%.

WHEN plane polarized light is propagated through a medium placed in a steady magnetic field, the plane of polarization of the light is observed to rotate. This is the Faraday effect. If the magnetic field $\mathbf{B}_0$ is constant in space and in the $\mathbf{k}$ direction, and if the light is propagated in the $\mathbf{k}$ or $-\mathbf{k}$ direction, then the angle θ through which the plane of polarization is rotated is given for most materials and moderate magnetic fields by an expression

$$\theta = V\cdot B_0\cdot L, \qquad (1)$$

where V is the Verdet constant for the material, B_0 is the magnetic field strength, and L is the path length. The sense of the angle θ depends only on the direction of the magnetic field, and V is taken to be positive when the sense of the rotation is the same as the sense of the positive current causing the field.

The early quantum mechanical treatments of Rosenfeld[1] and Serber,[2] which consider the propagation of visible and ultraviolet light through various gaseous materials, predict a Verdet constant which varies approximately as the square of the frequency. Suitably chosen values for quantities which were difficult to calculate and which were therefore treated as parameters gave expressions which fit the experimental data well, except for the Verdet constant of O_2. For this molecule, the Verdet constant in the infrared region varies much less rapidly than the square of the frequency. The older data for oxygen were somewhat questionable,[2] but the recent measurements of Ingersoll

* National Science Foundation Predoctoral Fellow, 1956–1960.

[1] L. Rosenfeld, Z. Physik **57**, 835 (1929).
[2] R. Serber, Phys. Rev. **41**, 489 (1932).

and Liebenberg with a greatly improved technique have confirmed the disagreement between experiment and theory.[3] Rosenfeld and Serber considered the interaction of the magnetic moment of the material in the sample cell with the constant external magnetic field, and the interaction of the electric moment of the material with the electric field of the light wave, but neglected effects arising from the interaction of the magnetic moment of the material with the magnetic field of the light wave. The treatment below includes all three interactions, yielding an expression which fits the oxygen data well.

The quantum mechanical expression for the Verdet constant may conveniently be derived as follows. The expressions from first order perturbation theory for the wave functions Ψ_s and the energies E_s of the stationary states of a molecule in an external magnetic field in the z direction are

$$\Psi_s=\Psi_s^0-B_0\sum_{k\neq s}[(k\mid m_z\mid s)/(E_s^0-E_k^0)]\Psi_k^0$$

$$E_s=E_s^0-B_0(s\mid m_z\mid s), \tag{2}$$

where $\mathbf{m}$ is the magnetic moment of the molecule, Ψ_s^0 and E_s^0 are the unperturbed wave functions and energies. In the presence of electromagnetic radiation these states are further perturbed by an interaction $\mathcal{U}$ which for visible or infrared radiation has the form

$$\mathcal{U}=-\mathbf{p}\cdot\mathbf{E}-\mathbf{m}\cdot\mathbf{B}, \tag{3}$$

where $\mathbf{p}$ and $\mathbf{m}$ are the electric and magnetic dipole moment of the molecule respectively, $\mathbf{E}$ and $\mathbf{B}$ are the electric and magnetic fields of the light wave. For monochromatic, elliptically polarized light with frequency ν, $\mathbf{E}$ and $\mathbf{B}$ at a fixed point in space have the form

$$\mathbf{E}=\mathbf{A}\exp(-2\pi i\nu t)+\mathbf{A}^*\exp(+2\pi i\nu t),$$

$$\mathbf{B}=\mathbf{C}\exp(-2\pi i\nu t)+\mathbf{C}^*\exp(+2\pi i\nu t), \tag{4}$$

where $\mathbf{A}$ and $\mathbf{C}$ are constant vectors. By using time dependent perturbation theory the first order eigenfunctions Φ_s are found to be

$$\Phi_s=\Psi_s-(1/h)\sum_k\{[(k\mid\mathbf{p}\mid s)/(\nu_{sk}-\nu)]\cdot\mathbf{A}^*\exp[+2\pi it(\nu-\nu_{sk})]+[(k\mid\mathbf{p}\mid s)/(\nu_{sk}+\nu)]\cdot\mathbf{A}\exp[-2\pi it(\nu+\nu_{sk})]\}\Psi_k$$
$$-(1/h)\sum_k\{[(k\mid\mathbf{m}\mid s)/(\nu_{sk}-\nu)]\cdot\mathbf{C}^*\exp[+2\pi it(\nu-\nu_{sk})]+[(k\mid\mathbf{m}\mid s)/(\nu_{sk}+\nu)]\cdot\mathbf{C}\exp[-2\pi it(\nu+\nu_{sk})]\}\Psi_k, \tag{5}$$

where $h\nu_{sk}=E_s-E_k$. *The quantum states involved in the expression to the right of the equality are the stationary states in the external magnetic field.* Consequently both the wave functions and matrix elements differ from their zero field limits.

The expectation values for the electric and magnetic moments of the molecules fround from these wave functions, together with a Boltzmann population distribution and the molecular concentration determine the macroscopic polarization and magnetization as a function of the applied fields $\mathbf{E}$, $\mathbf{B}$ of the light wave, i.e., determine the constitutive equations for this medium. Solving the boundary value problem prescribed by Maxwell's equations for propagating light through the medium, one finds that the Verdet constant can be written as the sum of two terms

$$V=V_p+V_m, \tag{6}$$

if the wave functions are taken to be simultaneous eigenfunctions of the Hamiltonian and of the operator which reflects the coordinates of *all* particles through the origin. With this choice of wave functions the first term V_p arises solely from the interaction of the molecule with the external magnetic field and the electric field of the light wave. It is the contribution to the Verdet constant which is usually considered. The second term V_m arises solely from the interaction of the molecule with the external magnetic field and with the magnetic field of the light wave. V_m is given by

$$V_m=-(1/B_0)(4\pi^2\nu^2 i/hc)(N/Q)\sum_s\exp(-E_s/kT)\cdot\sum_k[1/(\nu_{ks}^2-\nu^2)]$$
$$[(s\mid m_x\mid k)(k\mid m_y\mid s)-(s\mid m_y\mid k)(k\mid m_x\mid s)], \tag{7}$$

where N is the molecular concentration and Q is the partition function. The states labeled by the indices k, s are eigenstates in the presence of the external magnetic field $\mathbf{B}_0$. This expression is exactly analogous to that obtained by Rosenfeld and Serber for V_p, except that $\mathbf{p}$ is replaced by $\mathbf{m}$. With the choice of wave functions given above there are no cross terms involving a simultaneous interaction with both the electric and magnetic field of the light wave.

The expression for V_p was applied to various atoms and molecules with the assumption that the large contributions to the sum arose from matrix elements between states k, s such that $\nu_{ks}^2\gg\nu^2$. It is clear from Eq. (7) that such an assumption leads to an approximately quadratic dependence of the Verdet constant on frequency, for V_m as well as for V_p. There is for O_2, however, an additional contribution to V_m arising from matrix elements of the magnetic moment $\mathbf{m}$ between the various spin-rotational states of the $^3\Sigma$ ground electronic state,[4] for which $\nu_{ks}^2\ll\nu^2$. Such a contribution will be approximately independent of frequency.

[3] L. R. Ingersoll and D. H. Liebenberg, J. Opt. Soc. Am. **44**, 566 (1954); **46**, 538 (1956); **48**, 339 (1958).

[4] M. Tinkham and M. W. P. Strandberg, Phys. Rev. **97**, 937 (1955).

TABLE I. Faraday dispersion of O_2.[a]

λ	V_{obs}	V_{calc}	Error
3635	11.69	11.69	...
4000	9.72	9.84	1.2%
4360	8.50	8.50	...
4500	8.05	8.07	0.2%
5000	6.87	6.84	−0.4%
5460	6.05	6.02	−0.5%
5500	5.98	5.96	−0.3%
5780	5.59	5.56	−0.5%
5893	5.45	5.42	−0.6%
6000	5.32	5.29	−0.6%
6500	4.78	4.78	...
7000	4.35	4.38	0.7%
7500	4.03	4.06	0.7%
8000	3.79	3.80	0.3%
8500	3.58	3.59	0.3%
9000	3.41	3.41	...
9875	3.14	3.16	0.6%

[a] λ is the wavelength in angstroms. V is the Verdet constant in μmin/cm·oersted.

The matrix elements of $\mathbf{m}$ in Eq. (7) above will be of the order of one Bohr magneton. The matrix elements of $\mathbf{p}$ in the corresponding expression for V_p will be of the order of one debye. Thus, a cursory glance at Eq. (7) suggests that the ratio of V_m to V_p will be approximately (Bohr magneton)^2/(debye)^2, or 10^{-4}, just as magnetic dipole radiation is usually 10^{-4} as intense as electric dipole radiation. The resonance denominator $(\nu_{ks}^2-\nu^2)^{-1}$ favors by a factor of 100 the contributions of the magnetic dipole transitions among the spin-rotational states, which occur in the microwave, over those of the electric dipole transitions in the far ultraviolet. This is evident if we set $\nu=10\,000$ cm^{-1}, ν_{ks} (magnetic dipole) $=1$ cm^{-1}, and ν_{ks}(electric dipole) $=100\,000$ cm^{-1}. The additional enhancement of the importance of the magnetic dipole transitions arises from the nature of first order wave function mixing under the influence of a perturbation, as suggested by the arguments below. The mixing coefficients for a system in a magnetic field $B_0\mathbf{k}$ are essentially the quantities $(k\mid m_z\mid s)/(E_s^0-E_k^0)$. A perturbed eigenfunction contains a larger admixture of its neighboring spin-rotational states than of states differing in electronic or vibrational quantum numbers because the energy denominators for the former mixing are much smaller than for the latter. The magnetic moment $\mathbf{m}$ has matrix elements between the various spin-rotational states and these matrix elements are therefore sensitive to the former type of mixing. The electric moment $\mathbf{p}$, on the other hand, has no matrix elements between states differing in spin quantum numbers and so is less sensitive to such mixing. Thus, the magnetic moment responds to wave functions which are mixed in with an energy denominator of about 10 cm^{-1}, while the electric moment responds to wave functions which are mixed in with an energy denominator of about 10 000 cm^{-1}. This evidently favors the $\mathbf{m}$ contribution over the $\mathbf{p}$ by a factor of 1000.

The frequency independent contribution can be calculated explicitly. Let only the rotational and spin-multiplet states of the ground vibrational state of the $^3\Sigma$ electronic ground state of the O_2 molecule have appreciable populations. Let the states in the summation over k also be chosen from this group of populated states, so that $\nu_{ks}^2\ll\nu^2$ and $(\nu_{ks}^2-\nu^2)^{-1}\cong-\nu^{-2}$. With this choice of states s and k, we see that

$$\sum_k \Psi_k(k\mid \mathbf{S}\mid s)\cong \mathbf{S}\Psi_s$$

$$\sum_k \Psi_k(k\mid \mathbf{L}\mid s)\cong \mathbf{r}\Lambda\Psi_s \qquad (8)$$

where $\mathbf{S}$ is the spin *operator* and Λ is the quantum *number* associated with the projection of the electronic orbital angular momentum $\mathbf{L}$ along the internuclear axis; $\mathbf{r}$ is the unit vector describing the instantaneous orientation of the internuclear axis in space, i.e., a multiplicative operator involving the rotational angle variables. Thus, since $\mathbf{m}=\beta\hbar^{-1}(\mathbf{L}+2\mathbf{S})$,

$$\sum_k[(s\mid m_x\mid k)(k\mid m_y\mid s)-(s\mid m_y\mid k)(k\mid m_x\mid s)]$$
$$\cong 4i\beta^2\hbar^{-1}(s\mid S_z\mid s), \qquad (9)$$

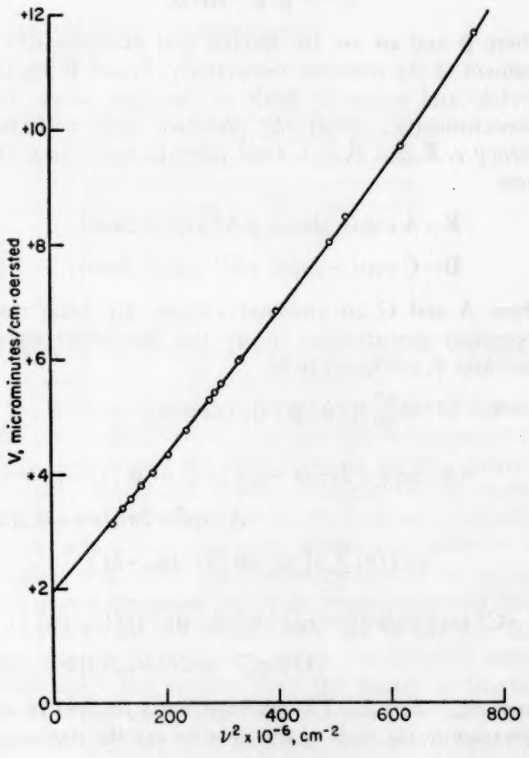

FIG. 1. The Verdet constancy of O_2 as a function of the square of the frequency.

and Eq. (7) becomes

$$V_m = -(1/B_0)(16\pi^2\beta^2/hc)(N/Q)\sum_s \exp-(E_s/kT) \times (s\,|\,\hbar^{-1}S_z\,|\,s). \quad (10)$$

Equation (10) is very similar to the expression for the magnetic susceptibility and can be treated as described by Van Vleck[5]. To the extent that the spin-multiplet and adjacent rotational levels are close compared to kT, the frequency independent contribution to V_m will have a spin-only value

$$V_m = (32\pi^2\beta^2N/3kThc)S(S+1). \quad (11)$$

For a temperature of 19°C and a concentration of 2.69×10^{19} molecules per cm³, the frequency independent contribution to the Verdet constant of O_2 (spin 1) is 1.95 μ min/cm·oersted. By combining this value with one term of the usual type, an expression is obtained which can be fitted to the experimental data[3] within 1%.

$$V = 1.95 + 8.93\nu^2/(77\times10^8-\nu^2), \quad (12)$$

where ν is in cm^{-1}, and V is in μ min/cm·oersted. Table I presents the observed values and those calculated from the formula above. Figure 1 displays the Faraday dispersion of O_2.

Equation (10) for the frequency independent part of V_m can also be applied to NO (§67 of reference 5). Because the doublet splitting of NO is *not* small compared to kT, we obtain an expression

$$V_m = (32\pi^2\beta^2N/3kThc)\frac{2(1-e^{-x})+xe^{-x}}{2x(1+e^x)}, \quad (13)$$

where x is the ratio of the doublet splitting of NO to kT. At room temperature $x=0.60$, which gives a frequency independent contribution of 0.64 microminute/cm·oersted. The frequency dependent part of the Verdet constant of NO is much larger than that of O_2, however, so that this very small relative contribution to the Verdet constant cannot be detected experimentally.

[5] J. H. Van Vleck, *Electric and Magnetic Susceptibilities* (Oxford University Press, New York, 1932), §46.

ACKNOWLEDGMENTS

I am deeply indebted to the late Professor William Moffitt, who suggested both this problem and the method of solution. I am also grateful for the valuable advice and criticism given me by Professor J. H. Van Vleck. This work was carried out during the tenure of a National Science Foundation Fellowship.

Calculation of the Heat of Solution of Copper in Germanium from Diffusion Measurements

M. TANENBAUM

Bell Telephone Laboratories, Incorporated, Murray Hill, New Jersey

(Received December 9, 1959)

The diffusion of substitutional copper in germanium below 700°C has been explained by a dissociation mechanism proposed by Frank and Turnbull. It is shown that this mechanism provides a means for estimating the heat of solution of copper in germanium by measuring the activation energies for substitutional copper diffusion and for self-diffusion in germanium.

FULLER and Struthers[1] have shown that copper will diffuse rapidly through single crystals of germanium. Van der Maesen and Brenkman[2] later proposed that much of the peculiar behavior of copper in germanium could be explained if an equilibrium existed between substitutional and interstitial copper. Following these observations, Frank and Turnbull[3] proposed a mechanism for the diffusion of copper in germanium which invoked the cooperation of substitutional copper, interstitial copper and lattice vacancies. Their theory suggests that the diffusion of copper in substitutional lattice positions will proceed by the dissociation of a substitutional copper atom into a vacancy and an interstitial copper atom. These two species will then diffuse independently until the interstitial copper atom combines with a vacancy and becomes substitutional again. These considerations lead to a relation for the effective diffusion coefficient of substitutional copper, D_s, given by

$$D_s = D_v(c_v/c_v + c_s), \tag{1}$$

where D_v is the diffusion coefficient of vacancies, c_v is the concentration of vacancies, and c_s is the concentration of substitutional copper atoms.

Equation (1) is based on the assumption that $c_v \ll c_i$ where c_i is the concentration of interstitial copper. Tweet[4] has determined that the ratio of substitutional copper to interstitial copper in germanium at 715°C is approximately 6 ± 2. With this ratio, the concentration of interstitial copper in germanium as a function of temperature can be estimated from the solid solubility of substitutional copper which has been determined by Fuller *et al.*[5] and by Woodbury and Tyler.[6] If it is further assumed that the activation energy for the formation of vacancies in germanium is 46 kcal per mole,[7] the concentration of vacancies in germanium as a function of temperature can be estimated. These estimates show that at temperatures up to 700°C, the assumption that $c_v \ll c_i$ is valid.

At first appearance, Eq. (1) seems to suggest that D_s will be a function of the instantaneous concentration of substitutional copper. However, Tweet[4] has observed that D_s is constant during the precipitation of copper from supersaturated solid solutions of copper although the concentration of copper is changing by more than a factor of ten during precipitation. This observation can be explained in the following manner. First it is noted from the discussion above that since $c_s > c_i$, then $c_s \gg c_v$ and Eq. (1) can be simplified to

$$D_s = D_v(c_v/c_s). \tag{2}$$

It is now assumed that the nonequilibrium concentrations of vacancies, substitutional copper and interstitial copper are related by the mass action constant K, which relates their equilibrium concentrations so that

$$c_s/c_i c_v = K = c_s'/c_i' c_v', \tag{3}$$

where the primes indicate thermal equilibrium values. If it is further assumed that the high diffusivity of interstitial copper (estimated as 4×10^{-3} cm^2/sec)[3] maintains $c_i \approx c_i'$, then Eq. (3) requires that

$$c_v/c_s \approx c_v'/c_s'. \tag{4}$$

Thus, Eq. (2) can be rewritten in terms of equilibrium values as

$$D_s = D_v(c_v'/c_s') = D_{Ge}/c_s', \tag{5}$$

where D_{Ge} is the self-diffusion coefficient of germanium in a pure crystal. Frank and Turnbull have derived Eq. (5) with similar assumptions by a slightly different algebraic path. Furthermore, Penning[8] has given further support to the dissociative diffusion mechanism in the form of Eq. (5) by demonstrating that values of D_{Ge} derived by studying the precipitation of copper in germanium agree with values of D_{Ge} measured directly by radiotracer techniques.

Equation (5) states that the effective diffusion coefficient of substitutional copper, D_s, is inversely proportional to the equilibrium concentration of the substitutional copper. This provides a means for determin-

[1] C. S. Fuller and J. D. Struthers, Phys. Rev. **87**, 526 (1952).
[2] F. Van der Maesen and J. A. Brenkman, J. Electrochem. Soc. **102**, 229 (1955).
[3] F. C. Frank and D. Turnbull, Phys. Rev. **104**, 617 (1956).
[4] A. G. Tweet, Phys. Rev. **106**, 221 (1957).
[5] C. S. Fuller, J. D. Struthers, J. A. Ditzenberger, and K. B. Wolfstirn, Phys. Rev. **93**, 1182 (1954).
[6] H. H. Woodbury and W. W. Tyler, Phys. Rev. **105**, (1957).
[7] H. Reiss and C. S. Fuller, *Semiconductors* (Reinhold Corporation, New York, 1959), p. 264.
[8] P. Penning, Phys. Rev. **110**, 586 (1958).

ing the equilibrium concentration of substitutional copper by measuring diffusion coefficients.

It is perhaps more enlightening to examine the temperature variation rather than the absolute magnitudes of the quantities in Eq. (5). If it is assumed that D_s, D_{Ge}, and c_s' can be represented by simple Arrhenius type expressions, then

$$K_1 \exp(-\Delta H_D/RT) = K_2 \exp(-\Delta H_{Ge}/RT) K_3 \exp(\Delta H_{Cu}/RT), \quad (6)$$

where K_1, K_2, and K_3 are constants, ΔH_D is the heat of activation for the effective diffusion of substitutional copper, ΔH_{Ge} is the heat of activation for the self-diffusion of germanium, and ΔH_{Cu} is a heat term which describes the variation of c_s' with temperature. If these quantities are evaluated in a temperature range where the germanium crystal is in equilibrium with a copper phase of approximately constant composition (i.e., below the eutectic temperature of 640°C) and if the solid solutions obey Henry's law, then ΔH_{Cu} is the heat of solution of copper in germanium.

Equation (6) leads to the relation

$$\Delta H_{Cu} = \Delta H_{Ge} - \Delta H_D. \quad (7)$$

Tweet[4] has obtained ΔH_D by measuring the precipitation of copper from supersaturated solutions in germanium from ~700°C to ~400°C. He obtained a value of 29.9 kcal/mole. The scatter of the published data suggests an uncertainty in this value of ±10%. The heat of activation for the self-diffusion of germanium has been measured by Letaw, Portnoy, and Slifkin[9] as 68.5±0.96 kcal/mole. From these values and Eq. (7), the heat of solution of copper in solid germanium is 38.6±4 kcal/mole.

The heat of solution of copper in germanium below the eutectic can also be obtained from the solubility measurements of Fuller *et al.*[5] and of Woodbury and Tyler.[6] The slope of these solubility curves below 640°C should give this quantity and the measured slopes are 41 kcal/mole and 44 kcal/mole, respectively. From the published data it appears that the errors in the slopes are not more than ±10% or ±4 kcal/mole. The agreement between this direct determination of the heat of solution and the value estimated from the diffusion measurements is satisfying.

Thus, the copper-germanium system provides an unusual example where the heat of an equilibrium reaction, the solution of copper in germanium, can be calculated from the heat of activation of two kinetic processes, the effective diffusion coefficient of copper in germanium and the self-diffusion coefficient of germanium. This situation arises because the effective diffusion coefficient of copper is a sensitive function of the equilibrium concentration of copper in the germanium crystal as evidenced by Eq. (5). The agreement between the measured heats of activation of the diffusion coefficients and the independently measured heat of solution of copper is a further substantiation of the Frank and Turnbull dissociative mechanism for copper diffusion in germanium. This result combined with the work of Penning cited above leaves little doubt that the dissociative mechanism is an adequate description of the diffusion of copper in germanium.

ACKNOWLEDGMENTS

The author wishes to acknowledge helpful discussions with F. A. Trumbore and C. D. Thurmond.

[9] H. Letaw, W. M. Portnoy, and L. Slifkin, Phys. Rev. **102**, 636 (1956).

Mass Spectrometric Studies of Ionic Intermediates in the Alpha-Particle Radiolysis of Ethylene

C. E. MELTON AND P. S. RUDOLPH

Chemistry Division, Oak Ridge National Laboratory, Oak Ridge, Tennessee*

(Received September 25, 1959)

Two techniques were used for the elucidation of ion-molecule reaction mechanisms in the alpha radiolysis of C_2H_4 in the new alpha-particle mass spectrometer. The corresponding variations in the percent of primary, secondary, and tertiary ions over a tenfold pressure range (to 0.1 mm) were used to postulate the reaction mechanisms. Mixtures of the C_2 hydrocarbons were employed to increase the relative concentrations of a specific reactant ion, thus independently confirming the postulated mechanisms. Polymeric ions as large as $C_5H_9^+$ were observed. Conclusions as to reaction mechanisms drawn from this study are compared to those drawn from the appearance potential technique used in the electron impact studies. Values of the rate constants are also compared for several secondary reactions.

INTRODUCTION

IN recent alpha-radiolysis studies at this laboratory,[1,2] wherein an alpha source replaced the electron source as an ionization medium in a mass spectrometer, polymeric ionic intermediates formed in acetylene were reported and their modes of formation discussed. In those investigations acetylene was studied over a tenfold pressure range to a maximum pressure of 0.1 mm. From those pressure studies, the mechanisms for the formation of the observed ions were elucidated.

The present study on the alpha radiolysis of ethylene in the alpha-particle mass spectrometer was undertaken to investigate the existence of and mode of formation of ionic intermediates in this gas. Reaction mechanisms are postulated for the ions observed in the pressure studies of ethylene and are substantiated by employing mixtures which increased the concentration of specific reactant ions. The alpha-induced ion-molecule reactions in ethylene are compared to the previously reported[3] electron impact-induced ion-molecule reactions. Differences were anticipated between the present alpha-bombardment studies and previous electron-impact studies since considerably higher pressures and lower temperatures are used in this investigation in addition to the obviously different ionizing medium. Not only are the experimental conditions different in the present study, but also the techniques used in elucidating the reaction mechanisms. Field *et al.*[3] interpret their results by means of appearance potential studies, whereas the present workers employ pressure studies identical to those used in their acetylene work[2] as well as studies of gaseous mixtures in the interpretation of their results.

EXPERIMENTAL

The alpha-particle mass spectrometer, the experimental conditions and techniques and the C_2H_2 used in this study were previously reported.[1,2] The other reactant gases were C_2H_4 (99.96%) and C_2H_6 (99.75%). Mixtures of the C_2 hydrocarbons in varying proportions were investigated at a pressure of 0.11 mm in addition to the study of C_2H_4 as a function of pressure.

RESULTS

Percent of ionic intermediates (parent ions, degradation ions, polymeric ions, etc.) are reported in Table I as a function of pressure. Values for ions having a percent less than 0.5 are not tabulated. It is obvious that ions containing more atoms of either carbon and/or hydrogen than the parent ion ($C_2H_4^+$) are produced by ion-molecule reactions.[1] Table I shows that polymeric ions containing both even and odd numbers of carbon atoms are observed. This is in contrast to the results from the acetylene study,[2] wherein polymeric ions containing only even numbers of carbon atoms were observed.

The percent of every ionic species varies with pressure as shown in Table I. This variation suggests that each of these ionic species is either depleted by or enhanced by ion-molecule reactions. The pressure dependence is shown more vividly in Fig. 1 for three ions which are involved in consecutive reactions. That $C_2H_4^+$ is a precursor for $C_3H_5^+$ which in turn is a precursor for $C_5H_9^+$ is shown by the corresponding variations in the slopes of their curves. A more detailed treatment of the ion-molecule reactions deduced from these pressure studies is summarized in Table III.

To corroborate the reactions deduced from the pressure studies, specific mixtures of the C_2 hydrocarbons which would increase the relative concentration of a postulated reactant ion were investigated. Nine mixtures in varying proportions of these gases were studied. Data for the two most elucidating mixtures are presented in Table II. For example, reactions

* Operated for the U.S. Atomic Energy Commission at the Oak Ridge National Laboratory by Union Carbide Corporation.

[1] C. E. Melton and P. S. Rudolph, J. Chem. Phys. **30**, 847 (1959).

[2] P. S. Rudolph and C. E. Melton, J. Phys. Chem. **63**, 916 (1959).

[3] F. H. Field, J. L. Franklin, and F. W. Lampe, J. Am. Chem. Soc. **79**, 2419 (1957).

TABLE I. Percent of ionic species in C_2H_4 as a function of pressure.

Mass	+ Ion	Approximate pressures (mm) 0.01	0.02	0.03	0.04	0.05	0.06	0.07	0.08	0.09	0.10
26	C_2H_2	9.9	9.4	8.6	7.1	6.5	5.2	4.1	3.7	3.3	2.5
27	C_2H_3	21.6	19.6	16.9	15.4	12.0	10.6	9.7	8.6	7.4	7.0
28	C_2H_4	59.3	50.7	44.3	39.9	32.5	27.8	24.9	21.9	20.1	17.6
29	C_2H_5		7.2	8.3	10.3	10.1	9.7	10.8	12.1	11.4	12.0
39	C_3H_3			1.8	3.2	3.0	3.6	3.5	3.3	3.7	4.0
41	C_3H_5	9.3	16.0	20.2	24.1	27.5	32.4	33.8	35.8	36.8	38.3
53	C_4H_5					1.8	2.2	3.2	3.0	3.4	3.3
55	C_4H_7					3.1	3.6	4.3	4.3	4.6	4.6
56	C_4H_8								0.7	1.3	1.2
69	C_5H_9					3.5	4.8	5.6	6.6	8.2	9.4

involving $C_2H_2^+$ were substantiated by mixtures containing C_2H_2 which increased the relative concentration of $C_2H_2^+$. In order to increase the concentration of $C_2H_4^+$ relative to C_2H_4, C_2H_6 [the predominant ion of which is $C_2H_4^+$ (49.4%)] was admixed with C_2H_4. These data are used in Table III to substantiate the reactions postulated from the pressure studies.

The probable reactions by which all the observed ionic species are formed, together with the substantiating evidence for these reactions, are summarized in Table III. The values for ΔH as calculated from data in Field and Franklin[4] and Pauling[5] would indicate that some of the postulated reactions are endothermic. This

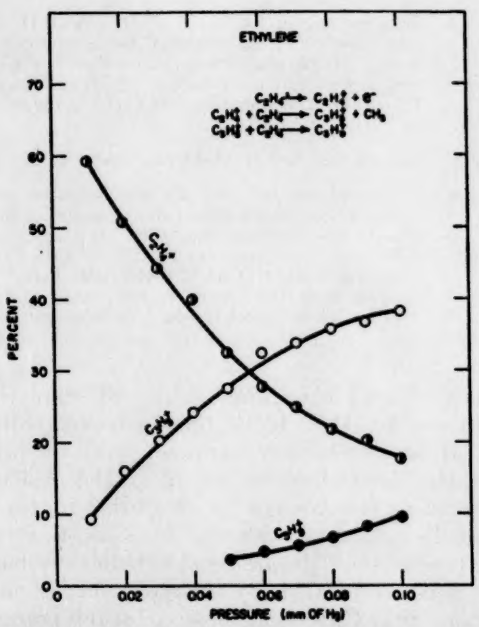

FIG. 1. Typical curves showing the variation in percent abundance for ions involved in a series of consecutive reactions.

discrepancy can be explained by one or more of the following:

1. The data used for these calculations represent ground state transitions whereas the observed transitions may involve excited states.

2. Neither the structures of the observed ions nor the structures of the ions for which the appearance potentials are given are known. Hence, it is possible that structurally different ions are compared.

3. The present technique gives no information on the structure or energetics of the neutral species. The neutral products of the postulated reactions were deduced by material balance. This also holds true of the data used in making the ΔH calculations. Hence, it is possible that the ΔH's for different neutral products are compared.

From a perusal of the probable reactions in Table III, the sequence of the consecutive reactions of the ionic intermediates can be followed. For example, consider

TABLE II. Percent of total ions at a pressure of approximately 0.1 mm.

1 Mass	2 + Ion	3 $1C_2H_4$ $10C_2H_6$	4 $10C_2H_2$ $1C_2H_4$
26	C_2H_2	1.3	13.1
27	C_2H_3	5.1	5.0
28	C_2H_4	40.1	4.1
29	C_2H_5	22.5	
30	C_2H_6	8.9	
39	C_3H_3		10.1
40	C_3H_4		0.7
41	C_3H_5	15.8	1.0
42	C_3H_6	0.6	
43	C_3H_7	2.2	
50	C_4H_2		14.4
51	C_4H_3		31.2
52	C_4H_4		4.2
53	C_4H_5		4.2
54	C_4H_6		
55	C_4H_7	1.8	
56	C_4H_8	0.5	
57	C_4H_9	0.7	

[4] F. H. Field and J. L. Franklin, *Electron Impact Phenomena* (Academic Press, Inc., New York, 1957), pp. 243 ff.
[5] L. Pauling, *Nature of the Chemical Bond* (Cornell University Press, Ithaca, New York, 1944), 2nd ed., pp. 53, 131.

TABLE III. Ionic intermediates in the radiolysis of C_2H_4 at a pressure of approximately 0.1 mm Hg.

Mass	Positive ion	Percent	Probable reaction	ΔH ev	Remarks
26	C_2H_2	2.5	$C_2H_4 \text{—}vv\text{→} C_2H_2^+ + H_2 + e^-$	13.5	Primary ionization and dissociation.
27	C_2H_3	7.0	$C_2H_4 \text{—}vv\text{→} C_2H_3^+ + H + e^-$	14.0	Primary ionization and dissociation.
			$C_2H_2^+ + C_2H_4 \rightarrow C_2H_3^+ + C_2H_3$	−0.2	The ratio, % $C_2H_3^+$/% $C_2H_4^+$, in a $10C_2H_2$:$1C_2H_4$ mixture (Table II, col. 4) is higher than the same ratio in pure C_2H_4 (Table I, 0.01 (5/4 vs 2/6)) thus indicating that the postulated reaction is probable.
28	C_2H_4	17.6	$C_2H_4 \text{—}vv\text{→} C_2H_4^+ + e^-$	10.5	Primary ionization.
29	C_2H_5	12.0	$C_2H_3^+ + C_2H_4 \rightarrow C_3H_5^+ + C_2H_2$	−0.7	The % of $C_3H_5^+$ increases with increasing pressure while the % of $C_2H_3^+$ decreases (Table I) thus suggesting an interrelationship.
39	C_3H_3	4.0	$C_3H_2^+ + C_2H_4 \rightarrow C_3H_3^+ + CH_3$	−1.8	In the mixture of $10C_2H_2$ to $1C_2H_4$ (Table II, col. 4) $C_3H_3^+$ was 10% of the total ion intensity. A corresponding decrease was observed for $C_4H_2^+$ and $C_4H_3^+$ which are also secondary reactions from $C_2H_3^+$. These observations indicate that $C_2H_2^+$ and C_2H_4 are necessary for the production of $C_3H_3^+$.
41	C_3H_5	38.3	$C_2H_4^+ + C_2H_4 \rightarrow C_3H_5^+ + CH_3$	−0.25	The decrease in the % of $C_2H_4^+$ parallels the increase in the % of $C_3H_5^+$ with increasing pressure (Fig. 1 and Table I). In a $10C_2H_6$:$1C_2H_4$ mixture (Table II, col. 3), the % of $C_3H_5^+$ is high relative to the % observed at the same partial pressure of C_2H_4 (Table I, 0.01). The observations are consistent with the postulated mechanism since $C_2H_4^+$ is the predominant ion in C_2H_6 (49.4%).
53	C_4H_5	3.3	$C_3H_3^+ + C_2H_4 \rightarrow C_4H_5^+ + CH_2$	1.4	$C_4H_5^+$ is observed in a mixture of $10C_2H_2$ to $1C_2H_4$ (Table II, col. 4) when the % of $C_3H_3^+$ is large, but $C_4H_5^+$ is not observed when $C_3H_3^+$ is absent (col. 3). These observations support the postulated mechanism.
55	C_4H_7	4.6	$C_3H_5^+ + C_2H_4 \rightarrow C_4H_7^+ + CH_2$	2.4	In a mixture of $10C_2H_6$ to $1C_2H_4$ (Table II, col. 3) where the % of $C_3H_5^+$ is high, $C_4H_7^+$ is observed. However, $C_4H_7^+$ is not detected when the % of $C_3H_5^+$ is low, as shown by the $10C_2H_2$ to $1C_2H_4$ mixture (Table II, col. 4). This indicates that $C_3H_5^+$ is the precursor for $C_4H_7^+$.
56	C_4H_8	1.2	$C_2H_4^+ + C_2H_4 \rightarrow C_4H_8^+$	−2.7	Percent too small to substantiate the process.
69	C_5H_9	9.4	$C_3H_5^+ + C_2H_4 \rightarrow C_5H_9^+$	−1.4	The increase in the % of $C_3H_5^+$ with increasing pressure is drastically reduced when $C_5H_9^+$ appears, as shown in Fig. 1. This indicates that $C_3H_5^+$ is a precursor for $C_5H_9^+$. The summation of the %'s of $C_2H_4^+$ (a precursor of $C_3H_5^+$), $C_3H_5^+$, $C_4H_7^+$ and $C_5H_9^+$ is ~ constant over the entire pressure range (Table I). This further substantiates the postulated mechanism.

a series of consecutive reactions, *viz.*,

$$C_2H_4 \rightarrow C_2H_2^+ + H_2 + e^- \quad (1)$$

$$C_2H_2^+ + C_2H_4 \rightarrow C_3H_3^+ + CH_3 \quad (2)$$

$$C_3H_3^+ + C_2H_4 \rightarrow C_4H_5^+ + CH_2 \quad (3)$$

which were postulated from pressure studies. The percent of $C_2H_2^+$ formed by (1) should be independent of pressure. However, if $C_2H_2^+$ is depleted by reaction (2), its percent should decrease with increasing pressure. Thus the continuous decrease in the percent of $C_2H_2^+$ (Table I) with increasing pressure suggests reaction (2). Since the percent of $C_3H_3^+$ does not continue to increase with increasing pressure once $C_4H_5^+$ appears, the formation of $C_4H_5^+$ from $C_3H_3^+$ is implied as per (3).

The postulated ion-molecule reactions are substantiated by the mixture studies. By employing a mixture of $10C_2H_2$ to $1C_2H_4$, the relative concentration of $C_2H_2^+$ is considerably increased, hence the percent of $C_3H_3^+$ should increase [cf. (2)]. This is actually observed as can be seen by comparing the data in Table II, column 4, with that in Table I, $P=0.01$. The pressures of C_2H_4 are equal in both cases but the concentration of $C_2H_2^+$ is markedly higher in the mixture. Since $C_3H_3^+$ is not observed at this pressure in C_2H_4 but is 10% of the total ions in the mixture, it is apparent that the $C_3H_3^+$ must be attributed to the increased concentration of $C_2H_2^+$. The confirmation for (3) is deduced by analogous reasoning using corresponding data (Table I, $P=0.01$, and Table II, column 4). Similar logic for the other "Probable reaction" in Table III is indicated in the "Remarks" column.

DISCUSSION

Differences in the ions resulting from ion-molecule reactions induced by electron impact[3] as compared to those reported in the present study can be explained. The electron-impact studies report ions ($C_4H_2^+$ and $C_4H_3^+$) produced by ion-molecule reactions involving degradation ions (C_2^+ and C_2H^+, respectively) and reactant molecules. Since these degradation ions were not abundant enough to report in the alpha-induced study, product ions formed by these precursors could not be observed. Polymeric ions of mass greater than 55 ($C_4H_7^+$) which were observed in this study at the higher pressures were not reported in the electron-impact studies. This difference can be attributed to the much higher pressures used in the current investigation. Both the electron-impact study[3] and the present alpha-bombardment study agree that $C_2H_2^+$ and $C_2H_4^+$ are the precursors for $C_4H_5^+$ and $C_4H_7^+$, respectively. In the previous study the product ions were postulated as being formed by competing simultaneous bimolecular reactions, whereas, in the present study it is postulated that these ions are formed by consecutive bimolecular reactions as shown in Table III. It is possible that both the simultaneous and consecutive bimolecular reactions contribute to formation of $C_4H_5^+$ and $C_4H_7^+$.

Values for rate constants obtained in this study are compared to those previously reported[3] in Table IV for the three reactions given. These values agree within experimental error for the reactions producing $C_3H_3^+$ and $C_3H_5^+$. However, the values for the reaction producing $C_2H_5^+$ disagree by a factor of 2. This discrepancy can not be explained at the present time.

The polymeric ions observed in the acetylene study[2] were formed without the elimination of carbon (e.g., $C_2H_2^+ + C_2H_2 \rightarrow C_4H_3^+ + H$). However, polymeric ion formation in ethylene is usually ($\sim$70%) accompanied by the elimination of carbon as shown in Table III (e.g., $C_2H_4^+ + C_2H_4 \rightarrow C_3H_5^+ + CH_3$). Hence, the ions containing more than two carbons observed in the present work are probably produced by reactions forming a carbon to carbon bond between the reacting species. The polymeric ions observed in these studies differ from the "ionic clusters" postulated by Lind *et al.*[6] from their early alpha-radiolysis studies of these gases. Their "ionic clusters" were postulated to consist of neutral molecules held around a central ion by attractive forces, whereas the polymeric ions observed in these investigations involve carbon to carbon bonding.

TABLE IV. Rate constants for some C_2H_4 reactions.

Probable reaction	$K \times 10^{10}$ cc molecule^{-1} sec^{-1} This work	F.F.L.[a]
$C_2H_3^+ + C_2H_4 \rightarrow C_3H_5^+ + C_2H_3$	3.8	6.4
$C_2H_2^+ + C_2H_4 \rightarrow C_3H_3^+ + CH_3$	2.5	2.5
$C_2H_4^+ + C_2H_4 \rightarrow C_3H_5^+ + CH_3$	4.1	5.3

[a] See reference 3.

The probable reactions produced by the radiolysis of C_2H_4 in the alpha-particle mass spectrometer are corroborated by two independent experimental techniques. These techniques (pressure studies and mixture studies) are elucidating for the distinction of intermediate steps in consecutive ion-molecule reactions, whereas previously used appearance potential techniques are not.

ACKNOWLEDGMENT

The authors would like to acknowledge valuable suggestions stemming from stimulating discussions with Professor P. H. Emmett of Johns Hopkins University; Professors M. Burton and J. L. Magee, of Notre Dame University, and R. Baldock and E. H. Taylor, of this Laboratory.

The authors are happy to have this opportunity to express their gratitude to Dr. S. C. Lind whose encouragement and interest in this work were a source of inspiration.

[6] S. C. Lind, D. C. Bardwell, and J. H. Perry, J. Am. Chem. Soc. **48**, 1556 (1926).

Calculation of the Dissociation Energy of NH by a Semiempirical Interpolative Method*

AUDREY L. COMPANION† AND FRANK O. ELLISON

Department of Chemistry, Carnegie Institute of Technology, Pittsburgh, Pennsylvania

(Received August 17, 1959)

Simple valence bond wave functions (using hybridized orbitals) are constructed for the CH, NH, and OH molecules. The intraatomic energy is evaluated by Moffitt's atoms-in-molecules method. The interatomic energy is approximated by: (1) replacing heavy-atom 1*s* electrons by point charges at their nuclei; (2) restricting exchange energy contribution to permutation of bonding electrons; (3) using Mulliken approximation to reduce exchange and hybrid integrals to Coulomb and overlap types; (4) evaluating one-center integrals by the Pariser approximation and by a new method which utilizes the virial theorem; and (5) expressing two-center integrals by simplified expressions which give correct semiempirical values at $R=0$ limit and which contain two arbitrary parameters. The latter are adjusted so as to yield correct dissociation energies of CH and OH. The dissociation energy of NH is then found to be 3.61 ev, which lies within the uncertainty of the best experimental result 3.7±0.5 ev. Calculated degrees of hybridization agree well with previous estimates.

INTRODUCTION

AT the present time, there is no well-established value for the dissociation energy of the NH molecule. Pannetier and Gaydon[1] obtained $D_0=4.0$ ev using a linear Birge-Sponer extrapolation of two points, but Gaydon[2] recommends 3.7±0.5 ev. Because of the inherent difficulty of present-day quantum mechanical calculations, no reliable theoretical estimates of the NH dissociation energy have yet been obtained[3]; semiempirical studies suggest values from 3.4 to 4.2 ev.[4]

The semiempirical valence bond treatment of NH here described is an attempt to transform the chemist's traditional picture of a chemical bond into semiquantitative language without the inconsistent neglect and reintroduction of overlap integrals, without sacrificing the possibly relevant Coulombic interactions, and without invoking empirical data at the level of the bond itself, but rather at the more basic level of its intrinsic structure.

OUTLINE OF METHOD

A brief summary of the method follows: (a) Given electron configurations $k^2\phi_0^2(\phi_1\cdot h)^2\pi^n$ for CH, NH, and OH ($n=1$, 2, 3, respectively), where $\phi_0=cs-(1-c^2)^{\frac{1}{2}}\sigma$ and $\phi_1=(1-c^2)^{\frac{1}{2}}s+c\sigma$ are hybrid orbitals constructed from 2*s* and 2*pσ* AO's on the heavy atom, k and π are 1*s* and 2*pπ* AO's on that atom, and h is a 1*s* hydrogen atom AO, one constructs the corresponding valence bond state functions $^2\Pi$ for CH, $^3\Sigma^-$ for NH, and $^2\Pi$ for OH; e.g., for CH,

$$\Omega=2^{-\frac{1}{2}}[\,|\,k\bar{k}\phi_0\bar{\phi}_0\pi\phi_1\bar{h}\,|-|\,k\bar{k}\phi_0\bar{\phi}_0\pi\bar{\phi}_1h\,|\,],^6 \qquad (1)$$

where the conventional symbol for a determinantal wave function has been employed. (b) The total energy is separated into its intraatomic and interatomic parts by Moffitt's atoms-in-molecules method,[5] and the intraatomic energy is evaluated by an approach previously described.[7-8] Simplification of the interatomic part is effected by assuming that the influence of k electrons can be approximated by two negative point charges located at the heavy nucleus, and by restricting exchange energy contributions to those due to permutation of bonding electron pairs, i.e., electrons are permuted only between ϕ_1 and h.[9]

The many interaction integrals are evaluated by invoking the following approximations:

(1) The Mulliken approximation[10] is utilized to reduce all one- and two-electron exchange and hybrid integrals to Coulombic and overlap integrals (SCF overlap integrals were used exclusively).[11]

(2) One-center two-electron repulsion integrals involving more than two hybridized AO's are found by

* Supported in part by a research grant from the National Science Foundation.

† Present Address: Department of Chemistry, Illinois Institute of Technology, Chicago, Illinois.

[1] G. Pannetier and A. G. Gaydon, J. Chem. Phys. **48**, 221 (1951).

[2] A. G. Gaydon, *Dissociation Energies and Spectra of Diatomic Molecules* (Chapman and Hall, Ltd., London, England, 1953), second ed.

[3] See J. Higuchi, J. Chem. Phys. **24**, 535 (1956); M. Krauss, *ibid.* **28**, 1021 (1958).

[4] G. W. King, J. Chem. Phys. **6**, 378 (1938); G. Glockler, *ibid.* **16**, 602 (1948); **19**, 124 (1951).

[5] W. Moffitt, Proc. Roy. Soc. (London) **A210**, 245 (1951).

[6] A. C. Hurley, Proc. Roy. Soc. (London) **A248**, 119 (1958), has shown in a semiempirical way that ionic structures A^-H^+ are important for CH, NH, and OH. Such structures have not been introduced into the present work; we tentatively assume that our empirically and interpolatively obtained integrals should give some account for differences in ionicity, but refined studies of this problem are in progress.

[7] A. L. Companion and F. O. Ellison, J. Chem. Phys. **28**, 1 (1958).

[8] For AH-type molecules, it was found that the intraatomic energy at equilibrium internuclear distance was approximated to within 0.05 ev by using the promotional energy evaluated at infinite internuclear distance, for all values of the hybridization coefficient.

[9] Our treatment here deviates from the conventional simple VB approach: we retain all Coulombic interactions, which the conventional neglects; we neglect all exchange interaction between nonbonding electrons, which the conventional retains.

[10] R. S. Mulliken, J. Chim. Phys. **46**, 500, 521 (1949).

[11] P-O. Lowdin, Phys. Rev. **90**, 120 (1953).

TABLE I. Semiempirical electron repulsion integrals involving hybridized orbitals.[a]

Integral	Atom	A	B	C
$(\phi_\sigma\phi_\sigma \mid \phi_\sigma\phi_\sigma)$	C	0.39419	0.22576	−0.19956
	N	0.47648	0.26300	−0.22082
	O	0.53688	0.26526	−0.23018
$(\phi_\sigma\phi_\sigma \mid \phi_1\phi_1)$	C	0.35301	−0.09978	0.09978
	N	0.41286	−0.12868	0.10747
	O	0.45822	−0.11474	0.11509
$(\phi_1\phi_1 \mid \phi_1\phi_1)$	C	0.42030	0.17330	−0.19961
	N	0.52858	0.14896	−0.20029
	O	0.57186	0.19520	−0.23018

[a] Integrals are listed in the form $(\phi_i\phi_i \mid \phi_j\phi_j)=A+Bc^2+Cc^4$, where c is the hybridization coefficient, and integrals are expressed in hartree units (1 hu=27.204 ev).

applying the Pariser approximation[12] directly to atomic valence states involving the appropriate hybrids; these integrals may be found in Table I. Those integrals involving less than three hybridized AO's are evaluated by expanding the integral in terms of integrals over pure AO's, listed in Table II, and then applying the Pariser approximation.[13]

(3) One-center one-electron nuclear attraction integrals of the type $(A:aa)$ are found by first expanding in terms of integrals over pure AO's to yield terms $(A:ss)$ and $(A:s\sigma)$ (see Table II) which, in turn, are evaluated by considering appropriate processes such as $C(s^2\sigma\pi)\rightarrow C^+(s^2\pi)+1e^-$, for which $\Delta E=I_v$ (valence state ionization potential), and for which the change in *potential energy* is $\Delta V\sim Z_c(C:ss)-2(ss:s\sigma)-(s\sigma:\pi\pi)$.[14] From the virial theorem,[15] $\Delta E=\frac{1}{2}\Delta V$, so that $(C:s\sigma)\sim 2[I_v+(ss:s\sigma)+\frac{1}{2}(s\sigma:\pi\pi)]/Z_c$.

(4) Two-center one-electron nuclear attraction integrals of the type $(A:bb)$ are approximated by the expression

$$(A:bb)=[1-(1+\alpha R)\exp(-\beta R)]/R, \qquad (2)$$

TABLE II. Semiempirical integrals involving pure atomic orbitals.[a]

Integral	C	N	O	H
$(hh \mid hh)$				0.47226
$(ss \mid ss)$	0.42434	0.53905	0.57258	
$(s\sigma \mid s\sigma)$	0.38722	0.46780	0.52083	
$(ss \mid s\sigma)$	0.36150	0.42987	0.46212	
$(s\sigma \mid \pi\pi)$	0.34504	0.42038	0.45331	
$(A \mid ss)$	0.64826	0.75405	0.80458	
$(A \mid s\sigma)$	0.46723	0.53989	0.58168	
$(H \mid hh)$				1.00000

[a] Integrals expressed in hartree units (1 hu=27.204 ev).

[12] R. Pariser, J. Chem. Phys. **21**, 568 (1953).

[13] On expansion in terms of integrals over pure AO's, repulsion integrals involving more than two hybridized AO's yield terms such as $(s\sigma \mid s\sigma)$, for which we have no semiempirical approximation; neglecting such terms causes the original integral to behave unreasonably upon variation of the hybridization coefficient c.

[14] $Z_c=Z$(nucleus)-2 to account for the k electrons.

[15] Eyring, Walter, and Kimball, *Quantum Chemistry* (John Wiley and Sons, Inc., New York, 1944), p. 355.

where β is an arbitrary parameter and α is chosen to satisfy the requirement that $(A:bb)$ approaches its correct semiempirical limit for $R=0$; i.e., $\alpha=\beta-(B:bb)$.

(5) Two-center two-electron repulsion integrals $(aa:bb)$ are approximated by an expression exactly like Eq. 2, but with new parameters δ and γ replacing α and β, respectively; γ is a second arbitrary parameter, and δ is chosen so that the integral $(aa:bb)$ approaches a reasonable semiempirical limit for $R=0$; *viz*, $\delta=\gamma-\frac{1}{2}[(aa:aa)+(bb:bb)]$.

RESULTS

On using experimental bond lengths for CH(1.120 A), NH (1.038 A) and OH (0.971 A), the parameters β and γ were found to be 3.525 and 2.507, respectively, by simultaneous fitting of the experimental dissociation energies of CH and OH. In each of the cases, the energies were variationally minimized with respect to the hybridization coefficient c. Then the calculations were repeated for the NH molecule. The hybridization coefficients, the traditional Coulomb, exchange, and promotional energy contributions J, K, and P, respectively, and the dissociation energies are given in Table III. Our predicted D_0 for NH is 3.61 ev, which lies well within the uncertainty of Gaydon's suggested value 3.7±0.5 ev.

TABLE III. Summary of results.[a]

	CH	NH	OH
c	0.965	0.975	0.987
$-J$	0.691	1.230	2.019
$-K$	3.934	4.021	3.493
P	0.971	1.439	0.930
D_e[b]	3.65	3.81	4.58
D_0	3.47[c]	3.61	4.35[c]

[a] Except for the hybridization coefficient c, all quantities are expressed in ev.

[b] $D_e=-(J+K+P)$=energy of separated atoms in ground electronic states minus energy at minimum of molecular potential energy curve.

[c] From reference 19.

Mulliken[16] has predicted the s character of the bonding CH orbital to be about 15.5%, corresponding to a hybridization coefficient $c=0.92$, which is not far from our 0.965. For CH, NH, and OH, Moffitt[17] predicted the s character of bonding AO's to be roughly 9.39, 6.05, and 4.02%, respectively, which would correspond to $c=0.95$, 0.97, and 0.98.

The method presented in this paper has also been applied directly to the hydrogen molecule Heitler-London type wave function using the same parameters β and γ given above; the calculated D_0 is 4.51 ev,[18] which is remarkably (and probably somewhat fortuitously) close to the experimental 4.48 ev.[19]

[16] R. S. Mulliken, J. Phys. Chem. **56**, 295 (1952).

[17] W. Moffitt, Proc. Roy. Soc. (London) **A202**, 548 (1950).

[18] $J=-0.607$ ev, $K=-4.176$ ev, $P=0$; zero-point energy=0.269 ev.

[19] G. Herzberg, *Molecular Spectra and Molecular Structure* (D. Van Nostrand Company, Inc., Princeton, New Jersey, 1950).

Mayer's Ionic Solution Theory Applied to Electrolyte Mixtures

HAROLD L. FRIEDMAN*

Faculté des Sciences, Université Libre de Bruxelles

AND

Department of Chemistry, University of Southern California, Los Angeles

(Received June 11, 1959)

For solutions of a mixture of two electrolytes with a common ion, the characteristic free energy function is $\Delta_m G^{ex}$, the change in excess free energy on forming the solution from solutions of the single electrolytes. This is closely related to $\Delta_m \mathcal{G}$, where $\mathcal{G}$ is the cluster integral sum of the Mayer theory. For systems that conform to Harned's rule the contributions of most of the cluster integrals to $\Delta_m \mathcal{G}$ are negligible. The form of the principle contribution to $\Delta_m \mathcal{G}$ depends on whether the two electrolytes have the same charge type (symmetrical mixtures) or not.

The equations for symmetrical mixtures which nearly conform to Harned's rule are developed in detail, first for the general case in which the components of the potential of average force are arbitrary and then for the special case of hard sphere ions, designated as the primitive model for electrolyte solutions. The leading term of $\Delta_m \mathcal{G}$ is determined by the difference in short-range interaction of pairs of ions of the same charge and does not depend at all on the common ion. Another general result is that $\Delta_m G^{ex}/I^2$ does not vanish as $I \to 0$, as has sometimes been expected on the basis of the Brønsted principle of specific ion interaction, but approaches a finite value in a way that is governed by a higher-order limiting law.

Comparison with experiment is made on the basis of the primitive model. The results are roughly consistent with the free energy effects in alkali metal chloride mixtures if it is assumed that the effective radii of the alkali metal ions are about double their crystal radii.

1. INTRODUCTION

MAYER's ionic solution theory[1] is derived from the theory of the virial coefficients of imperfect gases and is entirely independent of the Debye-Hückel theory and free of the physical and mathematical inconsistencies of the earlier theory. Frank and Tsao[2] have pointed out the great success of the application of Mayer's theory to dilute solutions of a single electrolyte.[3] We consider here the application of this theory to relatively concentrated solutions of two electrolytes with a common ion.

In applying Mayer's ionic solution theory[1,4] to a problem it is natural to calculate the thermodynamic properties of a solution from a molecular model in two steps:

Molecular model for the solution

↘ A

Potentials of average force of sets of ions in the solvent as functions of the center-of-mass coordinates of the ions

↘ B

Thermodynamic properties of the solution.

The calculation of step A is very difficult, except in the case of the *primitive model* in which the solvent is represented as an ideal structureless dielectric whose properties are independent of electric field strength, and the ions are represented as hard spheres with the same dielectric constant as the solvent and with the charge in an arbitrary but fixed spherical distribution within each ion. (The Debye-Hückel theory is limited to the treatment of this simplest model, and even this is treated in a fashion that is consistent only for extremely dilute solutions.)

It is important to note that each potential of average force of a set of ions *in the solvent* (=potential of average force at infinite dilution) that is referred to in the present paper is an average over the internal coordinates of the ions of the set and over all of the coordinates of the solvent molecules. This potential of average force of a set of ions in the solvent corresponds to the reversible work in the following thought experiment. Start with the set of ions at effectively infinite distance from each other, but all immersed in a body of solvent which is confined by rigid walls and is in contact with a thermostat. Now, supposing each ion to be held at its center of mass by an idealized handle which permits the ion to deform and to twist and turn

* Address: I.B.M. Research Center, Yorktown Heights, N. Y.

[1] J. E. Mayer, J. Chem. Phys. **18**, 1426 (1950).

[2] H. S. Frank and M. S. Tsao, Ann. Rev. Phys. Chem. **4**, 43 (1953).

[3] However, there are two important errors in their review. Their first equation, expressing the assumption that the potential of average force is the sum of pairwise contributions, is not, as stated, essential to the theory. This is shown by Friedman (reference 4). The other error is the statement that Poirier's equations give exactly the thermodynamic properties of the primitive model. In fact Poirier neglected terms corresponding to $\mathcal{G}_3$, $\mathcal{G}_4$, $\mathcal{G}_5$, , , in the terminology of the present paper.

[4] H. L. Friedman, Molecular Phys. **2**, 23 (1959).

around the center of mass, slowly manipulate the handles to bring the n ions to any specified set of coordinates, $\{n\}$. It is clear that for two ions the potential of average force will be a function of the distance between their centers, for three ions the potential of average force will be a function of the three distances between their centers, etc. These potentials of average force of sets of ions in the solvent are not to be confused with the potential of average force of a subset of the ions in a *solution* which requires an average over the coordinates of all of the solute molecules and ions that are not in the subset in addition to the average over the internal coordinates of the ions in the subset and the coordinates of the solvent.

Mayer's ionic solution theory amounts to a series expansion for the calculation of step B. It is convenient to write this expansion in the following way[4]:

$$\mathfrak{S}=\kappa^3/12\pi+\sum\mathfrak{S}_u, \qquad u=2, 3, 4, \cdots, \quad (1.1)$$

where $\mathfrak{S}$ is a thermodynamic function that is closely related to the excess free energy[5] of the solution; κ is the Debye parameter, $\kappa^2=\lambda\sum c_s z_s^2$; $\lambda=4\pi\epsilon^2/DkT$; c_s is the particle number density (molecules/unit volume) of solute species, s (assumed ionic in this paper); and $z_s\epsilon$ is the electric charge on an ion of species s.

D is the macroscopic dielectric constant of the pure solvent at pressure P_0 and temperature T,

$$\mathfrak{S}_u=\sum \mathbf{c}^{\mathbf{u}} I^{(\mathbf{u})}/\mathbf{u}!, \quad (1.2)$$

where $\mathbf{c}=c_1, c_2, \cdots c_s, \cdots$, the set of solute particle number densities (volume concentrations); $\mathbf{u}=u_1, u_2, \cdots u_s, \cdots$, a set of ions, u_1 of species 1, u_2 of species 2, etc., with $u_s\geq 0$ for each s; $\mathbf{c}^{\mathbf{u}}=c_1^{u_1}c_2^{u_2}c_3^{u_3}\cdots$, the product of exponentials; $\mathbf{u}!=u_1!u_2!u_3!\cdots$, the product of factorials.

The sum in Eq. (1.2) is over all sets, $\mathbf{u}$, such that

$$u=u_1+u_2+\cdots+u_s+\cdots$$

and such that $\mathbf{u}$ is a subset of all the ions in the solution. $I^{(\mathbf{u})}$ is a sum of irreducible cluster integrals on clusters (sets) of the composition, $\mathbf{u}$. The integrands of these integrals are products of cluster functions, each of which is a function of the potentials of average force of the set $\mathbf{u}$, or of a subset of $\mathbf{u}$, in the solvent. The general and complete definition of $I^{(\mathbf{u})}$ is complicated,[4] but one property of this function is of special importance for the present paper: $I^{(\mathbf{u})}$ is completely determined for a particular model if in addition κ and λ are fixed. Some examples of $I^{(\mathbf{u})}$ are given in Secs. 4 and 6 of this paper.

Not only is it very difficult to perform the calculation of step A for a realistic model but also, even if one is given the potentials of average force in the solvent, only the simplest $I^{(\mathbf{u})}$ in step B can be calculated with a reasonable amount of labor. These problems certainly impede the application of the Mayer theory but it seems inevitable that similar difficulties will be found in any theory of the equilibrium properties of electrolyte solutions of finite concentration.

[5] H. L. Friedman, J. Chem. Phys. (to be published).

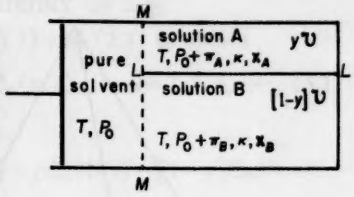

FIG. 1. Experiment corresponding to the definition of $\Delta_m\mathfrak{S}$. The partition, MLM, is permeable only to solvent species. The piston is adjusted during the experiment to maintain P_0 at a predetermined value.

Now we observe that in the isochoric isothermal process in which we mix two solutions in the same solvent with the same κ, each $I^{(\mathbf{u})}$ behaves only as a constant coefficient. On this basis, it is possible to learn something about the change in $\mathfrak{S}$ in this process, $\Delta_m\mathfrak{S}$, without evaluating the cluster integrals. In this paper we exploit this observation and then calculate the leading term in $\Delta_m\mathfrak{S}$ on the basis of the primitive model.

The change in excess free energy, $\Delta_m G^{ex}$, when we mix two solutions of the same molal ionic strength in an isothermal isobaric process[5] is closely related to $\Delta_m\mathfrak{S}$. However, the exact relation is intricate to derive because the concentrations, c_s, are those which pertain to the solution under its own osmotic pressure. This relation is obtained in the following section in order to enable us to use certain generalizations based on experiment.

2. THERMODYNAMIC CONSIDERATIONS

Consider the experiment represented in Fig. 1 in which two different solutions with the same solvent are in osmotic equilibrium with a reservoir of solvent which is maintained in the state, T, P_0. We define the solute fraction of species s as

$$x_s=c_s/\sum c_s=c_s/c, \quad (2.1)$$

and then the composition of a solution may be specified by giving κ and the set, $\mathbf{x}$.

$$\mathbf{x}=x_1, x_2, \cdots x_s, \cdots. \quad (2.2)$$

We assign a single definite index to each solute species so that $\mathbf{x}_A=\mathbf{x}_B$ if and only if the solutes in the two solutions of Fig. 1 are the same. The (extensive) volumes of the two solutions are $y\mathcal{V}$ and $[1-y]\mathcal{V}$.

In the mixing process in which the partition $L-L$ is removed and osmotic equilibrium is reestablished with the original solvent state, T, P_0, there is a change in $\mathfrak{S}$ that is given by[6]

$$\Delta_m\mathfrak{S}(y,\kappa)=\mathfrak{S}(y,\kappa)-y\mathfrak{S}(1,\kappa)-[1-y]\mathfrak{S}(0,\kappa), \quad (2.3)$$

where $\mathfrak{S}(1, \kappa)$ applies to solution A and $\mathfrak{S}(0, \kappa)$ to

[6] In this paper, parentheses are used in mathematical expressions to indicate functional dependence, as $d(x)$.

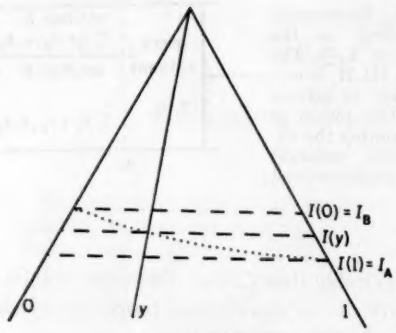

FIG. 2. Schematic relation of I to y at constant κ. —— line of constant y. ----- line of constant I. ····· line of constant κ. For a given solution corresponding to a point, y, I, of this graph, the function κ pertains to the solution at the pressure $P_0+\pi(y, I)$, where π is the osmotic pressure.

solution B. We assume that κ is unchanged in the process.

Now we employ the thermodynamic relation[5] of $\mathfrak{S}$ to G^{ex}, the excess free energy of the same solution at T, P_0:

$$2\lambda\mathfrak{S}/\kappa^2=-G^{ex}/IRT+B, \tag{2.4}$$

where B is defined so that $\frac{1}{2}B\sum x_s z_s^2$ is equal to the right-hand side of Eq. (4.16) of reference 5. As discussed there, B is of the nature of a small correction term whose main contribution comes from the difference in concentration scales of $\mathfrak{S}$ and G^{ex}.

Although the three solution states corresponding to the three terms on the right of Eq. (2.3) have the same value of κ, they do *not* in general have the same value of I, the molal ionic strength. This is because $\mathfrak{S}$ is a property of a solution of definite $\mathbf{x}$, κ, and T, but the amount of solvent in the solution of given volume is determined by the osmotic equilibrium with the solvent at P_0 and is therefore not an independent variable in the formulation of $\mathfrak{S}$. The situation is illustrated in Fig. 2. The coordinates of a point in this diagram are y, I and therefore we will express the excess free energy as a function of two variables: $G^{ex}(y, I)$. The other variables, namely T, P_0, $\mathbf{x}_A$, and $\mathbf{x}_B$, are constant in this problem. We designate the value of I at a particular y of the κ=constant curve as I_y and obtain

$$2\lambda\Delta_m\mathfrak{S}(y, \kappa)/\kappa^2=-\Delta_m G^{ex}(y, I_y)/I_y RT + \Delta_m B(y, I_y)+E(y, I_y), \tag{2.5}$$

where $\Delta_m G^{ex}$ and $\Delta_m B$ apply to the isobaric mixing process at constant I:

$$\Delta_m G^{ex}(y, I_y)=G^{ex}(y, I_y)-yG^{ex}(1, I_y) -[1-y]G^{ex}(0, I_y) \tag{2.6}$$

$$\Delta_m B(y, I_y)=B(y, I_y)-yB(1, I_y)-[1-y]B(0, I_y). \tag{2.7}$$

The remaining term in Eq. (2.5) is

$$E(y, I_y)=[y/RT]\{[G^{ex}(1, I_1)/I_1]-[G^{ex}(1, I_y)/I_y]\} +[[1-y]/RT]\{[G^{ex}(0, I_0)/I_0]-[G^{ex}(0, I_y)/I_y]\} -y\{B(1, I_1)-B(1, I_y)\} -[1-y]\{B(0, I_0)-B(0, I_y)\}. \tag{2.8}$$

Each of the differences in braces in this equation refers to a change in a function of I, either from I_y to I_1 on the $y=1$ line of Fig. 2, or from I_y to I_0 on the $y=0$ line. Each such function may be expanded in a Taylor series in I about I_y. For instance,

$$G^{ex}(1, I_1)/I_1=[G^{ex}(1, I_y)/I_y] +[I_1-I_y]\frac{\partial(G^{ex}/I)}{\partial I}+\tfrac{1}{2}[I_1-I_y]^2\frac{\partial^2(G^{ex}/I)}{\partial I^2}+\cdots,$$

where each derivative is evaluated at I_y. We may also represent the variation of I_y on the constant κ curve of Fig. 2 as

$$I_y=I_0+y[I_1-I_0]+\Delta_m I(y, \kappa),$$

where this Δ_m applies to the process at constant κ. With these substitutions, (2.8) becomes

$$E(y, I_y)=y[1-y][(I_0-I_1)/I_y^2 RT] \cdot[G_w^{ex}(1, I_y)-G_w^{ex}(0, I_y)]+\cdots, \tag{2.9}$$

where $G_w^{ex}(y, I)$ is[5] the excess partial free energy of the solvent in the state y, I and where the higher terms which are omitted are negligible compared to the first, at least for mixtures of solutions of 1–1 electrolytes.

It is convenient to introduce the expansion of $\Delta_m G^{ex}$ as before,[5]

$$\Delta_m G^{ex}(y, I)=I^2 RTy[1-y][g_0+g_1 Y+g_2 Y^2+\cdots], \tag{2.10}$$

where

$$Y=1-2y, \tag{2.11}$$

and the g_p coefficients are closely related to the Harned coefficients.[5] We expand $\Delta_m B$ and E in a similar way:

$$\Delta_m B(y, I)=y[1-y]I[b_0+b_1 Y+\cdots] \tag{2.12}$$

$$E(y, I)=y[1-y]I[e_0+e_1 Y+\cdots]. \tag{2.13}$$

The coefficients of (2.12) and (2.13) can also be determined by experiment although at this time there is no system for which all of the necessary data are available. Finally, we expand the change in cluster integral sum in the same way:

$$\Delta_m\mathfrak{S}(y, \kappa) =-\tfrac{1}{2}[\kappa^2/\lambda]^2 y[1-y][\mathfrak{s}_0+\mathfrak{s}_1 Y+\mathfrak{s}_2 Y^2+\cdots]. \tag{2.14}$$

In Sec. 3 we consider the theoretical expression for $\mathfrak{s}_0$. In the remainder of the present section, we consider the relation of the theoretical $\mathfrak{s}_p$ coefficients to the experimental g_p coefficients.

It must be noted that the $\mathcal{G}_p$ coefficients are independent of Y for variations at constant κ at the osmotic pressure (i.e., along the dotted curve of Fig. 2), but the coefficients g_p, b_p, and e_p are independent of Y for variations at constant I at the pressure P_0 (i.e., along a horizontal line of Fig. 2). Therefore, in the procedure of substituting Eqs. (2.10), (2.12), (2.13), and (2.14) into Eq. (2.5) and equating the coefficients of equal powers of Y, we must take into account the fact that for variation at constant κ we have

$$I(Y)=I(Y=0)+(\partial I/\partial Y)_\kappa Y+\tfrac{1}{2}(\partial^2/\partial Y^2)_\kappa Y^2+\cdots \tag{2.15}$$

$$g_0(Y)=g_0(Y=0)+(\partial g_0/\partial Y)_\kappa Y+(\partial^2 g_0/\partial Y^2)_\kappa \tfrac{1}{2}Y^2+\cdots$$

$$(\partial g_0/\partial Y)_\kappa=(\partial g_0/\partial I)(\partial I/\partial Y)_\kappa,$$

$$(\partial^2 g_0/\partial Y^2)_\kappa=(\partial g_0/\partial I)(\partial^2 I/\partial Y^2)_\kappa + (\partial^2 g_0/\partial I^2)(\partial I/\partial Y)_\kappa^2,$$

and similarly for the other experimental coefficients. In this way we obtain the desired relations:

$$[\kappa^2/\lambda I]\mathcal{G}_0=g_0-b_0-e_0 \tag{2.16}$$

$$[\kappa^2/\lambda I]\mathcal{G}_1=g_1-b_1-e_1 + (\partial \ln I/\partial Y)_\kappa(\partial/\partial I)\{I[g_0-b_0-e_0]\} \tag{2.17}$$

$$[\kappa^2/\lambda I]\mathcal{G}_2=g_2-b_2-e_2 + \tfrac{1}{2}[\partial \ln I/\partial Y]_\kappa^2(\partial/\partial I)\{I^2(\partial/\partial I)[g_0-b_0-e_0]\} + [1/2I][\partial \ln I/\partial Y]_\kappa(\partial/\partial I)\{I^2[g_1-b_1-e_1]\} + [1/2I][\partial^2 I/\partial Y^2]_\kappa(\partial/\partial I)\{I[g_0-b_0-e_0]\}. \tag{2.18}$$

In these equations, $\kappa^2\mathcal{G}_p$ is independent of Y and the remaining functions pertain to the ionic strength characteristic of $Y=0$ at the given κ.

Now we consider the special case in which there is a single electrolyte with two species of ions in solution A and another binary electrolyte in solution B, with either the anion species or the cation species the same in both solutions. In the majority of such systems, which have been investigated experimentally, it is found that Harned's rule[5] is nearly obeyed in the mixing process. In our nomenclature, this means that in such systems $|g_0|$ is much larger than $|g_1|$, $|g_2|$, etc.[5] It is also found in the cases for which we have the required data that the right side of Eq. (2.16) is nearly equal to g_0, the right side of Eq. (2.17) is nearly equal to g_1, etc. When a system conforms to all these conditions then it must also be true that $|\mathcal{G}_0|$ is large compared to $|\mathcal{G}_1|$, $|\mathcal{G}_2|$, etc. We use this result in the following section to simplify the theoretical calculation of $\mathcal{G}_0$ and the usefulness of these calculations therefore depends upon the generality of this behavior. Although it seems likely that it is as general as the approximate validity of Harned's rule, further work is required to establish this.

3. THEORY OF $\Delta_m\mathcal{G}$

We combine Eqs. (1.1) and (2.3) to obtain

$$\Delta_m\mathcal{G}(y,\kappa)=\sum\Delta_m\mathcal{G}_u(y,\kappa), \qquad u=2,3,4,\cdots, \tag{3.1}$$

where

$$\Delta_m\mathcal{G}_u(y,\kappa)=\mathcal{G}_u(y,\kappa)-y\mathcal{G}_u(1,\kappa)-[1-y]\mathcal{G}_u(0,\kappa). \tag{3.2}$$

We define the function (see the definitions of the set nomenclature following Eq. (1.2)),

$$\Delta_m\mathbf{c}^u=[\mathbf{c}(y,\kappa)]^u-y[\mathbf{c}(1,\kappa)]^u -[1-y][\mathbf{c}(0,\kappa)]^u \tag{3.3}$$

and combine Eqs. (1.2) and (3.2) to obtain

$$\Delta_m\mathcal{G}_u=\sum I^{(u)}\Delta_m\mathbf{c}^u/\mathbf{u}!, \tag{3.4}$$

where we have taken advantage of the fact that $I^{(u)}$ is not a function of y in the mixing process of Fig. 1. The range of the summation in Eq. (3.4) is exactly the same as that in Eq. (1.2).

Our objective is to obtain an expansion of the form of Eq. (2.14) by combining (3.1) and (3.4). The functional dependence on y must come from $\Delta_m\mathbf{c}^u$. We represent the concentration set in solution A as

$$\mathbf{c}(1,\kappa)=c_1, 0, c_3[1+\mathfrak{r}] \tag{3.5}$$

and in solution B as

$$\mathbf{c}(0,\kappa)=0, c_2, c_3[1-\mathfrak{r}]. \tag{3.6}$$

Thus, species 3 is the common ion and the *hetero* ion is species 1 in solution A and species 2 in solution B. The term, $\mathfrak{r}$, is to allow for the fact that if species 1 and 2 do not have the same charge, then the concentration of species 3 will not be the same in the two end solutions. The arithmetic mean of the concentration of species 3 in the end solutions is c_3 and from the condition of constant κ we find

$$\mathfrak{r}=[z_1-z_2]/[2z_3-z_1-z_2]. \tag{3.7}$$

Species 3 may be either a cation or an anion, but we note that both z_1z_3 and z_2z_3 are always negative.

It follows that in a mixture the concentration set is

$$\mathbf{c}(y,\kappa)=yc_1, [1-y]c_2, [1-\mathfrak{r}Y]c_3. \tag{3.8}$$

We also introduce the two functions,

$$\iota(x,p)=1+x+x^2+\cdots+x^p, \quad \text{if } p\geq 0, \tag{3.9}$$
$$=0, \quad \text{if } p<0;$$
$$\langle p\rangle=0, \quad \text{if } p \text{ is even},$$
$$=1, \quad \text{if } p \text{ is odd} \tag{3.10}$$

and then we may express the y dependence of $\Delta_m\mathbf{c}^u$ in the following concise way:
If $u_1>0$, $u_2>0$, $u_3\geq 0$, then

$$\Delta_m\mathbf{c}^u=y^{u_1}[1-y]^{u_2}[1-\mathfrak{r}Y]^{u_3}c_1^{u_1}c_2^{u_2}c_3^{u_3}. \tag{3.11}$$

TABLE I. Sets that contribute to $\mathfrak{s}_{0u}$.

	$\mathfrak{s}_{02}$	$\mathfrak{s}_{03}$	$\mathfrak{s}_{04}$
$\mathfrak{r}\neq 0$	1, 1, 0 0, 1, 1 2, 0, 0 1, 0, 1 0, 2, 0 0, 0, 2	none	none
$\mathfrak{r}=0$	1, 1, 0 2, 0, 0 0, 2, 0	1, 1, 1 2, 0, 1 0, 2, 1	1, 1, 2 2, 0, 2 0, 2, 2

If $u_1=0$, $u_2>0$, $u_3\geq 0$, then

$$\Delta_m\mathbf{c}^{\mathbf{u}}=-y[1-y]c_2^{u_2}c_3^{u_3}\sum_{p=0}^{u_3}\binom{u_3}{p}[-\mathfrak{r}]^p \times\{2[1-y]^{u_2-1}l(Y,p-1)+l(1-y,u_2-2)\}. \quad (3.12)$$

If $u_1>0$, $u_2=0$, $u_3\geq 0$, then

$$\Delta_m\mathbf{c}^{\mathbf{u}}=-y[1-y]c_1^{u_1}c_3^{u_3}\sum_{p=0}^{u_3}\binom{u_3}{p}\mathfrak{r}^p \times\{2y^{u_1-1}l(-Y,p-1)+l(y,u_1-2)\}. \quad (3.13)$$

If $u_1=0$, $u_2=0$, $u_3>1$, then

$$\Delta_m\mathbf{c}^{\mathbf{u}}=-4y[1-y]c_2^{u_3}\sum_{p=2}^{u_3}\binom{u_3}{p}\mathfrak{r}^pY^{(p)}l(Y^2,\tfrac{1}{2}p-1-\tfrac{1}{2}\langle p\rangle). \quad (3.14)$$

In these equations

$$\binom{n}{m}$$

is the binomial coefficient and $\mathfrak{r}^0=1$ even if $\mathfrak{r}=0$. The four special cases arise because either, neither, or both $[\mathbf{c}(1,\kappa)]^{\mathbf{u}}$ and $[\mathbf{c}(0,\kappa)]^{\mathbf{u}}$ may vanish, depending on the composition of the set, $\mathbf{u}$. It would obviously be more satisfactory to express $\Delta_m\mathbf{c}^{\mathbf{u}}/y[1-y]$ as a power series in Y, inasmuch as the objective is to obtain an equation of the form of (2.14), but the forms given above seem to be as far as we can go in this direction without greatly increasing the complexity of the expressions.

It is apparent upon examining these results together with Eqs. (2.14), (3.1), and (3.4) that every set, $\mathbf{u}$, makes a contribution to $\mathfrak{s}_0$ but that most sets contribute also to some of the higher $\mathfrak{s}_p$. It is convenient to classify the terms of $\mathfrak{s}_0$ on the basis of this observation. Let $\mathfrak{s}_{0u[p]}$ be the sum of the contributions to $\mathfrak{s}_0$ of all sets that contain u particles and that do not contribute to any of the terms, $\mathfrak{s}_{p+1}$, $\mathfrak{s}_{p+2}$, etc. Then we have

$$\mathfrak{s}_0=\sum_{u>1}\sum_{p=0}^{u-2}\mathfrak{s}_{0u[p]}. \quad (3.15)$$

Inspection of Eqs. (3.11) to (3.14) shows that if a given set, $\mathbf{u}$, contributes to $\mathfrak{s}_p$, $p>0$, as well as to $\mathfrak{s}_0$ then its contribution to $\mathfrak{s}_p$ is at least of the same order of magnitude as its contribution to $\mathfrak{s}_0$. Therefore, if we are to have the usual relation for a Harned's rule system

$$|\mathfrak{s}_0|>|\mathfrak{s}_p|, \qquad p>0,$$

as discussed in the last paragraph of Sec. 2, then there are certain restrictions on the contributions of the various sets to the $\mathfrak{s}_p$ coefficients. We may have one or both of the following restrictions: (1) There is a nearly complete cancellation of the contributions of various sets, $\mathbf{u}$, to each $\mathfrak{s}_p$, except $\mathfrak{s}_0$. (2) Those sets that contribute to any $\mathfrak{s}_p$ in addition to $\mathfrak{s}_0$ make negligible contributions to $\mathfrak{s}_0$ and every other $\mathfrak{s}_p$.

Now we *assume* that restriction (2) correctly describes the relations in Harned's rule systems. Some evidence in support of this assumption may be put forward, both on the basis of the cluster integrals and on the basis of certain experimental observations but, inasmuch as the evidence is incomplete and relatively complicated to apply, it seems wise to omit developing it here. Of course, the deduction of either restriction from the theory would be equivalent to a deduction of the approximate validity of Harned's rule.

The assumption that we have made is equivalent to the approximation

$$\mathfrak{s}_0\cong\sum\mathfrak{s}_{0u[0]}=\sum\mathfrak{s}_{0u} \qquad u=2,3,4,\cdots, \quad (3.16)$$

where, in the third member, we have indicated that the subscript, [0], will be omitted in the sequel.

The sets that contribute to the first few $\mathfrak{s}_{0u}$ are readily found from Eqs. (3.11)–(3.14) with the results shown in Table I. Some details of the contributions to $\mathfrak{s}_{02}$ are shown in Table II.

We also use the stoichiometric relations,

$$c_1=[\kappa^2/\lambda]/z_1[z_1-z_3] \quad (3.17)$$

$$c_2=[\kappa^2/\lambda]/z_2[z_2-z_3] \quad (3.18)$$

$$2\mathfrak{r}c_3=[\kappa^2/\lambda][z_1-z_2]/z_3[z_2-z_3][z_1-z_3] \quad (3.19)$$

and so obtain the equation,

$$-\mathfrak{s}_{02}=\frac{2I(1,1,0)}{z_1z_2[z_1-z_3][z_2-z_3]}-\frac{I(2,0,0)}{z_1^2[z_1-z_3]^2}-\frac{I(0,2,0)}{z_2^2[z_2-z_3]^2} +\frac{z_1-z_2}{z_3[z_1-z_3][z_2-z_3]}\left[\frac{2I(0,1,1)}{z_2[z_2-z_3]}-\frac{2I(1,0,1)}{z_1[z_1-z_3]} -\frac{[z_1-z_2]I(0,0,2)}{z_3[z_1-z_3][z_2-z_3]}\right]. \quad (3.20)$$

Note that the integral $I^{(\mathbf{u})}$ is written $I(\mathbf{u})$ when the set, $\mathbf{u}$, is written out as in the preceding equation where $\mathbf{u}=u_1,u_2,u_3$.

For the case, $\mathfrak{r}\neq 0$ (unsymmetrical mixtures), $\mathfrak{s}_{02}$ is the only nonvanishing $\mathfrak{s}_{0u}$. For the case, $\mathfrak{r}=0$ (symmetrical mixtures), the last three terms in Eq. (3.20)

TABLE II. Contributions to $\mathcal{E}_{0u}$.

u	1, 1, 0	2, 0, 0	0, 2, 0	0, 1, 1	1, 0, 1	0, 0, 2
$\Delta_m c^u/y[1-y]$	c_1c_2	$-c_1^2$	$-c_2^2$	$2\tau c_2c_3$	$-2\tau c_1c_3$	$-4\tau^2c_3^2$
u!	1	2	2	1	1	2

vanish, but the higher $\mathcal{E}_{0u}$ do not vanish. In fact, we have

$$-\mathcal{E}_{0,n+2}=\left[\frac{\kappa^2}{\lambda}\right]^n\frac{1}{n!}\frac{2I(1,1,n)-I(2,0,n)-I(0,2,n)}{z_1^2z_3^n[z_3-z_1]^{n+2}},$$
$$\text{if } \tau=0,\ n\geq 0,$$
$$=0, \qquad \text{if } \tau\neq 0 \text{ and } n>0. \tag{3.21}$$

The following sections present more detailed calculations based on Eqs. (3.20), and (3.21), leading finally to numerical calculations based on the primitive model. It seems useful to point out here that $I^{(u)}$ has the dimensions of [length]$^{3u-3}$ and that

$$\kappa^2/\lambda=1.2048\ 10^{-3}IV_\pi^{-1}\text{A}^{-3}, \tag{3.22}$$

where I is the molal ionic strength and V_π is the number of liters of solution per kg of solvent when the solution is at the pressure $P_0+\pi$, where π is the osmotic pressure.

4. SYMMETRICAL MIXTURES, GENERAL RELATIONS

We will consider here the first two terms of $\mathcal{E}_0$, namely $\mathcal{E}_{02}$ and $\mathcal{E}_{03}$. It is convenient for the purposes of this and the following section to introduce a different set notation. The set, ij, written without separating commas, denotes one ion of species i and one of species j. Then, the set consisting of two ions of species i is designated as ii. The same principle will also be employed for larger sets.

The definition[4] of $I^{(u)}$ for $u=2$ is

$$I(ij)=4\pi\int_0^\infty\Phi_{ij}'''r^2dr, \tag{4.1}$$

where

$$\Phi_{ij}=[1+k_{ij}]\exp(q_{ij}) \tag{4.2}$$
$$\Phi_{ij}'''=\Phi_{ij}-1-q_{ij}-q_{ij}^2/2 \tag{4.3}$$
$$1+k_{ij}=\exp(-w_{ij}^*(r)/kT) \tag{4.4}$$
$$q_{ij}=-z_iz_j\lambda\exp(-\kappa r)/4\pi r. \tag{4.5}$$

The potential, w_{ij}^*, is defined by the equation,

potential of average force of ions i and j in the pure solvent at separation r $=w_{ij}^*+z_iz_je^2/Dr.$ (4.6)

Therefore, w_{ij}^* includes various effects such as short-range repulsion that are introduced by a specific model for the solution, but rapidly vanish at large r where the effects of solute and solvent molecular structure on the interionic force are negligible.

Now we substitute Eq. (4.1) in (3.21) with $n=0$, and note that in this case ($\tau=0$), we have $q_{11}=q_{12}=q_{22}$ and therefore,

$$-\mathcal{E}_{02}=4\pi z_1^{-2}[z_1-z_3]^{-2}\int_0^\infty\delta k e^{q_{11}}r^2dr, \tag{4.7}$$

where we have introduced the operator δ that in this case denotes

$$\delta k=2k_{12}(r)-k_{11}(r)-k_{22}(r). \tag{4.8}$$

In general, the δ operator denotes

$$\delta f(\mathbf{w})=2f_{12}(\mathbf{w})-f_{11}(\mathbf{w})-f_{22}(\mathbf{w}), \tag{4.9}$$

where $f_{ij}(\mathbf{w})$ is a function of the set of variables, $\mathbf{w}$, the function being characteristic of a set containing two hetero ions. In some cases, it will be clear that there are other ions in the set, but if so this remaining part of the set is the same for f_{11}, f_{12}, and f_{22}.

We note that unlike[7] the integral $I(ij)$, the integral in (4.7) is not singular at $\kappa=0$. Eq. (4.7) can be given a relatively simple physical interpretation. We write (4.1) as[8]

$$I(ij)=4\pi\int_0^\infty\Phi_{ij}r^2dr-4\pi\int_0^\infty[1+q_{ij}+\tfrac{1}{2}q_{ij}^2]r^2dr. \tag{4.10}$$

The second term on the right of (4.10) is the limiting value of $I(ij)$ for a pair of ions as one or both of them become infinite in size. (i.e., as the strongly repulsive part of w_{ij}^* extends to larger and larger distance). This limiting value is always negative and it contributes a negative, or repulsive term to $\mathcal{E}$. We use repulsive here in the sense that a negative contribution to $\mathcal{E}$ is a positive contribution to G^{ex}, and hence, contributes to the free energy in the way characteristic of a repulsive interaction between the components of the system. The first integral in (4.10) is, in this sense, attractive and measures the reduction in free energy corresponding to the fact that neither of the ions of the pair is infinite in size. In the process of calculating $\delta I^{(2)}$, the contribution of the repulsive integral in (4.10) vanishes identically and we may read Eq. (4.7) as saying that $\mathcal{E}_{02}$ is negative if the attractive part of the 1–2 interaction is greater than the arithmetic mean of the attractive parts of the 1–1 and 2–2 interactions. As we shall see, this is usually the case, and is indeed always the result obtained from the primitive model.

[7] H. L. Friedman, Molecular Phys. 2, 190 (1959); 2, 436 (1959).

[8] This divides Eq. (4.1) into two terms, each of which is singular for any κ. By an alteration of this procedure it is possible to avoid these infinities but this would complicate the discussion and obscure the point of interest.

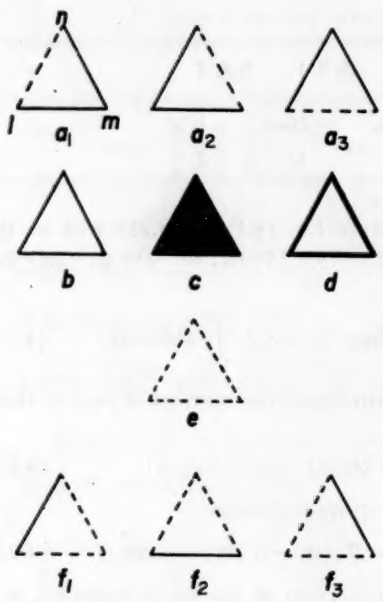

FIG. 3. Terms of $I(lmn)$. ------ q bond. —— Φ'' bond. —— Φ' bond.

Another point of interest is that we have

$$-d\mathfrak{g}_{02}/d\kappa=4\pi z_1^{-2}[z_1-z_3]^{-2}\int_0^\infty \delta k[z_1^2\lambda/4\pi] \cdot\exp(q_{11}-\kappa r)r^2dr \quad (4.11)$$

because k_{ij} is independent of κ. In the limit of $\kappa=0$, neither $\mathfrak{g}_{02}$ nor $d\mathfrak{g}_{02}/d\kappa$ vanishes in general, but we have the limiting relation,

$$d\mathfrak{g}_{02}/d\kappa=[z_1^2\lambda/4\pi]\mathfrak{g}_{02}, \qquad \kappa=0. \quad (4.12)$$

At higher concentrations, the concentration dependence of $\mathfrak{g}_{02}$ depends on the nature of the k_{ij} functions in a more complicated way. The behavior for the primitive model is investigated in Sec. 5.

As a result of investigation[7] of the singularities of the cluster integrals of the Mayer theory it follows that

$$\lim_{\kappa\to 0}\mathfrak{g}_0=\lim_{\kappa\to 0}\mathfrak{g}_{02}, \quad (4.13)$$

and also that

$$\lim_{\kappa\to 0}d\mathfrak{g}_0/d\kappa=\lim_{\kappa\to 0}d\mathfrak{g}_{02}/d\kappa. \quad (4.14)$$

Therefore, the following limiting law for symmetrical electrolyte mixtures at vanishing I may be deduced from Eq. (4.12),

$$d\ln\mathfrak{g}_0/d(I)^{\frac{1}{2}}=[z_1^2\lambda/4\pi][\kappa^2/\lambda I]^{\frac{1}{2}} =[z_1^2\lambda^{\frac{1}{2}}/4\pi][1.2048\times 10^{-3}/V_w]^{\frac{1}{2}}, \quad (4.15)$$

where V_w is the specific volume (liters/kg) of pure solvent. This is a general result of Mayer's ionic solution theory (with the assumptions of reference 7) and does not depend on the choice of a model for the calculation of the potentials of average force at infinite dilution nor on the validity of Harned's rule at finite concentrations. By appropriate differentiation, corresponding limiting laws may be obtained for $\Delta_m H^{ex}$, $\Delta_m V^{ex}$, etc. Unfortunately, the experimental techniques which are needed to investigate the validity of Eq. (4.15) or its derivatives seem to be far out of the range of present-day attainments. Nevertheless, it is interesting to observe that the Debye-Hückel limiting law is not unique but is only the simplest of a series of limiting laws which owe their existence to the long range of the interionic forces. The common characteristic of these limiting laws is that each is a relation that is independent of the details of the short-range ionic interactions and that cannot be deduced from the laws of thermodynamics.

The higher $\mathfrak{g}_{0u}$ are much more difficult to calculate and we will discuss only the first of these. This illustrates the problems which arise and also provides a basis for the numerical calculation of $\mathfrak{g}_{03}$ for the primitive model.

We may represent $I^{(u)}$ for $u=3$ as[4]

$$I(lmn)=3_{a1}+3_{a2}+3_{a3}+3_b+3_c, \quad (4.16)$$

where the terms on the right correspond to the integrals that are represented as graphs in Fig. 3. The correspondence of graphs to integrals in the case of graphs with only pairwise bonds is illustrated by the equation,

$$3_{a1}(lmn)=\iint \Phi_{lm}''\Phi_{mn}''q_{nl}dR_{lm}dR_{mn}, \quad (4.17)$$

where R_{lm} and R_{mn} are vectors from l to m and from m to n, respectively, and where the integration is over all orientations and lengths of these vectors. The function, Φ_{ij}'', is

$$\Phi_{ij}''=\Phi_{ij}-1-q_{ij}$$

and, like q_{ij}, is a function of the distance between the two particles but does not otherwise depend on the vector from one to the other. The other graph is

$$3_c(lmn)=\iint[\exp(-w_{lmn}/kT)-1]\Phi_{lm}\Phi_{mn}\Phi_{nl}dR_{lm}dR_{mn}, \quad (4.18)$$

where w_{lmn} is the third component of the potential of average force of the set, lmn, in the solvent.[4] It depends on the configuration of the centers of mass of the three ions and is obtained from the total potential of average force of the three ions in this configuration by subtracting the three pairwise potentials of average force.

It is readily verified that Eq. (4.13) may also be written in the following way (again refer to the graphs in Fig. 3).

$$I(lmn)=3_c+3_d-3_e-3f_1-3f_2-3f_3 \quad (4.19)$$

This reduces the number of three-center integrals that cannot be evaluated by analytical methods. Our ob-

jective is to evaluate

$$\delta I^{(3)}=2I(1,1,1)-I(2,0,1)-I(0,2,1)$$
$$=2I(123)-I(113)-I(223), \quad (4.20)$$

where the right side has been written out for both forms of the set notation (see the first paragraph of Sec. 4).

Now we note that 3_e may be written as

$$3_e(lmn)=z_l^2z_m^2z_n^2Q^*(\kappa,\lambda) \quad (4.21)$$

where Q^*, the integral remaining after factoring out the ionic charges, is independent of the set, *lmn*. We find at once that the integrals, 3_e, make a contribution to δI^4 of

$$\delta 3_e=-[2z_1^2z_2^2z_3^2-z_1^4z_3^2-z_2^4z_3^2]Q^*(\kappa,\lambda)=0. \quad (4.22)$$

The graphs with two q bonds may be reduced to two-center integrals in the following way. A chain of two q bonds, as in 3_{f1}, corresponds to the integral

$$\int q_{lm}q_{ln}dR_{lm},$$

where we suppose that R_{mn} is fixed so that

$$R_{ln}=R_{lm}+R_{mn}$$

is not independent of R_{lm}.

The integral on a chain of two q bonds may be evaluated by a convolution method[7] to give

$$z_mz_l^2z_n\lambda^2\exp(-\kappa\mid R_{mn}\mid)/8\pi\kappa$$

and so we may write 3_{f1} as

$$3_{f1}=z_mz_l^2z_n\lambda^2[2\kappa]^{-1}\int_0^\infty[1+k_{mn}]\exp(q_{mn}-\kappa r)r^2dr. \quad (4.23)$$

After making the same transformation for 3_{f2} and 3_{f3}, we find the contribution of these three integrals to $\delta I^{(3)}$ to be

$$\delta_{3f}=-z_1^2z_3^2\lambda^2[2\kappa]^{-1}\int_0^\infty\delta k\exp(q_{11}-\kappa r)r^2dr. \quad (4.24)$$

So we find that only 3_e and 3_d contribute three-center integrals to $\delta I^{(3)}$. The contribution of the former cannot be further simplified and is designated $\delta 3_e$. For the latter, we have

$$\delta 3_d=\int[2\Phi_{12}'\Phi_{13}'\Phi_{23}'-\Phi_{11}'\Phi_{13}'^2-\Phi_{22}'\Phi_{23}'^2]d\{3\}, \quad (4.25)$$

where $\{3\}$ represents the appropriate set of coordinates and

$$\Phi_{ij}'=\Phi_{ij}-1. \quad (4.26)$$

We now make the additional rearrangement,

$$\delta 3_d=B_s+B_{13}+B_{23}, \quad (4.27)$$

where

$$B_s=-\int\Phi_{12}'[\Phi_{13}-\Phi_{23}]^2d\{3\} \quad (4.23)$$

$$B_{13}=-\int[\Phi_{11}-\Phi_{12}]\Phi_{12}'^2d\{3\} \quad (4.29)$$

$$B_{23}=\int[\Phi_{12}-\Phi_{22}]\Phi_{23}'^2d\{3\}. \quad (4.30)$$

We combine these calculations to obtain

$$-\mathfrak{s}_{03}=[\kappa^2/\lambda][z_1^2z_3[z_3-z_1]^3]^{-1}[\delta 3_c+\delta 3_f+B_s+B_{13}+B_{23}]. \quad (4.31)$$

On the basis of the investigation[7] of the singularities of the cluster integrals it is deduced that as $\kappa\to 0$, $\mid\mathfrak{s}_{03}\mid$ goes to zero as $-\kappa^2\ln\kappa$. However, the individual terms, δ_{3f}, B_{13}, and B_{23}, are each $O(\kappa^{-1})$ at $\kappa=0$. Therefore, the rearrangement of $I(lmn)$ corresponding to the change from Eqs. (4.16) to (4.19) is not appropriate to an investigation of $\mathfrak{s}_{03}$ at small κ.

At large κ, it is expected that $\mid B_s\mid$ will usually be much larger than $\mid B_{13}+B_{23}\mid$ because the difference bonds, $\Phi_{13}-\Phi_{23}$, $\Phi_{11}-\Phi_{12}$, and $\Phi_{12}-\Phi_{22}$, are only different from zero when the pair of vertices they connect are close together, corresponding to ions which are close together. In the case of B_s, this implies strong attractive forces in such a configuration because in B_s the difference bonds are attractive, i.e., they connect ions of opposite sign. Thus, $q_{13}(=q_{23})$ is positive, $e^{q_{13}}$ is larger than unity, and so $\Phi_{13}-\Phi_{23}$ tends to be a large magnitude except at distances such that $k_{13}=k_{23}$. By the same reasoning, we find that both $\Phi_{12}-\Phi_{22}$ and $\Phi_{11}-\Phi_{12}$ tend to be small even when $k_{12}\neq k_{22}$.

5. SYMMETRICAL MIXTURES, PRIMITIVE MODEL

In this section, we compare certain experimental data for symmetrical electrolyte mixtures with calculations from the Mayer theory made on the basis of the primitive model. It is interesting to see to what extent the primitive model, in spite of its shortcomings, succeeds in this application. Another use of this comparison is that the values of the ion size parameters that are required to give rough numerical agreement with the data may be helpful in deciding what features of the real solution structure must be included to obtain a useful higher approximation than the primitive model. Finally, the mathematical techniques that are used in this section can be used with a more complicated model if the function, k_{ij}, yielded by the model is smoothed to give a sectionally constant function.

We consider first the methods of calculating $\mathfrak{s}_{02}$ and $\mathfrak{s}_{03}$ from the primitive model, and then the comparison with experimental data.

Calculation of $\mathfrak{s}_{02}$

In this special case, the k bonds are

$$k_{ij}(r)=-1 \quad \text{if} \quad r<a_{ij}$$
$$=0 \quad \text{if} \quad r>a_{ij}, \quad (5.1)$$

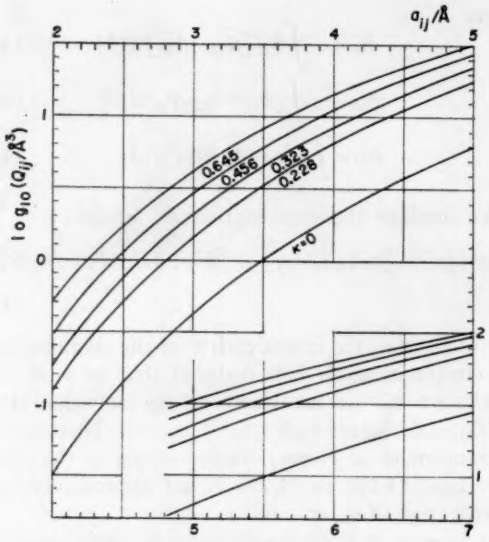

FIG. 4. The function Q_{ij}. Curves of constant κ.

and $\mathfrak{F}_{02}$ becomes [cf. Eq. (4.7)]

$$\mathfrak{F}_{02}=4\pi z_1^{-2}[z_1-z_3]^{-2}\delta Q, \tag{5.2}$$

where [cf. Eq. 4.9)]

$$Q_{ij}=\int_0^{a_{ij}} \exp(q_{11})r^2dr, \quad i=1 \text{ or } 2, \quad j=1 \text{ or } 2, \tag{5.3}$$

because for symmetrical mixtures $q_{11}=q_{12}=q_{22}$.

In Fig. 4 we show Q_{ij} as a function of a_{ij} and κ for $z_1=1$ and water at 25° as the solvent. In this case, $z_1^2\lambda=4\pi 7.135_1$ A. Several methods have been employed in the calculation of these curves. For small κa_{ij} we have the convergent expansion,

$$Q_{ij}=\sum b_n A_{ij}^n \mathrm{E}_{n+1}(z_i^2\lambda/4\pi A_{ij}), \quad n=3,4,5,\cdots, \tag{5.4}$$

where

$$b_n=[-n\kappa]^{n-3}/[n-3]! \tag{5.5}$$

$$A_{ij}=a_{ij}\exp(ka_{ij}), \tag{5.6}$$

$$\mathrm{E}_n(x)=\int_1^\infty \exp(-tx)t^{-n}dt. \tag{5.7}$$

This expansion is convergent only if $e\kappa A_{ij}<1$. Tables of the generalized exponential integral, $\mathrm{E}_n(x)$, have been prepared by Placzek.[9] Tables of a closely related function,

$$g_n(x)=x^3\mathrm{E}_{n-3}(nx)/4(n-1)! \tag{5.8}$$

have been given by Poirier.[10] The mathematical properties of $\mathrm{E}_n(x)$ are discussed by Placzek[9] and Erdeli et al.[11] For larger values of κa_{ij}, numerical integration of (5.3) is employed. Finally, for $\kappa a_{ij}\gg 1$ the power series expansion of $e^{q_{11}}$ may be used in the extension of tables of Q_{ij} to higher values of κa_{ij}.

Calculation of $\mathfrak{F}_{03}$

For the primitive model, we have $w_{ijk}=0$ and hence, $\delta 3_c=0$. The term, $\delta 3_f$, is similar in form to $\delta I^{(2)}$ and may be evaluated in a similar way. Referring to Eq. (4.24), we write

$$\delta 3_f=z_1^2z_3^2\lambda^2 \mid 2\kappa \mid^{-1}\delta Q_{ij}', \tag{5.9}$$

where

$$Q_{ij}'=\int_0^{a_{ij}} \exp(q_{11}-\kappa r)r^2dr. \tag{5.10}$$

This is simply related to the integral of Eq. (5.3):

$$Q_{ij}'=[4\pi/z_1^2\lambda][\partial Q_{ij}/\partial\kappa]_{\lambda,a_{ij}} \tag{5.11}$$

In Fig. 5 are given values of Q_{ij}' for $z_1^2\lambda=4\pi 7.1351$ A, the value for $z_1=1$ and water at 25°. These curves were constructed by numerical integration rather than by applying Eq. (5.11). Note that

$$\lim_{\kappa\to 0} Q_{ij}'=\lim_{\kappa\to 0} Q_{ij}$$

so the $\kappa=0$ curve is the same in both Fig. 4 and 5.

We have for the next term in Eq. (4.31),

$$B_s=-\tfrac{1}{2}\int \Phi_{12}'[\Phi_{13}-\Phi_{23}]^2d\{3\}. \tag{5.12}$$

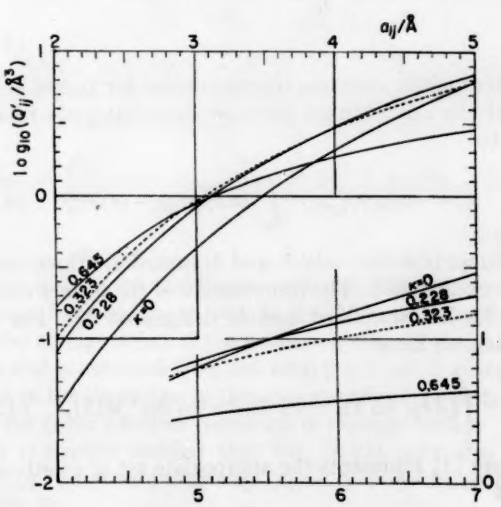

FIG. 5. The function Q_{ij}'. Curves of constant κ.

[9] G. Placzek, National Research Council of Canada, Division of Atomic Energy, Document No. MT-1 (NRC 1547), 1946.
[10] J. Poirier, J. Chem. Phys. **21**, 972 (1953).
[11] A. Erdelyi, W. Magnus, F. Oberhettinger, and F. Tricomi, *Higher Transcendental Functions* (McGraw-Hill Book Company, Inc., New York, 1953), Vol. 2, p. 134.

TABLE III. Properties of the system LiCl, CsCl, H_2O at 25°.[a]

I/molal	0.5	1	2	4	6
g_0/molal^{-1}			−0.198	−0.233	−0.251
b_0/molal^{-1} [b]			−0.001	−0.002	−0.002
e_0/molal^{-1} [c]			−0.012	−0.024	−0.036
$[g_0-b_0-e_0]$/molal^{-1}			−0.185	−0.207	−0.213
$[\kappa^3/\lambda I]\mathcal{E}_{02}$/molal^{-1}	−0.146	−0.162	−0.163	−0.158	
$[\kappa^3/\lambda I]\mathcal{E}_{03}$/molal^{-1} δ_3	0.014	0.010	0.005	−0.002	
$[\kappa^3/\lambda I]\mathcal{E}_{03}$/molal^{-1} B_s	−0.025	−0.028	−0.033	−0.041	
$[\kappa^3/\lambda I][\mathcal{E}_{02}+\mathcal{E}_{03}]$/molal^{-1}	−0.157	−0.181	−0.193	−0.199	

[a] The entries in this table are dimensionless.
[b] The volume data used here are from W. Geffken, Z. physik. Chem. **A155**, 1 (1931).
[c] The osmotic coefficients are from Robinson and Stokes, *Electrolyte Solutions* (Butterworths Scientific Publications, London, 1955).

This may be written out in bipolar coordinates[12] as

$$B_s=-8\pi^2\int_0^\infty[\Phi_{12}(x)-\Phi_{23}(x)]x\,dx \cdot\int_0^x[\Phi_{13}(y)-\Phi_{23}(y)]y\,dy\int_{x-y}^{x+y}\Phi_{12}'(z)z\,dz, \quad (5.13)$$

where we have made use of the symmetry of the integrand of B_s to combine the two integrals that one ordinarily obtains upon converting to bipolar coordinates.[12] In this equation, the length variable is specified for each cluster function. For the primitive model and $z_1=z_2$ we have

$$\Phi_{13}(x)-\Phi_{23}(x)=0, \quad 0<x<a_{13},$$
$$=\exp[q_{13}(x)], \quad a_{13}<x<a_{23}, \quad (5.14)$$
$$=0, \quad a_{23}<x,$$
$$\Phi_{12}'(z)=-1, \quad z<a_{12},$$
$$=\exp[q_{12}(z)]-1, \quad a_{12}<z, \quad (5.15)$$

and, for the case $a_{23}<a_{12}+a_{13}$; $a_{12}<2a_{13}$:

$$B_s=4\pi^2\int_{a_{13}}^{a_{23}}\exp[q_{13}(x)]x\,dx\int_{a_{13}}^{x}\exp[q_{13}(y)]y\,dy \cdot\left[\int_0^{a_{12}}z\,dz-\int_{a_{12}}^{x+y}\{1-\exp[-q_{12}(z)]\}z\,dz\right]. \quad (5.16)$$

For a rough calculation it is helpful to make the approximations

$$\exp[q_{13}(x)]=b_{13}/x^2, \qquad a_{13}<x<a_{23},$$
$$\exp[q_{12}(z)]-1=-b_{12}\exp(-\kappa z)/z, \quad a_{12}<z<a_{13}+a_{23}, \quad (5.18)$$

where the parameters, b_{13} and b_{12}, can be chosen to make the graphs of the approximate functions coincide as nearly as possible with those of the exact functions in the range of interest or to obtain upper or lower limits to B_s. In terms of these approximations, we find

$$B_s=4\pi^2b_{13}^2\{[a_{12}^2+2b_{12}\exp(-\kappa a_{12})/\kappa][\ln(a_{23}/a_{13})]^2 +2[a_{23}-a_{13}]^2-[a_{23}^2-a_{13}^2]\ln(a_{23}/a_{13}) -2b_{12}\kappa^{-1}[E_1(\kappa a_{23})-E_1(\kappa a_{13})]^2\} \quad (5.19)$$

where $E_1(x)$ is the exponential integral [Eq. (5.7)].

Equation (5.19) is the basis of the calculated values of B_s given in Table III. Similar results have been obtained by other approximate methods of evaluating B_s for the primitive model. A similar procedure, when applied to the calculation of B_{13} and B_{23} of Eq. (4.31) confirms the expectation that these are numerically small compared to B_s in the range of ionic strength, 0.5 to 4M.

Comparison with Free-Energy Data

Here it is often useful to use the approximation,

$$g_0=\mathcal{E}_{02}\kappa^2/\lambda I, \quad (5.20)$$

in place of the exact Eq. (2.16). A numerical comparison of the terms of Eq. (2.16) for the system LiCl, CsCl, H_2O, 25°, is given in Table III. This system has been chosen for the most detailed investigation because it exhibits the largest mixing effects.

The g_0 values for this system and for the other alkali chloride mixtures are derived from Robinson's[13] measurements of the water activity by the isopiestic method. From the composition and water activity of a solution we may calculate[5] G_w^{ex}. From G_w^{ex} for a mixture and the end solutions of the same ionic strength we may calculate $\Delta_m G_w^{ex}$. Proceeding in the usual way, we write

$$\Delta_m G_w^{ex}=RTI^2y[1-y][w_0+w_1Y+\cdots]$$

as the equation defining a set of w_p coefficients. The α coefficients used by Robinson to describe his results are related to w_0 by the equation,

$$w_0=2.303[\alpha_1+\alpha_2],$$

[12] T. Hill, *Statistical Mechanics* (McGraw-Hill Book Company, Inc., New York, 1956), p. 203.

[13] R. A. Robinson, J. Am. Chem. Soc. **74**, 6035 (1952). "Electrochemical Constants," Nat. Bureau Standards Circ. 524, 191 (1953); Trans. Faraday Soc. **49**, 1147 (1953). Robinson and Lim, *ibid.* **49**, 1144 (1953).

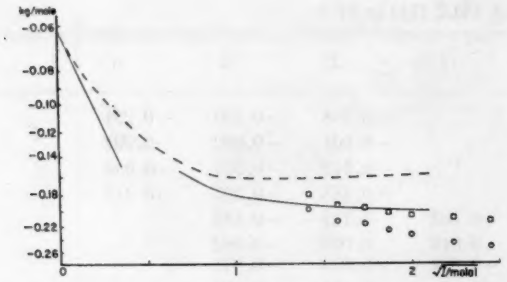

FIG. 6. The system LiCl—CsCl—H_2O at 25°. ○ g_0, experimental. □ $g_0-b_0-e_0$, experimental. ------ $[\kappa^2/\lambda I]\mathfrak{S}_{02}$. —·— $[\kappa^2/\lambda I][\mathfrak{S}_{02}+\mathfrak{S}_{03}]$. The scale of ordinates is logarithmic.

and w_0 is related to g_0 by the thermodynamic equations,

$$g_0=-I^{-1}\int_0^I w_0 dI \tag{5.21}$$

$$=-\sum_{n\geq 0}\{[-I]^n/[n+1]!\}(d^n w_0/dI^n), \tag{5.22}$$

where (5.22) is obtained from (5.21) by repeated integration by parts.

The g_0 values in Table III have been calculated from Robinson's corrected Harned coefficients using Eq. (6.9) of reference 5. This is equivalent to using (5.22), neglecting all $n>1$, and using a single average value of dw_0/dI over the whole experimental ionic strength range. These assumptions, which enter into Robinson's calculation of the Harned coefficients *defined* in terms of the activity coefficients of the solutes, seem reasonable when one considers the trends and uncertainties of the data but it is found that there is, in fact, a considerable range of g_0 values that may be calculated from the data using various sets of assumptions that are equally consistent with the data. This will be illustrated below, but for the present it is sufficient to emphasize the tentative nature of all of these g_0 values and the fact that *for the purposes of this paper*, the difference between g_0 values calculated in different ways is not important.

The estimation of b_0 is based on the approximation (reference 5, Table B-1)

$$B=-2\ln(V(m,0)/V(0,0)), \tag{5.23}$$

where $V(m, 0)$ is the volume of solution per kg of solvent for the solution of total molality, m, and pressure, P_0 (effectively zero or 1 atm) In the present notation (Sec. 2) this may be written

$$B(y,I_y)=-2\ln(V(y,I_y)/V(0,0)), \tag{5.24}$$

where both volumes apply at pressure P_0. Now we introduce the definitions of the v_p coefficient [cf. Eqs. (2.6) and (2.10)],

$$\Delta_m V(y,I_y)=V(y,I_y)-yV(1,I_y)-[1-y]V(0,I_y)$$
$$=y[1-y]I^2[v_0+v_1 Y+\cdots], \tag{5.25}$$

and combine Eqs. (2.12), (5.24), and (5.25) to obtain

$$\tfrac{1}{2}b_0=-Iv_0\bar{V}^{-1}-\tfrac{1}{2}[V(1,I_y)-V(0,I_y)]^2/\bar{V}^2 I+\cdots, \tag{5.26}$$

where $\bar{V}$ is the arithmetic mean of $V(1, I_y)$ and $V(0, I_y)$.

The experimental quantity, v_0, has not been determined for any system that is of interest here but we note that $|v_0|/\bar{V}$ is less than 10^{-4} for those few systems for which it has been investigated.[14] Therefore, although the term in v_0 has been neglected in arriving at the values of b_0 in Table III, it is unlikely that this is important for the present purpose.

The estimation of e_0 is based on Eq. (2.9). In this case, it is found by direct calculation that the next larger terms in e_0 contribute less than 11% of the total value of e_0.

Evidently, for this system, g_0 is similar in sign, magnitude, and concentration dependence to $g_0-b_0-e_0$. Table III also furnishes evidence that $\mathfrak{S}_0$ is approximately equal to $\mathfrak{S}_{02}$. Other systems that have been examined show similar behavior and this is the basis of our use of the approximation, Eq. (5.20), in the less detailed comparison of the theory with the data for other systems.

The remaining rows of Table III present values of the first two of the terms on the left of (2.16) [cf. Eq. (3.16)] as calculated on the basis of the primitive model with the following choices for the parameters, a_{ij}. In the case of interaction of two ions of the same sign, a_{ij} was chosen to be twice the sum of the crystal radii[15] of the ions. In the case of the interaction of oppositely charged ions, the a parameter of the modified Debye-Hückel theory[16(a)] was used for a_{ij}. This use of different ionic radii for the interaction of ions of the same sign than for interaction of ions of opposite sign is an extension of the primitive model, an aspect that is discussed in Sec. 7. It seems clear that the appropriate choice of a_{ij} for interaction of ions of opposite sign is determined by experiments with solutions of a single electrolyte. On the other hand, the present calculations are most sensitive to the choice of a_{ij} for the interaction of ions with the same sign, and as the following figures show, choosing a_{ij} equal to twice the sum of Pauling radii works surprisingly well for all of the alkali-metal ion pairs. This choice has been used in the remainder of this section, except where it it noted otherwise.

The comparison of theory and experiment for the LiCl–CsCl system is shown in more detail in Fig. 6. The results of the calculations at low I are included in this figure to illustrate two of the most novel features of

[14] T. F. Young and M. B. Smith, J. Phys. Chem. **58**, 716 (1954).
[15] L. Pauling, *The Nature of the Chemical Bond* (Cornell University Press, Ithaca, New York, 1945), p. 346.
[16] H. S. Harned and B. B. Owen, (a) *The Physical Chemistry of Electrolyte Solutions* (Reinhold Publishing Corporation, New York, 1958), 3rd ed., Table 12-5-2, second column ; (b) *ibid.*, Chap. 14.

the theory. These do not depend on the primitive model and they are noted here only to allow us the benefit of a definite example. The first of these features is the nonzero intercept of g_0 at $I=0$. This intercept depends on the short-range pairwise interactions, w_{ij}^*, of the hetero ions. The other feature is the approach of g_0 to its limiting value at $I=0$, as governed by the higher-order limiting law, Eq. (4.15). Of course, the Debye-Hückel limiting law does not appear here because g_0 is a parameter of the process in which mixing occurs at constant I. Note also that these calculations indicate that only for $I<0.01$ molal may g_0 be expected to conform reasonably closely to the higher order limiting law.

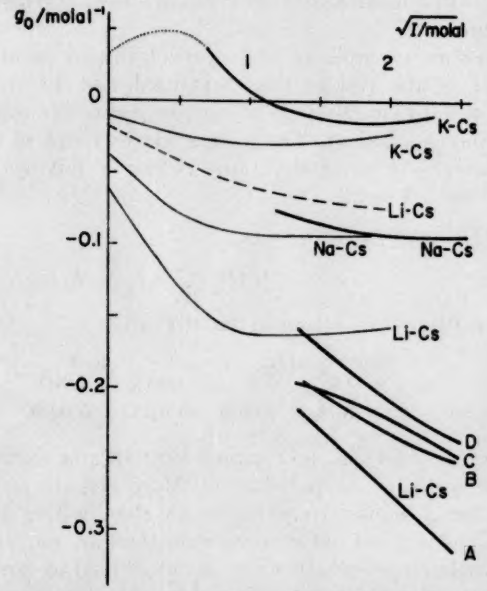

FIG. 7. Comparison of g_0 values calculated from the primitive model and from experiment for several mixtures of aqueous alkali-metal chloride solutions at 25°. — calculated. —— experimental. ····· a possible extrapolation to conform with the limiting law. ------ calculated on the assumption that the ionic radii are 1.5× the crystal radii. If 1× the crystal radii is used, the curve obtained is similar in shape to the 1.5× curve, but with about ½ the ordinate at each I. The four "experimental" curves for the LiCl—CsCl system illustrate the effect of calculating g_0 from the w_0 data by using different approximations in applying Eqs. (5.21) and (5.22):

A: $g_0=-w_0$ (used for the other systems here and in Fig. 8)

B: $g_0=-w_0+\frac{1}{2}\langle I dw_0/dI\rangle_M$

C: $g_0=(5/I)[-w_0+(I/2)(dw_0/dI)-(I^2/6)(d^2w_0/dI^2)]_{I=5}$
$-(1/I)\int_0^I w_0 dI$

D: $g_0=(2/I)[-\frac{3}{4}w_0]_{I=2}-(1/I)\int_2^I w_0 dI.$

Methods A and B have been discussed in the text. Method C corresponds to calculating g_0 by Eq. (5.22) at $I=5$ molal, where the data are most accurate, and then using (5.21) to get to other ionic strengths. Method D corresponds to taking the average of two extremes for the I dependence below $I=2$. One is $dw_0/dI=0$, which leads to $g_0=-w_0$ at $I=2$. The other is $w_0\propto I$, which gives $g_0=-\frac{1}{2}w_0$ at $I=2$. Then (5.21) is used to get to other ionic strengths.

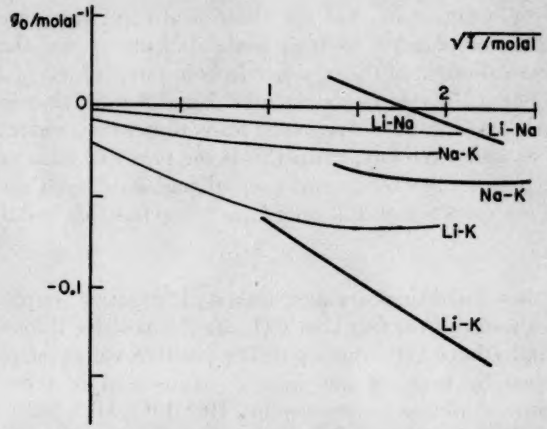

FIG. 8. Comparison of g_0 values calculated from the primitive model and from experiment for several mixtures of aqueous alkali-metal chloride solutions at 25°. — calculated. —— experimental.

The results calculated from the model agree with the experimental values within 20% and show a qualitatively similar concentration dependence. The agreement could doubtless be improved by adjustment of the various a_{ij} parameters, but it seems pointless to do so because of the uncertainty in the g_0 values and because of the shortcomings of the primitive model.

More evidence that the primitive model plus the Mayer theory gives at least a qualitative interpretation of the g_0 values is given in Figs. 7 and 8. Here, we see that the calculated g_0 values change in magnitude from system to system in the same way as the experimental values. It must be noted that the calculations on which these figures are based are much less complete than those underlying Fig. 6. In the first place, we are now comparing the left and right sides of (5.20) so that the terms $\mathfrak{G}_{02}$, b_0 and e_0 are neglected. In the second place, $\kappa^2/\lambda I$ is assumed to be the same at any I as at $I=0$, thus neglecting the dependence of V on composition and pressure. In fact, the variation of $\kappa^2/\lambda I$ is less than 15% for the systems of interest here. In the third place, we have made the approximation, $g_0(\text{expt})=-w_0$, thus neglecting all terms in (5.22) for $n>0$. The effect of this approximation is illustrated in Fig. 7, where we have plotted the results of calculating g_0 from w_0 by various methods. The differences certainly are not negligible compared to the uncertainty in w_0. On the other hand, the agreement with the calculated $[\kappa^2/\lambda I]\mathfrak{G}_0$ is not significantly different for the various g_0 curves. Moreover, the only adjustable parameter in the calculations, namely the factor of two multiplying the crystal radii of the ions, was selected on the basis of a comparison of the calculations with g_0 to the approximation $g_0=-w_0$. A slightly different factor would give better agreement for any higher approximation to g_0.

It is possible to avoid these difficulties in estimating g_0 from w_0 by calculating w_0 from the model. This has been done for the LiCl-CsCl system and the degree of agreement with experiment is about the same as for

the g_0 comparison, but the theoretical expressions are more complicated so it is more difficult to see the physical origin of the mixing effects in terms of w_0.

The calculated curves in Figs. 7 and 8 show that in each case the primitive model leads to negative values of $\mathfrak{g}_{02}$ and, therefore, when this is the principle term in g_0, to a net attractive effect on mixing. This result for $\mathfrak{g}_{02}$ is always obtained if each k_{ij} is a step function and if

$$a_{12}=\tfrac{1}{2}[a_{11}+a_{22}].$$

If these conditions are met, then $\mathfrak{g}_{02}$ is negative simply as a result of the fact that d^2Q_{ij}/da_{ij}^2 is positive if ions i and j have the same sign. The positive values of g_0 shown by some of the systems represented in these figures as well as by the systems, HCl–LiCl, HCl-NaCl, and HCl–KCl[16(b)], therefore demonstrate that if $\mathfrak{g}_{02}$ is the principal term, then such systems cannot be adequately represented by the primitive model, even for a qualitative purpose. It is not surprising, however, that the primitive model is less successful in representing the differences in interaction of sets of ions including hydrogen ion than sets of alkali metal ions alone, but it is also observed that when the alkali metal ions are most nearly the same size the differences in interaction are again not accounted for with significant accuracy by the primitive model. In this connection, it is interesting that the system HCl–CsCl behaves in a way that is qualitatively in accord with the primitive model: g_0 is negative.

In one respect, the general theory, Eq. (4.15), which does not depend on a model at all, also tends to be inconsistent with some of the data. This equation requires that g_0 (or w_0) have the same sign as dg_0/dI (or dw_0/dI) in the limit of $I=0$. As an example, the KCl-CsCl data are inconsistent with the theory unless the sign of the slope changes at low I as suggested by the dotted line.

One feature of the present theory is that g_0 is determined mainly by $\mathfrak{g}_{02}$ and is, therefore, nearly independent of the common ions, species 3. Unfortunately, the systems which are similar to those discussed above, except in the use of Br^- or I^- instead of Cl^-, have not been investigated except for the enthalpy determinations referred to in the next section. However, free energy data are available[17] for the systems, KOH, KCl, H_2O and NaOH, NaCl, H_2O at 25° and $I=1$ molal. The g_p parameters that we calculate from these[18] data are:

	NaOH, NaCl	KOH, KCl
g_0/molal^{-1}	−0.081	−0.105
g_1/molal^{-1}	0.003	0.017.

This discrepancy between the two g_0 values is clearly outside of the experimental error but this may be an unfavorable case for this comparison because $\mathfrak{g}_{03}$ may be more important compared to $\mathfrak{g}_{02}$ in this system than in alkali halide mixtures because of the unsymmetrical charge distribution in the ion, OH^-. Note that for these systems the hetero ions are OH^- and Cl^- and the common ion is Na^+ or K^+. The contributions to g_1 also seem to be unusually large in these systems, although not so large as might be expected on the basis of a casual inspection of the original Harned coefficients.[17] (For the system NaOH, NaCl at $I=0.5$ molal, $g_0=-0.088$ and $g_1=0.031$, so the comparison at $I=1$ molal may be misleading in suggesting that g_1 is much less important if Na^+ rather than K^+ is the common ion.) An examination of the integrals that contribute to $\mathfrak{g}_1$ leads us to suggest that the same factors that make $\mathfrak{g}_{03}$ so large compared to $\mathfrak{g}_{02}$ also makes $\mathfrak{g}_1$ large.

Another example of this sort of disagreement is found in the results that Scatchard and Prentiss[19] obtained by freezing point measurements on mixed electrolyte solutions. The g_0 function in terms of the coefficients of their equations is, for a mixture of electrolytes 1 and 2,

$$g_0=12I[D_{112}+D_{122}-D_{111}-D_{222}]+12\sqrt{2}I^{\frac{1}{2}}[E_{112}+E_{122}-E_{111}-E_{222}].$$

The g_0 values at $I=1$ molal and 0°C are:

	$LiNO_3$— KNO_3	LiCl KCl	LiCl— $LiNO_3$	KCl— KNO_3
g_0(0°C)	−0.1075	−0.0649	0.0218	0.0000.

Again, the effect of the common ion indicates that $\mathfrak{g}_{03}$ is not negligible compared to $\mathfrak{g}_{02}$. Moreover, the equation for g_0 is not consistent with the limiting law [Eq. (4.15)], but unfortunately the data are not suitable to determine whether g_0 does indeed tend to vanish as $I\rightarrow 0$.

Comparison with Enthalpy Data

The equations for testing the primitive model are easily developed and applied with the aid of the integrals already evaluated (Figs. 4 and 5). We define h_p coefficients, analogous to the g_p coefficients, as follows:

$$\Delta_m H^{ex}(y)=I^2y[1-y]RT\sum h_pY^p, \qquad p=0, 1, 2, \cdots, \tag{5.27}$$

where $\Delta_m H^{ex}=\Delta_m H$, the increase in enthalpy on mixing at constant pressure and ionic strength. Comparison with Eq. (2.10) shows that

$$h_p=-T[\partial g_p/\partial T]. \tag{5.28}$$

Substitution of Eq. (2.16) yields

$$h_0=T(\kappa^2/\lambda I)\{(\partial\mathfrak{g}_0/\partial T)-\mathfrak{g}_0[\partial \ln V(I,\pi)/\partial T]\}-(T/I)[(\partial b_0/\partial T)+(\partial e_0/\partial T)], \tag{5.29}$$

[17] H. S. Harned and M. A. Cook, J. Am. Chem. Soc. **59**, 1890 (1937).

[18] Calculated by using Eq. (6.9) of reference 5.

[19] G. Scatchard and S. S. Prentiss, J. Am. Chem. Soc. **56**, 2320 (1934).

which, to the order of approximation of Eq. (5.2), simplifies to

$$h_0=\frac{4\pi T\kappa^2}{\lambda I z_1^2[z_1-z_3]^2}\{\delta(Q_T)-\mathcal{E}_{02}(\partial \ln V(I,\pi)/\partial T)\}$$
$$-(T/I)[(\partial b_0/\partial T)+(\partial e_0/\partial T)], \quad (5.30)$$

where Q is the function defined in Eq. (5.3) and $Q_T=\partial Q/\partial T$. We have the general relation

$$Q_T=Q_\lambda \partial\lambda/\partial T+Q_\kappa \partial\kappa/\partial T+Q_a \partial a/\partial T, \quad (5.31)$$

where Q is regarded as a function of the three variables λ, κ, and a, and $Q_\kappa=(\partial Q/\partial\kappa)_{\lambda,a}$, etc. Note that Q_a is simply the integrand of Q [Eq. (5.3)] and that the primitive model implies $\partial a/\partial T=0$. We also have the identity,

$$3Q_{ij}=[\lambda Q_\lambda+\kappa Q_\kappa-a_{ij}Q_{a_{ij}}]4\pi/\lambda z_i z_j. \quad (5.32)$$

The preceding three equations are now combined to obtain

$$h_0=\frac{4\pi\kappa^2}{\lambda I z_1^2[z_1-z_3]^2}\{[3\delta Q+\tfrac{3}{2}\kappa\delta Q_\kappa-\delta(aQ_a)]$$
$$\cdot[-T\partial \ln(DT)/\partial T]-\tfrac{1}{2}\kappa\delta Q_\kappa T[\partial \ln V(I,\pi)/\partial T]\}$$
$$-(T/I)(\partial b_0/\partial T)+(\partial e_0/\partial T)]. \quad (5.33)$$

For water at 25° we have $-T\partial \ln(DT)/\partial T=0.371$ and $T\partial \ln(V(0,0)/\partial T)=0.060$, so as a rule, the first term in brackets is more important than the second. However, for the parameters that are used in this paper we find that in many cases

$$3\delta Q+\tfrac{3}{2}\kappa\delta Q_\kappa \simeq \delta(aQ_a)$$

and then, the calculation of h_0 depends on small differences among large quantities. Furthermore, if we neglect $\partial a_{ij}/\partial T$, we obtain the following values based on $2x$ Pauling crystal radii and $I=1$ molal:

Salt pair	LiCl, CsCl	NaCl, CsCl	LiCl, KCl
h_0/molal^{-1}, calc	0.001	−0.046	0.002
h_0/molal^{-1}, obs[20]	−0.320	−0.060	−0.107.

On the basis of this comparison, it seems most unlikely that one can fit the primitive model to the g_0 and h_0 data with a single set of a_{ij} parameters unless these parameters are allowed to be temperature dependent.

Finally, we note one respect in which the enthalpy data tend to support the present theory. If we assume that the term in $\partial\mathcal{E}_0/\partial T$ is the principal one in Eq. (5.29), and that the principal term in this derivative is $\partial\mathcal{E}_{02}/\partial T$, then we must conclude that h_0 is nearly independent of the common ion. Some measurements of Young, Wu, and Krawetz[20] show that h_0 is indeed nearly independent of the common ion when this is changed from Li^+ to Na^+ to K^+ for the pair of hetero ions, Cl^-, Br^-.

[20] T. F. Young, Y. C. Wu, and A. A. Krawetz, Discussions Faraday Soc. **24**, 37 (1957).

It is apparent that the calculation of h_0 from the theory is considerably more difficult than the calculation of g_0 to the same accuracy. The same is also true of v_0, which by the methods of the preceding section is found to be

$$v_0=\frac{4\pi\kappa^2}{\lambda I z_1^2[z_1-z_3]^2}\{[3\delta Q+\tfrac{3}{2}\kappa\delta Q_\kappa-\delta(aQ_a)](\partial \ln D/\partial P_0)$$
$$+[\tfrac{1}{2}\kappa\delta Q_\kappa+\delta Q][\partial \ln V(I,\pi)/\partial P_0]\}$$
$$-I^{-1}[\partial(d_0+e_0)/\partial P_0]. \quad (5.34)$$

For water at 25°, we have $\partial \ln D/\partial P_0=5.85\times10^{-5}$ atm^{-1} and $\partial \ln V/\partial P=-4.57\times10^{-5}$ atm^{-1}. Because of the cancellation noted above for the coefficient of the first of these derivatives, it is the term with $\partial \ln V/\partial P_0$ which is likely to be the more important in determining v_0. This gives values of v_0 of the order of 10^{-4} l mole^{-1} molal^{-1}, which is consistent with the few data that are available.

6. UNSYMMETRICAL MIXTURES

We start with Eq. (3.20) which cannot be simplified for unsymmetrical mixtures. However, we will consider only the particular case, $z_2=3$, $z_1=-z_3=1$. This corresponds to the systems HCl–$AlCl_3$ and HCl–$CeCl_3$, which have been investigated experimentally.[16] The systems HCl–$BaCl_2$ and HCl–$SrCl_2$ have also been investigated, but they do not exhibit any features that are qualitatively different from those of the 1,1–1,3 mixtures. It is unfortunate that there are no data for systems with an alkali metal chloride in place of HCl because at the present stage we must use the primitive model for comparison of theory and experiment and it seems likely that this is less satisfactory for solutions of H^+ than for any other simple ion. However, it is of interest to demonstrate that the theory correctly yields the feature, which qualitatively distinguishes the unsymmetrical mixtures from the symmetrical mixtures. This is the sign of the derivative, dg_0/dI. Compare Fig. 9 with Figs. 7 and 8.

On the basis of the primitive model, each of the pairwise cluster integrals in Eq. (3.18) may be represented as

$$I(ij)=4\pi\int_{a_{ij}}^{\infty}[\exp(q_{ij})-1-q_{ij}-q_{ij}^2/2]r^2dr. \quad (6.1)$$

We define the integral, J_{ij}, by the equation,

$$I(ij)=4\pi[-z_1z_j\lambda/4\pi]^3J_{ij}. \quad (6.2)$$

The series expansion,

$$J_{ij}=\sum_{n\geq0}\left[\frac{z_iz_j}{4\pi a_{ij}}\right]^n\frac{E_{n+1}(\kappa a_{ij}[n+3])}{[n+3]!},$$

where $E_n(x)$ is the generalized exponential integral [Eq. (5.7)], corresponds to the series evaluated by Poirier.[10] For some ranges of the variables, this series converges so slowly that it is more convenient to

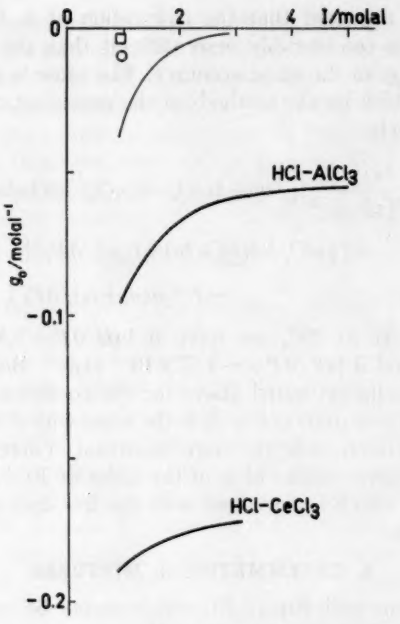

FIG. 9. Comparison of g_0 values calculated from the primitive model and from experiment for some unsymmetrical mixtures in water at 25°. —— experimental. —— calculated for all $a_{ij}=3$ A. ○ calculated for all $a_{ij}=4$ A. □ calculated for all $a_{ij}=5$ A.

evaluate the original integral by numerical integration.[21] Both methods have been employed in this application.

For our special case, Eq. (3.20) reduces to

$$-\mathfrak{G}_0=\pi[\lambda/4\pi]^3[J_{11}+20.25J_{22}-9J_{12}+4.5J_{23} -J_{13}+0.25J_{33}]. \quad (6.4)$$

This expression does not vanish for the case in which all of the a_{ij} are equal so we may expect that for unsymmetrical mixtures the first order contribution to $\Delta_m G^E$ comes from higher terms in the long-range electrostatic interactions (failure of the ionic strength principle) rather than from differences in the specific interaction of ions. Partly in order to illustrate this point, and partly because there is not much basis for assigning individual values to the a_{ij} for these systems, we only present numerical results for the case in which the a_{ij} are all the same (Fig. 9).

The magnitudes of the contributions of various sets to $\mathfrak{G}_0$ are illustrated for the case: all $a_{ij}=3$ A, $\kappa=0.323$ A^{-1}; by writing out the numerical values of the terms in Eq. (6.4) in the same order

$$-\mathfrak{G}_0=\pi[7.135]^3[9.74+93.61-68.87+87.26 -13.16+2.44]. \quad (6.5)$$

The prominence of the contributions of sets of like-charged ions is especially noteworthy. This may at first seem surprising but it must be recalled that in this approximation $\mathfrak{G}_0$ is determined by differences in long-range interactions rather than by differences in short-range specific interactions.

Evidently the theory does yield the negative values of dg_0/dI which distinguish unsymmetrical form symmetrical mixtures. The theory also requires that as $I\to 0$, g_0 goes to $-\infty$ as $\ln I$. There do not seem to be any data in dilute solution with which to compare this result.

7. DISCUSSION

Other Theories

The present theory is the first *molecular* theory of mixed electrolyte solutions and is therefore not really comparable with earlier theories which are part phenomenological and part empirical. However, one result of the present calculations is to show that a principal hypothesis of several of the earlier theories is less accurate than had formerly been supposed. This hypothesis is the Brønsted principle of specific ion interaction[22]: "In a dilute solution of constant total concentration, ions will be uniformly influenced by ions of their own sign."[23] This is a little vague, but it clearly requires that $\mathfrak{G}_{02}=0$ for symmetrical mixtures, and seems to imply $\mathfrak{G}_0=0$ and $g_0=0$ as well. This principle has been combined with the Debye-Hückel theory by Guggenheim[24] to provide a theory of dilute electrolyte mixtures. The comparison of the combined theory with experiment has been reviewed by Harned and Owen.[16(b)] The experiments at $I=0.1$ molal yield results in quantitative agreement with theory but there are numerous systems for which experiment shows that $g_0\neq 0$ at higher I. It remains to explain the low concentration data on the basis of the present theory, according to which g_0 does not approach zero as $I\to 0$.

This problem has not been completely investigated but a plausible interpretation is the following. The physical basis of the Brønsted principle is weakened at high ionic strength because of the shielding effect of the ionic atmosphere which appears as the $e^{-\kappa r}$ factor in the present theory. Therefore, it is not surprising that in some systems, such as LiCl–CsCl–H_2O, it is found that as I increases the sum of the Harned coefficients, $|\alpha_{12}+\alpha_{21}|$, becomes even larger than the difference of Harned coefficients, $|\alpha_{12}-\alpha_{21}|$. Recall that the former is a measure of g_0 while the latter is a measure of the difference in properties of the end solutions,[5] and therefore includes the difference in cation-anion interaction in the end solutions. On the other hand, at small I the shielding by the ion-atmosphere is less effective and just as this tends to reduce the magnitude of the integrals on clusters of two ions of the same sign (Figs. 6–8), it tends to increase the magnitude of the interaction of two ions of opposite

[21] E. Meeron, J. Chem. Phys. **27**, 1238 (1957).

[22] J. N. Brønsted, J. Am. Chem. Soc. **44**, 877 (1922).

[23] Brønsted's theory as first formulated included a salting-out interaction in addition to the specific ion interaction. The former has not been employed in the later theories referred to here.

[24] E. A. Guggenheim, Rept. of Scandinavian Sci. Congr. (Copenhagen, 1929), p. 298; Phil. Mag. **19**, 588 (1935).

sign. Thus, as I becomes smaller so does

$$|\alpha_{12}+\alpha_{21}|/|\alpha_{12}-\alpha_{21}|,$$

and the Brønsted principle becomes more accurate. On the basis of the present theory, one must say that it is only this sort of relative accuracy that is implied by the agreement of theory and experiment that is illustrated by Tables 14-7-1 and 14-7-2 of Harned and Owen.[16(b)]

A theory of the Harned coefficients has been proposed by Robinson and Stokes.[25] This theory is based on a correction to the Debye-Hückel theory for a scale-factor effect that is related to ionic hydration.[5] Their comparison of theory and experiment (their Table 15.1) shows rough agreement of calculated and experimental Harned coefficients, but if we form the sum, $\alpha_{12}+\alpha_{21}$, which is proportional to g_0,[5] we find no correlation between their calculated values and the observations. Therefore, their calculations are valid at most for $\alpha_{12}-\alpha_{21}$, a measure of the difference in properties of the end solutions.

In these earlier studies, there has been a failure to recognize that the free energy observations on electrolyte mixtures include large contributions from the difference in properties of the end solutions that may obscure the effects that are characteristic of the mixtures. If one is to learn anything from studying the mixtures that cannot be learned from purely thermodynamic calculations based only on the properties of the end solutions, then the thermodynamic data are best reduced to the extent of removing the contributions of the end solutions. When this is done it is $\Delta_m G^{ex}$ and its derivatives that remain.[5]

Primitive Model

From the point of view of the Mayer theory the characteristics of the primitive model are that it leads to a step function (Eq. (5.1) for k_{ij} and to vanishing higher components of the potentials of average force. But in addition, in order to know that the calculated thermodynamic properties are properties of a *physical* model, however idealized, we must regard the a_{ij} as made up of additive contributions from the radii of the ions. That is, only hard sphere ions can lead to the step function for k_{ij} and hard sphere ions have a_{ij} additive in the ion radii. Conversely, if a set of ionic radii can be found to fit all of the thermodynamic data for the simplest solutes, the alkali halides, then we may conclude that the equilibrium properties of these systems are indeed understandable in terms of the primitive model.

The a_{++} values used in this paper do form a set that is additive in the ionic radii. The a_{+-} values from the extended Debye-Hückel Theory, which are not very different from those required by the Mayer-Theory-plus-primitive-model,[26] form a set that is nearly additive in the ionic radii. The combined set of these a_{++} and a_{+-} values is clearly very far from additive in the ionic radii and it seems unlikely that one can find a combined set that is additive and is in even rough agreement with the data for both single and mixed electrolytes. The main difficulty is that the large g_0 values for the systems LiCl–CsCl, LiCl-KCl, and NaCl–CsCl require considerably larger differences in radii among the cations than are consistent with the a_{+-} values. (Note that the a_{++} values used in this paper correspond to an increase in radius from Li^+ to Cs^+, contrary to the trend of the a_{+-} values, but that the calculation of g_0 is only affected to a small degree if we assume instead that the radii increase from Cs^+ to Li^+. The reason for this is that δk for Eq. (4.7) is unchanged if we interchange the designations of the ions.)

It appears from these observations that the free energy data for alkali halide solutions would be reasonably consistent with a model which led to potentials of average force that are similar to those deduced from the primitive model in very respect save one. This would be that a_{++}, a_{+-}, and a_{--} would each be composed of additive contributions from a set of radii, but that the set of radii would be different in each of the three cases. It will be interesting to see what extent the solvent structure must be invoked to obtain this behavior. Note that the most sophisticated model yet investigates[27] provides only a small step in this direction.

ACKNOWLEDGMENTS

I wish to acknowledge the benefit of many discussions with Professor I. Prigogine concerning this research, and also the financial assistance of the John Simon Guggenheim Memorial Foundation.

[25] R. A. Robinson and R. H. Stokes, *Electrolyte Solutions* (Butterworths Scientific Publications, London, 1955).

[26] Unpublished work by Tsao described in reference 2.

[27] S. Levine and H. E. Wrigley, Discussions Faraday Soc. **24**, 43 (1957).

Structure of Glass Forming Halides. I. Liquid Beryllium Fluoride

J. D. MACKENZIE

General Electric Research Laboratory, Schenectady, New York

(Received November 5, 1959)

Viscosity and electric conductivity measurements have been made on liquid beryllium fluoride over the temperature range 700–950°C. The high specific resistance and viscosity and the magnitude of the corresponding energies of activation indicate that the classical random network structure for glasses is applicable. Liquid BeF_2, similar to liquid GeO_2 and SiO_2, is highly associated even at elevated temperatures. At a temperature 200° above the melting point, the energy of activation for viscous flow is greater than the heat of vaporization. The ease of glass formation is attributed to the network structure of the liquid.

INTRODUCTION

LIQUIDS having high viscosity and low electric conductivity at elevated temperatures are obtained from the fusion of certain oxides, for instance, boron trioxide,[1] germanium dioxide,[2] and silica.[3] These molten oxides constitute a special class of highly associated or "network" liquids which are easily undercooled to the glassy state. Conversely, the melts of most ionic halides are very fluid although wide variations of electric conductances may be encountered. The formation of halide glasses is uncommon, a well-known exception being that of beryllium fluoride which is easily rendered into the vitreous state. The possibility thus arises that the structure of a liquid halide may be similar to those of the highly associated liquid oxides. A network structure in the liquid, however, is not the only criterion for glass formation.[4] Direct structural information is needed before conclusions regarding the nature of the kinetic barrier to crystallization can be drawn. In the case of the network liquid oxides, transport studies have been particularly informative.[1,2] Viscous flow and electric conductivity measurements were therefore undertaken in the present study on liquid BeF_2.

EXPERIMENTAL

Beryllium fluoride (mp$\sim$540°C) was obtained from the Brush Beryllium Company with a quoted purity of at least 99% BeF_2. The maximum amounts of impurities present were: H_2O, 0.5; Al, 0.02; Fe and Mg, 0.01; Cr and Ni, 0.002; and Mn, 0.001%. The charge was contained in a Pt-20% Rh crucible and placed inside the apparatus overnight in a stream of dry N_2 (2 ppm H_2O). The apparatus was then evacuated to a pressure of about 10 mm Hg and the temperature was raised slowly to 200°C to remove the water present. When the temperature was increased to 700°C, dry N_2 was admitted. The melt was kept at 900°C for 1 hr before the commencement of measurements.

Viscosity was measured by the counterbalance technique employing a Pt–20% Rh bob. For electric conductivity measurements, the central suspension was adopted as one electrode and the crucible the other. The calibrations and other practical details of the apparatus are described elsewhere.[2,5] On account of the toxicity of BeF_2 the suction line of a specially designed vacuum cleaner was placed over the opening of the furnace. The former was in operation over the entire duration of the experiment except at intervals when viscosity measurements were being made.

At the conclusion of the experiment, less than 0.005% of N and Pt was found in the glassy BeF_2. The maximum over-all error in the viscosity results, arising mainly from the evaluation of the mean slope of the load-velocity plots and from uncertainty attached to the expansion of the apparatus, is estimated to be $\pm 8\%$. The similar estimate for the conductance data is $\pm 10\%$. The temperature gradient along the crucible was less than 2° and measurements by means of a calibrated Pt–10% Rh thermocouple were accurate to $\pm 1°$.

RESULTS

Measurements were made at alternate descending and ascending temperatures, over a range sufficiently wide to permit the evaluation of the activation energies for electric conduction and viscous flow. The lower temperature limit of 700°C was set by the high viscosity of the melt and the upper limit of about 950°C by the vapor pressure of BeF_2. The results for liquid BeF_2 over the temperature range 700–950°C, taken at 50° intervals from the smooth viscosity and conductivity against temperature curves, are presented in Table I. The approximate values at the melting temperature of 540°C,[6] obtained by extrapolation, are also included. No previous data have been reported to permit comparison.

The relationship between log viscosity and the reciprocal of the absolute temperature is illustrated in Fig. 1. The empirical equation,

$$\eta = A_\eta \exp(E_\eta/RT) \qquad (1)$$

[1] J. D. Mackenzie, Trans. Faraday Soc. **52**, 1564 (1956).
[2] J. D. Mackenzie, J. Chem. Phys. **29**, 605 (1958).
[3] J. O'M. Bockris, J. D. Mackenzie, and J. A. Kitchener, Trans. Faraday Soc. **51**, 1734 (1955).
[4] D. Turnbull and M. H. Cohen, J. Chem. Phys. **29**, 1049 (1958).
[5] J. D. Mackenzie, Rev. Sci. Instr. **27**, 297 (1956).
[6] D. M. Roy, R. Roy, and E. F. Osborn, J. Am. Ceram. Soc. **33**, 85 (1950).

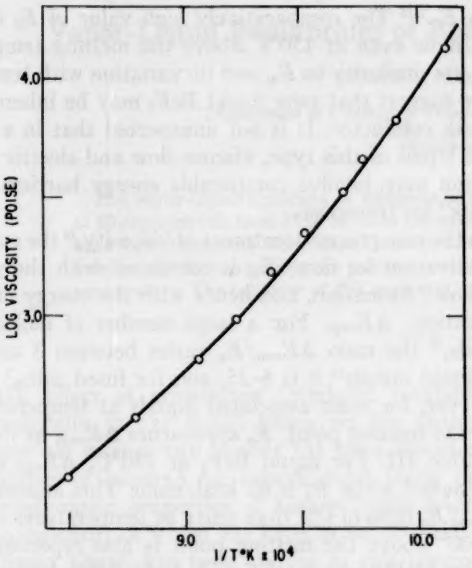

FIG. 1. Relation between log viscosity and $1/T$ for liquid BeF_2 at 700–900°C.

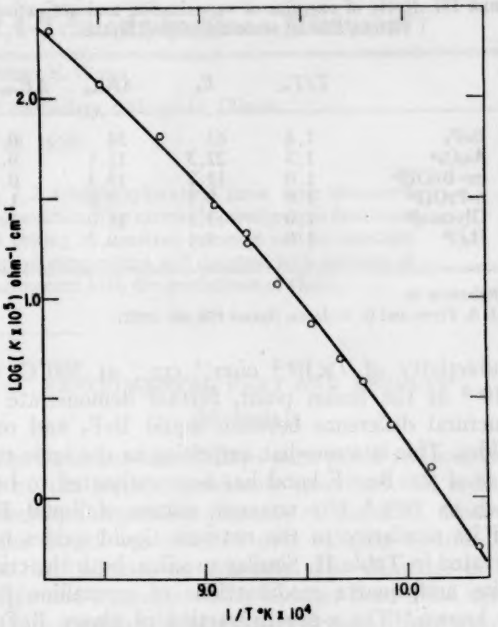

FIG. 2. Relation between log specific conductivity and $1/T$ for liquid BeF_2 at 700–950°C.

is not obeyed. The activation energies for viscous flow, E_η, decrease from 70 kcal/mole at 700°C to 38 kcal/mole at 920°C. The nonlinear relationship between log specific conductivity and $1/T$ is shown in Fig. 2. The activation energies for conduction, E_k, are 70 and 40 kcal/mole at 700 and 900°C, respectively. Over the range 2000–10 000 cps, conductance is independent of the frequency.

In the measurement of density by the Archimedean method, correction due to the effect of surface tension on the suspension wire may be eliminated by the use of two different bobs and a similar wire. The present results were based on measurements with the large bob alone. An attempt to obtain data with the small bob was unsuccessful on account of a suspension failure. In the absence of surface tension data, therefore, only approximate density results were obtained. By assuming the surface tension of liquid BeF_2 to be 200 dyne/cm, the corrected density at 800°C is 1.947 ± 0.010 g/cm³.

TABLE I. Electric conductivity and viscosity of liquid beryllium fluoride.

Temp (°C)	Sp conductivity (ohm^{-1} cm^{-1}) $\times 10^5$	Viscosity (poise) $\times 10^{-3}$
540 (mp)	$<10^{-3}$	$>10^4$
700	0.71	269
750	3.89	44.2
800	15.3	12.1
850	44.7	4.79
900	112	2.22
950	236	1.32

DISCUSSION

At 700°C, the viscosity of liquid BeF_2 is 2.7×10^4 poise and E_η is about 70 kcal/mole. The corresponding values extrapolated to the melting temperature are at least 10^6 poise and 100 kcal/mole, respectively. For most metallic halide melts at temperatures not far above the melting point, viscosity is in the order of 10^{-2} poise and E_η seldom exceeds 10 kcal/mole.[7] The low specific

TABLE II. Transport parameters of liquid BeF_2, typical halides, and network oxides.

	BeF_2	GeO_2[a]	B_2O_3[b]	$LiCl$[c,d]	$CdBr_2$[e,f]
T_m (°C)	540	1115	450	613	567
η (poise)	$>10^6$	10^7	10^5	0.02	0.03
E_η (kcal/mole)	>100	180	40	8.8	4.5
k (ohm^{-1} cm^{-1})	10^{-6}	$<10^{-6}$	$<10^{-6}$	5.6	1.0
E_k (kcal/mole)	>80	...	...	2.0	2.8
T_m+200°C					
η	10^3	10^5	10^3	0.01[g]	0.02[g]
E_η	60	160	30	8.8	4.5
k	10^{-5}	10^{-4}	10^{-6}	6.5[g]	1.5[g]
E_k	60	...	...	2.1	2.8

[a] Reference 2.
[b] Reference 11.
[c] Viscosity from C. E. Fawsitt, J. Chem. Soc. **93**, 1299 (1908).
[d] Conductance from E. R. Van Artsdalen and I. S. Yaffe, J. Phys. Chem. **59**, 118 (1955).
[e] Viscosity from H. Bloom, B. S. Harrap, and E. Heymann, Proc. Roy. Soc. (London) **A194**, 237 (1948).
[f] Conductance from H. Bloom and E. Heymann, Proc. Roy. Soc. (London) **A194**, 392 (1948).
[g] Extrapolated values,

[7] B. S. Harrap and E. Heymann, Chem. Revs. **48**, 45 (1951).

TABLE III. Ratio of energies of vaporization and activation for viscous flow of some associated liquids.

	T/T_m	E_η	ΔE_{vap}	$\Delta E_{vap}/E_\eta$
BeF_2	1.4	65	54	0.8
As_2O_3[a]	1.3	22.3	11.1	0.5
iso-BuOH[b]	1.0	11.2	10.3	0.9
n-PrOH[b]	1.0	9.7	9.8	1.0
Glycerol[b]	1.0	12.7	18.0	1.4
H_2O[b]	1.0	5.1	9.7	1.9

[a] Reference 14.
[b] J. A. Pryde and G. O. Jones, Nature **170**, 685 (1952).

conductivity of 7×10^{-5} ohm^{-1} cm^{-1} at 700°C, and $\sim10^{-8}$ at the fusion point, further demonstrate the structural difference between liquid BeF_2 and other halides. This is somewhat surprising as the ionic character of the Be—F bond has been estimated to be as much as 79%.[8] The nonionic nature of liquid BeF_2 and its similarity to the network liquid oxides is illustrated in Table II. Similar to silica, both the cristobalite and quartz modifications of crystalline BeF_2 are known.[9] The x-ray diffraction of glassy BeF_2 at room temperature has been studied by Warren and Hill.[10] Satisfactory agreement is obtained between the calculated and experimental scattering curves on the assumption of a random network structure in which each beryllium ion is tetrahedrally surrounded by four fluorines, and each fluorine is in turn bonded to two berylliums. This three-dimensional network is analogous to those present in vitreous SiO_2 and GeO_2. The present work is in agreement with the x-ray interpretations. Even at elevated temperatures, extensive association is still present in liquid BeF_2. The decrease of E_η from 70 kcal/mole at 700°C to 38 kcal/mole at 900°C, however, indicates that the degree of association decreases with increasing temperature.

The observed specific conductivity, as expected from the network structure of liquid BeF_2, is many orders of magnitude smaller than that for most ionic halide melts. It is not possible to conclude unequivocally if this is entirely due to small amounts of impurities present. In the network liquid oxides, however, when the observed conductance is due to commonly encountered impurities such as water or metal ions, E_k is independent of temperature and considerably smaller than E_η.[2,11] The comparatively high value of E_k of 70 kcal/mole even at 150°C above the melting temperature, its similarity to E_η, and its variation with temperature suggest that pure liquid BeF_2 may be inherently a weak conductor. It is not unexpected that in a network liquid of this type, viscous flow and electric conduction may involve comparable energy barriers and "units" for transport.

In the rate process treatment of viscosity,[12] the energy of activation for flow, E_η, is correlated with the work of "hole" formation, and hence with the energy of vaporization, ΔE_{vap}. For a large number of molecular liquids,[12] the ratio $\Delta E_{vap}/E_\eta$ varies between 3 and 4, for liquid metals[12] it is 8–25, and for fused salts,[7] 4–5. However, for some associated liquids at temperatures near the freezing point, E_η approaches ΔE_{vap}, as shown in Table III. For liquid BeF_2 at 750°C, ΔE_{vap} is 54 kcal/mole[13] while E_η is 65 kcal/mole. This anomalous $\Delta E_{vap}/E_\eta$ ratio of less than unity at temperatures some 50–100° above the melting point is also reported for another highly associated liquid, As_2O_3.[14] It is indicative that viscous flow in such network liquids can no longer be correlated simply with the mechanism of "hole" formation. Rather, a complex cooperative mechanism involving "entities" different from the vaporizing unit is more plausible.

For a pure liquid free of nucleating singularities, Turnbull and Cohen[4] have shown that crystallization will not take place if the kinetic barrier to nucleation, $\Delta G'$, exceeds 30 RT_m. The latter is 48 kcal/mole for liquid BeF_2. In a network liquid, interatomic bondings must be ruptured for flow to occur and the free energy of activation, ΔG_η^*, should be the same order of magnitude as $\Delta G'$. From the present viscosity data, ΔG_η^* is estimated to be 50 kcal/mole, and, hence, $\Delta G' > 30RT_m$. The ease of glass formation in beryllium fluoride is thus easily explained.

ACKNOWLEDGMENTS

The author is grateful to J. E. Burke for his interest and encouragement, to N. C. Cook for the beryllium fluoride, and to E. A. Aitken for his advice on safety precautions.

[8] L. Pauling, *The Nature of the Chemical Bond* (Cornell University Press, Ithaca, New York, 1945), p. 74.
[9] Roy, Roy, and Osborn, J. Am. Ceram. Soc. **36**, 185 (1953).
[10] B. E. Warren and C. F. Hill, Z. Krist. **89**, 481 (1934).
[11] J. D. Mackenzie, J. Phys. Chem. **63**, 1875 (1959).
[12] S. Glasstone, K. J. Laidler, and H. Eyring, *Theory of Rate Processes* (McGraw-Hill Book Company, Inc., New York, 1941), Chap. 9.
[13] K. A. Sense, M. J. Snyder, and J. W. Clegg, J. Phys. Chem. **58**, 223 (1954).
[14] I. Karutz and I. N. Stranski, Z. anorg. u. allgem. Chem. **292**, 330 (1957).

Vapor-Liquid Equilibrium of Benzene-2,2,4-Trimethylpentane Mixtures*†

STANLEY WEISSMAN AND SCOTT E. WOOD

Department of Chemistry, Illinois Institute of Technology, Chicago 16, Illinois

(Received September 22, 1959)

The vapor-liquid equilibria of solutions of benzene and 2,2,4-trimethylpentane have been measured at 10 deg intervals from 35 to 75° over the entire range of composition. The excess thermodynamic functions have been calculated from these data for the processes of mixing at constant pressure and at constant volume. All these functions are positive over the whole range of composition and decrease with increase of temperature. The behavior of this system is in qualitative agreement with the predictions of theory.

THE effect of orientation (hindered rotation) of molecules in the liquid phase on the change of entropy on mixing two liquids has been discussed in a number of papers.[1] An experimental study of the thermodynamic properties of binary liquid solutions, one component of which has little or no orientation in the liquid phase, has been started in this laboratory. Isooctane (2,2,4-trimethylpentane) has been chosen as this one component. This choice is a compromise between liquids which have spherically symmetric potential fields and those which have vapor pressures of suitable magnitudes in a convenient temperature range. It may be justified in terms of the difference of the heat capacity at constant volume of the pure liquid and that of the substance in the ideal gas state. Several workers[2] have suggested that this difference is a measure of the intermolecular orientation in the pure liquid. The value of this difference at 25° is 4.9 cal per mole deg for benzene and 1.0 cal per mole deg for isooctane.[3]

The volume of mixing of the benzene-isooctane system has already been reported.[1] This paper reports the vapor-liquid equilibria of the same system at ten degree intervals from 35 to 75° over the entire range of composition. The excess change of the thermodynamic functions over that of an ideal solution have been calculated from these data for the processes of mixing at constant pressure and constant volume. All these quantities are positive over the whole range of composition and decrease with an increase of temperature.

EXPERIMENTAL PART AND RESULTS[4]

Materials

The isooctane was Phillips pure grade and was purified by the method previously described.[1] In order to determine the possible presence of moisture, a portion of the liquid was refluxed over calcium hydride and then distilled into an ampoule. The densities of this sample and a sample which had not been dried agreed within experimental error, and it was therefore concluded that little or no moisture was present or that its effect was negligible. The density of the material used in the vapor pressure measurements was 0.68774 g cm^{-3}. This value is identical to that obtained by Wood and Sandus and is comparable to 0.68775 reported by Kretschmer *et al.*,[5] 0.68776 given by Brooks *et al.*[6] and 0.68779 given in the Selected Values of Properties of Hydrocarbons.[7]

Baker and Adamson, thiophene-free, A. C. S. grade, benzene was used. It was also purified by the methods previously described.[1] A portion of the purified product was dried over calcium hydride. Again, the densities of the dried and nondried samples agreed within experimental error. Consequently, the material used in the vapor pressure measurements was not treated with the hydride. The density of the product at 25° was 0.87365 g cm^{-3} in comparison to 0.87366 given in the Selected Values of Properties of Hydrocarbons.[7]

The water used to calibrate the pycnometers was obtained by distilling the tap water in a small Barnstead still. The distilled water was boiled prior to use to eliminate air and carbon dioxide.

Apparatus

A double-boiler still similar to those of Scatchard and co-workers was used.[8] Figure 1 gives a diagram of the

* Taken in part from a thesis by Stanley Weissman presented to the Graduate School, Illinois Institute of Technology, in partial fulfillment of the requirements for the degree of Doctor of Philosophy.

† Presented in part before the Division of Physical Chemistry of the American Chemical Society at its 136th meeting at Boston, Massachusetts (April, 1959).

[1] References to a number of such papers are given in S. E. Wood and O. Sandus, J. Phys. Chem. **60**, 801 (1956).

[2] J. A. Pople, Discussions Faraday Soc. **15**, 35 (1953); L. A. Staveley, K. R. Hart, and W. I. Tupman, Discussions Faraday Soc. **15**, 130 (1953); J. Frenkel, *Kinetic Theory of Liquids* (Oxford University Press, New York, 1947).

[3] S. E. Wood, O. Sandus, and S. Weissman, J. Am. Chem. Soc. **79**, 1777 (1957).

[4] A complete description of the apparatus and the experimental procedure is given in the thesis, written by Stanley Weissman, which is on file in the library of Illinois Institute of Technology.

[5] C. B. Kretschmer, J. Nowakowska, and R. J. Wiebe, J. Am. Chem. Soc. **70**, 1785 (1948).

[6] D. B. Brooks, F. L. Howard, and H. C. Crafton, J. Research Natl. Bur. Standards **24**, 33 (1940).

[7] "Selected values of properties of hydrocarbons," Natl. Bur. Standards Circ. No. C641 (Washington, D. C., 1947).

[8] G. Scatchard, C. L. Raymond, and H. H. Gilman, J. Am. Chem. Soc. **60**, 1275 (1938); G. Scatchard, G. M. Kavanaugh, and L. B. Ticknor, *ibid.* **74**, 3715 (1952).

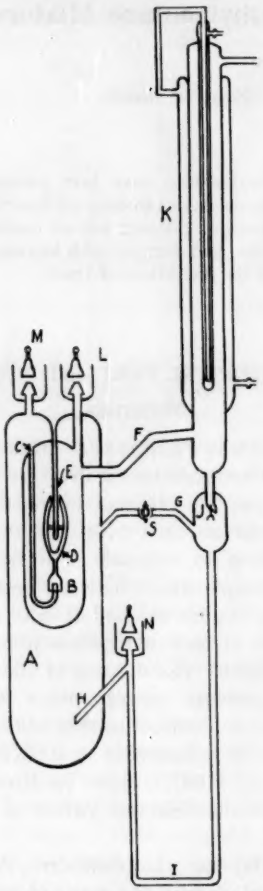

FIG. 1. Equilibrium still.

still. Liquid was placed in both the outer and inner boiler A and B. Electrical heaters were placed on the bottom of the still, on the tube F to prevent partial condensation of the vapor, and on the left-hand side of the trap I to bring the temperature of the condensate almost to its boiling point. Stopcock S was inserted so that large quantities of gas could be added to the still at the end of an experiment. It was not lubricated and leakage was prevented by packing it externally with Apiezon Q sealing compound. The operation of the still is apparent.

The pressure within the system was measured indirectly in terms of the known vapor pressure of pure isooctane. This was done by measuring the boiling point of a sample of pure isooctane under the pressure in the system. A still, identical to the solution still, was used for this purpose.

The two stills were connected through liquid nitrogen traps to a vacuum system and the auxiliary apparatus. This apparatus consisted essentially of a 100-liter steel tank used as a manostat and two one liter bulbs. The tank was thermostated to $\pm 0.01°$. The two bulbs were used in the adjustment of the pressure within the system until the temperature of the mixture of vapor and liquid on the thermocouple well of the solution still was that desired. Helium was used as the confining gas.

Two-junction copper-constantan thermels were used to measure the temperature in the equilibrium stills. These thermels were calibrated against two Leeds and Northrup resistance thermometers. The resistance thermometers were calibrated in turn at the triple point of water and the melting point of a sample of benzoic acid. The triple point apparatus was constructed and used according to the recommendations of the National Bureau of Standards.[9] The melting point standard was purchased from the National Bureau of Standards and certified by them. The δ constant of the Callendar equation was taken to be that given in the original certification of the thermometers. The reference junctions of the two thermals were kept at the triple point of water during an experiment. This triple point cell was a smaller version of that recommended by the National Bureau of Standards. Its temperature was constant during a given run to $\pm 0.004°$. The calibration of the thermels was reproducible to $\pm 0.005°$. It is believed that the measured temperatures are accurate to within $\pm 0.01°$.

In testing the operation of the stills it was found that, for the Cottrell pump to function properly, the boiling rate could be varied only within rather narrow limits. This rate was sufficient to replace the contents of the trap in approximately 5 min. Moreover, in varying the rate of boiling within these limits it was found that the temperature of the still did not change when the quantity of helium gas within the system was kept constant. This indicated that the pressure drop between the inner boiler and the condenser was either negligible or constant.

In further testing the operation of the stills, benzene was placed in both stills and the boiling temperatures were determined in each still for a given pressure. The thermels were then interchanged and the boiling temperatures redetermined. In each case, the temperatures of the two thermels agreed with each other within $\pm 0.01°$. Moreover, the temperature of each thermel in either still was the same within $\pm 0.01°$. These results indicated that the calibrations of the thermels were consistent with each other and further, that corrections

TABLE I. Vapor pressures of pure benzene and isooctane in mm of Hg.

t	Benzene	Isooctane
35	148.28	78.24
45	223.50	119.80
55	327.05	178.08
65	466.10	256.87
75	648.17	361.89

[9] H. F. Stimson, *Temperature, Its Measurement and Control in Science and Industry* (Reinhold Publishing Corporation, New York, 1955), Vol. 2, p. 141.

TABLE II. Vapor-liquid equilibria.

x_1	y_1	Deviation in y_1	P mm Hg	Deviation in P	$\Delta\bar{G}_2^E$ cal/mole	Deviation in $\Delta\bar{G}_2^E$
			35.00°C			
0.0886	0.2137	+0.0037	91.20	+0.27	23.9	+0.2
0.1601	0.3382	+0.0041	100.62	+0.38	41.1	+0.4
0.3343	0.5463	+0.0005	120.23	−0.04	74.9	−0.4
(0.4343)	(0.6242)	(+0.0030)	127.84	(+0.93)	(83.9)	(+2.8)
0.5061	0.6731	+0.0022	133.58	+0.32	91.4	+0.4
0.8375	0.8640	−0.0011	148.18	−0.05	60.4	0.0
0.9884	0.9865	+0.0002	148.62	+0.05	5.7	−0.2
			45.00°C			
0.0793	0.1894	−0.0004	136.44	+0.05	20.1	−0.1
0.1836	0.3643	+0.0004	156.19	−0.18	42.6	+0.6
0.3358	0.5364	+0.0024	179.71	+0.15	70.4	−0.7
0.3574	0.5558	+0.0026	182.66	+0.14	73.4	−0.9
0.5125	0.6738	+0.0016	200.62	+0.18	86.6	−0.2
0.5512	0.6998	+0.0001	204.21	+0.25	86.9	+0.7
0.8425	0.8691	−0.0008	222.71	−0.17	57.0	−0.5
0.9880	0.9865	+0.0003	223.89	−0.09	5.7	−0.1
			55.00°C			
0.0819	0.1869	−0.0008	201.74	−0.30	19.9	−0.7
0.2192	0.4065	−0.0048	236.86	−0.06	46.3	+0.7
0.3584	0.5509	+0.0001	266.04	−0.20	68.8	−0.5
0.3831	0.5748	−0.0020	270.73	−0.24	70.8	+0.4
0.5256	0.6786	+0.0012	293.36	+0.26	82.0	0.0
(0.5924)	(0.7293)	(−0.0072)	(302.07)	(+0.32)	(79.1)	(+3.8)
0.8478	0.8741	−0.0050	324.66	+0.03	52.5	0.0
0.9872	0.9863	+0.0001	327.39	+0.01	5.6	0.0
			65.00°C			
0.2230	0.4033	+0.0033	338.62	+0.28	44.6	+0.4
0.3981	0.5799	−0.0015	387.86	−0.58	69.2	−0.3
0.5460	0.6882	+0.0008	419.95	+0.05	78.6	−0.3
0.6060	0.7387	−0.0110	430.65	+0.20	73.4	+5.1
0.8548	0.8806	−0.0011	461.65	+0.09	48.1	+0.1
			75.00°C			
0.0879	0.1870	−0.0022	407.61	−0.52	18.6	+0.2
0.3862	0.5636	−0.0028	533.66	−0.33	64.9	−0.1
0.5558	0.6923	−0.0011	584.27	−0.34	74.8	+0.1
(0.6673)	(0.7670)	(−0.0042)	(610.11)	(−0.18)	(71.0)	(+1.9)
0.8590	0.8857	−0.0018	640.86	−0.32	44.8	+0.1
0.9875	0.9872	+0.0002	648.69	−0.37	5.4	−0.3

for the differences in the static heads in the two stills and the condensers and for the difference in the pressure drops between the stills and the condensers were negligible.

When a solution was used in the equilibrium still, it was possible to hold the temperature within the still to within ±0.02° for 2 hr and to within ±0.01° for 10 to 25 min. In this time, the contents of the trap would have been completely replaced many times. It is believed, therefore, that the steady state obtained in the still closely approximates the equilibrium state. Tests of the thermodynamic consistency of the data are discussed in a later section.

In the actual operation of the stills, the pressure within the system was adjusted by the addition and removal of helium until the desired temperature of the equilibrium still was obtained. When this temperature was maintained for at least 10 min (a longer time was used if possible) within ±0.01°, the temperature within the still containing the pure isooctane was determined, the heaters were shut off and helium added to the system as rapidly as possible. Samples of the liquid in the inner boiler and the trap were then taken. The composition of these samples was determined by density measurements by using the method and data of Wood and Sandus.[1]

Vapor Pressure of the Pure Components

The vapor pressure of pure isooctane was calculated by use of the Antoine equation.[7] The vapor pressures of the pure benzene were determined at the five desired temperatures by placing benzene in one still and iso-

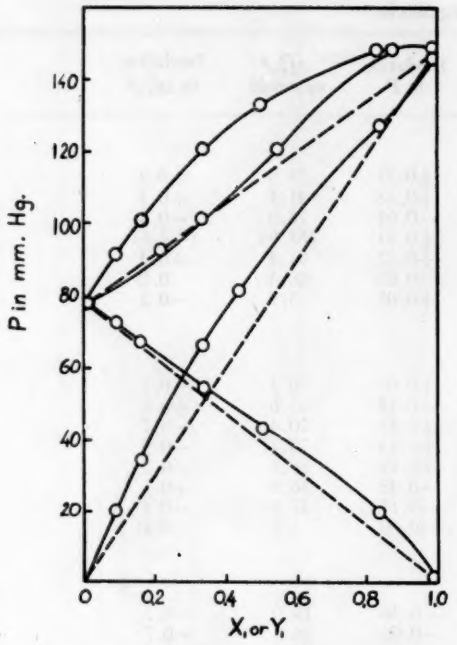

FIG. 2. Vapor pressure and partial pressures vs mole fraction of benzene.

octane in the other. The vapor pressures of benzene at these temperatures were then calculated from the measured temperatures in the still containing the isooctane by use of the Antoine equation. The values thus determined agree within ±0.08 mm with those given by Brown and Ewald,[10] Everett and Penny,[11] Scatchard *et al.*,[12] and the "Selected values of properties of hydrocarbons and related compounds."[7] The values in mm of Hg of the vapor pressures of the pure components which were used in the thermodynamic calculations are given in Table I.

Vapor-Liquid Equilibria

The experimental data for the vapor-liquid equilibria at the five temperatures are given in Table II. The first column gives the mole fraction of benzene[13] in the liquid phase, the second column the mole fraction of benzene in the vapor phase, and the fourth column the total pressure. The other columns will be described in a later section of this paper. The entries in parentheses in this table are quantities which were not used in the determination of the thermodynamic functions nor in the smoothing process because the deviations of these quantities from the smoothed values appeared to be quite large.

[10] I. Brown and A. H. Ewald, Australian J. Sci. Research **A4**, 198 (1951).
[11] D. H. Everett and M. F. Penny, Proc. Roy. Soc. (London) **A212**, 169 (1952).
[12] G. Scatchard, S. E. Wood, and J. M. Mochel, J. Am. Chem. Soc. **61**, 3206 (1939).
[13] The subscript 1 is used to designate benzene and the subscript 2 to designate isooctane.

The results at 35° are illustrated in Fig. 2. In this figure, the solid lines represent values which have been obtained by the smoothing process described in the next section. The circles represent the experimental data. The curves give the smoothed total pressure as a function of the mole fraction of the liquid and of the vapor and the smoothed partial pressures as a function of the mole fraction of the liquid. The dotted lines illustrate the Raoult's law lines. It is evident that this system exhibits rather large positive deviations from the ideal solutions laws. An azeotrope obviously exists but the composition of the azeotrope and the maximum pressure was not determined or calculated. Horsley[14] has reported an azeotrope for this system at 1 atm pressure and 80° at a mole fraction of benzene of 0.981.

THERMODYNAMIC FUNCTIONS

The change of the thermodynamic functions for mixing at constant pressure have been calculated for the change of state in which x_1 moles of benzene at 1 atm pressure and the chosen temperature T and x_2 moles of isooctane at the same conditions are mixed to form one mole of solution under the identical conditions. The excess chemical potentials defined by the relation

$$\Delta\mu_1^E=\mu_1-\mu_1^0-RT\ln x_1 \qquad (1)$$

were first calculated with the use of the equation,

$$\Delta\mu_1^E=RT\ln(Py_1/P_1^0x_1)+(\beta_{11}-\bar{V}_1^0)(P-P_1^0)+(\delta(1-y_1)^2P+(\bar{V}_1-\bar{V}_1^0)(1-P). \qquad (2)$$

The same equation with a change of subscripts is valid for the second component. In these equations, P is the total vapor pressure, P^0 the vapor pressure of the pure component, x and y the mole fraction of the component in the liquid and vapor phases, respectively, $\bar{V}$ and $\bar{V}^0$ the partial molar volume of the component in solution and the molar volume in the pure liquid, respectively, β_{11} the second virial coefficient and $T=273.15+t$. The quantity δ is defined by the relation $\delta=2\beta_{12}-\beta_{11}-\beta_{22}$. The equation of state for the vapor used in the derivation of this equation is the virial equation only to the second virial coefficient. The terms involving the molar and partial molar volumes correct the chemical potentials from the experimental pressures to 1 atm.

Berthelot's equation was used to determine the second virial coefficients. Lambert *et al.*[15] found that the second virial coefficients calculated from the Berthelot equation agree with the experimental values for a number of nonpolar organic substances including benzene. They also point out that the Berthelot equation is in excellent agreement with the temperature dependence of the virial coefficients derived from the Lennard-Jones potential. The second virial coefficients

[14] L. H. Horsley, Ind. Eng. Chem., Anal. Ed. **19**, 508 (1947).
[15] J. P. Lambert, G. A. H. Roberts, J. S. Rowlinson and V. J. Wilkinson, Proc. Roy. Soc. (London) **A196**, 113 (1949).

then are given by the equation,

$$\beta_{ii}=B_{ii}-(A_{ii}/T^2), \tag{3}$$

where $A=27RT_c^3/64P_c$ and $B=9RT_c/128P_c$. The quantity, β_{12}, was calculated from the assumed combining laws

$$B_{12}=\tfrac{1}{8}(B_{11}^{1/3}+B_{22}^{1/3})^3 \tag{4}$$

$$A_{12}=(A_{11}A_{22})^{\frac{1}{2}}. \tag{5}$$

For this particular system, the values thus obtained are almost identical to those obtained by assuming that β_{12} is the geometrical mean between β_{11} and β_{22}. The values of the critical temperature and critical pressure of benzene used in these calculations were 288.5° and 47.9 atm, respectively, given by Timmermans[16] and those of isooctane were 271.15° and 25.5 atm given by Beattie and Edwards.[17] The values β_{11}, β_{12}, β_{22} and δ used in the calculations are given in Table III. These virial coefficients for benzene agree with the experimental values reported by Lambert and his co-workers[15] and also with those obtained by Allen *et al.*[18] with the use of the Clapeyron equation.

The molar excess change of the Gibbs free energy on mixing at constant pressure was calculated from the excess chemical potentials according to the equation

$$\Delta\tilde{G}^E=x_1\Delta\mu_1^E+x_2\Delta\mu_2^E. \tag{6}$$

These values are listed in the sixth column of Table II. Smooth values of these quantities were obtained according to the method of least squares by use of the equation

$$\Delta\tilde{G}^E=x_1x_2[a+b(x_1-x_2)+c(x_1-x_2)^2] \tag{7}$$

suggested by Guggenheim.[19] The coefficients of these equations were then fitted to functions of the temperature, again according to the method of least squares. The resulting equations are[20]

$$a=2428.10-10.9940T+0.013961T^2 \tag{8}$$

$$b=-1113.1+7.662T-0.01207T^2 \tag{9}$$

$$c=33-0.027T. \tag{10}$$

The deviations of the smooth values from the observed values are given in the last column of Table II. The data at 65° were not used in these calculations because only four points were obtained which were thought to be reliable. It was possible to fit Eq. (7) to these four points, but the values of the coefficients deviated markedly from the curve obtained by plotting the values of the other coefficients against the temperature. The quadratic equation of b is fully justified by a study of the deviations of the calculated values from the observed values although it is possible to obtain a fair fit with a linear equation.

TABLE III. Second virial coefficients in cm³ mole⁻¹.

t	$-\beta_{11}$	$-\beta_{22}$	$-\beta_{12}$	δ
35	1281	2182	1671	121
45	1198	2039	1562	114
55	1122	1910	1463	106
65	1053	1791	1372	100
75	989	1683	1289	94

A further test of the adequacy of the smoothed quantities was made by calculating the total pressure and mole fraction of the vapor at each experimental point by Eqs. (7) to (10). For simplicity in these calculations, the corrections for the nonideality of the vapor phase and for the change from the experimental pressure to one atmosphere were taken to be the same as those obtained for the experimental values. The deviation of the calculated total pressure from the observed are given in the fifth column of Table II and those for the mole fraction in the third column of Table II. These deviations are only a little larger than those which were estimated from the experimental methods and are believed to be quite satisfactory.

The thermodynamic consistency of the data was checked in two ways. The first method was that proposed by Redlich and Kister[19] which requires that

$$\int_0^1(\Delta\mu_1^E-\Delta\mu_2^E)\,dx_1=0. \tag{11}$$

Figure 3 presents such a test for the data at 75°. The solid line represents the values of $(\Delta\mu_1^E-\Delta\mu_2^E)$ determined from Eqs. (7) to (10). This line must satisfy the condition because Eq. (7) must satisfy the Gibbs-Duhem relation on which the condition is based. The points represent the experimental values. The agreement appears to be excellent. The points at the other four temperatures show even better agreement. In a slightly different test based on the same condition, a smooth curve was drawn through the experimental points which had been plotted on a large scale. The ratio of the areas above and below the zero axis was then estimated; these ratios are 1.015 at 35°, 1.026 at 45°, 1.027 at 55°, and 1.042 at 75°.

A more stringent test is based on the requirement that Gibbs-Duhem equation must be satisfied in each phase at each experimental point if thermodynamic equili-

[16] J. Timmermans, *Physico-Chemical Constants of Pure Organic Compounds* (Elsevier Publishing Company, Inc., Princeton, New Jersey, 1950).
[17] J. A. Beattie and D. Edwards, J. Am. Chem. Soc. **70**, 338 (1951).
[18] P. Allen, D. H. Everett, and M. F. Penney, Proc. Roy. Soc. (London) **A212**, 149 (1952).
[19] E. A. Guggenheim, Trans. Faraday Soc. **33**, 151 (1937); see also O. Redlich and A. T. Kister, Ind. Eng. Chem. **40**, 345 (1948).
[20] The number of significant figures given in these equations has been set so that the values of the excess free energy can be calculated to 0.1 cal per mole. The root-mean-square deviation of the calculated values from those determined from the experimental data is ±0.4 cal per mole. The uncertainties in the temperature derivatives of these functions will be somewhat larger. See footnote 21.

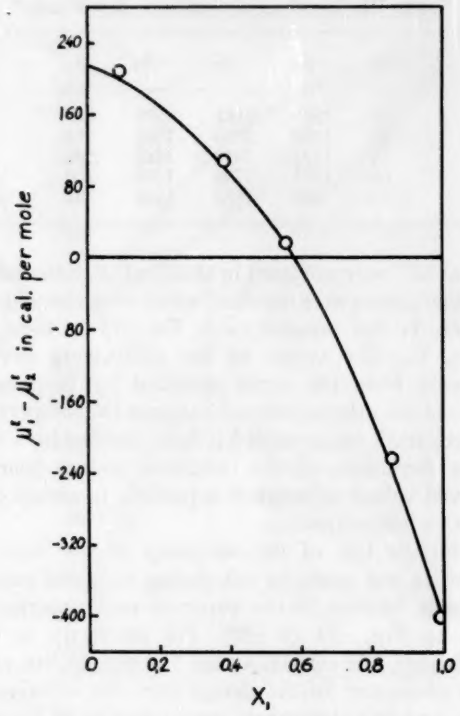

FIG. 3. $\mu_1^E - \mu_2^E$ vs mole fraction of benzene at 75°C.

brium is obtained. At constant temperature, this equation is

$$\tilde{V}dp + x_1 d\mu_1 + x_2 d\mu_2 = 0. \tag{12}$$

The chemical potential of one component in the vapor phase may be written as

$$\mu_1 = RT \ln P y_1 + \beta_{11} P + \delta y_2^2 P + \mu_1^0, \tag{13}$$

where μ_1 is the chemical potential of the component at the pressure of the experiment and μ_1^0 is the chemical potential of the pure gas in the ideal gas state at 1 atm pressure, both at the temperature of the experiment. A similar equation with subscripts changed may be written for the second component. The expression

$$\frac{dP}{dy_1} = \frac{(y_1 - x_1)[(RT/y_1 y_2) - 2\delta P]}{(RT/P) + x_1\beta_{11} + x_2\beta_{22} + (x_1 y_2^2 + x_2 y_1^2) - \tilde{V}_l} \tag{14}$$

is obtained by combining the two Gibbs-Duhem equations, one for each phase, and the two equations for the chemical potentials. The test of the thermodynamic consistency of the data then involves the comparison of dP/dy_1 calculated from the actual experimental data with the same quantity calculated from the smoothed data, which of necessity must obey the Gibbs-Duhem relation. Such a comparison is given in Table IV for the data at 35° and 75°. The first column gives the mole fraction of benzene in the liquid phase, the second column the observed values of dP/dy_1, the third column the smoothed values of dP/dy_1, and the last column the difference. Better agreement is obtained at 35° than at 75° as might be expected but the agreement is very good even at 75°. On the basis of these two tests, it is concluded that the experimental data are thermodynamically consistent.

The change of the enthalpy and the excess change of the entropy on mixing at constant pressure have been calculated by the usual methods from Eqs. (7) to (10) at 40 and 70° and at even tenth mole fractions. These quantities together with the excess change of the Gibbs free energy are given in the second, third, and fourth columns of Table V[21] and are illustrated in Fig. 4. All three functions are positive over the whole range of composition and decrease with an increase of temperature. The maxima of the curves for the enthalpy of mixing and the excess entropy of mixing shift toward the benzene-rich side as the temperature increases.

The difference between the change of the thermodynamic functions on mixing at constant pressure and on mixing at constant volume have been calculated by Sandus.[22] The initial state for the process of mixing at constant volume is the pure components at 1 atm pressure and the temperature T and the final state is the solution at the additive volume of the pure components and at the same temperature. The equations developed by Scatchard[23] and the same assumptions made in previous calculations[24] were used in these

TABLE IV. Calculated and observed values of dP/dy_1.

x_1	dP/dy_1 observed	dP/dy_1 calculated	Difference
	35.00°C		
0.0886	0.0907	0.0921	0.0014
0.1601	0.1066	0.1088	0.0022
0.3343	0.1369	0.1372	0.0003
(0.4343)	(0.1381)	(0.1415)	(0.0034)
0.5061	0.1352	0.1377	0.0025
0.8375	0.0444	0.0423	−0.0021
0.9884	−0.0280	−0.0261	0.0019
	75.00°C		
0.0879	0.3615	0.3568	−0.0047
0.3862	0.5258	0.5164	−0.0094
0.5558	0.5114	0.5065	−0.0049
(0.6673)	(0.4617)	(0.4398)	(+0.0219)
0.8590	0.2236	0.2089	+0.0147
0.9874	−0.0196	−0.0114	+0.0084

[21] The uncertainties for the change of the enthalpy and the energy are estimated to be one cal per mole and for the excess change of the entropies to be 0.003 cal per mole deg based on the deviation of the excess free energy from the smoothed values. The actual uncertainties are probably considerably larger, but they are difficult to estimate because of the uncertainties in the virial coefficients and their temperature derivatives as well as their dependence on the particular functions of the temperature used to express the experimental data analytically.

[22] O. Sandus, "The volume of mixing of benzene-2,2,4-trimethylpentane (isooctane) mixtures," Ph.D. thesis, Illinois Institute of Technology.

[23] G. Scatchard, Trans. Faraday Soc. **33**, 160 (1937).

[24] S. E. Wood and J. A. Gray, III, J. Am. Chem. Soc. **74**, 3729 (1952).

calculations. The coefficients of expansion of benzene and isooctane were determined from the data of Wood and Sandus.[1] The coefficient of compressibility and its temperature derivative for benzene were taken from Wood and Austin.[25] For isooctane, the coefficient of compressibility and its temperature derivative were taken from the data of Felsing and Watson.[26] The values of α_0, β_0, and $d\ln\beta/dT$ for the two components are given in Table VI.

The excess change of the Helmholtz free energy, the energy of mixing, and the excess change of the entropy of mixing, all at constant volume, have been calculated from the thermodynamic functions at constant pressure and the differences outlined in the previous paragraph at 40° and 70°. These quantities are given in the last three columns of Table V. As in other systems, the energy of mixing and the excess entropy of mixing at constant volume are smaller than the corresponding quantities for mixing at constant pressure. The two free energies are almost identical. The asymmetry of the excess entropy of mixing at constant volume is similar to that at constant pressure and the maximum shifts in the same direction with increase of temperature.

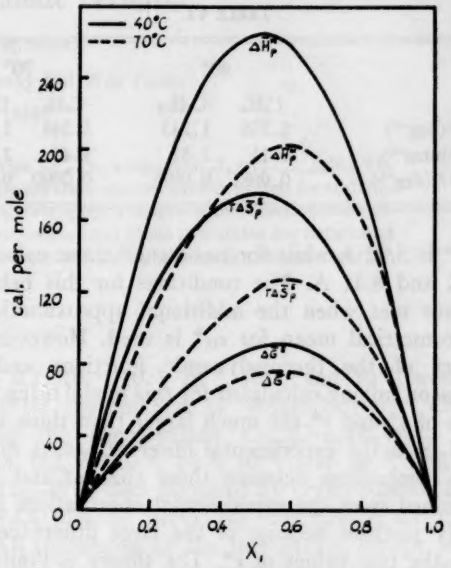

FIG. 4. Excess thermodynamic functions vs mole fraction of benzene when the parameter b is expressed as a quadratic function of temperature.

DISCUSSION

The experimental value of the energy of mixing at constant volume can be compared with those calculated according to the Scatchard-Hildebrand equation. The solubility parameters used in these calculations at 40° and 70° are 8.95 and 8.51 for benzene and 6.61 and 6.38 for isooctane, respectively. The values of the energy of mixing at half mole fraction then are 148.5 cal per mole at 40° and 139.6 at 70°. These quantities are to be compared with 231.2 cal per mole at 40° and 162.5 at 70°, which are the smoothed values determined from the experimental data. As in many other systems, the values calculated from the Scatchard-Hildebrand equation are smaller than the experimental values. It is interesting to note that the differences between the two sets of values decrease markedly with the increase of temperature.

TABLE V. Excess thermodynamic functions in cal per mole.

x_1	$\Delta\tilde{G}_p^E$	$\Delta\tilde{S}_p^E$	$\Delta\tilde{H}_p^M$	$\Delta\tilde{A}_v^E$	$\Delta\tilde{S}_v^E$	$\Delta\tilde{E}_v^M$
			40°			
0.1	25.9	0.212	92	25.9	0.179	82
0.2	48.3	0.372	165	48.3	0.312	146
0.3	66.6	0.482	218	66.7	0.400	192
0.4	80.3	0.545	251	80.5	0.447	221
0.5	88.6	0.563	265	88.8	0.455	231
0.6	90.2	0.535	258	90.4	0.426	224
0.7	83.9	0.465	229	84.1	0.363	198
0.8	68.0	0.352	178	68.1	0.268	152
0.9	40.7	0.197	102	40.8	0.144	86
			70°			
0.1	21.5	0.084	50	21.5	0.054	40
0.2	40.2	0.168	98	40.2	0.113	79
0.3	55.7	0.246	140	55.8	0.170	114
0.4	67.5	0.310	174	67.6	0.220	143
0.5	74.9	0.353	196	75.0	0.255	163
0.6	76.7	0.369	203	76.8	0.270	169
0.7	71.7	0.349	190	71.8	0.252	158
0.8	58.4	0.287	157	58.5	0.212	132
0.9	35.2	0.173	95	35.2	0.128	79

The excess changes of the various thermodynamic functions as well as the volume of mixing are all positive over the entire range of composition. According to the average potential model for solutions of spherically symmetric molecules developed by Prigogine and his co-workers,[27] this behavior should be exhibited by binary systems under the conditions that

$$\epsilon_{11}^* = \epsilon_{22}^* = \epsilon_{12}^*$$

and

$$r_{11}^* \neq r_{22}^* \neq r_{12}^*$$

with the usual assumption that

$$r_{12}^* = \tfrac{1}{2}(r_{11}^* + r_{22}^*).$$

In these equations, ϵ^* and r^* are the two constants in the Lennard-Jones expression of the potential energy between two molecules. For benzene[28], ϵ^*/k is 440°K

[25] S. E. Wood and A. E. Austin, J. Am. Chem. Soc. **67**, 480 (1945).
[26] W. A. Felsing and G. M. Watson, J. Am. Chem. Soc. **63**, 898 (1941).
[27] I. Prigogine, A. Bellemans, and V. Mathot, *The Molecular Theory of Solutions* (Interscience Publishers, Inc., New York, 1957).
[28] J. A. Hirshfelder, C. F. Curtiss, and R. B. Bird, *Molecular Theory of Gases and Liquids* (John Wiley & Sons, Inc., New York, 1954).

TABLE VI.

	40°		70°	
	C_6H_6	C_8H_{18}	C_6H_6	C_8H_{18}
$\alpha_0 \times 10^3 (\text{deg}^{-1})$	1.256	1.243	1.348	1.361
$\beta_0 \times 10^4 (\text{atm}^{-1})$	1.11	1.81	1.43	2.33
$d \ln\beta/dT (\text{deg}^{-1})$	0.0081	0.0078	0.0090	0.0090

and r^* is 5.92 A while for isooctane[29] these values are 409°K and 8.41 A. The conditions for this behavior are thus met when the additional approximation of the geometrical mean for ϵ_{12}^* is used. However, the changes of the thermodynamic functions and the volume on mixing calculated for this model using these values of ϵ^* and r^* are much larger than those determined from the experimental observations. A quantitative comparison between these changes and those determined from the experimental observations is not entirely justified because of the large differences between the two values of r^*. The theory is limited to those systems for which the percentage difference between the values of r^* is about 10% or less while the percentage difference for this system is about 30% when benzene is used as the reference substance.

The excess entropy of mixing, both at constant pressure and at constant volume, is considerably larger than that of the three binary systems composed of benzene, carbon tetrachloride, and cyclohexane. The Flory-Huggins approximation, in which the entropy change is expressed in terms of the logarithm of the volume fraction rather than the mole fraction accounts for approximately only one-fourth of the observed excess entropy at 40° and about one-half at 70°. It is premature to discuss the excess entropy in terms of the effect of orientation until other systems in which isooctane is one of the components have been studied. However, a study of an extension of the Hildebrand-Scatchard equation is being made in this laboratory at the present time. Preliminary results clearly show that the decrease of the excess entropy with increase in temperature at one atmosphere pressure depends primarily on the increase of volume rather than on the increase of temperature. Such a decrease of the entropy with an increase of volume can be ascribed to a decrease in the orientation of the molecules in the pure components when the volume is increased. Little can be said about the asymmetry of the curve for the excess entropy as a function of the mole fraction except that it depends in a somewhat complicated manner upon the orientation effects and on the molar volumes of the components.

[29] C. R. Mueller and J. E. Lewis, J. Chem. Phys. **26**, 286 (1957).

ACKNOWLEDGMENTS

The financial assistance of the National Science Foundation in the support of this research is gratefully acknowledged. The authors also wish to thank Dr. Rubin Battino for many helpful discussions.

Emission Spectra of Trivalent Terbium

L. G. VAN UITERT AND R. R. SODEN

Bell Telephone Laboratories, Inc., Murray Hill, New Jersey

(Received October 8, 1959)

The luminescent emission spectra of the members of the series $Y_{1-x}Tb_x$ antipyrene $_6I_3$ and $Ca_{1-2x}Na_xTb_xWO_4$ have been measured and compared. The antipyrene complexes show spectra similar to that for terbium octahydrosulfate which is a simple inverted multiplet. The tungstate spectra results from emissions originating from two electronic levels. The relative intensities of the emissions from these two states are dependent upon the terbium concentration. In $Na_{0.5}Tb_{0.5}WO_4$ the usual spectral bands are by far the stronger. In $CaWO_4$:$Tb_{0.0001}$ the situation is reversed.

INTRODUCTION

LUMINESCENT emission spectra, which are due to emission from more than one electronic energy level of trivalent terbium, have been reported but not identified as such in the past. The resulting complex emission patterns of terbium in calcium tungstate and in aluminum oxide were reported by de Rohden[1] in 1915. A pattern for terbium in a calcium-yttrium fluoride mineral, similar to that found in calcium tungstate, was reported by Przibram[2,3] (1934). However, Chatterjee[4] (1939) did not obtain the same results on synthetic calcium-yttrium fluoride containing terbium. The complex spectra found for trivalent terbium in calcium tungstate have also been reported for this ion in strontium sulfide.[5]

The simple multiplet spectrum of terbium octahydrosulfate, which involves only one emitting state, was first reported by Tomaschek[6] (1933) and resolved into an energy diagram involving an inverted multiplet of $^7F_{0-6}$ terminal levels by Gobrecht[7] (1937). Geisler and Hellwege[8] (1953) from their studies on $Tb(BrO_3)_3 \cdot 9H_2O$ have proposed that the simple spectrum results from emission from the $^5D_4$ level.

It has been found that emission from this and higher order levels can be resolved by varying the concentration of terbium in the calcium tungstate structure and comparing the resulting emission patterns to those found for terbium octahydrosulfate, terbium hexa-antipyrene triiodide (Tb-HAPI) and terbium in aluminum oxide.

MATERIALS

Terbium octahydrosulfate was prepared from Tb_2O_3 (99.9+% pure) and sulfuric acid. Colorless, well-formed crystals of $Y_{1-x}Tb_x$ antipyrene$_6I_3$, where $x=1$, 0.5, 10^{-1}, 10^{-2}, 10^{-3}, 10^{-4}, and 10^{-5}, were prepared by the method of Wilkes-Dörfurt.[9] Crystals having the compositions $Ca_{1-2x}Na_xTb_xWO_4$, where $x=0.5$, 0.2, 5×10^{-2}, 10^{-2}, 10^{-3}, and 10^{-4}, and $Na_{0.5}Y_{0.49}Tb_{0.01}WO_4$ were prepared by crystallization from a $Na_2W_2O_7$ flux, as previously described.[10] Crystals of $CaWO_4$ containing all the rare earths, except No. 61, were also prepared for spectra comparison. All the above tungstates have the scheelite structure.

Corundum boules containing 1 mole % terbium oxide were prepared by F. W. Swanekamp of these Laboratories employing the Verneuil technique.

MEASUREMENTS

Measurements were made with a Gaertner high dispersion spectrometer adapted with an AMINCO photomultiplier microphotometer, which employed a 1P22 photomultiplier tube. Slit widths were 10 mils. The apparatus was calibrated for nonlinearity against a tungsten filament. Prior to each measurement, the microphotometer was adjusted to read full scale for the the 5450-A line of a standard sample of $Na_{0.5}Tb_{0.5}WO_4$.

Emission spectra were excited by illuminating samples 1 in. long by $\frac{1}{2}$ in. wide by $\frac{1}{4}$ in. deep with a 3660-A rich H^4 spotlight through a Corning 5874 filter. A long wave uv excitation source was selected to avoid broad-band emission by the tungstate host lattice.

MULTIPLE EMISSION LEVELS

The photomultiplier response to the emission of terbium octahydrosulfate versus wavelength in angstrom units is shown in Fig. 1. The seven bands corresponding to the $^7F_{0-6}$ terminal states are so designated. These data are in good agreement with that of Gobrecht.[7]

Figure 2 shows the photomultiplier response to the emission of calcium tungstate, in which 1% of the calcium has been replaced by terbium. This is essentially the spectrum seen by de Rohden[1] on calcium tungstate, and by Przibram[2] in a natural calcium-

[1] M. Ch. de Rohden, Ann. Chem. **3**, 338–366 (1915).
[2] H. Haberlandt, B. Karlik, and K. Przibram, Wien Ber. **IIa 142**, 235 (1933); and **IIa 143**, 151+591 (1934).
[3] P. Pringsheim, *Fluorescence and Phosphorescence* (Interscience Publishers, New York, 1949), p. 662.
[4] N. Chatterjee, Z. Physik **113**, 96 (1939).
[5] S. P. Keller and G. D. Pettit, J. Chem. Phys. **30**, 434–441 (1959).
[6] R. Tomaschek and O. Deutschbein, Z. Physik **8**, 309 (1933).
[7] H. Gobrecht, Ann. Physik 5F–B28, 8 (1937).
[8] H. F. Geisler and K. H. Hellwege, Z. Physik **136**, 293–302 (1953).
[9] Wilkes-Dörfurt and Schliephake, Z. anorg. u. allgem. Chem. **170** (1928).
[10] L. G. Van Uitert and R. R. Soden, J. Appl. Phys. **31**, 328 (1960).

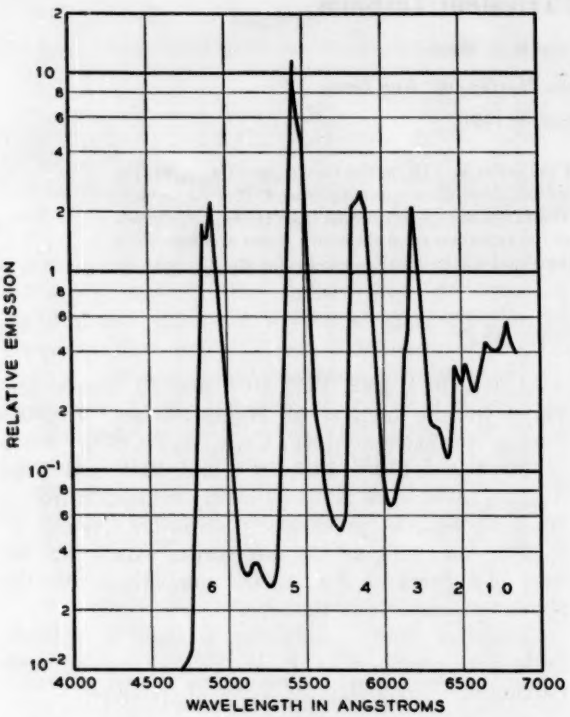

FIG. 1. The emission spectrum of $Tb_2(H_2O)_8(SO_4)_3$.

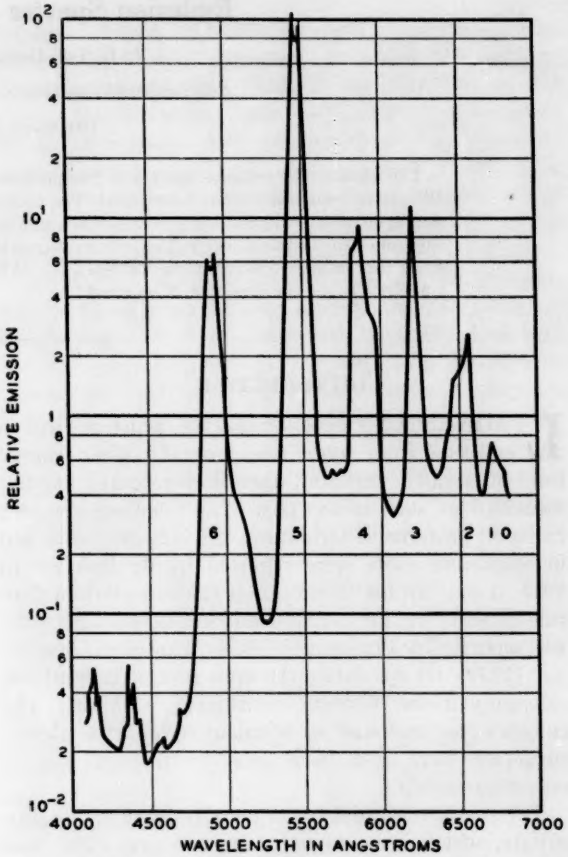

FIG. 3. The emission spectrum of $Na_{0.5}Tb_{0.5}WO_4$. At high C_{Tb} the low frequency spectrum predominates.

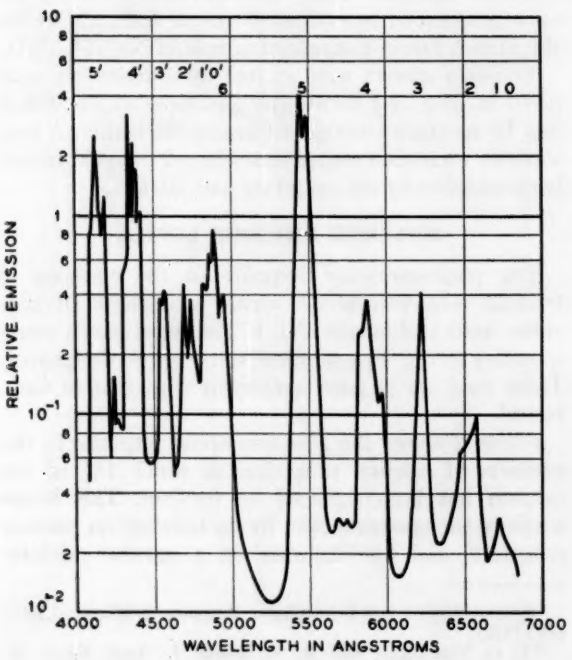

FIG. 2. The emission spectrum of $CaWO_4:Tb_{0.01}$.

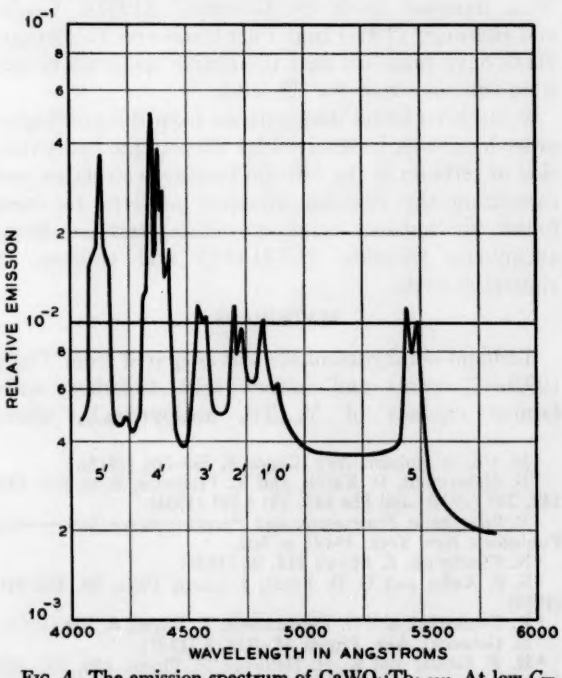

FIG. 4. The emission spectrum of $CaWO_4:Tb_{0.0001}$. At low C_{Tb}, the high frequency spectrum predominates.

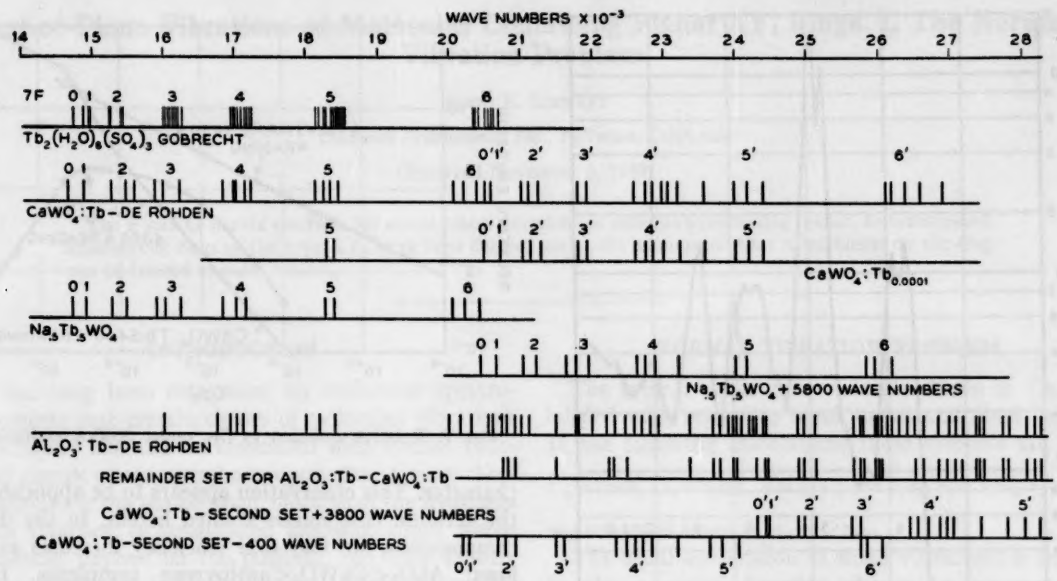
WAVE NUMBERS X10⁻³
14 15 16 17 18 19 20 21 22 23 24 25 26 27 28
7F 0 1 2 3 4 5 6
Tb₂(H₂O)₆(SO₄)₃ GOBRECHT
0 1 2 3 4 5 6 0'1' 2' 3' 4' 5' 6'
CaWO₄:Tb-DE ROHDEN
5 0'1' 2' 3' 4' 5'
CaWO₄:Tb₀.₀₀₀₁
0 1 2 3 4 5 6
Na₅Tb₅WO₄
0 1 2 3 4 5 6
Na₅Tb₅WO₄+5800 WAVE NUMBERS
Al₂O₃:Tb-DE ROHDEN
REMAINDER SET FOR Al₂O₃:Tb-CaWO₄:Tb
CaWO₄:Tb-SECOND SET+3800 WAVE NUMBERS
0'1' 2' 3' 4' 5'
CaWO₄:Tb-SECOND SET-400 WAVE NUMBERS
0'1' 2' 3' 4' 5' 6'

FIG. 5. The emission spectra of terbium in several environments and their resolution by emitting states.

yttrium fluoride.[11] This spectrum can be readily resolved into two components by varying the terbium concentration. At high concentration, a set of bands comparable to those obtained for terbium octahydrosulfate dominates, as shown for $Na_{0.5}Tb_{0.5}WO_4$ in Fig. 3. At low concentrations, the other bands dominate, as shown for $CaWO_4$:$Tb_{0.0001}$. The six bands of this second set indicated, plus an additional band which has been shown by de Rohden[1] to occur around 3800 A, and which is seen in strontium sulfide,[5] constitute a second set of seven bands whose energies match those of the first set when the latter are increased by 5800 wave numbers (see Fig. 4). The occurrence of this second set of bands shows that terbium has at least two energy levels from which luminescent emissions can originate in calcium tungstate. Since the more familiar of these levels lies approximately 20 700 wave numbers above the ground state,[7] the other must be at about 26 500 wave numbers.

The possibility of still higher emission levels for Tb^{3+} is suggested by the cathodoluminescence data obtained by de Rohden upon aluminum oxide containing a small quantity of terbium,[1] as shown in Fig. 4. The absence of spectral lines other than for terbium in the data for his tungstate sample is evidence of the purity of de Rohden's terbium source. The presence of a characteristic spectrum for terbium in combination with aluminum oxide was confirmed by photomultiplier measurements employing a boule of Al_2O_3 prepared from source materials which contained 1 mole % Tb_2O_3. The emission was very weak ($<10^{-3}$ of that for $CaWO_4$:$Tb_{0.01}$), but the main lines of the complex spectrum discussed above were detected. The more detailed spectrum of de Rohden is rich in lines at the higher frequencies. It is not surprising that the weaker low-frequency lines were not observed in de Rohden's material for neither were these seen in the dilute tungstates (refer to Fig. 5). By deducting the lines that can reasonably be related to those appearing in calcium tungstate (small changes due to structural effects being considered) a remainder set is obtained, which may be accounted for by lines corresponding to the first six bands that would result from emission from a level at about 30 300 wave numbers (higher frequency lines were beyond cutoff for de Rohden's apparatus), and a full set of bands that would result from emission from a level at about 26 100 wave numbers.

[11] It is possible that a small oxygen content in the fluoride mineral accounts for the presence of a high frequency spectrum as described herein, since it was not seen in the comparable synthetic material of Chatterjee.[4]

EMISSION INTENSITIES

Figure 6 shows the emission pattern for Tb HAPI. As in the case of the octahydrosulfate, no indications of higher emission levels are evident. Dilutions of terbium by yttrium in steps to 1 part in 10^5 in these materials were examined. There is no change in the basic emission pattern with concentration of terbium in these materials. The relative emission intensities of these samples and the tungstate samples as a function of the concentration of terbium (C_{Tb}) are shown in Fig. 7. The coordinates on the concentration axes are in terms of the number of terbium ions per formula volume of calcium tungstate. Since Tb HAPI has one terbium ion per unit cell[12] of 1751 A^3, and calcium tungstate has four calcium ions per unit cell of 312 A^3, the formula volume ratio is 22.4. Thus, the value $C_{Tb}=0.045$ corresponds to the 100% Tb HAPI, and C_{Tb} corresponds to 100% $Na_{0.5}Tb_{0.5}WO_4$.

[12] R. G. Treuting (private communication).

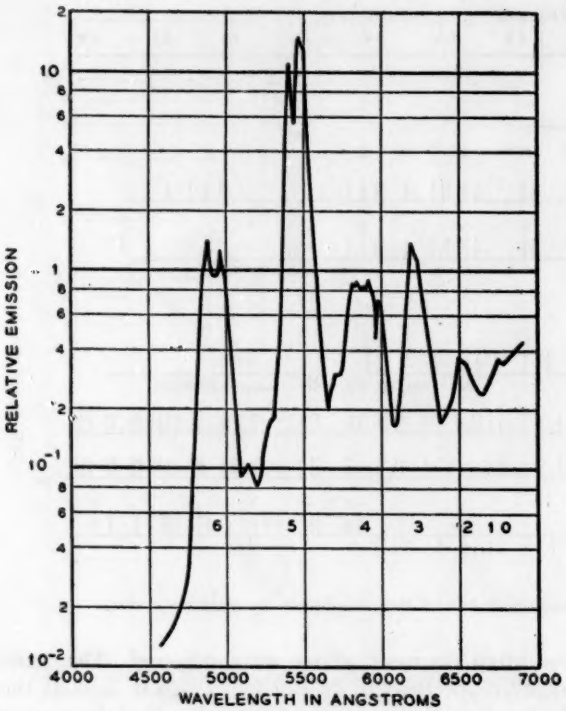

FIG. 6. The emission spectrum of Tb HAPI.

The high-frequency spectrum shown by the tungstates is characterized by the 4360-A emission and the low-frequency set by 5450-A emission. At high values, the dependence of intensity of emission of the low-frequency spectrum upon C_{Tb} is the same as in the $Y_{1-x}Tb_x$ HAPI series. Below $C_{Tb}=0.05$, the intensity of emission falls off much faster in the tungstates than in the metal organic complexes. As C_{Tb} is reduced, the relative prominence of the intensity of emission from the high-frequency spectrum increases. At $C_{Tb}=0.05$, the emission appears green to the eye, while at $C_{Tb}=0.01$ it appears blue.

DISCUSSION

Weissman[13] has related the luminescent efficiencies of a number of complexes of europium to their covalent character. This observation appears to be applicable to the terbium compounds studied herein. In the dilute compositions, we find that efficiency increases as follows: $Al_2O_3<CaWO_4<$antipyrene complexes. However, at high terbium concentrations, the tungstate compares favorably to Tb HAPI. Further, it takes on the emission characteristics of Tb HAPI in its intensity dependence on concentration and number of emission states. This suggests that there is an increase in the strength of the bonding between terbium and its surroundings as C_{Tb} increases. This may come about through the increased incidence of terbium in adjacent calcium sites[14] which can result in the development of exchange coupling[15] between these magnetic ions. Comparable results are obtained by substituting terbium for yttrium in $Na_{0.5}Y_{0.5}WO_4$, showing that the effects described are not the result of substituting trivalent ions for calcium.

[13] S. I. Weissman, J. Chem. Phys. **10**, 214–17 (1942).

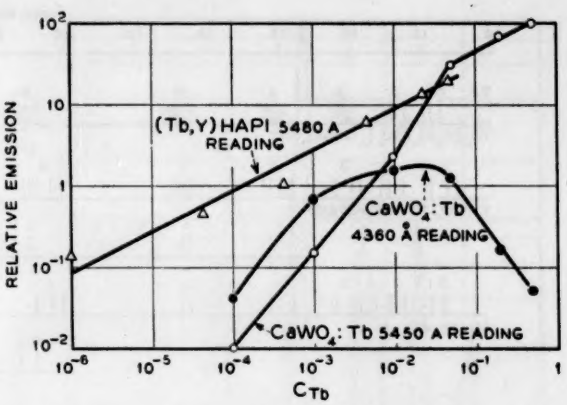

FIG. 7. Relative emission vs C_{Tb} under 3660-A excitation.

ACKNOWLEDGMENTS

The authors are indebted to C. G. B. Garrett and A. L. Schawlow for their helpful discussions.

[14] Paramagnetic resonance studies on $CaWO_4$ and $Na_{0.5}Y_{0.5}WO_4$ containing rare earth ions by C. F. Hempstead and K. D. Bowers of these Laboratories have shown that narrow line widths can be obtained in $CaWO_4$, while those for $Na_{0.5}Y_{0.5}WO_4$ are broad. This is evidence of a nonordered distribution of sodium and yttrium ions in the structure.

[15] A. L. Schawlow, D. L. Wood, and A. M. Clogston, Phys. Rev. Letters **3**, No. 6, 271 (1959).

Out-of-Plane Vibrations of Molecules Containing Planar XY_4 Rings. I. The Normal Vibration Problem

JAMES E. STEWART

Beckman Instruments, Inc., Fullerton, California

(Received November 6, 1959)

The **F** and **G** matrix elements for out-of-plane vibrations of molecules containing planar, five-membered heterocyclic rings of the type XY_4 have been derived under the assumption that substituents on the ring can be treated as point masses.

INTRODUCTION

IT has long been recognized by molecular spectroscopists that certain classes of molecular vibrations are localized and can be associated with specific functional groups or structural arrangements. Among these vibrations are the out-of-plane motions of the hydrogen atoms attached to substituted aromatic rings, whose frequencies depend on the position, but only slightly on the nature of the substituents. These vibrations have been studied theoretically by a number of workers[1-3] and it is generally agreed that force constants determined for the benzene molecule can be used to predict vibrational frequencies in satisfactory agreement with those determined experimentally for substituted benzenes.

There is very good evidence[4-6] that the out-of-plane vibrations of substituted thiophenes are also determined primarily by the position of substituents and it is reasonable to suppose that similar molecules, such as pyrrole, furan, and selenophene behave in this manner also. However, it is not likely that a sufficiently large number of variously substituted forms of some of these molecules will be available for experimental determination of the range of characteristic frequencies. The purpose of the investigation reported in this and following papers is (1) to determine the force field which will reproduce the out-of-plane vibrational frequencies of simple five-membered heterocyclic molecules; (2) using this force field, to calculate the frequencies of substituted compounds and compare the calculated frequencies with available experimental values; (3) to predict the frequencies of substituted compounds which are not available for experimental study. The first step in this program is to derive the equations describing the molecular vibrations.

NORMAL VIBRATION PROBLEM

The typical cyclic XY_4 molecule shown in Fig. 1 is labeled with regard to bond angles and bond lengths. In the following calculations these symbols are used:

$C_\alpha=\cos\theta_\alpha$, $S_\alpha=\sin\theta_\alpha$, $\sigma=1/r_s$, $\tau=1/r_0$, $\tau_1=1/r_1$, $\tau_2=1/r_2$,

$m_A=$ mass of atom A, $\mu_A=1/m_A$.

The usual assumption of small vibrations is implicit in the potential function chosen to represent the valence force field for out-of-plane motion of the molecule:

$$V_\perp=\tfrac{1}{2}A_1[(\Delta\gamma_1)^2+(\Delta\gamma_4)^2]+\tfrac{1}{2}A_2[(\Delta\gamma_2)^2+(\Delta\gamma_3)^2]$$
$$+\tfrac{1}{2}B_1[(\Delta\delta_1)^2+(\Delta\delta_5)^2]+a_1(\Delta\gamma_1\Delta\gamma_2+\Delta\gamma_3\Delta\gamma_4)$$
$$+a_2\Delta\gamma_2\Delta\gamma_3+b_3\Delta\delta_1\Delta\delta_5+c_1(\Delta\gamma_1\Delta\delta_1-\Delta\gamma_4\Delta\delta_5). \quad (1)$$

Additional valence force constants which might be included in (1) are found to be inoperative because of the symmetry of the molecule and the choice of redundant symmetry coordinates.

The assumption that the potential function can be split into an in-plane and out-of-plane part is valid provided the molecule has at least C_s symmetry and this will be true if the Z_i's can be treated as point masses.

In Eq. (1), $\Delta\gamma_1$, for example, represents an angular displacement of bond Y_1-Z_1 out of the $X-Y_1-Y_2$ plane and $\Delta\delta_1$ represents a twisting of the $X-Y_1$ bond measured by the dihedral angle between the plane containing Y_4, X, Y_1 and the plane of X, Y_1, Y_2. The coordinates δ_1, δ_2, δ_4, and δ_5 are defined such that $\delta_1\rightarrow-\delta_5$ and $\delta_2\rightarrow-\delta_4$ under a reflection through the symmetry plane perpendicular to the plane of the ring. This is contrary to the usual way of treating six-membered rings, but is consistent with the behavior of δ_3 under this reflection, $\delta_3\rightarrow-\delta_3$.

The vibration problem is treated by the conventional **FG** matrix method.[7] One of the features of this method is the simplification of the problem afforded by the use of symmetry coordinates. Molecules in which $Z_1=Z_4$ and $Z_2=Z_3$ (e.g., thiophene and the symmetrically di-, and tetrasubstituted thiophenes) belong to point group C_{2v} provided the Z_i's can be considered point masses.

[1] R. P. Bell, H. W. Thompson, and E. E. Vago, Proc. Roy. Soc. (London) **192A**, 498 (1948).
[2] A. R. H. Cole and H. W. Thompson, Trans. Faraday Soc. **46**, 103 (1950).
[3] T. Shimanouchi, Y. Kakiuti, and I. Gamo, J. Chem. Phys. **25**, 1245 (1956); Y. Kakiuti and T. Shimanouchi, J. Chem. Phys. **25**, 1252 (1956).
[4] F. P. Hochgesang in *Thiophene and Its Derivatives*, by H. D. Hartough (Interscience Publishers, Inc., New York, 1952), Chap. IV.
[5] John F. Zack, Jr., thesis, University of Illinois (1956).
[6] A. Hidalgo, J. Phys. Rad. **16**, 366 (1955).
[7] E. B. Wilson, J. C. Decius, and P. C. Cross, *Molecular Vibrations* (McGraw-Hill Book Company, Inc., New York, 1955).

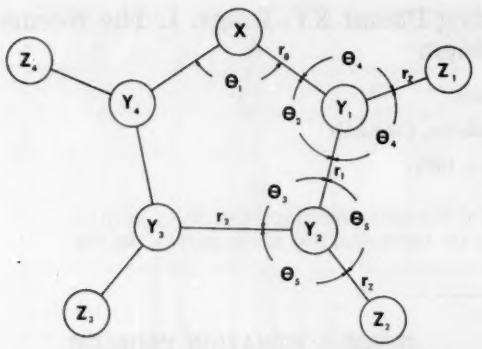

FIG. 1. Bond parameters of molecule containing planar XY_4 ring.

Symmetry coordinates appropriate to this group can be constructed as follows:

$$A_2: S_1=(\gamma_1-\gamma_4)/\sqrt{2}$$
$$S_2=(\gamma_2-\gamma_3)/\sqrt{2}$$
$$S_3=(\delta_1+\delta_5)/\sqrt{2}$$
$$S_4=[(r_1/r_2)(\delta_2+\delta_4)+(r_0/r_1)\delta_3]/[2(r_1/r_2)^2+(r_0/r_1)^2]^{\frac{1}{2}} \quad (2)$$
$$S_5=[(\delta_1+\delta_5)+(r_1/r_2)(\delta_2+\delta_4)+(r_0/r_1)\delta_3]/[2+2(r_1/r_2)^2+(r_0/r_1)^2]^{\frac{1}{2}}$$
$$B_2: S_1=(\gamma_1+\gamma_4)/\sqrt{2}$$
$$S_2=(\gamma_2+\gamma_3)/\sqrt{2}$$
$$S_3=(\delta_1-\delta_5)/\sqrt{2}$$
$$S_4=(\delta_2-\delta_4)/\sqrt{2}.$$

As there are only three modes of vibration of species A_2 and three of B_2, two of the A_2 and one of the B_2 symmetry coordinates are redundant. By manipulating these coordinates it can be demonstrated that $S_4(A_2)$ is equivalent to $S_3(A_2)$, $S_4(B_2)$ is proportional to $S_3(B_2)$, and $S_5(A_2)$ is identically zero. Coordinates $S_4(A_2)$, $S_5(A_2)$, and $S_4(B_2)$ are therefore redundant and the corresponding rows and columns of the symmetry factored **F** and **G** matrices are omitted in subsequent calculations. The molecular motion described by $S_3(B_2)$ is a folding of the ring about an axis through Y_1 and Y_4. $S_3(A_2)$ is an out-of-the-plane folding about an axis through **X** and Y_3 with an into-the-plane folding about an axis through **X** and Y_2. These motions are shown pictorially by Hidalgo.[6]

The elements of the symmetry factored force constant matrix for C_{2v} molecules are, for species A_2

$$F_{11}=A_1$$
$$F_{12}=a_1$$
$$F_{13}=c_1$$
$$F_{22}=A_2-a_2$$
$$F_{23}=0$$
$$F_{33}=B_1+b_3 \quad (3)$$

and for species B_2

$$F_{11}=A_1$$
$$F_{12}=a_1$$
$$F_{13}=c_1$$
$$F_{22}=A_2+a_2$$
$$F_{23}=0$$
$$F_{33}=B_1-b_3. \quad (4)$$

The elements of the unfactored **g** matrix which occur in the symmetry factored forms have been calculated from the displacement vectors, and are given in Table I. The symmetry factored **G** matrix elements for C_{2v} molecules are, for species A_2

$$G_{11}=g_{11}-g_{14}$$
$$G_{12}=g_{12}-g_{13}$$
$$G_{13}=g_{15}+g_{19}$$
$$G_{22}=g_{22}-g_{23}$$
$$G_{23}=g_{25}+g_{29}$$
$$G_{33}=g_{55}+g_{59} \quad (5)$$

and for species B_2

$$G_{11}=g_{11}+g_{14}$$
$$G_{12}=g_{12}+g_{13}$$
$$G_{13}=g_{15}-g_{19}$$
$$G_{22}=g_{22}+g_{23}$$
$$G_{23}=g_{25}-g_{29}$$
$$G_{33}=g_{55}-g_{59}. \quad (6)$$

TABLE I. g matrix elements in G matrices of C_{2v} and C_s molecules.

$g_{11}=\mu_{Z_1}\sigma^2+\mu_{S\tau}{}^2S_{42}{}^2+\mu_C(A^2+S_{42}{}^2\tau_1{}^2)=g_{44}-\mu_{Z_4}\sigma^2+\mu_{Z_1}\sigma^2$
$g_{12}=-\mu_C\tau_1(AS_{53}+CS_{42})=g_{34}$
$g_{13}=\mu_C\tau_1\tau_2S_{42}S_{53}=g_{24}$
$g_{14}=\mu_{S\tau}{}^2S_{42}{}^2$
$g_{15}=\mu_{S\tau}{}^2B-\mu_C(AD-\tau_1{}^2S_{42}/S_2)=-g_{49}$
$g_{19}=-\mu_{S\tau}{}^2B-\mu_C\tau A/S_1=-g_{45}$
$g_{22}=\mu_{Z_2}\sigma^2+\mu_C[C^2+S_{53}{}^2(\tau_1{}^2+\tau_2{}^2)]=g_{33}-\mu_{Z_4}\sigma^2+\mu_{Z_1}\sigma^2$
$g_{23}=-2\mu_C\tau_2S_{53}C$
$g_{25}=\mu_C\tau_1(DS_{53}-C/S_2)=-g_{39}$
$g_{29}=\mu_C\tau_1S_{53}(\tau/S_1-\tau_2/S_2)=-g_{35}$
$g_{55}=\mu_{S\tau}{}^2B^2S_{24}{}^2+\mu_C(\tau^2/S_1{}^2+\tau_1{}^2/S_2{}^2+D^2)$
$g_{59}=-\mu_{S\tau}{}^2B^2S_{24}{}^2+2\mu_C\tau D/S_1$

Where:

$S_{ab}=S_a/S_b$
$A=S_{42}(\sigma S_{24}+\tau+\tau_1)$
$B=S_{42}(1/S_1+C_2/S_2-C_1/S_1)$
$C=S_{53}(\sigma S_{35}+\tau_1+\tau_2)$
$D=\tau(C_2/S_2-C_1/S_1)-\tau_1/S_2$

It is of interest to note that the G matrix for the A_2 vibrations does not contain the mass of the hetero atom.

Mono- and trisubstituted and unsymmetrically disubstituted molecules lose the C_{2v} symmetry of their more symmetric relatives. They do, however, retain C_s symmetry to the extent that the substituents can be treated as point masses, and this symmetry insures that the six out-of-plane vibrations are separable from the fifteen in-plane modes. In this case the appropriate out-of-plane symmetry coordinates are

$$\begin{aligned} S_1&=\gamma_1\\ S_2&=\gamma_2\\ S_3&=\gamma_3\\ S_4&=\gamma_4\\ S_5&=(\delta_1+\delta_5)/\sqrt{2}\\ S_6&=(\delta_1-\delta_5)/\sqrt{2} \end{aligned} \tag{7}$$

after deletion of the redundant coordinates as in Eq. (2).

The nonvanishing elements of the F matrix for C_s molecules are

$$\begin{aligned} F_{11}&=F_{44}=A_1\\ F_{12}&=F_{34}=a_1\\ F_{15}&=F_{16}=-F_{45}=F_{46}=c_1/\sqrt{2}\\ F_{22}&=F_{33}=A_2\\ F_{23}&=a_2\\ F_{55}&=B_1+b_3\\ F_{66}&=B_1-b_3. \end{aligned} \tag{8}$$

The elements of the symmetry factored G matrix for C_s molecules are

$$\begin{aligned} G_{11}&=g_{11}\\ G_{12}&=G_{34}=g_{12}\\ G_{13}&=G_{24}=g_{13}\\ G_{14}&=g_{14}\\ G_{15}&=-G_{45}=(g_{15}+g_{19})/\sqrt{2}\\ G_{16}&=G_{46}=(g_{15}-g_{19})/\sqrt{2}\\ G_{22}&=g_{22}\\ G_{23}&=g_{23}\\ G_{25}&=-G_{35}=(g_{25}+g_{29})/\sqrt{2}\\ G_{26}&=G_{36}=(g_{25}-g_{29})/\sqrt{2}\\ G_{33}&=g_{33}\\ G_{44}&=g_{44}\\ G_{55}&=g_{55}+g_{59}\\ G_{56}&=0\\ G_{66}&=g_{55}-g_{59}. \end{aligned} \tag{9}$$

THE JOURNAL OF CHEMICAL PHYSICS VOLUME 32, NUMBER 4 APRIL, 1960

Magnetic Investigations of Spin-Free Cobaltous Complexes. II. Tetrahedral Complexes

RICHARD H. HOLM* AND F. ALBERT COTTON

Department of Chemistry, Massachusetts Institute of Technology, Cambridge 39, Massachusetts

(Received November 9, 1959)

The magnetic moments of 17 tetrahedral complexes of Co(II) have been carefully measured, most of them over a temperature range. The Curie-Weiss law is found to hold in all cases where the temperature dependence was studied. The variations of the orbital contribution to the moment are shown to be in accord with expectation from ligand field theory (Schlapp and Penney), and the utility of the results in correlating magnetic properties, spectra, and structures of Co(II) complexes is briefly discussed.

INTRODUCTION

In Part I[1] of this series we have illustrated how the relative magnitudes of the magnetic moments of tetrahedral cobaltous complexes can be interpreted and predicted using a model based on ligand field theory. The model was illustrated with perhaps the simplest examples, the tetrahalo ions. In Part II we wish to present, by use of nearly all tetrahedral Co(II) complexes now known, additional and more diverse examples of the general utility of the theory. A set of empirically derived rules correlating structure and magnetism is presented together with a spectrochemical series derived from the magnetic data.

The occurrence of the tetrahedral configuration in spin-free quadricoordinate Co(II) complexes is widespread. Simple ligand field theory indicates that Co(II), of all the spin-free divalent ions of the first transition series, is conspicuously likely to give tetrahedral complexes.[2] If the separation between the lowest two levels in T_d symmetry is taken to be $-40/9\ Dq$, then the ligand field stabilization energy is $16/3\ Dq$. For the weakest tetrahedral complex, CoI_4^{2-}, this stabilization amounts to $\sim$1500 cm^{-1} or $\sim$4.3 kcal mole^{-1} when $Dq \approx 280$ cm^{-1}.

A series of spin-free quadricoordinate cobaltous complexes has been prepared whose spectral and magnetic properties cannot be rationalized with a tetrahedral structure;[3] at the present time these appear to be the only cases in which a tetrahedral configuration cannot be assigned with certainty to spin-free quadricoordinate Co(II) complexes.

Table I lists those Co(II) complexes whose tetrahedral structures have been definitely established from x-ray investigations, and includes available magnetic moments of such compounds. Structural information on the tetrahalo ions has previously been summarized.[1] While the compounds of Table I are the only ones whose tetrahedral structures have been authenticated, comparison of their spectral and magnetic characteristics with those of the complexes of Table II leaves no doubt that those in the latter group are also tetrahedral, as the following discussion will show.

EXPERIMENTAL

Preparation of Compounds

The preparation and analysis of the following compounds used in this study have been described elsewhere: dihalobis(triphenylphosphine oxide) cobalate(II), $Co(\phi_3PO)_2X_2$, X=Cl$^-$, Br$^-$, I$^-$[4]; tetrakis (triphenylphosphine oxide) Co(II) perchlorate, $Co(\phi_3PO)_4(ClO_4)_2$[5]; tetrakis [tri(*p*-dimethylaminophenyl) phosphine oxide] Co(II) perchlorate, $Co[(p\text{-}Me_2N\cdot C_6H_4)_3PO]_4(ClO_4)_2$[5]; tetrakis(trimethylphosphine oxide)Co(II) $(ClO_4)_2$; dinitratobis(triphenylphosphine oxide)colbaltate(II), $Co(\phi_3PO)_2(NO_3)_2$.[6]

Dihalobis(*p*-toluidine)cobaltate(II), $Co(C_7H_9N)_2X_2$, X=Cl$^-$, Br$^-$, I$^-$[4]: Some of these compounds were reported briefly by Ablov *et al.*[7] We obtained them in good yield by mixing absolute ethanol solutions of amine and anhydrous CoX_2. The resulting crystalline precipitates were washed well with absolute ethanol and were recrystallized from this medium.

Analysis. Calculated for $Co(C_7H_9N)_2X_2$: X=Cl$^-$: Co, 17.13; Cl, 20.60; N, 8.14; X=Br$^-$: Co, 13.61; Br, 36.91; N, 6.47; X=I$^-$: Co, 11.18; I, 48.16; N, 5.32. Found: X=Cl$^-$: Co, 17.3; Cl, 20.63; N, 7.86, X=Br$^-$: Co, 13.7; Br, 36.90; N, 6.40; X=I$^-$; Co, 11.14; I, 47.96; N, 5.40.

$K_2Co(NCS)_4\cdot 4H_2O$: The compound was prepared following the procedure of Rosenheim and Cohn.[8]

Analysis. Calculated: Co, 13.35; N, 12.69. Found: Co, 13.5; N, 13.01. $K_2Co(NCS)_4$: The compound was obtained by heating the tetrahydrate *in vacuo* at 140°K for 24 hr.

Analysis. Calculated: Co, 15.95; N, 15.17. Found: Co, 15.9; N, 15.05.

---

* Present address: Department of Chemistry, Harvard University, Cambridge 38, Massachusetts.

[1] R. H. Holm and F. A. Cotton, J. Chem. Phys. **31**, 788 (1959).

[2] C. K. Jørgensen and J. Bjerrum, Acta Chem. Scand. **9**, 180 (1955).

[3] R. H. Holm and F. A. Cotton, J. Am. Chem. Soc. (to be published).

[4] F. A. Cotton, R. D. Barnes, and E. Bannister, J. Chem. Soc. (to be published).

[5] E. Bannister and F. A. Cotton, J. Chem. Soc. (to be published).

[6] E. Bannister and F. A. Cotton, J. Chem. Soc. (to be published).

[7] A. V. Ablov, Z. P. Burnasheva, and E. G. Levitskaya, Zhur. Neorg. Khim. **1**, 2465 (1956).

[8] A. Rosenheim and R. Cohn, Z. anorg. Chem. **27**, 289 (1901).

$HgCo(NCS)_4$: The compound was prepared according to Figgis and Nyholm.[9] CoO–ZnO mixed crystals: A sample of approximately 3% CoO in ZnO was obtained from Dr. D. S. McClure, RCA Laboratories, Princeton, New Jersey. The Co^{2+} content was determined polarographically with the method of Watters and Kolthoff.[10] Another sample of 0.74% Co proved too dilute for accurate bulk susceptibility measurements.

Magnetic Measurements

Bulk susceptibility measurements at room temperature and below were made by the Gouy method as previously described,[1] using Mohr's salt and $CuSO_4 \cdot 5H_2O$ as standards. Freshly boiled conductivity water was used as the standard for the solution measurement and its gram susceptibility was interpolated from the data of Auer.[11] Baker dichloromethane, used without further purification, was found to have a gram susceptibility of -0.550×10^{-6}. The moment of $Co(\phi_3PO)_2 \cdot (NO_3)_2$ in CH_2Cl_2 may be ~0.1 B.M. low due to solute precipitation during the measurement. For measurements of CoO–ZnO mixed crystals the gram susceptibility of ZnO was taken to be 0.25×10^{-6}.[12] The magnetic moments quoted in Table II are accurate to ±1% (0.04–0.05 B.M.) maximum error.

DISCUSSION

There are several common transition metal ions which, either in an octahedral or a tetrahedral ligand field, have orbitally nondegenerate ground states. The more important ones are octahedral Cr(III), octahedral Ni(II), and tetrahedral Co(II). In these cases, however, the magnetic moments still may, and do, differ from the spin-only values. This phenomenon was first accounted for, we believe, by Schlapp and Penney,[13] explicitly for the Co(II) case, but, of course, implicitly for any analogous case. They pointed out that to the extent that Russell-Saunders coupling fails to hold, spin-orbit coupling interactions will decompose the orbitally degenerate T_1 and T_2 levels into levels of which some have the same symmetry in the appropriate double group as does the A_1 ground level. Then, mixing of levels will introduce some orbital angular momentum into the ground state and hence an orbital contribution into the magnetic moment. By second-order perturbation theory it can be shown that the g value will then be given by the equation

$$g=2.00-8\lambda'/\Delta, \qquad (1)$$

where 2.00 is the (nonrelativistic) g value of the free electron, λ' is the value of the spin-orbit coupling constant in the complex, which, according to Owen,[14] may be about 20–40% lower than the free ion value in complexes with common ligands, and Δ is by definition the separation between the one-d-electron E and T levels in the ligand field.

As a matter of practical importance, this phenomenon is significant only for tetrahedral Co(II) and Ni(II)

TABLE I. Structure-magnetism correlations for tetrahedral Co(II).

Compound	Structure	μ_{eff}(B.M.)
$M_2Co(NCS)_4 \cdot 4H_2O$ ($M=K^+, NH_4^+$)	Tetrahedral $Co(NCS)_4^{2-}$, Co—N bonds, H_2O's not coordinated[a]	4.50 ($M=K^+$)
$Na_2Co(NCS)_4 \cdot 8H_2O$	Same[b]	[k]
$K_2Co(NCS)_4$	Tetrahedral $Co(NCS)_4^{2-}$, above structure not changed on dehydration[a]	4.43[l]
$HgCo(NCS)_4$	CoN_4, HgS_4 distorted tetrahedra[c]	4.44[l]
Cs_3CoCl_5	Double salt, slightly distorted $CoCl_4^{2-}$ tetrahedra[d]	4.70
Cs_2CoCl_4	Slightly distorted $CoCl_4^{2-}$ tetrahedra[e]	[m]
$[(CH_3)_4N]_2CoCl_4$	Isomorphous with the tetrahedral Zn compound[f]	[m]
Cs_2CoBr_4	Analogous to corresponding chloride compound[e]	
$Co(C_7H_9N)_2Cl_2$	Discrete molecules CoN_2Cl_2, tetrahedra[g,h]	4.72
$Co(\phi NH_2)_2Cl_2$	Same[h]	[m,n]
$Co(C_7H_9N)_2I_2$	Discrete molecules, CoN_2I_2 tetrahedra[h,i]	4.80
$Co(p\text{—}IC_6H_4NH_2)_2I_2$	Same[h]	[k]
α—$Co(py)_2Cl_2$	Discrete molecules, CoN_2Cl_2 tetrahedra[h]	4.51[m,n]
$Co(NH_3)_4(ReO_4)_2$	Isomorphous with tetrahedral Cd compound.	[k]

[a] G. S. Zdanov and Z. V. Zvonkova, Z. Fiz. Khim. **24**, 1339 (1950).
[b] A. P. Tshermak, Tshermak's mineral u. petrog. Mitt. **3**, 376 (1953).
[c] J. W. Jeffery, Nature **159**, 610 (1947).
[d] H. M. Powell and A. F. Wells, J. Chem. Soc. **1935**, 359.
[e] M. A. Porai-Koshits, Trudy Inst. Krist., Akad. Nauk S.S.S.R. **10**, 117 (1954); Kristallografiya **1**, 291 (1956); G. N. Tischenko and Z. G. Pinsker, Doklady Akad. Nauk S.S.S.R. **100**, 913 (1955).
[f] B. Morosin and E. C. Lingafelter, Acta Cryst. **12**, 611 (1959).
[g] G. B. Bokii, T. I. Malinovskii, and A. V. Ablov, Kristallografiya **1**, 49 (1956); T. I. Malinovskii, *ibid.* **2**, 734 (1957).
[h] Result quoted in M. A. Porai-Koshits, Russ. J. Inorg. Chem. (English translation) **4**, 332 (1959).
[i] T. I. Malinovskii, Kristallografiya **3**, 364 (1958).
[j] K. Pitzer, Z. Krist. **93**, 131 (1935).
[k] No data available.
[l] Measurement at room temperature only.
[m] No accurate data available but moments may be presumed to be those for analogous salts in Table II (see ref. 1).
[n] See reference 30.

[9] B. N. Figgis and R. S. Nyholm, J. Chem. Soc. **1958**, 4190.
[10] J. I. Watters and I. M. Kolthoff, Anal. Chem. **21**, 1466 (1949).
[11] H. Auer, Ann. Physik **18**, 593 (1933).
[12] J. Turkevich and P. W. Selwood, J. Am. Chem. Soc. **63**, 1077 (1941).
[13] R. Schlapp and W. G. Penney, Phys. Rev. **42**, 666 (1932).
[14] J. Owen, Proc. Roy. Soc. (London) **227A**, 183 (1955).

TABLE II. Magnetic data for tetrahedral Co(II) complexes.[a]

Compound	T, °K	$X_{corr}^{M} \cdot 10^6$	Diamagnetic correction $\times 10^6$	θ, °K	μ_{eff} (B.M.)
$(C_9H_8N)_2CoCl_4$				−11	4.80[b]
$(C_9H_8N)_2CoBr_4$				−10	4.87[b]
$(C_9H_8N)_2CoI_4$				−16	5.01[b]
$Co(C_7H_9N)_2Cl_2$	296.5	8 932			
	194.7	13 500	−212	−12	4.72
	73.2	32 400			
$Co(C_7H_9N)_2Br_2$	299.3	8 807			
	195.0	13 180	−232	−13	4.72
	73.7	31 350			
$Co(C_7H_9N)_2I_2$	298.6	9 290			
	195.1	14 050	−266	−10	4.80
	74.1	34 180			
$Co(\phi_3PO)_2Cl_2$	299.6	9 191			
	195.1	13 890	−418	−9	4.79
	73.6	34 110			
$Co(\phi_3PO)_2Br_2$	298.4	9 446			
	194.6	14 220	−438	−10	4.84
	74.1	34 490			
$Co(\phi_3PO)_2I_2$	302.2	9 737			
	197.4	14 560	−470	−13	4.98
	74.0	34 550			
$Co(\phi_3PO)_2(NO_3)_2$	299.2	8 841			
	196.1	13 620	−406	−8	4.69
	75.1	33 290			
in CH_2Cl_2	297.4	8 526			4.52
$Co(\phi_3PO)_4(ClO_4)_2$	299.5	9 030			
	195.4	13 950	−788	−6	4.72
	75.1	34 270			
$Co[p\text{-}(Me_2N \cdot C_6H_4)_3PO]_4(ClO_4)_2$	297.3	9 336			
	194.6	14 240	−1167	−5	4.76
	73.6	34 790			
$Co[(CH_3)_3PO]_4(ClO_4)_2$	299.5	7 418			
	196.8	11 060	−340	−15	4.34
	74.0	25 780			
$K_2Co(NCS)_4 \cdot 4H_2O$	297.8	8 320			
	194.6	13 140	−198	−3	4.50
	74.1	32 180			
$K_2Co(NCS)_4$	298.3	8 142	−146	...	4.43
$HgCo(NCS)_4$	294.7	8 132	−155	...	4.44
2.90% CoO–97.1% ZnO	295.9	7 455			
	194.4	11 000	−24	−12	4.26
	74.0	24 720			

[a] All data on solids.
[b] Complete data were given in reference 1.

but not for octahedral Cr(III).† This is because for Cr(III) complexes λ' is <87 cm^{-1}, while Δ is generally about 2×10^4 cm^{-1}; hence $2.00-g$ will be about 0.04 and variations in μ through the normal range of variation in Δ are too small to measure accurately or to be of importance. For Ni(II), $-\lambda'$ is <335, while Δ is generally $0.7\text{–}1.2\times10^4$; hence $g-2.00$ will be about 0.1–0.5. Hence the variations in g through the range of Δ values found in real complexes should be detectable in accurate measurements, but the presently available data[15] do not always reflect the expected trends.

† *Note added in proof.* We should perhaps have mentioned also tetrahedrally coordinated V(III). A few presumably tetrahedral tetrahalo complexes of V(III) have recently been prepared by D. E. Scaife (Abstracts of Papers presented at the International Conference on Co-ordination Chemistry, London, April, 1959, Abstract 71), but no spectral or magnetic data have as yet been published. It might be expected that in these cases the orbital contributions will exceed those in octahedral Cr(III), but that they would still be relatively small and difficult to assess precisely using bulk susceptibility measurements.

[15] G. Foex, *Constantes Sélectionees Diamagnétisme et Paramagnetisme* (Masson et Cie., Paris, 1957), pp. 243–246.

For tetrahedral Co(II) the spin-orbit coupling effect as given by Eq. (1) is of sufficient magnitude to provide a useful tool for correlating magnetic and structural properties. For Co(II) complexes $-\lambda' \approx$ 150–180 cm^{-1}, while Δ is about $2-6\times10^2$; hence $g-2.00$ values in the range of 0.4 to 1.2 B.M. may be expected. Standard methods of measurement, carefully applied, can readily provide data sufficiently accurate to be used in correlating structures, spectra, and magnetic moments.

That tetrahedral Co(II), at least in the $CoCl_4^{2-}$ ion, does indeed have an orbitally nondegenerate ground state is supported by the internal consistency of our data, and independently by the essentially zero anisotropy of the susceptibilities of Cs_3CoCl_5 and Cs_2CoCl_4.[16]

The magnetic data obtained in this work are given in Table II. All compounds exhibited satisfactory dependence on the Curie-Weiss law, $X^M = C/(T-\theta)$, as evidenced from plots of $1/X^M$ vs T. C and θ were determined graphically and the magnetic moments calculated from the relation $\mu_{eff} = 2.84\ C^{\frac{1}{2}}$.

The data of Table II are best discussed with reference to the spectrochemical series[17] which orders ligands in their relative abilities to effect ligand field splittings. The following series has been derived empirically from a large body of existing spectral data[18,19]:

$$I^- < Br^- < Cl^- < OH^- < NO_3^- < F^- < C_2O_4^{-2} \lesssim H_2O < py \lesssim NCS^- < NH_3 < en \lesssim NO_2^- < o\text{-phen} \lesssim dip \ll CN^-.$$[20]

This series has been derived principally from spectral data on variously substituted hexacoordinated Co(III) and Cr(III) complexes and it is not to be regarded as necessarily invariant with metal ion. From oxalate to ammonia especially, the series must not be taken too literally. The series as written above simply represents what is believed to be the best approximate order and nothing more. The ligand field splittings increase from I^- to CN^- so that on the basis of the model of the preceding section the orbital contribution should decrease in this direction. That the tetrahalo ions conform with this expectation has been demonstrated.[1] It now remains to be investigated whether or not this series will serve as a guide for predictions of relative orbital contributions in a much wider variety of tetrahedral Co(II) complexes which will offer a more severe test than did the tetrahalo ions. However, a number of tetrahedral complexes containing some or all of the ligands given in the above series could not be prepared, so that consideration of different complexes is necessary.

The complexes of the general type ML_4(L=ligand donor atom) will be considered first. Assuming effective T_d symmetry for the ligand field, the argument of the preceding section will be rigorously in force. Clearly the moments of $Co(NCS)_4^{-2}$, relative to those of CoX_4^{-2}, are in accord with the series. The moment at 300°K of 4.96 B.M. given by Janes[21] for $K_2Co(NCS)_4\cdot4H_2O$ must be regarded as incorrect. He attributed this moment to a predominantly cubic field produced apparently by additional coordination of water molecules. This is not an unreasonable conclusion since hexacoordinated spin-free Co(II) complexes have moments in the range of 4.7 to 5.2 B.M.[22–24] However, comparison of room temperature susceptibilities for the tetrahydrate and the rigorously anhydrous $K_2Co(NCS)_4$ and $HgCo(NCS)_4$ shows that no water molecules are coordinated, as had previously been proven by x-ray work (cf. Table I).

From the preceding series it would be predicted that complexes of the type $Co\text{-}O_4$, in which Co(II) is tetrahedrally surrounded by four oxygens, would possess moments lying between those for $CoCl_4^{2-}$ and $Co(NCS)_4^{2-}$. No such compounds were known until recently, when $Co(\phi_3PO)_4(ClO_4)_2$[6] and its p-dimethylamine analog[25] were isolated.[26] The two compounds both have orbital contributions within the expected limits, although possibly slightly higher than for a "normal" $Co\text{–}O_4$ tetrahedral arrangement, as, for example, in hypothetical tetrahedral $Co(H_2O)_4^{2+}$. This effect can reasonably be ascribed to decreased basicity of the donor oxygens due to conjugation with $3d\pi$ orbitals of the phosphorus and the bulkiness of the ligand itself which, while tending to force a tetrahedral configuration, may not allow a normal Co-O distance to be attained. That the steric effect upon the Co–O distance may be of some consequence can be illustrated by the moment of $Co[(CH_3)_3PO]_4^{2+}$, in which the more intense ligand field is almost certainly a result of decreased steric hindrance of ligand molecules and the electron-releasing tendency of methyl groups. Indeed, this moment is nearly as low as that for Co(II) in ZnO, in which the cobaltous ions may be assumed to replace zinc substitutionally in the host lattice and hence to occupy tetrahedral holes. The moment of 4.26 B.M. is in good agreement with other results[27,28] for Co(II) in tetrahedral oxide holes and may be taken as a lower limit for tetrahedral $Co\text{–}O_4$ complexes.

A number of complexes of the type $ML_2L'_2$ have been examined. In this case the ligand field possesses at best C_{2v} symmetry if the pair of M–L and M–L′

[16] K. S. Krishnan and A. Mookherji, Phys. Rev. **51**, 528, 774 (1937).
[17] L. E. Orgel, J. Chem. Phys. **23**, 1004 (1955).
[18] R. Tsuchida, J. Chem. Soc., Japan **59**, 586, 731, 819 (1938).
[19] Y. Shimura, Bull. Chem. Soc. Japan **25**, 49 (1953).
[20] py=pyridine, en=ethylenediamine, o-phen=1,10-o-phenanthroline, dip=α,α'-dipyridyl.
[21] R. B. Janes, Phys. Rev. **48**, 78 (1935).
[22] A. Bose and S. C. Mitra, Indian J. Phys. **26**, 393 (1952).
[23] R. S. Nyholm, Quart. Revs. (London) **7**, 402 (1953).
[24] R. H. Holm and F. A. Cotton (unpublished work).
[25] F. A. Cotton, R. D. Barnes, E. Bannister, and R. H. Holm, Proc. Chem. Soc. 158, 1959.
[26] Other Co—O_4 complexes have been isolated but are very probably not tetrahedral.[3]
[27] P. Cossee, thesis, Leiden (1956); Rec. trav. chim. **75**, 1089 (1956); J. Inorg. & Nuclear Chem. **8**, 483 (1958).
[28] J. Richardson and L. W. Vernon, J. Phys. Chem. **62**, 1153 (1958).

distances are each equal. X-ray data on $Co(C_7H_9N)_2X_2$ (cf. Table I) show that these distances are equal. Therefore, the first excited state in T_d symmetry is, strictly speaking, decomposed into $^4A_2+^4B_1+^4B_2$. The $^4A_2$ ground state is not directly affected by the lowering of ligand field symmetry except through repulsion with the new $^4A_2$ state. Because all these upper states, including those coming from the tetrahedral $^4T_2$ level, are not orbitally degenerate, it would appear that no mixing of upper state eigenfunctions with that of the ground state can introduce any amount of orbital contribution into the latter. However, if the departure from T_d symmetry is small, the C_{2v} symmetry component can be treated as a small perturbation on the original tetrahedral component and the essential features of the model will still be preserved, even in $ML_2L'_2$ complexes.

The data of Table II prove that the orbital contributions are still quite substantial in ML_2X_2 complexes[29] and that the interpretation of the magnetic moments based on tetrahedral symmetry can be successfully, although less rigorously, applied. Here it is appropriate to utilize the concept of an average ligand field in which each ligand provides to the over-all ligand field strength a contribution relative to its position in the spectrochemical series, and to assume a ligand field symmetry higher than that actually present. In the series bis-(*p*-toluidine)CoX_2 and bis(triphenylphosphine oxide) CoX_2 the moments should be between the limiting moments for $Co(C_7H_9N)_4^{2+}$ (as yet unprepared) and $Co(\phi_3PO)_4^{2+}$ and for CoI_4^{2-}, and the moments in the first series should be somewhat less than those of the second series when X is the same if the spectrochemical series given above is applicable here. Both of these expectations are confirmed. Furthermore, the moments within each of the series ought to increase in the order $X=Cl^-<Br^-<I^-$, and this is also seen to be the case. Significantly, the data of Nyholm[30] reflect the same effect in the series bis(aniline)CoX_2, $X=Cl^-$ (4.40), Br^- (4.46), I^- (4.61). The moment of $Co(\phi_3PO)_2(NO_3)_2$ is nicely in accord with expectation for a $Co-O_4$ complex of this type; the $Co-O_4$ formulation is supported by infrared data indicating coordinated nitrate.[6] However, the visible absorption spectrum consists of a band whose absorption frequency and band contour are somewhat dissimilar to spectra of other tetrahedral complexes.[24] The spectrum is the same in both the solid and in CH_2Cl_2 solution where the magnetic moment is 4.52 B.M. Thus we cannot say that the entire body of results for this compound leads to an unequivocal conclusion about its structure.

Certain general conclusions may now be drawn which render the orbital contribution in spin-free cobaltous complexes a useful tool for inferring stereochemistry.

1. Because I^- provides the smallest Dq of any ligand, the moment of CoI_4^{2-}, 5.01±0.05 B.M., is a maximum for tetrahedral complexes.

2. Because no ligand except Br^- is known to occur between I^- and Cl^- in the spectrochemical series, the moment[1] of $CoCl_4^{2-}$, 4.76±0.05 B.M., is a maximum for tetrahedral complexes of the type ML_4 in which L is not a halide.

3. Complexes of the type $ML_2L'_2$ possess moments which lie between those for ML_4 and ML'_4.

It has been found that the spectrochemical series quoted above yields correct predictions of the relative moments of tetrahedral Co(II) complexes even though it was derived from measurements principally on Co(III) and Cr(III) complexes. A number of the ligands in that series are not represented among the Co(II) complexes we have studied and, conversely, several of the ligands in the Co(II) complexes we have studied are not in that series. The data of Table II allow us to arrange all of the ligands which do occur in the complexes we have measured in the following series:

$$I^-<Br^-<Cl^-<\phi_3PO<NO_3^-<p\text{-}CH_3—C_6H_4NH_2$$
$$<NCS^-<(CH_3)_3PO<O^{2-}.$$

ACKNOWLEDGMENTS

Financial support to R. H. H. in the form of a Charles Coffin Fellowship is gratefully acknowledged, as is the loan of the CoO-ZnO mixed crystals by Dr. D. S. McClure. We are also very grateful for financial support from the National Science Foundation.

[29] Conductimetric and spectral evidence proves the mixed ligand formulation ML_2X_2 as opposed to the salt formulation $[ML_4][MX_4]$.

[30] R. S. Nyholm, Rept. to Tenth Solvay Council, Brussels (1956), p. 35.

Collision of a Gas Atom with a Cold Surface*

ROBERT W. ZWANZIG

National Bureau of Standards, Thermodynamics Section, Washington, 25, D. C.

(Received September 17, 1959)

The collisional transfer of kinetic energy from a gas atom to a cold solid is investigated in a simple model. (The solid is one-dimensional; classical mechanics is used throughout; and simplified interactions are assumed.) In two limiting cases the combined equations of motion of the atom and the lattice are solved exactly. The efficiency of energy transfer obtained from these calculations is much higher than that which is predicted from Lennard-Jones' single phonon approximation.

I

THIS article is concerned with the role of energy conservation in the theory of collisions between a gas atom and a solid surface.

In a long series of papers Lennard-Jones and his co-workers have presented a detailed quantum mechanical theory of such collisions.[1] In their work an approximation is introduced which implies that collisions in which more than one vibrational mode of the solid lattice is excited, or a single phonon produced, are improbable. Since the normal mode frequency spectrum of the lattice has an upper limit at the Debye frequency ν_m (where $\theta_D = h\nu_m/k$ is the Debye characteristic temperature), this means that only a limited amount of energy can be transferred to the solid. Especially, it means that if the kinetic energy of the gas atom normal to the surface is appreciably greater than $k\theta_D$, the atom will probably be reflected from the surface, and will not be adsorbed.

Most experimental evidence on this point is equivocal, because it is hard to distinguish between an inelastic collision with reflection, and an adsorption followed at a much later time by reevaporation. (Wexler surveys the experimental literature in his review[2] on the deposition of atomic beams.) However, some pertinent data exists. In particular, Devienne has shown[3] that when the surface temperature is lowered, so that evaporation is inhibited, the condensation coefficient can increase markedly. In some cases it approaches unity. For example, when gold atoms effusing from a furnace at 1670°K struck a copper surface at 300°K, 0.90 to 0.99 of the gold atoms remained on the surface. Since θ_D for copper is about 315°K, a sticking collision involves the production of at least six phonons. The high probability of its occurrence cannot be explained on the basis of the single phonon picture.

In a review of quantum theories of adsorption,[4] Bonch-Bruevich criticizes unfavorably almost everything that was done by the Lennard-Jones group, with the exception of the assumption which leads to the single phonon picture. This assumption is that when the energy of interaction of a gas atom with a solid is expanded in powers of displacements of lattice atoms from their equilibrium sites, only linear terms are important. An interaction which is linear in lattice displacements is also linear in lattice normal coordinates, and when first order perturbation theory is used it leads automatically to single phonon processes.

Bonch-Bruevich argues that this linearization is legitimate since one is dealing with a crystal and not a liquid. The argument is based on the notion that one can talk of crystalline structure only when thermal lattice vibrations have small amplitudes. This may be reasonable for thermal equilibrium, but it is not a valid argument for excluding large *transient* deformations of a lattice, of the sort that occur in a collision. This linearization of the interaction seems to be an essential flaw in Lennard-Jones' treatment. In view of the importance of energy conservation, it is a qualitatively more severe assumption than those which are criticized by Bonch-Bruevich.

In this article it will be shown, in a simple model, that large (meaning many phonon) amounts of energy can be transferred from a gas to a solid. In a quantum mechanical theory this can be attempted in two rather obvious ways: one is to use the linearized interaction in high orders of perturbation theory, and the other is to use the total interaction in low orders. Either of these procedures leads to very complicated equations, in which essential features are obscured by mathematical detail. This complication is avoided here by using a strictly classical model. While a classical theory cannot be expected to be quantitatively correct, the equivalent of a many phonon process can be handled easily. Also, the dynamics can be more easily visualized. The discussion is restricted to a one-dimensional lattice. This, too, is quantitatively unsatisfactory, but the gain in mathematical simplicity is worthwhile.

* This research was performed under the National Bureau of Standards Free Radicals Research Program, supported by the Department of the Army.

[1] J. E. Lennard-Jones and C. Strachan, Proc. Roy. Soc. (London) **A150**, 442 (1935); J. E. Lennard-Jones and A. F. Devonshire, *ibid.* **A156**, 6 (1936); A. F. Devonshire, *ibid.* **A158**, 269 (1937); C. Strachan, *ibid.* **A158**, 591 (1937).

[2] S. Wexler, Revs. Modern Phys. **30**, 402 (1958).

[3] F. M. Devienne, Compt. rend. **238**, 2397 (1954).

[4] B. L. Bonch-Bruevich, Uspekhi Fiz. Nauk. **40**, 369 (1950) (Technical Translation TT-509, National Research Council of Canada).

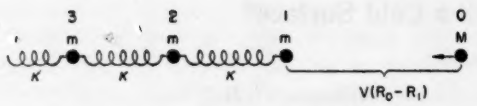

FIG. 1. The one-dimensional lattice and the gas atom. M and m are the masses of the gas atom and the lattice atoms. The lattice force constant is $\mathcal{K}$. Displacements from equilibrium positions are measured in the positive R direction. The interaction of the gas atom with the end of the lattice is $V(R_0-R_1)$.

II

It is instructive to begin by contrasting qualitatively some properties of the collision of a gas atom with a solid and with a diatomic molecule. A naive extension of the well-known theory of vibrational energy transfer between small molecules is bound to be incorrect because of certain fundamental differences.

When small molecules collide, vibrational energy transfer is most efficient for fast "nonadiabatic" collisions. The argument supporting this goes back to Landau and Teller.[5] An atom hitting a diatomic molecule (in a head-on collision) compresses the bond connecting its two atoms and thereby does work on the molecule. If this energy of compression is to be permanently transferred to the molecule, the atom has to get away before the bond expands again. The competition between the time spent by the atom in the neighborhood of the molecule, and the period of vibration of the molecule, is the basis of the Landau-Teller theory.

The situation is fundamentally different when a gas atom hits a solid. The atom still does compressional work. But this energy can either be transferred back to the atom (to give an elastic collision) or it can propagate away from the impact as a sound wave. The energy that goes into sound waves is permanently transferred, and cannot get back into the atom. In a sufficiently slow collision the energy of compression is therefore dissipated as fast as it is produced. The gas atom can even be brought to a complete halt in this way; it is then adsorbed.

A distinction has already been made between collisions where gas atoms are inelastically reflected and where an adsorption may be followed by later evaporation. It is hard to define the distinction precisely, except at 0°K where evaporation does not occur. At any nonzero temperature evaporation is the inverse of adsorption: sound waves in the lattice collect together by chance and impart so much energy to a particular surface atom that it can break loose. Although this process can be handled, in the following model, by techniques similar to those used by N. B. Slater in his theory of unimolecular reaction rates,[6] it will not be done here. In the following discussion the solid is always initially at rest.

[5] L. Landau and E. Teller, Phys. Z. Sowjetunion **10**, 34 (1936).
[6] N. B. Slater, Proc. Roy. Soc. (London) **A194**, 112 (1948).

III

Consider the straight-line collision of a gas atom with a one-dimensional crystal lattice (see Fig. 1). The atoms of the lattice are identical and have mass m. The lattice is semi-infinite. The equilibrium position of each atom is fixed, and the displacement of the jth atom ($j=1, 2, 3, \cdots$) from equilibrium is R_j. R_1 is the displacement of the end atom of the lattice. Assume only nearest neighbor interactions, with a force constant $\mathcal{K}$.

The gas atom has mass M. Its position, relative to the equilibrium position of the end of the lattice, is R_0. It interacts according to a potential energy $V(R_0-R_1)$ with the end atom of the lattice. All this is summed up in the equations of motion of the combined gas atom-lattice system,

$$M(d^2R_0/dt^2)=-\partial V(R_0-R_1)/\partial R_0 \quad (1)$$

$$m(d^2R_1/dt^2)=+[\partial V(R_0-R_1)/\partial R_0]-\mathcal{K}(R_1-R_2) \quad (2)$$

$$m(d^2R_j/dt^2)=\mathcal{K}(R_{j-1}-2R_j+R_{j+1}); \quad j=2, 3, \cdots (3)$$

These simultaneous equations can be partially integrated, leading to a single equation for the relative displacement R_0-R_1. The partial integration involves generating function techniques which were introduced by Schrodinger and extended by Rubin.[7] Details are presented in the Appendix; at this point we shall give only an outline of the derivation.

When Eqs. (1) and (2) are subtracted, one gets

$$(d_2R_0/dt^2)_1-(d^2R_1/dt^2)_1=-[(1/m)+(1/M)]V'(R_0-R_1)+(\mathcal{K}/m)(R_1-R_2). \quad (4)$$

If R_1-R_2 is constant in time (or the lattice is incompressible), an elastic binary collision occurs; there is no transfer of energy. But the lattice is compressible and will respond to the force exerted on it by the gas atom. The response takes the form of traveling lattice waves.

The time dependence of R_0-R_1 can be determined by a self-consistency argument in which effects of lattice oscillations are eliminated. We assume that R_0-R_1, and hence the force, is a known function of time; we calculate the response of the lattice to this force, obtaining in particular the corresponding $R_1(t)-R_2(t)$; and we put this into Eq. (4). The resulting equation must then be solved self-consistently for $R_0(t)-R_1(t)$. Since many variables have been eliminated, many constants of integration will appear. These may conveniently be taken to be initial conditions for the lattice. Since we wish to avoid the complications of reevaporation, we shall give here only the result when the lattice is initially at 0°K, i.e., when all atoms of the lattice are initially at rest in their equi-

[7] R. J. Rubin, *Proceedings of the International Symposium on Transport Processes in Statistical Mechanics*, held in Brussels, August 27–31, 1956 (Interscience Publishers, Inc., New York, 1958), pp. 155–160.

librium positions. The general result is given in the Appendix.

It is convenient to use new units and symbols:

$$\text{mass ratio } \mu = M/m \tag{5}$$

$$\text{frequency } \omega = (\mathcal{K}/m)^{\frac{1}{2}} \tag{6}$$

$$\text{reduced time } \tau = 2\omega t \tag{7}$$

$$\text{relative distance } u(\tau) = R_0(t) - R_1(t) \tag{8}$$

$$\text{reduced force } F(u) = -V'(R_0 - R_1)/\mathcal{K}. \tag{9}$$

In this notation the equation for the relative displacement is

$$\frac{d^2u(\tau)}{d\tau^2} = \frac{1+\mu}{4\mu} F[u(\tau)] - \tfrac{1}{2}\int_0^\tau ds \frac{J_2(s)}{s} F[u(\tau - s)] \tag{10}$$

where $J_2(s)$ is the Bessel function of order 2.

The integral in Eq. (10) represents a nonconservative force due to lattice compressibility. The acceleration at time τ depends on the entire past history of the system, going back to the atom's initial position and velocity. (It would be useful to be able to convert the nonconservative force term into a velocity-dependent friction, but this does not seem possible.)

IV

This equation has been solved exactly in a few special cases. The first one to be discussed provides a model for the trapping of an atom on a surface. We use a truncated harmonic oscillator interaction, as shown in Fig. 2(a),

$$V = \begin{cases} \tfrac{1}{2}\mathcal{K}(R_1 + a - R_0)^2; & R_0 - a - R_1 < R_c \\ \tfrac{1}{2}\mathcal{K}R_c^2; & R_0 - a - R_1 > R_c. \end{cases} \tag{11}$$

The force constant $\mathcal{K}$ is, for convenience, the same one that appears in the nearest neighbor lattice interaction. The distance a locates the equilibrium position of the trapped atom on the end of the lattice. Since the equation of motion is invariant to the substitution of R_0 for $R_0 + a$, we may as well set $a = 0$. The critical distance R_c defines the range of the interaction. Before a collision the separation is larger than R_c and the gas atom approaches as a free particle. The collision begins when the separation just reaches R_c. (This is a convenient origin for the time scale.) During the collision the gas atom is actually a part of the lattice; it takes part in harmonic lattice vibrations. The collision ends, and the gas atom is reflected, when the separation again reaches R_c. If the separation never returns to R_c, the atom is permanently trapped.

(The above criterion for reflection is not entirely correct. It is rigorous only when the gas atom is lighter than a lattice atom; but when $\mu > 1$ a difficulty arises. A heavy gas atom can move into the region of interaction, bounce off the lattice, and move out of range—but the vibrating lattice can catch up with the atom so that a second "collision" occurs. This process does not have any physical significance, since it is entirely a result of the abrupt cutoff of the interaction. In order to avoid this essentially mathematical complication, we shall restrict the discussion to the case $\mu \leq 1$.)

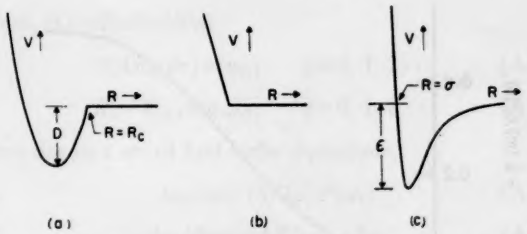

FIG. 2. (a) Truncated harmonic oscillator potential, Eq. (11). (b) Interaction in Eq. (14). (c) Lennard-Jones potential, Eq. (19).

The resulting equation of motion can be formally integrated by Laplace transforms. However, the transform of $u(\tau)$ which appears in the formal solution can be inverted in terms of tabulated functions only for mass ratios $\mu = \frac{1}{2}$ and $\mu = 1$. We give here only the result of this calculation.

At time $\tau = 0$, the position is $u(0) = R_c$ and the initial velocity $\dot{u}(0)$ is arbitrary but negative. The following equations for the separation hold only until the first return to $u = R_c$; after this, the gas atom is free from the lattice.

$\mu = 1$;

$$u(\tau) = 2\dot{u}(0)[J_1(\tau) + J_3(\tau)] + u(0)[J_0(\tau) - J_4(\tau)] \tag{12}$$

$\mu = \frac{1}{2}$;

$$u(\tau) = 2\dot{u}(0)\, J_1(\tau) + u(0)[J_0(\tau) - J_2(\tau)]. \tag{13}$$

In these equations $J_n(\tau)$ is the Bessel function of order n.

To proceed, we just solve for the smallest positive root of $u(\tau) = u(0)$. There is clearly always a root if the initial velocity of approach is large enough; and there is a critical velocity below which no root exists. The only way in which the velocity appears is in the ratio $\dot{u}(0)/u(0)$. When one converts back to the original dimensional variables, the condition for existence of a root is most conveniently expressed in terms of the depth of the potential well, $D = \frac{1}{2}\mathcal{K}R_c^2$, and the initial kinetic energy $K = \frac{1}{2}M(dR_0/dt)^2$. Then there is a critical kinetic energy K_c such that all incident gas atoms with $K < K_c$ will be trapped, and all atoms with $K > K_c$ will be reflected. The numerical values are

$$\mu = \tfrac{1}{2}; \qquad K_c/D = 2.394\cdots$$

$$\mu = 1; \qquad K_c/D = 24.54\cdots.$$

We have also calculated that in the limit of a very small mass ratio, K_c/D is of the order of μ^3. The values

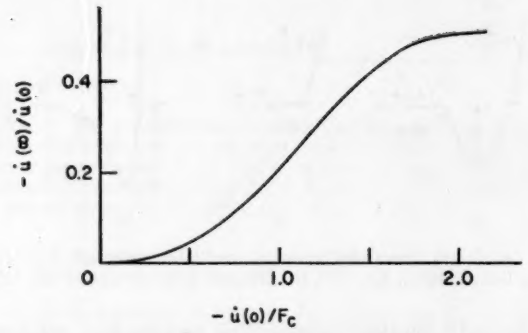

FIG. 3. Velocity transfer when the interaction is given by Eq. (14). The incident velocity is $\dot{u}(0)$, the reflected velocity is $\dot{u}(\infty)$, and F_c is the parameter of Eq. (14).

for $\mu=\frac{1}{2}$ and $\mu=1$, and this limiting case, show that there is a strong mass dependence. For a given amount of initial kinetic energy, a heavy gas atom is more easily trapped than a light atom. However, in view of the assumption in this model that the atom-surface interaction is identical with the internal lattice interaction, the exact form of the mass dependence is not particularly interesting.[8]

V

Another case for which Eq. (10) has been solved exactly provides a model for energy transfer without the possibility of trapping. We use the interaction shown in Fig. 2(b),

$$V=\begin{cases}0; & R_0-R_1>a\\ -F_c\mathcal{K}(R_0-R_1-a); & R_0-R_1<a,\end{cases} \tag{14}$$

where F_c is a positive constant. Again we can drop the a since it does not appear in the equation of motion or in the results. The reduced force for this interaction is a repulsion $F(u)=F_c$ for negative u, and the force vanishes for positive u. The equation of motion can be solved by Laplace transforms. As in the case of the truncated harmonic oscillator, the calculation is simplest when $\mu\leq 1$, so we present final numerical results for this case only.

We find that the velocity of the gas atom long after the impact, $\dot{u}(\infty)$, is related to the velocity before the impact by

$$\dot{u}(\infty)-\dot{u}(0)=F_c\tau_c/4\mu, \tag{15}$$

where τ_c is the total time during which $u<0$. This "collision time" is the smallest positive root of

$$-\dot{u}(0)/F_c=[\tau_c+\mu K(\tau_c)]/8\mu, \tag{16}$$

where the function $K(x)$ is

$$K(x)=4\left\{\frac{J_0(x)-1}{x}-J_1(x)+\int_0^x dy J_0(y)\right\}. \tag{17}$$

When $\mu\leq 1$, the ratio of reflected to incident velocities turns out to be

$$-\dot{u}(\infty)/\dot{u}(0)=[\tau_c-\mu K(\tau_c)]/[\tau_c+\mu K(\tau_c)]. \tag{18}$$

So, we determine τ_c from given values of $\dot{u}(0)$, F_c, and μ; we then use this to get $\dot{u}(\infty)$. In Fig. (3) numerical results are shown for the case $\mu=1$.

It will be instructive to convert the results of this calculation back into real variables, so that orders of magnitude can be estimated. Consider the Lennard-Jones potential, shown in Fig. 2(c),

$$V(R)=4\epsilon[(\sigma^{12}/R^{12})-(\sigma^6/R^6)], \tag{19}$$

where ϵ and σ are parameters characteristic of the interacting particles. A sensible choice for the force F_c is the slope of the L-J curve,

$$F_c=-V'(\sigma)/\mathcal{K}=24\epsilon/\sigma\mathcal{K}, \tag{20}$$

evaluated at the crossover $R=\sigma$. This takes reasonable account of the repulsive part of the L-J interaction.

The lattice force constant is related to the Debye characteristic temperature θ_D (in a one-dimensional lattice) by

$$\mathcal{K}=m\omega^2$$

$$\omega=k\theta_D/2\hbar. \tag{21}$$

Since the initial velocity in ordinary units is $v_0=2\omega\,|\,\dot{u}(0)\,|$, the ratio $\dot{u}(0)/F_c$ becomes

$$\dot{u}(0)/F_c=-(k\theta_D/\epsilon)(\sigma m/96\hbar)v_0. \tag{22}$$

By direct calculation one discovers that when the mass ratio is limited by $0.5\lesssim\mu\lesssim 1.0$, and the velocity ratio satisfies $|\,\dot{u}(0)\,|/F_c\lesssim 1.7$, then at least 75% of the incident kinetic energy is transferred to the lattice. The real velocity, in cm/sec, below which at least 75% transfer occurs is given approximately by

$$v_0\simeq(\epsilon/k\theta_D)\cdot(1/m\sigma)\times 10^7 \text{ cm/sec}, \tag{23}$$

where m is the mass in atomic weight units and σ is measured in angstroms. Another way of putting this is to use an effective gas temperature T_g,

$$\tfrac{1}{2}Mv_0^2=\tfrac{1}{2}kT_g, \tag{24}$$

so that

$$T_g\simeq(\epsilon/k\theta_D)^2(M/m^2\sigma^2)\times 10^6\ ^\circ\text{K}, \tag{25}$$

[8] In conversations on this problem, J. L. Jackson has pointed out an extremely simplified model which illustrates the main features of energy transfer and trapping. In Jackson's model the harmonic lattice is replaced by a linear array of billiard balls, which are initially at rest and do not touch one another. The gas atom interacts with the end of the lattice according to a square well potential whose depth is D. In the initial impact, velocity is transferred from the gas atom to the end of the lattice. This velocity is then carried away by successive rigid sphere collisions in the lattice and is forever lost to the gas atom. It is easy to show that if $\mu<1$, the criterion for trapping is

$$K/D<4\mu/(1-\mu)^2,$$

and if $\mu\geq 1$, the gas atom is always trapped, since it never has its velocity reversed in a collision.

where M is also in atomic weight units. In collisions of a rare gas with its own crystalline phase, where $M=m$, typical values of T_g are of the order of thousands of degrees.

According to this argument, the transfer of energy from a hot gas to a cold surface is very efficient under a wide variety of experimental conditions.

VI

Three major approximations have been made in the formulation of the preceding models. Classical mechanics is used, the models are one-dimensional, and the interactions are not realistic. Because of these approximations the results cannot be quantitatively correct; but the qualitative features which appear ought to be reliable.

The error introduced into these calculations by using classical mechanics is difficult to estimate. However, we feel that it should not be serious except perhaps for very light molecules.

In this model the main function of the lattice is to remove energy and momentum from the gas atom. The important feature is that lattice waves are set up, and that they can propagate away from the point of impact with a finite velocity. This property holds for one- and three-dimensional lattices. The use of a one-dimensional model should not give qualitatively wrong results.

More serious than the preceding approximations is the use of unrealistic interactions. The truncated harmonic oscillator potential is far too "soft" on the repulsive side. However, the dependence on "softness" is partially calibrated by the non trapping interaction of Eq. (14), where the strength of the repulsion can be made more realistic. In both cases the efficiency of energy transfer is very much higher than one would predict from the single phonon picture.

ACKNOWLEDGMENT

I wish to thank Dr. R. J. Rubin for many valuable discussions, and Dr. J. L. Jackson for telling me about his simple model.

APPENDIX

The reduction of the many body equations of motion to a single equation in relative displacement will be described here. First the equations of motion, Eqs. (1)–(3) are rewritten in the units defined by Eqs. (5)–(9),

$$4\mu(d^2R_0/d\tau^2)=F(R_0-R_1) \tag{A1}$$

$$4(d^2R_1/d\tau^2)=-F(R_0-R_1)-(R_1-R_2) \tag{A2}$$

$$4(d^2R_j/d\tau^2)=R_{j-1}-2R_j+R_{j+1};\qquad j=2,3,\cdots. \tag{A3}$$

Next, the substitutions

$$2(dR_j/d\tau)\equiv u_{2j};\qquad j=0,1,2\cdots \tag{A4}$$

$$R_j-R_{j+1}\equiv u_{2j+1};\qquad j=0,1,2,\cdots \tag{A5}$$

give rise to a set of first order equations,

$$du_0/d\tau=(1/2\mu)F(u_1) \tag{A6}$$

$$du_2/d\tau=-\tfrac{1}{2}F(u_1)-\tfrac{1}{2}u_3 \tag{A7}$$

$$du_j/d\tau=\tfrac{1}{2}(u_{j-1}-u_{j+1});\qquad j\neq 0,2. \tag{A8}$$

In particular take $j=1$ and differentiate a second time to get

$$d^2u_1/d\tau^2=\tfrac{1}{4}[1+(1/\mu)]F(u_1)+\tfrac{1}{4}u_3. \tag{A9}$$

The rest of the derivation deals with u_3.

Introduce the generating function

$$\mathfrak{G}(z,\tau)\equiv\sum_{n=1}^{\infty}u_n(\tau)z^n. \tag{A10}$$

A differential equation for $\mathfrak{G}$ can be obtained by calculating $d\mathfrak{G}/d\tau$ from the equations for $du_j/d\tau$. This equation can be integrated immediately in terms of the as yet unknown functions $u_0(\tau)$ and $u_1(\tau)$. The result is

$$\mathfrak{G}(z,\tau)=[\exp\tfrac{1}{2}(z-z^{-1})\tau]\mathfrak{G}(z,0)+\tfrac{1}{2}\int_0^\tau ds[\exp\tfrac{1}{2}(z-z^{-1})(\tau-s)]\times\{(1-z^2)u_1(s)+zu_0(s)-z^2F[u_1(s)]\}. \tag{A11}$$

By picking out the coefficient of z^3 in the power series expansion of this equation (and recognizing that

$$\exp\tfrac{1}{2}(z-z^{-1})\tau=\sum_{-\infty}^{+\infty}J_n(\tau)z^n \tag{A12}$$

generates the Bessel functions), $u_3(\tau)$ is obtained in terms of $u_0(\tau)$, $u_1(\tau)$, and $u_m(0)$ for $m\geq 1$. The appearance here of $u_0(\tau)$ is inconvenient, but it can be removed by further manipulation. In the power series expansion, select the coefficient z^{-1}, which does not appear in $\mathfrak{G}$. This relates $u_0(\tau)$, $u_1(\tau)$, and $u_m(0)$, and the term in $u_0(\tau)$ is just the one to be eliminated from $u_3(\tau)$. The final result of all this is

$$u_3(\tau)=-2\int_0^\tau ds\frac{J_2(\tau-s)}{\tau-s}F[u_1(s)]+4\frac{J_2(\tau)}{\tau}u_2(0)-\sum_3^{\infty}(-)^m[J_{m-3}(\tau)-J_{m+1}(\tau)]u_m(0). \tag{A13}$$

If the lattice is initially at rest, all $u_m(0)=0$ for $m\geq 2$, and the result quoted earlier has been derived.

Electronic Energy Levels and Crystal Quantum States of Tm (IV)

JOHN B. GRUBER AND JOHN G. CONWAY

Lawrence Radiation Laboratory, University of California, Berkeley, California

(Received April 3, 1959)

To date limited agreement has been obtained between theory and experiment for $4f \rightarrow 4f$ transitions for Tm (IV) ($4f^{12}$). It is clear from the considerations that have appeared so far in the literature that intermediate coupling is important in the case of Tm (IV). Solutions of the intermediate field equations yield $\zeta_{4f} = 2700$ cm^{-1}, $F_2 = 450$ cm^{-1}, and $\chi = (\zeta/F_2) = 3$. Experimental agreement to ± 200 cm^{-1} was obtained.

INTRODUCTION

EXPERIMENTAL investigations together with the theoretical considerations of Van Vleck[1] and Bethe[2] indicate that the sharp absorption lines of the rare earth ions in the visible and near-infrared spectra are due to $4f \rightarrow 4f$ transitions. The case of Tm IV (Tm^{3+} ion) should yield to complete theoretical and experimental treatment, since it is a relatively simple problem of 12 f electrons. To date there have been many papers dealing with the absorption spectrum of Tm IV.[3-9] Spedding has made the intermediate calculations for Tm IV using the ratios of F_4/F_2 and F_6/F_2 as derived from La II.[6] The disagreement between Spedding's calculated and observed values averages about 1500 cm^{-1}. Jørgensen, who has made similar calculations, disagrees with Spedding on the assignments of the $^3F_2$, $^1I_6$, and $^3P_2$ levels.[7] It would seem reasonable that better agreement should exist, particularly since very good agreement between theory and experiment has been obtained for Pr IV.[10-13]

A. GENERAL THEORY

The electronic configuration of Tm IV in the ground state is sometimes written as [Xe core] $4f^{12}$ where there are essentially two "holes" in the $4f$ shell. It is easily seen that Tm IV spectroscopically is quite similar to Pr IV, which has only two electrons in the $4f$ shell. According to the Pauli equivalence theorem, both ions should have the same number of electronic states. The only difference, as described by Hund's rules, would be that the multiplets are inverted.

Following the coupling scheme of Russell and Saunders, one may couple 12 equivalent f electrons to obtain

$$^1S\ ^3P\ ^1D\ ^3F\ ^1G\ ^3H\ ^1I.$$

The calculations for pure electrostatic interactions for Tm IV (f^{12}) are the same as for Pr IV (f^2). In an earlier paper[14] the authors have developed in stepwise form the theory for the electronic energy levels of Tm IV in the intermediate coupling case,[14] following the methods outlined by Condon and Shortley,[15] and Spedding.[6] The electrostatic results are given in Table I. In order to complete such calculations, it is necessary to consider which radial wave equations should be put into the Slater integrals F_k. The $4f$ hydrogenic wave functions will not describe very satisfactorily the f electrons in the Tm ion. A self-consistent field approximation would be necessary in order to obtain better radial functions. However, the ratio of F_k integrals is reasonably insensitive to the choice of the actual radial distribution function. One of the members of our group (John D. Axe) has calculated F_4/F_2 and F_6/F_2 ratios for the unlikely "square" radial distribution of $4f$ electrons and has obtained values that are not far from those obtained by Elliott, Judd, and Runciman[16] for a hydrogenic distribution. We have calculated the ratios F_4/F_2 and F_6/F_2 using hydrogenic wave functions by straight integration methods and have obtained values identical with those of Judd.[17] When the electrostatic equations in terms of F_2 were normalized to ^3H as the ground state, the results were found to be in complete agreement with those obtained by Elliott *et al.*[16]

It has been found for many of the 3+ rare earth ions that intermediate coupling is important. Qualitatively the $L-S$ coupling scheme may predict the proper order of levels from the ground state in some cases where one is not too far out into intermediate coupling. In the case of Tm IV, certain levels such as the $^1G_4$ and $^3F_2$ are greatly effected by other levels of the same j value. In the crystal lattice, crystal quantum levels having the same quantum numbers or levels related

[1] J. H. Van Vleck, J. Phys. Chem. **41**, 67 (1937).
[2] H. Bethe, Z. Physik **60**, 218 (1930).
[3] W. Prandtl and K. Scheiner, Z. Anorg. u. allgen. Chem. **220**, 107 (1934).
[4] H. Gabrecht, Ann. Physik, Ser. 5, **31**, 600 (1935).
[5] H. Bethe and F. H. Spedding, Phys. Rev. **52**, 545 (1937).
[6] F. H. Spedding, Phys. Rev. **58**, 255 (1940).
[7] C. K. Jørgensen, Acta. Chem. Scand. **9**, 540 (1955).
[8] D. C. Stewart, Argonne National Laboratory Rept., ANL-5624 (October, 1956).
[9] U. Johnsen, Z. Physik **152**, 454 (1958).
[10] E. V. Sayre, K. M. Sancier, and S. Freed, J. Chem. Phys. **23**, 2060 (1955); *ibid.* **29**, 242 (1958).
[11] B. R. Judd, Proc. Roy. Soc. (London) **A241**, 414 (1957).
[12] G. H. Dieke and R. Sarup, J. Chem. Phys. **29**, 741 (1958).
[13] W. A. Runciman and B. G. Wybourn, University of Canterbury, Christ Church, New Zealand (private communication, to be published, 1959).
[14] J. B. Gruber and J. G. Conway, University of California Radiation Laboratory Rept. UCRL-8666 (March, 1959).
[15] E. U. Condon and G. H. Shortley, *The Theory of Atomic Spectra* (Cambridge University Press, New York, 1953).
[16] R. J. Elliott, B. R. Judd, and W. A. Runciman, Proc. Roy. Soc. (London) **A240**, 509 (1957).
[17] B. R. Judd, Proc. Roy. Soc. (London) **A228**, 123 (1955).

TABLE I. Pure electrostatic energy levels-f^{12} configuration.

Level	Electrostatic equations in terms of Slater integrals	Electrostatic equations in terms of F_2[a]	Energy levels normalized to $^3H=0$
^3H	$F_0-25\ F_2-51\ F_4-13\ F_6$	$F_0-32.3\ F_2$	$0.00\ F_2$
^3F	$F_0-10\ F_2-33\ F_4-286\ F_6$	$F_0-18.9\ F_2$	$13.4\ F_2$
^1G	$F_0-30\ F_2+97\ F_4+78\ F_6$	$F_0-15.5\ F_2$	$16.8\ F_2$
^1D	$F_0+19\ F_2-99\ F_4+715\ F_6$	$F_0+16.3\ F_2$	$48.4\ F_2$
^1I	$F_0+25\ F_2+9\ F_4+F_6$	$F_0+26.3\ F_2$	$58.6\ F_2$
^3P	$F_0+45\ F_2+33\ F_4-1287\ F_6$	$F_0+30.3\ F_2$	$62.6\ F_2$
^1S	$F_0+60\ F_2+198\ F_4+1716\ F_6$	$F_0+113.2\ F_2$	$145.5\ F_2$

[a] $F_4=0.138\ F_2$, and $F_6=0.0151\ F_2$.

to one another by selection rules will also be affected to a lesser extent. It is therefore necessary to introduce the spin-orbit interaction term (ζ) into the secular equations. The addition of the crystal-field interaction to the secular equations will be considered in a later paper.

Spedding has given the secular equations for f^2.[6] For the f^{12} configuration, one need change only the sign in front of each ζ value.[15] The authors divided each term and ζ value in Spedding's equation by F_2 and used the variable $\chi=\zeta/F_2$. The secular equations may be solved for energy/F_2 as a function of χ. Since all except the three-by-three equations were solved by hand, it is possible to give complete analytical expressions (see Table II). The values for the three-by-three equations were obtained from an IBM 650 program. The results of the calculations appear in Fig. 1.

B. EXPERIMENTAL STUDIES

Spectrographic Equipment

The spectra were taken on a Wadsworth spectrograph. Two gratings were used in this instrument—one with 30 000 lines-per-inch and another with 15 000 lines-per-inch—giving dispersions of 2.46 A/mm and 5.25 A/mm.

The light sources employed were an air-cooled high-pressure mercury lamp (BH6) and a commercially available Kistiakowsky-type hydrogen discharge lamp.[18] Quartz and Pyrex Dewars were used. Three types of polarizers were employed—a Nicol, an Ahrein with ultraviolet-transmitting cement, and a Wollaston. Iron and mercury lines served as wavelength references.

TABLE II. Analytical expressions for $E/F_2=f(\chi)$.

Levels	$E/F_2=f(\chi)$
$^3H_5$	χ
$^3F_3$	$13.4+\chi$
$^3P_1$	$62.5+\chi$
$^1S_0$	$104+\chi+\frac{1}{2}(196\chi^2-332\chi+6824)^{\frac{1}{2}}$
$^3P_0$	$104+\chi-\frac{1}{2}(196\chi^2-332\chi+6824)^{\frac{1}{2}}$
$^1I_6$	$29.3-2.5\chi+\frac{1}{2}(49\chi^2+586\chi+3440)^{\frac{1}{2}}$
$^3H_6$	$29.3-2.5\chi-\frac{1}{2}(49\chi^2+586\chi+3440)^{\frac{1}{2}}$

[18] G. B. Kistiakowsky, Rev. Sci. Instr. 2, 549 (1931).

The plates were measured on a precision screw-type comparator.

Crystals

The spectra of three crystals have been observed: $Tm(C_2H_5SO_4)_3\cdot 9H_2O$, $TmCl_3\cdot 6H_2O$, and $TmCl_3$ in $LaCl_3$. The ethylsulfate was prepared by mixing stoichiometric amounts of thulium sulfate and barium ethylsulfate. After the solutions were centrifuged to remove the $BaSO_4$, they were allowed to evaporate slowly at room temperature.

The hydrated chloride was grown by slow evaporation of a 6.0 N HCl solution. The $TmCl_3$ in anhydrous

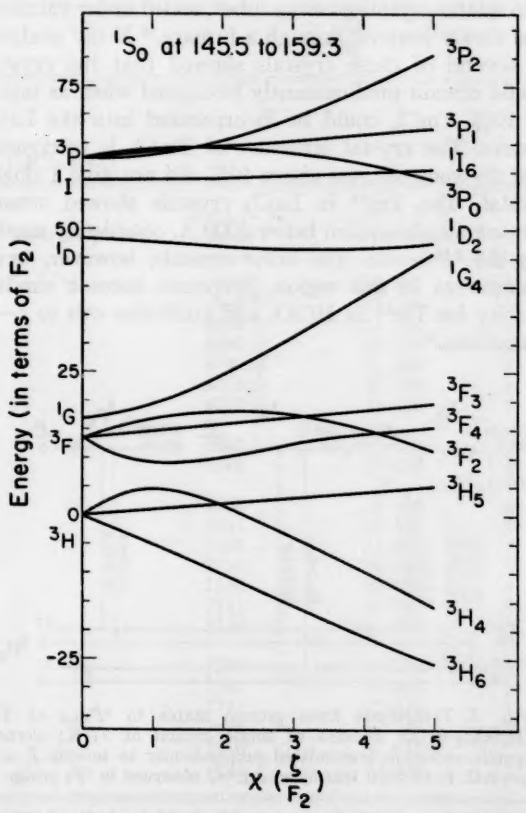

FIG. 1. Energy level diagram for Tm IV in intermediate coupling. The $^1S_0$ varies from 145.5, $\chi=0$, to 159.3 for $\chi=5$.

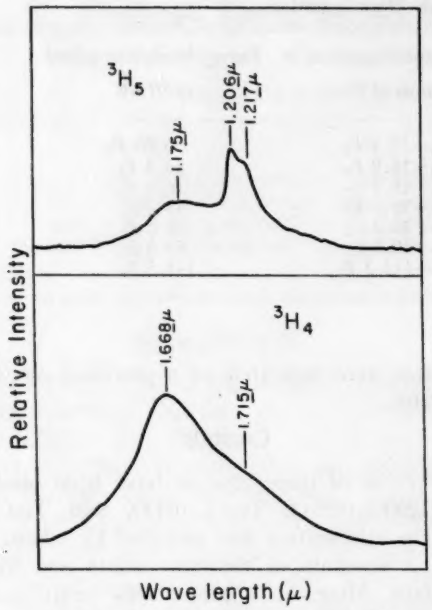

FIG. 2. The $^3H_5$ and $^3H_4$ multiplets in D_2O.

$LaCl_3$ crystal was prepared by sublimation of the mixed chlorides in vacuum. The purified mixture was melted into quartz crystal-growing tubes, sealed under vacuum, and slowly lowered through a furnace.[19] X-ray analysis of several of these crystals showed that the crystal would remain predominantly hexagonal when as much as 10% $TmCl_3$ could be incorporated into the LaCl matrix. The crystal structure of $TmCl_3$ is tetragonal and the compositions above 10% did not give a single crystal. The Tm^{3+} in $LaCl_3$ crystals showed strong continuous absorption below 3000 A, completely masking the ^3P levels. The other crystals, however, were transparent in this region. Jørgensen notes a similar opacity for Tm^{3+} in $HClO_4$ and attributes this to $f-d$ transitions.[20]

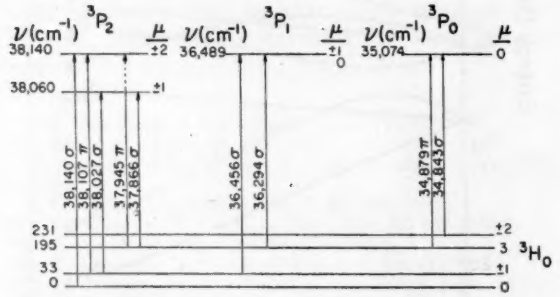

FIG. 3. Transitions from ground states to $^3P_{2,1,0}$ of Tm $(C_2H_5SO_4)_3 \cdot 9H_2O$. Spectra of single crystal at 77°K; electromagnetic radiation transmitted perpendicular to unique Z axis of crystal. Forbidden transition $3\pm\rightarrow 2$ observed in $^3P_2$ group.

[19] D. M. Gruen, J. G. Conway, and R. D. McLaughlin, J. Chem. Phys. **25**, 1102 (1956).
[20] C. K. Jørgensen, Acta Chem. Scand. **9**, 540 (1955).

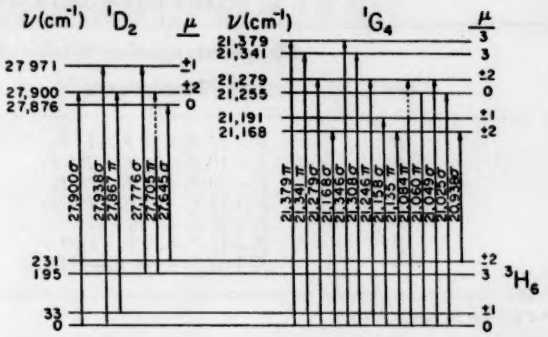

FIG. 4. Transitions from ground states to $^1D_2$ and $^1G_4$ of Tm $(C_2H_5SO_4)_3 \cdot 9H_2O$. Spectra of single crystal at 77°K; electromagnetic radiation transmitted perpendicular to unique Z axis of crystal. Forbidden transition $3\rightarrow\pm 2$ observed in $^1D_2$ and $^1G_4$ groups.

$^3H_4$ and $^3H_5$ Levels

The spectrum of 203.0 mg of anhydrous $TmCl_3$ in 10.0 ml of 0.10 M DCl in >98.5% D_2O was measured between 1 and 2 μ on a recording Cary 14 spectrophotometer. An acid solution was necessary in order to prevent the hydrolysis of the Tm^{3+} ion. Ordinary-water absorption bands appear around 1.4 μ and 1.8 μ, making it difficult to employ H_2O as a solvent for absorption studies in the region from 1 to 2 μ. In the case of D_2O, the isotope shift is far enough to the red (to about 2.2 μ) to make D_2O a useful solvent for studies in the region where the $^3H_5$ and $^3H_4$ levels are expected. Two peaks (1.175 μ and 1.206 μ) and one shoulder (1.217 μ) were found for the $^3H_5$, and one peak (1.668 μ) and one shoulder (1.715 μ) were found for the $^3H_4$ (see Fig. 2). The theoretical values calculated for $^3H_5$ and $^3H_4$ are 8520 cm^{-1} and 5320 cm^{-1}, which may be compared with the mean experimental values 8390 cm^{-1} and 5900 cm^{-1}, respectively.

C. RESULTS

Johnsen has identified the 0 and ± 1 crystal quantum levels of the $^3H_6$ ground state multiplet and the upper multiplets of $^3F_{2,3,4}$ and $^1G_4$. Our work confirms these

TABLE III. Comparison of theory with experiment.

	Values for energy levels (cm^{-1})	
Levels	Theory	Experiment
$^3H_6$	100	105
$^3H_4$	5320	5900
$^3H_5$	8520	8390
$^3F_4$	12 730	12 673[9]
$^3F_3$	14 550	14 446[9]
$^3F_2$	15 000	15 092[9]
$^1G_4$	21 120	21 275[9]
$^1D_2$	28 090	27 926
$^1I_6$	33 850	...
$^3P_0$	35 600	35 074
$^3P_1$	36 640	36 443
$^3P_2$	38 440	38 100
$^1S_0$	75 030	...

TABLE IV. Spectra, polarization, and crystal quantum transitions of $Tm(C_2H_5SO_4)_3 \cdot 9H_2O$.

Term assignment	Crystal quantum trans.	Wavelengths, intensities, and polarization 77°K (in air)	*I.*	*P.*	194°K (in air)	*I.*	*P.*	273°K (in air)	*I.*	*P.*	Wave numbers (in vacuum) 77°K	194°K	273°K
$^3P_2$	0→±2	2621.1	8[a]	σ	2621.7	6[c]	σ				38 140	38 132	
	±1→±2	2623.4	8[b]	π	2624.0	6[a]	π				38 107	38 099	
	±1→±1	2629.0	4[a]	σ	2629.3	6[a]	σ	2629.6	4[d]	σ	38 027	38 022	38 017
	3→±2	2634.6	4[a]	π	2635.1	6[a]	π	2635.4	5[d]	π	37 945	37 938	37 934
	3→±1	2640.0	1[b]	σ	2639.8	6[a]	σ	2640.1	6[d]	σ	37 866	37 870	37 866
$^3P_1$	±1→±1	2742.2	8[b]	σ	2743.1	5[a]	σ	2743.9	4[c]	σ	36 456	36 444	36 434
	3→±1,0	2754.4	3[b]	σ	2755.5	5[a]	σ				36 294	36 280	
$^3P_0$	3→ 0	2866.2	6[c]	π	2867.6	5[c]	π	2867.5	5[d]	π	34 879	34 863	34 862
	±2→ 0	2869.1	6[c]	σ	2870.4	5[d]	σ	2870.6	5[d]	σ	34 843	34 828	34 825
$^1D_2$	±1→±1	3578.3	9[d]	σ	3578.9	6[d]	σ	3579.0	6[d]	σ	27 938	27 934	27 933
	0→±2	3583.2	9[d]	σ							27 900		
	±1→±2	3587.4	9[c]	π	3587.9	6[c]	π	3589.7	4[d]	π	27 867	27 864	27 850
	3→±1	3599.2	5[a]	σ							27 776		
	3→±2	3608.6	4[a]	π	3608.7	6[a]	π	3608.4	8[a]	π	27 705	27 704	27 705
	±2→ 0	3616.2	3[a]	σ	3616.4	6[a]	σ	3616.9	8[a]	σ	27 645	27 644	27 640
$^1G_4$	0→ 3	4676.3	7[b]	π							21 379		
	±1→ 3	4683.4	7[a]	σ							21 346		
	0→ 3	4684.6	8[a]	π	4685.0	5[c]	π				21 341	21 339	
	±1→ 3	4691.8	6[d]	σ							21 308		
	0→±2	4698.2	5[d]	σ	4698.0	3[d]	σ				21 279	21 277	
	±1→±2	4705.5	6[b]	π	4708.7	3[d]	π				21 246	21 231	
	0→±2	4723.0	6[a]	σ							21 168		
	±1→±1	4725.0	6[a]	σ	4724.6	5[d]	σ				21 158	21 160	
	±1→±2	4730.2	6[a]	π							21 135		
	3→±2	4741.7	3[b]	π	4745.2	5[a]	π				21 084	21 068	
	3→ 0	4747.1	3[a]	π							21 060		
	±2→±2	4749.3	2[c]	σ							21 049		
	±2→ 0	4754.8	2[a]	σ							21 025		
	±2→±2	4774.5	2[b]	σ							20 938		

[a] Line width; 0.5 to 1.0 A.
[b] Line width; 0.1 to 0.5 A.
[c] Line width; 1.0 to 2.0 A.
[d] Line width; 2.0 to 4.0 A.

TABLE V. Spectra of $TmCl_3 \cdot 6H_2O$.

Term assignment	λ(A) 77°K (in air)	ν(cm⁻¹) 77°K (in vacuum)	*I*	Term assignment	λ(A) 77°K (in air)	ν(cm⁻¹) 77°K (in vacuum)	*I*
$^3P_2$	2590.9	38 585	8[a]	$^1G_4$	4629.2	21 596	8[c]
	2602.7	38 410	9[b]		4645.9	21 518	6[c]
	2611.5	38 281	8[a]		4649.5	21 502	9[b]
	2613.7	38 249	5[a]		4680.5	21 359	3[a]
	2622.0	38 127	4[c]		4709.8	21 226	4[a]
	2626.2	38 066	4[c]		4716.5	21 196	2[c]
					4719.8	21 181	1[a]
$^3P_1$	2734.3	36 562	4[c]				
	2743.5	36 439	6[d]	$^3F_2$[e]	.6567	15 220	5[b]
	2747.1	36 391	6[d]		6586	15 180	5[a]
$^3P_0$	2879.3	34 721	5[a]	$^3F_3$	7058	14 160	6[a]
					7064	14 150	9[b]
$^1D_2$	3552.7	28 140	6[c]		7104	14 070	7[c]
	3556.5	28 110	9[a]		7116	14 050	7[c]
	3560.0	28 082	9[a]		7140	14 020	4[c]
	3569.3	28 008	6[d]		7147	13 990	3[a]
	3573.2	27 978	6[d]		7159	13 970	3[a]
	3579.1	27 932	3[c]				
				$^3F_4$	7709	12 970	3[b]
					7781	12 850	3[b]
					7793	12 830	2
					7828	12 770	2
					7910	12 640	2
					7922	12 620	1

[a] Line width; 0.8 to 1.5 A.
[b] Broad complex of unresolved vibrational and electronic lines.
[c] Line width; 0.3 to 0.8 A.
[d] Line width; 0.1 to 0.3 A.
[e] $F_{2,3,4}$ measured to nearest 1 A.

TABLE VI. Spectra and polarization of anhydrous $TmCl_3$ in $LaCl_3$.

Term assignment	λ (A) 77°K (in air)	ν (cm⁻¹) 77°K (in vacuum)	P	I
$^1D_2$	3609.3	27 689	σ	5[a]
	3614.2	27 661	σ	5[a]
	3618.2	27 630	π	4[b]
	3621.6	27 604	σ	3[c]
	3626.3	27 569	σ	3[c]
	3630.9	27 534	π	4[a]
$^1G_4$	4708.0	21 234	π	4[a]
	4714.1	21 207	π	4[a]
	4733.0	21 122	σ	2[c]
	4636.1	21 109	σ	2[c]
	4740.6	21 088	π	3[b]
	4743.7	21 075	π	3[b]
	4752.0	21 038	σ	1[a]

[a] Line width; 0.1 to 0.5 A.
[b] Line width less than 0.1 A.
[c] Line width; 0.5 to 1.5 A.

ground state assignments for transitions to the ultraviolet multiplets of $^3P_{0,1,2}$ and $^1D_2$.

The symmetry of the Tm^{3+} ion in the ethylsulfate crystal is C_{3h} as given by Johnsen[9] and Ketelaar.[21] The crystal-quantum selection rules for this symmetry have been discussed previously.[10] The ultraviolet multiplets appear sharper than the $^3F_{2,3,4}$ group. As a result, one observes transitions from additional ground state crystal quantum levels to excited states. At 77, 194, and 273°K, the 3 and ±2 crystal quantum levels of the $^3H_6$ are populated. Transitions from these levels appear more intense as one goes from N_2 temperature (77°K) to CO_2 temperature (194°K). From the 3 and ±2 crystal quantum states the position of the $\mu=0$ level in $^1G_4$ was determined.

Figure 3 is the energy level diagrams for the $^3P_0$, $^3P_1$, $^3P_2$ multiplets; Fig. 4 is the diagram for the $^1D_2$ and $^1G_4$. The $^3F_{2,3,4}$ lines are too broad to permit an extension of the analysis. Polarized lines are observed between the $^3P_0$ and $^3P_1$ multiplets which are not due to impurities. These lines are probably due to the $^1I_6$ multiplet. The lines are faint and difficult to distinguish from vibrational lines of the $^3P_0$ and $^3P_1$. As many as ten vibrational lines per multiplet appear to the violet of the $^3P_2$ and $^1D_2$.

[21] J. A. A. Ketelaar, Physica **4**, 619 (1937).

Holmium and erbium ethylsulfate crystals were prepared and polarization spectra taken to determine if these impurities appeared in the Tm spectra. No lines of Er or Ho were observed in the Tm spectra taken.

The experimental data, including Johnsen's, were fitted to Fig. 1 and a good fit was obtained for $\chi=3$, $F_2=450$ cm⁻¹, and ζ_{4f} 2700 cm⁻¹. The spin-orbit interaction term ζ as used in Fig. 1 and in Spedding's work is one-half this value. From these parameters the calculated positions were obtained and are tabulated in Table III. Table IV includes the measured wavelengths, their intensity and polarization, and the crystal quantum transitions for the ethylsulfate.

Table V gives the wavelength and intensity for the lines appearing in the spectrum of $TmCl_3 \cdot 6H_2O$. The similarity in the spectra of the hydrated chloride and the ethylsulfate allows us to assign the multiplets, but the crystal quantum assignment cannot be made because the point symmetry of the Tm^{3+} ion is not known. Table VI gives the wavelengths and intensities for the $TmCl_3$ in $LaCl_3$. The only multiplets seen are the $^1D_2$ and $^1G_4$. The continuous absorption in the ultraviolet masks the ^3P levels, and the ^3F levels are too weak for good measurements.

DISCUSSION OF ERRORS

The spectral lines of the $^3P_{0,1,2}$ and $^1D_2$ groups are measured to ±0.1 A; the $^1G_4$ lines are measured to ±0.2 A. It is not possible to measure the positions of lines more accurately than this because line widths are considerable in many cases. In some cases the calculated energy levels (Table III) differ from the experimental value by as much as 200 cm⁻¹. This lack of agreement is due to (a) the theoretical calculations for the field-free ion are good only to 100 cm⁻¹, (b) the perturbing influence of the neighboring ligands in the crystal will shift the centers of the stark-split j levels from the field-free j level calculations, and (c) the center of gravity of the crystal-field split levels cannot be known without a detailed calculation of the crystal-field splitting.

ACKNOWLEDGMENT

We wish to acknowledge the help of B. B. Cunningham, R. D. McLaughlin, K. S. Pitzer, and J. D. Axe. This work was done under the auspices of the U.S. Atomic Energy Commission.

Application of a High-Speed Electronic Computer in Diffusion Kinetics. II. Depletion Effect in the Spherical One-Radical One-Solute Model*

HUGO FRICKE AND DAVID L. PHILLIPS

Chemistry and Applied Mathematics Divisions, Argonne National Laboratory, Lemont, Illinois

(Received October 30, 1959)

The earlier computations [D. A. Flanders and H. Fricke, J. Chem. Phys. 28, 1126 (1958)] on the Spherical One-Radical One-Solute model were extended by taking account of the transient dilution of the solute which occurs during the reaction. Although the drop in concentration of the solute near the center of the reaction zone may be considerable, its effect on the fraction of radicals combining with the solute is only of the order of one percent under the most unfavorable conditions likely to be encountered when the model is applied to γ-irradiated aqueous solutions.

THE first work[1] of this series was deficient in that it did not take into account the effect of the transient dilution of the solute which occurs due to its reaction with the radical. This problem has now been studied for the case of the spherical model by adding Eqs. (3a) and (4a) to the previous system of equations:

$$\partial C/\partial t = D_1(\partial^2 C/\partial r^2) + [(2D_1/r](\partial C/\partial r) - \beta C n \quad (3a)$$

$$t=0: \qquad C=C_0. \quad (4a)$$

C represents as before the concentration of the solute which is now a function of r and t; C_0 is the initial value of C; and D_1 is the coefficient of diffusion of the solute. Otherwise, the notation is the same as before.

The computation was essentially carried out as in reference 1 but instead of AVIDAC, we used the Argonne computer GEORGE which has eight times as large a word memory as AVIDAC and, in addition, computes twice as fast. A finer interval than before could therefore be used for R ($P=16$ and 32) and the values of I_S are now believed accurate to within 2/10%.

The problem can be defined by four dimensionless parameters. In addition to $E=\alpha N_0/\pi^{\frac{1}{2}}bD$ and $B=\beta C_0 b^2/4D$ of the foregoing model,[1] we used β/α and D_1/D. All computations were carried out with $E=2.50$, which is the approximate value obtained for E when the model is applied to γ-irradiated water.

As reflected in I_S, which represents the fraction of radicals which combine with the solute, the depletion effect was found to be small and it could be established only when β/α was relatively large. If it is assumed that the radicals combine at each encounter, the highest value to be expected for β/α is of the order of 2, which value might be obtained if radicals and solute molecules react at each encounter. Table I shows the values of I_S computed with this value of β/α, for the extreme case of $D_1/D=0$ and for different values of B. The depletion effect is obtained by comparing these values of I_S with those obtained with $D_1/D=\infty$. The latter case is that calculated in reference 1 but the calculation was repeated with greater accuracy and the values obtained are shown in Table I. It will be seen that even in this extreme case, the largest decrease in I_S owing to the depletion effect is little more than 1% (obtained with $B=0.1$).

When D_1/D is increased above zero, I_S remains nearly constant until values of D_1/D of the order of unity are reached. For values of D_1/D in the experimentally significant range around 0.2, I_S is at $B=0.1$ only 1/10% larger than the value obtained for $D_1/D=0$ (Table I). In its effect on the rate of reaction of radical with

TABLE I. Depletion effect in spherical reaction zone, $E=2.50$.

	$\frac{\beta}{\alpha}$	$\frac{D_1}{D}$	log B 1	0	−1	−2	−3
I_S	2	0	0.980	0.881	0.713	0.612	0.572
	2	0.01			0.713		
	2	0.2			0.714		
	2	1.			0.716		
	...	∞	0.980	0.886	0.722	0.615	0.573
	0.1	0			0.722		

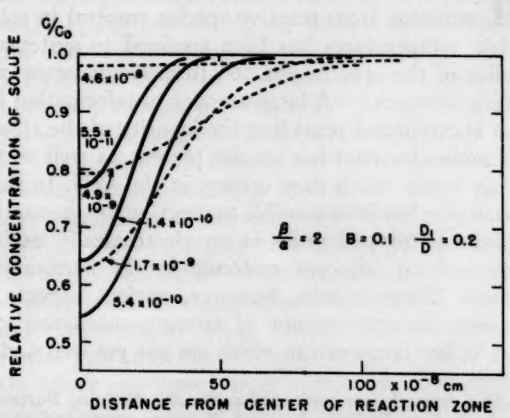

FIG. 1. Concentration of solute in spherical zone at different times (shown in seconds) during the reaction for $\beta/\alpha=2$, $D_1/D=0.2$, $B=0.1$. The radicals were produced instantaneously at zero time. The solid lines represent the concentration of the solute during the period in which the concentration is decreasing; the dashed lines represent the concentration during the period of recovery which begins when 44% of the radicals have been consumed in the reaction.

* Based on work performed under the auspices of the U. S. Atomic Energy Commission.

[1] D. A. Flanders and H. Fricke, J. Chem. Phys. 28, 1126 (1958).

solute, the depletion effect appears therefore to be of negligible importance in the γ irradiation of water.

The smaller the value of β/α, the higher is the concentration of solute required to obtain a fixed value of B, and the smaller the depletion effect would therefore be expected to be. The table includes the value of I_S computed for $\beta/\alpha=0.1$ and $D_1/D=0$, at $B=0.1$. No effect of the depletion can be seen.

In spite of the small effect of the depletion on I_S, the transient changes in concentration of the solute in the core of the expanding reaction zone may be quite large.

Figure 1 shows the concentration of the solute in the reaction zone at different times dur ng the reaction for $\beta/\alpha=2$, $D_1/D=0.2$ and $B=0.1$. To obtain the radius and time in absolute units we used $D=4.5\times10^{-5}$ cm^2 sec^{-1} and $b=18\times10^{-8}$ cm, which are reasonable values for these quantities when the model is applied to γ-irradiated water. In the center of the zone, the maximal drop in concentration of solute was 46%, reached after 0.46×10^{-9} sec, at which time 44% of the radicals had reacted. (The lowest curve in the figure was computed at 0.54×10^{-9} sec, slightly later than the time at which the maximal drop occurred.) After 4.6×10^{-8} sec, the concentration of the solute at the center of the zone has nearly returned to its original value, and the reaction has now been practically completed.

If I_S is plotted against log$B$, for $D_1/D=0$ and ∞, it will be seen that the depletion effect does not greatly affect the form of this curve. The curve for $D_1/D=0$ is displaced horizontally about 10% in B toward the side of larger B's, with respect to the curve for $D_1/D=\infty$. In other words, the depletion effect for $D_1/D=0$ is approximately equivalent to a decrease in concentration of the solute of 10%.

THE JOURNAL OF CHEMICAL PHYSICS VOLUME 32, NUMBER 4 APRIL, 1960

Spectra Emitted from Rare Gas-Oxygen Solids during Electron Bombardment*

L. J. SCHOEN AND H. P. BROIDA

National Bureau of Standards, Washington, D. C.

(Received November 2, 1959)

Light emission from rare gas solids containing small amounts of oxygen has been excited by an electron bombardment technique. The Herzberg bands of oxygen and a line group believed to be the $^1S\rightarrow{}^1D$ transition of the neutral oxygen atom form the strongest features of the observed spectra. In a neon matrix, the Second Negative system of O_2^+ has been identified. The effect of the various solids on the vibrational structure of the Herzberg bands is discussed.

I. INTRODUCTION

MUCH of the recent work concerned with light emission from reactive species trapped in solids at low temperatures has been confined to systematic studies of the spectra emitted from condensates containing nitrogen.[1–4] A large amount of information has been accumulated regarding the identity of the atomic and molecular emitting species present as well as the energy levels which they occupy in the solid. In some instances it has been possible to describe the interaction between a trapped atom in an electronically excited state and an adjacent molecule in the surrounding matrix.[5] There remain, however, various aspects of the emission spectroscopy of nitrogen-containing systems at low temperature which are not yet well understood. In order to obtain additional information concerning the interaction between a trapped species and its solid environment, an analogous study of several nitrogen-free systems containing oxygen was initiated. The matrices selected for this work were the rare gases, neon, argon, krypton, and xenon. It was thought that the type of information available from such a study would contribute to the general understanding of the nature of solids containing stabilized atoms or radicals at low temperatures.

In the current work, an electron bombardment technique was employed to produce electronically excited atoms and molecules in the deposit. In the absence of trace amounts of nitrogen, two systems dominate the observed spectra. The first, the Herzberg bands[6] of the oxygen molecule $C\,^3\Sigma_u^+\rightarrow X\,^3\Sigma_g^-$ have been observed in nitrogen and in the rare gas matrices with the exception of neon. The second, a diffuse line group near 5600 A is probably due to the $^1S\rightarrow{}^1D$ transition of the neutral oxygen atom. The similarities in gross

* This research was performed under the National Bureau of Standards Free Radicals Research Program, supported by the Department of the Army.

[1] A. M. Bass and H. P. Broida, Phys. Rev. **101**, 1740 (1956).

[2] M. Peyron and H. P. Broida, J. Chem. Phys. **30**, 139 (1959).

[3] E. M. Hörl, J. Mol. Spectroscopy **3**, 425 (1959).

[4] L. J. Schoen and R. E. Rebbert, J. Mol. Spectroscopy **3**, 417 (1959).

[5] M. Peyron, E. M. Hörl, H. W. Brown, and H. P. Broida, J. Chem. Phys. **30**, 1304 (1959).

[6] Referred to as the A bands in previous publications. Experiments with the O_2^{18} isotope have established the identification (H. P. Broida and M. Peyron, J. Chem. Phys. **32**, 1068 (1960)).

structure between this group and the analogous β transition in nitrogen solids[2] decrease as one goes from oxygen-neon to oxygen-xenon mixtures. Another strong system which appeared to be present only in neon-oxygen deposits has been identified as the $A\ ^2\Pi_u \rightarrow X\ ^2\Pi_g$ bands of O_2^+. This is the first electronically excited diatomic ion that we have observed in a low temperature solid. If a small quantity of nitrogen impurity is included in these rare gas-oxygen solids, in addition to the systems already described the $B\ ^2\Pi - X\ ^2\Pi$ bands of NO and the $A\ ^3\Sigma_u^+ \rightarrow X\ ^1\Sigma_g^+$ bands of N_2 may occur. The rare gas condensates without added gases have been found to emit light when subjected to bombardment at 4.2°K. These spectra consist of broad continua on which are superimposed a small number of emission lines most probably due to trace quantities of impurities.

II. EXPERIMENTAL

The experiments were carried out in a Pyrex glass Dewar of the type previously described.[7] Highest purity commercial gases estimated to contain several parts per hundred thousand or less of extraneous materials were employed without further purification. Details of the apparatus are shown in Fig. 1. Rare gas-oxygen mixtures of the desired composition, after passing through a flowmeter and a variable precision leak, were deposited on the wall of a liquid helium-cooled, electrically grounded copper cell. Deposition of the mixtures was carried out at gas flow rates less than 1 cm³/min (STP) for 3.5 min. A dc potential was then applied between either of two tungsten wire electrodes and the cell, the electrodes being maintained negative by about 5000 v. Currents were limited by means of a dropping resistor to approximately 100 μ. Temperature measurements were made by means of thermocouples mounted on the liquid helium cooled surface in the region where deposition took place. Although the temperature was not determined during bombardment, measurements made less than 0.5 sec after the termination of bombardment showed no detectable temperature rise. Under the conditions described, a relatively bright glow was excited in the solid, consisting in general of one or more bright patches or glowing areas. The locus of these bright regions in the solid appeared to depend on the orientation and previous history of the tungsten electrodes. The mechanism of excitation is thought to involve a field emission initiation process and subsequent electron bombardment of the deposit. Simultaneous negative ion bombardment of the solid can not be precluded under these conditions.

The emitted light was viewed through quartz windows on either side of the cold surface, and focused by quartz or glass lenses on the spectrograph slits. Two $f/10$ prism spectrographs, employing quartz and glass optics, respectively, were used. The former gave a resolution of about 0.5 A at 2600 A and the latter approximately 1.5 A at 5200 A. An $f/4$ quartz instrument having a resolution of about 0.8 A at 2600 A was employed for photographing several of the relatively weak spectral features. A few measurements also were made with an $f/0.625$ transmission grating spectrograph that could resolve approximately 6 A.

The majority of experiments were carried out at a temperature of 4.2°K by cooling the copper surface containing the deposited material with liquid helium at atmospheric pressure. By reducing the pressure above the liquid to a few hundred microns, temperatures of 1.2° K could be attained. Filling the Dewar with liquid hydrogen at atmospheric pressure allowed experiments to be carried out at 20.4°K.

III. RESULTS

A. General and Spectroscopic Observations

Oxygen in a Krypton Matrix

During bombardment of a 1% oxygen-in-krypton condensate at 4.2°K the glow observed from the solid was a deep yellow in color. Weak flashes occurring in the interior or on the surface of the deposit were visible at random intervals. The region of light emission varied in size and appearance from a great many small bright spots to one or more glowing areas of 1 to 1.5 cm². By adjusting the orientation of the tungsten electrodes with respect to the liquid helium cooled surface, it was always possible to cause these small glowing areas to coalesce into larger ones which would remain fixed in position for periods up to several hours. The electrode adjustments could conveniently be made by means of the glass ball joint mountings illustrated in Fig. 1.

The more prominent features of the spectra obtained from the 1% oxygen-in-krypton solid in the wavelength region 3500 to 7000 A are illustrated in Figs. 2(b_1) and 3(c). The observed wavelengths and relative intensities are summarized in Table I. Intensities are visual estimates of plate blackening ranging from 1 to 2450. An intensity of 1 indicates the weakest feature visible in an exposure time of 200 sec with the $f/4$ quartz spectrograph used with 103a-O plates. An intensity of 2450 represents the most intense feature which was photographed in less than 10 seconds by the $f/10$ glass instrument employing 103a-F plates. On this scale, the strongest band of the Herzberg system occurred with an intensity of approximately 100.

On heavy exposures taken during the excitation of oxygen-krypton solids at 4.2°K a relatively weak group of bands occurs in the region of the most intense Herzberg emission. These (denoted by an *s* in Table I) appear as satellites of the Herzberg bands, lying on both the short and long wavelength sides of members of the latter system as shown in Fig. 2(b_2). Although there appears to be some degree of regularity present

[7] L. J. Schoen, L. E. Kuentzel and H. P. Broida, Rev. Sci. Instr. 29, 633 (1958).

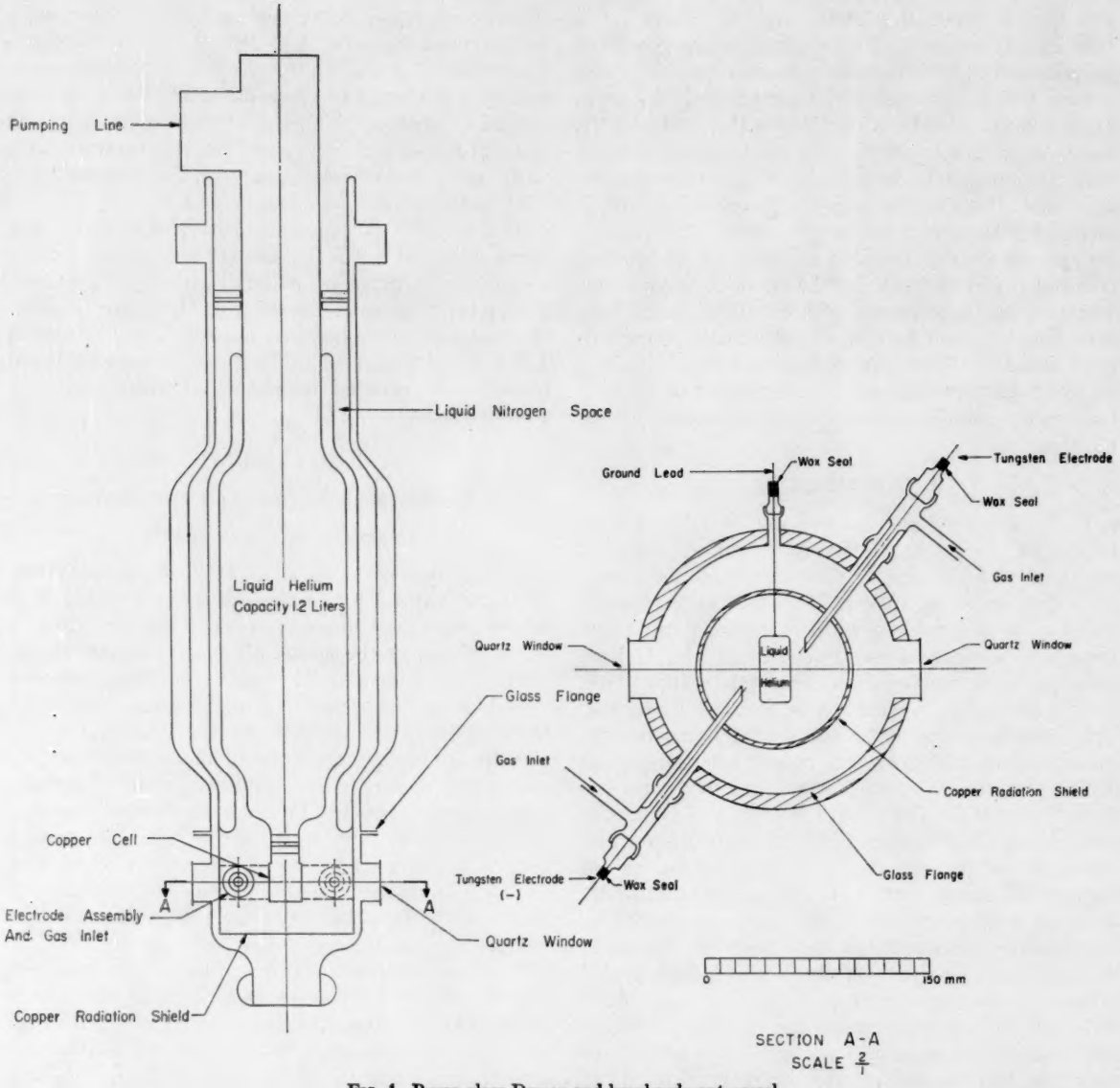

FIG. 1. Pyrex glass Dewar and bombardment vessel.

in their relationship to the Herzberg system, their identification has not been established.

An extremely weak, diffuse feature with unresolved structure appears near 2960 A in krypton (and in argon and neon) solids containing small amounts of oxygen. Because of the similarity of the wavelength region, it is possible that this group represents the $^1S \rightarrow {}^3P$ transition of the neutral oxygen atom which lies at 2972 A in the gas phase.

Oxygen in an Argon Matrix

The wavelengths and relative intensities obtained by bombardment of a 1% oxygen-in-argon solid at 4.2°K, were found to be similar to those listed in Table I for the oxygen-krypton system. The same strong spectral features seen in Fig. 3 were present. However, corresponding members of a given system may be shifted in wavelength with respect to the values obtained in matrices other than argon. The observed frequencies in cm^{-1} and relative intensities for the Herzberg bands of oxygen in the argon solid are given in Table IV. Some weak satellites appear near the stronger Herzberg bands (as in krypton but not in xenon). The glowing solid was pale blue in color, random flashes were observed, and as in the case of krypton, one or more relatively large zones of high intrinsic brightness could be formed.

Oxygen in a Xenon Matrix

Figures 2(c) and 3(d) illustrate the spectra obtained from a 1% oxygen-in-xenon solid at 4.2°K. A small amount of nitrogen impurity was undoubtedly present

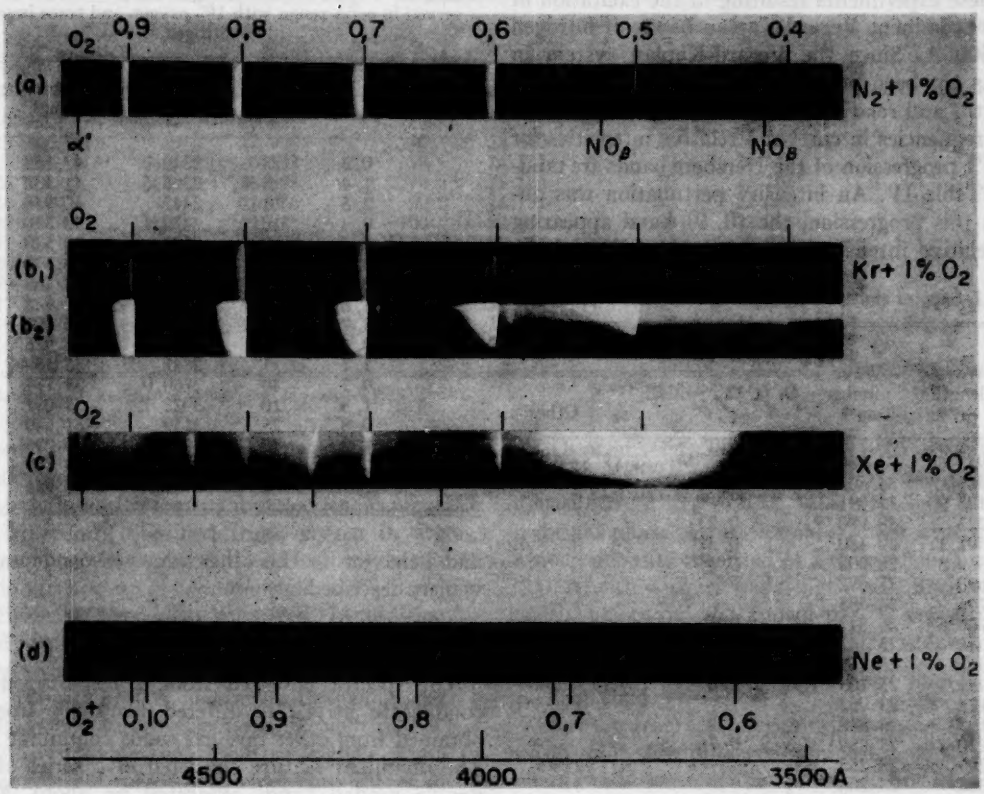

FIG. 2. Emission from oxygen-nitrogen and oxygen-rare gas solids; quartz prism spectrograph $f/10$; 103 a–O plates: (a) $N_2+1\%\ O_2$; (b_1) $Kr+1\%\ O_2$, exposure time 90 sec; (b_2) $Kr+1\%\ O_2$, exposure time 40 min; (c) $Xe+1\%\ O_2$; (d) $Ne+1\%\ O_2$.

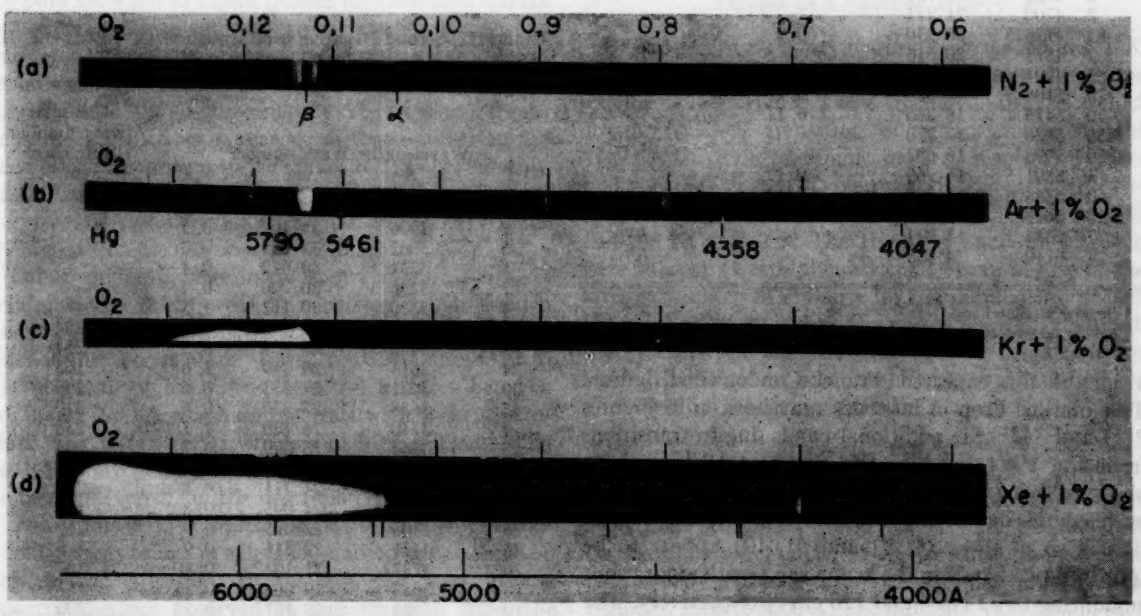

FIG. 3. Emission from oxygen-nitrogen and oxygen-rare gas solids; glass prism spectrograph $f/10$; 103 a–F plates: (a) $N_2+1\%\ O_2$; (b) $Ar+1\%\ O_2$; (c) $Kr+1\%\ O_2$; (d) $Xe+1\%\ O_2$.

during these experiments resulting in the excitation of the more prominent Vegard-Kaplan bands of nitrogen below 3500 A. Since the Vegard-Kaplan system in xenon has not been previously reported, the observed wavelengths and relative intensities are given in Table II. The frequencies in cm^{-1} and relative intensities for the (o, v'') progression of the Herzberg bands are tabulated in Table IV. An intensity pertubation was observed in this progression, the (0, 9) band appearing with a relative intensity approximately 1/250 of the value of the expected Franck-Condon distribution. This marked drop in intensity may be seen in Figures 2(c) and 3(d). Six additional bands due to transitions from the $v'=1$ level of the upper state have been observed lying approximately 1400 cm^{-1} to the short wavelength edge of the members of the main progression. Two of these (1, 9) and (1, 12) appear to be split into two bands in the xenon solid, with separations amounting to 32 cm^{-1} and 126 cm^{-1}, respectively. The latter separation is clearly shown in Fig. 3(d). The light emitted from the deposit was whitish-yellow in color; otherwise the solid was similar in appearance and behavior to the other rare gas condensates previously described.

TABLE I. Spectra emitted by 1% oxygen in solid krypton.

I	Wavelength A	Wave number cm^{-1}	Identification O_2 ($C\,^3\Sigma_u^+ \rightarrow X\,^3\Sigma_g^-$) v', v''	Other
1	2953–60	33 854–774		$O\,^1S \rightarrow {}^3P$?
3	2984	33 502		?
2	3125–90	31 991–339		continuum
5	3227	30 980	0, 2?	
10	3391.1	29 480	0, 3?	
30	3569.8	28 005	0, 4	
2	3690	27 092		s[a]
3	3746	26 688		s
50	3766.5	26 542	0, 5	
3	3941	25 367		s
5	3957	25 264		s
70	3982.5	25 103	0, 6	
3	4172	23 962		s
5	5192	23 848		s
85	4220.2	23 689	0, 7	
2	4299	23 255		s
3	4308	23 206		s
2	4422	22 608		s
2	4455	22 440		s
100	4483.5	22 298	0, 8	
3	4574	21 856		s
4	4593	21 766		s
2	4700	21 271		s
85	4776.5	20 930	0, 9	
2	4873	20 516		s
3	4904	20 386		s
70	5104.5	19 585	0, 10	
70	5473.1	18 266	0, 11	
2450	5626	17 770		$O\,^1S \rightarrow {}^1D$
1850	5993	16 682		$O\,^1S \rightarrow {}^1D$
m	5891.5	16 969	0, 12	
60	6368.6	15 698	0, 13	
20	6641	15 054		K[b]
7	6654	15 024		K[b]
4	6740	14 833		K[b]

[a] Denotes satellite lines.
[b] Similar features appear in solid argon at 6588, 6610, and 6720 A.

TABLE II. Vegard-Kaplan nitrogen bands ($A\,^3\Sigma_u^+ \rightarrow X\,^1\Sigma_g^+$) observed in solid xenon with 1% oxygen and trace impurity of nitrogen.

v', v''	I	Wavelength A	Wave number cm^{-1}
0, 3	3	2349.0	42 558
1, 4	3	2395.5	41 732
2, 5	1	2442	40 938
0, 4	10	2479.4	40 320
1, 5	2	2529	39 530
2, 6	2	2580	38 748
0, 5	25	2623.3	38 108
1, 6		not observed	
2, 7	2	2732	36 592
0, 6	30	2782.7	35 926
1, 7	1	2841	35 189
0, 7	40	2760.0	33 774
1, 8	10	3022	33 081
0, 8	25	3159	31 646
1, 9	25	3225.4	30 995
0, 9	15	3382	29 560
1, 10	15	3454	28 944

Oxygen in a Neon Matrix

The spectra observed from a 1% oxygen-in-neon condensate at 4.2°K differed markedly from those obtained from other rare gas solids containing oxygen. The dominant feature consisted of a series of diffuse double headed bands separated by about 200 cm^{-1} which have been identified as the Second Negative system of O_2^+ in the solid. The magnitudes of the observed wavelength shifts occurring when O_2^{18} is

TABLE III. Second Negative band system of O_2^+ ($A\,^2\Pi_u \rightarrow X\,^2\Pi_g$) emitted by 1% oxygen in solid neon.

I	Wavelength[a] A	Wave number cm^{-1}	v', v''	Gas-solid wave number difference[b] cm^{-1}
2	2906	34 402	0, 2	
5	3062	32 649	0, 3	
8	3234	30 912	0, 4	
7	3256	30 700	0, 4	
4	3320	30 112	1, 5	
9	3424	29 197	0, 5	224
8	3451	28 969	0, 5	254
4	3514	28 449	1, 6	163
20	3631	27 533	0, 6	206
15	3658	27 330	0, 6	210
4	3740	26 730	1, 7	238
25	3860	25 899	0, 7	203
20	3891	25 693	0, 7	206
25	4119	24 271	0, 8	220
20	4149	24 095	0, 8	194
25	4405	22 695	0, 9	219
25	4441	22 511	0, 9	215
20	4737	21 104	0, 10	267
10	5083	19 668	0, 11	187
10	5503	18 167	0, 12	200

[a] Wavelength measurements uncertain to 20 cm^{-1}.
[b] Gas values from Pearse and Gaydon, reference 8.

TABLE IV. Emission of $O_2(C\,^3\Sigma_u^+ \rightarrow X\,^3\Sigma_g^-)$ in the gas phase and in nitrogen and rare gas solids.

v', v''	Gas[a] cm^{-1}	Nitrogen I	Nitrogen cm^{-1}	Argon I	Argon cm^{-1}	Krypton I	Krypton cm^{-1}	Xenon I	Xenon cm^{-1}
0, 3	30 408	20	29 457						
0, 4	28 922	40	27 991	30	28 040	30	28 005		
0, 5	27 459	55	26 532	50	26 587	50	26 542	m	26 588
0, 6	26 019	70	25 093	70	25 160	70	25 103	65	25 144
0, 7	24 601	85	23 676	90	23 751	85	23 689	100	23 718
0, 8	23 206	100	22 281	100	22 360	100	22 298	50	22 325
0, 9	21 834	90	20 908	90	20 994	85	20 930	1/5	20 945
0, 10	20 484	55	19 560	60	19 648	70	19 585	40	19 595
0, 11	19 157	40	18 232	70	18 325	70	18 266	m	18 295
0, 12	17 853	20	16 932	70	17 021	m	16 969	not observed	
0, 13	16 571	15	15 662	60	15 741	60	15 698	m	15 739
0, 14	15 312			15	14 487?				

[a] Extrapolated from the calculated values given in reference 9.

substituted in the neon solid confirm the assignment. The bands are shown in Fig. 2(d), and wavelengths and relative intensities are tabulated in Table III.[8] Unlike the spectra obtained from oxygen in argon, krypton, and xenon matrices, the Herzberg bands of oxygen do not appear in neon deposits at 4.2°K under the conditions of excitation employed. In addition to the band system assigned to O_2^+ a group of twelve relatively weak but sharp lines have been observed between 3300 and 3750 A, identical with the line spectra arising from low lying transitions of Ne^+ in the gas phase. It is probable that these have their origin in the bombardment of vapor which has either been distilled from the surface of the solid during irradiation, or which has remained uncondensed in the interior of the Dewar. In this connection, the difficulty of depositing pure neon gas at liquid helium temperatures should be pointed out. Substantial rates of evaporation of the refrigerant have been encountered during deposition on glass or metal surfaces at 4.2°K. It has been found in the current work that approximately 1% of a more condensable gas such as oxygen or nitrogen added to the neon allows deposition to take place relatively smoothly and efficiently with essentially normal liquid helium loss rates. (An analogous effect has been observed for the deposition of hydrogen at 4.2°K.)

Other unidentified emission observed from the neon solid includes seven weak structureless bands (width about 50 cm^{-1}) between 3100 and 4100 A, three sharp lines (width about 5 cm^{-1}) at 2963, 3089, and 4370 A, and a group of ten diffuse spectral features between 6150 and 7950 A which do not shift with O_2^{18} substitution. The latter group which remained unchanged in both 1% nitrogen-neon and high purity neon is thought to be characteristic of the neon solid.

A band at 7943 A which did not shift with O_2^{18} substitution was found to exhibit a marked dependence on oxygen concentration. It was also the most intense spectral feature observed in the emission from the 1% O_2-neon solid. This band has been assigned to the (0, 0) transition of the atmospheric absorption bands of oxygen ($A\,^1\Sigma_g^+ \rightarrow X\,^3\Sigma_g^-$) which lies at 7594 A in the gas phase. An additional strong feature occurring in neon deposits consisted of a diffuse band just above 2537 A with a short wavelength tail. Both the wavelength region and the known partial pressure of mercury in the gas samples (about 1 μ) suggest that this is the $^3P \rightarrow {}^1S$ transition of the neutral mercury atom in the neon solid.

The glow from the oxygen-neon condensate was deep red in color. The observed luminosity slowly decreased with time because of the sputtering of metal from the tungsten cathode on to the deposit. This process was favored by the relatively high volatility of the neon condensate.

Oxygen in a Nitrogen Matrix

Irradiation of a 1% oxygen-in-nitrogen solid at 4.2°K led to the appearance of a number of spectral features previously reported.[2] These included the α and β groups ($^2D \rightarrow {}^4S$ transition of atomic nitrogen and $^1S \rightarrow {}^1D$ transition of atomic oxygen, respectively), as well as the Vegard-Kaplan bands of nitrogen, the Herzberg bands of oxygen (Table IV), bands of NH and the NO_β system. The Herzberg bands in nitrogen were sharper (width about 5 cm^{-1}) than in any of the rare gas matrices employed. The luminosity of the observed green glow was the most homogeneous of all the systems studied, the difference in brightness between the brightest and least bright regions being a minimum for the nitrogen solid.

Rare Gas Solids

Several experiments were performed in which neon, argon, krypton, and xenon solids were subjected to bombardment at 4.2°K. With the exception of neon, continua were observed for each rare gas in the general region of 2500 to 5000 A. The intensity variation in each continuum is of a complex nature and not easy to describe accurately. As an approximation to the

[8] R. W. B. Pearse and A. G. Gaydon, *The Identification of Molecular Spectra* (Chapman and Hall, Ltd., London, 1950).

TABLE V. Intensity distribution of continua emitted from rare gas solids.

	2500 A	2750 A	3000 A	3250 A	3500 A	3750 A	4000 A	4250 A	4500 A	4750 A	5000 A
Argon	10	9	5	3	8	4	7	7	6	5	4
Krypton	10	6	7	5	10	10	10	6	4	5	3
Xenon	9	7	10	10	9	10	10	6	4	2	1

observed distribution, estimated relative intensities based on an arbitrary scale of 0–10 for each rare gas solid are given in Table V at 250-A wavelength intervals. Representative regions of these continua are illustrated in Fig. 4(a)–(c). The variation in appearance of the continua with exposure time is illustrated in Fig. 4(c)–(e) for the case of the xenon continuum. When a small amount of oxygen was deposited on the surface of one of the rare gas condensates and the resulting two-layer solid subjected to irradiation, the continuum, was still present but reduced in intensity in the region of the Herzberg bands and at shorter wavelengths. This effect is illustrated in Fig. 4(f) for an oxygen-xenon solid.

B. Spectral Systems

Herzberg Bands

These bands of molecular oxygen ($C\,^3\Sigma_u^+ \rightarrow X\,^3\Sigma_g^-$) appear when oxygen is incorporated into all but one (neon) of the matrices employed in the current work. The sharpest bands are obtained from a nitrogen

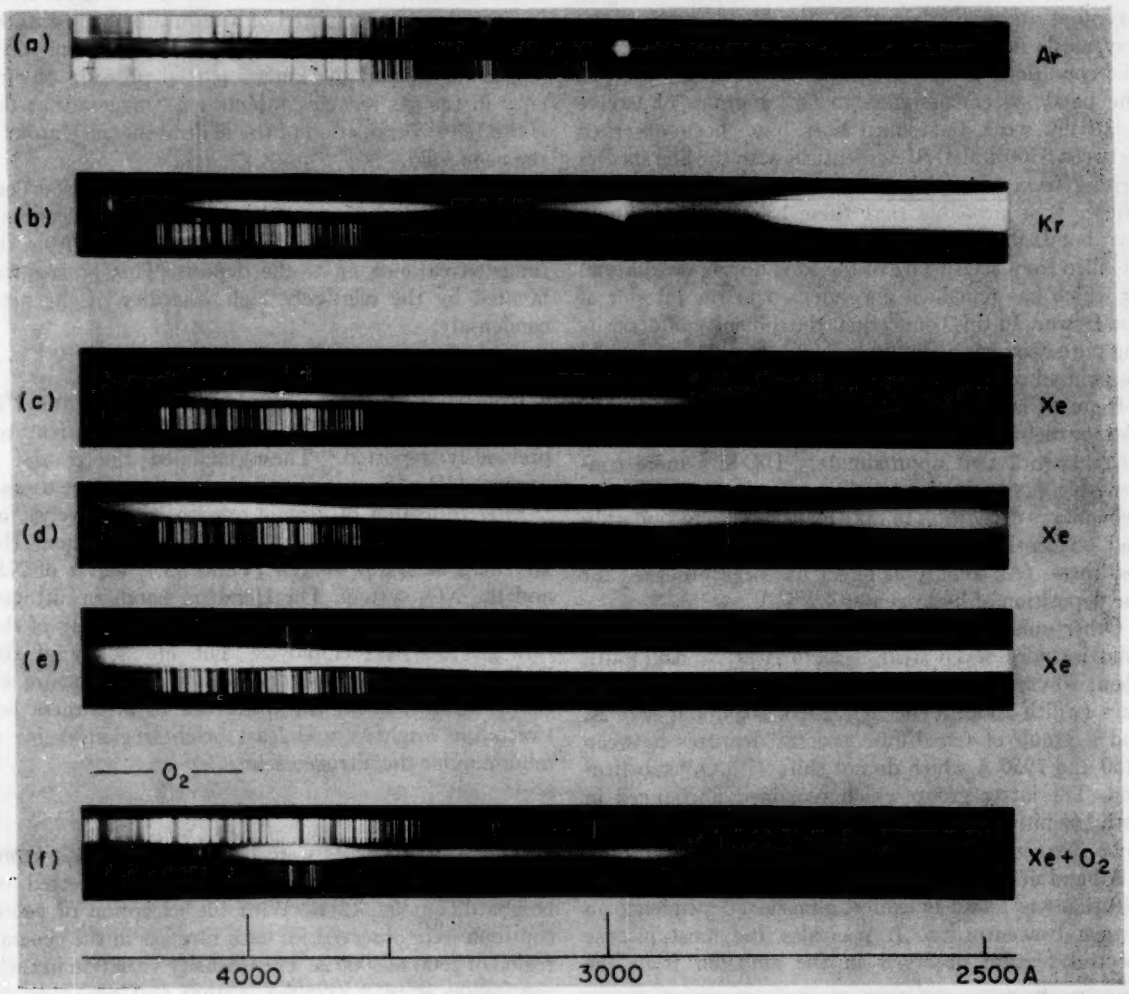

FIG. 4. Emission from rare gas solids; quartz prism spectrograph f/4; 103 a-O plates: (a) Argon; (b) Krypton; (c) Xenon, exposure time 15 sec; (d) Xenon, exposure time 45 sec; (e) Xenon, exposure time 135 sec; (f) Xenon plus a layer of oxygen, exposure time 15 sec.

matrix and the double head separation of about 40 cm^{-1} most clearly seen in the nitrogen solid. The frequencies in cm^{-1} from the absorption spectrum of oxygen in the gas phase[9] and the frequencies and relative intensities of emission for 1% oxygen in four different solids at 4.2°K have been summarized in Table IV. The vibrational numbering has been increased by one unit in the lower state[10] relative to the tentative numbering scheme proposed by Herzberg.[9] The group of six bands due to transitions from the $v'=1$ level of the upper state in the oxygen-xenon solid have not been included in the tabulation. Transitions from levels of the upper state other than the zero level have not been observed in the other oxygen-rare gas systems. It is apparent that in all four solids, each observed band undergoes a frequency shift to the red with respect to the corresponding gas phase value. The magnitudes of these shifts are displayed in Table VI. In all cases they decrease with increasing distance from the origin of the band system. For the argon, krypton, and nitrogen solids, a least squares method was employed to determine the constants in the equation

$$\nu=\nu_{00}+(\omega_e-\omega_e x_e)v-\omega_e x_e v^2,$$

where ν_{00} is the frequency in cm^{-1} of the (0, 0) band of the system, ω_e the equilibrium frequency of the molecule, x_e the anharmonicity constant, and v the vibrational quantum number in the ground state corresponding to the band of measured frequency ν. The results for the three solids together with the corresponding confidence factors are compared with the analogous gas values in Table VII.

O_2^+ *Bands*

In the 1% oxygen-neon solids, the bands of the Second Negative system ($A\,^2\Pi_u \rightarrow X\,^2\Pi_g$) are about 200 cm^{-1} wide, diffuse in appearance, and the heads not well defined. The bands are degraded toward the red, each band showing two heads with the average separation of 200 cm^{-1}. The main progression occurs from the zero vibrational level of the upper state. In addition, a few transitions from the $v'=1$ level were also observed.

TABLE VI. Wave number differences of Herzberg bands of oxygen in the condensed phase relative to the gas values ($\nu_{gas}-\nu_{solid}$).

v', v''	Nitrogen cm^{-1}	Argon cm^{-1}	Krypton cm^{-1}	Xenon cm^{-1}
0, 3	951			
0, 4	931	882	917	
0, 5	927	872	917	871
0, 6	926	859	916	875
0, 7	925	850	912	883
0, 8	925	846	908	881
0, 9	926	840	904	889
0, 10	924	836	899	889
0, 11	925	832	891	862
0, 12	921	832	884	
0, 13	909	830	873	832
0, 14		825?		

[9] G. Herzberg, Can. J. Phys. **30**, 185 (1952).
[10] H. P. Broida and A. G. Gaydon, Proc. Roy. Soc. (London) **A222**, 181 (1954).

TABLE VII. Constants of the $X\,^3\Sigma_g^-$ state of O_2 in nitrogen and rare gas solids compared with the gas phase values.

	ν_{00} cm^{-1}	ω_e cm^{-1}	$\omega_e x_e$ cm^{-1}
Gas[a]	35 000	1576.2	11.33
Argon	34 059	1557.8	10.62
Nitrogen	34 071	1577.2	11.47
Krypton	34 093	1581.5	11.88
Xenon[b]	34 257	1614.2	13.55
	±25	±6	±0.4

[a] Constants for the gas evaluated by a least squares fit of the values listed in column 2 of Table IV. Uncertainties approximately 1/10 those indicated at bottom of columns.
[b] Uncertainties for xenon 4 times those given at bottom of columns.

Vegard-Kaplan Bands

This system of the nitrogen molecule ($A\,^3\Sigma_u^+ \rightarrow X\,^1\Sigma_g^+$) was observed in 0.1% and 1% oxygen in nitrogen solids at 4.2°K, the bands occurring very weakly at the higher oxygen concentration. Although small amounts of added oxygen have been found efficient in quenching Vegard-Kaplan emission in nitrogen and nitrogen-argon deposits,[2] the bands are well developed in a 1% oxygen-xenon matrix containing less than 1% of nitrogen impurity. The bands are double headed in the xenon solid, with a separation of about 40 cm^{-1}. The shifts to the red in the solid[2-4,11] at 4.2°K with respect to the gas are given by

$$\nu_{gas}=\nu_{N_2}+135\ cm^{-1}=\nu_A+140\ cm^{-1}=\nu_{Kr}+220\ cm^{-1}$$
$$=\nu_{Xe}+300\ cm^{-1}=\nu_{N_2}+330\ cm^{-1},$$

where ν denotes the frequency in cm^{-1} of a particular band of the system and the differences represent averages between corresponding bands in the different matrices.

NO_β *Bands*

Eleven bands ($\beta\,^2\Pi \rightarrow X\,^2\Pi$) have been observed in a 1% oxygen-nitrogen solid at 4.2°K. In a 1% oxygen in argon matrix, six bands of the system have been identified. Under present conditions the bands appear in nitrogen with a sharp single head on the long wavelength side of a continuum about 130 cm^{-1} wide. In the nitrogen matrix, the system is also known to occur with double heads.[1,2] In the oxygen-argon solid there appear to be two heads overlapped by the continuum so that the structure is not easily resolved. The bands in argon are shifted an average of 75 cm^{-1} to the blue with respect to their position in the nitrogen matrix in agreement with previous observation.[4]

[11] See reference 2 for a representative list of Vegard's publications.

TABLE VIII. The β group in nitrogen and rare gas solids.

	I	Wavelength A	Wave number cm^{-1}
Nitrogen	300	5542	18 039
	175	5618	17 795
	150	5660	17 663
Neon	50	5577	17 913
	20	5587	
Argon	1000	5604	17 839
	750	5617	17 798
Krypton	2450	5626	17 770
	1850	5993	16 682
Xenon	2000	5766	17 308
	3300	6823	14 652

The β Group

The strongest feature in all of the observed oxygen-rare gas spectra (except neon) consists of a diffuse line group lying between 5500 and 7000 A designated as β in Fig. 3. The observed wavelengths and relative intensities are given in Table VIII. Although only two components of β occur in the rare gas solids whereas three are observed in nitrogen,[2] comparison of the wavelength region and general appearance of the two systems suggests that they are the same. In going toward the heavier rare gas solids, however, the β feature becomes progressively more intense and diffuse, and more difficult to reconcile with the structure observed in nitrogen. Along with these structural changes the center of gravity of the system simultaneously shifts toward longer wavelengths. A red shift of β with addition of argon or krypton to nitrogen matrices containing oxygen has previously been reported.[2] In view of the relative complexity of the β group in the various rare gas solids, the identification as the $^1S \rightarrow {}^1D$ transition of the oxygen atom is only a tentative one.

C. Afterglow and Warmup

When the electric power to the system is shut off, there is no persistence of any glow with a half-life in excess of 0.5 sec for the oxygen-rare gas solids that have been studied. In the case of oxygen in a nitrogen matrix, the typical green afterglow which has been described previously[2,5] is observed. The warmup glows are relatively weak with respect to those that occur after deposition at 4.2°K of the microwave discharge products of gases containing nitrogen, indicating little trapped energy. In several experiments with 1% oxygen-argon solids that had been subjected to bombardment, the Herzberg bands and the β group were the only spectral features observed during the warmup.

D. Effect of Concentration

A series of experiments were carried out to examine any possible dependence of the wavelengths of the Herzberg bands on the concentration of oxygen. The oxygen concentration was varied by a factor of 100 from 0.1% to 10% in a nitrogen matrix and each solid irradiated at 4.2°K. The resulting spectra showed no significant differences in the measured wavelengths. Although the Herzberg system occurred with greatly diminished intensity at the highest concentration, relative intensities remained unchanged.

E. Effect of Temperature

The temperature of deposition exerted a profound influence on the intensity of the Herzberg bands in the nitrogen matrix. At 1.2°K and 4.2°K the bands were easily visible with a few minutes exposure on the $f/10$ spectrograph. During irradiation of a sample of the same gas mixture condensed at 20.4°K, exposures up to 40 times as long failed to reveal any sign of this system. An analogous intensity dependence on deposition temperature has been observed for the NO_β bands in an argon matrix between 1.2 and 20.4°K. At this temperature, the bands appear relatively broad and diffuse with some less of sharpness in the short wavelength edge.

IV. DISCUSSION AND CONCLUSIONS

A study has been made of the spectra emitted by condensed gases containing small quantities of oxygen subjected to electron bombardment at low temperatures. Under the prevailing conditions, a large variety of spectral features was found to occur. A number of these have been identified, and their variation with the experimental parameters noted.

One system, the Herzberg bands of oxygen, common to argon, krypton, xenon, and nitrogen solids have been employed to investigate the degree of interaction between an excited diatomic species and its solid environment. The vibrational constants for the system in argon, krypton, xenon, and nitrogen matrices at 4.2°K have been compared with those for the gas in Table VII. The observed shifts to the red in the condensed phase are given by

$$\nu_{00_{gas}} = \nu_{00_{Xe}} + 743\ cm^{-1} = \nu_{00_{Kr}} + 907\ cm^{-1} = \nu_{00_{N_2}} + 929\ cm^{-1} = \nu_{00_A} + 941\ cm^{-1},$$

where ν_{00} represents the frequency in cm^{-1} of the (0, 0) band. It may be seen from Table VII that aside from the large difference in ν_{00} for the gas and ν_{00} for the four oxygen-containing solids, differences in the constants between the various solids as well as differences between the gas and the solid are small. In general, the magnitudes of these differences are of the order of the estimated limits of uncertainty involved in the determination of the constants. It should be noted, however, that the ν_{00}, ω_e, and $\omega_e x_e$ values do display a degree of self-consistency and a district trend as they increase in going from an argon to a xenon matrix. It is obvious from these results that measurements of higher precision than have been applied heretofore are

required to evaluate the small differences that exist between the vibrational constants for the systems studied. It is possible, however, that the acquisition of better data will be limited by the inherent nature of the trapping medium, in which the interactions between the emitting species and their nearest neighbors lead to spectra lacking in the sharpness necessary for precise measurement. Related to the need for improved precision is the question of reproducibility. In comparing the results of independent, self-consistent measurements of the Herzberg bands in the solid phase, differences of about 10 cm^{-1} per band are encountered. Thus far the basic reason for these discrepancies has not been uncovered. It may be that they are due to differences in the condensed solids whose structure may be peculiar to one set of deposition conditions or to the identity and nature of the surface on which condensation takes place. It should be noted that a concentration dependence of the observed wavelengths is ruled out by the present work.

The occurrence of the Second Negative system of O_2^+ in the oxygen-neon solid is of some interest. In order to observe this species in emission, approximately 17 ev are necessary—12.2 ev for the ionization of the oxygen molecule[12] plus about 4.8 ev for the excitation of the resulting ion. It should be pointed out that all the matrices employed, only neon atoms may be excited to metastable upper levels with energies close to the 17 ev required to produce excited O_2^+. Transitions from the $J=0$ and $J=2$ levels of the first excited state of NeI are not allowed for electric dipole radiation. Although the $J=0$ level is associated with an energy of only 16.7 ev in the gas phase,[13] it can be inferred from a recent investigation of the absorption spectra of xenon and krypton at 4.2°K,[14] that this level could be shifted as much as 0.3 ev toward higher energies in the neon solid. In order to explain the formation of excited O_2^+ in the oxygen-neon matrix, it then becomes attractive to postulate a mechanism of energy transfer involving intermediate participation of excited neon atoms. Alternatively, a singly ionized neon atom might act as an intermediate species, however, the required electron transfer and excitation processes then necessarily involve a corresponding higher degree of complexity.

ACKNOWLEDGMENT

The authors wish to thank Dr. Robert W. Zanwzig for many helpful discussions.

[12] C. A. McDowell and D. C. Frost, J. Am. Chem. Soc. **80**, 6183 (1958).

[13] C. E. Moore, *Atomic Energy Levels*, Natl. Bureau Standards Circ. No. 467, Washington, D. C., 1952.

[14] O. Schnepp and K. Dressler (to be published).

Electronic Structure of Carbon Monoxide*

HÉLÈNE BRION AND CARL MOSER

Centre de Mecanique Ondulatoire Appliquée, 155 Rue de Sèvres, Paris 15

(Received May 4, 1959)

The LCAO—MO SCF orbitals for carbon monoxide have been calculated with 1*s*, 2*s*, and 2*p* Slater atomic functions, using best atom (Roothaan) exponents. All atomic integrals have been calculated. While all the orbitals are orthogonal, the inner shells have been given a fixed form. The calculated binding energy (using these SCF orbitals for the molecular energy and the same atomic functions for atomic energy) is about 40% of that observed. A limited configuration interaction calculation gives about 55% of the observed binding energy. Both the single determinant and the CI wave function predict a dipole moment which is in agreement with the observed sign C^-O^+, but the error in magnitude is rather large. The atomic populations suggest the sign of the dipole moment to be C^+O^-, in agreement with Malone's rule.

The ionization energies have been calculated and the agreement with experiment is very satisfactory. Some of the observed lower electronic transitions can be understood by using single configurations constructed from these SCF orbitals, but, before a more complete analysis of the spectrum can be attempted, it may be necessary to introduce atomic functions from the *M* shell.

I. INTRODUCTION

AN LCAO-MO SCF calculation on CO has been given by Sahni.[1] However, in this calculation, the atomic integrals were taken from those used by Mulligan[2] for CO_2. The carbon-oxygen distances in the two molecules are not quite equal, and the values of some of the integrals used by Mulligan[2] were only approximated. The molecular orbitals calculated by Sahni are not orthogonal to the core orbitals, and it seems to be clear now that this nonorthogonality can have a large effect on some of the computed properties.[3,4] Thus, it seemed of interest to repeat the SCF calculation of CO using computed integrals appropriate to the molecule and keeping the orbitals strictly orthogonal to the core.[5]

A perturbation method has been used to calculate the SCF orbitals, and the procedure is given in some detail in this paper.

Finally, we shall discuss some of the properties of CO which are predicted by wave functions built on the SCF orbitals.

II. CALCULATIONS

The carbon-oxygen distance is taken to be the experimental value 1.128 A (2.131_9 a.u.) The usual (1*s*), (2*s*), and (2*p*) Slater atomic functions were used with the following exponents[6] which are those (to two decimal places) which minimize the energies of the atoms:

	Carbon	Oxygen
Z_{1s}	5.67	7.66
Z_{2s}	1.61	2.25
Z_{2p}	1.57	2.23.

The nonorthogonal $(2s)^*$ functions was transformed to the orthogonal (2*s*) function using the usual formula,

$$(2s)=(1-S^2)^{-\frac{1}{2}}[(2s)^*-S(1s)] \qquad (1)$$

where *S* is the overlap integral between the (1*s*) and $(2s^*)$ functions.

Dr. A. C. Hurley (Melbourne) has kindly furnished us with the values of the atomic integrals. He will publish these values in due course, but it will be desirable to indicate here that these integrals were obtained by machine programs from the Solid State and Molecular Physics Group, Massachusetts Institute of Technology, and the Laboratory of Molecular Structure and Spectra, University of Chicago.

From the atomic functions, six molecular orbitals of σ symmetry can be built which are linear combinations of the functions $(1s_C)$, $(1s_O)$, $(2s_C)$, $(2s_O)$, $(2p_{\sigma C})$ and $(2p_{\sigma O})$, two molecular orbitals of π symmetry, combinations of the $(2p_{xC})$ and $(2p_{xO})$ functions, and, finally, two molecular orbitals of $\bar{\pi}$ symmetry from the $(2p_{yC})$ and $(2p_{yO})$ functions.

The $^1\Sigma^+$ ground state of CO can be represented by the configuration,[3]

$$(1\sigma)^2(2\sigma)^2(3\sigma)^2(4\sigma)^2(1\pi)^4(5\sigma)^2.$$

As the (1*s*) functions are concentrated largely near the respective nuclei, no important error will be introduced by taking:

$$1\sigma=1s_O, \qquad 2\sigma=1s_C. \qquad (2)$$

In order that the other σ orbitals are strictly orthogonal to 1σ and 2σ, they will have to be linear combinations of the six atomic functions $(1s)_C\cdots(2p_{\sigma O})$.

As the ground state configuration contains only closed shells, the SCF orbitals could be determined by

* Part of this paper was read before the Conference on Wave Mechanics, University of Colorado, Boulder, June 23–27, 1959.

[1] R. C. Sahni, Trans. Faraday Soc. **49**, 1246 (1953).

[2] J. F. Mulligan, J. Chem. Phys. **19**, 347 (1951).

[3] C. W. Scherr, J. Chem. Phys. **23**, 569 (1955).

[4] H. Brion, C. Moser, and M. Yamazaki, J. Chem. Phys. **30**, 673 (1959).

[5] Since this work was completed, B. J. Ransil, J. Chem. Phys. **30**, 1113 (1959), has given a preliminary report of a calculation on CO.

[6] C. C. J. Roothaan, Technical Rept., Lab. of Molecular Structure and Spectra, University of Chicago (1955), p. 24.

solving the Roothaan equations.[7] We have, however, used a perturbation procedure.[8] This method starts from a set of orthogonal orbitals which are assumed to be reasonably close to the SCF orbitals. The occupied orbitals then are "corrected" by the unoccupied orbitals in an iterative procedure, until no further corrections can be made. In order to maintain orthogonality to the first order among the set of orbitals, the unoccupied orbitals must be corrected at the same time. As 1σ and 2σ have fixed forms in our calculation, only 3σ, 4σ, 5σ, among the σ occupied orbitals, need be calculated. For the orbitals of π symmetry, 1π and $1\bar{\pi}$ are occupied, 2π and $2\bar{\pi}$ unoccupied.

The orbitals of the $(n+1)$ iteration are given in terms of the orbitals of the nth iteration by the formulas,

$$\left.\begin{aligned}\phi_i^{(n+1)}&=\phi_i^{(n)}+c_{i6}\phi_6^{(n)}\\ \phi_6^{(n+1)}&=\phi_6^{(n)}-\sum_i c_{i6}\phi_i^{(n)}\end{aligned}\right\}\begin{matrix}i=3\sigma,\,4\sigma,\,5\sigma\\ 6=6\sigma\end{matrix}$$

$$\left.\begin{aligned}\phi_1^{(n+1)}&=\phi_1^{(n)}+c_{12}\phi_2^{(n)}\\ \phi_{\bar{1}}^{(n+1)}&=\phi_{\bar{1}}^{(n)}+c_{\bar{1}\bar{2}}\phi_{\bar{2}}^{(n)}\\ \phi_2^{(n+1)}&=\phi_2^{(n)}-c_{12}\phi_1^{(n)}\\ \phi_{\bar{2}}^{(n+1)}&=\phi_{\bar{2}}^{(n)}-c_{\bar{1}\bar{2}}\phi_{\bar{1}}^{(n)}\end{aligned}\right\}\begin{matrix}1=1\pi\\ 2=2\pi\\ \bar{1}=1\bar{\pi}\\ \bar{2}=2\bar{\pi}\end{matrix}\qquad(3)$$

(π and $\bar{\pi}$ are real molecular orbitals).

At each iteration we will wish to keep a one-determinant wave function which corresponds to the ground state configuration. To do this, 1π and $1\bar{\pi}$ must be degenerate, and this can be insured by arbitrarily taking $c_{12}=c_{\bar{1}\bar{2}}$.

There are a number of different ways of determining the corrections c_{ij}, but the most rapid convergence will be found from solving the following set of linear nonhomogeneous equations:

$$\begin{aligned}&\epsilon_{i6}+c_{i6}(\epsilon_6-\epsilon_i+3\zeta_{i6}{}^{i6}-\zeta_{66}{}^{ii})\\ &\qquad+\sum_{j\neq i}c_{j6}(3\zeta_{j6}{}^{i6}-\zeta_{66}{}^{ij}-\epsilon_{ij})\\ &\qquad+(c_{12}+c_{\bar{1}\bar{2}})(4\zeta_{12}{}^{i6}-\zeta_{26}{}^{1i}-\zeta_{2i}{}^{16})=0,\\ &\epsilon_{12}+\sum_i c_{i6}(4\zeta_{12}{}^{i6}-\zeta_{26}{}^{1i}-\zeta_{2i}{}^{16})+c_{12}(\epsilon_2-\epsilon_1+3\zeta_{12}{}^{12}\\ &\qquad-\zeta_{22}{}^{11}+4\zeta_{\bar{1}\bar{2}}{}^{12}-\zeta_{\bar{1}}{}^{2\bar{2}}-\zeta_{\bar{2}}{}^{2\bar{1}})=0,\\ &\epsilon_{\bar{1}\bar{2}}+\sum_i c_{i6}(4\zeta_{\bar{1}\bar{2}}{}^{i6}-\zeta_{\bar{2}6}{}^{\bar{1}i}-\zeta_{\bar{2}i}{}^{\bar{1}6})+c_{\bar{1}\bar{2}}(\epsilon_{\bar{2}}-\epsilon_{\bar{1}}\\ &\qquad+3\zeta_{\bar{1}\bar{2}}{}^{\bar{1}\bar{2}}-\zeta_{\bar{2}\bar{2}}{}^{\bar{1}\bar{1}}+4\zeta_{12}{}^{\bar{1}\bar{2}}-\zeta_{1\bar{2}}{}^{\bar{1}2}-\zeta_{2\bar{2}}{}^{1\bar{1}})=0,\\ &\qquad i,j=3\sigma,\,4\sigma,\,5\sigma\\ &\qquad 6=6\sigma\\ &\qquad 1=1\pi\\ &\qquad 2=2\pi\\ &\qquad \bar{1}=1\bar{\pi}\\ &\qquad \bar{2}=2\bar{\pi}\end{aligned}$$

[7] C. C. J. Roothaan, Revs. Modern Phys. **23**, 69 (1951).
[8] R. Lefebvre and C. Moser, J. chim. phys. **53**, 393 (1956).

TABLE I. SCF orbitals for CO calculated by Sahni.[a]

Orbitals
$\phi_{3\sigma}=0.270\ 2s_C+0.675\ 2s_O+0.227\ 2p\sigma_C+0.231\ 2p\sigma_O$
$\phi_{4\sigma}=0.4926\ 2s_C-0.7176\ 2s_O+0.168\ 2p\sigma_C+0.6065\ 2p\sigma_O$
$\phi_{5\sigma}=0.6145\ 2s_C+0.187\ 2s_O-0.7626\ 2p\sigma_C-0.189\ 2p\sigma_O$
$\phi_{6\sigma}=0.971\ 2s_C-0.973\ 2s_O+1.055\ 2p\sigma_C-1.0\ 2p\sigma_O$
$\phi_{1\pi}=0.4162\ 2p\pi_C+0.8145\ 2p\pi_O$
$\phi_{2\pi}=0.9425\ 2p\pi_C-0.631\ 2p\pi_O$

[a] From reference 1.
[b] The notation has been made to conform to that used in this paper.

where

$$\epsilon_{kl}=\int\phi_k^*(H^N+\sum_m 2J_m-K_m)\phi_l d\tau \qquad (5)$$

(m=occupied orbitals),
and

$$\zeta_{iu}{}^{rs}=\int\phi_r^*(1)\phi_s(1)\,(1/r_{12})\phi_i^*(2)\phi_u(2)d\tau. \qquad (6)$$

When the orbitals are finally self-consistent, they will obey, for the closed-shell single determinant function, the conditions $\epsilon_{mn}=0$. (m=occupied orbitals; n=unoccupied orbitals.) Thus the terms ϵ_{i6}, ϵ_{12}, and $\epsilon_{\bar{1}\bar{2}}$ disappear, and the c_{ij}'s become zero.

It should be noted that the new orbitals obtained after one iteration, using Eq. (3), are only orthogonal to the first order. Before proceeding with a new iteration, it is necessary to transform them into a rigorously orthonormal set. As the lack of orthogonality is usually small, Lowdin's procedure[9] is very useful.

The self-consistent orbitals in this way do not completely diagonalize the H^{SCF} operator. Once the self-consistent orbitals are known, one can carry out the necessary unitary transformation between occupied orbitals in a straightforward manner.

The convergence, using this method, is very rapid. Starting from Sahni's orbitals for CO (Table I) properly orthogonalized to the ($1s$) atomic functions, three iterations were sufficient to obtain the orbitals given in Table II, which completely diagonalize the H^{SCF} operator.

III. DISCUSSION

A. Binding Energy

The data for calculated and observed atomic and molecular energies and binding energy of CO are given in Table III. The error in the calculated molecular energy is less than 1%, which is a fairly general result of SCF calculations for diatomic molecules.

The calculated binding energy is at least 40% of the observed, for the experimental binding energy is not

[9] P. O. Löwdin, J. Chem. Phys. **18**, 365 (1950).

TABLE II. SCF orbitals and orbital energies for CO.

$\phi_{1\sigma}=1s_O$

$\phi_{2\sigma}=1s_C$

$\phi_{3\sigma}=-0.05725\ 1s_C-0.02447\ 1s_O+0.21976\ 2s_C+0.74766\ 2s_O$
$+0.15584\ 2p\sigma_C+0.23803\ 2p\sigma_O$

$\phi_{4\sigma}=-0.02094\ 1s_C-0.03171\ 1s_O+0.52538\ 2s_C-0.63552\ 2s_O$
$+0.06031\ 1p\sigma_C+0.63494\ 1p\sigma_O$

$\phi_{5\sigma}=0.03552\ 1s_C+0.01062\ 1s_O+0.74299\ 2s_C+0.04002\ 2s_O$
$-0.56125\ 1p\sigma_C-0.45146\ 1p\sigma_O$

$\phi_{6\sigma}=0.13581\ 1s_C-0.15966\ 1s_O+0.98106\ 2s_C-1.14162\ 2s_O$
$+1.28356\ 1p\sigma_C-0.94553\ 1p\sigma_O$

$\phi_{1\pi}=0.46172\ 2p\pi_C+0.77088\ 2p\pi_O$

$\phi_{*\pi}=0.93047\ 2p\pi_C-0.69620\ 2p\pi_O$

	(a.u.)
$\epsilon_{1\sigma}$	−20.79896
$\epsilon_{2\sigma}$	−11.43646
$\epsilon_{3\sigma}$	− 1.53465
$\epsilon_{4\sigma}$	− 0.75914
$\epsilon_{5\sigma}$	− 0.50512
$\epsilon_{6\sigma}$	0.86242
$\epsilon_{1\pi}$	− 0.61037
$\epsilon_{2\pi}$	0.22500

known with absolute certainty. It may be as low as 9.14 ev, although it seems more likely to be 11.108 ev. The SCF calculation for CO gives a higher percentage of calculated binding energy than has been reported for other diatomic molecules in this region of the periodic table using SCF functions. For example, for O_2 the SCF calculation gives only 15% of the binding energy, for N_2 12% and Li_2 11%. Negative binding energies have been found for F_2[10] and NO[4].

One evident difference between this calculation on CO and other SCF calculations is that we have taken an exponent for the $(2p)$ orbital different from the $(2s)$. All exponents are those which minimize the energy of the atoms, not those calculated from Slater's rules. Scherr[3] suggests that using these "improved" exponents should produce negligible differences in molecular calculations, but these are not enough results in the literature to be certain. It seems to make little difference in HF[11] and Li_2.[12–14]

It is interesting to compare the *absolute* errors found in the molecular calculations and in the sum of atomic energies for the various diatomic molecules for which SCF calculations which have been reported. Figure 1 summarizes the data. First of all, it can be seen that the error increases with the number of electrons both for the sum of the atomic energies and for the molecular calculations. But if the error is plotted against number of electrons, it is found that the slopes of the curves for atomic and molecular errors are not the same, and all the points do not fall on the curve. The hydrides give curves quite separate from those for other kinds of diatomic molecules.

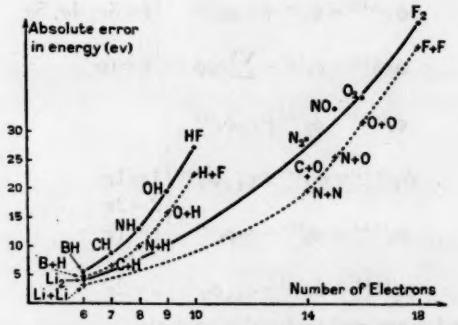

FIG. 1. Absolute error (in ev) found in some SCF calculations as a function of number of electrons. Molecular calculation:—; sum of atoms calculation:···. The errors in the molecular calculations for CO and N_2 are nearly the same. The data for the hydrides is taken from M. Krauss, J. Chem. Phys. **28**, 1021 (1958). The references for the other molecules have been given.

A study of the graph shows that the greater percentage of binding energy calculated for CO as compared to the isoelectronic molecule N_2 is not due, to a better molecular calculation (the error is nearly the same), but to the fact that the error in the calculated energy of separated atoms is about 2 ev greater in CO than in N_2.

The reverse situation appears to hold in NO. The error in the molecular calculation for NO is nearly as large for O_2 (which has one more electron) and much

TABLE III. Calculated and observed binding energies in CO.

	Energy of separated atoms (in a.u.)	Total molecular energy (in a.u.)	Binding energy[a] (ev)
Calculated	−112.16268	−112.32705	4.47
Observed	−112.96431[b]	−113.37751	11.108[c,d]
Percentage	99.29%	99.07%	40.24%

[a] 1 au=27.207 ev.

[b] C. E. Moore, Natl. Bur. Standards (U.S.) Circ. No. 467 (1949).

[c] Includes zero point energy of 0.134 ev.

[d] See, e.g., H. Herzberg, *Molecular Spectra and Molecular Structure; Spectra of Diatomic Molecules* (D. Van Nostrand Company, Inc., Princeton, New Jersey, 1950), 2nd ed.

[10] J. Eve, Proc. Roy. Soc. (London) **A246**, 582 (1958).

[11] A. M. Karo and L. C. Allen, J. Chem. Phys. **31**, 968 (1959).

[12] E. Ishiguro, K. Kayama, M. Kotani, and Y. Mizuno, J. Phys. Soc. Japan **12**, 1355 (1957).

[13] J. E. Faulkner, J. Chem. Phys. **27**, 369 (1957).

[14] Since this paper was prepared, Ransil [Molecular Physics Conference, University of Colorado, June 23–27 (1959)] has reported that, using Slater values for the exponents, a molecular energy of −112.34357 a.u. is found. This is about 0.017 a.u. better than we have found, which indicates that the "best-atom" exponents are not necessarily best for the molecule. Using the exact "best-atom" coefficients Ransil has found a molecular energy of −112.32604 a.u. This is a difference of about 0.001 a.u. from the calculation reported in this paper. But as all these total energies are about 1 a.u. from the observed values, it will be seen that small changes in the values of the exponents are not very important for the total energy. Small changes in exponents, however, may be more significant for the calculation of other properties like dipole moment.

TABLE IV. Determinantal wave functions used in configuration interaction calculation.

Function	Coefficient	1σ	2σ	3σ	4σ	5σ	6σ	$1\pi^+$	$1\pi^-$	$2\pi^+$	$2\pi^-$
ψ_0	1	+−	+−	+−	+−	+−		+−	+−		
ψ_1	$1/\sqrt{2}$	+−	+−	+−	+−	+−		+−			+−
	$+1/\sqrt{2}$	+−	+−	+−	+−	+−			+−	+−	
ψ_2	$\frac{1}{2}$	+−	+−	+−	+−	+−		+	−	+	−
	$+\frac{1}{2}$	+−	+−	+−	+−	+−		−	+	−	+
	$-\frac{1}{2}$	+−	+−	+−	+−	+−		−	+	+	−
	$-\frac{1}{2}$	+−	+−	+−	+−	+−		+	−	−	+
ψ_2'	$1/\sqrt{3}$	+−	+−	+−	+−	+−		+	+	−	−
	$+1/\sqrt{3}$	+−	+−	+−	+−	+−		−	−	+	+
	$-1/(12)^{\frac{1}{2}}$	+−	+−	+−	+−	+−		+	−	+	−
	$-1/(12)^{\frac{1}{2}}$	+−	+−	+−	+−	+−		−	+	−	+
	$-1/(12)^{\frac{1}{2}}$	+−	+−	+−	+−	+−		−	+	+	−
	$-1/(12)^{\frac{1}{2}}$	+−	+−	+−	+−	+−		+	−	−	+
ψ_3	$1/\sqrt{2}$	+−	+−	+−	+−			+−	+−	+	−
	$+1/\sqrt{2}$	+−	+−	+−	+−			+−	+−	−	+

larger than for N_2 (which has one less electron). The error in the energy of the separated atom falls, of course, in the middle between N_2 and O_2, and thus a negative binding energy is found.

We have carried out a limited configuration interaction calculation on the ground state of CO. As we build the excited configurations using the virtual orbitals calculated in the SCF procedure, all monoexcited configurations will have a zero-matrix element with the ground state.[15] In our CI calculation 1σ, 2σ, 3σ, and 4σ are always doubly occupied. Of the other configurations, we have retained only those which, by second-order perturbation theory, cause a lowering of the ground state by more than 0.007 a.u. The wave functions which were kept are given in Table IV. The configuration interaction function is:

$$\Psi = 0.97321\psi_0 - 0.09111\psi_3 + 0.12659\psi_2 - 0.14059\psi_1 + 0.09363\psi_2'.$$

The energy associated with this function is lower by 2.14 ev than that associated with the SCF function.

TABLE V. Improvement in binding energy of some diatomic molecules after configuration interaction.

Molecule	Improvement (ev)
N_2[a]	2.22
O_2[b]	2.6
NO[c]	3.3
F_2[d]	1.96
CO[e]	1.64

[a] A. C. Hurley, Proc. Phys. Soc. (London) A69, 767 (1956).
[b] M. Kotani, Y. Mizuno, K. Kayama, and E. Ishiguro, J. Phys. Soc. Japan, 12, 707 (1957).
[c] H. Brion, C. Moser, and M. Yamazaki, J. Chem. Phys. 30, 673, (1959).
[d] J. Eve, Proc. Roy. Soc. (London) A246, 582 (1958).
[e] Our data.

[15] L. Brillouin, *Les Champs self-consistents de Hartree et de Fock* (Hermann & Cie, Paris, France, 1934), p. 36.

While there is only one ^3p state of the oxygen atom which can be built from $(1s)$, $(2s)$, and $(2p)$ functions (with the restriction that $(1s)$ is always doubly filled), there are two configurations for the carbon atom both of which generate a ^3P state: $(1s)^2(2s)^2(2p)^2$ and $(1s)^2(2p)^4$. Calculation shows that the energy of C is lowered by 0.5 ev from this interaction, so that the increase of binding energy due to configuration interaction is 1.64 ev. As the choice of configurations is not always the same, it is somewhat difficult to compare this result with other CI calculations of diatomic molecules; it is interesting to observe that those reported in the literature for similar molecules give energy lowerings which are of the same order of magnitude as that found here (Table V). Hydrides have not been included.

B. Dipole Moment

The calculation of this physical quantity is particularly interesting, as both the sign and the magnitude are known experimentally. The results are collected in Table VI. Those calculated have been obtained using the atomic integrals given in Table VII.

TABLE VI. Dipole moment of CO.

Type of calculation	Magnitude (a.u.)	Sign
Our SCF LCAO–MO	0.2404	$C^- O^+$
Our CI	0.3097	$C^- O^+$
Sahni SCF LCAO–MO	0.394	$C^- O^+$
Malone's rule	0.394	$C^+ O^-$
Mulliken's population analysis	0.352	$C^+ O^-$
Ransil (using Slater exponents)[a]	0.2873	$C^- O^+$
Ransil (using exact "best atom" exponents)[b]	0.2328	
Observed	0.047[c]	$C^- O^{+d}$

[a] B. J. Ransil, J. Chem. Phys. 30, 1113 (1959).
[b] Presented before Molecular Physics Conference, Boulder, Colorado, June 23–9 (1959).
[c] R. C. Sahni, Trans. Faraday Soc. 49, 1246 (1953).
[d] B. Rosemblum, A. H. Nethercot, and C. H. Townes, Phys. Rev. 109, 400 (1958).

TABLE VII. Dipole moment integrals.

x_1	x_2	$\vec{x_1 Z_C x_2}$
$1s_C$	$1s_O$	0.00013
$1s_C$	$2s_O$	0.01030
$1s_C$	$2p\sigma_C$	0.06708
$1s_C$	$2p\sigma_C$	0.01609
$1s_O$	$2s_C$	0.10392
$1s_O$	$2p\sigma_C$	0.17694
$1s_O$	$2p\sigma_O$	−0.05324
$2s_C$	$2s_O$	0.58758
$2s_C$	$2p\sigma_C$	0.91495
$2s_C$	$2p\sigma_O$	0.17203
$2s_O$	$2p\sigma_C$	0.88342
$2s_O$	$2p\sigma_O$	−0.64963
$2p\sigma_C$	$2p\sigma_O$	0.22549
$2p\pi_C$	$2p\pi_O$	0.35334

Both of our results and those of Sahni[1] give the sign C^- O^+ which is in agreement with experiment, though the agreement in magnitude is somewhat better with our wave functions than with Sahni's. The agreement is worse with the CI function, than with the SCF function.

The atomic population analysis[16] gives for CO:

$$(1s_C)^2(2s_C)^{1.664}(2p\sigma_C)^{0.930}(2p\pi_C)^{1.238}(1s_O)^2(2s_O)^{1.862}$$
$$(2p\sigma_O)^{1.543}(2p\pi_O)^{2.762}.$$

If we could relate the atomic population to the distribution of electronic charge, then this analysis would predict the sign to be C^+ O^-, in agreement with electronegativity considerations. As one often is interested mainly in the sign of the dipole moment, it would be very desirable to have a simple method for determining at least the general pattern of the electronic distribution; it is disappointing that this cannot be found from the atomic population analysis.

C. Ionization Potentials

Table VIII gives the lowest vertical ionization potentials, calculated from our SCF calculation and those of Sahni. The observed potentials have been corrected for verticality from considering the most intense transitions. We have, as usual, used Koopmans' theorem[17] as applied to molecules[18] in calculating the ionization potentials so that successive ionization energies are simply the negative of the values of the diagonal elements of the Hartree-Fock operator.

TABLE VIII. Vertical ionization potentials (ev).

Upper state	Observed	Calc in this paper (i.e. ϵ)	Calc by Sahni
$X\,^2\Sigma^+$	14.01[a]	13.74	13.37
$^2\Pi$	16.92[b]	16.60	15.97
$^2\Sigma^+$	19.66[b]	20.65	20.01

[a] F. H. Field and J. L. Franklin, *Electron Impact Phenomena and the Properties of Gaseous Ions* (Academic Press, New York, 1957), p. 110.

[b] *Données Spectroscopiques concernant les Molécules Diatomiques* (Hermann and Cie, Paris, 1951), p. 69. The vertical correction has been made by considering the most intense transitions.

[16] R. S. Mulliken, J. Chem. Phys. **23**, 1833 (1955).

In both calculations, it will be observed the agreement is quite good as the error is never more than about 5%. As the molecular orbitals are rather different (cf. Table I and Table II), it would seem that the ionization potentials are rather insensitive to the exact form of the wave function.

D. Transition Energies

The electronic spectra of CO has been studied carefully and a number of different transitions have been identified. In most of these, it is easy to determine the energy of the vertical excitation, which is, of course, the most intense transition. In Table IX we have collected this experimental data with the usual spectroscopic notation. Then we have tried to see how far we can understand these transitions from a simple one-particle excitation calculation. We have constructed the excited states using the virtual orbitals obtained in the SCF calculation. The particular monoexcitation involved is indicated in column 3 and it is straightforward to construct the corresponding wave function. Only one configuration has been used to describe each upper state.[19]

TABLE IX. Vertical electronic transitions in CO.[a]

Upper state	Observed energy (ev)	Assumed monoexcitation	Calculated energy (ev)	Equilibrium distance (in A)
$X\,^1\Sigma^+$	0	$5\sigma\rightarrow 2\pi$	0	1.128
$a\,^3\Pi$	6.22	$5\sigma\rightarrow 2\pi$	6.17	1.209
$a'\,^3\Sigma^+$	8.25	$1\pi\rightarrow 2\pi$	7.41	1.359
$e\,^3\Sigma^-$	8.68–8.91	$1\pi\rightarrow 2\pi$	9.56	1.393
$A\,^1\Pi$	8.74	$5\sigma\rightarrow 2\pi$	9.23	1.235
$d\,^3\Pi$	8.96	$1\pi\rightarrow 6\sigma$	24.2	1.396
$^3\Delta$		$1\pi\rightarrow 2\pi$	8.48	
$B\,^1\Sigma^+$	10.8	$1\pi\rightarrow 2\pi$	23.14	1.12
$C\,^1\Sigma^+$	11.4	$5\sigma\rightarrow 6\sigma$	27.37	1.125
$b\,^3\Sigma^+$	10.39	$5\sigma\rightarrow 6\sigma$	23.05	1.088
$F\,^1\Pi$	12.37	$1\pi\rightarrow 6\sigma$	25.97	

[a] Data taken from Y. Tanaka, A. S. Jursa, and F. Le Blanc, J. Chem. Phys. **26**, 862 (1957) and H. Herzberg, *Molecular Spectra and Molecular Structure; Spectra of Diatomic Molecules* (D. Van Nostrand Company, Inc., Princeton, New Jersey, 1950), 2nd ed.

We have tried to make a correspondence between the observed and calculated order of states of given symmetry. The correspondence for the first four transitions is surprisingly good, considering the simple method which has been used. Particularly striking is the agreement with the singlet-triplet separation $A\,^1\Pi - a\,^3\Pi$.

[17] T. Koopmans, Physica **1**, 104 (1933).

[18] G. G. Hall and J. E. Lennard-Jones, Proc. Roy. Soc. (London) **A202**, 155 (1950).

[19] The details of this kind of calculation are given in reference 3.

The calculated separation of somewhat more than 3 ev is not greatly different from the observed value of 2.5 ev. The agreement for these transitions seems to indicate that we essentially have described correctly the monoexcitations with our orbitals 5σ, 1π, and 2π.

However, for the other transitions, the difference between calculations and experiment is so large that the correspondence breaks down. A similar discrepancy has been observed in the corresponding transitions in N_2.[3] Mulliken[20] has suggested that in CO, the state which is usually called $d^3\Pi$, is, in fact, a $^3\Delta$ state. If this is so, then the monoexcitation would be $1\pi \rightarrow 2\pi$ and the calculated values (8.48 ev) would be in very good agreement with the observed value. A possible explanation for the transitions $B\,^1\Sigma^+$, $C\,^1\Sigma^+$ and $b\,^3\Sigma^+$ is that both the upper levels of σ and π symmetry are not the 6σ or 2π orbitals which we have calculated, but orbitals which are made up largely of bonding ($3s$) orbitals or bonding (3π) (or $3\pi+3d$) orbitals, respectively. The observed equilibrium distance of the excited states (column 5) seems to substantiate this explanation for they are about the same here as in the ground state.

In any event, it seems that if we are to attempt a more complete analysis of the observed electronic spectra, it may well be necessary to introduce in the calculation more than one configuration to describe the upper states or to introduce atomic orbitals of higher quantum number.

[20] R. S. Mulliken, Can. J. Chem. **36**, 11 (1958).

ACKNOWLEDGMENTS

We are grateful to Dr. A. C. Hurley for transmitting the values of the atomic integrals for CO. We are happy to acknowledge our indebtedness to Professor R. Daudel and Dr. R. Lefebvre for useful and stimulating discussions. A part of this work has been supported by a grant from the U. S. Public Health Service.

THE JOURNAL OF CHEMICAL PHYSICS VOLUME 32, NUMBER 4 APRIL, 1960

Higher Ionization Potentials of Linear Triatomic Molecules. I. CO_2

Y. TANAKA, A. S. JURSA, AND F. J. LEBLANC

Geophysics Research Directorate, Air Force Cambridge Research Center, Air Research and Development Command, Laurence G. Hanscom Field, Bedford, Massachusetts

(Received September 8, 1959)

Four new Rydberg series, in addition to series already known, have been observed. One of them, which corresponds to the vibration series of Henning's series, converged to 18.23 ev, while the other three converged to a value of 19.38 ev and yielded an additional higher ionization potential. All the observed values were compared with the theoretically calculated values. Several new progressions of absorption bands were also observed.

INTRODUCTION

HENNING[1] discovered two Rydberg absorption series converging to 18.00 ev,[2] and, shortly after, Rathenau[3] confirmed the series. By assuming this value as the ionization energy of the $2\sigma_u$ electron and combining it with other known experimental data from the emission spectra of CO_2^+ in the near ultraviolet region, Mulliken[4,5] proposed several other ionization energies including the first (lowest) ionization potential. Shortly after, Price and Simpson[6] discovered another series converging to a limit which is very close to Mulliken's value for the ionization value of the $1\pi_g$ electron. Mulligan[7] made theoretical calculations for the ionization energies of this molecule, but his values disagree with Mulliken's. The purpose of the present work was to find new ionization potentials by means of analyzing Rydberg series and to compare them with the theoretical results.

EXPERIMENTAL

A Hilger normal incidence vacuum spectrograph equipped with a grating, 2 m in radius of curvature and with 15 000 lines per inch, was used. Two sources, the helium[8] and the argon[9] continua, were employed as

[1] H. J. Henning, Ann. Physik **13**, 599 (1932).
[2] This value should be changed to 18.07 ev because of the difference of the conversion factor used (see Table II).
[3] G. Rathenau, Z. Physik **87**, 32 (1934).
[4] R. S. Mulliken, J. Chem. Phys. **3**, 720 (1935).
[5] R. S. Mulliken, Revs. Modern Phys. **14**, 204 (1942).
[6] W. C. Price and D. M. Simpson, Proc. Roy. Soc. (London) **A169**, 501 (1938).
[7] J. F. Mulligan, J. Chem. Phys. **19**, 347 (1951).
[8] Y. Tanaka, A. S. Jursa, and F. J. LeBlanc, J. Opt. Soc. Am. **48**, 304 (1958); Y. Tanaka, Sci. Papers Inst. Phys. Chem. Research (Tokyo) **39**, 465 (1942).
[9] Y. Tanaka, J. Opt. Soc. Am. **45**, 710 (1955).

TABLE I. Rydberg series converging to the first ionization potential of CO_2.

	Main series (1)			Main series (2)			Minor series (1)			Minor series (2)			Vibration series		
n	ν(cm^{-1})	I	n^*	ν(cm^{-1})	I	n^*	ν(cm^{-1})	I	n^*	ν(cm^{-1})	I	n^*	ν(cm^{-1})	I	n^*
2	88 535	10	2.21	88 530[a]	10	2.20	91 827	6					89 993	3	
	89 111	10					91 886	10					90 678	2	
3	100 570	7	3.15	100 940	5	3.20	101 920	7	3.41	99 331	5	3.02			
	100 650	5													
4	105 060	5	4.25	104 980	4	4.32	105 710	4	4.45	104 560	3	4.03	106 680	4	4.34
	105 140	5													
5	107 150	5	5.11	106 980[a]	4	5.00	107 560	3	5.37	106 980	3	5.18	108 660	4	5.39
	107 220	2													
6	108 460	4	6.45	108 320	3	6.35	108 660	3	6.52	108 200	2	6.00	109 750	3	6.26
	108 500	4													
7	109 150	3	7.45	109 010[a]	3	7.78	109 330	2	7.92	109 010	2	6.77	110 470	3	7.39
8	109 580	2	8.16	109 400	2	8.08	109 670	1	8.63	109 580	1	8.23	110 920	2	8.34
9	109 920	2	9.50	109 750[a]	3	9.67	109 960	3	8.99	109 920	3	9.53	111 240	1	9.09
10	110 140	1	10.40	109 960[a]	3	10.20	110 220	1		110 140[a]	1		111 490	1	
11	110 310	1	10.60	110 140[a]	1										
12	110 470	2	12.50												
13	110 550	1	13.50												
14	110 670	1													
	IP=111 240 cm^{-1} =13.78$_7$ ev[b]			IP=111 060 cm^{-1} =13.76$_5$ ev			IP=111 250 cm^{-1} =13.78$_8$ ev			IP=111 250 cm^{-1} =13.78$_8$ ev			IP=112 510 cm^{-1} =13.94$_5$ ev		

[a] These are also identified as other band.
[b] Difference from Price and Simpson's value, 13.73 ev, is due to the difference of conversion factors used.

background to cover the regions 600–1100 A and 1070–1650 A, respectively. The sources are strong and 3–5 min of exposure were sufficient with a 20-μ slit width. No window was used, and the rare gas which leaked into the spectrograph through the slit was continuously pumped out.

Commercial tank CO_2, purified several times by fractional distillation, was maintained at a desired partial pressure within the spectrograph by controlling its flow with a needle valve. Most of the Rydberg bands were so strong that 0.1 μ of partial pressure of CO_2 in a pathlength of 4 m was sufficient to record them, while for most of the non-Rydberg bands 1–10 μ pressure was required.

RESULTS

Rydberg Bands

As shown in Table I, main series (1), Price and Simpson's (PS) series[6] has been extended to $n=14$; the members of the series are expressed by the following equation:

$$\nu_n = 111\,240 - [R/(n+0.35)^2], \quad n=2, 3, 4, \cdots. \quad (1)$$

Although the average quantum defect in the equation is a little larger than that of PS, which is 0.21, the average value of the ionization potential which we observed is very close to their value.[10] As one can see in the table, the individual values of the effective quantum numbers (n^*) are rather irregular, but as mentioned by PS, the intensities and appearance of the bands seem to satisfy the necessary requirements for belonging to a Rydberg series. Because the ground state of CO_2^+ is $^2\Pi_g$ and its doublet separation is approximately 160 cm^{-1},[11] another series must exist whose converging limit differs from the PS series by an amount of 160 cm^{-1}. We observed that series, and our results are shown in Table I, main series (2). As one can see in the table, many of the higher members of the series are superimposed with other bands. The identification is our best effort at present, but there remains some uncertainty because of the irregularity of the quantum defect. The main source of error originates in the broad appearance of individual bands caused by a relatively broad slit width[12] necessary because the background (He continuum) was very weak in this region. However, we believe that the present value of the ionization potential is quite accurate, within an error of ± 0.03 ev. The ionization continuum appeared very close to our ionization value when the pressure was increased.

Without listing any individual bands, Price and Simpson also gave formulas for two other series:

$$\nu_n = 111\,250 - [R/(n+0.43)^2], \quad n=3, 4, 5, \cdots, \quad (2)$$

[10] Their original value expressed in ev is 13.73 ev but this should be changed to 13.79 ev because of the change of conversion factor.

[11] S. Mrozowski, Phys. Rev. **60**, 730 (1941); **62**, 270 (1942); **72**, 682 (1947).

[12] In this particular case a 40-μ slit width was adopted.

$$\nu_n = 111\,250 - [R/(n+0.03)^2], \quad n=3, 4, 5, \cdots. \quad (3)$$

The corresponding bands which we observed are listed under minor series (1) and (2) in Table I. The agreement between the observed values and the values calculated with Eqs. (2) and (3) is very good except for the first member ($n=2$) of the minor series (1). Because this band at 91 886 cm^{-1} was extremely strong[13] compared with other bands which appeared in the vicinity, we believe that it does belong to minor series (1) although its deviation from its calculated value is fairly large. The existence of the $n=2$ band in the minor series (2) is questionable. One of the bands which we observed at 86 470 cm^{-1} [14] and 87 000 cm^{-1} [14] might possibly be this member; however, we can not be certain of this because of their weak intensity and of their large deviations from their calculated values.

In addition to the four series just mentioned, we observed another series whose wavelengths are also shown in Table I, under "vibration series." It is expressed by the following equation:

$$\nu_n = 112\,510 - [R/(n+0.30)^2], \quad n=4, 5, 6, \cdots. \quad (4)$$

The average wave number difference between the members of the new series and the corresponding members of the main series (1) is 1410 cm^{-1}, and the difference between the two series limits is 1260 cm^{-1}. Although the two values differ by 150 cm^{-1}, both are fairly close to the frequency of the stretching vibration of the ground state of CO_2, as well as to that of the ground state of CO_2^+.[15] This indicates that the series is most probably the vibration series $(v''=0)\rightarrow(v_1=1)$. A point difficult to understand is that the intensity of the $n=2$ band was abnormally weak compared with that of the higher members.

The known Rydberg series which converge to the next higher energy value beyond that of Price and Simpson's are Henning's series.[1] These are two series, one sharp, the other diffuse, which are stronger than any other series observed for this molecule. A second order spectrum of our series corresponding to Henning's is reproduced in Fig. 1. As one sees in the figure, it is

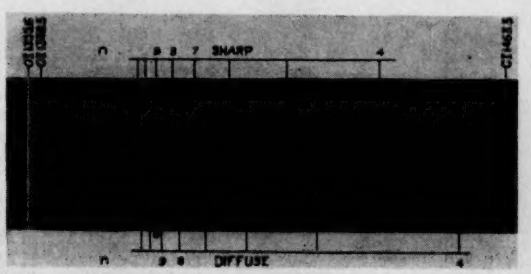

FIG. 1. Henning's Rydberg series of CO_2. Second order spectrum with helium continuum as a background.

[13] E. C. Y. Inn, K. Watanabe, and M. Zelikoff, J. Chem. Phys. 21, 1648 (1953).
[14] They belong to one of the Rathenau progressions (see Table IV, progression VI).
[15] S. Mrozowski, Phys. Rev. 72, 691 (1947).

TABLE II. Rydberg series converging to the higher ionization potentials of CO_2.

	Henning diffuse series			Henning sharp series			Vibration series			Absorption series			Absorption series			Apparent emission series		
n	ν (cm^{-1})	I	n^*	ν (cm^{-1})	I	n^*	ν (cm^{-1})	I	n^*	ν (cm^{-1})	I	n^*	ν (cm^{-1})	I	n^*	ν (cm^{-1})	I	n^*
3	130 380	10	2.66	132 900	10	2.80				146 490	3	3.35	144 100[b]	3	2.99	147 280	5	3.45
4	137 700	8	3.70	139 380	8	4.25				150 580	3	4.35	149 500	2	3.98	150 950	3	4.50
5	140 760	7	4.65	141 440	7	5.05				152 550	2	5.30	152 000	2	5.07	152 720	2	5.45
6	142 390	6	5.75	142 760	6	6.05				153 670	2	6.45	153 300	1	6.02	153 770	2	6.42
7	143 310	5	6.60	143 550	5	7.00				154 340	1	6.98	154 100	1	6.68	154 440	1	7.40
8	143 920	4	7.70	144 080	6	8.05	145 330	2	8.00	154 880	1		154 700	1		154 880	1	
9	144 330	3	8.65	144 430	3	9.10	145 690	2	8.97									
10	144 610	2	9.45	144 680	2	9.90	145 950	1	10.00									
11	144 840	2	10.75	144 880	2	11.35	146 140	1										
12	144 990	2		145 010	1	11.40												
13	145 140	1		145 140	1													
14	145 220	1		145 220	1													
	IP = 145 780 cm^{-1} = 18.06$_8$ ev[a]			IP = 145 860 cm^{-1} = 18.07$_8$ ev			IP = 147 050 cm^{-1} = 18.22$_4$ ev			IP = 156 350 cm^{-1} = 19.37$_8$ ev			IP = 156 400 cm^{-1} = 19.38$_4$ ev			IP = 156 410 cm^{-1} = 19.38$_4$ ev		

[a] Difference from Henning's value; 18.00 ev is due to the difference of conversion factors used.
[b] Superimposed with Henning sharp series, $n=8$.

difficult to tell which way the individual bands are shaded, but the bands belonging to one series are much broader than those of the other series. The measured results are listed in Table II. The sharp and the diffuse series are represented by Eqs. (5) and (6) respectively:

$$\nu_n = 145\,860 - [R/(n-0.01)^2], \quad n=3, 4, 5, \cdots, \quad (5)$$

$$\nu_n = 145\,780 - [R/(n-0.34)^2], \quad n=3, 4, 5, \cdots, \quad (6)$$

The separation of the corresponding bands in the two series decreases rapidly with larger n values and they converge to the same limit, 18.08 ev, within experimental error. The present measurements for the diffuse series[16] agree with Henning's except for his member $n=3$ at 132 900 cm^{-1}. Actually, this band is $n=3$ of the sharp series, and the $n=3$ of the diffuse series should be the one at 130 380 cm^{-1} as shown in the table; this is very close to the value, 130 390 cm^{-1}, suggested by Price and Simpson.[6] The identification of the $n=2$ bands was very difficult in both series. We suggest that the band observed at 960.5 A is probably the one for the diffuse series because of its position, intensity, and diffuse nature. If we assume the same quantum defect as for the $n=3$ band, the expected position of the $n=2$ band of the sharp series is 893 A. This is slightly below the first ionization potential (899 A) and no conspicuous band was observed near this position, nor below this wavelength. Perhaps this band falls in the region 915–930 A where several strong bands remain unidentified.

In the region near the limit of Henning's series four weak bands were observed which also fit well in a Rydberg series. Unfortunately, its lower members, $n<8$, are superimposed with some of Henning's bands, and the higher members, $n>11$, are obscured by a diffuse band at 146 490 cm^{-1} which belongs to another series (see Table II). The spectrum of this region is reproduced in Fig. 2. The wavenumbers of the four bands are listed in Table II under "vibration series" and they are represented by the following equation:

$$\nu_n = 147\,050 - [R/(n-0.01)^2], \quad n=8, 9, 10, \cdots. \quad (7)$$

The wave number differences between the sharp series and this particular series for corresponding n numbers are almost constant and give the average value of $\Delta\nu=1260$ cm^{-1}. As already mentioned, this value approximates the frequency of the stretching vibration of the ground state of CO_2. Also, as one can see in the table, the two series, the sharp and the present series, have similar quantum defects. Consequently, this is the vibration series belonging to Henning's sharp series.

Below the convergent limit of Henning's series, three new Rydberg series were observed (see Fig. 2). Two of them (one is much weaker than the other) are absorption series but the other appears to be an apparent

[16] Neither Hennig nor Rathenau listed the data for the sharp series.

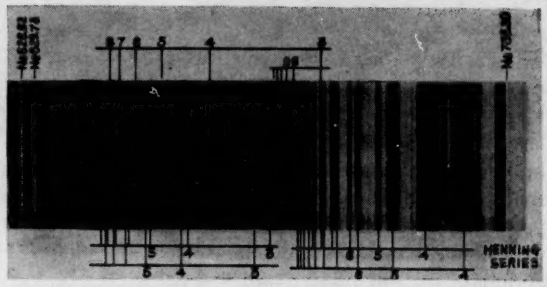

FIG. 2. Rydberg series of CO_2. The series which converge to the highest observed IP are shown at the left. The vibration series which is accompanied by Henning's series is shown in the center.

emission series, all being much weaker than Henning's series. Their wave numbers are listed in Table II and they are represented by the following equations:

$$\nu_n = 156\,350 - [R/(n+0.29)^2], \quad n=3, 4, 5, \cdots, \quad (8)$$

$$\nu_n = 156\,400 - [R/(n-0.05)^2], \quad n=3, 4, 5, \cdots, \quad (9)$$

$$\nu_n = 156\,410 - [R/(n+0.44)^2], \quad n=3, 4, 5, \cdots. \quad (10)$$

All three converge to the same limit, 19.39 ev, within experimental error. This is the highest ionization potential observed in the present work, and no other series or progression of bands was observed below this point although the background available extended to 600 A (20.66 ev). Henning[1] and Rathenau[3] did not observe these series, probably because they are weak in intensity.

Non-Rydberg Bands

In the region below about 850 A, Henning[1] observed two progressions of absorption bands. We tentatively call them the first and second progressions, and we extend them somewhat to shorter wavelengths in the present work as shown in Table III. Both are strong

TABLE III. Henning progressions of absorption bands of CO_2.

First progression			Second progression		
ν(cm^{-1})	I	$\Delta\nu$	ν(cm^{-1})	I	$\Delta\nu$
127 040	5		127 440	2	
128 190	7	1150	128 580	5	1140
129 300	7	1110	129 650	6	1070
130 380	7	1080	130 750	7	1100
131 490	6	1110	131 830	7	1080
132 590	6s	1110	132 950	6	1120
133 740	5s	1150	134 090	5s	1140
134 870	5s	1130	135 180	3s	1090
135 960	4s	1090	136 310	5s	1130
137 100	3s	1140	137 430	5s	1120
138 220	2s	1120	138 550	4s	1120
139 380	3s	1160	139 670	3s	1120
140 500	1s	1120	140 730[a]	10s	1060
			141 890	2s	1160
			143 000	1s	1110
		$\Delta\nu_{Av}$ =1120			$\Delta\nu_{Av}$ =1110

[a] Superimposed with other band.

TABLE IV. Other progressions of absorption bands of CO_2 including Rathenau's.

I (weak and narrow)			II (weak and broad)			III (Rathenau, broad)		
ν(cm^{-1})	I	$\Delta\nu$	ν(cm^{-1})	I	$\Delta\nu$	ν(cm^{-1})	I	$\Delta\nu$
119 900	0		120 050	0		96 600	6	
121 000	1	1100	121 350	1	1300	97 940	6	1340
121 850	1	850	122 440	2	1090	99 240	7	1300
122 880	1	1030	123 470	2	1030	100 570	7	1330
123 890	1	1010	124 380	1	910	101 890[a]	6	1320
124 830	2	940				103 190[b]	2	1300
125 770	2	940						
		$\Delta\nu_{Av}$ = 980			$\Delta\nu_{Av}$ = 1080			$\Delta\nu_{Av}$ = 1320
IV (Rathenau, strong)			V (Rathenau, weak)			VI (Rathenau, double, strong)		
91 830[a]	6		92 360	5		85 160	1	
93 000	5	1170	93 620	5	1260	86 470	3	1310
94 260	9	1260	94 840	3	1220	87 000[a]	5	1230
95 390	5	1130	96 040	2	1200			
96 520	5	1130	97 320[a]	2	1280			
			98 560	2	1240			
		$\Delta\nu_{Av}$ = 1172			$\Delta\nu_{Av}$ = 1240			$\Delta\nu_{Av}$ = 1270
VII (Rathenau, double, weak)								
85 840	1							
87 050	2	1210						
88 170[a]	2	1120						
		$\Delta\nu_{Av}$ = 1165						

[a] Superimposed with other band.
[b] Superimposed with emission line.

progressions, and their strongest bands are almost as strong as the Rydberg bands in the same region. In the first progression, the last eight bands are somewhat sharper than the first five bands. The same phenomenon was also observed in the second progression, namely, all the bands below the 752 A (134 090-cm^{-1}) band are sharper than those of the rest of the progression. We have no adequate explanation for this at this moment. Possibly, there might be two progressions in each; one diffuse, the other sharp. However, we classified them as a single progression because the $\Delta\nu$ values are fairly constant throughout each progression as shown in the table. Rathenau[3] observed two additional weak bands at 125 740 cm^{-1} and 124 710 cm^{-1} in the first progression. They are included in our progression I (see Table IV), which is much weaker than the two progressions already mentioned. In the same region as progression I, we observed another weak progression, II, which is very similar to I in intensity, appearance, and frequency differences. Energetically, these two (I, II) appear close to the region where a progression of the forbidden transition, $(\pi_g^4)\ ^1\Sigma_g^+ - (\pi_g^3\sigma_g)\ ^1\Pi_g$, $^3\Pi_g$, is expected. The excitation energy of the upper state of the transition is 14.6 ev (=850 A) according to Mulligan.[17]

In the narrow region, 735–700 A, a large number of absorption bands were observed in addition to portions of Henning's series and of his progressions (Table III). They appear to be very sharp and perhaps they belong to a Rydberg series arising from the excitation of the $^1\pi_u$ electron whose ionization energy is 17.09 ev (=725 A) according to Mulliken[4] (see Fig. 3). If this is so, Henning's two progressions might belong to that series. The values of $\Delta\nu$ of Henning's progressions are very close to Mrozowski's value of ν_1 of the $^2\Pi_u$ state

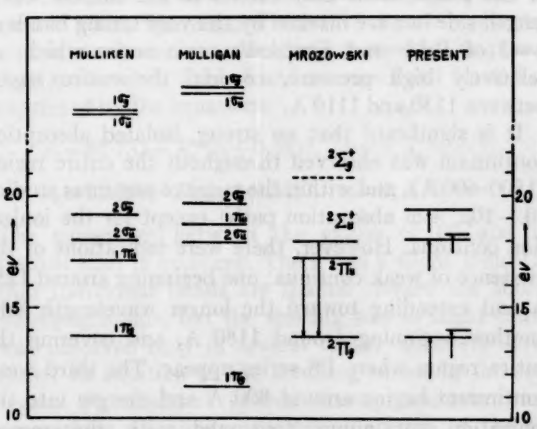

FIG. 3. Energy level diagram of CO_2^+. The energy level of Mrozowski's ground state, $^2\pi_g$, was adjusted to our first ionization potential.

[17] J. F. Mulligan, J. Chem. Phys. 19, 1428 (1951); see also reference 18.

of CO_2^+ [15] which is formed by removing the $^1\pi_u$ electron from the neutral molecule. This evidence strongly supports the "Rydberg series" suggestion stated in the foregoing. Actually, we were unable to identify any such Rydberg series because of the complex appearance of the spectrum in this region and because of the small dispersion of our instrument. We intend to study this region of the spectrum in the near future using an instrument of larger dispersion. Energetically, the upper state (16.3 ev=760 A) of Mulligan's[17] proposed transition, $(\pi_g^4)\ ^1\Sigma_g^+ - (\pi_g^3\sigma_u)\ ^1\Pi_u$, also falls close to this region; however, he suggested that Rathenau's strong progression (see Table IV) may correspond to this transition.

In the region between 970 and 1170 A, Rathenau[8] listed five progressions, some strong and others weak. We confirmed his observations and our data are listed in Table IV. Progression III is a strong progression. Its individual members are degraded toward the red except for the first band at 96 600 cm^{-1}, which showed somewhat violet shading. Actually this is a close doublet, and one component at 96 520 cm^{-1} is identified as a member of progression IV. The third, 99 240 cm^{-1}, and the fourth, 100 570 cm^{-1}, also showed a doublet appearance, and one component of each is identified as $n=3$ of Price and Simpson's minor series (2) and of the main series (2), respectively (see Table I). Progression IV is also a strong progression and its individual bands showed a weak degradation towards the red. The first band at 91 830 cm^{-1} was also identified as the $n=2$ of Price and Simpson's minor series (1). Actually, this is a close doublet, 91 830, 91 890 cm^{-1}, and three other bands, 91 710, 91 630, 91 520 cm^{-1}, also appeared close to its longer wavelength side. The appearance of progression V is similar to that of IV and the first two bands appeared as strong as those of IV, although Rathenau classified this as a weak progression. The last two short progressions (VI) and (VII), are rather weak, particularly the latter. Both of of the progressions may extend to the shorter wavelength side but are masked by the very strong bands of $n=2$ of Price and Simpson's main series which, at relatively high pressure, covered the entire region between 1130 and 1110 A.

It is significant that no strong, isolated absorption continuum was observed throughout the entire region (1500–600 A), and within the range of pressures studied (0.1–10μ, 4-m absorption path) except for the ionization continua. However, there were indications of the existence of weak continua; one beginning around 1250 A and extending toward the longer wavelength side, another beginning around 1180 A, and covering the entire region where PS series appear. The third weak continuum begins around 800 A and merges into the ionization continuum associated with the second ionization potential.

The non-Rydberg bands which appear in the region above 1300 A are discussed by Mulliken[18] in detail, but not those described in the foregoing which are below 1300 A.

Discussion of Rydberg Bands

The energy level diagram of CO_2^+, with the theoretical calculations and the spectroscopic results, is shown in Fig. 3. Mulliken[4,5] proposed several ionization energies for this molecule based on experimental data and his rough theoretical calculations. He identified Henning's series limit as the ionization energy of the $2\sigma_u$ electron. By interpreting the emission bands at 2900 A as caused by the transition $(\sigma_u)^{-1} - (\pi_g)^{-1}$ of CO_2^+, and combining this with Henning's ionization value he obtained 13.72 ev for the ionization energy of the $1\pi_g$ electron, which corresponds to the first ionization potential of this molecule. His value agrees well with Price and Simpson's value and with our present value. Mulligan[7] also made theoretical calculations for the ionization energies of the molecule. His value for the $1\pi_g$ electron is 11.5 ev, which is far smaller than the value discussed in the foregoing. We examined our plates carefully, but were unable to find any Rydberg series which converged to, or near, his value.

Mulligan's value for the $2\sigma_u$ electron agrees well with Henning's series limit. Our newly observed value at 18.23 ev may not correspond to Mulligan's value for the $1\pi_u$ electron; although the two values are fairly close to one another. Instead, as discussed earlier, it corresponds to the limit of the vibration series (stretching vibration) belonging to Henning's sharp series. For the $1\pi_u$ electron, Mulliken proposed an ionization value of 17.09 ev under the assumption that the emission bands of CO_2^+ at 3660 A are due to the transition $(\pi_u)^{-1} - (\pi_g)^{-1}$; the lower state being the ground state $^2\Pi_g$. As mentioned previously, the spectrum observed in the corresponding region (730 A) showed a complicated appearance, and we had difficulty in identifying any Rydberg series that might have been present. If there is a Rydberg series which converges to Mulliken's value, it must be a doublet with a separation of about 100 cm^{-1} at the series limit.[15]

The highest ionization potential which we observed, 19.39 ev, agrees fairly well with Mulligan's value for the $2\sigma_g$ electron. Mulliken's value for this electron is 19.1 ev which also agrees with our present value. Mrozowski[19] suggested a $^2\Sigma_g^+$ state at about 20.9 ev,[20] which he calculated from the observed Λ doubling in the $^2\Pi_{\frac{1}{2},g}$ state, by using Van Vleck's theory and by assuming a relation of "pure precession" between these two states. This is slightly beyond the lower limit of our background (600 A). We did not observe any absorption bands below 640 A; instead, a continuous absorption

[18] R. S. Mulliken, Can. J. Chem. **36**, 10 (1958).

[19] S. Mrozowski, Revs. Modern Phys. **14**, 216 (1942); see also references 11 and 15.

[20] As Mrozowski did not give a numerical value we estimated this value from his figure.

extended into this region from the shorter wavelength side.

Apparent Emission Series

The apparent emission series were observed not only with CO_2 but with other linear triatomic molecules which we studied. Hopfield[21] and others[22] also observed such a phenomenon in N_2. We believe that such series are not real emission series but are caused by a photographic effect brought about by closely related absorption bands of a very diffuse nature. More detailed experimental results and a discussion of this phenomenon will be published elsewhere at a later date.

The writers are indebted to Professor R. S. Mulliken for his interest and considerate discussions on this work.

[21] J. J. Hopfield, Phys. Rev. **36**, 789 (1930).
[22] T. Takamine, T. Suga, and Y. Tanaka, Sci. Papers Inst. Phys. Chem. Research (Tokyo) **34**, 854 (1938).

THE JOURNAL OF CHEMICAL PHYSICS VOLUME 32, NUMBER 4 APRIL, 1960

Higher Ionization Potentials of Linear Triatomic Molecules. II. CS_2, COS, and N_2O

Y. TANAKA, A. S. JURSA, AND F. J. LEBLANC

Geophysics Research Directorate, Air Force Cambridge Research Center, Laurence G. Hanscom Field, Bedford, Massachusetts

(Received September 8, 1959)

Four ionization potentials for the CS_2 molecule, three for the COS, and three for the N_2O were determined by an analysis of Rydberg series of the respective molecules. Our value for the first ionization potential of CS_2 agrees very well with the previous spectroscopically determined value; however, there was disagreement between our value for the first ionization potential of N_2O and that determined previously.

Several progressions of absorption bands for each of the molecules were also observed.

INTRODUCTION

THE first (or lowest) ionization potential of CS_2 and of N_2O has been reported, from spectroscopic observations, by Price and Simpson[1] and by Duncan,[2] respectively; however, none has been reported for COS. To our knowledge, no report is available concerning the higher ionization potentials of those molecules. As we reported in part I of this series[3] for CO_2, we observed three of its ionization potentials including the lowest one. Because the three present molecules have structures similar to that of CO_2, an attempt was made to find new Rydberg series for these three molecules which converge to their higher ionization potentials.

EXPERIMENTAL

The experimental apparatus and procedure were exactly the same as that used for CO_2 and described in the preceding paper[3]; the only difference being in purification methods. For CS_2, an ordinary grade of commercial CS_2 was evaporated in vacuum and introduced into the spectrograph without further purification. Commercial tank COS and N_2O were both purified by fractional distillation several times before use. For CS_2 and N_2O, no impurity bands were observed, but, for COS, weak CO_2 bands always appeared as an impurity. A pressure range of 0.1–10 μ was used for all these gases.

[1] W. C. Price and D. M. Simpson, Proc. Roy. Soc. (London) **A165**, 272 (1938).
[2] A. B. F. Duncan, J. Chem. Phys. **4**, 638 (1936).
[3] Y. Tanaka, A. S. Jursa, and F. J. LeBlanc, J. Chem. Phys. **32**, 1199 (1960), this issue.

RESULTS

CS_2

A. Rydberg Bands. Price and Simpson (PS)[1] observed two strong Rydberg series for this molecule; one converging to 10.130 ev[4] and the other to 10.076 ev.[4] This is the first ionization potential of the molecule. According to them, the difference between the two limits corresponds to the doublet separation of the ground state, $^2\Pi_{g,3/2,1/2}$, of the CS_2^+ ion. We observed the two series and extended both to $n=18$. The present data are listed in Table I under series I and II, and are expressed by the equations

$$\nu_n = 81\,735 - R/(n+0.54)^2, \quad n=3, 4, 5, \cdots, \quad (1)$$

$$\nu_n = 81\,299 - R/(n+0.56)^2, \quad n=3, 4, 5, \cdots. \quad (2)$$

The agreement between the values of PS and the present ones is excellent. There was a slight indication that individual bands are shaded toward the shorter wavelength side, but the shading was so slight that it was observed only in several earlier members of the series. In addition to the Rydberg series, in the same region we observed several strong doublets whose separations are similar to the separation of the two

[4] The conversion factor which we used differs from theirs. Their original values for the series limits expressed in ev are 10.083 and 10.027 ev.

TABLE I. Rydberg series of CS_2.

	I Strong absorption			II Strong absorption			III Strong absorption			IV Strong absorption		
n	ν(cm^{-1})	I	n^*	ν(cm^{-1})	I	n^*	ν(cm^{-1})	I	n^*	ν(cm^{-1})	I	n^*
2							89 550	10	2.03	96 570	8	2.30
							89 920	10		97 120	7	
3	73 048	10	3.57	72 564	10	3.55	104 240	8	2.92	107 300	6	3.37
							104 780	8		107 800	4	
4	76 405	10	4.53	75 975	10	4.53	109 950	6	4.22	111 110	5	4.66
							110 560	5		111 700	3	
5	78 165	8	5.53	77 730	8	5.54	112 390	5	4.99	113 030	5	5.44
6	79 182	7	6.59	78 740	7	6.55	113 740	5	6.02	114 090	5	6.38
7	79 803[a]	8	7.51	79 373	7	7.51	114 540	4	7.03	114 770	4	7.45
8	80 234	5	8.61	79 803	8	8.69	115 060	4	8.16	115 210	4	8.43
9	80 526	4	9.51	80 088	5	9.50	115 400	3	8.85	115 520	3	9.35
10	80 746	3	10.65	80 308	5	10.70	115 670	3	10.20	115 750	3	10.40
11	80 905[a]	3	11.25	80 465	3	11.48	115 850	2	11.15	115 920	2	
12	81 041	3	12.60	80 593	4	12.10	115 990	2				
13	81 139	2	13.60	80 703	2	13.70	116 120	1				
14	81 217	2	14.55	80 780	3	14.85						
15	81 281	2	16.30	80 840	2							
16	81 327	2	16.55	80 905	2							
17	81 371	1	17.45	80 932	1							
18	81 409	1		80 976	0							
	IP=81 735 cm^{-1} =10.130 ev			IP=81 299 cm^{-1} =10.076 ev			IP=116 760 cm^{-1} =14.47$_1$ ev			IP=116 760 cm^{-1} =14.47$_1$ ev		

	V Strong absorption			VI Apparent emission			VII Apparent emission			VIII Weak absorption[b]		
n	ν(cm^{-1})	I	n^*	ν(cm^{-1})	I	n^*	ν(cm^{-1})	I	n^*	ν(cm^{-1})	I	n^*
2							113 420	5	2.53			
3	120 580	10	3.39	117 780	4	2.93	121 740	3	3.53	144 350	3	3.01
4	124 430	6	4.25	123 450	3	3.92	125 200	2	4.48	149 660	3	4.02
5	126 530	5	5.16	126 050	3	4.90	127 010	1	5.54	152 090	2	5.32
6	127 760	5	6.23	127 470	2	5.95	128 020	1		153 220	2	5.83
7	128 490	4	7.23	128 300	2	6.72				154 120	1	7.12
8	128 970	4	8.16	128 890	1	8.00				154 620	1	8.00
9	129 310	3	9.23	129 250	1					154 980	1	
10	129 550	3	10.20									
11	129 730	2	10.88									
12	129 880	1										
	IP=130 540 cm^{-1} 16.17$_9$ ev			IP=130 600 cm^{-1} =16.18$_7$ ev			IP=130 610 cm^{-1} =16.18$_8$ ev			IP=157 390 cm^{-1} =19.50$_7$ ev		

[a] Superimposed with another absorption band.
[b] Absolute intensity of this series is approximately 100 times weaker than other absorption series.

corresponding members (with same n) in the series already described. They are listed in Table II, but we have no adequate explanation for them at the moment.

The second ionization potential observed was 14.47 ev where, within experimental error,[5] two strong series converge. They are listed in Table I under series III and IV and are expressed by Eqs. (3) and (4), respectively,

$$\nu_n = 116\,760 - R/(n+0.06)^2, \quad n=2, 3, 4, \cdots, \qquad (3)$$

$$\nu_n = 116\,760 - R/(n+0.42)^2, \quad n=2, 3, 4, \cdots. \qquad (4)$$

Part of the series is reported in Fig. 1, together with other series which will be described shortly. The earlier members (n=2, 3, 4) of both series were observed as narrow doublets (see Table I) with an approximate separation of 500–600 cm^{-1}. Probably, one band of each

[5] Actually, the two values coincided accidentally (see Table I).

TABLE II. Absorption bands associated with series I and II of CS_2.

n	Series I and II ν(cm^{-1})	Associated bands ν(cm^{-1})		
3	72 564	74 051	75 436	...
	73 048	74 482	75 907	77 308
4	75 975	77 460	78 942	80 403
	76 405	...	[a]	80 618
5	77 730	[a]	80 703[b]	
	78 165	79 599	81 041[b]	
6	78 740	80 234[b]		
	79 182	80 618		
7	79 373	80 780		
	79 803	81 281		

[a] Superimposed with an emission line.
[b] Superimposed with another ansorption band.

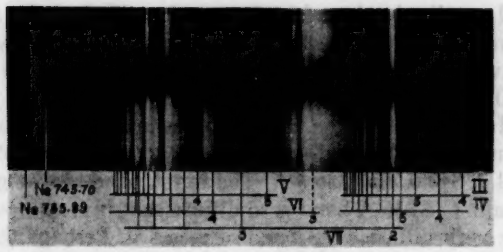

FIG. 1. Rydberg series of the CS_2 molecule converging to the second and third ionization potentials.

doublet (that of the shorter wavelength) is the vibration band ($v'=1$); however, we used the average value of the doublet in calculating the ionization potential. Again, it was very difficult to tell which way the individual bands were shaded even with the earllier members of the series. In analogy with CO_2^+, the state to which the present two series converge in CS_2^+ is most probably the $^2\Sigma_u^+$ state which corresponds in CO_2^+, to the state to which Henning's series converge. The intensity of the band at 1117 A ($n=2$ of III) is extraordinarily strong, as is that of the CO_2 band at 1088 A[6] mentioned in our previous paper.[3] Because it appeared stronger than that of the CO_2 band, under similar experimental conditions, its absorption coefficient will exceed 4000 cm^{-1}.[7]

The third ionization potential observed was 16.18 ev where three series converged. One is a strong absorption series but the other two are apparent emission series.[8] They are listed in Table I under series V, VI, and VII and are expressed, respectively, by Eqs. (5), (6), and (7),

$$\nu_n=130\,540-R/(n+0.19)^2,\quad n=3,4,5,\cdots, \quad (5)$$

$$\nu_n=130\,600-R/(n-0.10)^2,\quad n=3,4,5,\cdots, \quad (6)$$

$$\nu_n=130\,610-R/(n+0.52)^2,\quad n=2,3,4,\cdots. \quad (7)$$

The spectrum of this region is reproduced in Fig. 1. As can be seen in the figure, the individual bands of series V show more or less violet shading while those of VI show red shading if we consider them as absorption. Furthermore, the separation of corresponding members of the two series V and VI, particularly at a larger n, becomes less. Consequently, the portion between the bands of the two series resembled an emission series. The wavelengths for series VI were measured at the longer wavelength edge of the apparent emission series. Perhaps the best explanation at the moment for the rather strange features of series VI is that the individual bands, which were originally weak and red-shaded in absorption, became extremely diffuse, because of the effect of preionization which produced a "less-absorbed" portion between the bands under consideration and the corresponding bands of series V which were also affected in a like manner. The bands with $n=3$, 4 of series V are very diffuse[9] which tends to support this statement. Series VII is also an apparent emission series, but its individual bands are much narrower than those of the apparent emission series VI. The explanation proposed for VI is applicable for the appearance of this series of bands, namely, each apparent emission band, in this case, was produced by two absorption bands which are situated close to each other, thus leaving a less absorbed portion between them; although in this case it is not easy to recognize the absorption bands responsible for the effect as such. If this explanation is accepted, it implies that there are two absorption series converging to the same limit as series VII. In analogy with CO_2^+, the state to which the present three series converge in CS_2^+, will correspond to the state of CO_2^+ whose observed energy is 19.38 ev [measured from the ground state of CO_2 (see reference 3)].

The fourth ionization potential observed in this molecule was 19.51 ev where one absorption series converges. It is listed in Table I under series VIII and is expressed by the following equation:

$$\nu_n=157\,390-R/(n+0.05)^2,\quad n=3,4,5,\cdots. \quad (8)$$

Compared with all the previous ones, this is a very weak series and was observed only when the pressure was relatively high ($\sim 10\,\mu$). However, its individual bands were narrow in appearance and enabled us to measure them fairly accurately to $n=9$. No corresponding series was observed in CO_2 because of the lack of background radiation in the appropriate region.

B. Non-Rydberg Bands. Price and Simpson[1] observed two progressions of bands in the region 2300–1650 A. These are out of range of the background (argon continuum) in our present work. They also listed four groups of bands in the region 1621–1550 A, most of which are very strong bands; but no regularity was mentioned. We observed the same bands, and, in addition, four additional groups were observed in the region 1530–1360 A, and are listed in Table III. Their intensities and features are very similar to the groups observed by PS.

Three progressions were identified in this region (see Table III). Progression (1), which begins at 88 834 cm^{-1}, is composed of strong, but very diffuse, bands with an average interval of 490 cm^{-1}. Progression (2) has an average interval of 590 cm^{-1}. Compared with (1), the individual bands of progression (2) are weaker and much narrower. Actually, this progression is not as simple as described in the foregoing, but each band is closely associated with several weak bands which we

[6] This band of CO_2 belongs to the Rydberg series which converges to the first ionization potential, while the 1117 A band of CS_2 belongs to the series converging to the second ionization potential.

[7] K. Watanabe, M. Zelikoff, and E. C. Y. Inn, AFCRC Technical Report No. 53-23, Geophysical Research Papers, No. 21, June, 1953.

[8] See section entitled "Apparent Emission Series" in footnote 3.

[9] The $n=3$ band, particularly, was very strong and diffuse even at low pressure.

TABLE III. Progressions and groups of absorption bands of CS_2.

Groups of Bands						Progressions of Bands											
1525 A Group		1444 A Group		1420 A Group		1385 A Group		1. Diffuse			2. Weak but sharp			3. Very weak			
ν(cm^{-1})	I	ν(cm^{-1})	I	ν(cm^{-1})	I	ν(cm^{-1})	I	ν(cm^{-1})	I	$\Delta\nu$	ν(cm^{-1})	I	$\Delta\nu$	ν(cm^{-1})	I	$\Delta\nu$	
65 584	5	69 248	5	70 449	5	72 192	2	88 834	2		100 300	1		140 410	0		
65 738	5	69 493	6	70 585	6	72 319	6	90 293	6	3×486	100 910	3	610	141 000	1	590	
65 781	4	69 611	2	70 630	5	72 564*	10	90 818	5	525	101 510	3	600	141 560	1	560	
65 853	5	69 662	2	70 796	7	72 597	4	91 333	4	515	102 090	3	580	142 130	2	570	
66 115	7	69 703	2	70 925	10	72 680	10	91 819	3	486	102 680	2	590	142 670	2	540	
66 271	3	69 783	3	71 292	5	72 717	4	92 293	2	474	103 250	1	570	143 250	2	580	
66 376	6	69 904	4	71 352	5	72 795	10	92 782	2	489				143 800	3	550	
66 571	3			71 390	5	72 956	7	93 266	1	484				144 340	3	540	
						73 048*	10							144 930	2	590	
										$\Delta\nu_{av}$ = 492			$\Delta\nu_{av}$ = 590	145 450	0	520
																$\Delta\nu_{av}$ = 560	

* Superimposed with Rydberg band.

did not list in the table. Progression (3) includes ten bands. It is very weak but shows a good regularity in wave number differences with an average value of 560 cm^{-1}.

In addition to the three progressions already mentioned, we observed four prominent bands at 849.1, 844.2, 840.6, and 836.3 A. The 844-A band is strongest of all. The 836-A band is so diffuse that it merges with the very diffuse $n=3$ band of series V. Perhaps these four also form a progression whose average interval is approximately 600 cm^{-1}.

As in our work with CO_2, we did not observe any strong and isolated continuous absorption for this molecule throughout the entire region except for the ionization continua. However, there was evidence of some weak continua existing, but they were so weak and were superimposed with many bands[10] that it was very difficult to locate the positions of their maximum intensity.

COS

A. Rydberg Bands. We searched, in the region 1070–1300 A (11.6–9.5 ev), to find a Rydberg series which converged to the first ionization potential of this molecule. Because of the complicated appearance of the band spectrum in this region, we were unable to locate such a series with certainty. Several bands seem to form the end of two series at about 1112 A; however, an extension of that series to the longer wavelength side proved very difficult. Nevertheless, we listed these in Table IV, under series I and II and they are roughly expressed by the equations

$$\nu_n = 90\,610 - R/(n+0.62)^2, \quad n=7, 8, 9, \cdots, \quad (9)$$

$$\nu_n = 90\,740 - R/(n+0.56)^2, \quad n=7, 8, 9, \cdots. \quad (10)$$

The bands are doublets, each member of which forms a series with limits of convergence of 11.23 and 11.25 ev. In addition, there are two strong doublets, one at 1399.9 and 1385.8 A, and one at 1293.0 and 1281.9 A; the former belongs to one of PS[1] progressions (see Table V) and the latter belongs to one of the newly identified progressions (see Table V). They are very strong, actually the strongest bands in this region, and they possibly form a Rydberg series; although the higher members could not be identified. If these are the earlier members ($n=2$, 3) of a Rydberg series, the series limit comes roughly at 10.5 ev. At any rate, we failed to find the first ionization potential of this molecule and the values mentioned in the foregoing are only in the nature of suggestions.

The second ionization potential observed was 16.04 ev where, within experimental error, four series converge. They are all in absorption as shown in Fig. 2, and wave numbers are listed in Table IV under series III, IV, V,

[10] No measurement was made for these bands. They are very weak and are observed only at high pressure.

TABLE IV. Rydberg series of COS.

n	I Absorption ν(cm^{-1})	I	n^*	II Absorption ν(cm^{-1})	I	n^*	III Absorption diffuse ν(cm^{-1})	I	n^*	IV Absorption diffuse ν(cm^{-1})	I	n^*	V Absorption sharp ν(cm^{-1})	I	n^*	VI Absorption sharp ν(cm^{-1})	I	n^*	VII Apparent emission ν(cm^{-1})	I	n^*
2							107 250	8	2.19	112 060	7	2.52									
							107 790	5		112 640	5										
										113 170	3										
3	[a]						119 320	6	3.28	120 530	6	3.51	116 130	8	2.85	116 970	8	2.96			
4	85 530	4	4.54				123 540	5	4.31	124 030	5	4.55	122 230	7	3.93	122 500	5	3.98	138 100	3	4.16
5	87 280	3		87 380	3		125 550	4	5.35	125 770	3	5.50	124 820	6	4.94	125 000	4	5.19	140 390	3	4.83
6	[a]			[a]			126 660	3	6.32	126 800	3	6.49	126 210	4	5.87	126 210	4		141 860	2	6.11
7	88 730	3	7.64	88 840	3	7.58	127 360	3	7.17	127 450	2		127 070	3	6.80				142 630	2	7.17
8	89 140	4	8.63	89 260	3	8.85	127 850	2	8.34	Higher members are			127 640	2	7.92	Higher members are			143 120	1	8.25
9	89 430	3	9.67	89 530	2	9.25	128 170	2	9.23	superimposed with			128 010	2		superimposed with			143 450	1	
10	89 640	3		89 770	2		128 410	1	10.63	those of series III.						those of series V and					
11							128 570	1								III.					
12							128 680	1													
	IP=90 610 cm^{-1} =11.23 ev			IP=90 740 cm^{-1} =11.25 ev			IP=129 400 cm^{-1} =16.03$_8$ ev			IP=129 400 cm^{-1} =16.03$_8$ ev			IP=129 390 cm^{-1} =16.03$_7$ ev			IP=129 330 cm^{-1} =16.02$_9$ ev			IP=144 680 cm^{-1} =17.93$_1$ ev		

[a] Superimposed with an emission line.

TABLE V. Progressions of absorption bands of COS.

1. Diffuse ν(cm^{-1})	I	$\Delta\nu$	2. Sharp ν(cm^{-1})	I	$\Delta\nu$	3. Sharp ν(cm^{-1})	I	$\Delta\nu$	4. Sharp ν(cm^{-1})	I	$\Delta\nu$	5. Sharp ν(cm^{-1})	I	$\Delta\nu$	6. Sharp ν(cm^{-1})	I	$\Delta\nu$	7. Sharp ν(cm^{-1})	I	$\Delta\nu$
63 720	4		70 907	4		71 435	5		71 531	1		71 696	2		71 785	3		71 887	3	
63 800	4																			
64 630	6	920[a]	71 631	4	724	72 162	6	727	72 234	4	703			2×723	72 504	2	719	72 631	2	744
64 730	6																			
65 490	7	870[a]	72 345	5	714	72 880	5	718	72 969	5	735	73 141	2		73 241	2	737	73 328	2	697
65 600	7																			
66 350	8	850[a]	73 052	4	707	73 581	6	701	73 659	3	690	73 853	2	712	73 965	2	724	74 020	2	692
66 440	8																			
		2×760[a]	73 724	3	690	74 268	5	687	74 378	3	719	74 555	2	702	74 674	2	709	74 674	2	654
67 910	5		74 449	2	707	74 975	4	707				75 237[b]	1	682	75 357	1	683	75 278	1	604
68 630	3	720	75 182	2	733	75 686	3	711				75 694	1	727	76 043	1	686	75 857	1	579
69 320	2	690	75 899	1	717	76 364	3	678												

8. Sharp ν(cm^{-1})	I	$\Delta\nu$	9. Sharp ν(cm^{-1})	I	$\Delta\nu$	10. Sharp ν(cm^{-1})	I	$\Delta\nu$	11. Sharp ν(cm^{-1})	I	$\Delta\nu$	12. Sharp ν(cm^{-1})	I	$\Delta\nu$	13. Sharp ν(cm^{-1})	I	$\Delta\nu$	14. Sharp ν(cm^{-1})	I	$\Delta\nu$
72 774	5		77 273	10		79 286	8		80 845	5		81 227	6		77 109	1		77 434	4	
73 506	6	732	78 012	8	739	79 993	7	707	81 551	4	706	81 945	4	718	77 797	4	688	78 156	3	722
74 223	6	717	78 719	7	707	80 682	3	689	[b]			82 629	4	684	78 497	3	700	78 850	3	694
74 909	3	686							82 851	3	2×650				79 199	3	702	79 548	2	698
75 581	3	672							83 569	3	718				79 884	2	685	80 216	2	668
76 245	2	664													80 566	1	682			
															81 227	1	661			

[a] Average between the two doublets.
[b] Superimposed with another band.

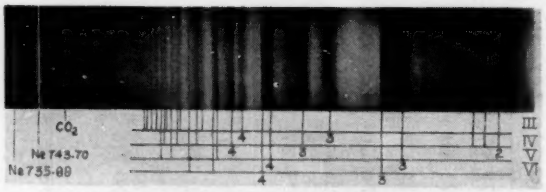

FIG. 2. Rydberg series of the COS molecule converging to the second ionization potential.

and VI, which are expressed, respectively, by the equations

$$\nu_n = 129\,400 - R/(n+0.32)^2, \quad n=2, 3, 4, \cdots, \quad (11)$$

$$\nu_n = 129\,400 - R/(n+0.51)^2, \quad n=2, 3, 4, \cdots, \quad (12)$$

$$\nu_n = 129\,390 - R/(n-0.12)^2, \quad n=3, 4, 5, \cdots, \quad (13)$$

$$\nu_n = 129\,330 - R/(n+0.04)^2, \quad n=3, 4, 5, \cdots. \quad (14)$$

The bands of series III are diffuse and show almost no indication of shading, but those of series IV show a distinct shading toward the shorter wavelengths. Both series V and VI are much sharper compared with the previous two series. The bands of series V have no shading while those of series VI show sharp heads and degrade toward longer wavelengths. All four series are of roughly equal intensity; although series V and VI appeared a little stronger because of their sharpness.

The energy state of COS^+ to which the present four series converge is probably the $^2\Sigma$ which may be considered to correspond to the $2\sigma_u^{-1}\ ^2\Sigma_u^+$ of CO_2^+.[3]

The third ionization potential observed was 17.93 ev where an apparent emission series converges. It is listed in Table IV under series VII and is expressed by the equation

$$\nu_n = 144\,680 - R/(n+0.10)^2, \quad n=4, 5, 6, \cdots. \quad (15)$$

This is a very weak series and is somewhat confusing because of Henning's series of CO_2 which, in this case, appears as an impurity. However, because CO_2 has no apparent emission bands in this region, we are certain that the series is due to the COS molecule. The energy state of COS^+ as determined by the convergence limit of the present series (series VII) may be assumed to correspond to that one of CO_2^+ (to which three weak series converged[3]) whose energy is 19.38 ev measured from the ground state of CO_2.

B. Non-Rydberg Bands. In the region between 1565 and 1250 A, Price and Simpson[1] observed eight progressions whose frequency differences fall in the range 700 to 790 cm^{-1}. We confirmed all of them, and, in addition, also observed several other similar progressions in the same region. All the observed progressions are listed in Table V. It is interesting that the frequency difference of about 750 cm^{-1} is so prevalent; actually no

TABLE VI. Rydberg series of N_2O.

	I Absorption			II Absorption			III Absorption			IV Absorption			V Absorption		
n	ν(cm^{-1})	I	n^*	ν(cm^{-1})	I	n^*	ν(cm^{-1})	I	n^*	ν(cm^{-1})	I	n^*	ν(cm^{-1})	I	n^*
2	84 633	7	2.35	84 960	10	2.36	99 710	10	1.80						
3	94 751	5	3.44	94 916	7	3.45	119 650	9	2.94	117 930	7	2.77			
4	98 452	5	4.57	98 608	7	4.54	125 270	8	3.96	124 520	6	3.79			
5	100 170	4	5.35	100 360	6	5.37	127 810	8	5.03	127 390	4	4.78			
6	101 280	3	6.28	101 460	5	6.14	129 130	7	5.92	128 910	4	5.82			
7	101 990	3	7.39	102 220	4	7.07	129 970	5	7.02	129 790	3	6.72			
8	102 440	2	8.63	102 730[a]	3		130 490	5	8.00	130 380	3		131 740	3	7.71
9	102 730[a]	2	9.36				130 850	3	8.97				132 140	3	9.26
10	102 960	1	10.20				131 110	3	10.20	Higher members are			132 380	2	9.67
11	103 140	1	11.43				131 290	2	11.15	superimposed with			132 590	2	
12	103 270	1					131 430	1		those of series III.			132 800	1	
	IP=104 000 cm^{-1} =12.88$_9$ ev			IP=104 300 cm^{-1} =12.92$_7$ ev			IP=132 210 cm^{-1} =16.38$_6$ ev			IP=132 250 cm^{-1} =16.39$_1$ ev			IP=133 490 cm^{-1} =16.54$_4$ ev		

	VI Absorption			VII Absorption			VIII Apparent emission			IX Apparent emission		
n	ν(cm^{-1})	I	n^*	ν(cm^{-1})	I	n^*	ν(cm^{-1})	I	n^*	ν(cm^{-1})	I	n^*
2							141 580	3	2.30	142 900	3	2.36
3	147 340	6	2.74	149 600	8	2.94	152 210	2	3.32	152 910	2	3.43
4	154 130	5	3.69	155 220	7	3.99	156 300	1	4.34	156 640	1	4.48
5	157 190	5	4.76	157 710	6	4.91	158 280	0		158 450	0	
6	158 730	4	5.73	159 120	5	5.97						
7	159 650	3	6.43	159 940	4	6.93						
8	160 320	2	7.71	160 480	3	7.92						
9	160 720	2	8.48	160 850	3							
10	161 030[a]	2	10.00	161 030[a]	2							
11	161 220[a]	2		161 220[a]	2							
	IP=162 130 cm^{-1} =20.09$_5$ ev			IP=162 200 cm^{-1} =20.10$_5$ ev			IP=162 200 cm^{-1} =20.1$_0$ ev			IP=162 160 cm^{-1} =20.1$_0$ ev		

[a] Superimposed with another band.

other frequency difference was observed. Another interesting observation is that the bands of progression (1) have a very diffuse nature, while the bands belonging to the rest of the progressions are very sharp and show almost no indication of shading. The bands which were proposed as being the earlier members of a Rydberg series, mentioned in a previous paragraph, are actually members of the present progression; namely, $n=2$, at 71 435, 72 162 cm^{-1}, belongs to progression (3) and $n=3$, at 77 273, 78 012 cm^{-1}, belongs to progression (9).

No strong bands were observed in the region of the helium continuum (600–1050 A) except for the Rydberg bands which we mentioned earlier. However, at high pressure, many weak bands, mostly diffuse, begin to appear, in particular, in the region above about 900 A. As with the previous two molecules, CO_2, CS_2, no strong continuum was observed in the entire region except for the ionization continua.

N_2O

A. Rydberg Bands. The Rydberg series observed in our present work are listed in Table VI. The corresponding bands with the same n of series I and II form close doublets and converge to 12.89 ev and 12.93 ev, respectively. This is the first ionization potential observed in this molecule and it agrees with the values obtained by other methods.[11] The two series mentioned in the foregoing are expressed by the equations

$$\nu_n = 104\,000 - R/(n+0.40)^2, \quad n=2, 3, 4, \cdots, \quad (16)$$

$$\nu_n = 103\,300 - R/(n+0.32)^2, \quad n=2, 3, 4, \cdots. \quad (17)$$

It was difficult to say which way the individual bands were shaded, but the $n=2$ bands of both series showed a distinct shading toward the red. Duncan[2] observed five absorption bands below 1058 A and arranged four of them in a Rydberg series and included two continua, D and F, as its earlier members. His value of the series limit is 102 567 cm^{-1} (12.712 ev) which disagrees with ours. Our present series does not include any continuum. The $n=2$ band of our series II is exceptionally strong as is the case with the corresponding bands in CO_2 (at 1088 A)[3] and CS_2 (at 1117 A). Duncan observed the band but mentioned that this might be the first member of a Rydberg series which converges to a higher ionization potential lying at λ below 850 A. According to our observation, none of the series which converged to higher ionization potentials included this band (see Table VI). The difference of the two series limits mentioned above is 300 cm^{-1}, which is greater than the estimated experimental error. This indicates that the ground state of N_2O^+ is $^2\Pi$ and that its doublet separation is approximately of this magnitude.

The second ionization potential observed was 16.39 ev to which two absorption series, III and IV, converge; each is represented by the following equations, respectively,

$$\nu_n = 132\,210 - R/(n+0.00)^2, \quad n=2, 3, 4, \cdots, \quad (18)$$

$$\nu_n = 132\,250 - R/(n-0.22)^2, \quad n=3, 4, 5, \cdots. \quad (19)$$

Series III is much stronger than series IV, and their individual bands showed almost no shading. Both series are associated with vibration bands which are shown in Table VII. One can see from the table, that the vibration frequencies of the upper states in both series are approximately 1300 cm^{-1} which approaches the value of ν_1(1288.5 cm^{-1}) of the ground state of this molecule.

Series V, in which only five bands were identified near its limit, converges to 16.54 ev and is expressed by the equation

$$\nu_n = 133\,490 - R/(n-0.11)^2, \quad n=8, 9, 10, \cdots. \quad (20)$$

The difference between the two limits of series III and V is 1280 cm^{-1} which is very close to one of the fundamental frequencies, $\nu_1=1288.5$ cm^{-1}, of the ground state. Furthermore, the average difference between the two corresponding bands (with same n) of series III

TABLE VII. Vibration bands associated with series III and IV of N_2O.

n \ v'	Series III 0	1	2	Series IV 0	1	2
2	99 710 99 890					
3	119 650 119 910 1290 1350	120 940 121 260 1090	122 350	117 930 1290	119 220 1260	120 480
4	125 270 125 400 1320	126 590 1220	127 810	124 520 1300	125 820	
5	127 810			127 390 1340	128 730	

[11] K. Watanabe, J. Chem. Phys. **26**, 542 (1957).

TABLE VIII. Progressions of absorption bands of N_2O.

1. Weak			2. Weak			3. Strong, diffuse			4. Weak, diffuse			5. Weak, diffuse		
ν(cm^{-1})	I	$\Delta\nu$	ν(cm^{-1})	I	$\Delta\nu$	ν(cm^{-1})	I	$\Delta\nu$	ν(cm^{-1})	I	$\Delta\nu$	ν(cm^{-1})	I	$\Delta\nu$
84 400	2		86 130	3		86 690	4		112 210	3		112 880	2	
85 730	2	1330	87 660	2	1530	87 420	4	730	113 510	2	1300	114 160	1	1280
87 070	1	1340	89 080	5	1420	88 270	4	850	114 680	1	1170	115 230	1	1070
88 430	1	1360	90 680	4	1600	89 080	5	810	115 890	1	1210	116 410	1	1180
89 710	1	1280	92 200	2	1520	89 970	5	890						
						90 680	4	710						
						91 660	3	980						
						92 400	1	740						
		$\Delta\nu_{Av}$ =1328			$\Delta\nu_{Av}$ =1518			$\Delta\nu_{Av}$ =816			$\Delta\nu_{Av}$ =1227			$\Delta\nu_{Av}$ =1177

and V is also close to this value. Consequently, series V is the vibration series associated with series III. The vibration bands attached to the earlier members of series III (see Table VII) is actually the extension of series V, and the members between $n=4$ and 8 are not listed in Tables (VI and VII) because they are superimposed with other bands. Energetically, the state of N_2O^+, where series III and IV converge, may be assumed to correspond to the $^2\Sigma_u^+$ state of CO_2^+ where Henning's two series converge.[3]

The third ionization potential observed was 20.10 ev to which, within experimental error, four series, VI, VII, VIII, and IX, converge. They are listed in Table VI and are expressed, respectively, by the equations

$$\nu_n = 162\,130 - R/(n-0.31)^2, \quad n=3, 4, 5, \cdots, \quad (21)$$

$$\nu_n = 162\,200 - R/(n-0.06)^2, \quad n=3, 4, 5, \cdots, \quad (22)$$

$$\nu_n = 162\,200 - R/(n+0.32)^2, \quad n=2, 3, 4, \cdots, \quad (23)$$

$$\nu_n = 162\,160 - R/(n+0.42)^2, \quad n=2, 3, 4, \cdots. \quad (24)$$

Series VI and VII are absorption but VIII and IX are apparent emission. A reproduction of the spectrum of this region is shown in Fig. 3. As one sees in the figure, series VII is stronger than VI, and the doublet structure can be seen clearly in the earlier members ($n=3$, 4). Perhaps series VI also has doublet structure because the $n=4$ band showed, slightly, just such an indication. However, the doublet separation, in both cases, diminishes rapidly toward higher n values. Because of their appearance, we identified series VIII and IX as apparent emission series. Actually they are absorption series whose individual bands have sharp heads at the long wavelength edge of the apparent emission and degrade toward the long wavelengths. (See Fig. 3) We believe that the peculiar appearance of this series (apparent emission) is brought about by preionization and for the same reason as was discussed in a earlier paragraph which dealt with the Rydberg series of CS_2. It is difficult to state whether or not the energy state of N_2O^+, to which the present four series converge, can be considered to correspond to the state of CO_2^+ whose energy is 19.38 ev[3] measured from the ground state of CO_2.

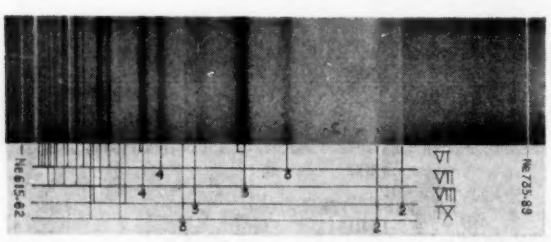

FIG. 3. Rydberg series of the N_2O molecule converging to the third ionization potential.

B. Non-Rydberg Bands. Duncan[2] observed several sharp bands in the region 1550–1400 A and arranged them in a progression. He called it the *C* region, and we confirmed his observation. He also observed a strong continuum with its center at about 1284 A and called it the *D* region.[12] Zelikoff and others[7,13] made an absorption coefficient measurement in this region and observed a single strong peak at 1292 A close to the continuum maximum. They attributed the peak to the $n=3$ band of Duncan's Rydberg series. We carefully investigated

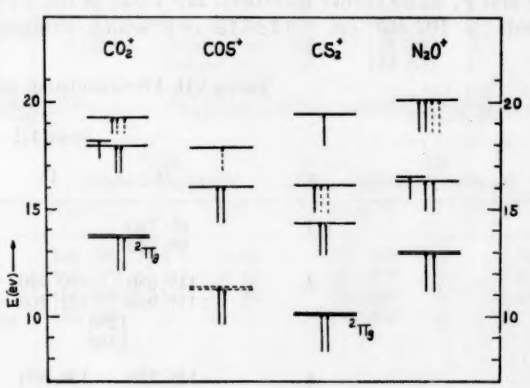

FIG. 4. Observed energy level diagram of CO_2^+, COS^+, CS_2^+, and N_2O^+.

[12] The continuum is the $n=3$ member of his Rydberg series.
[13] M. Zelikoff, K. Watanabe, and E. C. Y. Inn, J. Chem. Phys. **21**, 1643 (1953).

TABLE IX. Ionization potentials of linear triatomic molecules, CO_2, CS_2, COS, and N_2O.

	Electron impact[a]		Spectroscopic and photoionization	Present[b]
	Obs. (ev)	Elemental processes		
CO_2	14.4	$CO_2 \rightarrow CO_2^+$	13.788[c]	13.788 13.95 ($v''=0 \rightarrow v'=1$)
	19.6	$CO_2 \rightarrow CO+O^+$		
	20.4	$CO_2 \rightarrow CO^++O$	18.071[d]	18.068 18.23 ($v''=0 \rightarrow v'=1$)
	28.3	$CO_2 \rightarrow C^++O+O$		19.38
CS_2	10.4	$CS_2 \rightarrow CS_2^+$	10.076[e] 10.130	10.076 10.130
	14.0	$CS_2 \rightarrow CS+S^+$		14.47
	14.7	$CS_2 \rightarrow CS^++S$		16.18
	21.5	$CS_2 \rightarrow C^++S+S$		19.51
COS				11.23 11.25 16.04 17.93
N_2O	12.9	$N_2O \rightarrow N_2O^+$	12.71[f]	12.89
	15.3	$N_2O \rightarrow NO^++N$		12.93
	16.3	$N_2O \rightarrow N_2+O^+$		16.39 16.54 ($v''=0 \rightarrow v'=1$)
	21.4	$N_2O \rightarrow NO+N^+$		20.10

[a] W. de Gnoot and F. M. Penning, *Handbuch der Physik* (1933) Bd 23/I, p. 23. E. Friedländer, H. Kallmann, W. Lasareff, and B. Rosen, Z. Physik **76**, 70 (1932); H. D. Smyth and J. P. Blewett, Phys. Rev. **46**, 276 (1934); see also H. Sponer, *Molekül Spektren und ihre Anwendung auf Chemische Probleme* (Verlag Julius Springer, Berlin, 1935), p. 131, Tabellen I.

[b] Present values do not necessarily correspond to the elemental processes shown in column 3.

[c] W. C. Price and D. M. Simpson, Proc. Roy. Soc. (London) **A169**, 501 (1938).

[d] H. J. Henning, Ann. Physik **13**, 599 (1932); G. Rathenau, Z. Physik **87**, 32 (1934).

[e] Footnote 1.

[f] Footnote 2.

the continuum but were unable to observe the strong sharp band in it. Furthermore, our present Rydberg series I and II do not include a band whose wavelength is approximately 1292 A. We were unable, also, to observe the weak and diffuse bands which they mentioned as occurring on the long wavelength slope of the continuum. However, we cannot comment definitely on the existence of the weak bands because of the inferiority of the photographic method as compared with the photoelectric method for the detection of weak and diffuse bands, particularly when superimposed with a strong continuum such as in the present case.

In the *E* region (1190–1130 A), we observed several bands in addition to those observed by Duncan, and they are arranged in three progressions, (1), (2), (3), in Table VIII. He also observed a strong continuum with the maximum at 1096 A and called it the *F* region.[14] Actually, in our present work, the continuum appeared to be fairly weak, and instead, many strong and relatively narrow bands occupied the region from the end of the argon continuum (~1070 A) to about 1110 A. Some of them are included in progressions (2) and (3), but the majority of them are not identified.[15]

[14] This continuum is the $n=4$ of his Rydberg series.

[15] They were not identified mainly because of experimental difficulty. The He continuum is extremely weak in this region, while the A continuum is extremely strong. Actually, in the latter case, this region was covered by the broadened portion of the resonance line, 1066.6 A.

There is a group of weak and diffuse bands in the region 860–890 A. They probably form two short progressions (4) and (5) as proposed in Table VIII, but their frequency intervals are not consistent.

Unlike the three molecules described previously (including CO_2), N_2O showed strong and isolated continuous absorption at 1284 and 1096 A; the former was so strong that it was observed even at a pressure of 0.1 μ, whereas the latter began to appear at about 1 μ pressure.

The observed energy levels diagram of the molecular ions studied in our present work is shown in Fig. 4 which also includes the energy levels of CO_2^+. In the figure, the energy is measured from the ground state of the respective neutral molecule. A solid arrow indicates an absorption Rydberg series and a dotted arrow indicates an apparent emission series. As one can see in the figure, the energy levels of the first three molecules, CO_2^+, COS^+, and CS_2^+, run "parallel" to each other; if one compares the energy of the corresponding levels, it decreases as the molecular weight increases. This implies that the corresponding levels of the molecules result by removal of a similar electron from their neutral ground states. The same implication can be applied to the observed levels of N_2O.[+]

By using present values of the ionization energies, one can expect several systems of emission bands in these molecular ions including those around 2819 A and

2854 A for CS_2^+, and 3542 A and 3581 A for N_2O^+, both of which can be considered to correspond to the well-known transition, $^2\Sigma_u^+ - {}^2\Pi_g$, of CO_2^+ whose (0, 0) bands appear at 2882 A and 2896 A.

In Table IX, the present values of ionization potentials are compared with those obtained by different methods.

ACKNOWLEDGMENT

The writers are indebted to Professor R. S. Mulliken for his interest and considerate discussions on this work.

THE JOURNAL OF CHEMICAL PHYSICS VOLUME 32, NUMBER 4 APRIL, 1960

Exchange of Radiochlorine between Hydrogen Chloride and Carbon Tetrachloride. "Red Form" of Solid Hydrogen Chloride*

IRVING M. PEARSON† AND CLIFFORD S. GARNER

Department of Chemistry, University of California, Los Angeles, California

(Received November 4, 1959)

Radiochlorine-36 has been used to investigate the HCl*—CCl_4 exchange in systems of high purity at 22–35°C in the dark and in sunlight for exchange times up to 200 and 117 days, respectively, with solutions 0.14–0.18 *f* in HCl and 10 *f* in CCl_4. The exchange rate law is not known, but results have been presented in terms of an assumed bimolecular rate law, $R=k(\mathrm{HCl})(CCl_4)$. For the dark exchange, $k \leqslant 2\times10^{-11}$ liter mole^{-1} sec^{-1}, an upper limit which is about 4×10^7 times smaller than the upper limit set by earlier workers. There is no evidence that the exchange is accelerated in sunlight. The so-called "red form" of solid HCl was observed during the work, as well as solid HCl which was yellow. An apparent red-inducing impurity was found separable from most of the HCl by slow vacuum distillation of the latter from a −140°C bath to a trap at −196°C. The solid HCl distillate was colorless and failed to develop a red color even in six flash freezings at −196°C, whereas the pale yellow HCl residue from the distillation gave a rose-red color on being flash frozen at −196°C. Volatility characteristics of the latter apparent impurity suggest that, if it be an oxide of nitrogen as proposed by Clusius and Haimerl, it is probably not NO but rather N_2O or possibly N_2O_3. If the red color arises from imperfection color centers in the crystal lattice of HCl, as suggested by Johnston and Martin, generation of the color seems to require both reasonably rapid freezing at or near −196°C and the presence of an impurity separable from the HCl by a proper distillation. Consequently the flash-freeze test for traces of HCl in other substances must be interpreted with caution.

IN 1942 Clusius and Haimerl[1] reported that no exchange occurred within their experimental error in a gas mixture of 97% HCl^{35}—3% HCl^{37} (normal isotopic composition, 75.5% HCl^{35}—24.5% HCl^{37}) at 10 mm partial pressure and CCl_4 at 48 mm partial pressure kept at 20°C for 15 hr. From statements made[2] regarding the precision of the gas-density-balance determinations of the isotopic composition of the HCl from the exchange experiment of Clusius and Haimerl, we estimate that the bimolecular rate constant could have been as large as 8×10^{-4} liter mole^{-1} sec^{-1}. Apparently the only other report in the literature on HCl*–CCl_4 exchange is that of Horiuti and Tanabe,[3] who mixed 1-ml aliquots of aqueous HCl (310 000-year Cl^{36} label; *p*H 0–9.6) with 1.5-ml aliquots of CCl_4 and heated the mixtures at 97–98°C for 7–8 hr in 6- to 12-ml sealed tubes (water and liquid CCl_4 phases present in addition to vapor phase) and observed no exchange within their experimental error.

In connection with a study[4] of the Cl_2*–CCl_4 exchange, we were interested in the HCl*–CCl_4 exchange rate in order to correct for exchange with traces of HCl in our Cl_2*–CCl_4 system. For this reason, and because of the limited nature of previous work on the HCl*–CCl_4 exchange, we have investigated this exchange in CCl_4 solution in the dark and in sunlight for periods up to 200 days and 117 days, respectively, at room temperature.

We also give here some observations which bear on the nature of the so-called "red form" of solid HCl which has been reported[1,5–8] to appear under certain conditions when HCl is frozen at liquid-N_2 or liquid-air temperatures.

* Work partly supported under contract between the U.S. Atomic Energy Commission and the University of California.

† Present address: Electronics Division, The National Cash Register Company, Hawthorne, California.

[1] K. Clusius and H. Haimerl, Z. physik. Chem. **51B**, 347 (1942).

[2] W. Schanzer and K. Clusius, Z. physik. Chem. **190A**, 241 (1942).

[3] J. Horiuti and K. Tanabe, Proc. Japan Acad. **28**, 127 (1952).

[4] I. M. Pearson, Ph.D. thesis, University of California at Los Angeles (1960).

[5] W. F. Giauque and R. Wiebe, J. Am. Chem. Soc. **50**, 101 (1928).

[6] L. B. Loeb, Proc. Natl. Acad. Sci. U.S. **12**, 35 (1926).

[7] W. H. Johnston and R. E. Martin, J. Chem. Phys. **20**, 534 (1952).

[8] R. E. Martin, Dissertation Abstracts **14**, 936 (1954).

EXPERIMENTAL

Radioactive Hydrogen Chloride

Matheson tank HCl was dried by passage through $Mg(ClO_4)_2$ drying tubes into an evacuated Pyrex bulb, then frozen with liquid N_2, pumped on with a high vacuum, and finally passed through an evacuated $Mg(ClO_4)_2$ drying tube into an evacuated Pyrex bulb. This supply was labeled by admixture with HCl labeled with 310 000-year Cl^{36}, the source and testing of which has been described elsewhere,[4] and which had been purified in a similar manner to that used for the inactive HCl. The labeled solid condensate at −196°C had a faint pale yellow coloration, so the condensate was warmed to −130°C (*n*-pentane slush bath) and distilled into a trap at −196°C. Visible traces of moisture remained behind in the −130°C bulb, but the solid distillate at −196°C still had the faint pale yellow color. The distillate was then distilled from a 40% ether-60% ethanol slush bath at −140°C over a 2.5-hr period into a bulb at −196°C, leaving behind about 10% of the HCl. The new solid distillate was colorless and was used without further purification. A sample absorbed in aqueous KI gave a negative test for Cl_2, indicating the HCl contained less than 0.01% Cl_2.

"Red Form" of Solid Hydrogen Chloride

The colorless purified label HCl described above did not give a red color even in six flash freezings at −196°C. The pale yellow HCl residue from the last distillation made at −140°C was flash-frozen three times with liquid N_2, giving a solid with a rose-red color each time. This solid was vaporized and the gas passed into a tube containing activated charcoal; the HCl coming through (about 5% of the total) gave a colorless solid on repeated flash freezing at −196°C, whereas the HCl subsequently desorbed from the charcoal always gave a rose-red solid on repeated flash freezing at −196°C.

Additional experiments were made with inactive HCl taken from a different Matheson tank. All colors noted were observed independently by at least three observers, and each slow freeze (**SF**) and fast freeze (**FF**) test[9] was repeated at least six times, giving the same result each time. The HCl was passed at atmospheric pressure through a $Mg(ClO_4)_2$ drying tube into a trap. The solid formed on **SF** or **FF** at −196°C was colorless, and remained so even when pumped on with a high vacuum, then vaporized and refrozen by **SF** or **FF**. The HCl was next distilled *in vacuo* through $Mg(ClO_4)_2$ and then gave a deep yellow solid on **SF** or **FF** at −196°C (the yellow seemed to be most intense in the first portions of HCl solidifying). This solid was vaporized and subjected to the same kind of −130°C fractionation described earlier. The distillate collected at −196°C was pale yellow with a slight pink coloration at the top, and on vaporization followed by **SF** or **FF** at −196°C gave the same colors. The residue, examined when it was about 85, 20, and 10% of the total HCl, was pale yellow at −130°C and on **SF** or **FF** at −196°C gave colors ranging from an intense yellow to yellow-orange to a pale yellow. The distillate was vaporized and fractionated at −140°C in the manner described earlier, giving a new distillate and a new residue, each examined when the distillate was about 10 and 95% of the total HCl. The HCl distillate at both stages gave only a colorless solid on **SF** or **FF** at −196°C. The HCl residue, at the 10% distillation stage, was pale yellow at −140°C and on **SF** or **FF** at −196°C; at the 95% distillation stage, the HCl residue, although only a very pale yellow at −140°C, gave a pronounced rose-red solid on **SF** or **FF** at −196°C. At no time was a visible color noted in the HCl when it was in the liquid or vapor state.

[9] The **FF** test was made by continued immersion of the trap in the refrigerant bath. The **SF** test consisted of repeated short immersions until freezing was complete, actually not a "slow" freezing except by comparison with the **FF** procedure.

Carbon Tetrachloride

Baker's "analyzed" CCl_4 was purified and handled as described earlier.[4] All other chemicals were reagent grade.

Exchange Runs

The exchange solutions were prepared in the same manner as described for the Cl_2*–CCl_4 exchange study.[4] One was processed immediately as a "zero-time" sample, two others were kept in the dark (wrapped in aluminum foil) at room temperature for 40 and 200 days, respectively, and the remaining two were kept at room temperature for approximately these same times, but were exposed to indirect sunlight during the days and to laboratory fluorescent light for about 16 hr per day to test the effect of normal illumination on the exchange rate.

After the indicated exchange time, each tube was weighed (to permit checking the volume of CCl_4), the contents frozen with liquid N_2, the tip of the tube broken off, and the remainder inserted quickly into a g.s. flask containing 100 ml of freshly boiled and cooled conductivity water. After the CCl_4 had thawed, the system was titrated with standard NaOH (phenolphthalein endpoint) to determine the HCl. Each analyzed mixture was acidified slightly with HNO_3, and the phases separated carefully with a separatory funnel for radioassay.

Specific Radioactivity Determinations

A 10-ml aliquot of each aqueous phase (HCl fraction) was dip-counted with a G–M tube in a cell sealed with a plastic collar, and the net activity of each entire aqueous phase (*ca.* 200 ml) computed. Each entire CCl_4 phase (*ca.* 10 ml) was dried for 1 day over $Mg(ClO_4)_2$, filtered, diluted to 10 ml with inactive CCl_4, and dip-counted; in two cases the resulting solutions were distilled, distillate volumes measured,

TABLE I. HCl*—CCl_4 exchange in CCl_4 solution at 22–35°C.

Illum.	Exchange time, days	(HCl), M	Net cpm[a] in HCl	Net cpm[a] in CCl_4
Dark	0	0.141	3252±35	1.2±0.9
	40	0.165	4746±50	0.5±0.9[c]
	200	0.144	3432±40	0.0±1.0
Light[b]	23	0.175	4178±45	2.1±1.4[d]
	117	0.175	4581±48	1.7±1.0

[a] Error given is standard deviation computed from combining the net statistical counting error (square root of sum of squares of standard deviations of sample and background counting rates) with an estimate of the aliquot error.
[b] Indirect sunlight plus fluorescent room lights; times given do not include the dark intervals (about 40% of total exchange time).
[c] Activity after distillation of CCl_4 phase (1.1±0.8 cpm before distillation).
[d] Activity after distillation of CCl_4 phase (4.0±0.7 cpm before distillation).

and the distillates diluted to 10 ml with inactive CCl_4 and dip-counted. The statistical counting error was kept below 2% standard deviation. Background corrections of about 24–27 counts per minute (cpm) were made, using solutions of essentially the same composition but without radiochlorine present. Coincidence errors were less than 1% even at the highest counting rates (about 300 cpm). Counting rates in CCl_4 were converted to an "aqueous" basis by use of a factor of 1.03 empirically determined. The precision of the counting and HCl analyses is indicated by the fact that the mean standard deviation from the mean of the total cpm per mole of HCl in the five exchange solutions assayed was only 0.9%.

RESULTS AND DISCUSSION

HCl*—CCl_4 Exchange

The relationships[10,11]

$$R=-[4ab/(4a+b)t]\ln(1-F) \quad (1)$$

$$F=(4a+b)x/4ay_0 \quad (2)$$

may be used to compute values for R, the constant rate of exchange of Cl atoms (active plus inactive) between CCl_4 and HCl in gram-atoms liter^{-1} sec^{-1} in a given exchange solution a molar in CCl_4 and b molar in HCl; F is the fraction exchange, and x and y_0 are the net radioactivities (cpm) of the initially inactive CCl_4 at time t and of HCl, at zero time, respectively, in the exchange solution. The data are presented in Table I.

It is clear that only an upper limit for the exchange rate can be set, and that there is no evidence for acceleration of the exchange in sunlight. The exchange rate law cannot be deduced from these data, nor from those of earlier studies[1,3] made over much shorter exchange times. If we assume the rate law to be $R=k(\mathrm{HCl})\ (CCl_4)=kab$, we may take $k\leqslant 2\times10^{-11}$ liter mole^{-1} sec^{-1} as a conservative upper limit[12] at room temperature, a value about 4×10^7 times smaller than the upper limit set by earlier workers. Because of the possibility of incomplete removal of the highly radioactive aqueous phase from the CCl_4 phase or of radiocontamination of the latter, the actual reaction rate may well be much less.

"Red Form" of Solid Hydrogen Chloride

A so-called "red form" of solid HCl has been observed by several investigators when HCl is frozen at liquid-air or liquid-N_2 temperatures. The effect was apparently first reported by Giauque and Wiebe,[5] who observed a "reddish-pink" color in solid HCl only when it was condensed by liquid air *in vacuo*. They attributed the color to an unstable crystalline modification of HCl. Clusius and Haimerl[1] noted a "pink" color (rosafärbung") in their solid HCl which they interpreted as arising from the presence of nitrogen oxides, expecially NO; they were apparently able to remove the impurity and the color by distillation of the HCl (they reported no details). Johnston and Martin[7,8] reported that tank anhydrous HCl was white at liquid-N_2 temperature; when purified by vacuum distillation it became "pink" or "red" when frozen quickly by liquid N_2, but not when frozen too slowly. The red color disappeared on warming the solid to −175°C, the transition temperature between two crystalline modifications of HCl. Mass spectrographic analyses before and after the purification showed <0.1% of any impurity peak from mass 6 to 100. Addition of $10^{-4}-10^{-5}$ mole-fraction of NO intensified the red color, whereas NO_2, H_2, H, N_2, Cl_2, Cl, ClO_2, CO_2, O_2, He, and Hg had no effect. Johnston and Martin felt that their experiments appeared to rule out separable impurities as the cause of the red color, which they ascribed to imperfection color centers in the crystal lattice of HCl, with traces of NO favoring the production of these imperfections.

Our observation that slow vacuum distillation of HCl from a −140°C bath to a trap at −196°C gave a colorless HCl distillate that failed to develop a red color even in six flash freezings at −196°C, and an HCl residue (containing a yellow impurity concentrated about 10–20 times by the distillation) which gave a rose-red color each time on **FF** (or even on **SF**) six times at −196°C, indicates that the "red form" of solid HCl is associated with a separable impurity. This is not to say that the impurity is itself red at −196°C, but rather that it induces production of either an unstable red modification of solid HCl or, more likely, crystal-imperfection color centers in solid HCl.

We have not attempted to identify chemically the red-inducing impurity. Our above observation suggests

[10] H. A. C. McKay, Nature **142**, 997 (1938).
[11] O. E. Myers and R. J. Prestwood, *Radioactivity Applied to Chemistry*, edited by A. C. Wahl and N. A. Bonner (John Wiley & Sons, Inc., New York, 1951), Chap. 1.

[12] Taken as four times the largest value of k (computed from the 117-day run, using the upper value 2.7 net cpm in the CCl_4 without subtracting off the zero-time activity); a corresponding calculation based on the 200-day dark run gives an upper limit three times smaller.

that the red-inducing impurity and the yellow-inducing impurity are less volatile than HCl at −140°C; the relative volatilities at −130°C are not clear-cut, although the appearance of pink colorations in the distillates but not in the residues suggests that the red-inducing impurity is more volatile than HCl at −130°C (vapor pressures of HCl at −130° and −140°C are about 20 and 7 mm, respectively). The fact that a yellow color apparently has not been previously reported in solid HCl samples which gave red colors suggests that the red-inducing impurity and the yellow-inducing impurity are not the same substance, as does the fact that our −140°C distillation residue, left after about 95% of the HCl was distilled away, developed rose-red solid HCl on FF at −196°C but had a less intense yellow color at −140°C than the earlier residue left after only about 10% of the HCl was distilled away, which residue gave only yellow solid on FF at −196°C. NO (−164°C mp, −152°C bp), proposed by Clusius and Haimerl[1] as probably responsible for the red color and by Johnston and Martin[7,8] as intensifying the red color, presumably would have distilled over quantitatively with the HCl in the −130° and −140°C distillations (unless vaporized NO readsorbs on active sites of the small fraction of solid HCl remaining); hence NO was probably not the red-inducing impurity in our HCl, although it may have been in the HCl of these other investigators. If the red-inducing impurity be an oxide of nitrogen, the volatility behavior suggests N_2O (−102°C mp, −91°C bp, vapor pressure about 12 mm at −130°C, about 2 mm at −140°C) or possibly N_2O_3 (−102°C mp, 4°C bp) as more probable inducers of the color. The former was found by Johnston and Martin not to intensify a red color already present (whereas NO did).

It is interesting to note that Cl_2 contaminated with 0.6 mole % of HCl was observed in the course of our Cl_2–CCl_4 exchange work[4] to give a rose-red color on FF at −196°C, but not on SF. Downs[13] implies possibly having observed a red color when testing his Cl_2 for HCl impurity by the flash-freeze technique, since he stated the Cl_2 had a red color which was "either very faint or entirely absent." In view of our findings that generation of the red color in solid HCl depends both on reasonably rapid freezing at or near −196°C and on the presence of an impurity, a negative flash-freeze test need not necessarily imply the absence of HCl in other materials.

[13] J. J. Downs, Ph.D. thesis, Florida State University (1954), p. 14.

On the Nature of Solvent Effects in the Proton Resonance Spectra of Unsaturated Ring Compounds. I. Substituted Benzenes*

T. SCHAEFER† AND W. G. SCHNEIDER

Division of Pure Chemistry, National Research Council, Ottawa, Canada

(Received September 4, 1959)

The relative chemical shift between the resonances of ortho and meta hydrogens in certain para-disubstituted benzenes are markedly dependent on solvent and concentration. This behavior, which is observed also in other substituted benzenes, is characterized by a pronounced shift of some proton signals to low field in acetone solution and to high field in benzene solution. In compounds of the type

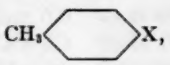

where X is an electron-withdrawing substituent, the resonance signals of protons meta to the X substituent are displaced selectively in donor solvents. When the CH_3 group is replaced by F, both ortho and meta hydrogens show pronounced shifts. The observations can be interpreted in terms of a specific molecular association involving hydrogen bonding. Although generally these bonds appear relatively weak, for some compounds the hydrogen-bond strength is estimated to be comparable to those formed by chloroform in donor solvents. These effects offer a valuable practical aid in proton resonance measurements since in such compounds, within limits, it is possible to alter the relative chemical shifts by a suitable adjustment of solvent conditions.

IT has been observed that the proton resonance spectra of certain aromatic compounds are strongly solvent dependent and are affected both by the nature of the solvent and the degree of dilution. In different solvent environments, the resonance signals of some protons of the solute molecule become displaced more than others, causing a change in the relative chemical shift (or "internal" chemical shift) of the solute protons and a marked change in the over-all appearance of the NMR spectrum. An understanding of the nature of these effects is basic to a better understanding of solute-solvent molecular interactions generally, as well as the various factors which contribute to the NMR chemical shift.

Solvent and concentration dependent chemical shifts hitherto have been encountered either with hydrogen-bonded systems,[1] or with systems involving an aromatic solvent or an aromatic solute.[2–4] In hydrogen-bonded systems, usually only the protons directly involved in hydrogen bonds show large solvent and concentration-dependent shifts. On the other hand, the dilution shifts involving aromatic compounds is due to the "ring current" effect,[5] dilution causing an identical shift for all protons in the solute molecule, unless a specific molecular association is involved.[3,4] The systems to be considered here, for example, the substituted benzenes,[6] generally are not regarded as involving either hydrogen bonding or any other specific molecular association. Yet the variation in the "internal" chemical shifts in some of these compounds in different solvents is surprisingly large. Thus, for example, in *p*-methylnitrobenzene the chemical shift between ortho and meta protons is 35 cps in a dilute acetone solution and 72 cps in a dulute benzene solution (see Fig. 1). The present work was undertaken to study the nature of the solvent interactions in these systems.

EXPERIMENTAL PROCEDURE

In order to simplify the measurements, the compounds initially chosen for study were para-disubstituted benzenes in which one of the substituents was either a CH_3 group or fluorine. The reasons for this choice are twofold:

(1) The para-substituted compounds give rise to an almost symmetrical spectrum (A_2B_2), which, when the chemical shifts between ortho and meta protons are fairly large, approximate to a simple four-line AB spectrum. From this, the chemical shifts are readily extracted without the necessity of a detailed analysis.

(2) The fluorine atom or methyl group in the para position give rise to a spin-spin interaction with the protons in the benzene ring. This coupling is strongest with the two hydrogens ortho to the fluorine or methyl groups, thus permitting the signals of the ortho and meta hydrogens in the ring proton spectrum to be identified separately.

The solvents employed were, for the most part, *n*-hexane, acetone, benzene. Hexane may be regarded as

* Issued as N.R.C. Contribution No. 5601.

† Research Associate, summer 1959. Permanent address: Chemistry Department, University of Manitoba, Winnipeg.

[1] J. T. Arnold and M. E. Packard, J. Chem. Phys. **19**, 1608 (1951).

[2] J. R. Zimmerman and M. R. Foster, J. Phys. Chem. **61**, 282 (1957).

[3] A. A. Bothner-By and R. E. Glick, J. Chem. Phys. **26**, 1651 (1957).

[4] L. W. Reeves and W. G. Schneider, Can. J. Chem. **35**, 251 (1957).

[5] J. A. Pople, J. Chem. Phys. **24**, 1111 (1956).

[6] We exclude from consideration here substituents containing hydrogen-bonding groups, such as OH, NH_2, and COOH.

a relatively inert solvent, capable only of interacting by ordinary van der Waals forces. Acetone is a strong *n*-type donor solvent by virtue of lone-pair electrons on the oxygen atom, while benzene, an aromatic molecule, is a weak π-electron donor.

Dilute solutions of the compounds in each solvent were made up, for convenience, to a uniform concentration of 5 mole %. All measurements were made at 60 Mcps. The spectra were measured relative to an external chloroform reference, contained in a sealed capillary. Bulk susceptibility corrections were applied to all measurements. Diamagnetic susceptibilities for some of the compounds, which were not known, were evaluated with the aid of Pascal's constants.

Several of the compounds, which are solids at room temperature, were measured in the form of the melt about 10–20°C above the melting point. For *p*-methylnitrobenzene, the spectra of the pure compound and of 18- and 50-mole % solutions in acetone and in benzene were measured as a function of temperature with a sample heating arrangement previously described.[7]

RESULTS

Figure 1 shows illustrative spectra of *p*-methylnitrobenzene in 5-mole % solutions of hexane, acetone, and benzene, as well as the spectra for the pure compound. The signals of the hydrogens meta to the NO_2 group are broader due to spin coupling with the methyl group. The chemical shifts derived from similar measurements for a number of para-disubstituted compounds are summarized in Table I. These shifts are seen to be quite different in the three solvents. To illustrate these changes more clearly, we choose the ortho and meta proton shifts in the hexane solution as an arbitrary reference point[8] and then enquire how these shifts are altered in magnitude and direction (i.e., to higher or lower magnetic field) in the corresponding acetone and benzene solutions. The results are displayed in Fig. 2. It is evident that the resonances (compared to those observed in hexane) are displaced to higher magnetic field in benzene and to lower magnetic field in acetone. Moreover, in most cases, the signals of meta hydrogens are displaced to a much greater extent than those of the ortho hydrogens, causing an apparent change of the "internal" chemical shift, i.e., the actual separation of the ortho and meta hydrogen signals of a compound in a given solvent. The values for each compound in each of the three solvents, summarized in Table II, show a surprisingly large variation, as much as 36 cps. It is quite clear, therefore, that the determination of the relative chemical shifts of protons in such compounds has little meaning unless solvent conditions (type of solvent and degree of dilution) are specified.

[7] Schneider, Bernstein, and Pople, J. Chem. Phys. **28**, 601 (1958).

[8] As discussed, it is assumed that specific solvent interactions in the inert solvent hexane are negligible apart from the ordinary van der Waals interaction.

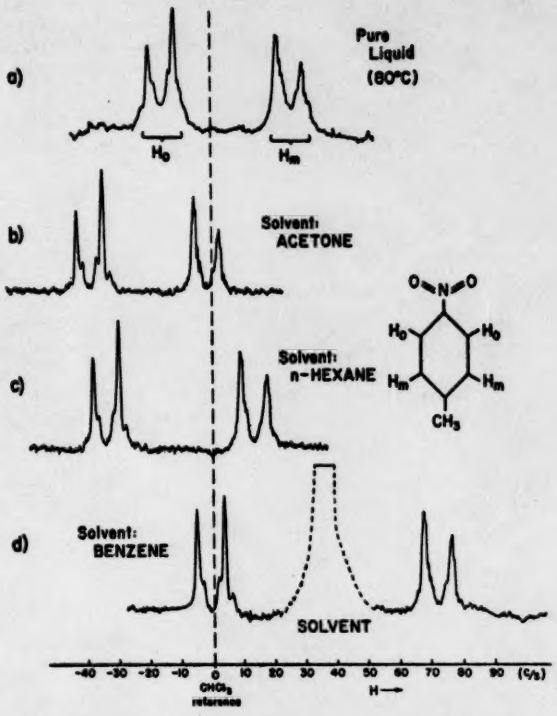

FIG. 1. Proton resonance spectra at 60 Mcps of *p*-methylnitrobenzene, (a) pure liquid at 80°C, (b) 5-mole % acetone solution, (c) 5-mole % hexane solution, and (d) 5-mole % benzene solution. The spectra are shown on a common scale (corrected for bulk susceptibility differences) relative to a chloroform reference signal.

DISCUSSION

In interpreting the observed data, it is reasonable to assume that in the relatively inert solvent, *n*-hexane, solute-solvent interactions are negligible. The observed chemical shifts of the ortho and meta hydrogens of each compound in a 5-mole % solution in hexane then may be regarded as the true chemical shifts for the "isolated" molecule. (Although, strictly speaking, the shifts obtained at "infinite dilution" more nearly approach this state, the 5-mole % solution is a sufficient approximation for the present purpose.) On this basis there are two important features of the observed results to be explained:

(1) Relative to the observed shifts in hexane, the resonance signals of ortho and meta hydrogens in the para-disubstituted compounds are shifted to *lower* magnetic field in acetone solution and to considerably *higher* field in benzene (cf. Figs. 1 and 2).

(2) In most compounds, the solvent interaction shifts arising in acetone and benzene solutions are substantially greater for meta hydrogens than for ortho (Fig. 2). It is this difference which gives rise to the different "internal" chemical shifts in the three solvents (Table II).

To explain these effects several possible contributing factors must be considered: (a) a purely magnetic con-

TABLE I. Ring proton chemical shifts, $\Delta\nu$, of para-disubstituted benzenes (in cps at 60 Mcps relative to external $CHCl_3$ reference and corrected for differences in bulk susceptibility).

Compound[a]	Pure liquid		5-mole % solution in Hexane		Acetone		benzene	
	ortho	meta	ortho	meta	ortho	meta	ortho	meta
	...	...	−34.4	14.6	−38.2	−2.6	−0.3	71.9
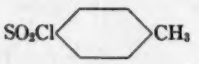	...	...	−23.8	7.2	−33.0	−8.8	8.7	69.3
	−4.9	35.3	−19.5	19.5	−25.4	9.2	3.1	53.1
	0	15.0	3.0	16.4	−10.9	4.7	42.2	58.4
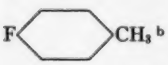	27.6	26.6	38.9	28.3	27.8	16.4	62.2	62.2
	20.2	33.2	19.6	29.0	10.9	16.1	43.0	66.0
	20.4	44.8	9.8	31.6	1.8	18.0	34.9	70.3
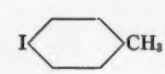	...	...	−3.6	37.0	−10.7	25.1	21.8	76.8
	...	...	−12.2	18.5	−26.2	4.0	42.5	70.9
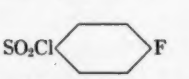	...	...	−35.3	16.5	−49.3	−9.1	20.7	88.7
	18.7	47.3	5.1	36.3	−8.6	18.8	48.3	80.9

[a] Protons are designated ortho and meta with respect to the left-hand substituent.
[b] Meta hydrogen signal appears at lower field than the ortho signal.

tribution arising from solute-solvent interactions in a magnetic field; (b) steric effects arising from bulky substituents on the benzene ring influencing solute-solvent interactions; (c) polar interactions of solute and solvent molecules influenced by the dielectric constant of the solvent; (d) a specific molecular interaction involving complex formation and a preferred mutual orientation of solute and solvent molecules.

It is well known that dilution by benzene causes the proton resonances of an aliphatic solute to be displaced to high field.[3,9] This is due to the "ring current" effect which arises from the induced diamagnetic circulation of the mobile π electrons in the benzene ring.[5] The resulting secondary magnetic field displaces the resonances of aliphatic solutes to high field (at infinite dilution in benzene) by 0.6 to 0.7 ppm[9] or about 38 cps at 60 Mcps. On the other hand, when the solute is a substituted benzene molecule, it generates a ring effect of its own, and if it had the same molecular volume as benzene itself, no dilution shift in benzene would be observed. In actual fact, nearly all substituted benzenes have a greater molecular volume than benzene (the distance of approach of neighboring molecules, on the average, is larger), so that dilution in benzene will cause a slight shift to high field. This explains why

[9] Pople, Schneider, and Bernstein, *High Resolution Nuclear Magnetic Resonance* (McGraw-Hill Book Company, Inc., New York, 1959), p. 424.

the proton signals in benzene solution appear to higher field relative to those of the pure solute (Table I). (Note that the relative shift between ortho and meta hydrogens are not generally the same in the two cases.) Dilution in an aliphatic solute, such as hexane, causes the resonances of the protons of the aromatic solute molecules to be shifted to lower field, since now the molecules are separated, and the ring current effect due to neighboring aromatic molecules is absent. However, when the aromatic compound is diluted in benzene, the magnetic interaction of neighboring benzene molecules shifts the proton resonances to high field relative to their position in the hexane solution. As a "calibration" of the magnitude of this effect for a para-disubstituted benzene we may choose *p*-xylene, in which all four ring protons are equivalent. The displacement of the ring proton resonances in the benzene solution, relative to their position in the hexane solution, is indicated by the dotted line in Fig. 2. It is immediately evident that the shifts in benzene solution for the other compounds shown in Fig. 2 are very much larger, and these differences cannot be accounted for in terms of differing molecular volumes of the solutes.

Shifts in benzene, in excess of those to be expected for the simple "ring current" effect, are observed only when specific molecular interaction of the solute with benzene occurs, for example, in the benzene-chloro-

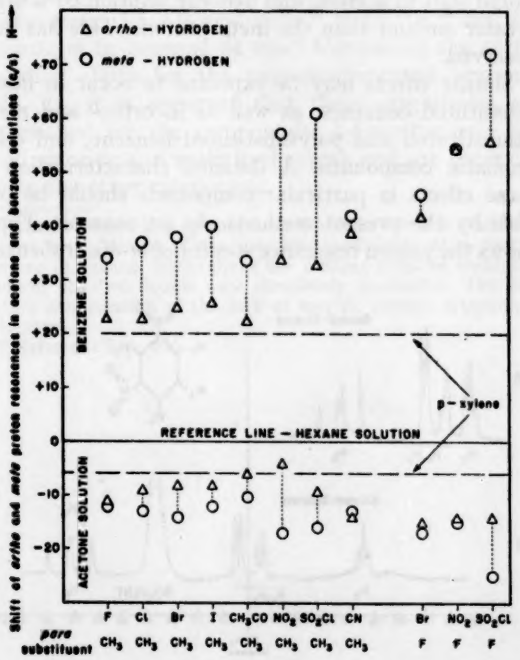

FIG. 2. Shifts of the ortho and meta proton signals of para-disubstituted benzenes in dilute acetone and benzene solutions relative to their position in the field for a dilute *n*-hexane solution. The shifts are given in cps for a fixed measuring frequency of 60 Mcps. The corresponding shifts of the ring protons of *p*-xylene in acetone and benzene solutions are indicated by the two dotted horizontal lines.

TABLE II. Internal chemical shifts $\nu_{meta}-\nu_{ortho}$, of para-disubstituted benzenes (in cps at 60 Mcps).

Compound[a]	5-mole % solution in Hexane	Acetone	Benzene
NO_2–C$_6$H$_4$–CH_3	49.1	35.9	72.2
SO_2Cl–C$_6$H$_4$–CH_3	31.0	24.2	60.7
CH_3CO–C$_6$H$_4$–CH_3	39.0	34.6	50.0
CN–C$_6$H$_4$–CH_3	13.5	15.6	16.3
F–C$_6$H$_4$–CH_3[b]	−10.7	−11.5	0
Cl–C$_6$H$_4$–CH_3	9.4	5.3	23.1
Br–C$_6$H$_4$–CH_3	21.9	16.2	35.4
I–C$_6$H$_4$–CH_3	40.6	35.8	55.0
NO_2–C$_6$H$_4$–F	30.7	30.2	28.4
SO_2Cl–C$_6$H$_4$–F	51.8	40.2	68.0
Br–C$_6$H$_4$–F	31.2	27.4	32.6

[a] Protons are designated ortho and meta relative to the left-hand substituent.
[b] Meta-hydrogen signal appears at lower field than the ortho signal.

form system.[3,4] The strongest indication, however, that a specific solute-solvent interaction is involved, is the greater benzene dilution shift of the meta hydrogens relative to those of ortho hydrogens. This again cannot be accounted for on the basis of the simple "ring current" effect, which should give rise to *identical* (averaged) benzene dilution shifts for all proton signals of the solute molecule.

At first sight, it may appear reasonable that the greater benzene dilution shifts of the meta protons could be ascribed to possible steric effects arising from bulky substitutents. It is conceivable that a bulky substituent might prevent a neighboring benzene solvent molecule from approaching the ortho hydrogen as closely, on the average, as a meta hydrogen, and thus the high field displacement due to the "ring current" effect would be less for ortho hydrogens. If we examine the ortho and meta hydrogen shifts in benzene (Fig. 2) for the *p*-

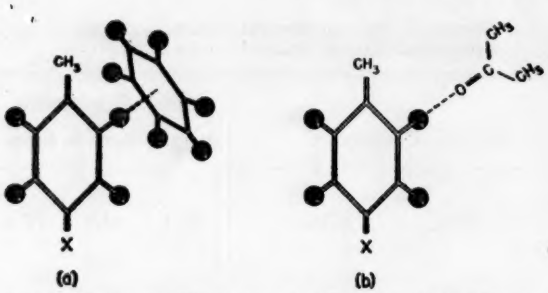

FIG. 3. Schematic illustration of the preferential hydrogen-bonding interactions of the protons meta to the X substituent in benzene and acetone.

halotoluenes, involving the substituents, F, Cl, Br, and I, the magnitudes of the shifts in benzene are almost equal, in spite of the varying size of the substituent. Furthermore, in the compound *p*-fluoronitrobenzene, the benzene solution shifts for the ortho and meta hydrogens are almost identical in magnitude, although the fluorine atom is very much smaller than the nitro group. As a further test of possible steric effects, *p-tert*-butyl toluene was examined. In this molecule, strong polar groups are absent, but the *t*-butyl group is much larger than the methyl group and might be expected to hinder the close approach of solvent molecules to the protons ortho to it, whereas the meta protons would not be so hindered. Actually both types of protons were shifted by the same amount in benzene (17.4 cps) relative to *n*-hexane, as well as in acetone (−6.4 cps) relative to *n*-hexane. It does not appear possible, therefore, to attribute the present effects to steric hindrance by the substituents.

Most of the solute molecules employed in the present experiments are polar and may be expected to interact with the surrounding solvent molecules which provide the "reaction field." The contribution of such polar interaction effects on the proton screening becomes significant only with solvents of high dielectric constant.[10,11] It can be shown,[10] for example, that for *p*-methylnitrobenzene in acetone, the ortho proton signals are shifted somewhat to higher applied field whereas the meta protons are displaced to lower applied field. In the low-dielectric-constant solvents, hexane and benzene, the correspondings shifts are negligibly small. The different shifts of the ortho and meta protons in benzene solution, therefore, cannot be explained on the basis of polar interactions. Polar effects will, however, be important in the pure liquid state of the substituted benzenes because of their large dipole moments. Thus, the proton spectrum of such compounds will be modified by the polar interactions of neighboring molecules (as well as by the effects due to their aromatic rings).

All the present observations are consistent with the assumption of a specific molecular association between solute and solvent molecules in the benzene and acetone solutions. There is, in fact, a very close parallel with the behavior of the proton resonances of the present compounds and those of chloroform in the same solvents. Chloroform is known to form hydrogen bonds with acetone and as a result the chloroform proton is shifted to *lower* field.[12,13] In benzene, the chloroform forms a hydrogen bond with the π electrons of the benzene ring in which the C—H bond of the chloroform tends to be directed at right angles to the plane of the ring with the proton adjacent to the ring.[4] Because of this interaction, the proton is drawn closer to the ring and accordingly, its resonance signal suffers a greater displacement to *high* field by the "ring effect" than it would have in the absence of a preferred interaction of this kind.

The observed proton shifts of the substituted benzenes can be accounted for satisfactorily if, by analogy with chloroform, the protons are assumed to interact by weak hydrogen bonding with acetone and benzene and this interaction is favored at the meta protons. This suggests a preferred mutual orientation of molecules as indicated schematically in Fig. 3. Implied in this suggestion is a polarization of the C—H sigma bond at the meta position by the electronegative substituent so as to favor hydrogen-bonding interactions. With an electropositive substitutent, such as $-N(CH_3)_2$, the polarizing field may be expected to be reversed, and under these conditions the ortho protons would shift in acetone and benzene solution by a much greater amount than the meta protons. This has been observed.

Similar effects may be expected to occur in monosubstituted benzenes, as well as in ortho- and meta-disubstituted and polysubstituted benzene, and other aromatic compounds. A detailed characterization of these effects in particular compounds should be possible by the present methods. As an example, Fig. 4 shows the proton resonance spectra of *m*-dinitrobenzene

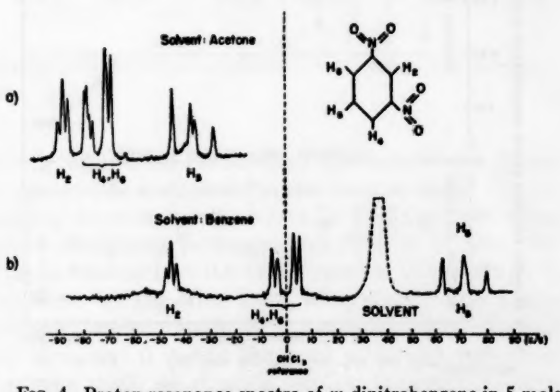

FIG. 4. Proton resonance spectra of *m*-dinitrobenzene in 5-mole % solution of (a) acetone and (b) benzene at 60 Mcps relative to $CHCl_3$ reference.

[10] A. D. Buckingham, Can. J. Chem. (in press).

[11] Buckingham, Schaefer, and Schneider, J. Chem. Phys. **32**, 1227 (1960), this issue.

[12] Huggins, Pimentel, and Shoolery, J. Chem. Phys. **23**, 1244 (1955).

[13] G. Korinek and W. G. Schneider, Can. J. Chem. **35**, 1157 (1957).

in a 5-mole % solution of acetone and benzene. In this compound one hydrogen (at position 5) finds itself meta with respect to two NO_2 groups, and accordingly it may be expected to have a greater tendency to form hydrogen bonds than the remaining protons, which are ortho to the NO_2 groups. The proton spectra and the solvent shifts in acetone and benzene are consistent with this interpretation.[14] The assignment of proton signals in the spectrum was confirmed by deuteration.

If acetone and benzene solutions of substituted aromatic compounds involve association by hydrogen bonding, a characteristic temperature dependence of the proton resonance signals should be observable. This was confirmed for benzene solutions containing 18- and 50-mole % concentrations of *p*-methylnitrobenzene. The measured change in "internal" shift between ortho and meta proton signals was found to have a temperature coefficient of approximately 0.07 and 0.03 cps per degree centigrade for the 18- and 50-mole % solutions, respectively. The temperature variation of the acetone solution was smaller but detectable.

Assuming an approximate proportionality between hydrogen-bond strength and the magnitudes of the proton chemical shifts resulting from hydrogen bonding, a rough indication of the relative hydrogen-bond strengths is possible. Thus, for comparison, the "hydrogen-bond" shift of chloroform in acetone, for which the hydrogen-bond strength has been estimated to be in the range 2.5–4.0 kcal/mole,[12] is 45 cps,[15] and for chloroform in benzene 84 cps.[9] Comparing the corresponding shifts for the para-disubstituted benzenes (Fig. 2), it is apparent that these magnitudes are approached for the compounds, *p*-fluorobenzene sulfonyl chloride and *m*-dinitrobenzene and are generally less in the other compounds.

The tentative interpretation of the results presented here, although somewhat speculative, is evidently consistent with all details of the experimental observations. The conclusion that a highly specific solute-solvent interaction is involved appears inescapable in view of the results of the benzene solutions. Perhaps some other type of interaction, than what has been termed "hydrogen bonding" here, may be formulated to account for the present observations. But in any interpretation of this kind, progress is limited by a lack of understanding of the detailed electronic effects of substituents in aromatic rings, and the way these effects alter the measured proton screening constants. The additional changes in proton screening arising from solvent interactions then conceivably could be interpreted in terms of an appropriate perturbation of the primary substituent effects.

The present results suggest a useful application in NMR studies generally in that, in compounds of this type and within limits, the chemical shift can be varied at will by adjusting the solvent environment. This is a useful aid in signal assignments and in studying the nature of spin-coupling interactions in the limit when the chemical shift approaches zero. A detailed study of this kind, to be published shortly,[16] has been made for the proton resonances of *p*-fluorotoluene. In this compound, contrary to the other para-substituted toluenes studied, the signals of the protons ortho to the F atom occur at *highest* field in hexane solution. Since association with benzene is favored at the meta hydrogens, the signal of the latter is shifted to higher field to a greater extent than the ortho hydrogen signal. Thus by adjusting the benzene concentration, the relative chemical shift between ortho and meta hydrogens can be reduced to zero and ultimately reversed.

The authors are indebted to Mr. Yves Lupien for assistance in the experimental measurements and to Dr. L. C. Leitch for the preparation of several deuterated compounds.

[14] The corresponding spectrum in *n*-hexane solution could not be measured because of the complete insolubility of *m*-dinitrobenzene in hexane. Even above the melting point of *m*-dinitrobenzene, the two liquids were completely immiscible. This is a further confirmation of the lack of specific solvent interactions in hexane.

[15] Reference 9, p. 406.

[16] T. Schaefer and W. G. Schneider, Can. J. Chem. (in press).

On the Nature of Solvent Effects in the Proton Resonance Spectra of Unsaturated Ring Compounds. II. Heterocyclic Compounds*

T. SCHAEFER† AND W. G. SCHNEIDER

Division of Pure Chemistry, National Research Council, Ottawa, Canada

(Received September 4, 1959)

In unsaturated heterocyclic compounds, the relative chemical shifts of the protons bonded to the ring are strongly dependent on solvent and concentration. In 6-membered ring compounds, as for example 4-picoline, the β hydrogens show a pronounced shift to low field in acetone solutions and to high field in benzene solutions. This behavior is similar to the behavior found for *p*-substituted toluenes (preceding paper). In the 5-membered heterocyclic compounds, for example pyrrole, the behavior of α and β hydrogens is reversed, the proton signals of α hydrogens being displaced selectively in acetone and benzene. The results can be interpreted in terms of a preferential hydrogen bonding of the α protons with the donor solvent molecules.

IT was shown in the preceding paper,[1] hereafter referred to as I, that the pronounced shift of the ring proton signals of para-disubstituted benzenes in dilute acetone and benzene solutions, relative to their position in *n*-hexane, could be interpreted in terms of a specific molecular association involving preferential hydrogen bonding of some of the aromatic ring protons to the solvent molecules. The present paper reports measurements of solvent effects on a number of unsaturated heterocyclic compounds.

The solvents used and the general experimental procedure were similar to those described in I. Figure 1 shows the ring proton spectra of pyrrole in 5-mole % solutions in *n*-hexane and acetone and in 5- and 20-mole % solutions in benzene. In the acetone and hexane solutions, the quartet at lower field arises from the α protons. The separation of this signal from that of the corresponding β protons is considerably greater in the acetone solution than in the inert solvent hexane. In the 20-mole % benzene solution, the α proton signals are shifted to higher field to such an extent that the α and β signals begin to overlap. This shift is even more pronounced in the 5-mole % benzene solution, where the chemical shift between α and β protons is very small.

Table I gives the shifts of the α and β ring protons for seven heterocyclic compounds relative to an external chloroform reference. These values have been corrected for bulk susceptibility differences. In Fig. 2, the proton shifts in *n*-hexane are taken as a reference point, and

TABLE I. Ring proton chemical shifts, $\Delta\nu$, of some heterocyclic compounds (in cps at 60 Mcps relative to external $CHCl_3$ reference; corrected for differences in bulk susceptibility).

Compounds		5-mole % Solution in Hexane α	Hexane β	Acetone α	Acetone β	Benzene α	Benzene β
Pyrrole		56.1	78.4	40.4	81.5	84.2	87.3
N-*n*-butyl pyrrole		59.8	87.1	45.4	86.0	76.5	85.1
Thiophene		15.8	27.0	−1.1	17.8	50.2	58.9
Furan		9.3	71.8	−6.1	61.6	44.0±3	103.6
4-Methylpyridine		−5.6	32	−59	17	−41	71
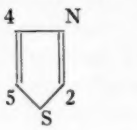	2:	−76.2		−96.7		−33.0	
	4:	13.9		−13.4		66.7	
	5:	−26.3		−32.2		3.1	
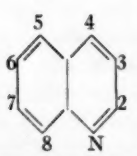	2:	−79.2		−85.3		−52.9	
	3:	19.5		1.3		66.1	
	4:	−26.6		−37.0		20.6	
	8:	−36.0		−48.4		−24.9	

* Issued as NRC Contribution No. 5611.

† Research Associate, summer, 1959. Permanent address: Chemistry Department, University of Manitoba, Winnipeg, Canada.

[1] Schaefer and W. G. Schneider, J. Chem. Phys. **32**, 1218 (1960), this issue.

the alteration of the shifts in the acetone and benzene solutions are plotted for all the compounds. Table II gives the "internal" chemical shifts in the three solvents and in some of the pure liquids. The variation in "internal shift" is seen to be very large in some cases. It amounts to 45 cps for two of the protons in thiazole.

4-PICOLINE AND QUINOLINE

In 4-picoline, the β hydrogens (those ortho to CH_3) are shifted most in benzene and acetone solution (Fig. 2). In fact, the solvent effects in this molecule have the same sign and magnitude as in para-substituted toluenes (see I) and also can be accounted for by preferential hydrogen bonding of the β protons with the solvent. In quinoline, it is protons 3 and 4 whose shifts are most solvent dependent.[2] Proton 2 is shifted by about the same amount as the α proton in 4-picoline. Proton 8 is affected least by dilution in benzene.

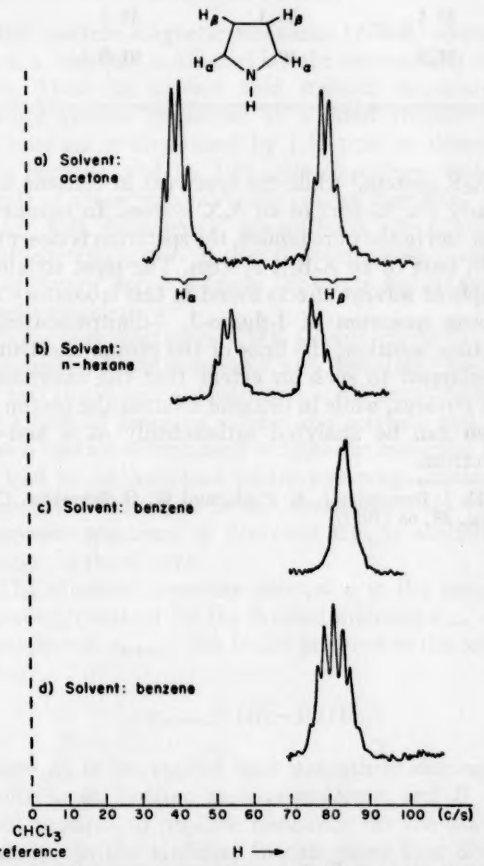

FIG. 1. Proton resonance spectra at 60 Mcps of the ring protons in pyrrole: (a) 5-mole % acetone solution, (b) 5-mole % hexane solution, (c) 5-mole % benzene solution, and (d) 20-mole % benzene solution. The spectra are shown on a common scale (corrected for the bulk susceptibility differences) relative to a chloroform reference signal.

[2] Protons 5, 6, and 7 cannot be assigned unequivocally in the proton spectrum of quinoline. However, measurements on a series of methyl- and ethyl-substituted quinolines showed that their shifts in benzene relative to *n*-hexane fall close to +30 cps, i.e., between 10 and 20 cps less than for protons 3 and 4.

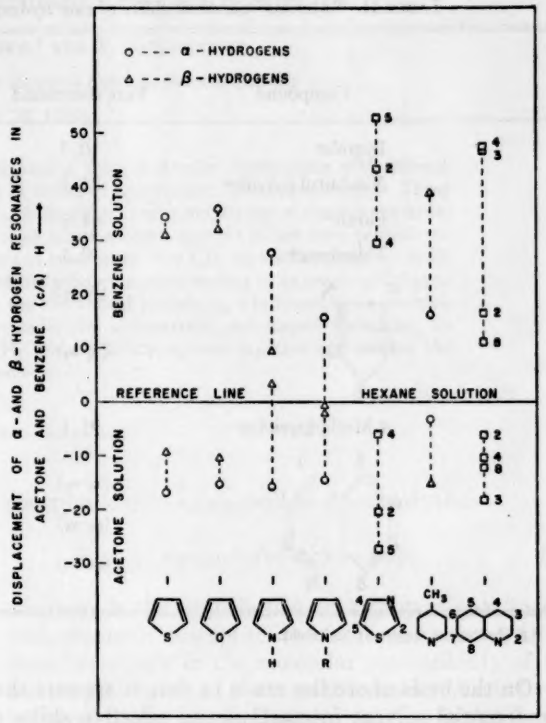

FIG. 2. Shifts of the ring hydrogens of some heterocyclic compounds in dilute acetone and benzene solutions relative to their position in the field for a dilute *n*-hexane solution. The shifts are given in cps for a fixed measuring frequency of 60 Mcps.

FIVE-MEMBERED HETEROCYCLICS

As can be seen from Fig. 2, both thiophene and furan behave like pyrrole and *N*-*n*-butylpyrrole in that the proton signals of the α hydrogens show a greater solvent shift in acetone and benzene than do the β hydrogens. Thus, in contrast to the behavior of 4-picoline and the substituted benzenes, it is now the protons nearest the electronegative atom, the α protons, which give rise to the strongest solvent interaction. In thiazole, proton 5, the farthest removed from the nitrogen, shows the largest solvent effect. The effect is larger than in other five-membered rings and approaches that for the C—H proton of chloroform in benzene and acetone. Proton 2 is affected more than proton 4.

It is known that hydrogen-bonding interactions involving the N—H group occur in pure pyrrole. In dilute solution in the donor solvents, benzene and acetone, the N—H group presumably forms hydrogen bonds to the solvent molecules, and this interaction gives rise, in turn, to changes in shielding at the α and β protons. These effects might be expected to be greater at the α positions. The extent to which effects of this kind influence the results can be seen by comparing the solution results of pyrrole and *N*-*n*-butylpyrrole (Fig. 2). In the latter compound, the N—H group is absent, but the preferential hydrogen bonding of α protons still is apparent.

TABLE II. "Internal" chemical shifts of ring hydrogens in some heterocyclic compounds (in cps at 60 Mcps).

Compound	Pure compound	5-mole % Solution in Hexane	Acetone	Benzene
Pyrrole[a]	10.5	22.3	41.1	3.1
N-*n*-butyl pyrrole[a]	23.7	27.3	40.6	8.6
Furan[a]	64.1	62.5	67.7	59.6
Thiophene[a]	9.3	11.2	18.9	8.7
	($\nu_5-\nu_2$)	90.1	83.3	99.7
	($\nu_5-\nu_4$)	40.2	18.8	63.6
4-Methylpyridine	91.1	88	76	112
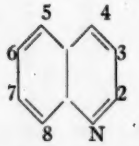	($\nu_3-\nu_2$)	98.7	86.6	119.0
	($\nu_3-\nu_4$)	46.1	38.3	45.5
	($\nu_3-\nu_8$)	55.5	49.7	91.0

[a] β Hydrogens appear at high field.

On the basis of studies made to date it appears that preferential solvent interaction and selective shifts of certain protons in a molecule may be anticipated generally if the molecule is unsaturated and contains, in addition, strongly electronegative or electropositive substituents. Small effects of this kind are observable with olefinic compounds, such as the vinyl halides, but they tend to be more pronounced in larger conjugated systems and particularly in aromatic compounds. A practical use of the solvent effects reported here is as a help in spectra analyses, as has been noted in I. The ring-proton spectrum of pyrrole in acetone, for instance, can be treated as the A_2X_2 part of an A_2X_2R system,[3] while the spectrum in benzene is very nearly the A_4 part of an A_4X system. In hexane solution and in the pure liquids, the spectrum is closer to the A_2B_2 part of an A_2B_2X system. The most striking example of solvent effects found in this laboratory is the proton spectrum of 1-fluoro-2, 4-dinitro-benzene. In acetone solution, the lines of the proton spectrum are overlapped to such an extent that the assignment is not obvious, while in benzene solution the proton spectrum can be analyzed satisfactorily as a first-order spectrum.

[3] H. J. Bernstein, J. A. Pople, and W. G. Schneider, Can. J. Chem. **35**, 68 (1957).

Solvent Effects in Nuclear Magnetic Resonance Spectra*

A. D. BUCKINGHAM,† T. SCHAEFER,† AND W. G. SCHNEIDER

Division of Pure Chemistry, National Research Council, Ottawa, Canada

(Received October 20, 1959)

Contributions to nuclear screening (chemical shifts) arising from molecular interactions with solvent molecules (excluding hydrogen bonding) are discussed in terms of appropriate theoretical models. These include contributions from van der Waals interactions σ_w, from the magnetic anisotropy of the solvent molecule σ_a, and from polar effects σ_E. By a suitable choice of solute-solvent systems it has been possible to demonstrate each of these effects experimentally for proton resonances. For CH_4 as a solute, σ_w was in all cases negative, its magnitude varying with the nature of the solvent and amounting to as much as 0.6 ppm for high molecular weight solvents. In agreement with the theoretical models, σ_a was found to be positive for disk-shaped solvent molecules and negative for cylindrically symmetrical rod-shaped molecules, its magnitude in extreme cases reaching 0.75 ppm. For CH_3CN as a solute, σ_E was negative and showed the expected dependence on the dielectric constant of the solvent.

I. INTRODUCTION

THE nuclear magnetic resonance (NMR) spectrum of a molecule is affected by the surrounding molecules. Thus the applied field strength necessary to produce proton resonance at a fixed frequency in methane gas is diminished by 1.13 ppm on dissolving it in benzene, and by 1.99 ppm in carbon disulfide. A part of these "solvent shifts" arises from the "long-range" bulk diamagnetic susceptibility effect, but the most interesting part is due to interactions involving "short-range" forces between the solute and its nearest solvent neighbors.

Early work relating to NMR solvent effects has been discussed by Pople, Schneider, and Bernstein.[1] Bothner-By and Glick[2] and Zimmermann and Foster[3] examined the effects of aromatic solutes and solvents and have shown that an environment of aromatic molecules tends to lead to an increased solute screening constant of from 0.3 to 0.7 ppm. Evans[4] found that the fluorine resonance spectrum of dissolved CF_4 is sensitive to changes in the solvent.

The observed *screening constant* σ is the sum of a screening constant for the isolated molecule σ_{gas}, and a contribution $\sigma_{solvent}$, due to the presence of the solvent. Thus

$$\sigma_{solvent}=(H_0-H)/H_0, \tag{1}$$

where H_0 is the applied field strength producing resonance in an isolated gaseous molecule, and H is the field required to produce resonance (at the same frequency) in the medium. In this paper four different contributions to $\sigma_{solvent}$ will be discussed; thus

$$\sigma_{solvent}=\sigma_b+\sigma_a+\sigma_w+\sigma_E, \tag{2}$$

where σ_b is the contribution to σ proportional to the bulk magnetic susceptibility of the medium; σ_a arises from anisotropy in the molecular susceptibility of the solvent molecules; σ_w is due to the van der Waals forces between the solute and solvent; and σ_E is the "polar effect," caused by the charge distribution in the neighboring solvent molecules leading to an electric field E acting on the solute, thereby perturbing its electronic structure and hence the nuclear screening constant.

It is found that σ_b and σ_w are negative (that is, they lead to resonance at lower applied field strengths), σ_a is positive for disk-shaped solvents (like benzene) and negative for rod-shaped ones (like carbon disufide), while σ_E can be either positive or negative, depending on the position of the nucleus relative to the polar groups in the solute molecule.[5]

Strong specific interactions, such as those in intermolecular hydrogen bonds,[6] are not dealt with though they may be regarded as an extreme form of σ_E type screening.

II. THEORY

(i) Bulk Susceptibility Effect σ_b

The solvent molecules at large distances from the resonant nucleus interact with it as if they formed a continuum having the macroscopic properties of the solvent. In the presence of an external magnetic field H, they will be diamagnetically polarized and this polarization may produce a magnetic field at the nucleus and thus contribute to its screening constant σ. This secondary field depends upon the shape of the sample and is zero for a sphere.

---

* Issued as NRC contribution No. 5612.

† Research Associate, summer, 1959.

[1] J. A. Pople, W. G. Schneider, and H. J. Bernstein, *High Resolution Nuclear Magnetic Resonance* (McGraw-Hill Book Company, Inc., New York, 1959), Chap. 16.

[2] A. A. Bothner-By and R. E. Glick, J. Chem. Phys. **26**, 1651 (1957).

[3] J. R. Zimmerman and M. R. Foster, J. Phys. Chem. **61**, 282 (1957).

[4] D. F. Evans, Proc. Chem. Soc. (London) **1958**, 115.

[5] A. D. Buckingham, Can. J. Chem. **38**, 300 (1960).

[6] T. Schaefer and W. G. Schneider, J. Chem. Phys. **32**, 1218, 1224 (1960) this issue.

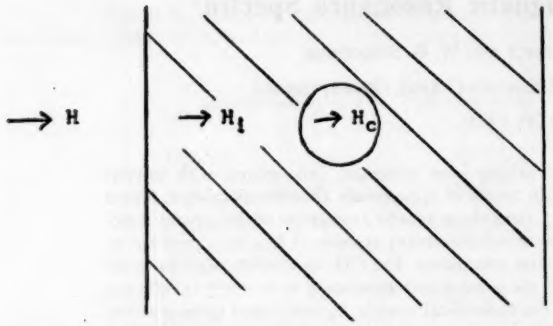

To calculate the magnetic field that would act on the molecule if there were no short-range interactions, consider a macroscopic spherical cavity—small relative to the size of the whole sample—hollowed out of the medium surrounding the active molecule. If the primary magnetic field is H, the field H_i in the medium is uniform and parallel to H if the sample is either spherical or cylindrical. An application of classical magnetostatics leads to the results:

$$\text{Sphere:}\quad H_i=[3/(\mu^*+2)]H=[1/(1+\tfrac{4}{3}\pi\chi_v)]H$$
$$\text{Cylinder:}\quad H_i=[2/(\mu^*+1)]H=[1/(1+2\pi\chi_v)]H, \tag{3}$$

where μ^* is the magnetic permeability of the medium and $\chi_v=(1/4\pi)(\mu^*-1)$ its volume susceptibility. Also, the effective field inside the cavity is

$$H_c=[(\mu^*+2)/3]H=(1+\tfrac{4}{3}\pi\chi_v)H, \tag{4}$$

so that, from (1), (3), and (4),

$$(\sigma_b)_{\text{sphere}}=(H-H_c)/H=0. \tag{5}$$

Similarly, neglecting terms in χ_v^2, (which is reasonable, for $\chi_v\sim10^{-6}$ for diamagnetic liquids, and the smallest significant screening constants are $\sim10^{-8}$),

$$(\sigma_b)_{\text{cylinder}}=\tfrac{2}{3}\pi\chi_v \tag{6}$$

and this is the well-known result first deduced by Dickinson.[7]

Ordinarily, chemical shift measurements are made in cylindrical sample tubes. Hence, in order to investigate solvent effects arising from short-range molecular interactions, σ_b must be subtracted from σ—that is, the "bulk susceptibility correction" must be applied. For gaseous samples at moderate pressures the correction is negligible (for CH_4 at 25°C at a pressure of P atm, $\chi_v=-5.0\times10^{-10}P$, so that for $P=10$, $\sigma_b=-0.01$ ppm]. In the remainder of this paper, it will be assumed that this "correction" has been applied to all liquid samples.

(ii) Anisotropy in the Susceptibility of the Solvent σ_a

It is well known[1-3] that aromatic solvents tend to produce high-field shifts in the solute. This has been interpreted by Bothner-By and Glick[2] in terms of the "disk" shape of these molecules combined with their large diamagnetic anisotropies. Benzene rings have large induced magnetic moments only when the ring is at right angles to the field; also, their disklike shape enables them to lie closer to the solute when they are in the configuration a(i) than when in the configuration a(ii) of Fig. 1. Since the secondary magnetic field due to this induced magnetic moment is proportional to the inverse third power of the separation, effect a(i) may be expected to dominate leading to a mean diminution of the external field at the solute proton and a resulting shift to *high field*. Similarly, it is to be expected that rod-shaped solvent molecules, like carbon disulfide or acetylene, whose largest diamagnetic susceptibility is along the axis of the rod, would lead to *low-field* shifts, for in this case configuration b(ii) is the most important one and it leads to an enhancement of the applied field.

If $\chi_{\alpha\beta}$ is the molecular susceptibility tensor of a molecule, then in the presence of a uniform magnetic field H_0 (having components $H_{0\beta}$, where $\beta=x, y, z$), the α component of the total magnetic field H_α at the origin is

$$H_\alpha=H_{0\alpha}+R^{-5}\sum_{\beta,\gamma=x,y,z}\{3R_\alpha R_\beta-R^2\delta_{\alpha\beta}\}\chi_{\alpha\beta}H_{0\gamma}, \tag{7}$$

where $\mathbf{R}$ (whose magnitude must be large compared to molecular dimensions) is the vector from the origin to the center of the molecule, and $\delta_{\alpha\beta}$ is the Krönecker delta ($=1$ if $\alpha=\beta$, $=0$ if $\alpha\neq\beta$). In NMR experiments, it is the time-average value of $\mathbf{H}$ in the direction of H_0 which is significant, and from (7) this is

$$\bar{H}=H_0+\tfrac{1}{3}R^{-5}\sum_{\alpha,\beta}\{3R_\alpha R_\beta-R^2\delta_{\alpha\beta}\}\chi_{\alpha\beta}H_0 \tag{8}$$

(we have averaged over all directions of $\mathbf{H}_0$, but this is equivalent to averaging over all orientations of $\mathbf{R}$). For an axially symmetric molecule

$$\chi_{\alpha\beta}=(\chi_{\parallel}-\chi_\perp)l_\alpha l_\beta+\chi_\perp\delta_{\alpha\beta}, \tag{9}$$

where $\mathbf{l}$ is the unit vector in the direction of the axis, and $\chi_\parallel$ and $\chi_\perp$ are the magnetic susceptibilities parallel and at right angles to the axis. From (8) and (9)

$$\bar{H}=H_0+[(\chi_\parallel-\chi_\perp)/3R^3](3\cos^2\theta-1)H_0 \tag{10}$$

where $\cos\theta=\mathbf{R}\cdot\mathbf{l}/R$ is the cosine of the angle between $\mathbf{R}$ and the axis of the solvent molecule.

If the solute is a hard sphere of radius r, and the solvent molecules are hard cylinders of diameter $2L_1$ and length $2L_2$, then if there are no orientationally dependent attractive forces, $(3\cos^2\theta-1)$ will average to zero for $R>r+L$, where L is the larger of L_1 and L_2. However, for $r<R<r+L$, shape effects will cause $(3\cos^2\theta-1)$ to be positive if $L_1>L_2$, and negative for $L_1<L_2$. The screening constant σ_a is given by

$$\sigma_a=-n[(\chi_\parallel-\chi_\perp)/3R^3](3\cos^2\theta-1), \tag{11}$$

[7] W. C. Dickinson, Phys. Rev. **81**, 717 (1951).

where n is the number of molecules in the relevant range of R. Equation (11) is equivalent to a result derived by Stephen.[8]

For disks close to the solute, $\theta\sim0°$ and $(3\cos^2\theta-1)\sim2$, while for rods $\theta\sim90°$ and $(3\cos^2\theta-1)\sim-1$ (actual mean values of $(3\cos^2\theta-1)$ for the nearest neighbor solvent molecules will in both cases have smaller magnitudes). Hence for

Disk-shaped solvents:

$$\sigma_a=-2n(\chi_{\parallel}-\chi_{\perp})/3R^3$$

and for

Rod-shaped solvents:

$$\sigma_a=n(\chi_{\parallel}-\chi_{\perp})/3R^3, \qquad (12)$$

and if the appropriate r is the mean of the two extremes, that is, $R=r+[(L_1+L_2)/2]$, it is found that for CH_4 in benzene

$$(\chi_{\parallel}-\chi_{\perp}=-9\times10^{-29}\text{ erg gauss}^{-2},$$

$$n\sim2,\ R\sim4.5\text{ A})\ \sigma_a=1.3\text{ ppm.}$$

For CH_4 in carbon disulfide $(\chi_{\parallel}-\chi_{\perp}=-5\times10^{-29}$, $n\sim2$, $R\sim4$ A) $\sigma_a=-0.5$ ppm. These screening constants are of the observed order of magnitude (thus relative to CH_4 in hexane as a reference, σ for CH_4 in benzene is 0.33 ppm, and for CH_4 in CS_2, $\sigma=-0.42$) but precise agreement with experiment cannot be expected because of the severe approximations inherent in the model.

As the size of the solute or solvent molecules increases, n/R^3 tends to decrease (approximately as $1/R$) leading to smaller values of σ_a.

Since σ_a is primarily due to strong short-range repulsive forces causing the mean of $(3\cos^2\theta-1)$ to differ from zero, changes in temperature (at constant density) should be ineffective in altering σ_a.

The shape of the solute molecule is probably also important; thus disk-shaped solutes, like NH_3 and $CHCl_3$, probably have enhanced σ_a screening constants in disk-shaped solvents, and rod-shaped solutes, like HCN, C_2H_2, and CH_3Cl, probably have enhanced low-field shifts in rod-shaped solvents, that is, large negative values of σ_a.

(iii) van der Waals Forces σ_w

Interactions between molecules perturb their electronic structure, and the resulting distortion leads to a solvent-dependent nuclear screening constant. In the absence of polar effects, these interactions are of the type leading to the well-known London dispersion forces. The associated contribution to σ_{solvent} will be denoted by σ_w.

Two effects may contribute to σ_w:

(a) Interaction between the solute and the solvent *in its equilibrium configuration* causes a distortion of the electronic environment of the nucleus. This distortion is probably an expansion (as the electrons are attracted by the nuclei of neighboring molecules). The diamagnetic screening is thereby diminished, leading to nuclear resonance at lower field strengths. The diminution should increase as the charges on the solvent nuclei rise, so that a rough correlation between σ_w and the number of electrons in a solvent molecule might be expected.

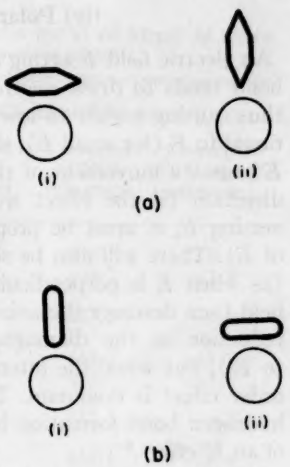

FIG. 1. Relevant arrangements for (a) disks and (b) rods in relation to a spherical solute molecule.

(b) Departures from the equilibrium solvent configurations will lead to a "buffetting" of the solute and hence to a time-dependent distortion of the electronic structure. If the solute is an atom in an S state (e.g., He^3, Xe^{129}) these distortions must destroy the symmetry and hence introduce a negative paramagnetic screening. This effect will be greatest in atoms, but may also effect proton screening constants, for X—H bonds are usually at least approximately axially symmetric, and this symmetry may be destroyed in interactions.

Effect (a) is independent of temperature at constant density, but since departures from the equilibrium configuration become more important as T increases, effect (b) will lead to an increased low-field shift as T rises (at constant density). Measurements on CH_4 in CCl_4 at $-27°$C and at 95°C, indicated that effect (b) is unimportant for CH_4. However, molecules whose X—H bonds are more exposed to sideways attack" (e.g. HCl, C_2H_2, HCN) which may destroy the axial symmetry, should show larger shifts due to effect (b).

Atoms, such as Xe^{129}, should show the largest temperature-dependent σ_w values due to effect (b).

When effect (b) is dominant, nuclei in symmetrical electronic environments should have larger negative σ_w constants than they would have in less symmetrical structures. Thus the C^{13} nucleus in $H—C^{13}\equiv C—H$ would have a negative shift relative to $H_2C^{13}=CH_2$ in changing the solvent from say neopentane to carbon tetrachloride. Similarly, because the hydrogen-bonded proton in salicylaldehyde is not in an axially symmetric environment, effect (b) should be small, while (a) presumably still operates.

[8] M. J. Stephen, Mol. Phys. 1, 223 (1958).

(iv) Polar Effect σ_E

An electric field E acting along the axis of an X—H bond tends to draw electrons away from the proton, thus causing a shift to low field.[5] This shift is proportional to E (for small E), since a reversal of the sign of E causes a movement of the electrons in the opposite direction (if the effect would be unchanged by reversing E, it must be proportional to an even power of E). There will also be screening proportional to E^2 (as when E is perpendicular to the X—H bond; the field then destroys the axial symmetry, and leads to a reduction in the diamagnetic shielding proportional to E^2), but when the interactions are weak, the first-order effect is dominant. The large negative shift on hydrogen bond formation has been discussed in terms of an E^2 effect.[9]

An approximate calculation,[5] leads to the following equation for σ_E:

$$\sigma_E=-2\times10^{-12}E_z-10^{-18}E^2, \qquad (13)$$

where E_z is the component of the total field E along the X—H bond.

When a polar molecule is dissolved, it polarizes its surroundings, and this polarization leads to an electric field—the "reaction field" $\mathbf{R}$—at the solute. If the solute is sufficiently symmetrical, the mean $\mathbf{R}$ will be parallel and proportional to μ, the permanent dipole moment of the solute molecule. In the Onsager model,[10] the solute is represented by a sphere of radius r, containing a point dipole of moment μ at its center, and the solvent by a continuum of dielectric constant ϵ, and $\mathbf{R}$ is given by

$$\mathbf{R}=[2(\epsilon-1)/2\epsilon+1](\mathbf{m}/r^3)$$
$$=[2(\epsilon-1)(n^2-1)/3(2\epsilon+n^2)](\boldsymbol{\mu}/\alpha), \qquad (14)$$

where $\mathbf{m}=\boldsymbol{\mu}+\alpha\mathbf{R}$ is the total dipole moment of the solute in the medium, $\alpha=[(n^2-1)/(n^2+2)]r^3$ is the polarizability of the sphere and n the refractive index of the pure solute as a liquid or solid. Thus $n^2\sim2.5$ and $\mathbf{R}$ is approximately given by

$$\mathbf{R}=[(\epsilon-1)/(2\epsilon+2.5)](\boldsymbol{\mu}/\alpha) \qquad (15)$$

Thus, from (13) and (15),

$$\sigma_E=-2\times10^{-12}[(\epsilon-1)/(2\epsilon+2.5)](\mu\cos\phi/\alpha)$$
$$-10^{-16}[(\epsilon-1)/(2\epsilon+2.5)]^2(\mu^2/\alpha^2), \qquad (16)$$

where ϕ is the angle between $\boldsymbol{\mu}$ and the X—H bond. When $\cos\phi$ is positive, increasing the dielectric constant of the solvent will tend to shift proton signals from polar molecules to lower fields.

For CH_3CN, $\mu/\alpha=1.0\times10^6$ and $\cos\phi=\frac{1}{3}$, so that in n-hexane $\sigma_E=-0.11$ and in acetone $\sigma_E=-0.50$ ppm.

The various protons in a molecule may have different values of σ_E. Thus in 2,6-dinitrobenzene, for which $\mu/\alpha=0.26\times10^6$, $(\sigma_E)_1=0.22$, $(\sigma_E)_3=-0.13$, and $(\sigma_E)_4=-0.24$ ppm in acetone, where the subscript refers to the position of the hydrogen atom on the benzene ring. As ϵ increases, the H_1 and H_4 signals should separate, the H_4 signal going to lower field relative to H_1 (and H_3).

Protons are normally on the "surface" of a molecule and are therefore exposed to direct contact with the surrounding molecules, so that the Onsager field (14) is probably not normally a good approximation to the actual reaction field acting on a proton; it should however reasonably accurately describe the field in the interior of the molecule, so that C^{13} resonances in substituted methanes should be approximately described by (16). Local solvent effects due to polar groups near a proton are probably important—thus in the nonpolar molecule 1,4-dinitrobenzene, fields resulting from the induced charges on the solvent molecules near the highly polar nitro groups lead to a nonzero σ_E, even though R, as given by (14) and (15), is zero. The reaction field gradient R' for a model analogous to Onsager's is[5,11]

$$R'=[6(\epsilon-1)/(3\epsilon+2)](\Theta/r^5) \qquad (17)$$

where Θ is the molecular quadrupole moment. For a molecule with two opposed dipole groups of moment μ separated by a distance d, $\Theta=2\mu d$. Thus for 1,4-dinitrobenzene $\Theta\sim20\times10^{-26}$ esu and for acetylene $\Theta\sim3\times10^{-26}$ esu. The protons in 1,4-dinitrobenzene experience a reaction field—$\sqrt{3}R'\,r/4$ along the C—H bonds, so that in hexane $\sigma_E=-0.08$, and in acetone $\sigma_E=-0.23$ ppm.

Thus protons near polar groups undoubtedly experience "local" electric fields as well as the over-all uniform field (15). Thus the value $(\sigma_E)_1=0.22$ for 2,6-dinitrobenzene deduced from (16) for acetone as solvent is probably too large and should be diminished by a local field. Fortunately both R and R' are approximately proportional to $(\epsilon-1)/(\epsilon+1)$, so that screening constants should vary smoothly with this solvent parameter.

III. EXPERIMENTAL RESULTS

In general, the individual solvent effects, outlined in the previous section, are most easily investigated by choosing a simple nonpolar solute whose magnetic resonance can be examined in a variety of nonassociated solvents. In order to eliminate solute-solute interactions a high degree of dilution in each solvent must be employed. The most desirable reference state is the chemical shift in the gaseous state, where all solvent effects are absent. In the present work methane was chosen as the common solute molecule for most of the experiments, and for the investigation of polar

[9] W. G. Schneider, H. J. Bernstein, and J. A. Pople, J. Chem. Phys. **28**, 601 (1958).
[10] L. Onsager, J. Am. Chem. Soc. **58**, 1486 (1936).
[11] A. D. Buckingham, J. Chem. Phys. **30**, 1580 (1959).

effects, (requiring a polar solute) the additional solute molecule CH_3CN was used. Although the effect of solvents on proton chemical shifts were investigated only in the present study, a similar analysis will also apply to resonances of other nuclei. In particular the fluorine resonances of fluorine-containing solutes should show analogous effects but their magnitude may be expected to be greater than those encountered in proton resonances.

The individual CH_4 solution samples were contained in cylindrical glass tubes (5-mm o.d., 3-mm i.d.) and were prepared on a vacuum line. A constant amount of solvent (~0.4 cc) was introduced into each sample tube and CH_4 gas was subsequently added with the aid of liquid nitrogen, after which the tube was sealed off. The amount of CH_4 gas introduced was measured volumetrically in the vacuum system and was calculated to produce a pressure of 10 atm in the volume of the sample tube not occupied by the solvent. (This condition is realized when the liquid nitrogen freezing medium is removed and the CH_4 vaporizes while the solvent remains frozen.) After warming to room temperature the tube was shaken to dissolve the gas in the liquid solvent. Depending on the solubility the concentration of methane in the final solution may vary with different solvents but estimates based on solubility data[12] indicated that it did not exceed 5-mole % in any of the solutions. Each sample tube also contained a sealed capillary with chloroform in it and this was used throughout as the external reference for the chemical shift measurements. The chemical shift between liquid chloroform and methane gas was measured over a range of temperatures in a separate experiment. In this case the chloroform was contained in a capillary which was introduced into a 5-mm o.d. sealed sample tube containing methane gas at a pressure of 10 atm.

For the solute CH_3CN 5-mole % solutions were made up by weighing. The chemical shift of the solute in solutions of this concentration was considered to yield a sufficiently close approximation to the "infinite dilution" chemical shift for the present purpose.

All measurements were made at approximately 30°C with a Varian High Resolution Spectrometer at a fixed frequency of 60 Mcps. The observed proton signal separation of the solute molecule and the reference was measured with a frequency counter. The measurements of the CH_4 solutions are summarized in Table I, and those of the CH_3CN solutions in Table II. The greatest single uncertainty in the results derives from the bulk susceptibility correction. Values of the bulk susceptibility employed for each solvent, listed in the second column of each table, were derived from molar susceptibility and density data given in the *Handbook of Chemistry and Physics*.[13] Where the susceptibility data were unavailable values were obtained with the aid of Pascal's constants and by interpolation of data from related compounds. For the CH_4

TABLE I. Proton chemical shifts (in cps at 60 Mcps) of dilute solutions of CH_4 in various solvents.

Solvent	$-\chi_v$ ($\times 10^6$)	Chemical shifts (cps) Measured ($CHCl_3$ reference)	Corrected ($CHCl_3$ reference)	Corrected [CH_4 (gas) reference]
1. CH_4 (gas)	0	538.2	446.5	0
2. Neopentane	0.554[a]	460.9	438.7	−7.8
3. Cyclopentane	0.661[a]	445.9	437.1	−9.4
4. *n*-Hexane	0.586	452.9	434.7	−11.8
5. Cyclohexane	0.631	445.2	432.7	−13.8
6. *trans*-Butene-2	0.475[a]	469.4	437.3	−9.2
7. *cis*-Butene-2	0.475[a]	468.2	436.1	−10.4
8. Acetone	0.460	469.9	435.9	−10.6
9. Ethyl ether	0.547	458.1	435.0	−11.5
10. Ethyl acetate	0.547	455.9	432.9	−13.6
11. Ethyl nitrate	0.485[a]	463.4	432.7	−13.8
12. Triethylamine	0.610[a]	449.0	433.8	−12.7
13. Propyne	0.470[a]	460.6	427.9	−15.6
14. Acetonitrile	0.486[a]	449.6	418.9	−27.6
15. Butyne-2	0.519[a]	448.5	421.9	−24.6
16. Carbon disulfide	0.681	418.8	412.5	−34.0
17. Diacetylene	0.401[a]	450.0	408.7	−37.8
18. Dicyanoacetylene	0.417[a]	440.5	401.2	−45.2
19. Benzene	0.626	470.5	457.3	+10.8
20. Toluene	0.631	466.8	454.3	+7.8
21. Chlorobenzene	0.707	456.3	453.3	+6.8
22. Nitrobenzene	0.598	479.3	462.6	+16.1
23. Nitromethane	0.473[a]	476.8	444.4	−2.1
24. Nitroethane	0.497	469.2	440.0	−6.5
25. Bromine	1.17[a]	369.4	424.6	−21.9
26. CH_3Br	0.73[b]	424.5	424.5	−22.0
27. CH_3I	0.918	395.2	418.6	−27.9
28. CH_2Cl_2	0.733	425.5	425.7	−20.8
29. CH_2Br_2	0.946	392.0	419.0	−27.5
30. CH_2I_2	1.16	350.2	404.1	−42.4
31. $CHCl_3$	0.731	423.1	423.1	−23.4
32. $CHBr_3$	0.913	383.9	406.7	−39.8
33. CCl_4	0.684	427.2	421.3	−25.2
34. CBr_4 (100°C)	0.863[c]	396.0	412.5	−34.0
35. CH_2ClBr	0.839[a]	408.4	421.9	−24.6
36. $CHClBr_2$	0.792[a]	396.8	404.4	−42.1
37. CCl_3Br	0.752[a]	415.5	418.1	−26.4
38. $SiCl_4$	0.796	426.1	434.2	−12.3
39. $SnCl_4$	0.986	395.8	427.8	−18.7

[a] Estimated from Pascal's constants and interpolation of data of related compounds.
[b] From A. A. Bothner-By and R. E. Glick, J. Chem. Phys. 26, 1647 (1957).
[c] Density measured at 100°C, 2.943 g/cc.

[12] Hildebrand and Scott, *Solubility of Non-Electrolytes* (Reinhold Publishing Corporation, New York, 1950), Chap. XV.
[13] Published by Chemical Rubber Publishing Company, Inc., Cleveland, Ohio, 1957.

TABLE II. Proton chemical shifts (in cps at 60 Mcps) of CH_3CN in 5-mole % solutions of various solvents (relative to $CHCl_3$ reference signal).

Solvent	$-\chi_v$ ($\times 10^6$)	Chemical shift Measured	Chemical shift Corrected
1. *n*-Hexane	0.586	358.7	340.5
2. Cyclohexene	0.576	353.7	334.3
3. *cis*-Butene-2	0.475[a]	367.3	335.3
4. *trans*-Butene-2	0.475[a]	371.3	339.3
5. Cyclohexene	0.576	353.7	334.3
6. Trimethylamine	0.610[a]	344.8	329.6
7. Ethyl ether	0.547	353.2	330.1
8. Ethyl formate	0.537	350.3	326.0
9. Cyclohexanone	0.614	338.3	323.7
10. Acetone	0.460	357.0	323.0
11. Acetaldehyde	0.393	369.1	326.8
12 Carbon tetrachloride	0.684	323.8	317.9
13. Chloroform	0.731	319.2	319.2
14. Methylene chloride	0.733	320.9	321.1
15. Ethyl chloride	0.664[a]	341.3	332.9
16. Acetonitrile	0.486[a]	344.8	314.1
17. Nitromethane	0.473[a]	366.6	334.2
18. Benzene	0.626	434.2	421.0
19. Mesitylene	0.652[a]	417.8	407.8
20. Nitrobenzene	0.598	364.8	348.1
21. Bromobenzene	0.771	376.2	381.2
22. Benzonitrile	0.658	361.4	352.3

[a] Estimated from Pascal's constants and interpolation of data of related compounds.

solutions the corrected chemical shifts are shown relative to both the liquid $CHCl_3$ and CH_4 gas reference.

IV. DISCUSSION

(i) Nonpolar Solvent Interactions

The shift of the proton resonance signal ($\sigma_{solvent}-\sigma_b$), of CH_4 dissolved in various solvents, relative to the proton signal in gaseous CH_4 (where the molecule is isolated) is a measure of the short-range molecular interaction of the methane molecule with the surrounding solvent molecules. For a symmetrical, nonpolar molecule such as methane, these interactions will involve only the universal van der Waals forces and, for some solvents, an additional interaction of magnetic origin due to a large diamagnetic anisotropy of the solvent molecules, as discussed in Sec. II. For solvent molecules having negligible diamagnetic anisotropy we may expect a simple linear correlation between the "solution-gas" CH_4 proton shift and the van der Waals interaction energy. This energy, which depends on the number of electrons in the molecule and their configuration and polarizability, cannot be evaluated reliably in any direct manner. For the present purpose we have chosen instead a relevant molecular property, the heat of vaporization of the solvent at the boiling point,[14] as an indirect measure of molecular interaction energy. While this is primarily a measure of the interaction between like solvent molecules, a close proportionality of the corresponding interaction of the solvent molecules with the common solute molecule CH_4 may be expected if the interactions are of the simple van der Waals type.

The heat of vaporization H_b at the boiling point T_b was evaluated from the empirical relation

$$H_b = 17.0T_b + 0.009T_b^2$$

due to Hildebrand and Scott,[15] and is essentially a modification of Trouton's rule. Figure 2 shows a correlation plot of the CH_4 proton shifts in the various solvents (relative to CH_4 gas) against the heat of vaporization of the solvent. In this plot the magnetic anisotropy effects of certain solvents are revealed in a rather striking manner and amply substantiate the theoretical models (Sec. II). Rod-shaped solvent molecules with cylindrical symmetry, such as the acetylenes, nitriles, and CS_2, give rise to an excess shift of the CH_4 resonance to low field. The disk-shaped aromatic molecules, benzene, and substituted benzenes, give rise to the well-known excess shifts to high field. An additional effect of this kind, indicated by Fig. 2, appears to arise from the NO_2 group (cf. nitromethane and nitroethane). This is a planar, roughly disk-shaped group and when added to a benzene ring appears to enhance significantly the diamagnetic anisotropy of the latter. The remaining solvents shown in Fig. 2 are clustered about a line with negative slope showing the expected increasing shift of the CH_4 resonance to low field with increasing interaction with the solvent molecules. This behavior is evidently characteristic of purely van der Waals interaction.

In the correlation plot of Fig. 2 the series of solvents (25–37, cf. Table I) consisting of liquid Br_2 and halogen substituted methanes have been omitted. The corresponding points for these solvents were uniformly displaced below the common correlation line of the

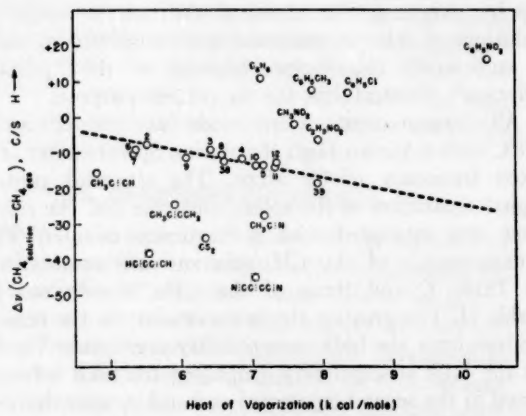

FIG. 2. Plot of the proton resonance shift of CH_4 (in cps at 60 Mcps relative to gaseous CH_4) in dilute solution in various solvents against the heat of vaporization of the solvent. The points corresponding to different solvents are numbered as in Table I.

[14] The heat of vaporization at the boiling point, rather than at some other arbitrary temperature, was chosen to approximate "corresponding" states.

[15] Reference 12, p. 427.

other solvents. This is illustrated in Fig. 3, where the upper dotted line corresponds to the mean line of Fig. 2. It is at present not possible to determine whether this is a significant difference or merely a result of the inadequacy of the particular type of correlation plot employed.

(ii) Polar Effect

This effect can be demonstrated with the aid of the experimental data for the polar solute, CH_3CN (Table II). It is necessary however to separate out, as far as possible, effects due to magnetic anisotropy of the solvent and van der Waals interactions, since these may partially mask the polar effect. Accordingly we exclude from consideration aromatic solvents, solvents whose molecules are rod-shaped and halogenated molecules. To allow for the shift due to van der Waals interactions, at least approximately, we choose the 5% solution of CH_3CN in *n*-hexane as our reference state and examine how the solute resonance is shifted in the other solvents, both polar and nonpolar. According to Eq. (16) these shifts should be related to the dielectric constant of the solvent and specifically to the quantity $(\epsilon-1)/(2\epsilon+2.5)$. The relevant data are shown plotted in Fig. 4. The dotted line drawn through the points corresponds to the theoretical slope (−40 cps) given by Eq. (16). The experimental points, which cover a range of shifts up to about 20 cps, confirm the theoretical model for the polar effect. Some of the scatter of the points in this and the preceding plots is probably due to the inaccuracies of available bulk susceptibility data for many of the solvents used. The crudeness of the theoretical model as well as the assumptions made regarding van der Waals forces will of course also contribute to the inaccuracies. The latter assumption implies in fact that the contribution due to van der Waals forces is the same for all solvents plotted and is equal to that in *n*-hexane. It may be seen from Fig. 2 that this may introduce errors of as much as 5 cps in some cases.

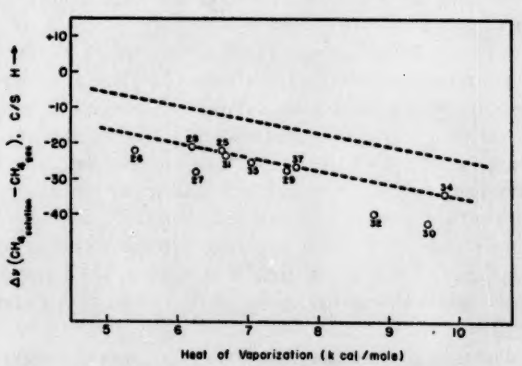

FIG. 3. Plot of the proton resonance shift of CH_4 (in cps at 60 Mcps relative to gaseous CH_4) in dilute solution in a series of halogenated solvents against the heat of vaporization of the solvent. The solvents are identified according to the numbers in Table I.

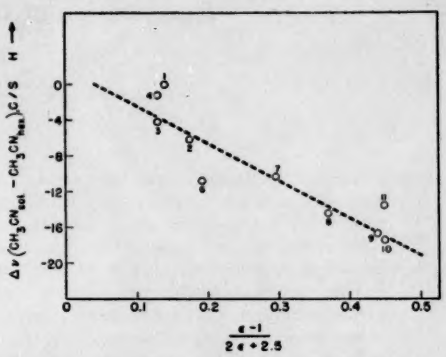

FIG. 4. Plot of the proton resonance shift of the polar solute CH_3CN in 5-mole % solution in various solvents (in cps at 60 Mcps relative to CH_3CN in a 5-mole % *n*-hexane solution) against $(\epsilon-1)/(2\epsilon+2.5)$. The solvents are numbered as in Table II.

(iii) Conclusion

On the basis of the present study together with previous work on hydrogen bonding effects[6] some general conclusions can be drawn about the contribution of molecular interactions and solvent effects to the measured proton chemical shifts. It is clear there are four effects which may make significant contributions to the corrected chemical shift or screening constant of a solute proton in solution, *viz*; (i) hydrogen bonding σ_{HB}, (ii) van der Waals interaction σ_w, (iii) diamagnetic anisotropy of the solvent molecules σ_a, and (iv) polar effects σ_E. With the exception of σ_a for disk-shaped solvent molecules and possibly σ_E in some molecules, all of these contributions to the screening constant are negative, causing a solvent shift of the solute proton signal to lower field. The extent to which any or all of these effects contribute depends on the nature of the solute-solvent system. σ_{HB}, which requires a somewhat acidic proton in the molecule,[6] is generally the largest of the four contributions. σ_w, which is always present in liquid systems, appears to be somewhat enhanced for halogenated solvents. For solvents with large diamagnetic anisotropies, and in the absence of hydrogen bonding, σ_a is appreciably larger than the σ_w and σ_E contributions. For polar molecules in solvents with high dielectric constants the σ_E contribution may amount to 1 ppm and in some cases may be indistinguishable from weak hydrogen bonding effects. If a σ_{solvent} value is observed which is not explicable in terms of Eq. (2), we should consider this evidence for some specific interaction, e.g., hydrogen bonding or "chemical association." Equation (2) may be regarded as describing the purely "physical effects" to be expected.

ACKNOWLEDGMENT

We are greatly indebted to Mr. Yves Lupien for assistance in the preparation of samples for the NMR measurements.

Dissociation of C_6H_5T Following Beta Decay*

THOMAS A. CARLSON

Oak Ridge National Laboratory, Oak Ridge, Tennessee

(Received May 15, 1959)

The relative abundance of the various charged fragments formed following beta decay of monotritiated benzene was measured with a specially designed mass spectrometer. In nearly every case the C—He bond was ruptured, the charge remaining with $C_6H_5^+$. In 28% of the events the $C_6H_5^+$ species were further excited to produce more than 30 different charged fragments. Comparison of this spectra with the electron impact data on benzene is made to arrive at an estimate of the energies involved in the initial excitation and the results are found to be in essential agreement with those of other tritiated hydrocarbons. The molecular excitation of benzene following beta decay is then shown to result probably from a sudden electronic perturbation following the formation of the doubly charged He^3 nucleus.

Some results on the dependence of the collection efficiency of a given ion on its kinetic energy are also discussed.

WHEN a radioactive atom in a molecule emits a β^- particle, the molecule is left with at least one + charge. Further ionization and molecular disruption may also subsequently occur. If these events take place in a mass spectrometer at low pressure, the ions can be collected without intermolecular collisions. Since the time of collection, about 10^{-4} to 10^{-5} sec, is long compared to the half-lives of allowed radiative transitions, about 10^{-8} sec, and to periods of vibration, about 10^{-14} sec, the energy involved in the molecular excitation has had time to distribute itself and one is in a position to evaluate the excitation of a molecule as a consequence of beta decay. Studies have recently been made on $C^{14}O_2$, CH_3T[1(a)] and HT[1(b)] by Snell and Pleasonton, and on C_2H_5T, $C_2H_2Br_2$[80 2(a)], *n*- and *i*-C_3H_5T[2(b)], and HT and TT[2(c)] by Wexler *et al.* It was thought useful to investigate a more complex molecule, and in particular an aromatic species, to contrast with the compounds previously studied. The simplest of the aromatic family, benzene, was chosen. Most recently, Wexler has also presented data on four monotritiated toluenes to fill out the picture.[2(d)]

EXPERIMENTAL

Monotritiated benzene was prepared for us by the New England Nuclear Corporation. The preparation was accomplished by the addition of tritiated water diluted with about 20 parts of normal H_2O to phenyl magnesium bromide. To check the purity of the preparation, the T benzene in one preparatory run was diluted with purified nonradioactive benzene, and the product distilled. Aliquots from the distillation indicated a homogeneity of product of at least 98%. A run made with the mass spectrometer a week after preparation, when compared with one made three months later, showed no apparent change in the hydrocarbon spectra due to production of foreign species caused by self-ionization. Mass 4, which was measured three months after preparation, (cf. Table I), represents the upper limit of HT contamination, HeH^+ being the principal product of HT decay.[1(b),2(c)]

The tritiated benzene was allowed to leak at a steady rate into a specially designed mass spectrometer previously described by Pleasonton and Snell,[3] Fig. 1. The total pressure in the source volume was held at about 3×10^{-6} mm Hg. Differential pumping was employed so as not to deplete the gas in the source volume too quickly, but still allow for fast pumping near the detector so that the radioactivity would not contribute considerably to the background. Ions formed within the region of the field rings are collected, focused, and accelerated to an energy of about 5000 v into the magnetic analyzer. The spread of energies in 99.5% of the ion beam thus formed is less than 1%. Subjected to analysis by deflection through 96.5° in a two-directional focusing magnetic spectrometer, the ions, after acceleration through a further 2000 v, are then counted by means of an electron multiplier.

The counting rate was taken at different e/m settings with repeated reference to mass 77. Because of the constancy of peak shapes over a wide range of e/m and recoil energy values and because of the narrowness of the peaks relative to the slit width at the detector, the counting rate at the peak maximum can be taken as proportional to the integrated value of the collected ion. Furthermore, the accuracy in the location of a peak is at least a few tenths of a percent of the e/m value while the width of the peak at half maximum is 2%.

For neighboring masses above 30, it was necessary to apply a correction for overlap. Shapes obtained from the ionization of N_2 and from the +7 peak from the decay of Kr^{79} were used for the purpose. Corrections

* This document is based on work performed for the United States Atomic Energy Commission at the Oak Ridge National Laboratory.

[1] (a) A. H. Snell and F. Pleasonton, J. Phys. Chem. **62**, 1377 (1958); (b) A. H. Snell, F. Pleasonton, and H. E. Leming, J. Inorg. & Nuclear Chem. **5**, 112 (1957).

[2] (a) S. Wexler and D. C. Hess, J. Phys. Chem. **62**, 1382 (1958); (b) S. Wexler and D. C. Hess, ANL–5818 (October–December, 1957), p. 82; (c) S. Wexler (to be published); (d) G. R. Anderson, L. A. Singer, and S. Wexler, ANL–5911 (August–September, 1958), p. 13.

[3] A. H. Snell and F. Pleasonton, Phys. Rev. **111**, 1338 (1958).

were small in most instances, and mass 78 was in agreement with that calculated from the average amount of C^{13} present in a benzene molecule. However, the presence of the principal peak mass 77 left the evaluation of mass 76 in doubt. Also the presence of mass 38 and mass 37 made the determination of the doubly charged species difficult, though the fact that the doubly charged ions were collected with twice the efficiency of the singly charged ones, rendered the task easier than might be expected from the relative amounts reported.

RESULTS

The results are presented in Table I. As with the previous studies made on monotritiated hydrocarbons,[1,2] the C—He bond is severed following beta decay in nearly every case and the charge is left with the organic fragment. This initial parent fragment remains intact in about 70% of the events while in the remaining situations it fractures into one of a large variety of ions forming a spectrum similar in complexity to that found after electron impact.[4,5] Pictorially the reaction seems to be the following:

$$C_6H_5T \xrightarrow{\beta^-} C_6H_5He^+ \longrightarrow C_6H_5^+ + He$$

$$\Big\downarrow\ 30\%$$

$$\swarrow\ \downarrow\ \searrow$$

$$\sim 30 \text{ fragments.}$$

The ions, $C_2H_5^+$, $C_3H_5^+$, and $C_4H_5^+$, seem spurious although minute traces of them have been found in some electron impact studies.[5] The presence of the obviously spurious $e/m = 1/54$, however, casts suspicion on the results of ions in very low yield.

DISCUSSION

Electron impact studies produce fragment spectra similar in the complexity and types of species as are found with the studies on T hydrocarbons, and Wexler[2(a)] has suggested that the fragment ions, formed following β^- decay, decompose in the same manner as the fragment ions formed from electron impact. That is, there would be substantially no difference in a $C_6H_5^+$ ion formed following the β^- decay of T benzene from one formed following the electron impact on benzene, except for the total amount of energy that each might have received. Evidence for the independence of the site of excitation following the decay of T hydrocarbons is given by the fact that each of four different toluenes, tritiated respectively on the methyl group and on the positions *o*, *m*, and *p* to the methyl group, gave substantially identical fragmentation patterns.[2(d),6]

As another example of the correspondence between electron impact studies and studies on T hydrocarbons, it is interesting to compare the yield of $C_4H_4^+$, $C_3H_2^+$ from electron impact on benzene with that from T benzene. $C_3H_2^+$ is found in relatively large yield in the T

TABLE I. Fragment spectra of T benzene.

M/e	Species	(Corr. for C^{13}) Abundance	Error[a]
80	$C_6H_5He^{3+}$	0.0	±0.2
79	$C_6H_4He^{3+}$	0.1	±0.2
78	$C_6H_6^+$	0.0	±0.7
77	$C_6H_5^+$	100.0	±1.0
76	$C_6H_4^+$	?	...
75	$C_6H_3^+$	0.7	±0.3
74	$C_6H_2^+$	3.5	±0.2
73	C_6H^+	1.8	±0.2
72	C_6^+	0.4	±0.2
65	$C_5H_5^+$	0.0	±0.02
64	$C_5H_4^+$	0.0	±0.06
63	$C_5H_3^+$	0.0	±0.06
62	$C_5H_2^+$	0.23	±0.06
61	C_5H^+	0.93	±0.10
60	C_5^+	0.75	±0.08
54	...	0.11	±0.02
53	$C_4H_5^+$	0.11	±0.03
52	$C_4H_4^+$	0.0	±0.07
51	$C_4H_3^+$	3.6	±0.2
50	$C_4H_2^+$	4.7	±0.2
49	C_4H^+	4.8	±0.1
48	C_4^+	0.86	±0.09
42	...	0.03	±0.03
41	$C_3H_5^+$	0.15	±0.04
40	$C_3H_4^+$	0.0	±0.05
39	$C_3H_3^+$	0.5	±0.08
38½	$C_6H_5^{++}$	0.8	±0.11
38	$C_3H_2^+$	3.8	±0.14
37½	$C_6H_3^{++}$	0.2	±0.12
37	C_3H^+	4.7	±0.14
36½	C_6H^{++}	0.6	±0.11
36	C_3^+	1.7	±0.10
30	...	0.0	±0.06
29	$C_2H_5^+$	0.20	±0.03
28	$C_2H_4^+$	0.0	±0.04
27	$C_2H_3^+$	0.50	±0.07
26	$C_2H_2^+$	0.69	±0.07
25	C_2H^+	0.66	±0.08
24	C_2^+	0.51	±0.08
17	...	0.02	±0.03
16	CH_4^+	0.02	±0.03
15	CH_3^+	0.08	±0.03
14	CH_2^+	0.09	±0.03
13	CH^+	0.19	±0.03
12	C^+	0.38	±0.04
4	HHe_3^+, TH^+	0.37	±0.05
3	H_3^+, He^{3+}	0.17	±0.06
2	H_2^+	0.0	±0.06
1	H^+	0.49	±0.08

[a] Statistical error in counting.

[4] A. Hustrulid, P. Kush, and J. T. Tate, Phys. Rev. **54**, 1037 (1938).

[5] (a) Mass spectral data, Am. Pet. Inst. Research Project **44**, No. 175, 250; (b) mass spectral data, *ibid.* **44**, No. 1; (c) mass spectral data, *ibid.* **44**, No. 2.

[6] The electron impact results of Seymour Meyerson and Paul N. Rylander [J. Chem. Phys. **27**, 901 (1957)] suggest that a 7-membered ring ion may serve as an intermediate species in the breakdown of toluene and thus give a specific model for explaining the identical behavior of the different T toluenes. This, however, does not diminish the argument for the ability of the organic fragment to distribute partially at least some of its energy throughout the molecule before decomposition.

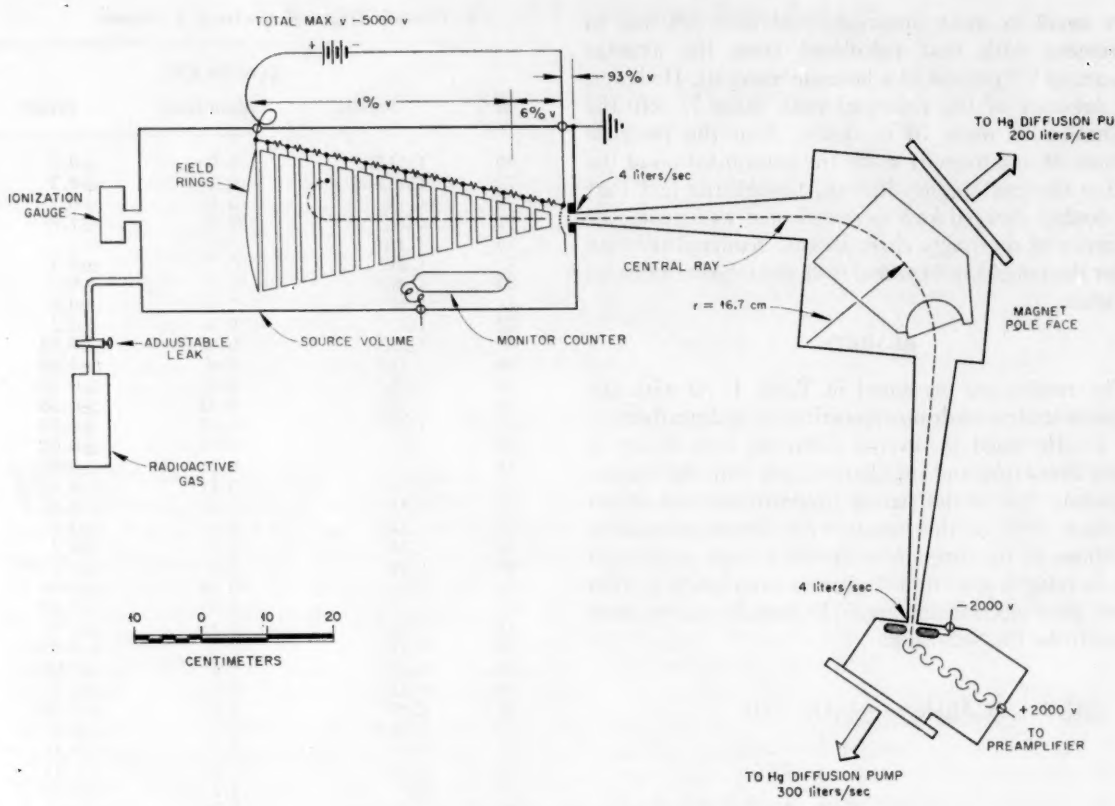

FIG. 1. Mass spectrometer for radioactive gases.

benzene study while $C_4H_4^+$ is not found at all. In the electron impact study on benzene both ions are found in relatively large abundances. This suggests that $C_4H_4^+$, formed from electron impact on benzene, comes directly from $C_6H_6^+$ while $C_3H_2^+$ comes via $C_6H_5^+$. This conclusion was also reached by Franklin and Field[7] on comparing heats of formation and appearance potential data.

Electron impact data coupled with the use of the Rosenstock *et al.*,[8] theory of unimolecular decomposition have been used by Wexler to evaluate the energy distribution following the decay of C_2H_5T. On using the Rosenstock rate equation for a similar calculation on T benzene, we found that it was impossible to fit any energy distribution to this calculation which would give rise to the observed fragment spectra. The Rosenstock equation is $k=\nu[(E-\epsilon)/E]^N$ where k is the rate constant, E is the total energy available for excitation, ϵ is the energy required for decomposition, N is the number of vibrational degrees of freedom in the activated complex, and ν is the frequency factor. Besides the difficulties in evaluating the frequency factors from estimates of the vibrational frequencies of the parent ion's activated complex, we also encountered problems peculiar to large molecules. Some of our difficulties may be understood from the following considerations. The general agreement in the literature, even for molecules larger than benzene, between the calculated energies of decomposition using appearance potential data and those using heats of formation suggests that a given ion will be observed as soon as its parent ion has enough energy to decompose. However, the Rosenstock rate equation seems to indicate that for parent ions having a large number of degrees of freedom, the energy required before this ion can decompose in 10^{-5} sec be in a large excess of the decomposition energy. For example, in the case of benzene for $C_6H_6^+ \rightarrow C_6H_5^+ + H$, we have calculated, using the methods outlined by Rosenstock *et al.*[8] for evaluating rate constants, that 175 kcal/mole of initial excitation would have to be present to produce even a decomposition of 0.01% of the parent ion, while the experimentally observed appearance potential is 120 kcal/mole. A change of a millionfold in the frequency factor will only reduce the value to 150 kcal/mole. Furthermore, branching ratios or the ratios of the number of times that an ion breaks up along a given path to the total number of ruptures it undergoes, as calculated from the Rosenstock rate equation would not even allow one to account for the existence of some of the observed fragments from the electron impact

[7] J. L. Franklin and F. H. Field, J. Chem. Phys. **21**, 2082 (1953).
[8] H. M. Rosenstock, M. B. Wallenstein, A. L. Wahrhaftig, and H. Eyring, Proc. Natl. Acad. Sci. U. S. **38**, 667 (1952).

studies on benzene or the study on T benzene. Even using the frequency factor parametically did not alleviate all the problems. This difficulty in using the Rosenstock theory to explain the decomposition data of larger molecules has been discussed extensively by Chupka.[9]

Some estimate, however, of the energies involved in the β^- decay of tritiated hydrocarbons can be made without recourse to the Rosenstock theory. Examination of the appearance potentials of the ions formed from electron impact on benzene[10] reveals that in 72% of the decays of T benzene the energy possessed by the $C_6H_5^+$ for decomposition must be lower than 4 ev, the difference in appearance potentials between $C_6H_5^+$ and the first daughter ion, while presence of such ions as C_4^+ suggests that energies up to at least 30 ev are present, the difference between the appearance potentials of C_4^+ and $C_6H_5^+$. The appearance in the fragment spectra of C_6H_5T of numerous other species, which possess a variety of intermediate appearance potentials, when formed from electron impact on benzene, indicates that there may be also excitation between 4 and 30 ev available for the decomposition of $C_6H_5^+$ following β^- decay. For example, such an ion as $C_4H_3^+$ which can be formed from $C_6H_5^+$ with 4 ev of excitation and which in turn will itself decompose with about 3 ev of excitation will probably not be observed if the parent ion $C_6H_5^+$ has an initial excitation in large excess of the sum of these two energies.

Comparison of the data for T benzene with the other studies on T hydrocarbons shows analogies which suggest a similarity in the β^- excitation process for these hydrocarbons. A large variety of fragments is found in each case, and at least a small amount of those species requiring the largest energy for formation is noted. There is also a surprising uniformity in the percentage of the parent ion left intact after the dissociation of He. Table II gives the ratio of the number of initial parent ions to the total number of ions found, which in turn represents the number of decays resulting in little or no excitation. The results fall roughly between 70 and 80% except for the propanes, but it is interesting to note that the energy needed to break the first bond in propane, about 1.5 ev, is lower than in any of the other studies. It may be that some of the parent ions described as having little or no excitation may nevertheless have just enough to exceed the first energy barrier in the decomposition of propane. The inordinate amount of the first daughter fragments found in the T propanes lends weight to this suggestion.

We now have to explain the excitation in terms of the β^- decay process. Molecular excitation by β^- decay is derived principally from two sources. One source stems from the beta-neutrino recoil, and the other from the fact that the β^- particle leaves the nucleus with a velocity large compared to that of the orbital electrons, so that these electrons cannot adjust adiabatically to the sudden change in nuclear charge. Direct interaction between β^- ray and the orbital electrons as the β^- leaves the atom has been shown to be negligible.[11]

TABLE II. Percent of parent ion in fragment spectra.

Reactant	Parent ion	% of parent ion/total no. of ions formed
CH_3T	CH_3^+	83
C_2H_5T	$C_2H_5^+$	80
i-C_3H_7T	$C_3H_7^+$	56
n-C_3H_7T	$C_3H_7^+$	40
C_6H_5T	$C_6H_5^+$	72
α-C_7H_7T	$C_7H_7^+$	79
o-C_7H_7T	$C_7H_7^+$	78
m-C_7H_7T	$C_7H_7^+$	79
p-C_7H_7T	$C_7H_7^+$	76

If He^3 takes the full recoil of the beta decay, it will receive a spread of energies with 3.6 ev as a maximum and more than 90% below 2 ev. This excitation is much too small to account for the high energies needed to explain some of the observed spectra of the tritiated hydrocarbons. Furthermore, in the next section it will be shown that most of the recoil energy seems to be manifested as translational energy for the entire molecule.

Excitation from the nonadiabatic nature of the sudden change in nuclear charge does afford, however, an explanation for the energy spectrum that has been obtained from the fragmentation of T hydrocarbons. From hydrogenlike wave functions Migdal[11] has calculated expressions for the electronic excitation following β^- decay. His Eq. (6)[12] gives the relative probability of transitions from the ground state of H to the various states of He^+.

$$W_1^0,\ n=2^6\frac{[n(Z_1/Z)-1]^{2n-4}}{[n(Z_1/Z)+1]^{2n+4}}\times n^5(Z_1/Z)^3(Z_1-Z/Z)^2,$$

where Z_1 and Z are, respectively, the charge on the nucleus before and after the β^- decay and n is the principal quantum number for the final state.

For example, the transition probably to the first excited state of He^+, following β^- decay is:

$$W_1^0,\ 2=[2^6(2\cdot\tfrac{1}{2}-1)^0/(2)^8\times 2^5(\tfrac{1}{2})^3(-\tfrac{1}{2})^2=0.25.$$

The calculations reveal that for the decay $T\rightarrow He^+$, 70% of the transitions go to the ground state of He^+; 25% to the first excited level, 40.5 ev; 2.5% to states with energies up to 54.1 ev and 2.5% lead to He^{++}. Wexler[2(a)] has suggested that tritium on a hydrocarbon acts like a T^- and behaves independently of the molecule, so that the probability of transitions to excited states can be calculated from atomic wave functions.

[9] W. A. Chupka, J. Chem. Phys. **30**, 191 (1959).

[10] F. H. Field and J. L. Franklin, *Electron Impact Phenomena* (Academic Press, Inc., New York, 1957).

[11] A. Migdal, J. Phys. (U.S.S.R) **4**, 449 (1941).

[12] Dr. Sol Wexler (private communication) has pointed out a misprint for this equation in the original paper.

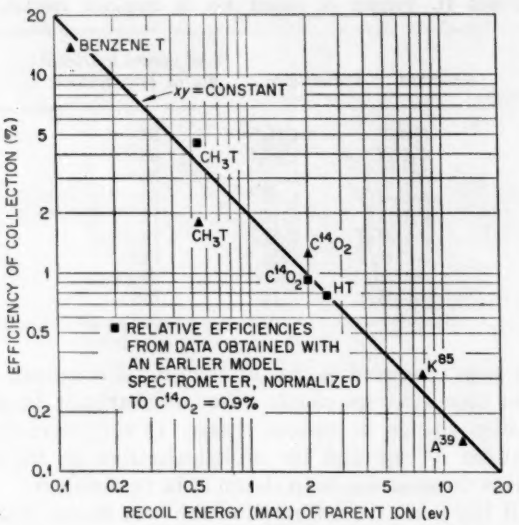

FIG. 2. Dependence of collection efficiency on recoil energy.

He proposes that the transition probabilities arising from $T^- \rightarrow He$ lie close to those calculated from Migdal's equation for $T \rightarrow He^+$ given in the foregoing and to those calculated for $He \rightarrow Li^+$ by Winther[13] from the wave functions of the helium atom and lithium ion, i.e., 67% to ground state and 17% to the first excited state. Thus one would expect an excitation of 20.2 ev, the first excited level of He, or more in about 30–35% of the T hydrocarbon decays, with no excitation in the remainder of the cases.

The analysis given in the foregoing suggests that the initial parent ions receive a distribution of energies which is discontinuous, having no energies between 0 and the first excited state of He^+ or He, rather than the probable occurrence of some energies of intermediate values which has been inferred from the experimentally observed large variety of fragments. A possible explanation for this is that the transference of energies from He to the organic fragment before it leaves may not be quantitative because of photo emission or losses to He either as atomic excitation or kinetic energy. There may also be some allowed transitions during the β^- decay to a spectrum of molecular electronic levels lying between the ground and first excited states of He.

That extrapolation from the calculation of atomic excitation to the molecular situation may not be at all unreasonable is substantiated by Wolfsberg's[14] calculations on the excitation following

$$C^{14} \xrightarrow{\beta^-} N^{14}$$

decay of $C^{14}H_3C^{14}H_3$ in which he found from quantum mechanical analysis that the probability of ground state transitions is to a first approximation the same in the molecular case as in the atomic one.

So far in this paper no mention has yet been made of the importance of the formation of multicharged ions and the production of more than one charged fragment per event. Migdal[11] predicts that 2.5% of the He be doubly charged following β^- decay of tritium, but incorporation of the T into a molecule makes extrapolation of this value uncertain. Some doubly charged species are found in the study of T benzene, but in small amounts (about 1.5%, though the value may be higher since some species are obscured by singly charged ones having the same e/m value), and are the same species which likewise occur in small amounts in the electron impact studies on benzene, so that perhaps the statement about the independence of the source of initial excitation may also be applicable to the doubly charged ions.

The possibility of rupturing a doubly charged ion into two singly charged species should also be taken into account in the analysis. However, since the repulsive forces involved in the breakup of two+ions should give rise to large kinetic energies, the absence of many high recoil energy fragments in electron impact studies argues against a large prevalence of reactions involving simultaneous formation of two charged ions. The process of an excited neutral fragment decaying to a charged one is also not ruled out experimentally, though such processes are not needed for a consistent picture and are generally not energetically as probable as the breakup into two neutral fragments.

RECOIL ENERGY

A digression should be made on kinetic energy. The collection efficiencies in electron impact[15] studies are greatly influenced by the recoil energies of the collected ions. To ascertain the importance of this effect in our studies, the collection efficiencies of various radioactive atoms or molecules having different recoil energies were measured. The radioactivities were sufficiently long lived to permit reasonable amounts of the materials to be put into the source volume. The purities of the gases were checked by mass analysis and their pressures were measured by an ionization gauge with suitable corrections for relative ionization efficiencies. From the volume of the source, the pressure of the gas, and the transmission of the slits, estimates of the collection efficiencies were made. Though the absolute values are quite crude, the relative values should be accurate to within ±50%. All the radioactive gases used for comparison were essentially pure β^- emitters with maximum β^- energies below 0.75 Mev. For simplicity, the maximum recoil energies of the ions were considered roughly proportional to their average. In the case of molecules, the recoil was considered as against the total mass of the molecule. As shown in Fig. 2 the plot of

[13] A. Winther, Kgl. Danske Videnskab. Selskab., Math.-fys. Medd. **27**, No. 2 (1952).
[14] M. Wolfsberg, J. Chem. Phys. **24**, 27 (1956).
[15] F. H. Field and J. L. Franklin, J. Chem. Phys. **24**, 92–105 (1956).

the maximum recoil energy vs the collection efficiency for each of the radioactive gases studied gave a fit over a large range of energies to a curve representing an inverse proportionality between collection efficiency and recoil energy. These findings are substantiated by a linear decrease of the collection efficiency with the lowering of the voltage on the field rings.

It will be noted that the recoil energies for T benzene and CH_3T which best fit the curve described in the foregoing require that the whole molecule receive the full recoil as kinetic energy. This is particularly in evidence since ions with smaller kinetic energies would be preferentially weighted.

A warning with regard to kinetic energy should be made in the interpretation of data in our studies and in the studies with electron impact. What we are concerned with is the conversion of some of the excitation energy into kinetic energy during molecular breakup which would cause the daughter fragments to be subsequently less efficiently collected than the parent ion. Though in large molecules the overlapping of electronic levels will keep energy confined to the electronic and vibrational states, in small molecules, particularly diatomic molecules, the electronic levels are widely spread and Franck-Condon transitions may occur to nonbinding states which lie above the energy needed for decomposition and so convert some of the excitation into kinetic energy. Furthermore, if excessive energy, more than that required to break a given bond, is present in that bond, translational energy may be expected for the fragments. This is probably of lesser importance for larger molecular ions. However, in breakage of a diatomic molecule, one can certainly expect at least some or most of the excess energy to be manifested as kinetic energy, since there is no longer a means for absorbing the excitation as vibrational energy.

In the fragmentation of large molecules the small neutral fragments will probably carry away most of the kinetic energy, and it is again the smaller ionic fragments which are more likely to exhibit translational energy. In confirmation of the foregoing discussion, the literature of electron impact phenomena reveals few cases of large molecular fragments with much recoil energy, but does show that recoil energy is quite prevalent with smaller fragments and is present in all diatomic ruptures.[15] Thus errors in collection efficiency are to be looked for in smaller fragments, and since they constitute the yardstick for high energy processes, this is the region in which there lies the greatest uncertainty. Fortunately, since in β^- decay the parent molecule already gets a "kick," the difference between its collection efficiency and that of the subsequent fragments is reduced. Studies which may be in considerable error, however, are those on HT, TT, and $C^{14}O_2$ where the daughter ions will carry off a sizable fraction of the kinetic energy and where the parent ion, or in the case of CO_2 where the first daughter ion, is diatomic.

To obtain a less ambiguous picture of molecular breakup following nuclear decay, some experiments should be carried out in field free sources[16] or under such strong collection fields that collection efficiencies are uniform. Concurrent measurements of the kinetic energy spectrum of each of the fragments should also be made to clarify phenomena of both the initial excitation and subsequent decomposition, as, for example, in the identification of the rupture of multicharged ions. Such experiments have been planned for the near future in this laboratory.

CONCLUSIONS

Though the assumptions involved in calculating the excitation following β^- decay of tritium do not allow for more than tentative conclusions with regard to details, a qualitative description of this process can be made with some confidence. Following beta decay, the helium does not remain bound to the organic molecule but leaves as a He atom. The remaining singly charged organic fragment is found in about 70% of the cases with little or no internal excitation. In the other 30% of the events the fragment is left with a spectrum of energy distributed from 0 up to a value high enough for extensive multiple bond breakage. The data from all the hydrocarbons thus far studied appear to be consistent with these generalizations, which in turn are consistent with the calculations concerning the nonadiabatic excitation following the atomic transition

$$T \xrightarrow{\beta^-} He^+.$$

ACKNOWLEDGMENTS

I should like to thank Dr. Arthur H. Snell and Frances Pleasonton for the use of their equipment and for the helpful discussions I have had with them. I should like to thank particularly Miss Pleasonton for her assistance in collecting some of the experimental data.

[16] See, for example, A. H. Snell and F. Pleasonton, Phys. Rev. **100**, 1396 (1955).

Absolute Infrared Intensities of the Ammonium Ion in Crystals*

C. C. FERRISO† AND D. F. HORNIG‡

Metcalf Chemical Laboratories, Brown University, Providence, Rhode Island

(Received October 26, 1959)

The absolute intensities of the two infrared active fundamentals of the ammonium ion, ν_3 and ν_4, have been studied in several environments. Dilute solid solutions of NH_4^+ ions in KCl, KI, CsCl, and CsI were studied and compared with pure NH_4I. After separating the effect of the net charge, the apparent bond moments ranged from 0.63 d to 0.80 d (av 0.71) and the bond dipole derivatives, $\partial\mu/\partial r$, from 2.06 d/A to 3.59 d/A (av 2.80 d/A). The bond moment is substantially the same as in NH_3.

INTRODUCTION

UP to the present time no direct experimental studies of the absolute infrared absorption intensities of ions in crystals have been carried out. Decius[1–3] has estimated dipole moment derivatives (from which intensities may be calculated) from the magnitude of the frequency splittings caused by intermolecular coupling, basing the calculation on the assumption that only dipole-dipole forces were important. Haas and Hornig[4] have computed intensities and dipole moment derivatives from the frequency difference between longitudinal and transverse waves in crystals, obtained either from Raman spectra or infrared reflection spectra. This calculation depends on the validity of the assumption of purely electrostatic interactions. It seemed important to us to obtain a direct measurement involving as few auxiliary assumptions as possible.

Straightforward measurement of single crystal specimens is exceedingly difficult because the thickness required to study fundamentals in ionic crystals is of the order of 10 μ or less. Techniques for producing such specimens have not yet been developed. In some cases, such as the ammonium salts, suitably thin samples can be made by sublimation. In order to measure intensities, the number of absorbing molecules per cm^2 of beam must be known. This might be determined by measuring the thickness and index of refraction of the film optically. Alternatively, if it is established that the film is of uniform thickness this same quantity can be found by quantitative chemical determination of the amount of material in the film. We have used the latter method to study the absolute infrared intensities of the two infrared active bands of the ammonium ion in films of ammonium iodide.

We have also studied the intensities of dilute solid solutions of ammonium ions in alkali halide crystals.[5] The ammonium ions can thus be placed in crystalline environments which closely approximate all of the phases of pure ammonium halides, but any complications produced by intermolecular coupling are avoided since in a dilute solution the ammonium ions are far apart. In addition, the specimens can be made conveniently thick. The integrated infrared absorption intensities of the NH_4^+ ion were therefore measured in KCl and KI, which have the NaCl structure characteristic of the high-temperature phases of the pure ammonium salts, as well as in CsCl and CsI which have the same structure as the low-temperature phases.

EXPERIMENTAL METHODS

(a) Sample Preparation

The NH_4I films were deposited on masked KBr plates by sublimation in a high vacuum. The KBr plates were cooled to about 0°C and the NH_4I heated to about 100°. The growth of the films was followed by observing the color of reflected light when they were illuminated with white light and in this way the thickness could be estimated accurately enough to prepare films for the intensity measurements. The fact that the color was relatively uniform over the entire film surfaces indicated that they were homogenous. The amount of material deposited was determined later by dissolving the specimen and analyzing for NH_4^+. Since the mask determined the coated area accurately, this was sufficient to give the concentration of NH_4^+ per cm^2.

The solid solutions were prepared by adding an aliquot of stock NH_4X solution to a saturated water solution of the corresponding alkali halide. Some of the material in the solution was then precipitated, either by evaporation or by the addition of ethanol, yielding crystals in which the ammonium ion replaced a small proportion of the alkali ions. No differences were noted between the spectra of samples prepared by the two methods.

* Based on a thesis submitted by C. C. Ferriso in partial fulfillment of the requirements for the Ph.D. degree, Brown University, 1956. This work was supported by the Office of Naval Research and presented at the Symposium on Molecular Structure and Spectroscopy, Ohio State University, Columbus, Ohio, June, 1955.

† Present address: Convair Astronautics, Applied Research, San Diego, California.

‡ Present address: Department of Chemistry, Princeton University, Princeton, New Jersey.

[1] J. C. Decius, J. Chem. Phys. **22**, 1941, 1946 (1954).

[2] J. C. Decius, J. Chem. Phys. **23**, 1290 (1955).

[3] W. C. Steele and J. C. Decius, J. Chem. Phys. **25**, 1184 (1956).

[4] C. Haas and D. F. Hornig, J. Chem. Phys. **26**, 707 (1957).

[5] All the systems studied form solid solutions at the concentrations used, e.g., R. W. Havighurst, E. Mack, Jr., and E. C. Blake, J. Am. Chem. Soc. **47**, 29 (1925). This is also evident from our spectra which are characteristically different from those of the pure phases.

The sample, usually about 7 to 8 g, was dried overnight at 115°C and then ground for 30 min in an agate mortar. The powder was then dried again overnight, ground once more for 15 to 30 min and stored in the oven until used. For study, this powder was pressed into pellets in a press of our own design and construction. The powder was placed in the mold and evenly distributed by inserting the plunger and rotating it several times. The mold was assembled, evacuated to about 20 μ Hg for 5 min, and the pellet formed by pressing at about 100 000 psi for 1 min or so. The pressing was repeated two or more times, rotating the mold 120° after each pressing. The resulting pellet was transferred with tongs to the absorption cell or a desiccator.

The pellets were of 20.6 mm diam and their thickness, measured with micrometers, was uniform to within 1 or 2% over the entire area. Their thicknesses were usually in the range 0.3 mm to 1.4 mm. The powdered alkali halides were pressed to within less than 1% of their theoretical densities. The pellets prepared in this way remained optically transparent for more than four months if stored in a desiccator.

(b) Pellet Press

Many evacuable molds which produce good quality pellets have been described in the literature;[6-8] however, some of them suffer from the fact that the pellet may be fractured and chipped when removed from the mold. The unique feature of our mold is the tapered lower die (3 degrees) which eliminates the problem of fracture when the pellet is removed from the mold. Figure 1 shows a section through the vacuum mold. The powder is pressed in the cylinder D between the polished surfaces of the quench hardened tool steel dies (E) and (F). Pressure is applied by means of the plunger A and supported by the lower anvil (C) which screws into the carbon steel body of the mold (B). The sample chamber (D) can be evacuated through the port (G) about 3/4-in. above the sample. The O rings on the plunger and anvil provide the vacuum seal. The pressure was delivered by a hydraulic ram which provided a total force of up to 55 000 lb, yielding a pressure up to 110 000 psi on the sample.

(c) Analysis of the Pellets

In order to measure the ammonium ion concentration, a weighed pellet was dissolved in 100 ml of water. The NH_4^+ was then determined as NH_3, using Nessler's reagent prepared as suggested by Winkler.[9] The colorimetric analysis was carried out utilizing a spectrophotometer as described by Kistiakowsky *et al.*[10] In order to obtain reproducible and accurate results it was found necessary to prepare fresh Nessler's reagent before each analysis and to carry out the spectrophotometric determination as soon as the color was fully developed, approximately 5 min after the addition of reagent to the solution being analyzed. The calibration curves were constructed by analyzing standard solutions containing from 10^{-7} to 10^{-8} mole of NH_4^+ per cc of water in the presence of from 0.01 cc to 0.001 cc of alkali halide per cc of water. It must be noted that by analogy to liquid solutions concentrations in the pellets were expressed in moles of NH_4^+ per cc of alkali halide, the alkali halide being treated as if it were a solvent. The alkali halides used included KCl, KI, and CsCl; no effect on the calibration curve depending on the salt was found. It was concluded from the study of standard solutions that the absolute error was within $\pm 1.0\times10^{-9}$ mole of NH_4^+ per cc of water. This represents an error of 1.5% in the crystal solutions.

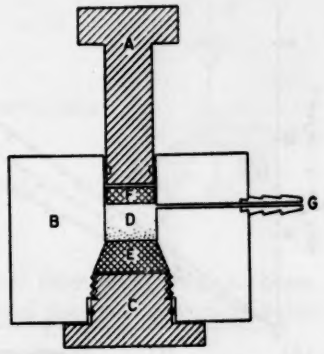

FIG. 1. Section through the vacuum mold.

(d) Measurement of Intensities

The absolute intensity is defined by the relation

$$A=(1/lc)\int_{\text{band}} \ln(I_0/I)_{\text{true}}\,d\nu,$$

where I_0 and I are the true values of the intensities of the incident and transmitted beams, l is the thickness and c is the concentration of NH_4^+ in the specimen. The quantity which can be measured is

$$B=(1/lc)\int_{\text{band}} \ln(T_0/T)_{\text{expt.}}\,d\nu,$$

which may differ from A because of the finite resolution of the spectrometer.[11] Here T is the apparent transmission measured by the spectrometer. It is readily shown that $B\rightarrow A$ as $lc\rightarrow 0$. Consequently, if Blc is plotted vs lc, $B=A$ in that region of lc where a straight line is obtained. Another test is also available in that

[6] V. Schiedt and H. Remwein, Z. Naturforsch. **7b**, 270 (1952).
[7] M. A. Ford and G. R. Wilkinson, J. Sci. Instr. **31**, 338 (1954).
[8] D. H. Anderson and N. B. Woodall, Anal. Chem. **25**, 1906 (1953).
[9] L. W. Winkler, Z. Untersuch. Nahr. u. Genussm. **49**, 164 (1925).
[10] G. B. Kistiakowsky, P. C. Manglesdorf, Jr., A. J. Rosenberg, and W. H. R. Shaw, J. Am. Chem. Soc. **74**, 5015 (1952).
[11] E. B. Wilson, Jr., and A. J. Wells, J. Chem. Phys. **14**, 578 (1946); A. M. Thorndike, A. J. Wells, and E. B. Wilson, Jr., *ibid.* **15**, 157, 868 (1947).

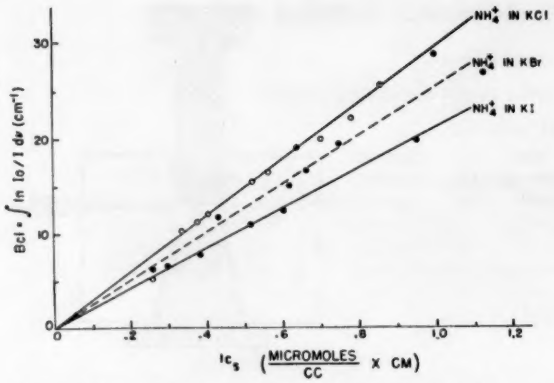

FIG. 2. Blc_s vs lc_s of coprecipitated mixtures in the 7μ band.

when $B \neq A$, B must depend on the resolution of the spectrometer.

The infrared spectra were obtained on a Perkin-Elmer Model 83 monochromator which was modified for use as a ratio-recording double beam instrument.[12] A CaF_2 prism, calibrated by the procedure of Dowie *et al.*,[13] was used. Intensities were measured for both infrared active fundamentals of NH_4^+, the triply degenerate stretching vibration, ν_3, and the triply degenerate bending vibration, ν_4. To obtain the base line corresponding to I_0, a spectral region through the absorption band was scanned, with a blank pellet made from the same salt substituted for the sample. In first order this procedure should have eliminated both reflection and scattering errors for solid solutions. The same is not necessarily true for the NH_4I films; however, the reflectivity is sufficiently small in bulk specimens, even at the ν_3 and ν_4 peaks, so that the correction should be negligible for films whose thickness is much smaller than the wave length of the radiation, since the reflection is still further attenuated. Measured intensities (B) were obtained by replotting the measured T_0/T as $\ln(T_0/T)$ vs frequency.

The measured intensities were very little influenced by changes in spectral resolution. When the resolution was decreased two- or threefold, the change in B was only 2 or 3%, the decrease in peak intensity being roughly compensated by the increase in band width. The spectral resolution used in the 7-μ region ranged from 6 to 15 cm^{-1} and that in the 3-μ region varied from 20 to 40 cm^{-1}.

As a second check on the extent to which B was equal to A, a series of pellets of varying thickness and concentration were prepared. These pellets were not analyzed but it was assumed that the concentration of NH_4^+ ion in each pellet was proportional to the ratio of NH_4^+ and alkali halide concentrations in the solution (c_s). The resulting plots of Blc_s vs lc_s for both ν_3 and ν_4 are shown in Figs. 2 and 3. It is seen that in all cases the points fall on a straight line passing through the origin so throughout this range of lc_s it may be concluded that $B=A$ and the measured intensities are reliable.

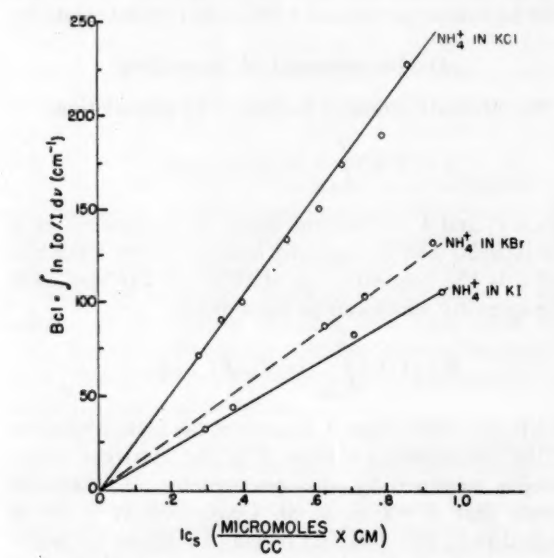

FIG. 3. Blc_s vs lc_s of coprecipitated mixtures in the 3μ band.

TABLE I.

System	c (moles/cc)	lc (μM/cm²)	$B(\nu_3)$[a]	$B(\nu_4)$[a]
NH_4^+—KCl	8.346×10^{-6}	0.771	259.8	28.9
NH_4^+—KI	12.353×10^{-6}	0.726	212.9	39.5
NH_4^+—CsCl	16.425×10^{-6}	1.257	117.9	20.9
NH_4^+—CsI	7.490×10^{-6}	0.770	106.4	22.4
NH_4I	1.732×10^{-2}	0.39	80	18

[a] Units: Darks=$cm^{-1}/\mu M\ cm^2\times10^{-3}$ [D. G. Williams, W. B. Person, and B. Crawford, Jr., J. Chem. Phys. **23**, 179 (1955).

The final experimental values, given in Table I, were determined from a set of three-intensity runs for each ammonium ion-alkali halide system, and for the pure NH_4I films from a set of ten films ranging from about 0.5 to 2.3 μ in thickness. All of these specimens were carefully analyzed to determine the NH_4^+ concentration. The magnitude of the absorption in each case placed them within the intensity range covered by Figs. 2 and 3.

It should be noted that the intensity measured for ν_3 includes that of the combination band, $\nu_2+\nu_4$, which is in Fermi resonance with it.[14] We assume that the major part of the intensity of the entire band derives from the fundamental.

[12] D. F. Hornig, G. E. Hyde, and W. A. Adcock, J. Opt. Soc. Am. **40**, 497 (1950).

[13] A. R. Dowie, M. C. Magoon, T. Purcell, and B. Crawford, Jr., J. Opt. Soc. Am. **43**, 941 (1953).

[14] E. L. Wagner and D. F. Hornig, J. Chem. Phys. **18**, 296, 305 (1950).

DISCUSSION OF EXPERIMENTAL RESULTS

The previous absolute intensities have been determined in a medium with refractive index differing from unity; they must be corrected for the fact that the effective field of the radiation is not that in free space. This problem has been considered by Polo and Wilson[15] for the case of a molecule embedded in a spherical cavity in a continuous dielectric medium and experiencing an Onsager reaction field. Their result was that

$$A_i=\frac{N\pi}{3cn}\left(\frac{n^2+2}{3}\right)^2\left(\frac{\partial\mu}{\partial Q_i}\right)^2, \tag{3}$$

where A_i is the absolute integrated intensity of the ith normal mode; N the number of absorbing molecules per cc, c the velocity of light in a vacuum, n the refractive index of the medium, and $\partial\mu/\partial Q_i$ the rate of change of vector dipole moment with normal coordinate Q_i. This expression should be a good approximation for an ion embedded in a cubic crystal. The resulting $\partial\mu/\partial Q_i$'s for the NH_4^+ ion in various lattices are given in Table II, together with the results of Haas and Hornig for comparison. The experimental intensities were divided by three since both modes are triply degenerate. The sign ambiguity is present because $(\partial\mu/\partial Q_i)$ appears as the square in Eq. (3).

TABLE II.

Substance	$\pm(\partial\mu/\partial Q_3)$	$\pm(\partial\mu/\partial Q_4)$
NH_4^+—KCl	305	101
NH_4^+—KI	256	110
NH_4^+—CsCl	193	81
NH_4^+—CsI	173	79
NH_4I	163	71
NH_4Cl[a] (−190°C)	...	99
NH_4Br[b] (−190°C)	...	104

[a] Reference 4, Raman frequency difference between longitudinal and transverse modes.
[b] Reference 4, infrared reflection spectrum.

The general agreement between the results obtained with two different methods in the present work and two dissimilar methods in reference 4 is very satisfying. The intensities obtained from solid solutions in the NaCl-type lattices were generally greater than in the CsCl-type lattices, but those for NH_4I, which has an NaCl lattice, were lower than in any of the solid solutions. It is hard to rule out systematic errors but presumably the differences reflect the differing local environment of the NH_4 ion in the various lattices.

Calculation of $\partial\mu/\partial R_i$

To obtain information about the N—H bonds in NH_4^+ the $\partial\mu/\partial Q$'s must be related to the change in moment during stretching and bending motions of

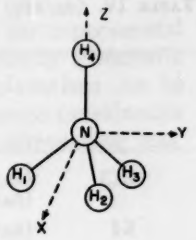

FIG. 4. Orientation of atoms for calculation of $\partial\mu/\partial R_i$.

known amplitude. Using the orientation of atoms shown in Fig. 4, we have employed the symmetry coordinates

$$R_{3a}=(r_1+r_2+r_3-3r_4)/(12)^{\frac{1}{2}} \tag{4}$$

and

$$R_{4a}=(\alpha_{12}+\alpha_{23}+\alpha_{13}-\alpha_{14}-\alpha_{24}-\alpha_{34})/(6)^{\frac{1}{2}} \tag{5}$$

for the infrared active species, where r_i is the change in length of the NH_i bond and α_{ij} is the change in the angle H_iNH_j. The coefficients in the transformation

$$\partial\mu/\partial R_j=\sum_k L_{kj}^{-1}(\partial\mu/\partial Q_k) \tag{6}$$

can be worked out by the method of Wilson.[16] The details of the calculation for a tetrahedral molecule have been given previously.[17] In order to carry it through it is necessary to know the force constants. Since there are three force constants, F_{33}, r_0F_{34}, and $r_0^2F_{44}$, in the most general potential function for the F_2 species of a tetrahedral molecule, the two frequencies of NH_4^+ are not enough to solve the problem. If the frequencies of ND_4^+ are also used, there are just enough frequencies to solve for all the force constants. The frequencies used in our calculation were as follows[14]:

	NH_4^+	ND_4^+
ν_3	3130 cm^{-1}	2350 cm^{-1}
ν_4	1400 cm^{-1}	1067 cm^{-1}.

Because of the anharmonicity, these frequencies do not follow the Teller-Redlich product rule, the frequency product differing from the harmonic oscillator

TABLE III. Summary of results for the ammonium ion in KCl.

	Set I	Set II
$(L^{-1})_{33}\times10^{-12}$	1.2439	1.2440
$(L^{-1})_{43}\times10^{-12}$	−0.0316	−0.0299
$(L^{-1})_{34}\times10^{-20}$	0.1262	0.1238
$(L^{-1})_{44}\times10^{-20}$	0.8668	0.8643
for $\frac{(\partial\mu/\partial Q_3)}{(\partial\mu/\partial Q_4)}=+$	$(\partial\mu/\partial R_4)=1.265$ d $(\partial\mu/\partial R_3)=3.759$ d/A	1.256 d 3.760 d/A
for $\frac{(\partial\mu/\partial Q_3)}{(\partial\mu/\partial Q_4)}=-$	$(\partial\mu/\partial R_4)=0.497$ d $(\partial\mu/\partial R_3)=3.823$ d/A	0.501 d −3.822 d/A

[15] S. R. Polo and M. Kent Wilson, J. Chem. Phys. **23**, 2376 (1955).

[16] E. B. Wilson, Jr., J. Chem. Phys. **7**, 1047 (1939); **9**, 76 (1941).

[17] P. N. Schatz and D. F. Hornig, J. Chem. Phys. **21**, 1516 (1953).

TABLE IV. $(\partial\mu/\partial R_i)$ for the ammonium ion in various alkali halides.

	$\frac{\partial\mu/\partial Q_3}{\partial\mu/\partial Q_4}=+$	$\frac{\partial\mu/\partial Q_3}{\partial\mu/\partial Q_4}=-$ *
KCl	$(\partial\mu/\partial R_4)=$ 1.27 d	0.50 d
	$(\partial\mu/\partial R_3)=+3.76$ d/A	-3.82 d/A
KI	$(\partial\mu/\partial R_4)$ 1.28 d	0.60 d
	$(\partial\mu/\partial R_3)$ $+3.16$ d/A	-3.23 d/A
CsCl	$(\partial\mu/\partial R_4)$ 0.95 d	0.46 d
	$(\partial\mu/\partial R_3)$ $+2.38$ d/A	-3.23 d/A
CsI	$(\partial\mu/\partial R_4)$ 0.91 d	0.47 d
	$(\partial\mu/\partial R_3)$ $+2.14$ d/A	-2.19 d/A
NH_4I	$(\partial\mu/\partial R_4)$ 0.82 d	0.41 d
	$(\partial\mu/\partial R_3)$ 2.00 d/A	-2.05 d/A

* Preferred solution.

value by about 3%. The anharmonicity resides largely in ν_3 since the first overtone of the bending vibration, $2\nu_4$, is found at almost exactly twice the fundamental frequency.

These frequencies therefore yield two sets of force constants. The first (I) is obtained from the two bending frequencies plus the NH_4^+ stretching frequency, ν_3. The other (II) is obtained from the two bending frequencies plus the ND_4^+ stretching frequency, ν_3. Taking $r_0=1.035$ A from nuclear magnetic resonance studies[18] the results obtained are as follows:

	Set I	Set II
F_{33}	5.380×10^5 dynes/cm	5.719×10^5 dynes/cm
r_0F_{34}	0.506	0.536
$r_0^2F_{44}$	0.539	0.541

The consistency of the two values of F_{44} and the differences in F_{33} tend to bear out the initial assumption that the anharmonicity resides in ν_3. In order to test the sensitivity of the $\partial\mu/\partial R$'s to these uncertainties in the force field, a complete calculation was carried out with both sets for NH_4^+ in KCl and the results are summarized in Table III. The two sets of force constants yielded such consistent results that only Set I was used in calculating the dipole derivatives in the other lattices; the results are given in Table IV. The two solutions result from the sign ambiguity arising because only $(\partial\mu/\partial Q)^2$ is measured.

In order to choose between the formal solutions it is important to note that positive R_3 and R_4 result in proton motions in opposite directions. Hence any model with an effective charge located on the protons will predict that $\partial\mu/\partial R_3$ and $\partial\mu/\partial R_4$ have opposite signs. Consequently, we feel that the last column of Table IV is most probably the correct one.

EFFECT OF DISPLACEMENT OF CENTER OF CHARGE

The results given in Table IV cannot be interpreted immediately in terms of bond characteristics since the dipole moment change includes the total charge times the displacement of the origin with respect to which dipole moment is measured. The magnitude of this effect (which does not occur in neutral species) can readily be estimated if the nitrogen atom is chosen as an origin for the definition of internal moments and the coupling of the internal vibrations to the lattice vibration is neglected. The extra apparent moment is then the electronic charge times the displacement of the nitrogen atom, yielding

$$(\partial\mu/\partial R_3)=(\partial\mu/\partial R_3)^0-(2e/3)(m_H/M)$$
$$=(\partial\mu/\partial R_3)^0-0.306\text{ d/A} \quad (7)$$
$$(\partial\mu/\partial R_4)=(\partial\mu/\partial R_4)^0-(2er_0/3)(m_H/M)$$
$$=(\partial\mu/\partial R_4)^0-0.319\text{ d}, \quad (8)$$

where m_H is the proton mass and M is the total mass of the ion. In Eqs. (7) and (8) it is assumed that the net effective charge on the protons is positive in both motions. Otherwise the sign of the second term, representing the displacement of the positive center of charge, must be changed. It would be possible to improve on these assumptions if the frequency and intensity of the Reststrahlen mode were also measured. If the additional assumption is now made of additive changes in bond moments, directed parallel to bonds when they are stretched and perpendicular when they are bent, we have also that

$$(\partial\mu/\partial r)=(\sqrt{3}/2)(\partial\mu/\partial R_3)^0$$
$$\mu_0=(\sqrt{3}/2)(\partial\mu/\partial R_4)^0.$$

The resulting dipole derivatives and bond moments are given in Table V.

Several points are worth noting. First, the bond moment is not high; interpreted as effective charge it corresponds to a charge $+0.14e$ on each proton and $+0.44e$ on the nitrogen.[19] It is interesting that the NH moment found is identical with the bond moment found in NH_3.[20]

Secondly, $\partial\mu/\partial r$, which also has the significance of an effective charge, is very much larger, corresponding to over $+0.6e$. This is presumably the case because

TABLE V. Bond moments and bond moment derivatives for ammonium ions in various crystals.

	$(\partial\mu/\partial R_3)^0$	$(\partial\mu/\partial R_4)^0$	$\partial\mu/\partial r$ (d/A)	μ_0 (d)
KCl	-4.13	0.82	3.59	0.72
KI	-3.54	0.92	3.08	0.81
CsCl	-3.54	0.78	3.08	0.69
CsI	-2.50	0.79	2.18	0.69
NH_4I (pure)	-2.36	0.73	2.06	0.64
av.	-3.21	0.81	2.80	0.71

[18] H. S. Gutowsky, G. E. Pake, and R. Bersohn, J. Chem. Phys. **22**, 643 (1954).

[19] L. Pauling, *Nature of the Chemical Bond* (Cornell University Press, Ithaca, New York, 1948).

[20] D. C. McKean and P. N. Schatz, J. Chem. Phys. **24**, 316 (1956).

the motion involved in the antisymmetric stretch corresponds roughly to the process $NH_4^+ \rightarrow H^+ + NH_3$ so that the polarity changes violently as the protons vibrate.

Thirdly, the differences between the various environments appear to be real and outside the experimental error. On the other hand, no particularly systematic trend appears and no immediate explanations can be given. It seems clear, though, that there is considerable polarization of the NH_4^+ ions by the surrounding ions.

THE JOURNAL OF CHEMICAL PHYSICS VOLUME 32, NUMBER 4 APRIL, 1960

Unimolecular Decomposition of Chemically Activated *sec*-Deuterobutyl Radicals from D Atoms plus *cis*-Burene-2*

R. E. HARRINGTON, B. S. RABINOVITCH, AND R. W. DIESEN

Department of Chemistry, University of Washington, Seattle 5, Washington

(Received November 2, 1959)

Chemically activated *sec*-deuterobutyl radicals were produced at 25°C by the reaction of D atoms with *cis*-butene-2. These vibrationally excited species contain an increment of energy above that of the corresponding light radicals as formed from H plus *cis*-butene-2 in a previous study [B. S. Rabinovitch and R. W. Diesen, J. Chem. Phys. **30**, 735 (1959)]. Apparent rate constants for the unimolecular decomposition to propylene of the deuterobutyl radicals were obtained as a function of pressure, relative to the collision induced stabilization process. Theoretical values for the rate constants at the limits of high and low pressures were calculated using a direct count for the density of vibrational energy levels. The calculated and experimental results are compared with one another, and with the results of the previous study of the *sec*-butyl radical decomposition. The expected energy effect is observed; the deuterobutyl radicals appear slightly more monoenergetic than the equivalent nondeuterated species.

VIBRATIONALLY excited alkyl radicals may be produced homogeneously in the gas phase by the addition of atoms or radicals to an olefin. The ensuing unimolecular decomposition and collisional stabilization processes can be studied concurrently under varying conditions of temperature and pressure. Although the method is restricted in some ways, it nevertheless provides a means of studying rapid unimolecular processes at low temperatures such that the excited species are nearly monoenergetic. Rabinovitch and Diesen (RD)[1] have described experimental and theoretical aspects of the method and its application to the formation of *sec*-butyl radicals, by addition of H atoms to *cis*-butene-2, and their decomposition to propylene plus methyl. Reference should be made to this work for details and for nomenclature used here.

It is of value to employ different addition reactions to produce the same (or virtually the same) species in different states of vibrational excitation. In this paper we present the experimental findings for the unimolecular decomposition of chemically activated *sec*-deuterobutyl radicals formed by addition of D atoms to *cis*-butene-2. The deuterobutyl radicals have a minimum energy, E_{min}, which is ~2 kcal/mole larger than that of butyl radicals produced with H atoms due to zero point energy factors. A comparison is made between this work and the earlier results. In the calculation of k_a, the average observed rate constant for decomposition, the semiclassical approximation of RD for the evaluation of the density and weights of vibrational energy levels, based upon expressions of Marcus and Rice,[2] has been replaced by direct count.

EXPERIMENTAL

Deuterium gas (purity 99.5%) was passed through a silica gel trap at −195°C and was used without further purification. Other experimental details were as previously.

Corrections to the Data

In addition to providing an experimental verification of the primary and secondary reaction mechanisms given by RD, the use of deterium atoms disclosed two additional complicating processes. The first was the contamination of the reaction products by CD_4. This arose from "cracking" to CD_4 of butene which effused into the discharge tube, followed by back-effusion of CD_4 into the reactor. The effect was most marked at the higher run pressures. Methane analyses were performed mass spectrographically; only light CH_4 was considered in the computation of stabilization products resulting from disproportionation of methyl and *sec*-butyl.

* Abstracted in part from a Ph.D. thesis by R. E. H. to be submitted to the Graduate School, University of Washington.

[1] B. S. Rabinovitch and R. W. Diesen, J. Chem. Phys. **30**, 735 (1959).

[2] R. A. Marcus and O. K. Rice, J. Phys. Colloid Chem. **55**, 894 (1951); R. A. Marcus, J. Chem. Phys. **20**, 352, 359 (1952).

TABLE I. Calculated and experimental k_a quantities for *sec*-butyl radical.

Model	Observed (corr.)	I	I′	I″	II
E_{min} kcal/mole		10	10	8	8
Complex		rigid	rigid	rigid	semi-rigid
$k_{a_{cc}}(25°)/k_{a_{cc}}(-78°)$	1.92	1.73	1.64	1.84	1.96
$k_{a_0}(25°)/k_{a_0}(-78°)$	1.44	1.36	1.38	1.44	1.47
$k_{a_{cc}}/k_{a_0}(25°)$	1.68	1.48	1.29	1.43	1.51
$k_{a_{cc}}/k_{a_0}(-78°)$	1.26	1.17	1.08	1.12	1.14
$k_{a_{cc}}(25°)10^6$ sec^{-1}	14.3	7.4	16.8	4.5	16.2
$k_{a_0}(25°)10^6$ sec^{-1}	8.8	4.3	13.0	3.1	10.7
$k_{a_{cc}}(-78°)10^6$ sec^{-1}	7.7	3.7	10.2	2.4	8.3
$k_{a_0}(-78°)10^6$ sec^{-1}	6.1	3.2	9.5	2.2	7.3

A second complication was the presence in the products of *n*-butane-d_2, in addition to *n*-butane-d_1 from butyl disproportionation. The amounts were appreciably larger (and increased at lower butene pressures, when the partial D atom pressure was higher, to >70% total butane) than had been estimated by RD for the process

$$D+CH_3CHD\dot{C}HCH_3 \rightarrow C_4H_8D_2^* \xrightarrow{M} C_4H_8D_2.$$

Fortunately, at the lower run pressures the principal stabilization products are not butane or octane, but largely isopentane. In determining the contribution of the *n*-butane to the stabilization process, *n*-butane-d_2 was counted as 1.6 to allow for any concomitant H abstraction (disproportionation) process, while the *n*-butane-d_1 was weighted by a factor of two. Any error in the arbitrary value 1.6 used is of small effect on absolute k_a values and quite negligible for relative values. Decomposition of an intermediate $C_4H_8D_2^*$ molecule does not appear to occur under present conditions.

A lesser amount of CH_3D, probably from $CH_3+D\rightarrow CH_3D$, also arose at lower pressures and was distinguished, and excluded, by mass spectral analysis.

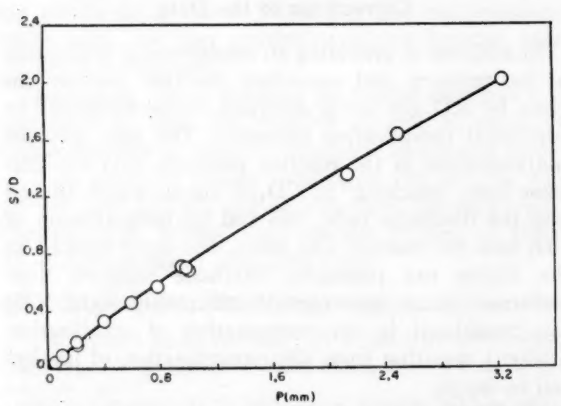

FIG. 1. S/D as a function of p for *sec*-deuterobutyl radical at 25°.

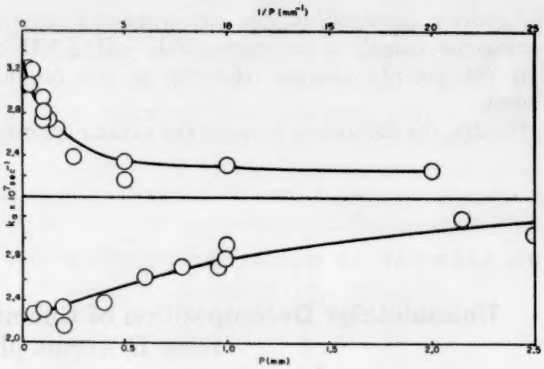

FIG. 2. Plot of k_a vs inverse pressure, and of k_a vs pressure for *sec*-deuterobutyl radical at 25°.

RESULTS AND DISCUSSION

The data of RD were recalculated with the previously mentioned corrections to the methane and *n*-butane. The revised k_a, which do not differ appreciably from the earlier values, are summarized in Table I for the limits of low and high pressure.

The composition of the products for the reaction of D atoms with *cis*-butene-2 at 25° was similar to that of the previous study, aside from more regular appearance of small amounts of *cis*-pentene-2, and need not be detailed here. The data are summarized in Fig. 1 which gives the S/D ratios as a function of pressure; extrapolation to the high and low pressure limits of k_a is made in Fig. 2. The limiting values are listed in Table II. Collision cross sections have been taken as previously and unit collisional efficiency for deactivation again assumed; additional information on this subject will be presented at a later time.

Disproportionation of Radicals

For the ratio of disproportionation/recombination by *sec*-butyl radicals, the value of 0.95 quoted in RD is lowered as a consequence of the new butane correction. The average value found in the present work is ~0.6, with some pressure dependence being manifested. The agreement with the value 2.3 of Kraus and Calvert[3] is not good.

TABLE II. Calculated and experimental k_a quantities for *sec*-deuterobutyl radical (25°).

	Observed	Model II
$k_{a_{cc}}10^7$ sec^{-1}	3.3	2.9
$k_{a_0}10^7$ sec^{-1}	2.2	2.0
$k_{a_{cc}}/k_{a_0}$	1.52	1.45
$k_{a_{cc}}(D)/k_{a_{cc}}(H)$	2.2	1.8
$k_{a_0}(D)/k_{a_0}(H)$	2.5	1.9

[3] J. W. Kraus and J. E. Calvert, J. Am. Chem. Soc. **79**, 5921 (1957). Agreement exists with the value 0.7 calculated by RD from data of F. E. Frey and H. J. Hepp.

The disproportionation/recombination ratio for methyl plus *sec*-butyl is less affected by correction for deuteromethane, and an average of 0.3 in the present work is the same value as found by us previously.

Calculation of k_a

In the calculations of RD the minimum energy of the butyl radical was $E_{min}=41$ kcal/mole; a minimum energy of the activated complex, E_{min}^+, of 10 kcal/mole was adopted there, based on a value of the activation energy for addition of methyl to propylene, E_{CH_3}, of 6 kcal/mole. More recently Brinton[4] found 8.7 kcal/mole for the addition of methyl to ethylene, while for the addition of ethyl to various terminal olefins James and Steacie[5] report values ~8 kcal/mole. Adoption of $E_{CH_3}=8$ kcal/mole makes $E_{min}^+=8$ kcal/mole.

For the deuterobutyl radical, E_{min} and E_{min}^+ alter in accordance with the zero point energy changes associated with the reduced deuterium vibration frequencies of the *association* complex and of the radical (Appendix I). The activation energy for addition of D to butene-2 is then $E_D=2.4$ kcal/mole (cf. $E_H=3.0$ kcal/mole previously), $E_{min}=42.8$ kcal/mole and, for $E_{CH_3}=8$ kcal/mole, $E_{min}^+=9.8$ kcal/mole.

Direct Count of Number and Density of Vibrational Energy Levels

The following expressions are given in RD where the treatment of Marcus[2] has been applied to this problem. The numbering of equations follows the earlier work.

The observed average rate constant for decomposition at a given pressure is

$$k_a=\omega\cdot D/S=\omega\frac{\int_{E_{min}}^{\infty}(k_E/[k_E+\omega])f(E)dE}{\int_{E_{min}}^{\infty}(\omega/[k_E+\omega])f(E)dE}, \quad (a)$$

where $f(E)dE$, the fraction of radicals formed in the energy range E to $E+dE$, is

$$f(E)dE=k_E'K'(E)dE\Big/\int_{E_{min}}^{\infty}k_E'K'(E)dE \quad (d)$$

and the specific rate constant for decomposition of radicals of energy E is

$$k_E=P_1^+N_E^+/hP_1^*N_E^*. \quad (e)$$

Calculation of k_a involves the evaluation of a number of quantities which enter into k_E and $f(E)dE$. These include N_E^+, the number of internal rotational and vibrational energy states at the total energy E^+ for the *decomposition* complex; $N_E^{+\prime}$, the corresponding quantity for the *association* complex; N_E^*, the density of the internal energy levels at the energy E for the energized radicals. These were given earlier as

$$N_E^+=\frac{P_r^+}{(kT)^{r+/2}(r^+/2)!}\cdot\sum_{E_v^+=0}^{E^+}P(E_v^+)(E^+-E_v^+)^{r+/2}\,(f)$$

with a similar expression for $N_E^{+\prime}$, and

$$N_E^*=\frac{P_r^*}{(kT)^{r*/2}(r^*/2-1)!}\cdot\sum_{E_v^*=0}^{E^*}P(E_v^*)(E^*-E_v^*)^{r*/2-1}. \quad (g)$$

Previous applications of this type of treatment have employed a semiclassical expression[1,2,6] for the evaluation of the summations in N_E^+ and N_E^*. $\sum P(E_v^{+\prime})$ is easily evaluated since $E^{+\prime}$ is always comparatively small. The classical evaluation leads not only to an overestimate for these quantities, which may be reduced by *ad hoc* correction factors,[1] but also to an incorrect variation of these quantities with variation of energy (experimentally, with variation of temperature and pressure.) Fortunately much of the error may cancel in the calculation of k_a and various ratios, but a direct evaluation is to be preferred. In this case the expression for k_a becomes

$$k_a=\frac{Q\int_0^{\infty}\frac{A\cdot A'\exp(-E^{+\prime}/RT)dE^{+\prime}}{B(QA/B+\omega)}}{\int_0^{\infty}\frac{A'\exp(-E^{+\prime}/RT)dE^{+\prime}}{(QA/B+\omega)}}, \quad (1)$$

where

$$A=\sum_{E_v^+=0}^{E^+}P(E_v^+)(E^+-E_v^+)^{r+/2},$$

A' is the corresponding expression for the *association* complex, and

$$B=\sum_{E_v^*=0}^{E^*}P(E_v^*)(E-E_v^*)^{r*/2-1}.$$

$Q=P_1^+P_R^+/hP_1^*P_R^*$ was defined previously; its numerical value is taken here as $1/h$; k_a has appropriate limiting values k_{a_0} and k_{a_∞} for ω tending to zero and infinity, respectively.

A simple systematic direct counting procedure was used in the present work for the calculation of N_E^+ and N_E^*. The complexity of such a calculation increases excessively with the number of vibrational degrees of freedom unless the procedure is simplified by grouping the vibrational frequencies into degenerate sets. The frequency of each set was taken as the rounded geometrical mean of the assigned frequencies constituting the set.

The calculation of $N_E^{+\prime}$ by direct count is easily performed at all points throughout the range since

[4] R. K. Brinton, J. Chem. Phys. **29**, 781 (1958).

[5] D. G. L. James and E. W. R. Steacie, Proc. Roy. Soc. (London) **A244**, 289 (1958).

[6] B. S. Rabinovitch, E. Tschuikow-Roux, and E. W. Schlag, J. Am. Chem. Soc. **81**, 1081 (1959).

$E^{+\prime}$ is a small quantity. However, because of the complicated nature of the direct calculations for $N_E{}^+$ (up to 20 kcal/mole), and particularly $N_E{}^*$ at the higher energies (up to 52 kcal/mole), these functions were only evaluated at discrete points which spanned the particular energy range in question, and logarithmic curves were constructed from which values of $N_E{}^+$ and $N_E{}^*$ could be read. At the energies at which these quantities were calculated, the level spacings are small and the functions are well represented by smooth curves. Trial variation of the molecular vibrations models showed that the simplified sets of frequencies are a good representation of the actual molecule.

Before discussing specific applications of the foregoing procedure to Eq. (1), some details and results of the model I of RD will be recalled: All vibrations for both *association* and *decomposition* were taken as active; r^+, $r^{+\prime}$ and r^* were all set equal to 2 and the internal rotations were taken as active; $E_{CH_3}=10$ kcal/mole was used; a semirigid complex was taken for the *association* complex, and a rigid model for the *decomposition* complex. Actually, RD found the computed values quite insensitive to the specification of the *association* model (this thereby introduces another adjustable parameter, namely E_D-E_H) and in the present paper no further variation of the model given in Appendix I need be considered. The earlier calculations of temperature and pressure ratios for k_a were also somewhat insensitive to the details of the *decomposition* complex although absolute values of k_a were more drastically affected.

In Table I, the calculational results for model I are compared with the same model (aside from grouping of frequencies, as in Appendix I) employing the direct count evaluation (model I′). The two sets of values are seen to have the same qualitative significance although the detailed quantitative differences in the ratios, etc. are somewhat larger than were previously found semiclassically by RD for more drastic changes in the assumptions about molecular vibrations models. In order to test this further for the quantum count procedure, the various k_a quantities were also evaluated for other assumptions. Two illustrations are given. Model I″: As in I′ but with E_{CH_3} set at the new value of 8 kcal/mole. Model II: A semirigid decomposition complex in which the four vibrations lost on rupture (CH_3 rock (2), CH_2 bend and skeletal bend, apart from a C—C stretching mode and the internal rotation of CH_3) were arbitrarily reduced to almost half their normal values. The quantities are shown in Table I. The k_a ratios are still not very sensitive qualitatively to the assumptions, although the absolute values of k_a are more affected. This is for the reason, given previously, that $E_{min}{}^+ \gg RT$. In the decomposition of ethyl-d_2 radicals, where $E_{min}{}^+=0$, a larger effect is noted.[7]

[7] B. S. Rabinovitch, D. H. Dills, W. H. McLain, and J. H. Current, J. Chem. Phys. **32**, 493 (1960).

Model II is considered here as showing the best concordance with experiment. Exact fit is not sought, since the variability of the experimental data and subjectivity of the extrapolations, as well as flexibility in the choice of models and parameters such as E_{CH_3}, E_H, etc., make such an endeavor fruitless. Substantial concordance of experiment and theory is all that is meaningful at present.

Model II has been applied to the results for *sec*-deuterobutyl and to the calculation of the isotopic energy effect (Table II). The agreement is satisfactory and could be improved at will. In comparing the expected behavior of deuterobutyl with butyl, two counteracting factors enter. First, for the deuteroradical the energy of the formation process is increased; the increased value of $E_{min}{}^+$ causes these radicals to appear relatively more monoenergetic. Second, the reduction of the deuterium frequencies (consequent on the changed chemical identity of the radical) and of vibrational quantum restrictions, tends to cause an increased effective thermal energy spread. At these temperatures, the first effect predominates and the deuterobutyl radicals appear slightly more monoenergetic than the light radicals, from a comparison of $k_{a_{CO}}/k_{a_0}$ values. A less complicated demonstration of the energy factor alone could be obtained by use of H plus *trans*-butene-2 or butene-1.

ACKNOWLEDGMENT

We thank the Office of Naval Research for their support of this work.

APPENDIX I

Molecular Vibration Models (cm^{-1})

A. H+*cis*-Butene-2.

Association activated complex. Models I′, I″, and II are the same as model I[1] with frequencies rounded and grouped: 3000 (8), 1400 (9), 1000 (7), 650 (4), 300 (2).

Butyl radical. Models I′, I″, II are the same as model I with frequencies rounded and grouped: 3000 (9), 1400 (9), 1000 (9), 750 (1), 300 (3).

Decomposition activated complex. Models I′ and I″: As for butyl radical, with one 1000 mode eliminated. Model II: 3000 (9), 1400 (9), 1000 (5), 600 (4), 300 (2), 150.

B. D+*cis*-Butene-2. Model II.

Association activated complex. As in A, with 650 (2) replaced by 450 (2); the insensitivity of the results to details of the model makes (E_H-E_D), and thus $E_{min}{}^+$, an additional adjustable parameter in effect within limits.

Deuterobutyl radical. 3000 (8), 2250, 1400 (8), 1000 (9), 750 (2), 300 (3).

Decomposition activated complex. 3000 (8), 2250, 1400 (8), 1000 (5) 600 (5), 300 (2), 150.

The lowering of these rounded, grouped frequencies for the deuterated species gives adequate conformity with the product rule.

Observations of the Thermal Behavior of Radicals in Gamma-Irradiated Ice*

SEYMOUR SIEGEL, LILLIAN H. BAUM, SOL SKOLNIK, AND JOHN M. FLOURNOY

Chemical Division, Aerojet-General Corporation, Azusa, California

(Received November 2, 1959)

Ice was subjected to γ radiation at 77°K and the EPR spectra of the radicals produced were examined as a function of temperature. The spectrum consisted essentially of a doublet centered at $g=2.008\pm0.002$ and split by 40 gauss; the corresponding spectrum of irradiated D_2O consisted of a triplet with approximately 6 gauss between adjacent lines. The doublet decayed rapidly above 100°K leaving a residual broad line which was thermally stable until approximately 145°K. The main spectrum has been attributed to the OH radical and the residual line assigned to the HO_2 radical. The decay process of the OH radicals was shown to follow the rate law $d(OH)/dt=-k(OH)^{\frac{1}{2}}$ where $k=8.5\times10^{12}\exp-6000/RT$ (liter/mole)$^{\frac{1}{2}}$ sec^{-1}. The magnitude of the rate constant was shown to be a function of the total irradiation damage experienced by the ice sample.

Stabilization of OH radicals at 77°K was studied as a function of total irradiation dosage; saturation is reached at an OH concentration of $1.8\times10^{-3}M$ or 0.003 mole %. The EPR spectrum of a frozen aqueous NO solution was also observed; it consisted of a broad line centered at approximately $g=2.08$.

I. INTRODUCTION

IN the last few years a great amount of effort has been expended in research on the stabilization of free radicals at low temperatures. However, little is known of the mechanism of the stabilization processes or of the forces which the radicals experience in the trapping matrix. It was thought at this laboratory that an important contribution to the understanding of the nature of the stabilizing forces might be obtained from isothermal kinetic studies on the stabilization and recombination of radicals trapped at low temperatures. Also, these experiments could shed light upon the nature and energetics of the diffusion process.

The kinetics was studied by following the growth and decay of the EPR spectrum of radicals produced by the γ irradiation of ice at 77°K. The use of EPR techniques was considered the most desirable method with which to obtain accurate data since the radicals can be observed continuously and the method of detection perturbs the observed systems only to a negligible extent. Also, observations of the line shape and width as a function of concentration and temperature yield information on the magnitude and nature of the matrix perturbations.

Irradiated ice was chosen as the first system to study because of the considerable amount of work done on the radiation chemistry of water at room temperature. It was hoped that the behavior of the radicals formed at low temperatures might be correlated with postulated mechanisms at room temperature. There is some controversy in the literature over the shape and interpretation of the spectrum of irradiated ice[1,2]; it was hoped that this study would help settle this question.

II. EXPERIMENTAL

Sample Preparation

Samples of distilled water weighing 0.4–0.6 g were degassed under high vacuum, frozen in cylindrical Pyrex molds, and transferred from the molds to the precooled microwave cavity with only slight melting on the surface. The samples were irradiated in the cavity at 77°K by means of an 800-curie cobalt-60 source at a dose rate of approximately 1.0×10^5 rep/hr. Most of the data were obtained from samples irradiated to a total dosage of approximately 1.6×10^6 rep (about 0.9×10^{20} ev/g).

Paramagnetic Resonance Equipment

Spectra were obtained with a Varian Associates V-4500 EPR Spectrometer equipped with a 12-in. magnet system and low temperature accessories. The output from the crystal detector is an ac signal (400 cps) which, after ac amplification, is passed through a phase detector to a graphic recorder; the recorder presentation is approximately the derivative of the resonance line. Most of the quantitative work was done at power levels which were shown by experiment to be low enough to avoid power saturation effects on the OH spectrum. The microwave frequency was near 9.4 kMc and was measured with a calibrated tunable cavity. The magnetic field was calibrated with respect to the six absorption lines of Mn^{++} in zinc-blende[3] and the resonance line of solid DPPH.[4]

Concentration Determinations

The concentrations of OH were estimated by a comparison between the values of (height×width^2) for the absorption derivative curves for OH and for a known

* This research is being supported by a contract with the Air Force Office of Scientific Research.

[1] M. S. Matheson and B. Smaller, J. Chem. Phys. **23**, 521 (1955).

[2] R. Livingston, H. Zeldes, and E. H. Taylor, Discussions Faraday Soc. **19**, 166 (1955).

[3] J. S. Van Wieringen, Discussions Faraday Soc. **19**, 118 (1955).

[4] A. N. Holden, W. A. Yager, and F. R. Merritt, J. Chem. Phys. **19**, 1319 (1951).

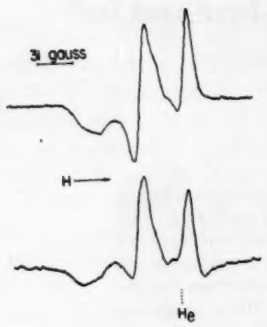

FIG. 1. Paramagnetic resonance spectrum of γ-irradiated H_2O at 77°K. The upper and lower spectra are the absorption and dispersion signals, respectively. In this and the following figures H_e represents the free electron resonance as given by the equation $h\nu = g_e\mu_0 H_e$ where $g_e = 2.0023$.

quantity of Wurster's blue perchlorate (WBP) dispersed in an ice sample of identical size and geometry at 77°K. The product of the height of an absorption derivative curve and the square of the width at maximum height is directly proportional to the area under the absorption curve, and the proportionality constant is a function of line shape only. Inspection of the shapes of the dispersion derivative curves for OH and WBP showed that the OH curve was very nearly Gaussian while the WBP line was very nearly Lorentzian. It can be shown that for two absorption derivative lines of identical area, one Lorentzian (L) and the other Gaussian (G), that $(hw^2)_G/(hw^2)_L = 3.49$. Using this correction factor, and allowing for both lines of the OH doublet, a comparison of (hw^2) for the two systems yielded a value of 8×10^{-4} moles/liter for the OH concentration after 16.5 hr of irradiation (1.6×10^6 rep). The absolute values of the concentrations are estimated to be good to within a factor of two.

They are in excellent agreement with values which we obtained in calorimetric studies of irradiated ice (to be published), based on the assumption that OH recombination ($\Delta H \cong -26$ kcal/mole OH) was[5] responsible for an exotherm observed on warming irradiated ice to 100°K.

Temperature Control

The EPR cavity was mounted in a double Dewar system designed for liquid helium. For temperatures above 77°K, the inner Dewar and its vacuum jacket were filled with nitrogen gas and the outer Dewar with liquid nitrogen. Warming of the cavity was accomplished by blowing a stream of dried nitrogen at room temperature into the volume surrounding the cavity but not impinging directly on the cavity. A calibrated copper-constantan thermocouple was in intimate contact with the lower part of the sample cavity and was insulated from the immediate surroundings by $\frac{1}{4}$-in. styrofoam. The thermocouple output was recorded continuously by a recording potentiometer. The potentiometer was fitted with electrical contacts which, though an electronic relay, caused a solenoid valve to open and close, controlling the warm nitrogen flow around the cavity. This control system was sensitive to about ±0.05°K (1μv) and maintained the sample temperature continuously to within ±0.2°K maximum variation at temperatures from 85° to 150°K. In one experiment, a second thermocouple was frozen directly into a sample inside the cavity; the temperature of the inner thermocouple was within 0.5°K of that of the outer control thermocouple.

Rate Measurements

After irradiation of a sample the concentration of stabilized OH was determined at 77°K for use as an initial value in the kinetic calculations. The sample was then warmed rapidly (about 10°/min) to the reaction temperature, and rate measurements were begun within about three minutes, the time required to retune the apparatus at the higher temperature. A reference portion of the absorption derivative spectrum was scanned repeatedly at 30–60 second intervals during decay at constant temperature. Occasional scans of the entire spectrum showed that no noticeable changes in line shape occurred before about 90% decomposition, after which perturbations from the overlapping spectra of other trace radicals became appreciable. Within the region of constant line width, relative OH concentrations were taken to be proportional to the height of the low-field component of the doublet.

III. RESULTS AND DISCUSSION

Description of the Observed Spectra in Irradiated Ice

A. H_2O

The EPR spectrum of degassed ice irradiated and observed at 77°K consists essentially of a partially resolved doublet and a broad hump at the low field end of the spectrum (Fig. 1). The doublet has a hyperfine splitting constant of 110±5Mc/sec and a g value of 2.008±0.002. The members of the doublet have a line width at half height of approximately 17 gauss. The line widths of the doublet components do not vary measurably with changes in the concentration of radicals present, which indicates that the line width is due to spin-matrix interactions rather than electronic spin-spin interactions. The doublet begins to disappear slowly at 90°K, and at 110°K the spectrum decays very rapidly. The broad side band has essentially the same temperature dependence as the doublet.

After the spectrum described above has disappeared, a weak, broad, unresolved line remains (Fig. 2) until the temperature reaches about 145°K, at which point the line begins to lose intensity measurably with time.

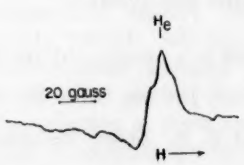

FIG. 2. Absorption spectrum of γ-irradiated H_2O at 77°K after annealing at 110°K.

[5] P. A. Giguère, J. Chem. Phys. **30**, 322 (L) (1959).

This line has a width of approximately 20 gauss. The height of the line relative to one of the peaks of the doublet depends upon the total irradiation dosage; the larger the dosage the greater the relative height. After a dosage of 0.9×10^{20} ev/g the relative height was ~4%, while after 2.7×10^{20} ev/g the relative height was ~8%.

B. D_2O

The EPR spectrum of a D_2O sample irradiated and observed at 77°K consists of a poorly resolved triplet and a broad band on the low field side of the spectrum (Fig. 3). The triplet has approximately the same g value as the doublet observed in the H_2O system and has a hyperfine splitting constant of 17 Mc/sec. The ratio of the observed splittings of the doublet and triplet is in excellent agreement, within experimental error, with the reported[6] free atom ratio of $H/D=6.5$.

The line widths of the triplet components are about 5 gauss. The ratio of the line widths in the spectra of irradiated H_2O and D_2O is in good agreement with the ratio of the magnetic moments of the proton and deuteron. This good agreement, together with the observations that the line width did not appreciably change with spin concentration or with temperature from 77° to 107°K, indicates that the main cause of line width is the magnetic interactions of the free electron and the nuclei of the matrix.

The field position of the broad band on the low field side of the spectrum is essentially the same as that of the broad band in the irradiated H_2O spectrum.

Interpretation and Assignment of Spectra

The transformation of the observed doublet in the spectrum of irradiated H_2O into a triplet in the spectrum of irradiated D_2O strongly indicates that the responsible paramagnetic species contains only one interacting hydrogen atom. The radicals containing one hydrogen atom that are most likely to be formed during the irradiation process are H, OH, and HO_2.

Matheson and Smaller,[1] using a 350 Mc/sec quarter-wave coaxial line oscillator detector, observed a doublet at $g=2.0$ in the spectrum of γ-irradiated ice which they attribute to strongly perturbed H atoms; this doublet is probably the same as the one reported here.[7] However, recently the spectra of ice, irradiated at 4°K with high voltage electrons and with γ rays, were observed at the Varian Associates Laboratory[8] and at this laboratory, respectively. The 4°K spectrum contains the doublet described above (split by 40 gauss) superimposed on a broad background; it also contains a doublet centered about $g=2.0$ and split by approximately 500 gauss. It seems very probable that the latter doublet, which has a hyperfine splitting constant very close to that of a free H atom, is due to trapped H atoms. Also, H atoms have been trapped in a variety of other matrices, at this laboratory and elsewhere, including acidified ice,[2,9] wet glass surfaces,[2] solid hydrogen,[8,10] and sodium *meta*-silicate. The EPR spectra of all these systems contained a doublet which was split within 20 Mc of the free hydrogen atom value. The maximum temperature at which the hydrogen atoms were stable in the various matrices varied from 40° to above 100°K; microwave power saturation studies indicated that the relaxation times for the trapped hydrogen atoms also varied appreciably. In view of the constancy of the splittings found for H atoms perturbed by their environment to considerably different extents, it seems very unlikely that the 40-gauss doublet is due to trapped hydrogen atoms.

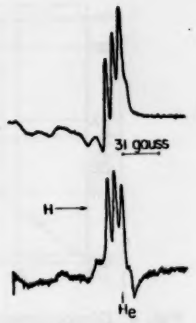

FIG. 3. Paramagnetic resonance spectrum of γ-irradiated D_2O at 77°K. The upper and lower spectra are the absorption and dispersion signals, respectively.

Several other investigators have reported spectra similar to the residual broad line left after the disappearance of the doublet[10,11]; they have, on various reasonable arguments, tentatively attributed this line to the HO_2 radical. The line shape is similar to that found for the corresponding salt NaO_2.[12] Examination of the EPR spectrum of a 0.01 M aqueous H_2O_2 solution irradiated at 77°K in our laboratory showed that the height of the broad line relative to that of the doublet was considerably greater (~30%) than in plain H_2O (~4%). Experiments performed here on frozen aqueous solutions have shown that considerable energy is released upon irradiation and that chemical reactions readily take place during irradiation even at 77°K.[13]

[6] J. E. Nafe and E. B. Nelson, Phys. Rev. **73**, 718 (1948).

[7] However, Matheson and Smaller report a splitting constant of 85.5 Mc/sec while the value reported here is 110±10 Mc/sec. The difference in the two values is larger than experimental error; the reason for the difference is not immediately obvious.

[8] L. H. Piette, R. C. Rempel, H. E. Weaver, and J. M. Flournoy, J. Chem. Phys. **30**, 1623 (1959).

[9] R. Livingston, H. Zeldes, and E. H. Taylor, Phys. Rev. **94**, 725 (1954).

[10] C. K. Jen, S. N. Foner, E. L. Cochran, and V. A. Bowers, Phys. Rev. **112**, 1169 (1958).

[11] R. Livingston, J. Ghormley, and H. Zeldes, J. Chem. Phys. **24**, 483 (L) (1956).

[12] J. E. Bennett, D. J. E. Ingram, M. C. R. Symonds, P. George, and J. S. Griffith, Phil. Mag. **46**, 443 (1956).

[13] Two degassed aqueous solutions, one 0.01 M in acrylamide and the other 0.01 M in $FeSO_4$, were irradiated at 77°K. Examination of their EPR spectra showed a marked decrease in the intensity of the observed doublet, as well as modifications in the shape of the spectra, compared to the spectrum observed from irradiated pure ice.

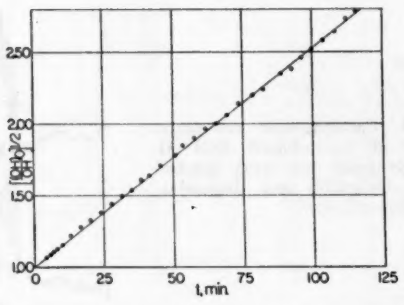

FIG. 4. Disappearance of OH radicals in ice at 100°K; OH_0= initial OH concentration.

Also, Foner and Hudson[14] have shown that the reaction $H_2O_2+OH \rightarrow H_2O+HO_2$ occurs readily in the gas phase. Thus it seems quite probable that the broad line is due to HO_2 and that the reaction stated above does take place during irradiation of the H_2O_2 solution. On this basis the doublet spectrum in irradiated ice and the triplet spectrum in irradiated D_2O can be readily attributed to the OH and OD radicals, respectively.

An important objection which might be raised to the above identification is that the ground electronic state of the OH radical in the gas phase is $^2\Pi$. Molecules in the $^2\Pi_{\frac{1}{2}}$ state should be essentially nonparamagnetic and those in the $^2\Pi_{\frac{3}{2}}$ state should have a g value appreciably different from $g=2.0$. However, an OH radical trapped in an H_2O lattice will experience quite intense crystalline fields. It would not be improbable for the crystalline field interactions to uncouple the spin and orbital angular momenta, yielding a spectrum centered about $g=2.0$ due to the residual Kramers' doublet. We have, in fact, observed a spectrum centered about $g=2.0$ for a frozen aqueous solution of NO ($^2\Pi$ electronic state) which tends to confirm that quenching of the orbital momentum can take place in an ice matrix. (The NO observations are discussed below.) For the remainder of the paper the identification of the doublet as the OH radical will be considered correct.

Kinetics

The rate law $d(OH)/dt=-k'(OH)^{\frac{3}{2}}$ was found to describe accurately the decrease of OH concentration with time in ice at temperatures from 92–107°K. The validity of the $\frac{3}{2}$ order law was confirmed in separate experiments in which the initial concentrations differed by a factor of 5.5. Figure 4 gives a plot of $(OH_0/OH)^{\frac{1}{2}}$ vs time obtained in one of the runs at 100°K.

The magnitude of the rate constant k' was found to depend upon the history of the sample. In order to assure a constant sample weight and geometry in the microwave cavity, some samples were used for several kinetic runs by warming the cavity (without melting the sample) to destroy the residual radicals, and then reirradiating at 77°K. It was found that the magnitude of the rate constant was a function of the cumulative dosage even at the same initial OH concentrations; an increase in cumulative dosage by a factor of more than 20, from 0.9×10^{20} to 20×10^{20} ev/g, resulted in an increase in the observed rate constant by a factor of 3.5. Corrections were therefore necessary in comparisons between rate constants for new and reirradiated samples. The uncertainty in the activation energy due to the incorporation of these corrections is only about 0.3 kcal/mole.

The uncorrected molar reaction rate constants (k') are tabulated in Table I, along with the constants (k) which are corrected for cumulative irradiation effects. The uncertainty in the 77°K rate constant is due to the possibility that the very slow decrease in spectral intensity (*ca.* 2%/day) may have been due in part to drift in the sensitivity of the EPR spectrometer. The uncertainty in the rate constants due to graphing errors is estimated at ±10%. An Arrhenius plot, illustrating the temperature dependence of the rate constant k, is given in Fig. 5. The corrected rate constant can be expressed by the following Arrhenius expression

$$k=8.5\times10^{12}\exp-6000/RT \text{ (liters/mole)}^{\frac{1}{2}}\text{ sec}^{-1}$$

over the entire temperature range studied, representing a maximum change in rate constant of a factor of 10^4. The uncertainty in the activation energy is estimated to be less than ±0.5 kcal.

Experiments involving OD in D_2O indicate that the activation energy for the deuterated system is, within experimental error, the same as that for OH in H_2O.

The most likely uncharged products formed during the irradiation of ice at 77°K are OH, HO_2, H_2O_2, and H_2; there may also be very small amounts of H atoms present ($<10^{12}$ spins/cc). An attempt to derive a $\frac{3}{2}$ order rate law for the disappearance of OH in terms of various reaction mechanisms using the above species was unsuccessful. One problem is that there is considerable doubt about the identities of the primary products from the OH decay. The concentration of H_2O_2 after melting the samples was found, using approximate colorimetric methods, to be considerably less than that predicted on the basis of the reaction $2OH \rightarrow H_2O_2$

TABLE I. Molar rate constants.

k', (liter/mole)$^{\frac{1}{2}}$ sec^{-1}	k,[a] (liter/mole)$^{\frac{1}{2}}$ sec^{-1}	T, °K	Total dosage,[b] ev/g$\times10^{-20}$
5×10^{-4}	2×10^{-4}	77	8.5
0.12	0.085	92.0	4.2
0.12	0.12	94.8	0.9
0.79	0.79	100.1	0.9
1.06	0.79	100.1	3.5
3.33	2.72	103.9	2.6
6.32	5.67	106.7	1.7

[a] These constants are corrected for cumulative irradiation damage; all values are normalized to a total dosage of 0.9×10^{20} ev/g.
[b] This quantity is the total irradiation dosage received by the sample.

[14] S. N. Foner and R. L. Hudson, J. Chem. Phys. **23**, 1364 (L) (1955).

alone. Ghormley and Stewart,[15] using more exact analytical methods, after melting the irradiated samples determined the concentration of H_2O_2 produced with irradiation dose rates of 3.0×10^{18} ev/g hr and 4.2×10^{19} ev/g hr (5.3×10^{18} ev/g hr was the dose rate in the experiments described in this paper). Their results indicated H_2O_2 concentrations which were a factor of 4 to 5 smaller than those predicted on the basis of the stabilized OH concentrations determined by the present authors for the same dosage. The yields of hydrogen and oxygen were found in our experiments to be somewhat smaller than the yields of stabilized hydroxyl radicals; however, the experimental conditions were such that the differences are not too significant. The significant fact is that the above products are not present in large excess of the stabilized OH radicals (see next section). The problem is further complicated by the fact that the analysis of products is made after melting the sample; thus effects due to reactions occurring during the melting process must also be considered.

An important and complicating feature of the system under consideration is that the reaction is taking place at low temperatures between species embedded in a solid matrix. The problem of encounter rates is much more difficult in the solid phase than in the liquid or gaseous phases. In the solid state there is no translational motion in the ordinary sense and mass transfer is accomplished by a limited degree of diffusion which probably depends upon complex mechanisms. Also, in a polycrystalline sample there is a considerable amount of internal surface area, as well as a large number of grain boundaries, which would be important in the diffusion process. The fractional order of the observed rate law could be due to the mechanism of mass transfer.[16] The observed increase in the rate constant with increased irradiation damage certainly suggests that the diffusional process is very important. An activation energy of 6 kcal/mole is consistent with the idea that the rate-controlling step is the diffusional process since hydroxyl radicals are probably involved in the elaborate hydrogen bond network in ice. The energy of a normal hydrogen bond in ice is approximately 5 kcal/mole.[17]

A kinetic run at 100°K was made on a sample of ice which was prepared from 0.01 M aqueous H_2O_2 and was irradiated to produce an OH concentration of 4×10^{-4} M. The peroxide concentration in this experiment

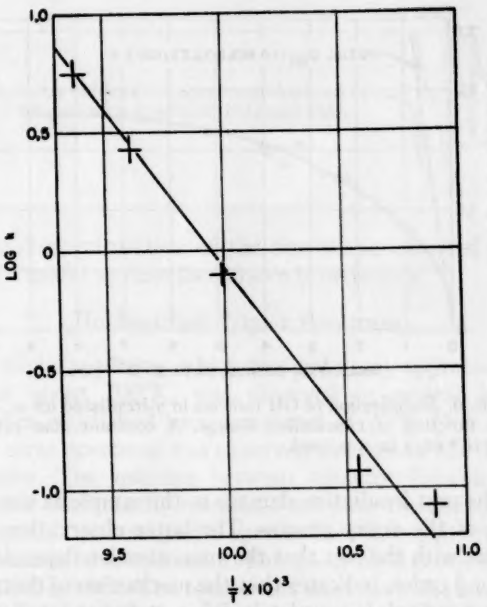

FIG. 5. Temperature dependence of rate of disappearance of OH in irradiated ice.

was nearly two orders of magnitude greater than the amount normally found after irradiation of pure ice, but the rate of disappearance of OH was only about twice the normal rate, initially, and approached the normal rate as the reaction proceeded. The relatively slight effect of the peroxide on the rate indicates that H_2O_2 is not a principal reactant in the rate determining step. However, the kinetics were somewhat perturbed, in that the peroxide run followed closely a second order rate law in OH, instead of the normal $\frac{3}{2}$ order law, during the two half-lives for which data were obtained. The effects of the peroxide are not well understood, but may be due to perturbation of the crystal lattice of the ice matrix which might affect the diffusion mechanism of OH.

Production of Stabilized Radicals

Stabilization of OH radicals at 77°K was studied as a function of total irradiation dosage. The irradiation was stopped at intervals and the EPR spectrum examined. The effect of stopping the irradiation at intervals was shown in separate experiments to be negligible. Since the line width did not change with concentration the peak height was taken to be proportional to concentration, and the absolute concentration was determined at only one point. The concentration of stabilized OH radicals is shown as a function of cumulative dosage in Fig. 6. "Saturation" is reached at an OH concentration of $1.8\times10^{-3}M$ or 0.003 mole %.

An attempt to fit the experimental curve to a rate law of the form $d(\mathrm{OH})/dt=a-k(\mathrm{OH})^n$, where a and n are empirical constants, showed that the best fit is obtained when $n=\frac{1}{4}$. The rate of stabilization was not sensitive

[15] J. A. Ghormley and A. C. Stewart, J. Am. Chem. Soc. 78, 2934 (1956).

[16] *Note added in illustration*: In the case of certain catalyzed, heterogeneous, diffusion-controlled, bimolecular reactions the apparent concentration dependence is $\frac{3}{2}$ order [P. H. Emmett, *Catalysis* (Reinhold Publishing Corporation, New York, 1955), Vol. II, p. 131]. It is not suggested that exactly the same conditions exist in the case under discussion; rather, the example is given only to illustrate the effect that the physical mass transfer process can have on the apparent concentration dependence of a chemical reaction.

[17] L. Pauling, *The Nature of the Chemical Bond* (Cornell University Press, Ithaca, New York, 1948), p. 301.

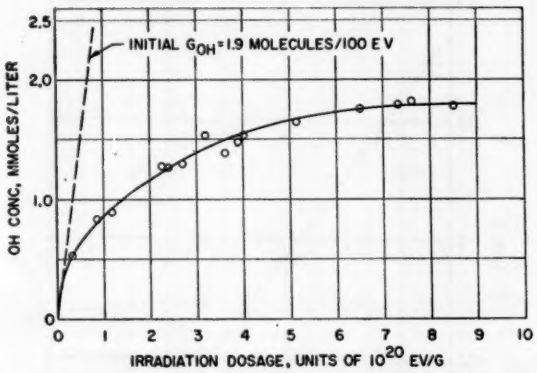

FIG. 6. Stabilization of OH radicals in γ-irradiated ice at 77°K as a function of cumulative dosage. A constant dose rate of 5.3×10^{18} ev/g hr was used.

to the past irradiation damage to the sample as was the case of the decay process. The latter observation, together with the fact that the concentration dependence is not $\frac{3}{2}$ order, indicates that the mechanism of destruction of radicals is completely different during irradiation from the mechanism during the decay process. Work is in progress on the effect of different irradiation levels and sample geometry; any further speculation on the mechanism of stabilization and the theoretical significance of the empirical rate law will be deferred until this work is completed.

An interesting feature of the stabilization curve is that the initial slope corresponds to an irradiation yield $G_{OH}=1.9$ radicals/100 ev; the corresponding value[18] for pure H_2O at 300°K is $G_{OH}=2.05$. This close agreement (even taking into account the uncertainty of the concentration determination) suggests that the mechanism of radical formation by ionizing radiation is essentially the same at 300° and 77°K. In water at 300°K molecular hydrogen and hydrogen peroxide are thought to form in regions of dense energy release, i.e., at the ends of the tracks of slow secondary electrons. The radicals H and OH diffuse out of the tracks from regions of less dense energy release; the radiation yield measures the number of radicals which do not recombine immediately.[19] Stabilization of essentially the same number of OH radicals at 77°K as survive to diffuse out of the "spurs" at room temperature illustrates the effectiveness of the ice matrix as a radical trap at low concentrations.

The initial slope of the OH stabilization curve (Fig. 6) represents a minimum value for the rate of formation OH (and H) during irradiation; it is of interest to consider the destruction reactions which are responsible for the decrease in yield of stable OH with prolonged irradiation. Toward this end, the final yields of the molecular products H_2 and H_2O_2 were determined, after melting, for a sample which had been irradiated to saturation with respect to OH ($1.8\times10^{-3}M$ after a dosage of 2×10^{21} ev/g). Extrapolation of the initial slope of Fig. 6 to this dosage indicated that at least 6×10^{-2} moles/liter of H and OH should have been formed during the irradiation. However, on the basis of the observed EPR spectra, 97% of the OH and 100% of the H had disappeared, presumably through the reactions:

$$2OH\rightarrow H_2O_2 \quad (1)$$

$$H+OH\rightarrow H_2O \quad (2)$$

$$2H\rightarrow H_2. \quad (3)$$

Analysis of the sample after melting showed that the final H_2O_2 and H_2 concentrations were both somewhat less than 10^{-3} M, i.e., of the order of 1% of the values which would have been expected if reactions (1) and (3) were predominant during irradiation. Thus, the destruction of OH apparently occurs principally through recombination with H. This conclusion is a reasonable one in view of the wide difference in stability between H and OH. The absence of stable H at 77°K indicates that H is more mobile than OH, the latter probably being strongly hydrogen-bonded in the ice matrix. Therefore reaction (1) is quite unfavorable with respect to (2) and (3). The relative importance of (2) and (3) depends on the concentration ratio (OH)/(H), which rapidly becomes quite large as OH accumulates, causing (2) to predominate after a short time. In evaluating these conclusions, it must be remembered that the product analysis was made after the sample melted. The desirability of product analysis at low temperatures is obvious; low temperature infrared techniques would be useful in this regard.

NO in Ice

It was thought that since NO has a similar ground electronic state to OH in the gas phase, the electron paramagnetic resonance spectrum of NO in a crystal matrix would be of great interest. Jen *et al.*[10] failed to observe a spectrum for NO either in an argon matrix at 4°K or in a CO_2 matrix at 77°K. The absence of a spectrum was attributed to crystal anisotropy coupled with the $^2\Pi$ state of NO. However, since the H_2O matrix would provide stronger electric fields than argon or CO_2 it seemed desirable to attempt to observe NO in an ice matrix.

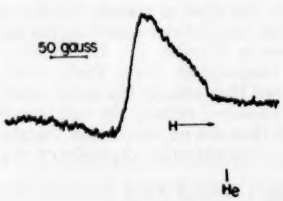

FIG. 7. Absorption spectrum of an aqueous NO solution at 77°K.

[18] C. J. Hochanadel and S. C. Lind, Ann. Rev. Phys. Chem. **7**, 83 (1956).
[19] J. L. Magee, J. Am. Chem. Soc. **73**, 3270 (1951).

Gaseous NO (fractionally distilled to remove most of the NO_2) was dissolved in previously degassed H_2O at room temperature. The resulting solution was quickly frozen under a partial pressure of NO of about 60 cm Hg, and the EPR spectrum was taken at 77°K (no irradiation). The observed spectrum is shown in Fig. 7.

The presence of a broad spectrum at $g=2.08\pm0.02$ indicates that the orbital angular momentum is largely uncoupled from the spin momentum since molecules in the $^2\Pi_{\frac{1}{2}}$ state would be nonparamagnetic and those in the $^2\Pi_{\frac{3}{2}}$ state would have a g value near $\frac{4}{3}$. However, the broad unresolved physiognomy of the spectrum and the deviation of g from 2.002 suggests that the quenching of the angular momentum is not complete. The fact that the line was not appreciably power saturated at the highest klystron power output available to us, more than 230 mw, confirms that the relaxation time is quite short, as would be expected for such a system. The line shape remained approximately constant from 77° to 180°K; it could not be ascertained accurately, because of tuning problems, whether or not the line was appreciably broadened at the higher temperatures.

The observation that the angular momentum of NO is only partly quenched in ice ($g=2.08$) while the angular momentum of OH is rather completely quenched ($g=2.008$) is at first somewhat surprising, since the two radicals are quite similar electronically in the gas phase. However, it must be remembered that the radicals are imbedded in an ice matrix and that the OH radical would be much more intimately involved in the hydrogen-bonded network than would NO. In fact, the structural description of the OH radical in ice is probably incomplete without inclusion of the hydrogen-bonding interactions between the hydroxyl oxygen atom and the H atoms belonging to the neighboring water molecules. The line width in the case of the OH radical was shown above to be largely determined by the magnetic perturbation produced by the magnetic moments of the matrix nuclei. Also, the magnitude of the line width did not appreciably change over the temperature range studied. The last observation strongly indicates that the OH radical is held tightly in the hydrogen bonded cage, since any appreciable motion of the radical would result in line narrowing as the temperature increased. If the line broadening is due primarily to spin-spin dipolar interactions between the free electron and two equivalent hydrogen-bonded hydrogen nuclei, then a line width of 17 gauss corresponds to an average distance of 1.1 A between the free electron and either of the interacting nuclei. This distance is noticeably shorter than Pauling's value of 1.7 A for the O···H separation in ice.[17] The hydrogen atom which is directly bonded to the oxygen atom on which the free electron is localized contributes a larger dipolar splitting, which together with the isotropic hyperfine splitting accounts for the observed splitting of 40 gauss.

FIG. 8. An unidentified spectrum observed in several samples of γ-irradiated H_2O and D_2O.

A detailed calculation of the line shape expected for such a model as described above is underway.

Unidentified Triplet Spectrum

A triplet spectrum, which does not decay appreciably below about 200°K, was observed in several H_2O samples which had been irradiated at 77°K (Fig. 8). The same spectrum was observed in some of the D_2O samples. The splitting between adjacent lines is 20 gauss in both the H_2O and D_2O samples; therefore, the responsible paramagnetic species does not contain an interacting hydrogen atom. The spectrum is centered at $g=2.002\pm0.001$. The component lines have line widths of approximately 3 gauss in both the H_2O and D_2O matrices; thus, the magnetic nuclei of the lattice are not interacting appreciably with the unpaired electron. Another interesting feature of the triplet spectrum is that the relative intensities of the lines change with temperature. At 77°K the relative intensities are 1:1.7:1.2, going from high to low field; as the temperature increases the relative intensities approach 1:2:1. Also, the absolute height of the lines increases with temperature while the line width does not decrease noticeably.

The conditions under which the triplet is formed upon irradiation are not well understood. In the degassed samples the triplet seldom occurred on short irradiations; when it did appear its intensity relative to the main spectrum (described above) was weak. Upon long irradiations the triplet increased in intensity. It was thought that the triplet might be due to residual gas left after imperfect degassing, although this seemed doubtful, or to O_2 formed during the irradiation process. However, H_2O samples which were frozen while saturated with air produced little or no triplet upon irradiation at 77°K. On the other hand, samples saturated with O_2, N_2, or Ar all produced a large amount of triplet after irradiation; in fact, with the O_2 saturated sample the normal spectrum was almost completely absent. This last series of experiments indicates that the species responsible for the triplet may be due to reactions involving the radicals responsible for the normal spectrum, i.e., OH radicals. The disappearance of the triplet upon warming above 200°K is an irreversible process since the spectrum fails to reappear on cooling again to 77°K. This confirms the fact that the spectrum is due to an unstable species formed during the irradiation.

IV. CONCLUSION

The growing importance of free radical research and low temperature reactions lends interest to the results described in this paper. The techniques described here can be used for investigating diffusion-controlled processes in a variety of systems. Correlation of line widths and thermal stability should give important information on the relaxation processes and on the binding forces present in the solid state. Further work is in progress at this laboratory along these lines.

THE JOURNAL OF CHEMICAL PHYSICS VOLUME 32, NUMBER 4 APRIL, 1960

Rate Constants at Low Concentrations. V. Mechanism of Reaction of Ozone with Photolyzing Nitrogen Dioxide in Presence of Excess Oxygen*

H. W. FORD,† G. J. DOYLE, AND N. ENDOW

Stanford Research Institute, Southern California Laboratories, South Pasadena, California

(Received October 16, 1959)

Trace concentrations of ozone and nitrogen dioxide in pure, dry air at atmospheric pressure were exposed to a known intensity of 3660 A radiation in a stirred flow reactor at 300°K. An increase of steady-state concentrations of ozone and nitrogen dioxide above their dark values was observed and measured. A value of $k_7K_{eq}=0.44$ sec^{-1} ($NO_3+NO\rightarrow 2NO_2$, k_7, $NO_2+NO_3\rightleftharpoons N_2O_5$, K_{eq}) was obtained from the data using a postulated mechanism. The good agreement between this value and the values of 1.0 sec^{-1} obtained by I. C. Hisatsune, B. Ogg, and R. A. Crawford [J. Am. Chem. Soc. **79**, 4648 (1957)] supports the validity of the proposed mechanism.

THE authors have reported the results of an investigation of the reaction of ozone with nitrogen dioxide[1] in which the following method was used. The reactants and pure, dry air were passed into a stirred flow reactor at measured flow rates. The steady-state effluent concentrations were measured both with the reactor dark and with irradiation. Checks were made on the equality of the influent and effluent concentrations of each of the reactants in the absence of the other.

Data obtained in those experiments with no irradiation allowed a calculation of the rate constant for reaction (4) in the following, previously reported.[1] However, the data obtained with these mixtures irradiated with a known light intensity at 3660 A have not been previously reported because the fate of atomic oxygen produced by photolysis of nitrogen dioxide was not sufficiently understood. Now that the reactions of atomic oxygen have been better established[2-4] we can propose a reaction mechanism and interpret the data with greater confidence.

The experimental results are shown in Table I. It is apparent that both reactants were consumed in the dark reaction, and this result can be accounted for by reactions previously discussed.[1] When the mixture was irradiated following attainment of dark steady state, both of the effluent reactant concentrations increased to irradiated steady-state values (see columns 3, 4, 6, and 7, Table I). Ozone effluent concentrations were higher than influent concentrations in two instances, whereas nitrogen dioxide did not attain its influent concentration. These small differences between influent and effluent dioxide concentrations can be used to estimate some of the reaction constants in the mechanism proposed below.

According to published rate constants,[2,4] atomic oxygen is important only in its reaction with molecular oxygen to form ozone when such a large excess of oxygen is present. The mechanism shown in Table II is proposed.

The steady-state stirred reactor equations were used to obtain a relationship between the reaction constants and the data. The residence time in the reactor was so long that the rate of removal by reactor flow of the species O, NO, and NO_3 was insignificant in comparison with their rate of reaction. By use of this assumption and after considerable algebraic manipulation, the expression

$$\frac{k_7k_6}{k_5}\left[\frac{Q/V}{k_6}+1\right]=\frac{\{2k_4(O_3)_{ss}(NO_2)_{ss}-[Q/V][(NO_2)_0-(NO_2)_{ss}]\}\{k_3(O_3)_{ss}(NO_2)_{ss}\}}{\{KI\phi(NO_2)_{ss}+[Q/V][(O_3)_0-(O_3)_{ss}]-k_4(O_3)_{ss}(NO_2)_{ss}\}\{(NO_2)_0-(NO_2)_{ss}\}}$$

* This work was supported by the American Petroleum Institute. Dr. P. A. Leighton of Stanford University, Dr. F. E. Blacet of the University of California at Los Angeles, Dr. J. N. Pitts of the University of California at Riverside, and Dr. L. M. Richards of Richfield Oil Company were consultants on the project.

† Present address: Jet Propulsion Laboratories, California Institute of Technology, Pasadena, California.

[1] H. W. Ford, G. J. Doyle, and N. Endow, J. Chem. Phys. **26**, 1336 (1957).
[2] S. W. Benson and A. E. Axworthy, Jr., J. Chem. Phys. **26**, 1718 (1957).
[3] H. W. Ford and N. Endow, J. Chem. Phys. **27**, 1156 (1957).
[4] H. W. Ford and N. Endow, J. Chem. Phys. **27**, 1277 (1957).

TABLE I. Results of the 3660 A photolysis of nitrogen dioxide-ozone mixtures.[a]

Run No.	Q/V[b]	$(NO_2)_0$[b]	$(NO_2)_s$[b]	$(NO_2)_{si}$	$(O_3)_0$[b]	$(O_3)_s$[b]	$(O_3)_{si}$
	$(sec^{-1})\times10^4$			$(moles\ liter^{-1})\times10^9$			
1	8.7	9.0	5.7	7.8	21.2	21.2	22.4
2	8.8	39.6	20.0	27.0	24.5	20.4	22.0
3	8.8	38.8	20.0	27.0	24.5	15.9	20.0
4	14.5	18.0	14.3	16.4	14.7	13.1	16.3
5	8.7	27.4	14.7	20.8	32.7	20.4	27.3
6	8.8	21.6	18.0	20.8	10.6	6.5	9.0

[a] Q is the flow rate through the reactor (1 sec^{-1} and V is the reactor volume (52 liters). A light intensity of 1.0×10^{16} quanta cm^{-2} sec^{-1} at 3660 was used. The subscript 0 refers to the influent concentrations, the subscript s to the steady-state concentrations in the dark, and the subscript si to the steady-state concentrations under irradiation conditions.
[b] From previously published data, reference 1.

TABLE II.

Reaction No.	Reaction	Rate constant at 300°K	Reference
(1)	$h\nu+NO_2\rightarrow NO+O$	$5.8\times10^{-3}sec^{-1}=KI\phi$[a]	4
(2)	$O+O_2+M\rightarrow O_3+M$	$2.4\times10^4\ sec^{-1}=k_2\ (M)\ (O_2)$	2
(3)	$O_3+NO\rightarrow O_2+NO_2$	1.25×10^7 liters $mole^{-1}$ $sec^{-1}=k_3$ 2.8×10^7 liters $mole^{-1}$ $sec^{-1}=k_3$	b 1
(4)	$O_3+NO_2\rightarrow O_2+NO_3$	4.3×10^4 liters $mole^{-1}$ $sec^{-1}=k_4$ 2×10^4 liters $mole^{-1}$ $sec^{-1}=k_4$	c d
(5)	$NO_3+NO_2\rightarrow N_2O_5$	3.5×10^9 liters $mole^{-1}$ $sec^{-1}=k_5$ 1.65×10^{-10} mole $liters^{-1}=(k_6/k_5)=K_{eq}$	5 5
(6)	$N_2O_5\rightarrow NO_3+NO_2$	$4.6\times10^{-2}\ sec^{-1}=k_6$	5
(7)	$NO_3+NO\rightarrow 2NO_2$	6×10^9 liters $mole^{-1}$ $sec^{-1}=k_7$	5

[a] K=absorption cross section of NO_2 at 3600 A cm^2, I=intensity quantum cm^{-2} sec^{-1} at 3660 A, and ϕ=quantum yield for photolysis, here set equal to 1.00.
[b] H. S. Johnston and H. J. Crosby, J. Chem. Phys. **22**, 689 (1954).
[c] H. S. Johnston and D. M. Yost, J. Chem. Phys. **17**, 386 (1949).
[d] H. W. Ford, G. J. Doyle, and N. Endow, J. Chem. Phys. **26**, 1337 (1957).

is obtained. Table III shows the values of the right side of this expression computed for each of the experiments of Table I. Values of k_6, obtained from recent data[5] or as estimated by Johnston,[6] indicate that $(Q/V)/k_6$ on the left side of the equation can be neglected for the values of Q/V used in these experiments. The values reported in Table III are therefore values of k_7K_{eq}

TABLE III. Reaction constants in the photolysis of ozone-nitrogen dioxide mixtures.

Run No.	$[k_7k_4/k_5][Q/Vk_6+1]$,[a] sec^{-1}
1	0.76
2	0.22
3	0.22
4	0.42
5	0.52
6	0.51

[a] Each number is the average of the four values derived from the four possible combinations of Johnston's and the authors' values of k_3 and k_4.

[5] G. Schott and N. Davidson, J. Am. Chem. Soc. **80**, 1841 (1948).
[6] H. S. Johnston, J. Am. Chem. Soc. **73**, 4542 (1951).

obtained from our data plus the values of k_4, k_3, K, and determined by a number of different authors.

The good agreement between the average value of $k_7K_{eq}=0.44$ sec^{-1} obtained in these experiments and the value of 1.0 sec^{-1} obtained by Hisatsune, Ogg, and Crawford supports the proposed mechanism and demonstrates the self-consistency of the set of rate constants used in each case.

Taking $K_{eq}=1.65\times10^{-10}$ mole $liter^{-1}$,[5] we obtain $k_7=2.7\times10^9$ $liter/mole^{-1}$ sec^{-1}, as compared with Schott and Davidson's 6×10^9.[5]

Our lower value of k_7K_{eq} would tend to remove some of the discrepancy between the estimates for the rate of $NO_2+NO_2\rightarrow NO_3+NO$, $k_8=26$, and the ratio $k_7/k_9=250$, where $NO_3+NO_2\rightarrow O_2+NO+NO_2$, k_9, discussed by Davidson and Schott[7] and Ashmore and Levitt.[8] However, the imprecision of our data leads to a factor of uncertainty of about 2 or 3 for the value of k_7K_{eq}, and therefore the apparent improvement may not be real.

[7] N. Davidson and G. L. Schott, J. Chem. Phys. **27**, 317 (1957).
[8] P. G. Ashmore and B. P. Levitt, J. Chem. Phys. **27**, 318 (1957).

Microwave Spectrum and Molecular Structure of Monochloroacetonitrile*

JACK D. GRAYBEAL†

Department of Chemistry, University of Wisconsin, Madison, Wisconsin

and

Department of Chemistry, West Virginia University, Morgantown, West Virginia

(Received September 28, 1959)

The microwave spectrum of monochloroacetonitrile has been measured and analyzed. By assuming certain molecular parameters the structure of the planar framework was determined from the moments of inertia of two isotopic species. The C—Cl and C—C bond lengths were found to be 1.767 A and 1.472 A, respectively. The CCCl angle was found to be 111°24′. The H···H distance was found to be 1.728 A. The chlorine nuclear quadrupole coupling constant along the C—Cl bond axis was calculated to be −76.36 Mc. The direction of the dipole moment was estimated to be between the C—Cl and C—CN bond directions, 28° from the latter. The observed C—Cl distance, in addition to the observed nuclear quadrupole coupling constants in the solid and gaseous molecules, are indications that there is very little double bond character in the C—Cl bond. The ionic character of the C—Cl bond was estimated to be 18%.

INTRODUCTION

MEYER and Gutowsky[1] have used double-bonded structures of the type

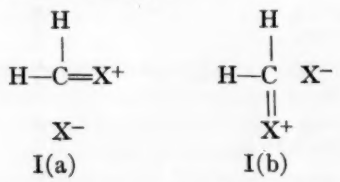

I(a) I(b)

to account for the variations of chemical shifts observed in nuclear magnetic resonance studies of a series of halogenated methanes. The presence of a CN group, with its very strong electron withdrawing power as indicated by nuclear quadrupole resonance spectra,[2] would lead one to expect that monochloroacetonitrile, CH_2ClCN, would be a favorable case for observing hyperconjugation involving a $C{=}Cl^+$ type bond, if such effects are important in substituted methanes. Yet the effect of CN group substitution on the quadrupole coupling constants of the chloromethanes suggested that the principal effect is that of changing the ionic character of the bond rather than contribution of double bond character in the bond.[2] The purpose of the present investigation is to determine molecular parameters of CH_2ClCN, such as bond length and quadrupole coupling constants, which can indicate the extent of double bond character in the C—Cl bond.

EXPERIMENTAL

The microwave spectrum of CH_2ClCN has been observed in two regions, 13.0–17.5 kMc and 22.5–24.5 kMc. The apparatus used was a 5-kc Stark modulated recording microwave spectrometer for the measurements in the 13.0–17.5-kMc region and a 100-kc Stark modulated recording microwave spectrometer for the measurements in the 22.5–24.5-kMc region. Frequency measurements in both cases were made by recording of frequency markers, derived from a standard compared to WWV, directly on the recordings of transitions. The absorption cell was equipped with dry ice containers arranged so that the temperature could be maintained at about 250°K, sufficiently cold to improve sensitivity but high enough to prevent the sample from freezing out. The CH_2ClCN used was obtained from Eastman Kodak Company and redistilled.

RESULTS

The observed transitions of CH_2ClCN that have been definitely assigned are given in Table I. All the lines listed in the table have hyperfine splittings in good agreement with those calculated for the transitions. In addition to the transitions listed in Table I numerous other transitions were observed in both regions. These are due to high J transitions and to transitions belonging to excited vibrational states. Cheng[3] has found that there are several low-lying vibrational states which would have appreciable populations at the temperature used for study, 250°K. No attempt was made to fit either the high J or excited state transitions. From the observed data the rotational constants and asymmetry parameters were determined for the two isotopic species as given in Table II.

Since only the hydrogens lie out of the ClCCN plane the H···H distance in the CH_2Cl group is determined from $I_a+I_b-I_c$. Due to the fact that small variations of either the C—H distance or the CCH angle have little effect on the reciprocal moments, especially B and C, assumed values were taken for these param-

* Based partly on a thesis submitted in partial fulfillment of the requirements for the Ph.D. degree at the University of Wisconsin, 1955. Part of this research was made possible by a National Science Foundation Grant.

† Present address: Department of Chemistry, West Virginia University, Morgantown, West Virginia.

[1] L. H. Meyer and H. S. Gutowsky, J. Phys. Chem. **57**, 481 (1953).

[2] J. D. Graybeal and C. D. Cornwell, J. Phys. Chem. **62**, 483 (1958).

[3] H. C. Cheng, Z. physik. Chem. (Leipzig) **B26**, 288 (1934).

eters and the structure of the planar framework calculated from the experimentally determined reciprocal moments of the two isotopic species. The assumed value for the C—H distance is that in CH_2Cl_2.[4] An additional assumption of 1.158 A for the C≡N bond distance was made. This assumption is justified by the relatively constant length observed for this bond in other molecules studied.[5] The assumed and calculated molecular constants are given in Table III.

The quadrupole coupling constants along the principal axes, calculated separately from the well-resolved components of the $5_{15}\rightarrow 6_{06}$ and the $11_{2,10}\rightarrow 12_{1,11}$ transitions, are given in Table III. If one assumes that the electric field at the Cl nucleus has cylindrical symmetry, and this assumption seems reasonable in view of the discussion to follow, then the quadrupole coupling constant along the C—Cl bond axis is −76.36 Mc, which is comparable to the value of −76.24 Mc found for the solid.[2]

Stark effect measurements on the observed transitions are difficult to make because of the hyperfine structure, and separate determinations of both the *a* and *b* components of the dipole moment were not possible. Measurements of the Stark effect of the unresolved Stark components of the $11_{2,10}\rightarrow 12_{1,11}$ transition, along with a previously measured value of the dipole moment in solution,[6] have been used to estimate the ratio, μ_a/μ_b, to be 0.65±0.05. This gives a dipole moment oriented at 57±3° with respect to the *a* axis, the sign of the angle being undetermined. By using bond moments one can reliably predict that the dipole moment will lie between the C—Cl bond direction and the C—CN bond direction. Using this to determine the sign of the angle one can estimate that the dipole moment will lie 28±3° off the C—CN bond direction toward the C—Cl bond.

TABLE I. Observed and calculated spectra (Mc).[a]

	$CH_2Cl^{35}CN$		$CH_2Cl^{37}CN$	
	ν_{obs}	ν_{calc}	ν_{obs}	ν_{calc}
a-type[b]				
$2_{12}\rightarrow 3_{12}$	17 550	17 549.40	17 177	17 179.03
$3_{03}\rightarrow 4_{04}$	23 974	23 975.39		
$3_{22}\rightarrow 4_{23}$	24 002	24 003.65		
$3_{21}\rightarrow 4_{22}$	24 011	24 012.09		
$3_{30}\rightarrow 4_{31}$	24 011	24 012.21		
$3_{21}\rightarrow 4_{22}$	24 036	24 034.28		
b-type[c]				
$5_{15}\rightarrow 6_{06}$	15 794.54	15 794.54	15 038.34	15 038.32
$10_{1,10}\rightarrow 9_{27}$	16 347.33	16 347.34	17 004.60	17 004.30
$11_{2,10}\rightarrow 12_{1,11}$	16 469.00	16 469.00	14 789.70	14 789.62
$6_{16}\rightarrow 7_{07}$	22 554.00	22 553.57		
$4_{04}\rightarrow 4_{13}$	23 829.80	23 830.09		

[a] No corrections for centrifugal distortion or rotation-vibration effects in calculated spectrum.
[b] Estimated uncertainity±1 Mc.
[c] Estimated uncertainity±0.2 Mc.

TABLE II. Rotational constants and asymmetry parameters of monochloroacetonitrile.

	$CH_2Cl^{35}CN$	$CH_2Cl^{37}CN$
A	25 284.77±0.50 Mc	25 135.17±0.50 Mc
B	3 151.61±0.20 Mc	3 081.77±0.20 Mc
C	2 849.90±0.20 Mc	2 790.84±0.20 Mc
δ	0.01345±0.00001	0.01302±0.00001

DISCUSSION

If one compares the observed value of the C—Cl bond length in gaseous CH_2ClCN, 1.767 A, to those of CH_3Cl, 1.781 A,[7] and CH_2Cl_2, 1.772 A,[4] one sees that the difference is barely above experimental error and may not exceed the magnitude of error introduced by zero-point vibrational effects. The C—Cl bond distance observed for vinyl chloride is 1.726 A.[8] Hyperconjugation has been reasonably well established as occurring in this molecule and a definite decrease in bond length is noticeable even for the small amount of double bond character in the C—Cl bond. On the basis of the observed length of the C—Cl bond in CH_2ClCN one can predict that there is little, if any, double bond character in this bond.

The observed C—C distance in CH_2ClCN is shorter than the accepted value for the normal C—C single bond, 1.54 A.[9] This indicates the presence of either some double bond character in the C—C bond, which could arise from a contributing resonance form such as

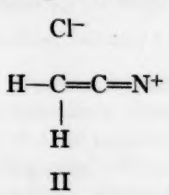

II

or the existence of some positive charge on the carbon atoms, which could be the result of contributing resonance forms such as

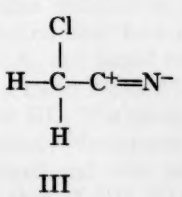

III

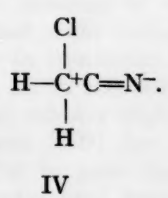

IV

[4] R. J. Myers and W. D. Gwinn, J. Chem. Phys. **20**, 1420 (1952).
[5] See, for example, *Tables of Interatomic Distances and Configuration in Molecules and Ions* (Burlington House, London, 1958), Sec. S, p. 17.
[6] M. T. Rogers, J. Am. Chem. Soc. **69**, 457 (1947).
[7] S. L. Miller, L. C. Aamodt, G. Dousmanis, C. H. Townes, and J. Kraitchman, J. Chem. Phys. **20**, 1112 (1952).
[8] D. Kivelson, E. B. Wilson, Jr., and D. R. Lide, Jr., J. Chem. Phys. **32**, 205 (1960).
[9] See footnote 5, Sec. S, p. 12.

TABLE III. Molecular constants of monochloroacetonitrile.

Assumed	
C≡N 1.158 A	∢ CCH 109°30′
C—H 1.070 A	
Calculated[a]	
C—Cl 1.767±0.005 A	∢CCCl 111°24′±30′
C—C 1.472±0.005 A	H···H 1.728±0.005 A
$\chi_{aa}=-30.45$ Mc	$\chi_{bb}=-7.73$ Mc

[a] The error listed allows for neglected vibration-rotation interactions in addition to experimental error.

Forms II and III are postulated by consideration of the strong electron withdrawing power of the CN group. The present data do not allow a choice as to which predominates.

Regardless of the structure of the remainder of the molecule, consideration can be given to three forms when discussing the C—Cl bond: (i) R—Cl covalent, (ii) R^+Cl^- ionic, (iii) $R^-{=}Cl^+$ π-bonded. Three factors now support the conclusion that iii is not an important form for this molecule: (a) There is an increase in the quadrupole coupling constant in the solid with increasing electron withdrawing power of a substituent. (b) The microwave data show little if any shortening of the C—Cl bond. (c) The quadrupole coupling constants for the gaseous molecule are consistent with the assumption of cylindrical symmetry for the field at the chlorine nucleus. Since CH_2ClCN would be a favorable case, among substituted chloromethanes, for observing double bond character in the C—Cl bond, one can expect little $C{=}Cl^+$ type character in other chloromethanes.

If one takes forms i and ii as being the principal contributing structures to the C—Cl bond, utilizes the method of Townes and Schawlow,[10] considers the C—Cl bond in form i as having 15% *s* character, and uses the calculated value for the quadrupole coupling constant along the C—Cl bond axis, one can estimate the total contribution of ionic structures to be about 18%.

In summary it can be said that the evidence available indicates that there is little double bond character in the C—Cl bonds in the chloromethanes and that perhaps one should be cautious about using hyperconjugated structures for any other halomethanes.

ACKNOWLEDGMENTS

The author wishes to thank Professor C. D. Cornwell, Department of Chemistry, University of Wisconsin, for many helpful suggestions during the course of this work. The author is indebted to the National Science Foundation for support during the latter part of this work. The author acknowledges the contribution of the use of computing facilities by the IBM Service, Office of the Registrar, West Virginia University.

[10] C. H. Townes and A. L. Schawlow, *Microwave Spectroscopy* (McGraw-Hill Book Company, Inc., New York, 1955), Chap. 9.

Letters to the Editor

THE Letters to the Editor section is subdivided into three parts entitled Communications, Comments and Errata, and Notes. These three sections are all subject to the same limitations on length. The textual material of each Letter is limited to a number of words equal to 950 minus the following: (a) 200 words for each average-sized figure; (b) 50 words for each displayed equation; (c) 7 words for each line of table including headings and horizontal rulings. No proof will be sent to the authors of "Communications" and "Comments and Errata." Proof will be sent to the authors of "Notes." The publication charge for Letters is $30 per page, with a minimum of $30 per Letter. If honored, the Institution will be entitled to 100 reprints without covers. See issues of May–September, 1957, for descriptions of categories.

Communications

Paramagnetic Resonance in Tetravalent Pa^{231}*

JOHN D. AXE AND RU-TAO KYI

Lawrence Radiation Laboratory, University of California, Berkeley, California

AND

H. J. STAPLETON

Department of Physics, University of California, Berkeley, California

(Received February 10, 1960)

THE paramagnetic resonance spectrum of tetravalent Pa^{231} has been observed in a single crystal of Cs_2ZrCl_6. A melt of Cs_2ZrCl_6 was "doped" with ~500 μg of anhydrous $Pa^{231}Cl_4$[1] and allowed to crystallize in an atmosphere of hydrogen by slow passage through a furnace. At 4.2°K and a frequency of 9457 Mcps, the observed resonance pattern consisted of four widely separated hyperfine components. The spectrum was isotropic to within the accuracy of the field measurements (~½%). These features are interpreted as the usual $\Delta M_S=\pm 1$, $\Delta M_I=0$ transitions between the eigenstates of the spin Hamiltonian

$$\mathcal{H}=g\beta\mathbf{H}\cdot\mathbf{S}+A\mathbf{I}\cdot\mathbf{S},$$

with $S=\frac{1}{2}$, $I=\frac{3}{2}$,

$$|g|=1.14\ (\pm 0.02),$$

and

$$|A|=0.0529\ (\pm 0.001)\ \text{cm}^{-1}.$$

The large hyperfine interaction necessitates the use of exact solutions for the energy levels.[2] No resonance was detected at 77°K.

The nuclear-spin value of $\frac{3}{2}$ is verified.[3] The paramagnetism can be most plausibly ascribed to a single 5*f* electron. A magnetically isotropic Kramers' doublet is expected to be the lowest lying as the result of the octahedral perturbation present at the zirconium site.[4,5] As an alternative, a $6d^1$ configuration is expected to give rise to a fourfold degenerate magnetically anisotropic level if octahedral symmetry is preserved,[6] or an anisotropic doublet if distortion is present.[7] Further work on the optical absorption spectra of this system is in progress and should allow amplification of the foregoing conclusions. An attempt to measure the nuclear magnetic moment of Pa^{231} by a "double-resonance" technique is likewise in progress. We wish to thank Professor C. D. Jeffries and Professor B. B. Cunningham for their invaluable advice.

* Supported in part by the U. S. Atomic Energy Commission and the Office of Naval Research.

[1] Prepared by the method of P. A. Sellers, S. M. Fried, R. E. Elson, and W. H. Zachariasen, J. Am. Chem. Soc. **76**, 5935 (1954).

[2] B. Bleaney, Phil. Mag. **42**, 441 (1951).

[3] H. Schüler and H. Gollnow, Naturwiss. **22**, 511 (1934).

[4] See for example J. S. Griffith and L. E. Orgel, J. Chem. Phys. **26**, 988 (1956).

[5] C. A. Hutchison and B. Weinstock, J. Chem. Phys. **32**, 56 (1960). These authors discuss paramagnetic resonance in another f^1 octahedral system, NpF_6.

[6] B. Bleaney, Proc. Phys. Soc. (London) **73**, 939 (1959).

[7] J. H. E. Griffiths, J. Owen, and I. M. Ward, Proc. Roy. Soc. (London) **A219**, 526 (1953).

Effect of Deuterium Substitution on the Lifetime of the Phosphorescent Triplet State of Naphthalene*

CLYDE A. HUTCHISON, JR., AND BILLY W. MANGUM†‡

Enrico Fermi Institute for Nuclear Studies and Department of Chemistry, University of Chicago, Chicago, Illinois

(Received February 12, 1960)

PROTON and deuteron hyperfine structures in the paramagnetic resonance absorption by the phosphorescent triplet state of naphthalene[1] are being investigated at the boiling point of liquid N_2. It has been observed that completely deuterated naphthalene in completely deuterated durene (DD) gives an extraordinarily intense resonance signal relative to ordinary naphthalene in ordinary durene (HH). Decays of the magnetic resonances after cessation of ultraviolet irradiation have been examined at the boiling point of liquid N_2 and found to obey an exponential decay law with a mean life of 2.1±0.1 sec for HH and 16.9±0.7 sec for DD. The mean life of ordinary naphthalene in completely deuterated durene (HD) has also been examined and does not differ by more than 0.5 sec from that of HH. These decays have been measured for periods from one to two mean lives in length. The decay of the paramagnetic resonance has been investigated with the static magnetic field along two of the

principal magnetic axes of HH and along all three of DD. The observed variation of lifetime with direction is no greater than the probable error of an individual measurement for both HH and DD. Inasmuch as the hyperfine structure is very anisotropic this shows that the change of lifetime is purely a mass effect rather than a nuclear hyperfine effect.

The lifetime of the phosphorescence of ordinary naphthalene in a rigid glass (EPA) has been found by McClure[2] to be 2.6±0.2 sec at 77°K. On the basis of their measurements of the absolute yields of fluorescence and phosphorescence, Gilmore, Gibson, and McClure[3] calculated the natural lifetime of the phosphorescent state to be 11 sec assuming that all the radiationless processes originate in the triplet state.

The large observed effect of deuterium substitution on triplet state lifetime may arise from the effect of mass of the hydrogen atoms (a) on singlet-triplet internal conversion rates; (b) on rate of conversion of vibrational energy to crystal energy; or (c) on rate of radiationless electronic energy transfers to the crystal.

We thank Professor Harden McConnell for pointing out to us in several stimulating discussions the possibility of nuclear hyperfine limited lifetimes and the significance of the measurements in various directions. We also thank Winifred M. Y. Huo for her assistance with this work.

* This work has been supported by the U. S. Atomic Energy Commission.
† National Science Foundation Predoctoral Fellow.
‡ Present address: The Clarendon Laboratory, Parks Road, Oxford, England.
[1] Clyde A. Hutchison, Jr., and Billy W. Mangum, J. Chem. Phys. **29**, 952 (1958).
[2] Donald S. McClure, J. Chem. Phys. **17**, 905 (1949).
[3] E. H. Gilmore, G. E. Gibson, and D. S. McClure, J. Chem. Phys. **20**, 829 (1952); J. Chem. Phys. **23**, 399 (1955).

Comments and Errata

Emission by Vibrational Fundamentals and Overtones in Shock Waves*

J. C. Decius

Oregon State College, Corvallis, Oregon

(Received January 14, 1960)

THE rate of vibrational excitation in CO in a shock wave has recently been studied by Windsor, Davidson, and Taylor,[1] who observed emission of the first overtone as a function of time. These authors analyzed their data using a three-state model ($v=0$, 1, 2) although they pointed out the fact that higher states influence the process to a certain extent. Subsequently Shuler[2] has given expressions for the time dependence of such a process in the form of the ratio of the populations of any two harmonic oscillator levels, taking into account the infinite set of vibrational levels. But at present experimental techniques limit such studies to observation of the superposed emission for all transitions corresponding to a given Δv, and it is pertinent to express the emission summed over all vibrational states.

If, as has generally been assumed, the collisional excitation is a one-quantum process, Montroll and Shuler[3] have shown that an initial Boltzmann distribution relaxes to a final Boltzmann distribution via a continuous sequence of such distributions. In such a case it is easy to obtain suitable expressions for the total emission due to a fundamental ($\Delta v=-1$), first overtone ($\Delta v=-2$), etc.

The total spontaneous emission for the fundamental transition is proportional to

$$I^{(1)}=(\tfrac{1}{2}\gamma^2)(\mu')\sum_{v=0}^{\infty}vn_v=(\tfrac{1}{2}\gamma^2)(\mu')^2[n/(1-\rho)\rho], \qquad (1)$$

whereas that for the first overtone is proportional to

$$I^{(2)}=(\tfrac{1}{6}\gamma^4)(\mu''+a\mu')^2\sum_{v=0}^{\infty}v(v-1)n_v$$
$$=(\tfrac{1}{6}\gamma^4)(\mu''+a\mu')^2n[\rho/(1-\rho)]^2. \qquad (2)$$

In the foregoing (cf. Crawford and Dinsmore[4]), γ^2 is $2B/\omega$, i.e., the ratio of rotational constant to fundamental vibration frequency; μ' and μ'' are, respectively, first and second derivatives of molecular dipole with respect to dimensionless internuclear distance; a is a cubic potential energy constant; n is the total number of molecules per unit volume; and ρ, the most significant part of the formulas, stands for $\exp(-h\nu/kT)$, T being the instantaneous vibrational temperature.

Since it is assumed that emission does not measurably affect the rate of change of level populations, the time dependence of ρ can be determined from the vibrational energy relaxation equation

$$E-E_\infty=(E_0-E_\infty)\exp(-\lambda t) \qquad (3)$$

in which

$$E=[nh\nu/(1-\rho)\rho] \qquad (4)$$

and

$$\lambda=(1-\rho_\infty)/\tau_{10} \qquad (5)$$

with τ_{10} as the reciprocal of the rate constant for the collisional deactivation $v=1\rightarrow v=0$. By combining Eqs. (1)–(4) one finds

$$I^{(1)}=I_\infty^{(1)}\{1+[(I_0^{(1)}-I_\infty^{(1)})/I_\infty^{(1)}]\exp(-\lambda t)\}, \qquad (6)$$

and

$$I^{(2)}=I_\infty^{(2)}\{1+[(I_0^{(2)}-I_\infty^{(2)})/I_\infty^{(2)}]\exp(-\lambda t)\}^2, \qquad (7)$$

from which it follows directly that plots of log

$$[1-(I/I_\infty)]$$

and log $\{1-[(I)^{\frac{1}{2}}/I_\infty]\}$ vs t should be linear in the respective cases and should yield λ.

Thus we may conclude that when account is taken of the upper states, the radiation decays with a rate constant of $k_{10}(1-\rho_\infty)$ just as does the total vibrational energy. If k_{10}(WDT) represents the value reported by Windsor *et al.* the true value of k_{10} is given by

$$k_{10}=k_{10}(\mathrm{WDT})/(1-\rho_\infty).$$

* Supported by Office of Naval Research.

[1] M. W. Windsor, N. Davidson, and R. Taylor, J. Chem. Phys. **27**, 315 (1957); Symposium on Combustion, 7th Symposium, Oxford, England, p. 80.
[2] K. W. Shüler, J. Chem. Phys. **30**, 1631 (1959).
[3] E. W. Montroll and K. E. Shuler, J. Chem. Phys. **26**, 454 (1957).
[4] B. L. Crawford, Jr., and H. L. Dinsmore, J. Chem. Phys. **18**, 983 (1950).

Dangers of the "Average Energy Approximation" in Perturbation Theory

A. D. McLachlan*

Gates and Crellin Laboratories of Chemistry,† California Institute of Technology, Pasadena, California

(Received December 8, 1959)

A DEVICE often used for obtaining second-order perturbation expansions in closed form is the replacement of the excitation energies E_n-E_0 by an average value ΔE and the subsequent use of the law of matrix multiplication:

$$\sum_n{}'[\langle 0\,|\,A\,|\,n\rangle\langle n\,|\,B\,|\,0\rangle/(E_n-E_0)]$$
$$=\Delta E^{-1}\{\langle 0\,|\,AB\,|\,0\rangle-\langle 0\,|\,A\,|\,0\rangle\langle 0\,|\,B\,|\,0\rangle\}. \quad (1)$$

Examples are Ramsey's formula for nuclear magnetic shielding,[1] and McConnell and Karplus' [2,3] theories of nuclear spin-spin couplings in molecules. This procedure leads to false conclusions unless the nature of the excited states in (1) is carefully examined in each case. In particular *there need not exist any positive value of* ΔE *for which* (1) *holds, unless*

$$\langle 0\,|\,A\,|\,n\rangle\langle n\,|\,B\,|\,0\rangle,$$

has the same sign for every excited state n. Thus (1) may not even predict the correct sign of the perturbation sum. As an example, consider how molecular orbital theory treats the changes δq_r of π-electron density in an alternant conjugated molecule when a substituent alters the Coulomb integral α_s at atom s. In standard notation[4]

$$\delta q_r=\sum_s \pi_{rs}\delta\alpha_s, \quad (2)$$

$$\pi_{rs}=-4\sum_{i=1}^{n}\sum_{j=n+1}^{2n}[c_{ri}c_{rj}c_{si}c_{sj}/(E_j-E_i)]$$
$$(-1/\Delta E)p_{rs}(2\delta_{rs}-p_{rs}) \quad (3)$$

according to (1). The approximate formula gives $\pi_{rs}=0$ when atoms r and s are separated by an even number of bonds, ($p_{rs}=0$), but the correct value is definitely negative, according to the law of alternating polarity. McConnell's statement that single configuration molecular orbital theory always leads to positive long-range contact nuclear spin-spin couplings rests on an argument similar to (3), and is not generally valid. In Eq. (45) of his paper[2] $1/\Delta E(\eta_{HH'})^2$ should be replaced by the mutual polarizability $\pi_{HH'}$ if one uses a one-electron Hamiltonian for the excited states. On the other hand, the use of (1) for the valence bond theory of nuclear couplings in *alternant* systems[5] does give the correct signs because of the special nature of the ground and excited state wave functions.[6] However, Karplus' calculation[3] may need critical examination as his molecules are not alternant.[7]

The author is grateful to Professor Harden M. McConnell for helpful discussions on the details of this Comment.

* Harkness Fellow of the Commonwealth Fund 1959–1961.
† Contribution No. 2532.

[1] N. F. Ramsey, Phys. Rev. **78**, 699 (1950).
[2] H. M. McConnell, J. Chem. Phys. **24**, 460 (1956).
[3] M. Karplus and D. H. Anderson, J. Chem. Phys. **30**, 6, 11 (1959).
[4] C. A. Coulson and H. C. Longuet-Higgins, Proc. Roy. Soc. (London) **A192**, 16 (1947).
[5] H. M. McConnell, J. Chem. Phys. **30**, 126 (1959).
[6] A. D. McLachlan, Mol. Phys. **2**, 223 (1959).
[7] Professor Karplus reports that he is already reexamining his calculations with variational and perturbation methods.

Notes

Solvent Effect on the Infrared Absorptions of N-Methylacetamide in the Region of the NH Stretching Frequency

I. Suzuki, M. Tsuboi, and T. Shimanouchi

Department of Chemisty, Faculty of Science, Tokyo University, Hongo, Tokyo, Japan

(Received November 16, 1959)

IN a previous paper[1] we showed that N-methylacetamide, when it is dissolved in benzene (or a solvent that consists of benzene and carbon tetrachloride), forms a complex with benzene in which its NH stretching frequency is a little lower than in that of its monomer in dulute carbon tetrachloride solutions. This complex may be considered to be formed by a hydrogen-bondlike interaction[2] between the NH group of N-methylacetamide and the π electrons of the benzene ring. The same kind of interaction has been found to be acting between the NH group and phenyl group within the N-methylphenylacetamide molecule.[3] In attempting to know more of the nature of this

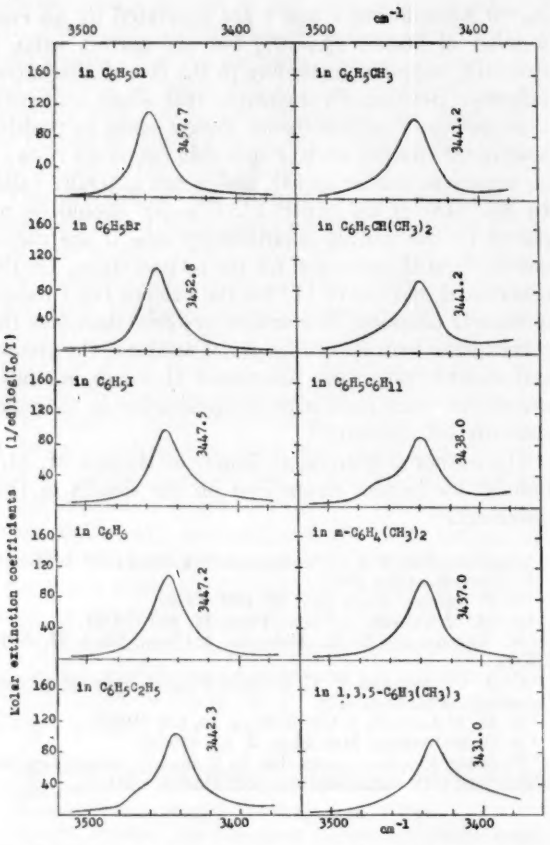

FIG. 1. Infrared absorption curves in the free NH stretching region of N-methylacetamide dissolved in various solvents. Positions of the absorption maxima are given in cm^{-1}.

kind of interaction, we observed the infrared absorptions in the NH stretching region of N-methylacetamide in various solvents having phenyl groups. The apparatus used was a Perkin-Elmer 112G grating spectrometer. The results are given graphically in Fig. 1.

It can be seen from the figure that the position of the absorption maximum of the NH band depends upon the π electron density in the phenyl group in the solvent molecule. When the π-electron density in the benzene ring of the solvent is lowered by substituting halogen atoms for hydrogen atoms, the maximum of the NH band shifts towards higher frequency. This is explained by considering that the interaction becomes a little weaker causing the NH frequency to approach towards that of the free NH (3472 cm^{-1} in CCl_4). On the other hand, when the π-electron density in the benzene ring in the solvent is elevated by substituting the hydrogen atoms with alkyl groups, the maximum of the NH band shifts towards lower frequency. This is explained by considering that the interaction becomes stronger.

Another interesting fact to be noted is concerned with the band shape. N-methylacetamide dissolved in benzene affords an NH band almost symmetrical with respect to its center, whereas the same substance dissolved in a substituted benzene affords an asymmetrical band. With halogenobenzene as the solvent, the slope of the band is less steep on its lower frequency side than on its higher frequency side. With alkylbenzene as the solvent, the slope is less steep on the higher frequency side. This fact may be explained by supposing that there is another NH band (a weak subband) superposed over the skirt of the main NH band, as was actually observed with phenylcyclohexane as the solvent. Such a subband may be attributed to the NH group of N-methylacetamide which is situated close to the substituents of the solvent molecules, but not close to the benzene ring.

[1] Suzuki, Tsuboi, Shimanouchi, and Mizushima, J. Chem. Phys. **31**, 1437 (1959).

[2] Similar interaction has been found between the OH or NH group and aromatic or olefinic π electrons by Oki, Iwamura and Urushibara [Bull. Chem. Soc. Japan **31**, 769 (1958); *ibid.* **32**, 567, 955 (1959)]; and also between phenolic OH group and olefinic or acetylenic π electrons by R. West [J. Am. Chem. Soc. **81**, 1614 (1959)].

[3] Suzuki, Tsuboi, and Shimanouchi (to be published).

Induced emf in Electrolytes

F. HEINMETS

Pioneering Research Division, Quartermaster Research & Engineering Center, U. S. Army, Natick, Massachusetts

(Received October 14, 1959)

USUALLY the effect of an electric field on the movement of ions in electrolytes is studied by direct application of the field by means of electrodes. It is of interest to expore the interaction between an induced electric field and ions in solution. Maxwell's law relating changing magnetic flux and electric field intensity is

$$(d/dt)\int_s \mathbf{B}\cdot d\mathbf{a} = -\oint_c \mathbf{E}\cdot d\mathbf{s},$$

where $d\mathbf{s}$ is an element of length along, and $d\mathbf{a}$ an element of area $\mathbf{s}$ enclosed by contour c. Faraday's experiments on induction, carried out with metallic circuits, led Maxwell to the theoretical formulation of the phenomenon. Maxwell's point of view was abstract and he defined his law for any arbitrary loops of conductors or nonconductors.[1]

The passage of current through electrolytes involves ionic transport. Since this differs from electron movement in metals, we wished to study the effect of a slowly varying magnetic flux on the induction of electric fields in solutions, where the following points should be noted: (a) Positive and negative charges are present and move simultaneously in opposite directions; (b) Ions have single or multiple charges and a mixture of ions may be present; (c) concentrations of ions can be varied; (d) the mechanism of ionic movement may differ (protons).

To study experimentally the effect of magnetic induction on ions in solution, an electric transformer (110 v ac) was modified. The primary winding was left intact but the secondary was removed. Two new windings were substituted: (a) a long piece of Tygon tubing (internal diameter 3 mm) wound around the iron core with both ends connected to glass funnels, or (b) a copper wire wound around the same iron case (reference winding). Tygon tube winding and funnels were filled with suitable electrolyte and platinum electrodes placed in the funnels. A 60-cycle alternating potential was applied to the primary winding and following measurements were made: primary current, primary potential, secondary potential, secondary winding resistance (electrolyte). Since resistance of the coil was high when it contained dilute electrolyte, secondary potentials had to be measured with a high input impedance vacuum tube voltmeter. Waveform was followed with an oscillograph. A series of measurements were carried out in different electrolytes (HCl, NaCl, KCl, $CuSO_4$, H_2SO_4) at various concentrations. The results can be summarized as follows: (a) the secondary potential induced in electrolyte does not depend on the character of the electrolyte and its concentration (provided that the potential is measured correctly at high dilutions); (b) there is no visible change in the sinusoidal wave form of the potential of the electrolyte coil provided that magnetic saturation of the iron core is avoided; (c) there is no phase shift when the potential of the electrolyte and the copper winding are compared.

Subsequently windings were reversed and potential was applied to the electrolytic coil which served as the primary. Induced potential in copper-secondary was again sinusoidal and its magnitude was proportional to the applied primary potential. This proves that ionic and protonic currents in electrolytes will induce emf in magnetically coupled metallic circuits. However, it is expected that differences in ionic and electronic movements will appear, when the frequency of varying magnetic flux is in the range of time of relaxation for ionic motion. Because of large energy losses at high frequencies in iron core, such experiments could not be carried out.

Our experiments confirm Maxwell's law of induction as valid in electrolytic media since the induced potential does not depend on (a) the magnitude and polarity of charges, (b) the velocity of charges, (c) the character of medium, or (d) the mechanism of charge transport (protons). The equivalence of electric and magnetic fields in certain geometric relations seems to be indicated.

One interesting feature of the induced potential is that an alternating potential can be produced in an electrolyte without electrodes. This may sometimes be desirable in certain experimental conditions, e.g., the elucidation of the mechanism of proton movement. It has been suggested[2] that the preferred direction of proton movement in water results from the proton sink at the cathode and not from an orientation of the water molecules and hydrated protons in the external electric field. By using an electrolytic transformer, a selective experiment was made. The electrolytic coil which contained 1*M* HCl solution served as secondary winding. Potential was applied to the primary and secondary current and was measured by a Clipp-On ac Microammeter (Quan-Tech, Model 301). The secondary coil was at first short circuited by an electrolytic bridge (1*M* HCl) and then by the metallic electrodes. Current values were the same for both cases. This suggests that the preferred direction of proton movement in water does not result from the proton sink at the cathode.

[1] J. C. Maxwell, *A Treatise on Electricity and Magnetism* (Oxford University Press, New York, 1892), 3rd ed., Vol. II.
[2] G. Kortum and J. O'M. Bockris, *Textbook of Electrochemistry* (Elsevier Publishing Company, New York, 1951).

Ionization Potentials and Electrostatic Polarization

NORMAN D. COGGESHALL
Gulf Research & Development Company, Pittsburgh, Pennsylvania

(Received March 17, 1959)

IT is assumed that the difference of ionization potential between two molecules differing only by a methyl substitution will be given approximately by the electrostatic polarization energy of the methyl group. The electric field results from the unbalanced charge at the center of the orbit of the electron removed to produce the ionization. If we add a methyl group at a distance r from the charge site, the field E there will be proportional to $1/r^2$. The energy of polarization will be αE^2 where α is the polarizability of the group. The difference of ionization potential should therefore be proportional to $1/r^4$.

It is not known whether or not the ionization of n-paraffins results from the removal of electrons from preferred sites. However, the addition of a further methyl group in going from a n-paraffin of $(n-1)$ carbon atoms to n carbon atoms will result in the addition of further polarizable C—H groups at a distance which will be a function of the total number of carbon atoms. The increment of ionization potential $\Delta E(n, n-1)$ should then be proportional to the inverse fourth power of a function of n. We may write this as $\Delta E(n, n-1)=k/[f(n)]^4$. By using Honig's values,[1] the $\Delta E(n, n-1)$ were obtained and the inverse fourth roots calculated. When plotted *vs* n the points all fell near a straight line except the one representing the difference in ionization potential of n-octane and n-heptane. This discrepancy corresponds to an apparent discrepancy in Honig's experimental results.

TABLE I. $\Delta E(n, n-1)$ values for n-paraffins in ev.

n	$\Delta E(n, n-1)$ calc	$\Delta E(n, n-1)$ (Honig's data)
4	0.43	0.41
5	0.21	0.25
6	0.12	0.12
7	0.07	0.08
8	0.05	0.11
9	0.03	0.03
10	0.02	0.02

Using the graph to determine the slope and making it a fit on the $n=6$ value, we may calculate the $\Delta E(n, n-1)$ values and compare them with those obtained from Honig's work (see Table I).

In olefins we would expect ionization to remove a pi electron from the double bond. Substitution at a definite distance from the double bond should result in an approximately constant increment of ionization potential. In Table II are given the changes in ionization potential for two different types of substitutions in several cases.

Olefin isomers with equal spatial distribution of C—H bonds from the double bond should have approximately equal ionization potentials. *Cis*-2-butene, *trans*-2-butene, and 2-methyl propene have ionization potentials of 9.31, 9.29, and 9.35 ev, respectively,[1] which confirms this.

If valid, this simple model should yield a value of polarizability of the right order of magnitude. We use the results under A of Table II to get an average of ΔE of 0.51 ev for a methyl group added to an olefinic carbon. We may use $\Delta E=\alpha q^2/r^4$ to calculate α. Using accepted bond distances and angles we obtain $\alpha=0.42\times10^{-24}$ cm^3. This compares with $\alpha=1.82\times10^{-24}$ cm^3 from molar refraction for a methylene unit.

The center of the benzene ring may be taken as the charge site for an alkyl benzene. From Morrison and Nicholson's data[2] we get a ΔE value of 0.29 ev for benzene and toluene. This should represent the polarization energy of substituting a methyl group on the benzene ring. This agrees quite well with a ΔE of 0.27 ev from Field and Franklin's data[3] for 1,3-dimethylbenzene and 1,3,5-trimethylbenzene.

TABLE II. ΔE values for different types of addition (Honig's data[a]).

A. Methyl group on olefinic carbon		B. Methyl group alpha to bond	
propene butene-2 (*cis* or *trans*)	0.55 ev	propene 1-butene	0.08 ev
propene 2-methyl propene	0.49	2-butene 2-pentene	0.13
2-methyl propene 3-methyl-2-butene	0.50	2-pentene 3-hexene	0.04

[a] Reference 1.

By using Morrison and Nicholson's data for toluene and ethylbenzene,[2] we may calculate α. This gives $\alpha=1.57\times10^{-24}$ cm^3 in better agreement with the molar refraction value of 1.82×10^{-24} cm^3 than obtained in the foregoing. Using the calculated value of α and applying it to 1,3-dimethylbenzene and 1,3,5-trimethylbenzene gives a predicted ΔE value of 0.30 ev which compares quite well with the experimental value of 0.27 ev.

With two methyl groups on a benzene ring, the interaction resulting from the induced dipoles will provide a positive increment $\Delta(\Delta E)$ to the ionization potential. The order of decreasing ionization potential should be *ortho*; *meta*; *para*. With one methyl group attached, the total field at the *ortho*, *meta*, and *para* positions can be calculated as the resultant of the coulomb field and the dipole field from the polarized methyl group. Comparison of this field with the coulomb field allows the calculation of the positive increment due to the second methyl substitution as a fraction of the negative increment ΔE due to adding the first methyl group. The total effect will be double due to the mutual effect of the two methyl groups upon each other. Using accepted molecular geometry and the molar refraction value of α we obtain $\Delta(\Delta E)_{ortho}=0.34\Delta E$; $\Delta(\Delta E)_{meta}=0.11\Delta E$; $\Delta(\Delta E)_{para}=0.03\Delta E$. Using $\Delta E=0.29$ ev from the foregoing, the calculated difference in ionization potential between *ortho* and *para* xylene should be 0.09 ev which agrees with the difference observed by Field and Franklin.[3] Their value for *m*-xylene does not fit the predicted trend. However, data obtained by Crable *et al.*[4] fit the predicted trend for the isomeric xylenes, phenols, and toluidines.

[1] R. E. Honig, J. Chem. Phys. **16**, 105 (1948).
[2] J. F. Morrison and A. J. C. Nicholson, J. Chem. Phys. **20**, 1021 (1952).
[3] F. H. Field and J. L. Franklin, J. Chem. Phys. **22**, 1895 (1954).
[4] G. F. Crable, G. L. Kearns, and M. S. Norris, Anal. Chem. **32**, 13 (1960).

Intermolecular Isotope Effect in Recoil Tritium Reactions with Hydrogen

J. K. LEE, BURDON MUSGRAVE, AND F. S. ROWLAND*
Department of Chemistry, University of Kansas, Lawrence, Kansas

(Received December 9, 1959)

OUR recent experiments show that recoiling tritium atoms from the nuclear reaction He^3 $(n, p)T$ show a preference for formation of HT over DT in reaction with mixtures of H_2 and D_2. An isotope effect has previously been reported in recoil tritium reactions only in the case of liquid isopropyl benzoate, deuterated in various positions.[1] In those experiments, intramolecular tritium distributions were observed in

each isotopic form of isopropyl benzoate and then compared with each other; a preference for tritium replacement of H over D by a factor of 1.41 in a methyl group and 1.16 in an aromatic ring was observed. In our system, the isotopic effect has been observed between two chemical species competing for the tritium recoil atoms in a single homogeneous gaseous system.

Gaseous mixtures of He^3 with H_2 and D_2 were sealed in Pyrex 1720 glass and irradiated in a thermal neutron flux of 3×10^9 neutrons/cm²/sec for two days. The radioactive products, HT and DT, were then separated by gas chromatography on a 10-ft column of 13 A molecular sieve at −160° C, using helium flow gas. After separation, methane was added to the flowing stream and the radioactivity content determined by passing the gas mixture through a proportional counter of 100 ml active volume.[2]

We have checked against possible isotopic exchange of hydrogen with the glass walls, and between H_2 and D_2 by analysis of the macroscopic composition of the gas mixtures after irradiation. This analysis was performed, again after gas chromatographic separation as already described, by detection of the hydrogen peaks with either a microcombustion tube plus thermal conductivity detector, or with an ionization detector using helium carrier gas. At −160° C, the order of elution is para-H_2, ortho-H_2, HD, and D_2, all in clean peaks. Less than 5% HD and no measurable deviations from the original H/D ratios were observed, indicating that the measured HT/DT ratios have not been materially altered by exchange reactions.

The isotopic ratios from a number of samples are shown in Table I.

TABLE I. HT/DT ratios in recoil tritium reactions with mixtures of gaseous H_2 and D_2.

Sample gas pressures (cm. Hg)				Obs ratio	Specific activity ratio
He^3	H_2	D_2	Other	HT/DT	HT/DT
1.5	28.5	32.1		1.33	1.49
1.5	14.5	31.9		0.72	1.58
1.7	12.0	58.1		0.35	1.68
1.7	39.6	31.0		1.97	1.55
1.7	61.2	9.0		9.93	1.45
1.0	30.4	32.1	4.3 NO	2.65	2.79
1.0	26.3	27.7	6.3 O_2	2.45	2.58

The isotopic preference for reaction with H_2 rather than D_2 is 1.55±0.06 for the runs in Table I in the absence of a free radical scavenger. The results are not yet accurate enough to indicate whether the observed ratios show any variation with composition. The observed HT/DT yields are clearly higher in the presence of the free radical scavengers, but the total radioactivity yield as molecular hydrogen is somewhat less. From other results in our laboratory, one can estimate that much of the recoil tritium in the oxygen run originally reacted with O_2; possible contributions to the observed HT and DT yields from secondary reactions cannot be accurately estimated for the scavenger runs. Since the presumed role of O_2 or NO is to compete especially well for those tritium atoms that reach lower energies without forming a chemical bond, the inference is strong that higher energy tritium atoms show the greater isotopic preference for reaction with H_2 rather than D_2.

The experimental ratio of the rate constants for the thermal reactions of H atoms with H_2 and D_2 is 1.8, and for D atoms with H_2 and D_2 is 1.7, all rates being measured at 1000°K.[3] These measurements, however, are based on reactions in temperature equilibrium, and cannot be compared directly with the reactions of the recoil atoms. The energetic tritium atoms usually react before attaining thermal energies and can be considered as a special case of a nonequilibrium kinetic process: the reaction of an atom of fixed velocity in a Maxwellian gas. The initial tritium velocity is fixed high enough that chemical reaction does not occur on collision, and then the velocity is degraded in successive collisions until reaction to form either HT or DT occurs. The calculation of collision frequencies for such a molecule as a function of the fixed velocity has been treated by Kennard[4]—assuming equal cross sections, the relative collision frequency with H_2 and D_2 in an equimolar mixture varies from 1.00 at high tritium atom velocity to 1.41 at very low tritium velocity. For a tritium atom of $\geq$1 ev kinetic energy in a Maxwellian gas of H_2 and D_2 at 300°K, the relative collision frequency is 1.0.

Another gas kinetic factor that must be considered here is the inequality in the fraction of energy available as internal energy for equal tritium velocity, because of differences in the motion of the center of mass. The maximum fraction of kinetic energy available as internal energy is 0.86 for D_2 and 0.60 for H_2. A lower internal energy should allow isotopic effects to show up more readily in the decomposition of a D_2T or H_2T complex, once formed, and should lead to a preferential formation of HT over DT.

The individual contribution of these and other factors remains to be established since the actual energy range of the tritium atom at the time of reaction to form HT or DT is still unknown. However, it seems to us that the recoil reactions of tritium atoms with molecular hydrogen can more profitably be examined as high energy extrapolations of ordinary kinetics, rather than through special "hot atom" mechanisms.

* Work supported by contract with the Geophysics Directorate of the U. S. Air Force.

[1] W. G. Brown and J. L. Garnett, Intern. J. Appl. Radiation and Isotopes **5**, 114 (1959).

[2] R. Wolfgang and F. S. Rowland, Anal. Chem. **30**, 903 (1958). The separation conditions are very similar to those used in separation and assay of HT and T_2 [P. Gant and K. Yang, Science **129**, 1548 (1959)].

[3] See R. Weston, J. Chem. Phys. **31**, 892 (1959); and G. Careri, Advances in Chem. Phys. **1**, 119 (1958).

[4] E. H. Kennard, *Kinetic Theory of Gases* (McGraw-Hill Book Company, Inc., New York, 1938), p. 107.

Infrared Studies of Crystal Benzene. III. Assignment of 705 cm^{-1} Band and Crystal Splitting of ν_{11}

WILLIS B. PERSON AND DOUGLAS A. OLSEN

Department of Chemistry, State University of Iowa, Iowa City, Iowa

(Received December 30, 1959)

THE assignment of the 705 cm^{-1} band in the infrared spectrum of crystal benzene[1-3] has been a real puzzle for a number of years. Recently Hexter and Dows[4] have explained this band as a combination between the very strong A_{2u} fundamental ν_{11} at 687 cm^{-1} and a low-frequency lattice rotational mode at 18 cm^{-1}. Since no other explanation has been suggested for this band, this assignment has, as yet, gone unchallenged by other spectroscopists.[3,5] However, Cruickshank[6] has recently questioned this assignment on the basis of the temperature factor found in x-ray diffraction studies.

As part of a study of the spectrum of crystal benzene underway in our laboratory,[3,5] we had begun a survey of the spectrum of benzene in a mixed crystal with benzene-d_6. We studied this region of the benzene spectrum in a crystal of 1 C_6H_6:10C_6D_6. At this ratio each benzene molecule in the crystal is, on the average, surrounded only by benzene-d_6 molecules. Thus the correlation-field coupling will be completely removed.[7,8]

The experimental techniques have been described earlier.[3,5] We used a modified Perkin-Elmer Model 12c spectrometer with a KBr prism. The cold cell was equipped with KBr windows except for the CsBr window on the cooling block. The spectra obtained in this region are shown in Fig. 1. This clearly indicates that the 705 and 687 cm^{-1} bands are components of

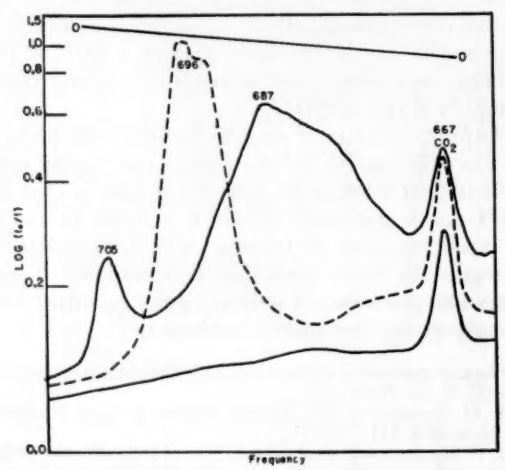

FIG. 1. The spectrum of ν_{11} in the benzene crystal and in a mixed crystal of 1 C_6H_6:10 C_6D_6. ——— pure benzene. - - - - benzene in the mixed crystal. These spectra are traced from the recorder chart, with the pertinent wave numbers in cm^{-1} shown on the drawing.

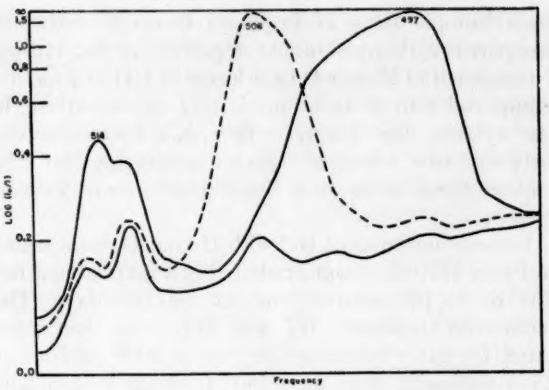

FIG. 2. The spectrum of ν_{11} in the benzene-d_6 crystal and in a mixed crystal of 1 C_6D_6:1 C_6H_6. ——— pure benzene-d_6. - - - - benzene-d_6 in the mixed crystal. These spectra are traced from the recorder chart with the pertinent wave numbers in cm^{-1} shown on the drawing.

a correlation-field doublet. The doublet structure has almost completely collapsed in the mixed crystal to give a singlet at 696 cm^{-1}, just as expected.[7,8] The relative intensities of the components of this correlation doublet are quite unusual; the 687 cm^{-1} component is about 10 times as intense as the 705 cm^{-1} component.[3] This unusual intensity ratio has undoubtedly been the factor which has led spectroscopists astray for so long. The polarization studies of Zwerdling and Halford[2] showed clearly that the 705 cm^{-1} band is polarized in the *c* direction and that at least part of the 687 cm^{-1} band is polarized in the *a* direction. It is true that the 687 cm^{-1} band also shows strong absorption in the *c* direction. However, it seems quite possible that their crystal may not have been as perfect as they had expected. These polarization results and the intensity ratio are difficult to explain under the new assignment, but it would seem that this difficulty is not great enough to suggest that it is wrong.

On discovering this surprising result, we decided to study the complementary solution of 1 C_6D_6:10 C_6H_6. The results are shown in Fig. 2 for the analogous pair of bands at 514 and 497 cm^{-1} in the C_6D_6 crystal.[9] As before, this doublet is replaced by a singlet coming at the mean of the two frequencies at 506 cm^{-1}, thus proving that these also form a correlation doublet.

In conclusion, the new assignment of the 705 cm^{-1} band in the spectrum of crystal benzene as a member of the correlation doublet of ν_{11} makes it unnecessary to postulate the existence of a low-frequency rotational mode at 17 cm^{-1}. This should make it easier to bring the calculated temperature factor into agreement with that observed in the x-ray diffraction studies.[6] Finally it should be noted that the correlation-field splitting of ν_{11} (18 cm^{-1}) is the largest splitting of this type to be observed in the crystal spectrum of benzene.[3,5]

Financial support from the Office of Ordnance Research, U. S. Army, is gratefully acknowledged. It

is a pleasure to acknowledge the discussion and correspondence with Dr. R. M. Hexter and Professor D. A. Dows.

[1] R. D. Mair and D. F. Hornig, J. Chem. Phys. **17**, 1236 (1949).
[2] S. Zwerdling and R. S. Halford, J. Chem. Phys. **23**, 2221 (1955).
[3] C. A. Swenson and W. B. Person, J. Chem. Phys. (to be published).
[4] R. M. Hexter and D. A. Dows, J. Chem. Phys. **25**, 504 (1956).
[5] C. A. Swenson, W. B. Person, D. A. Dows, and R. M. Hexter, J. Chem. Phys. **31**, 1324 (1959).
[6] D. W. J. Cruickshank, Revs. Modern Phys. **30**, 163 (1958).
[7] H. J. Hrostowski and G. C. Pimentel, J. Chem. Phys. **19**, 661 (1951).
[8] G. L. Hiebert and D. F. Hornig, J. Chem. Phys. **20**, 918 (1952).
[9] D. A. Olsen, Ph.D. thesis, State University of Iowa (1960).

Closed Crucible—A New Technique in High Temperature Chemistry. Its Application to Tantalum and Molybdenum Oxides

E. David Cater, Ernest R. Plante, and Paul W. Gilles

Department of Chemistry, University of Kansas, Lawrence, Kansas

(Received December 2, 1959)

MOST vapor pressure measurements at high temperatures employ the Knudsen effusion method. Despite its efficacy, the method has numerous pitfalls and difficulties, and it is unable to provide answers to all the questions that may arise in the course of a vaporization study.

A new type of experiment has been conceived and employed to help characterize vaporizing systems and to indicate the reliability of effusion measurements. The purposes of this report are to describe this type of experiment, to suggest some of its uses, and to present some results on the Ta–O and Mo–O systems that demonstrate its effectiveness.

In the experiment the desired sample, contained in a closed crucible rather than in one fitted with an orifice, is heated in vacuum to an appropriate temperature for an extended time. There are alternatives or modifications involving at least four pairs of conditions: (1) the crucible may be inert or reactive; (2) it may be isothermal, or there may be a temperature gradient; (3) it may be welded, or it may be fitted with a tight but removable lid, and (4) the sample may or may not be isotopically enriched for mass spectrographic or radiochemical analysis.

It might seem that permanent gases could not be removed during evacuation, but it has been our experience that crucibles with close fitting lids are not entirely closed. Suitable techniques for welding crucibles in vacuum could be devised, if desirable.

Some of the information that can be obtained from such an experiment follows. (1) Reaction between a sample and its crucible that would invalidate effusion measurements can be revealed by inspection or analysis following a prolonged heating of intimate mixtures of the sample and crucible substances. The closed crucible will prevent evaporation loss that could make this compatibility experiment impossible in an open crucible.

(2) The leaking of a liquid or the diffusion of a sample through the crucible walls that could render effusion studies involving weight loss measurements unreliable is readily indicated by a weight loss greater than that arising from the evaporation of the crucible material itself.

(3) If diffusion occurs, diffusion coefficients of the sample substance through the crucible material may be obtained approximately from the measured transport and reasonable assumptions about the concentration gradient. Self-diffusion coefficients could be measured if the sample were an isotopically enriched specimen of crucible material.

(4) If the sample does escape through the crucible, and if the heating is prolonged to dryness, the initial sample weight and total weight loss corrected for volatility of the crucible material may be used to calculate the average composition of the gases evaporating from the exterior of the crucible. This technique is much the same as that of Ackermann and Thorn[1] who used an effusion crucible. We have performed experiments with Ta_2O_5 in a closed Ta crucible, observing rapid transport of material through the wall at temperatures above the melting point of Ta_2O_5. At 2172°C all the oxygen escaped through the parts of the crucible in contact with liquid, leaving some sintered tantalum powder inside and an etched appearance on the exterior surface, and carrying away excess tantalum to give the ratio O/Ta=1.60 for the transported matter. The gaseous species in the Ta–O system have been identified mass spectrometrically as TaO and TaO_2 by Inghram *et al.*[2] Extrapolation of their data to 2172°C gives TaO_2/TaO=1.9 with an estimated uncertainty of a factor of 2.5, a value in agreement with the value 1.50 calculated from our O/Ta ratio.

(5) The experiment may be useful for the identification of migrating species, especially if tracers are used. The tantalum residue in the crucible indicates that either oxygen or a lower oxide migrates. Use of a sample of Ta_2O_5 enriched in one of the tantalum isotopes could enable a choice between these hypotheses by analysis of the crucible surface and the evaporated material.

(6) A nonisothermal experiment provides a sensitive test for the existence of two or more important gaseous species. Experiments with MoO_2 in a Mo crucible have shown that a lid cooler than the crucible gains weight because of MoO_2 deposition, but a hotter lid loses weight because of the reaction,

$$2\,MoO_3(g)+Mo(s)=3\,MoO_2(g), \qquad (1)$$

which occurs on the lid. Such transport can happen only if two or more gases are present. Burns, DeMaria, and Drowart[3] have recently observed these species over Mo–MoO_2. This experiment shows similarity to the

"iodide" process of metal purification and to the transport experiments of Schäfer and co-workers.[4]

(7) Thermodynamic information can be obtained from the same nonisothermal experiment. Even though effusion measurements in the Mo–MoO_2 system are difficult because of orifice clogging with a cool lid or disturbance of the MoO_2/MoO_3 ratio with a warm lid, the direction of transport indicates that reaction (1) is endothermic.

(8) Finally, the experiment may be used as a method of preparing crystals for x ray diffraction investigation. Twinned crystals of MoO_2 have been deposited in a cold orifice, and it is possible that single crystals could be obtained with carefully controlled conditions in a closed crucible.

We believe that the potentialities of the closed crucible technique are sufficiently great that it should be considered in any high temperature evaporation study.

We are pleased to acknowledge the support of the U.S. Atomic Energy Commission in this work.

[1] R. J. Ackermann and R. J. Thorn, Intern. Congr. Pure and Appl. Chem., 16th Congr., Inorganic Chem. Sec. 667 (1957).
[2] M. G. Inghram, W. A. Chupka, and J. Berkowitz, J. Chem. Phys. **27**, 569 (1957).
[3] See M. G. Inghram, International Symposium on High Temperature Technology, Stanford Research Institute (October, 1959).
[3] See M. G. Inghram and J. Drowart, *Proceedings of an International Symposium on High Temperature Technology*, Stanford Research Institute, Menlo Park, California. (Distributed by McGraw-Hill Book Company, New York, 1960), p. 219.
[4] H. Schäfer and K. Etzel, Z. anorg. u. allgem. Chem. **291**, 294 (1957); and earlier papers.

Stark Effect and Dipole Moment of CH_3CHF_2*

GEORGE H. KWEI† AND DUDLEY R. HERSCHBACH†

Mallinckrodt Chemical Laboratory, Harvard University, Cambridge, Massachusetts

(Received December 23, 1959)

IN the spectra of asymmetric rotor molecules, large deviations from a quadratic Stark effect can occur if the Stark perturbation terms connect pairs of nearly degenerate levels. This situation is expected for a molecule such as CH_3CHF_2, as it is a near *oblate* rotor with a large dipole component along the principal axis of least inertia (the *prolate*, or "*a* axis"). Severe nonquadratic perturbations were noticed in previous microwave studies,[1] but no analysis was attempted. We have measured nonquadratic Stark effects for the $M=1$, $J=1\rightarrow2$, "*a*-type" transitions, and also quadratic shifts which occur for the corresponding $M=0$ lines. The two types of transitions provided two independent determinations of the dipole moment and these agreed within experimental error. The values obtained for the principal axis components are $\mu_a=2.01\pm0.01$ debye and $\mu_c=1.12\pm0.03$ debye; the total dipole moment is $\mu=2.30\pm0.03$ debye and makes an angle of 46.3° with the C—C bond.

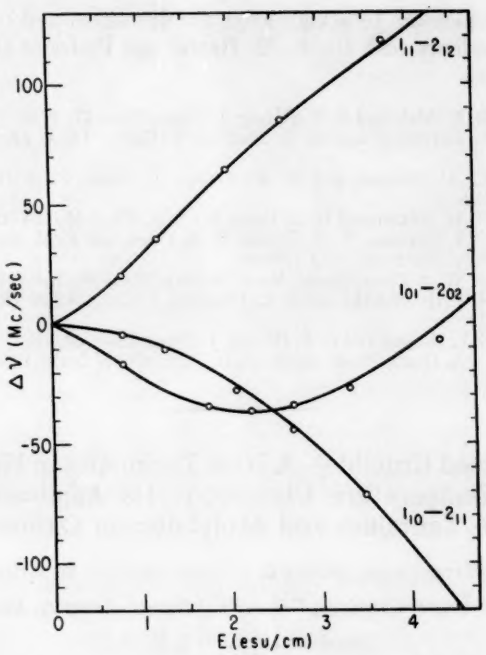

FIG. 1. Stark displacements of $M=1$ components.

The Stark shifts of the $M=1$ transitions are extremely rapid (see Fig. 1). The $1_{10}\rightarrow2_{11}$ transition is not far from quadratic, whereas the $1_{11}\rightarrow2_{12}$ line shows the approximately linear field dependence typical of near degeneracy. The boomerang-like trajectory of the $1_{01}\rightarrow2_{02}$ line corresponds very roughly to the difference in the shifts of the other two lines. The intensity of the $1_{01}\rightarrow2_{02}$ line grows by a factor of two during the outward journey, then fades quickly as the line returns to the vicinity of the zero-field line.

These extremely strong perturbations are satisfactorily accounted for by a slight extension of the treatment of Golden and Wilson.[2] The calculated curves are shown in Fig. 1. The special feature is that in the presence of large perturbations by *both* μ_a and μ_c the effective degeneracy of the zero-field rotational levels becomes quite high. Even for nonquadratic cases the Hamiltonian matrix for the rotational energy and Stark perturbation[2] can usually be factored in good approximation into blocks no larger than 2×2. In CH_3CHF_2, however, over most of the range of field values used all three of the $J=1$ rotational levels and all five of the $J=2$ levels must be treated as if they were degenerate. Application of a Van Vleck transformation[2] uncouples the blocks of different J to a sufficiently good approximation. The secular equations for each block may be expanded in polynomial form and solved by standard techniques. Another procedure is much more convenient for CH_3CHF_2 and can be applied in several other likely cases of highly degenerate Stark

TABLE I. Stark coefficients for $M=0$ transitions.[a]

Transition	$\Delta\nu/E^2$[Mc/(esu/cm)^2] Obs	Calc
1_{10}–2_{11}	0.443±0.01	0.433
1_{11}–2_{12}	1.008±0.01	0.999
1_{01}–2_{02}	−0.987±0.01	−0.996

[a] The Stark effect of OCS was used for the field calibration, with $\mu_{OCS}=0.7124$ debye.

effects.‡ As the important nondiagonal elements within each J block are just one step off the diagonal (the contributions from others may be incorporated into the diagonal elements as in the usual perturbation treatment[2]), the secular equations may be expanded in continued fraction form.[3] This is a considerable advantage when calculations are to be made for a range of field values and dipole components, because of the simple way the matrix elements enter into the continued fraction. Convergence difficulties do not arise unless the spacing of adjacent levels is extremely small; for the low J levels of asymmetric rotor molecules, this situation seldom occurs for more than a single pair of levels, so that the continued fraction treatment can be carried through until the size of the secular equation is reduced to 2×2.

Table I gives the Stark coefficients for the $M=0$ transitions, which are nicely quadratic and could be analyzed by the usual method.[2]

The deviation of the dipole moments of halogenated alkanes from the simple bond moment model is a favorite example of inductive effects.[4] Several treatments have been developed which approximate the inductive contributions by considering bond polarizabilities in addition to bond dipoles.[4,5] The model and parameters used by Smith *et al.*[5] to correlate the extensive data on other halogenated alkanes gives for CH_3CHF_2 a dipole moment of 2.33 debye oriented 43° from the C—C bond, in close agreement with the experimental results.

* The research reported in this paper was supported by a grant extended Harvard University by the Office of Naval Research under contract and by a grant from the California Research Corporation.

† Present address: Department of Chemistry, University of California, Berkeley 4, California.

[1] N. Solimene and B. P. Dailey, J. Chem. Phys. **22**, 2042 (1954); D. R. Herschbach, *ibid.* **25**, 358 (1956).

[2] S. Golden and E. B. Wilson, Jr., J. Chem. Phys. **16**, 669 (1948). The line strengths used were those tabulated by R. H. Schwendeman and V. W. Laurie, *Line Strengths of Rotational Transitions* (Pergamon Press, New York, 1958).

‡ For example, these will frequently occur for molecules which are nearly spherical tops, such as SO_2F_2, whose Stark effect has been studied by D. R. Lide, Jr., D. E. Mann, and R. M. Fristrom, J. Chem. Phys. **26**, 734 (1957).

[3] A continued fraction treatment due to W. E. Lamb of the Stark effect in a diatomic molecule is described by N. F. Ramsey, *Molecular Beams* (Clarendon Press, Oxford, 1956), p. 292.

[4] C. P. Smyth, *Dielectric Behavior and Structure* (McGraw-Hill Book Company, Inc., New York, 1955), pp. 235–239, 268–274.

[5] Smith, Ree, Magee, and Eyring, J. Am. Chem. Soc. **73**, 2263 (1951); R. P. Smith and E. M. Mortensen, *ibid.* **78**, 3932 (1956).

On Twisted Organic Crystals

A. L. MCCLELLAN

California Research Corporation, Richmond, California

(Received November 9, 1959)

IN a recent note Sears[1] describes twisted fibers of LiF and explains their shape in terms of equations due to Eshelby.[2,3] This letter reports the result of similar calculations for some micro-crystals of soap from lubricating grease, such as illustrated in Figs. 1 and 2. Two forms occur. Helicoid (or twisted ribbon) as in the Fig. 1 and true helix or two-strand "rope" as in Fig. 2. As examples, lithium-12-hydroxystearate often forms the first type and hydrated mixtures of calcium oleate and calcium stearate the second.

Measurements on 20 separate fibers of each kind give data which yield calculated Burger's vector (b) values. For helicoids b varies from 80 to 1600 A (corresponding roughly to about 0.8 to 16 unit cell lengths) with fairly even distribution throughout the length range. For ropelike crystals, on the other hand, five b values out of the 20 are larger than 200 A while 15 are between 80 and 200 A. These latter values of b represent one or two repeats of the unit cell.

FIG. 1. Electron micrograph of helicoid fiber of lithium 12-hydroxystearate grown in hydrocarbon, hexane washed, U shadowed, 8000 ×.

FIG. 2. Electron micrograph of helical fiber of hydrated mixed calcium oleate-calcium stearate prepared as in Fig. 1.

A value of b approximating a few multiples of molecular length is reasonable and in general agreement with electron micrographs of paraffin crystals[4] and stearic acid[5] which show step heights of the same magnitude. Probably the basic disruption of the lattice is by a single molecular length with higher steps caused by dislocations of multiple strength. In spite of the large value of b, the crystals do not have a hollow center. A similar fact was noted by Dawson and explained by Frank.[6]

Another point of agreement with Eshelby's equation is the variation of fiber twist with fiber width. As predicted, the pitch is greatest for the narrow portions of the crystal. This effect can be seen in Fig. 1 at the ends of the large, diagonally placed spiral.

It is further of interest to note that lithium-12-hydroxystearate crystals show this twisted shape when the common method of washing the oil out with a liquid solvent is used. When the oil is replaced by a series of successively lighter solvents and the last removed as a gas above its critical point, the fibers are not twisted.[7]

[1] G. W. Sears, J. Chem. Phys. **31**, 53–4 (1959).
[2] J. D. Eshelby, J. Appl. Phys. **24**, 176 (1953).
[3] J. D. Eshelby, Phil. Mag. **3**, 440 (1958).
[4] See, for instance, I. M. Dawson and V. Vand, Proc. Roy. Soc. (London) **A206**, 555–62 (1951) and A. R. Verma, *Crystal Growth and Dislocations* (Academic Press, Inc., New York, 1953), Chaps. 5 and 8.
[5] A. R. Verma and P. M. Reynolds, Proc. Phys. Soc. **B66**, 414 (1953).
[6] F. C. Frank, Acta Crystallographica **4**, 497–501 (1951).
[7] A. L. McClellan and J. Cortes, NLGI Spokesman **20**, No. 6, 12–16 (1956).

Proton NMR Spectra of the N,N-Dimethylformamide, N-Methylformamide, and N,N-Dimethylacetamide

VALDEMAR J. KOWALEWSKI* AND DORA G. DE KOWALEWSKI
Institute of Physics, University of Uppsala, Sweden

(Received June 26, 1959)

THE NMR proton spectrum of the N,N-dimethylformamide has been reported[1,2] to consist of one resonance line corresponding to the formyl hydrogen and two methyl resonances corresponding to the nonequivalent methyl groups.

We observed a further splitting in both peaks corresponding to different values of J couplings between the formyl hydrogen and the two methyl groups. These long-range interactions are observed at about the highest resolution obtainable using a Varian instrument at 40 Mc.

The methyl spectrum of the N,N-dimethylformamide with 30% water is shown in Fig. 1. From a series of several measurements, the two splittings were found to be 0.8 cps for the higher field methyl group and 0.5 cps for the lower field one. With water, the lines are sharper, allowing a better determination of the splittings.

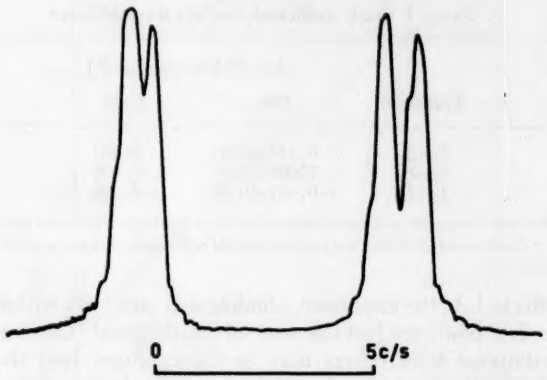

FIG. 1. NMR spectrum of the two methyl groups of the N–N-dimethylformamide, split by the C hydrogen. The field increases from left to right.

The methyl spectrum of the N,N-dimethylacetamide consists of two peaks due to the nonequivalence of the N-methyl groups and a single, rather broad line due to the C-methyl hydrogens. The NCH_3 peak shifted toward higher field is a quadruplet with a splitting of 0.5 cps due to the interaction with the C-methyl group. The interaction with the low field N-methyl group is too small to be resolved. These values agree with the corresponding ones of N-methylacetamide.[6]

The spectrum due to the methyl hydrogens of the N-methylformamide is a quadruplet (Fig. 2) with two narrow lines 4.1 cps apart and two broader lines 0.9 cps on each side of the central ones. Complete analysis of the spectrum in the ABX_3 approximation[3] was not possible because the NH signal was not observed and the octuplet corresponding to the CH appears as one line of about 3 cps half width without fine structure. An analysis of the behavior of the X_3 group at different frequencies[4] shows, like in the ABX case,[5] that the lines corresponding to transitions between pure states have a

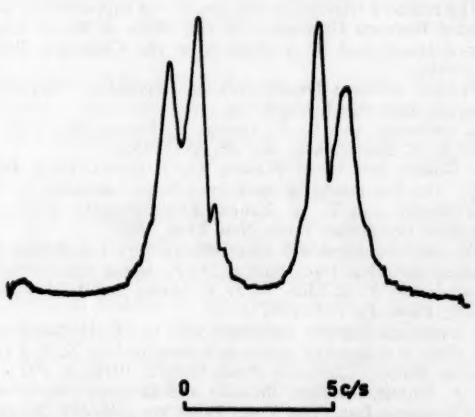

FIG. 2. Quadruplet due to the methyl hydrogens of the N-methylformamide, split by the C and N hydrogens.

separation equal to $|J_{AX}+J_{BX}|$ which is field independent and that at sufficiently high fields these lines lie outside the other ones if both J couplings are of the same sign and inside if they have opposite signs.

A study of the N-methylformamide at 60, 40, and 25 Mc. shows that both couplings are of different signs and that already at 40 Mc we can apply first order theory. This gives $J_{AX}=\mp 0.9$ cps and $J_{BX}=\pm 5.0$ cps. This last value is consistent with the one found in substances of similar structure like N-methylacetamide (5.1 cps[6]), N-ethylacetamide (5.6 cps[7]), and formylgycine (5.9 cps[7]).

As, according to infrared data,[8,9] the N-methylformamide has, at room temperatures, its formyl hydrogen trans to the NCH_3, the attribution of the 0.8 cps splitting of the N,N-dimethylformamide, the 0.5 cps of the N,N-dimethylacetamide, and 0.9 cps for the N-methylformamide to the trans coupling is consistent with the larger trans and smaller cis absolute values of J couplings observed for the C—N bond in the formamide[10] and similar to the C=C case.

We may conclude that in the dimethylamide compounds the N-methyl peak located towards higher fields should be assigned to the cis location relative to the carbonyl.

The authors wish to express their thanks to Professor K. Siegbahn for all facilities put at their disposal, to Professor R. Freyman for having run the spectra at 25 Mc and to Dr. R. Hoffman for helpful comments during the work.

* On leave of absence from Instituto de Física, Facultad de Ciencias Exactas, Universidad de Buenos Aires, Argentina.

[1] H. S. Gutowsky and C. H. Holm, J. Chem. Phys. **25**, 1228 (1956).
[2] W. D. Phillips, Ann. N. Y. Acad. Sci. **70**, 817 (1958).
[3] R. W. Fessenden and J. S. Waugh, J. Chem. Phys. **30**, 944 (1959).
[4] V. J. Kowalewski and D. G. de Kowalewski (to be published).
[5] Pople, Schneider, and Bernstein, *High Resolution Nuclear Magnetic Resonance* (McGraw-Hill Book Company, Inc., New York, 1959).
[6] Berger, Loewenstein, and Meiboom, J. Am. Chem. Soc. **81**, 62 (1959).
[7] V. J. Kowalewski (unpublished data).
[8] R. Lumley Jones, J. Mol. Spectroscopy **2**, 581 (1958).
[9] Mizushima, Shimanouchi, and Nagakura, J. Am. Chem. Soc. **72**, 3490 (1950).
[10] Piette, Ray, and Ogg, J. Mol. Spectroscopy **2**, 66 (1958).

Source of Green Bands from Boron-Containing Flames

W. E. Kaskan and R. C. Millikan
General Electric Research Laboratory, Schenectady, New York

(Received December 9, 1959)

In a study of gases from flames containing trimethyl borate, stabilized on flat porous metal burners, evidence has been obtained which contradicts the assignment of the "fluctuation" bands[1] to $B_2O_3(g)$.[2,3] The purpose of this Letter is to discuss this evidence and to point out that the data are consistent with the bands being due to the molecule BO_2. The existence of BO_2 does not appear to have been previously suggested.

The system and techniques were similar to those previously described.[4] Measurements were made of: infrared emission of HBO_2 (2040 cm^{-1}); absorption of one of the stronger of the fluctuation bands with a center at approximately 5470 A; and the concentration of OH by absorption; all as a function of distance (and, therefore, time) from the burner surface for a number of flames.

The behavior of OH was similar to that in flames not containing boron.[4] The OH concentration was highest, and in excess of equilibrium, nearest the flame, and it decayed downstream at essentially the same rate as in the absence of boron. The HBO_2 emission was high at the flame zone and rose only a few percent to an asymptotic value as the gas passed downstream. For a typical pair of flames, one lean and one rich, both at nearly the same temperature (1800°K±50°) the ratio of the asymptotic HBO_2 intensities was within experimental error equal to the ratio of the concentrations of HBO_2 at equilibrium, according to recent thermodynamic data.[5] Thus, HBO_2 was probably formed in the flame at nearly the equilibrium amount.

In contrast, the absorptivity at 5470 A in the lean flame was a maximum near the flame zone, and decreased to about 40% of this value 15 mm from the flame. In the rich flame it started at about the downstream value of the lean flame and decayed rapidly to an unobservably small value 10 mm from the flame. The calculated equilibrium $(B_2O_3)(g)$ was about 3% of the total boron for both flames.[5] If the 5470 A transition arises from $B_2O_3(g)$, then the far downstream absorptivity in the rich flame most nearly represents this equilibrium concentration of B_2O_3. However, the 50-fold difference between the far downstream 5470 A absorptivity in the rich flame and the maximum in the lean flame would mean that all of the boron was in the form of $B_2O_3(g)$ near the flame zone of the lean flame. This is inconsistent with the apparently reliable infrared data, which indicates that about 90% of the boron was in HBO_2 at this point. Thus we conclude that the 5470 band does not come from $B_2O_3(g)$.

Further investigation showed that in any flame, lean or rich, the 5470 absorptivity was always proportional to the OH concentration, and both decayed together. Thus, the unknown boron compound responsible for the green emission is involved in an equilibrated reaction with the free radicals present. Although there may be other ways to explain this, it appears that the simplest and most reasonable possibility is to postulate the existence of the molecule BO_2, which is equilibrated with OH via the rapid, approximately thermo-

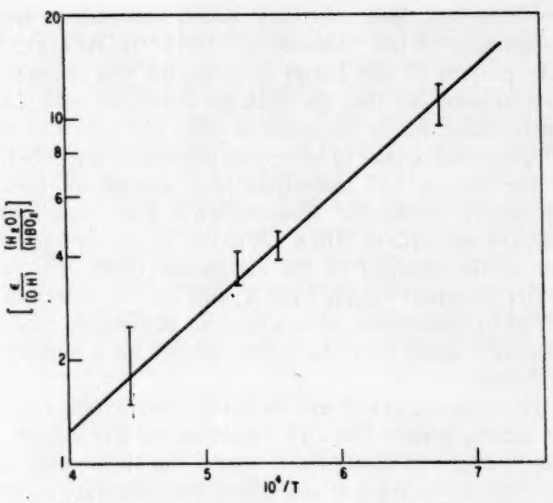

FIG. 1. Plot of logarithm of a quantity which is proportional to the equilibrium constant of reaction (1) against reciprocal temperature. ϵ is the absorptivity at the center of the 5470 A band as determined by using slits of 10 A band pass centered at 5470; (OH) is the concentration of hydroxyl measured at the same level above the burner as ϵ; (H_2O) and (HBO_2) are the computed equilibrium values, cf. reference 5.

neutral reaction,

$$OH+HOBO \rightleftharpoons HOH+OBO \qquad (1)$$

with BO_2 being the source of the fluctuation bands. This reaction would, in any case, appear to be a reasonable reaction to postulate, since it involves only the rupture of one O—H bond and the formation of another.

To further test the consistency of this idea, the temperature dependence of the equilibrium constant for reaction (1) was investigated and is shown in Fig. 1. Here each temperature corresponds to a single flame and the vertical heights of the data points indicate the spread in $\epsilon/(OH)$ where ϵ is the absorptivity at 5470 A. The assumption is made that ϵ is proportional to the concentration of BO_2. Errors in T are not indicated but may be 50°C. It can be seen that the data are consistent with a ΔH for reaction (1) of -16 kcal/mole. This gives a value of about 100 kcal/mole for the strength of the O—H bond in HBO_2, an entirely reasonable value.

In summary, the fluctuation bands characteristic of boron-containing flames almost certainly do not arise from $B_2O_3(g)$, but may have their origin in the free radical BO_2.

[1] R. W. B. Pearse and A. G. Gaydon, *The Identification of Molecular Spectra* (John Wiley & Sons, Inc., New York, 1950), 2nd ed., p. 60.
[2] J. R. Soulen, P. Sthapitanonda, and J. L. Margrave, J. Phys. Chem. **59**, 132 (1955).
[3] J. R. Soulen and J. L. Margrave, J. Am. Chem. Soc. **78**, 2911 (1956).
[4] W. E. Kaskan, Combustion & Flame **2**, 229, 286 (1958).
[5] D. White, P. N. Walsh, D. E. Mann, and A. Sommer, Ohio State University Research Foundation Tech. Rept. 4, R. F. Project 691 (July, 1959).

Spin Coupling between Protons of Different Rings in Aromatic Compounds

F. A. L. ANET

Department of Chemistry, University of Ottawa, Ottawa, Canada

(Received December 28, 1959)

INDIRECT spin-spin coupling does not appear to have been observed in polycyclic aromatic compounds between protons attached to different rings[1] and has often been assumed to be negligible.[2] We now wish to report two examples where such coupling is shown to occur. This observation is of interest in view of attempts to obtain coupling constants from theoretical calculations.[3–5] The compounds examined were 5,7-dichloroquinoline and 5,7-dimethylquinoline. The NMR spectra (Fig. 1) were taken on 10 to 20% solutions in carbon tetrachloride containing tetramethylsilane for reference, and were measured on a Varian

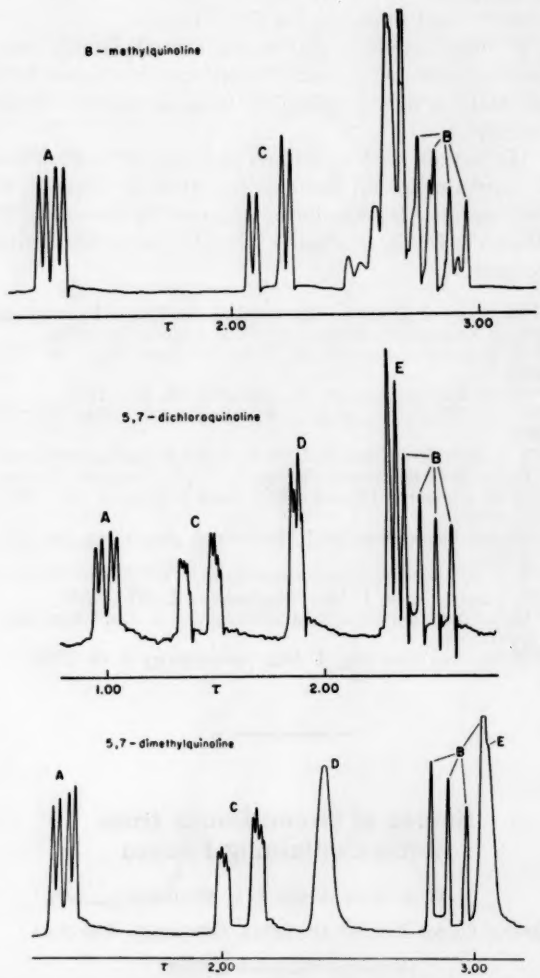

FIG. 1. Proton NMR spectra of quinoline derivatives. The methyl group resonances of 8-methylquinoline and 5,7-dimethylquinoline are not included.

TABLE I. Chemical shifts[a] (τ in ppm) and coupling constants (J in cps, signs indeterminate) for quinoline derivatives.

Compound	τ_2	τ_3	τ_4	τ_6	τ_8	τ_{methyl}	J_{23}	J_{34}	J_{24}	J_{48}	J_{68}
8-methylquinoline[b]	1.28	2.88	2.18			7.23	4.1	7.9	1.8		
5,7-dichloroquinoline[c]	1.18	2.66	1.61	2.50	2.05		4.2	8.5	1.6	0.8	2.0
5,7-dimethylquinoline[d]	1.38	2.95	2.09	3.08	2.43	7.65 7.57	3.9	8.6	1.7	0.8	

[a] $\tau = 10 - 10^6 \times [H_{SiMe_4} - H_{obs}) / H_{SiMe_4}]$ [Tiers, J. Phys. Chem. **62**, 1151 (1958)].
[b] Eastman Kodak White Label.
[c] Prepared according to A. Claus and A. Ammelburg [J. prakt. Chem. **51**, 415 (1895)].
[d] Sample kindly donated by Dr. L. Marion.

Model V-4302 spectrometer in the usual way. Fortunately, in the two compounds examined, hydrogens which are coupled together are sufficiently well chemically shifted that analysis of the spectra can be carried out by a first-order treatment.

The spectra of quinoline and certain derivatives have been discussed by Pople *et al.*[1] On the basis of their work and of our observations on other quinoline derivatives the following assignments may be made for the spectra of Fig. 1. In each case, the quartets *A* and *B* are due to the 2- and the 3-hydrogen, respectively. From these two signals the values of the coupling constants J_{24} and J_{34} were found and these must be the spacings of the band, which should be a quartet, due to 4-hydrogen. Band *C* is the only one which has these spacings; however, it is an octet having an additional spacing, and this must mean that the 4-hydrogen is coupled to the 2- and 3-hydrogens and to one other hydrogen. Since there are no other hydrogens in the pyridine ring there must be coupling between hydrogens in different rings. In the case of the dimethyl compound it is not possible to find directly whether this is the 6- or the 8-hydrogen as the bands of these hydrogens are broad and without observable structure, obviously due to unresolved coupling with the methyl groups. However, in the dichloro compound this complication is absent.

The band *D* may be assigned to the 8-hydrogen and the band *E* to the 6-hydrogen. Although these assignments are not rigorously proven they are consistent with the effect[1] of chlorine and methyl substituents on aromatic rings and the fact that the 8-hydrogen of quinoline is at much lower field than the 6-hydrogen. If these assignments are correct, then, at least in the dichloro compound, it is the 8-hydrogen only which is coupled with the 4-hydrogen as band *D* is a quartet whereas *E* is a doublet. That the 4-hydrogen is not coupled to the 5-, 6-, or 7-hydrogen is shown by the spectrum of 8-methylquinoline (Fig. 1), in which the 4-hydrogen is just a quartet.

The values of the various coupling constants and chemical shifts are given in Table I. Although no detailed study was carried out on the concentration dependence of the chemical shifts, it was observed that the position of some bands changed, especially at very high concentrations. Thus, in pure 5,7-dimethylquinoline, the signals of the 4- and 8-hydrogens overlapped while the signals of the 3- and 6-hydrogens were now well separated.

The values of 1:2 and 1:3 coupling constants are normal.[1] The inter-ring coupling constant (J_{48}) has the value of 0.8 cps. in both compounds studied. This value is comparable to the coupling between hydrogens separated by five bonds in *trans-trans-* and *cis-cis-*dimethyl muconate[7] ($J\alpha\delta$, 0.6 and 1.3 cps, respectively), in *trans-* and *cis-*2-butene[8] (J_{14}, 1.5 and 1.1 cps, respectively), in angelic and tiglic acids[9] (J_{14}, 1.5 and 1.2 cps, respectively), and in dimethylacetylene[10] (J, 2.7 cps). It is interesting that such long-range coupling in the quinoline derivatives studied is limited to the 4- and 8-hydrogens. It may be mentioned that the observation of such inter-ring coupling between chemically shifted hydrogens becomes much more difficult if either of the hydrogens concerned is also strongly coupled to another hydrogen from which it is only slightly chemically shifted. Then, due to averaging effects,[11] a splitting of only $J/2$ may occur with an inter-ring coupling of magnitude J.

[1] J. A. Pople, W. G. Schneider, and H. J. Bernstein, *High-resolution Nuclear Magnetic Resonance* (McGraw-Hill Book Company, Inc., New York, 1959).
[2] K. Ito, T. Isobe, and K. Sone, J. Chem. Phys. **31**, 861 (1959).
[3] H. M. McConnell, J. Chem. Phys. **24**, 460 (1956).
[4] J. A. Pople, Mol. Phys. **1**, 216 (1958).
[5] M. Karplus, J. Chem. Phys. **30**, 11 (1959).
[6] H. M. McConnell, J. Mol. Spectroscopy **1**, 11 (1957).
[7] J. A. Elvidge and L. M. Jackman, Proc. Chem. Soc. **1959**, 89.
[8] F. A. L. Anet (to be published).
[9] R. R. Fraser, Can. J. Chem. (to be published).
[10] N. Muller and D. E. Pritchard, J. Chem. Phys. **31**, 768 (1959).
[11] R. E. Richards and T. Schaefer, Mol. Phys. **1**, 331 (1958).

Ion-Molecule Reactions in Mass Spectrometric Studies of Alkali Halide Salts*

THOMAS A. MILNE
Stanford Research Institute, Menlo Park, California

(Received December 21, 1959)

IN mass spectrometric studies[1–4] of the species evaporating from the alkali halides, complex ions of

TABLE I. Ion intensity in arbitrary units.

Temp °K	Na^+	K^+	$NaCl^+$	KCl^+	Na_2Cl^+	K_2Cl^+	$NaKCl^+$ NaCl cell open	$NaKCl^+$ KCl cell open	$NaKCl^+$ Both open
926	94	330	82	67	75	47	0.17	0.028	0.37
943	120	370	*	*	84	51	0.37	0.29	0.66

* Not recorded.

the type M_2X^+ have been observed. These ions could arise either from an ion-molecule reaction such as

$$MX^+ + MX \rightarrow M_2^+ + X$$

or by the dissociative ionization of M_2X_2

$$M_2X_2 + e \rightarrow M_2X^+ + X + 2e.$$

Although Schissler and Stevenson[5] have shown that the cross section for the former type of reaction may be very high, the results of calculations and experiments by Chupka *et al.*[4,6] leave little doubt that under the usual mass spectrometer and Knudsen cell experimental conditions, the latter process accounts for the major fraction of the observed molecule-ions.

However, because of the uncertainty in the apparent reaction cross section to be expected for such ion-strong dipole reactions and because the conditions in the source region of our Bendix time-of-flight spectrometer[7] have not been investigated and are slightly different from the conventional spectrometer (i.e., the ions are produced at near zero drawing out potential and then subsequently pulsed into the accelerating region), it is difficult to estimate the extent of such reactions to be expected in our work. Consequently, in connection with a study of the vaporization of alkali chlorides from Knudsen cells and single crystals we have undertaken an experiment to demonstrate directly and sensitively the contribution of ion-molecule reactions to the observed intensities of M_2Cl^+ under our experimental conditions.

The basis of the experiment is the use of a double orifice cell containing pure KCl in one chamber and pure NaCl in the other. The slit geometry and shutter are so arranged that the two effusing beams may alternatively or simultaneously be allowed to travel into the mass spectrometer and through the ionizing electron beam. It has been shown in equilibrium experiments with LiCl-MX mixtures[8] that the ion $LiMCl^+$ is formed by ionization of the vapor in concentrations equal to or greater than Li_2Cl^+ or M_2Cl^+. In the experiment described here if ion-molecule reactions of the type postulated in the foregoing occur, then one would also expect the ion $NaKCl^+$ to be formed. The possibility of reaction in the neutral beams to form $NaKCl_2$, which would give $NaKCl^+$ on ionization, cannot be excluded in this simple experiment. However, the observed intensity of $NaKCl^+$ should give a measure of the upper limit for the contribution of ion-molecule reactions to the species M_2X^+.

The results reported here were obtained with the Bendix time-of-flight spectrometer using a two-channel pulse counter and electron multiplier to detect individual ions formed. The salts were in the form of optical grade $\frac{1}{4}$-in. diam single crystals sitting in two $\frac{1}{4}$-in. diam$\times$1-in. deep open holes drilled into a resistance heated copper block. The block was about 10-in. from the ionizing electron beam. Experiments were performed at temperatures up to 943°K.

The averaged results obtained in the two experiments at the highest temperatures are shown in Table I. All intensities represent the shutter dependent contribution to that particular mass number, and were obtained with an electron energy of 20 ev.

As shown in the last columns some $NaKCl^+$ was found. However, its shutter dependence with respect to the two cells shows that, within the scatter of the data at such low intensities, it can be accounted for as originating from either cell separately, so that there is no clear evidence of the ion-molecule reaction contribution to $NaKCl^+$. The source of the $NaKCl^+$ when only one cell was open could be due to impurities initially in the salts or to cross contamination during the experiment. The background at 39 was too large to detect any change in K^+ when the NaCl cell was opened or closed but the Na^+ count changed by 0.16 units when the KCl cell was opened or closed indicating directly some impurity in this cell.

By ignoring differences in ion-molecule reaction cross sections for KCl and NaCl and assuming that the probability of formation of M_2X^+ is proportional to $P_{MX}I_{MX+}$ for all combinations of neutrals and ions, then from the data in Table I, it is estimated that if ion-molecule reactions were the sole source of M_2X^+, the ratio $Na_2Cl^+/NaKCl^+$ should be about 0.5. Actually the observed ratio appears to be >1000, so that it seems safe to conclude that under our experimental conditions ion-molecule reactions account for less than 0.1% of the observed M_2X^+ species.

These preliminary experiments suggest that such dual molecular beam arrangements might be suitable for precise study of ion-molecule reactions under conditions where such reactions are more predominant, i.e., higher beam and ion intensities. It should then also be possible to distinguish, by varying certain ionization source

parameters, whether the mixed molecule-ions originate from neutral beam reactions or ion-molecule reactions.

* This research was supported by the U. S. Air Force through the Air Force Office of Scientific Research of the Air Research and Development Command under contract.

[1] N. E. Ionov, Doklady Akad. Nauk S.S.S.R. **59**, 468 (1948).
[2] L. Friedman, J. Chem. Phys. **23**, 477 (1955).
[3] T. A. Milne, H. M. Klein, and D. Cubicciotti, J. Chem. Phys. **28**, 718 (1958).
[4] J. Berkowitz and W. Chupka, J. Chem. Phys. **29**, 653 (1958).
[5] D. P. Stevenson and D. O. Schissler, J. Chem. Phys. **29**, 282 (1958).
[6] W. Chupka, J. Berkowitz and C. Giese, J. Chem. Phys. **30**, 827 (1959).
[7] W. C. Wiley and I. H. McLaren, Rev. Sci. Instr. **26**, 1150 (1955).
[8] T. A. Milne and D. Cubicciotti, J. Chem. Phys. **29**, 846 (1958).

Indium Sulfate: Raman Spectra and Incomplete Dissociation

B. McCarroll, *George Herbert Jones Laboratory, University of Chicago, Chicago, Illinois*

AND

M. H. Lietzke, *Oak Ridge National Laboratory, Oak Ridge, Tennessee*

(Received December 10, 1959)

IN aqueous solutions of $In_2(SO_4)_3$ there is evidence for the hydrolysis of the indium ion.[1,2] There is also evidence which indicates considerable association between In^{3+} and SO_4^{2+}. Ion exchange studies indicate $In(SO_4)_2^-$ and extraction studies of aqueous solutions show possibly three complex species.[3] Lietzke and Stoughton[4] have interpreted the solubility of Ag_2SO_4 in $In_2(SO_4)_3$ solutions to indicate that the latter salt behaves as a 1,1 electrolyte in concentrated solutions of $In_2(SO_4)_3$. They pointed out, however, that the variations of their emf and conductivity data indicate that $In_2(SO_4)_3$ behaves as a 1,2 electrolyte. For example, at 0.01 *M* the variation of the conductivity is consistent with

$$In_2(SO_4)_3 \leftrightarrows 2InSO_4^+ + SO_4^{2-}.$$

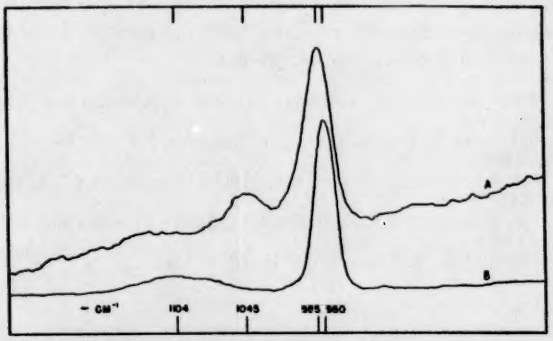

FIG. 1. Raman spectra of (A) 0.985 *M* $In_2(SO_4)_3$ and (B) 3.57 *M* $(NH_4)_2SO_4$.

TABLE I. Raman frequencies of $In_2(SO_4)_3$ and $(NH_4)_2SO_4$ in cm^{-1}.

$In_2(SO_4)_3$	$(NH_4)_2SO_4$
450±10	450
613±10	613
985	980
1045	...
1104±15	1104

Figure 1 is a reproduction of portions of the photoelectric Raman recordings of 0.985 *M* $In_2(SO_4)_3$ (upper trace) and 3.57 *M* $(NH_4)_2SO_4$ (lower trace). The amplification of the upper trace is three times that of the lower trace. The photoelectric Raman spectrometer has been described.[5] Except where noted, the frequencies reported in Table I are within ±5 cm^{-1}.

The shift and broadening of the main peak of the $In_2(SO_4)_3$ spectrum with respect to the 980 cm^{-1} peak of $(NH_4)_2SO_4$ may be caused by the foot of the 1045 cm^{-1} band overlapping the high-frequency side of the main peak. This effect and the 1045 cm^{-1} band are also evident in the spectrum of a 0.228 *M* $In_2(SO_4)_3$ solution.

A 0.924 *M* $In_2(SO_4)_3$ solution which is 1.44 *M* in added $(NH_4)_2SO_4$ has a 1045 cm^{-1} intensity about 20% higher than the 0.985 *M* solution (with no added sulfate). The increase in intensity, interpreted as an increase in the concentration of the species causing the 1045 cm^{-1} band, is consistent with either or both of the reactions

$$In^{3+} + SO_4^{2-} \rightleftarrows InSO_4^+$$

$$In^{3+} + 2SO_4^{2-} \rightleftarrows In(SO_4)_2^-.$$

At present, we are unable to ascertain which species causes the 1045 cm^{-1} band.

We are indebted to Professor T. F. Young for suggestions and for the use of his Raman instrument.

[1] R. P. Seward, J. Am. Chem. Soc. **55**, 2740 (1933).
[2] E. M. Hattox and T. De Vries, J. Am. Chem. Soc. **58**, 2126 (1936).
[3] N. Suden, Svensk Kem. Tidskr. **66**, 173, 345 (1954).
[4] M. H. Lietzke and R. W. Stoughton, J. Am. Chem. Soc. **78**, 4520 (1956).
[5] T. F. Young, Record Chem. Progr. (Kresge-Hooker Sci. Lib.) **12**, 81 (1951).

Note on the Equation of State for Hard Spheres*

O. K. Rice

Department of Chemistry, University of North Carolina, Chapel Hill, North Carolina

(Received November 13, 1959)

INTRODUCTION of a sphere of diameter *b* into a gas of hard spheres with diameter *a* is equivalent to

introduction of an *exclusion* sphere of *radius* $r=(a+b)/2$. The pressure exerted by the centers of the spheres of diameter a, at a number density ρ, against the exclusion sphere is $p_r=kT\rho G(r,\rho)$, where $\rho G(r,\rho)$ is the density of centers at the distance r from the center of (i.e., in contact with) the exclusion sphere. Reiss *et al.*[1] show that for $r\leq a/2$ we have, exactly, $G(r,\rho)=(1-\frac{4}{3}\pi r^3\rho)^{-1}$; they give arguments to support the contention that $G(r,\rho)$ should be given approximately by $1+\frac{2}{3}\pi a^3\rho G(a,\rho)+\alpha/r+\beta/r^2$, for $a/2\leq r<\infty$ (α and β are functions of ρ). By evaluating this at $r=a$, and comparing with $G(r,\rho)$ and its derivative at $r=a/2$ from the other expression, enough relations are obtained to eliminate α and β, the result being

$$G(a,\rho)=\frac{1}{4(1-\pi a^3\rho/6)}+\frac{3}{4(1-\pi a^3\rho/6)^2}+\frac{\pi a^3\rho}{8(1-\pi a^3\rho/6)^3}. \quad (1)$$

If expanded in powers of $\pi a^3\rho$, Eq. (1) gives excellent values for the first five virial coefficients; even the fourth virial coefficient is only about 3% high and the fifth about 5% high (the actual value of the latter is not too certain).

The approximations involved in Eq. (1) have been discussed in detail by Reiss *et al.* who noted that Eq. (1) holds best when ρ is not too large. When ρ becomes greater the approximations become less justified; Eq. (1) does not diverge until $\rho=6/\pi a^3$, which considerably exceeds the density, $\rho_0=2^{\frac{1}{2}}/a^3$, for close-packed spheres of diameter a. One of the factors in this behavior has not been explicitly discussed, and seems to be of some interest.

For spheres thrown together at random there is a limiting density $\rho_0'\sim\rho_0/1.15$. As a hard-sphere gas with this type of random configuration is compressed toward ρ_0' its pressure approaches infinity. This means, from the expression for p_r applied at $r=a$ and $r=\infty$, that $G(a,\rho_0')$ and $G(\infty,\rho_0')$ are both infinite. It is easy to see that this must be so, for at this limiting density neighbors are constantly held against any central sphere and against the wall and the pair-distribution function approaches a delta function. However, an exclusion sphere with radius sufficiently less than a but greater than $a/2$ can be introduced into various positions in the gas without touching the centers of any of the hard spheres. Once it is introduced, the centers of the hard spheres will occasionally collide with it and bounce off its surface, but clearly $G(r,\rho_0')$ will not be infinite. $G(r,\rho_0')$ will change from the value $(1-\frac{1}{6}\pi a^3\rho_0')^{-1}$ at $r=a/2$ to infinity at $r=a$ (or $r<a$), and then will remain infinite, so the expression for $G(r,\rho)$ cannot be used over the range between $r=a/2$ and $r=\infty$ for ρ near ρ_0'. Despite this, Eq. (1) holds well at densities only slightly less than ρ_0'. The following remarks apply to some relatively fine points, involving differences between different curves of around 10% in the pressure in the interesting density range.

Machine calculations of the equation of state of a gas of hard spheres have been made[2,3]; there are two branches, one corresponding to a random or fluid phase, the other corresponding to a regular or solid phase. The equation of state obtained from Eq. (1) goes nicely through the machine calculations for the random branch to as high densities as the latter go. An equation of state obtained by attempting to extrapolate the virial coefficients, assuming that beyond the fourth-power term of the series in powers of ρ/ρ_0' the coefficients remain the same (which would make the series diverge at the right value of ρ/ρ_0'), gives a curve which comes close to the random machine points at the lower densities but at larger densities goes above these points.[4] A curve which the author obtained by a special method of interpolation falls below the machine points at low densities and eventually goes above them, but not as much higher as the curve obtained from the extrapolation of the virial coefficients. Some arguments[4] that at low densities the random curve should be lower than that given by the machine calculations were based on the question of intersection with the corresponding curve for the regular phase and the density at which a transition might occur between these phases, which is closely related to the point of intersection. Lowering the random curve would make the transition occur at a greater density, which seemed more reasonable. It is not impossible that the machine points might lie too high, on account of the relatively small number of particles which could be considered. Equation (1), which passes through the machine points, gives fourth and fifth virial coefficients which appear to be slightly (but increasingly) too large. Thus Eq. (1) may also give too high a pressure at the lowest densities at which machine calculations were made, even though at greater densities it does not diverge soon enough. The exact course of the equation of state thus cannot be considered to be definitely settled, but the author feels that the evidence from the intersection and transition point cannot be ignored.

* This work was supported by the Office of Ordnance Research, U. S. Army.

[1] H. Reiss, H. L. Frisch, and J. L. Lebowitz, J. Chem. Phys. **31**, 369 (1959).

[2] Wood, Parker, and Jacobson, Nuovo Cimento Suppl. **9**, 133 (1958).

[3] B. J. Alder and T. E. Wainwright, Nuovo Cimento Suppl. **9**, 116 (1958).

[4] O. K. Rice, J. Chem. Phys. **31**, 987 (1959).